R-10-49

Site investigation SFR

Bedrock geology

Philip Curtis, Ingemar Markström
Golder Associates AB

Jesper Petersson
Vattenfall Power Consultant AB

Carl-Axel Triumf, Hans Isaksson, Håkan Mattsson
GeoVista AB

December 2011

Svensk Kärnbränslehantering AB
Swedish Nuclear Fuel
and Waste Management Co

Box 250, SE-101 24 Stockholm
Phone +46 8 459 84 00

ISSN 1402-3091
SKB R-10-49

Site investigation SFR

Bedrock geology

Philip Curtis, Ingemar Markström
Golder Associates AB

Jesper Petersson
Vattenfall Power Consultant AB

Carl-Axel Triumf, Hans Isaksson, Håkan Mattsson
GeoVista AB

December 2011

Keywords: SKBdoc 1254755, Kravdatabas SFR-utbyggnad (N2X-275).

Preface

The following people have contributed to the geological modelling work:

Deterministic modelling of rock domains – Jesper Petersson, Ingemar Markström, Hans Isaksson and Håkan Mattsson.

Deterministic modelling of deformation zones – Philip Curtis, Jesper Petersson, Carl-Axel Triumf with support from Johan Öhman, Diego Mas, Sakar Koyi and Sara Kvartsberg.

Reflection seismic data and interpretation – Christopher Juhlin.

The investigation of a possible relationship between deformation zone thickness and length (Appendix 10) – Aaron Fox.

Important contributions and internal review – Michael Stephens and Assen Simeonov.

External review – Geoffrey Milnes, Derek Martin and Raymond Munier.

Contents

Summary

SKB is currently carrying out an assessment of the future extension of the final repository for low and middle level radioactive operational waste, SFR. The planned SFR extension lies at a relatively shallow depth (–50 to –200 masl) compared with the planned Forsmark facility for spent nuclear fuel (–400 to –500 masl). The main aim of the multidisciplinary modelling project involving geology, hydrogeology, hydrogeochemistry and rock mechanical modelling is to describe the rock volume for the planned extension of SFR that was presented in /SKB 2008a/. The results of the modelling project in the form of a forthcoming site descriptive model will supply the basis for site-adapted design including engineering characteristics, in addition to a general assessment of the site suitability.

The current report presents the results of the geological work with the deterministic rock domain and deformation zone models (version 1.0) and forms a basis for the three other disciplines in the modelling work. The shallow depth of SFR and its proposed extension means that the facility lies partly within the rock volume affected by the effects of stress release processes during loading and unloading cycles, with an associated increased frequency of open sub-horizontal fractures in the near-surface realm (above –150 masl) compared with that observed at greater depths.

The main report describes the data input to the modelling work, the applied modelling methodology and the overall results. More detailed descriptions of the individual modelled deformation zones and rock domains are included in the appendices. The geological modelling work during version 1.0 follows SKB's established methodology using the Rock Visualisation System (RVS). The deformation zone model version 1.0 is a further development of the previous version 0.1 /Curtis et al. 2009/. While the main input to deformation zone model version 0.1 was older geological data from the construction of SFR, including drawings of the geological tunnel mapping and eleven drill cores remapped according to the Boremap system, input to model version 1.0 has included the results from eight new cored boreholes as well as a fuller integration of Forsmark site investigation data, a further more extensive review of the drill core from an additional 32 boreholes associated with the construction of the existing SFR facility and an updated mapping of the lower construction tunnel. The current modelling work has also reviewed the older SFR data and models. While details concerning the earlier zones lying in immediate contact with the existing SFR facility have been changed, the earlier overall position, orientation and number of these deformation zones is maintained. A significant difference concerns their thickness due to the contrasting methodologies used during the different campaigns.

In SFR model version 0.1, a single deformation zone model was produced, with a volume corresponding to the regional model volume. The model contained all the deformation zones modelled irrespective of size. Separate local and regional deformation zone models have been produced in SFR model version 1.0, following resolution criteria for the different model volumes. The local model contains zones with a minimum size of 300 m, while the regional model has structures that have a minimum size constraint of 1,000 m trace length at the ground surface. The selection of these size limits is related to the model volume maximum depth (local model –300 masl and regional model –1,000 masl) and the applied methodology that requires the same model resolution throughout the defined model volume (see Section 5.3.1). To assist hydrogeological modelling work, an updated combined model, including all structures from both the regional and local models, has also been delivered.

The existing SFR facility and the rock volume directly to the south-east, which is proposed for the new facility extension, lies within a tectonic block that is bounded to the north-east and south-west by two broad belts of concentrated ductile and brittle deformation (Figures S-1 and S-2). The central block is less affected by deformation than the bounding belts. Within the central block, in the rock volume for the planned extension, a series of WNW-NW trending deformation zones are included in the local model (Figure S-2). These are much smaller than the bounding belts and were initiated at a later stage in a brittle regime. Even smaller zones with the same general strike and character, below the current model resolution, are inferred to permeate the entire rock volume. A NE to ENE striking set of brittle deformation zones is also present (Figure S-2). Compared with the WNW-NW set they are generally thinner and shorter, due to termination against the broad WNW-NW trending deformation belts.

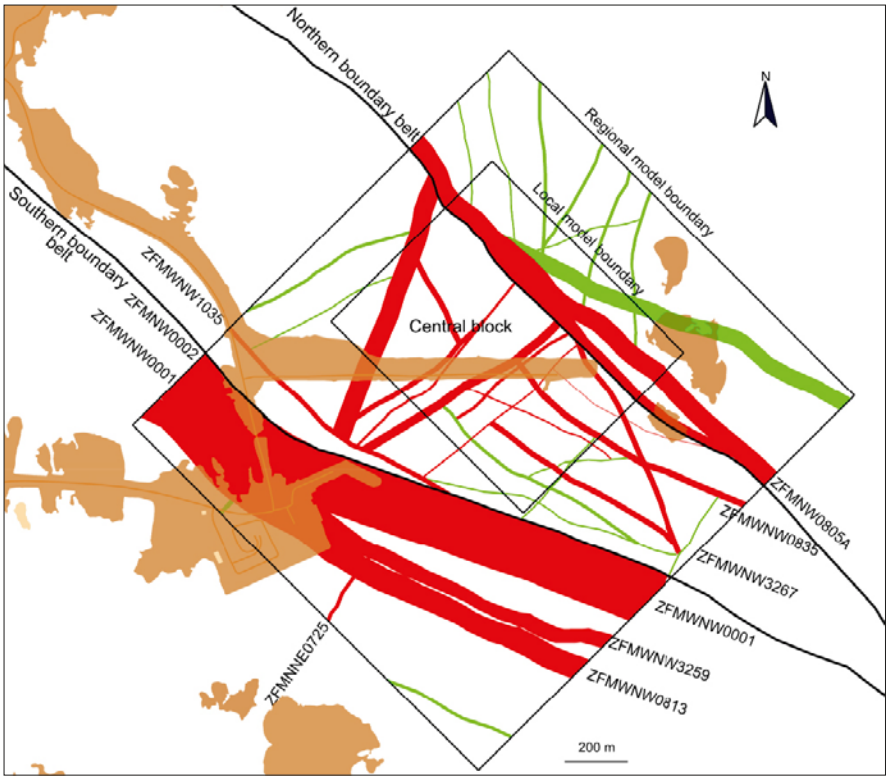

Figure S-1. *Intersection at the current ground surface of deformation zone traces of all sizes inside the regional model area, i.e. a combined model version. A northern and southern belt of with regional deformation zones and their major splays, form the general boundaries of the central SFR tectonic block. The northern belt consists of ZFMNW0805A/B and the southern belt of ZFMWNW0001, ZFMWNW0813, ZFMWNW3259 and ZFMNW0002 (see Chapter 5 for further details). Confidence in existence: high=red, medium=green.*

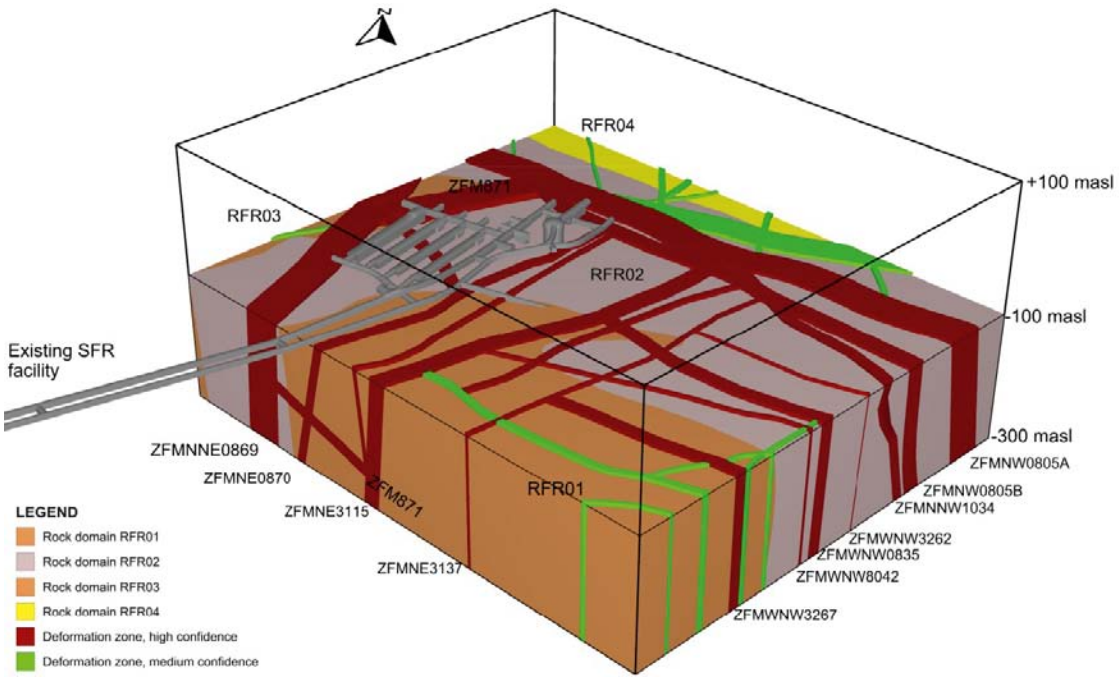

Figure S-2. *Rock domains and deformation zones included in the SFR local model, version 1.0. The relationship to the existing SFR underground facility is illustrated by a horizontal section at –100 m elevation, viewed to the north. Note that parts of the silo and lower construction tunnel (NBT) are beneath that level.*

The existence of gently dipping deformation zones was a particular focus of the project due to their previously identified engineering significance. No new significant gently dipping deformation zone was identified in the rock volume for the new extension. However, there is a relatively high frequency of sub-horizontal open fractures in the upper part of the rock volume (above c. –150 masl), which are inferred to have formed or to have been reactivated in connection with stress release processes during unloading and also by strike-slip movements along the bounding steeply dipping zones. These sub-horizontal to gently dipping structures make a more significant contribution to the pattern of local groundwater flow in the upper part of the bedrock than the steeply dipping deformation zones.

A rock domain model has been produced in SFR model version 1.0 for the local model volume. In the same way as the deformation zone model it is based on a mixture of old and new data. Four rock domains have been recognised in the local SFR model volume mainly on the basis of rock composition and degree of heterogeneity. High resolution magnetic total field data, in combination with fixed points along drill cores, have made a significant contribution to the definition of boundaries between domains. The rock volume for the planned extension is situated within two rock domains, RFR01 in the south-west and RFR02 in the north-east (Figure S-2). Rock domain RFR01 is modelled as a major fold structure characterised by a relatively high degree of homogeneity and dominated by pegmatitic granite and pegmatite with a poorly-developed ductile deformational fabric, whereas rock domain RFR02 is far more heterogeneous and dominated by fine- to finely medium-grained metagranodiorite (to granite), often with a well-developed planar ductile deformational fabric.

The model described in this report follows the earlier established conceptual understanding of the geological evolution in the Forsmark area. At the end of model version 1.0, the overall confidence level concerning the regional deformation history and the broad tectonic framework of the region is judged to be high. However, the overall confidence level in the rock volume of specific interest to the SFR project, lying between deformation zones ZFMWNW0001 and ZFMNW0805A, is inevitably somewhat lower due to scale-related issues and the distribution of available data as discussed in this report . While certain details concerning particular deformation zones have been modified, there is nothing resulting from the current modelling work that has any significant impact on the earlier reported results for the Forsmark project for the final repository for spent nuclear fuel.

Sammanfattning

SKB utvärderar för närvarande en planerad utbyggnad av slutförvaret för låg- och medelaktivt kortlivat radioaktivt avfall, SFR. Den planerade utbyggnaden skall förläggas relativt ytnära (–50 till –200 m.ö.h.) jämfört med det planerade djupförvaret för utbränt kärnbränsle i Forsmark (–400 till –500 m.ö.h.). Syftet med detta multidisciplinära modelleringsprojekt, som inkluderar geologi, hydrogeologi, hydrogeokemi och bergmekanisk modellering, är att karaktärisera den bergvolym för planerad utbyggnad som presenterades i /SKB 2008a/. I form av en kommande platsbeskrivande modell kommer projektet att utgöra grunden för platsspecifik projektering, samt en generell utvärdering av platsens lämplighet.

Föreliggande rapport presenterar resultaten från det geologiska modelleringsarbetet med de deterministiska bergdomän- och deformationszonsmodellerna (version 1.0), som utgör underlag för övriga discipliners modelleringsarbete. Det ytnära läget för SFR och den planerade utbyggnaden innebär att anläggningen delvis kommer att ligga i den del av bergmassan som påverkats av glacial av- och pålastning, med en förhöjd frekvens av öppna, subhorisontella sprickor som följd jämfört med större djup (under ungefär –200 m.ö.h.).

Huvudrapporten för den geologiska modelleringen beskriver underlagsdata, den tillämpade modelleringsmetodiken och modelleringsresultaten. Mer detaljerade beskrivningar av enskilda deformationszoner och bergdomäner presenteras i form av bilagor. Modelleringsarbetet under version 1.0 följer SKB:s vedertagna metodik med användandet av RVS. Modellversion 1.0 för deformationszonerna är en vidareutveckling av den tidigare version 0.1 /Curtis et al. 2009/. Medan modellversion 0.1 huvudsakligen var baserad på äldre geologisk data från byggnationen av SFR, inklusive geologisk tunnelkartering och elva borrkärnor som omkarterats med Boremap-systemet, så är modellversion 1.0 baserad på ytterligare resultat från åtta nya kärnborrhål, integration av data från Platsundersökning Forsmark, en genomgång av ytterligare 32 borrkärnor från byggnationen av SFR och en förnyad kartering av nedre byggtunneln. Modelleringsarbetet omfattar även en genomgång av äldre SFR-data och modeller. Medan detaljerna för äldre modellerade zoner i omedelbar anslutning till SFR har förändrats så har deras lägen, orientering och antal lämnats oförändrade i modellversion 1.0. En betydande olikhet, som resultat av metodikskillnader vid det två projekten, är dock zonernas tjocklek.

För SFR version 0.1 levererades endast en deformationszonsmodell, med en volym som motsvarar den regionala modellvolymen. Denna integrerade modell innehöll alla deformationszoner som dittills modellerats oberoende av storlek. För version 1.0 har både en separat lokal och en regional deformationszonsmodell levererats med de upplösningskriterier som gäller för de två olika modellvolymerna. Den lokala modellvolymen innehåller zoner med en undre storleksbegränsning på 300 m, medan den regionala modellen har strukturer med en undre storleksbegränsning på 1 000 m för den projicerade längden på markytan. Val av storleksbegränsning är ett direkt resultat av modellvolymernas maximala djup (i den lokala modellen –300 m.ö.h. och i den regionala modellen –1 000 m.ö.h.), samt att metodiken som tillämpats kräver enhetlig upplösning i hela modellvolymen (se underrubrik 5.3.1). För att underlätta arbetet med den hydrogeologiska modelleringen har även en uppdaterad kombinerad version av de lokala och regionala modellerna levererats.

Den befintliga SFR-anläggningen och anslutande bergvolym åt sydost, vilken föreslås rymma den utbyggda förvarsdelen, ligger i ett tektoniskt block som i nordost och sydväst begränsas av två breda stråk av förhöjd plastisk och spröd deformation (figurer S-1 och S-2). Det centrala blocket är följaktligen mindre påverkat av deformationen än de omgivande stråken. I den del av blocket som planeras rymma utbyggnaden har en serie västnordvästligt till nordvästligt strykande deformationszoner lagts in i modellen (figur S-2). Dessa är betydligt mindre än de omgivande, breda stråken och anses vara initierade något senare, i en spröd regim. Även mindre zoner med samma generella orientering och karaktär, men som understiger begränsningen för deterministisk modellering, antas förekomma i hela bergvolymen. En grupp med nordostligt till ostnordostligt strykande deformationszoner har modellerats (figur S-2). Jämfört med den västnordvästligt till nordvästligt strykande gruppen är de tunnare och kortare, till följd av trunkering mot de breda västnordvästligt till nordvästligt strykande deformationsstråken. Förekomsten av flackt stupande deformationszoner har varit en väsentlig fråga för projektet, på grund av deras tidigare belagda ingenjörsmässiga betydelse.

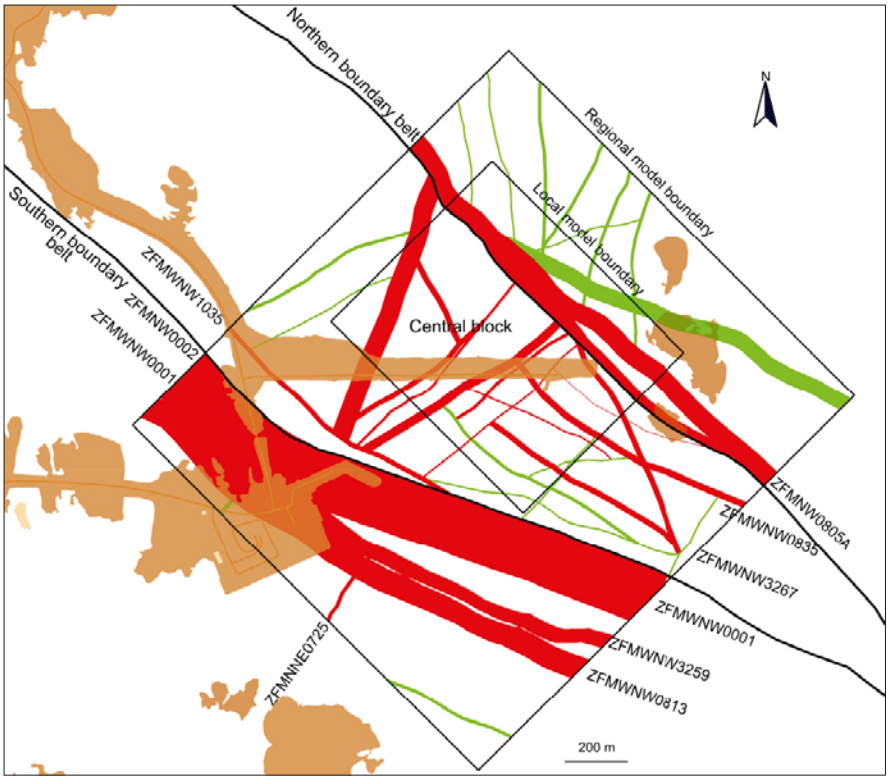

Figur S-1. *Skärningen med markyta för alla modellerade deformationszoner inom det regionala modellområdet oberoende av storlek , d v s. en kombinerad modellversion. Ett nordligt och ett sydligt stråk av regionala deformationszoner med associerade smärre zoner utgör begränsningar till ett centralt tektoniskt block. Det norra stråket utgörs av ZFMNW0805A/B och det södra stråket av ZFMWNW0001, ZFMWNW0813, ZFMWNW3259 och ZFMNW0002 (se kapitel 5 för ytterligare detaljer). Osäkerhet beträffande zonernas existens: hög konfidensgrad=röd, medium konfidensgrad=grön.*

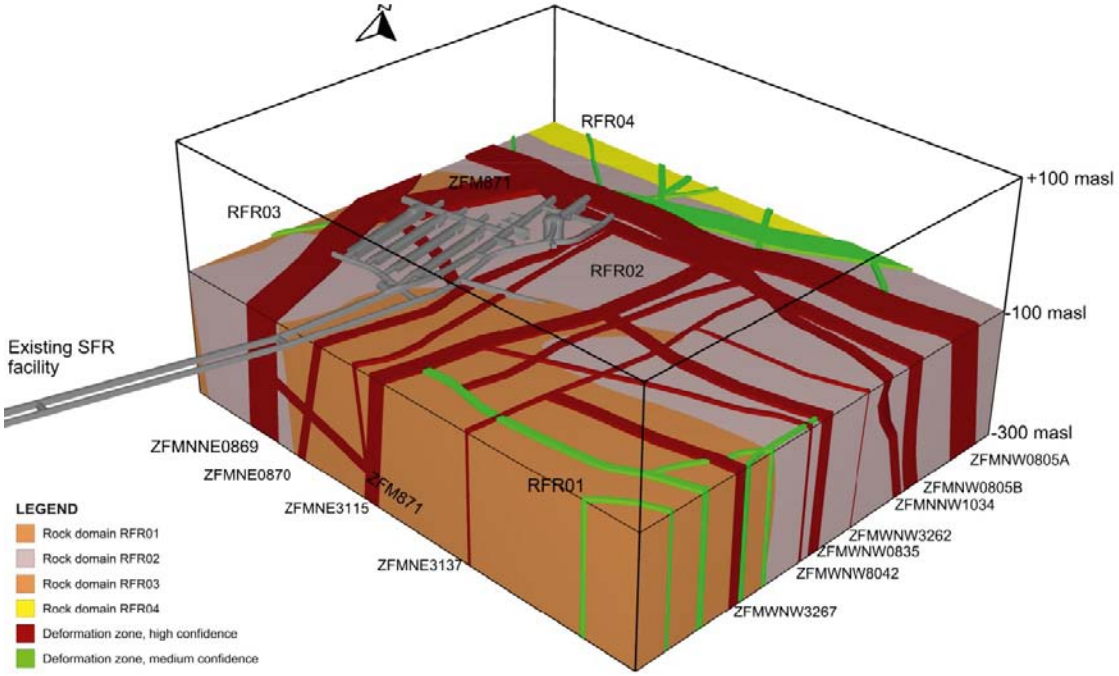

Figur S-2. *Bergdomäner och deformationszoner inkluderade iden lokala modellen, version 1.0. Relationen med befintlig underjordsdel av SFR illustreras i ett horisontellt snitt på en nivå av –100 m.ö.h. med vy mot norr. Notera att delar av silo och nedre byggtunneln (NBT) är belägna under denna nivå.*

Inga nya flackt stupande deformationszoner av betydelse har identifierats i bergvolymen för den tilltänkta utbyggnaden. Frekvensen av subhorisontella, öppna sprickor som antas vara bildade eller reaktiverade i samband med avlastning och till följd av förkastningsrörelser längs associerade brant stupande zoner är dock relativt hög i den ytnära bergvolym (över ungefär –200 m.ö.h.). Dessa strukturer är av större betydelse för det lokala grundvattenflödet än de brantstupande deformationszonerna.

En bergdomänmodell, motsvarande den lokala modellvolymen, ingår i SFR modellversion 1.0. På samma sätt som för deformationszonsmodellen baserar den sig på både gammal och ny data. Fyra bergdomäner har identifierats i den lokala modellvolymen, huvudsakligen på grundval av bergartssammansättning och heterogenitet. Högupplöst data för det magnetiska totalfältet har tillsammans med geologiska fixpunkter längs borrhål och tunnlar varit avgörande för att definiera domänernas begränsningar. Bergvolymen för den planerade utbyggnaden är belägen i två olika bergdomäner: RFR01 i sydväst och RFR02 i nordost (figur S-2). Bergdomän RFR01 är modellerad som en större veckstruktur som karaktäriseras av en relativt hög grad av homogenitet och domineras av pegmatitisk granit och pegmatit, medan bergdomän RFR02 är betydligt mer heterogen och domineras av fin- till fint medelkornig metagranodiotit (till granit), ofta med en distinkt plastisk planstruktur.

Föreliggande modell följer vedertagen konceptuell förståelse av den tektoniska och geologiska historien i Forsmarksområdet. Den övergripande konfidensnivån för deformationshistorien och regionens tektoniska ramverk bedöms mot slutet av modellversion 1.0 vara hög. Den övergripande konfidensnivån i bergmassan mellan deformationszonerna ZFMWNW0001 och ZFMNW0805A som är av specifikt intresse för utbyggnadsprojektet, bedöms däremot vara något lägre på grund av skalrelaterade problem och fördelningen av tillgänglig data, vilket även diskuteras i rapporten. Medan vissa detaljer för enskilda deformationszoner har modifierats har arbetet under den aktuella modelleringsfasen inte haft någon inverkan på tidigare rapporterade resultat från Platsundersökning Forsmark för slutförvaret av uttjänt kärnbränsle.

1 Introduction

1.1 Background

During 2008, the Swedish Nuclear Fuel and Waste Management Company (SKB) initiated an investigation programme for a future extension of the final repository for low and middle level radioactive operational waste, SFR /SKB 2008a/. The motivation for the extension was to provide room for the demolition waste from the closed reactors (Barsebäck, Studsvik and Ågesta) and the increased amount of operational waste caused by the extended operating time of the remaining nuclear power plants.

The programme was preceded by the site investigations for a deep repository for spent nuclear fuel, henceforth denoted the Forsmark site investigation /SKB 2008b/, and some systematisation and evaluation of the material from the construction of the nuclear power plant and SFR. Based on these data, a site descriptive model, version 0, was compiled for geology, rock mechanics, hydrogeology and hydrogeochemistry (see compilation in /SKB 2008a/).

SFR geological modelling work continued with version 0.1 /Curtis et al. 2009/, based on additional evaluation of older geological data from SFR and a revision of lineaments based on the interpretation of high resolution measurements of the magnetic total field covering most of the SFR area /Isaksson et al. 2007/. Only a deterministic deformation zone model was produced during version 0.1, no rock domain modelling work was undertaken.

This report covers the investigation and modelling work carried out in connection with the production of the SFR version 1.0 geological model. Both deformation zone and rock domain sub-models have been produced and these constitute the final model version for the SFR extension project. The final geological model provides the framework for the modelling work by other disciplines, including rock mechanics, hydrogeology and hydrogeochemistry as well as a foundation for the detailed design and the long-term safety assessment.

Model version 1.0 is based on the completed revision of magnetic lineaments in the model area, some reprocessing of earlier reflection seismic data, a further re-examination and integration of earlier SFR drilling and tunnel mapping results as well as the results from the surface and underground based boreholes of the latest drilling campaign. The work has followed SKB's established methodology for modelling /Munier et al. 2003/ using the Rock Visualisation System (RVS) /Curtis et al. 2007/.

The investigations for the extension of SFR differ in several aspects from the preceding Forsmark site investigation. Since it is desired that the new repository will connect with the existing facility, the target area for the location of the extension was already well-defined in the version 0 report /SKB 2008a/. Thus, the current SFR investigations supply the basis for site-adapted design in addition to a general assessment of the site suitability. Other significant differences are the repository type and depth, as well as the existence of data from the construction of SFR. Also the fact that the target area is located under the sea has implications for the investigations by limiting the number of bedrock exposures, possible drilling locations and the coverage of seismic surveys.

In order to aid comparative studies, the current report is structured in a similar manner as the stage 2.2 site descriptive model report for geology produced during the Forsmark site investigation /Stephens et al. 2007/. All figures containing geographical information within the report are published with permission from Lantmäteriet MS 2006/01789.

1.2 Objective and scope

The general aim of the geological modelling work is to provide deterministic deformation zone and rock domain models that fulfil the needs of the repository design and safety assessment groups. Since the deterministic geological models form the framework for the modelling work by other disciplines, including rock mechanics, hydrogeology and hydrogeochemistry, they have been developed successively, in tandem with the other models as new data from the SFR site investigation became available. The results from all of these modelling efforts are to be integrated into a comprehensive site description (SDM) of the SFR site.

The specific aim with the version 1.0 modelling work was to further develop the existing version 0.1 deterministic deformation zone model and create a new deterministic rock domain model, based on a reassessment of existing data from SFR and the Forsmark site investigation, along with integration of data from the latest drilling campaign.

The current report and modelling work has been restricted to the development of a geological model with a predefined maximum resolution of 300 m within the local model volume (see Section 1.4). This maximum resolution must be considered when using the model. The development of a geological Discrete Fracture Network (DFN) model or fracture domain model, covering smaller structures is not included in the scope of work for this project. In addition, the aim of the current work has not been to provide an engineering description of the rock mass but rather a strictly geological description at the predefined resolution. Consequently, engineering geological descriptions and evaluations have been excluded from the current report.

1.3 Geological setting

While the current project has increased the detailed knowledge concerning the geology in the SFR regional model area, in the immediate vicinity of the existing SFR facility, no new data or interpretations have been forthcoming that affect the earlier established interpretation of the regional geological setting as described by /Söderbäck 2008/ and that is summarised below.

The SFR facility is located in northern Uppland close to the Forsmark nuclear power plant within the municipality of Östhammar, about 120 km north of Stockholm. The area forms part of a crustal segment in the Fennoscandian Shield generally affected by high ductile strain that extends several tens of kilometres across the Palaeoproterozoic bedrock in northern Uppland. This crustal segment consists of sub-vertical belts affected by high ductile strain that strike WNW-ESE to NW-SE and anastomose around tectonic lenses affected by lower ductile strain (Figure 1-1). The deformation initiated under amphibolite-facies metamorphic conditions at mid-crustal levels during the Svecokarelian orogeny, and continued at lower metamorphic grade with the retrograde development of more discrete, sub-vertical deformation zones with similar strike, along which both ductile and brittle strain was focused. Other orientation sets of brittle deformation zones as well as further WNW-ESE to NW-SE zones, which are sub-vertical or gently dipping, formed during the later stages of or after the Svecokarelian orogeny.

The SFR area is situated within a high-strain belt that forms the north-easterly margin to the so-called Forsmark tectonic lens /SKB 2008b/. The north-western part of this tectonic lens hosts the target area for siting the potential repository for spent nuclear fuel. The rock volume that includes the SFR underground facility lies between two regional deformation zones of focussed ductile and brittle strain, the Singö deformation zone (ZFMWNW0001) and zone ZFMNW0805A (Figure 1-2). The rock types, their grouping and temporal relationship in this rock volume are virtually identical to that of the rocks in the adjacent Forsmark tectonic lens, but they are generally affected by a much higher degree of ductile strain and a well-defined WNW-ESE to NW-SE structural trend.

The strongly deformed rocks in the SFR area consist of a heterogeneous package of mainly felsic to intermediate metavolcanic rocks intercalated with biotite-bearing metagranodiorite (to granite). These rocks form the major components in an older igneous suite. They exhibit a penetrative foliation and are, in part, also lineated or banded, forming heterogeneous banded, foliated and lineated (BSL) tectonites. Due to the intense strain and recrystallization, these rocks are generally difficult to separate (see Chapter 4). Other subordinate rock types in this suite are amphibolite and aplitic metagranite. Lithological contacts between these rocks are generally aligned parallel to the ductile tectonic foliation. The steeply dipping planar structures and variable inclination of stretching lineation in the region west and south of Forsmark (Bergslagen) suggest development in a transpressive tectonic regime, with dextral strike-slip movement along sub-vertical structures that strike WNW-ESE to NW-SE /Stephens et al. 2009/.

These rocks have been intruded by a younger igneous suite of granite, pegmatitic granite and pegmatite during the waning stages of Svecokarelian orogenic activity. The rocks in this younger igneous suite occur typically as subordinate bodies and dykes. However, in the proximity to and at the scale of the SFR underground facility, they constitute a substantial volume of the rock mass (Figure 1-2).

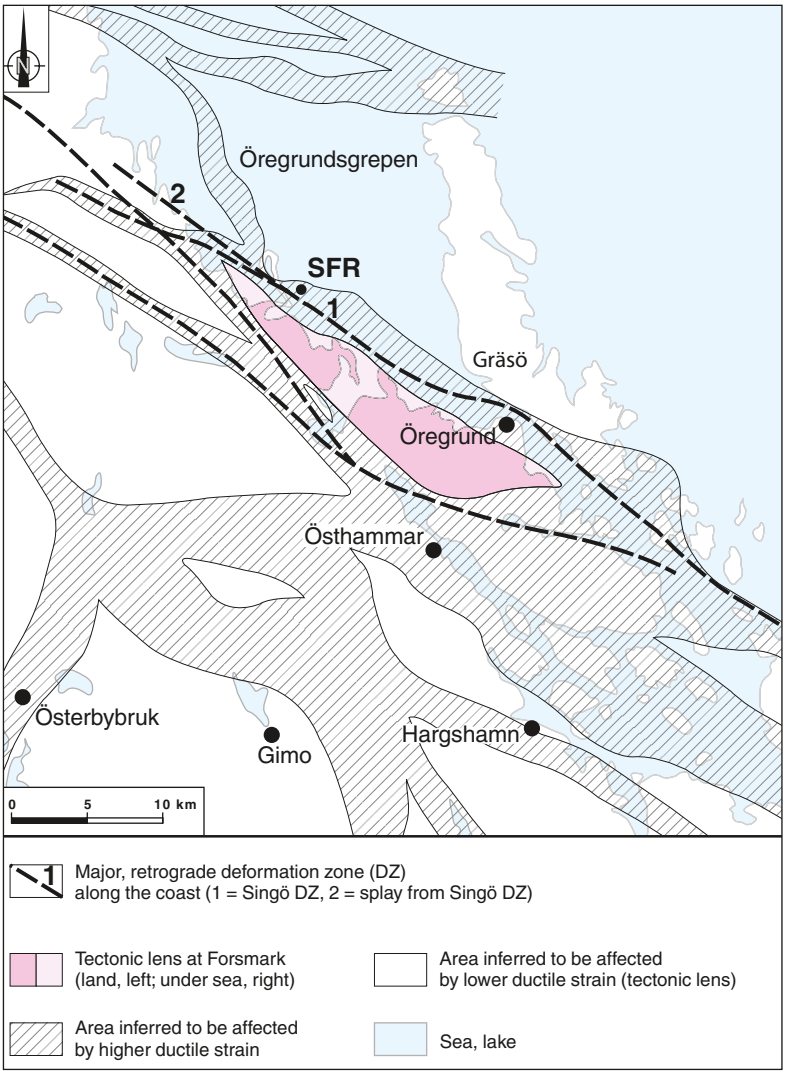

Figure 1-1. *Map showing the structural framework in the Forsmark area with ductile high-strain belts that anastomose around tectonic lenses of lower ductile strain. The major retrograde deformation zones surrounding the Forsmark tectonic lens are also shown. Modified after /Stephens et al. 2007/.*

In contrast to the Forsmark tectonic lens, where these rocks are only partly affected by the ductile deformation and metamorphism, in the SFR area a majority display a conspicuous stretching lineation and, locally, even a planar tectonic fabric. The grain-size is highly variable in the rocks of this suite and may range from fine- to coarse-grained and pegmatitic in a single occurrence. Another conspicuous feature is the anomalously high uranium content in the younger granites, consistent with that observed in the Forsmark tectonic lens and its surroundings to the south-west of the SFR area /SKB 2005, 2008b/.

Folding at different scales, with fold axes sub-parallel to the stretching lineation, has affected most rocks in the area. Based on structural data from the region, /Stephens et al. 2009/ propose that the folds initially developed by normal cylindrical folding and were progressively drawn out in the direction of the stretching lineation into sheath folds. The Singö deformation zone forms a regionally important, composite ductile and brittle zone in the SFR area. A conceptual model for the formation and reactivation of deformation zones in the Forsmark area has been provided in /Stephens et al. 2007/ and is summarised in Section 2.3.

Extensive geochronological data in the Forsmark area indicate that the bedrock formed and was affected by ductile deformation under amphibolite-facies conditions between 1.89 and 1.85 Ga, while ductile deformation along the more discrete zones continued until at least 1.8 Ga /Hermansson et al. 2007, 2008a, b/. The bedrock had cooled sufficiently to respond to deformation in a brittle manner sometime between 1.8 and 1.7 Ga /Söderlund et al. 2009/.

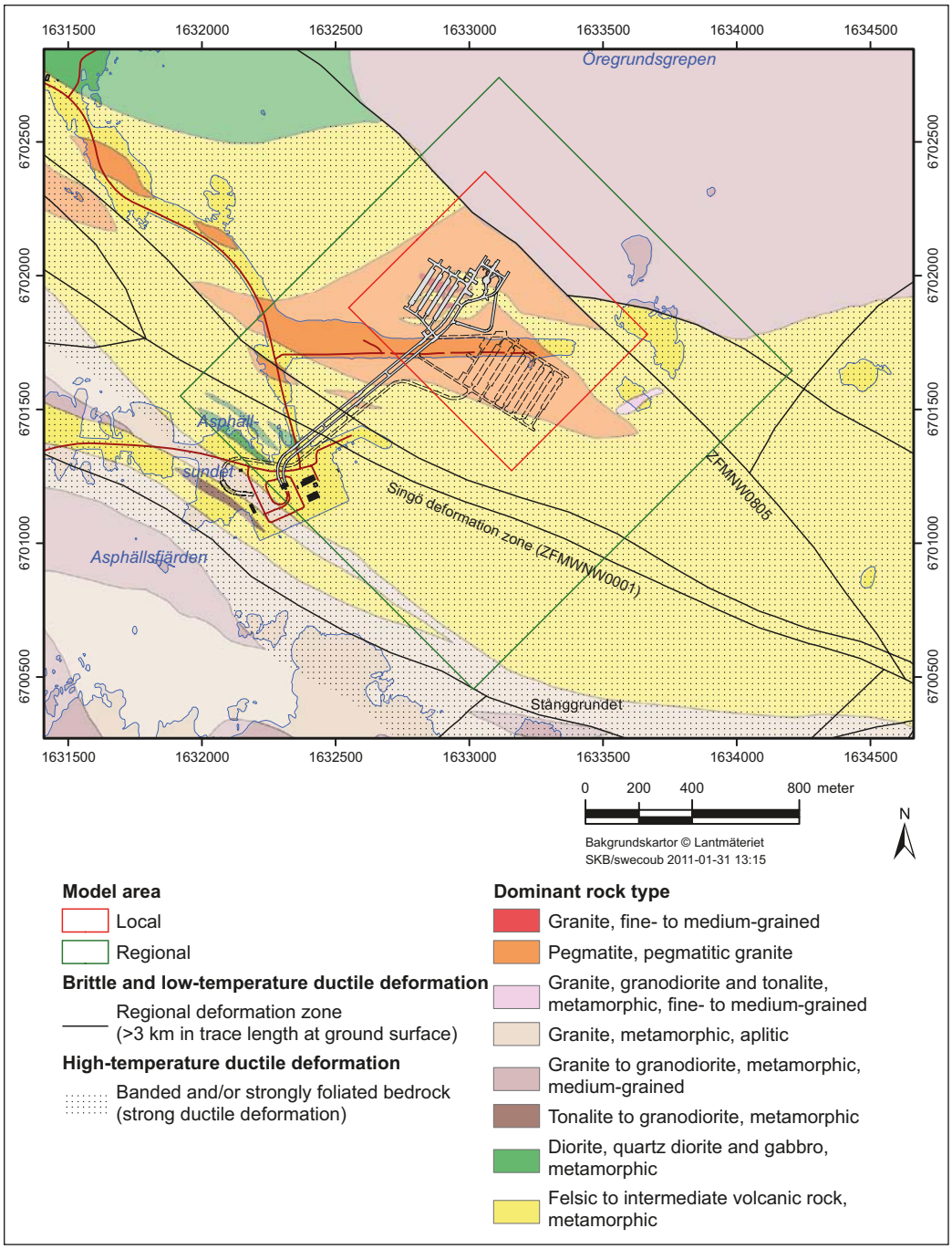

Figure 1-2. *Bedrock geological map of the area around SFR based on the bedrock geological map, Forsmark stage 2.3 /Stephens et al. 2008a/ produced during the Forsmark site investigation. Local and regional SFR model areas are also shown. The paler shades for each colour on the map indicate that the corresponding rock unit is covered by water. The outline of existing SFR tunnel system is shown by solid lines and a possible configuration of the planned facility is shown by dashed lines.*

1.4 Model volumes

In accordance with the geoscientific execution programme /SKB 2008a/, the deformation zone modelling work has been performed on two different scales, one regional and one local. The regional model contains all modelled deformation zones that have a trace length on the ground surface of ≥ 1,000 m, whereas the local model contains all ≥ 300 m. The local model covers the existing SFR facility and the rock volume for the planned SFR extension to the south-east (Figure 1-3).

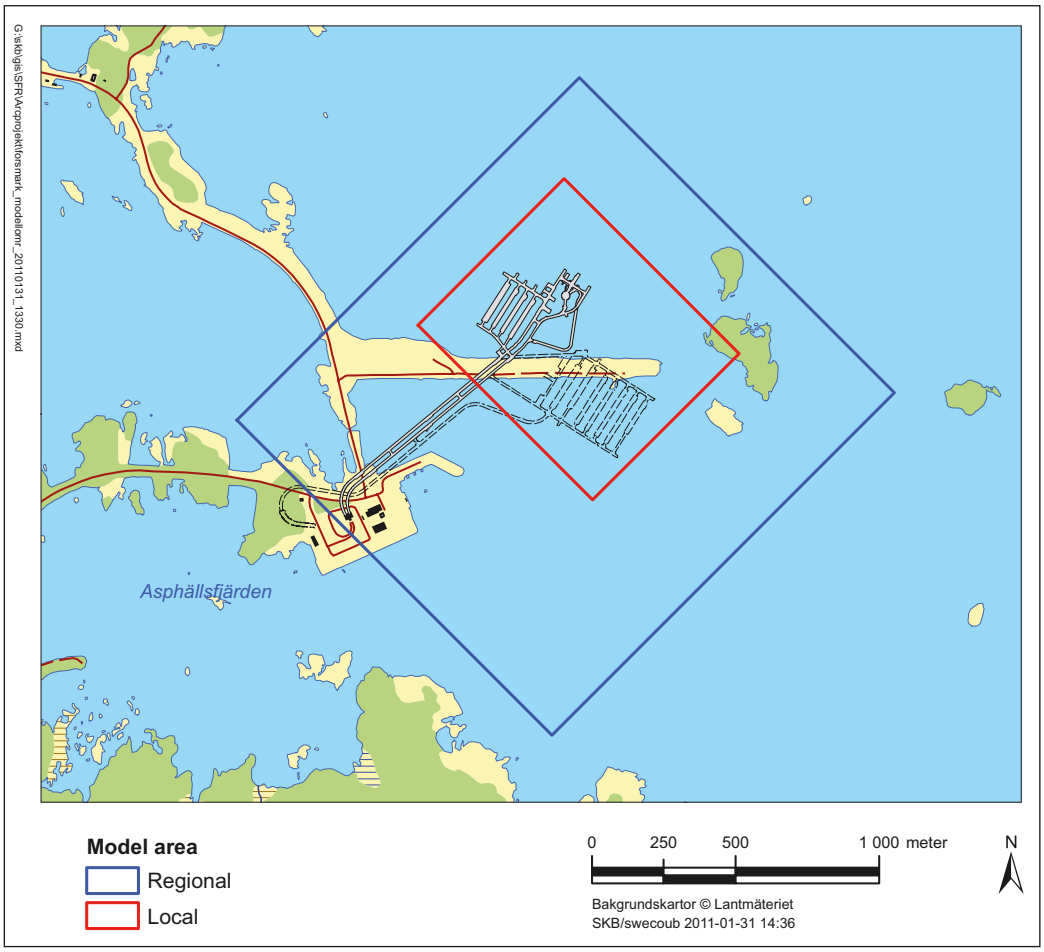

Figure 1-3. *Regional (blue) and local (red) model areas for SFR model version 1.0 relative to the existing SFR facility and the currently planned SFR extension to the south-east.*

For rock domain modelling work a single local model has been produced. The SFR model areas as well as the local model area in the Forsmark site investigation are shown in Figure 1-4. The SFR local model volume extends from elevation +100 masl (metres above sea level as defined by RHB70) to –300 masl, while the regional model volume extends from +100 masl to –1,100 masl. The coordinates defining the model areas are provided in Table 1-1.

A single deformation zone model was delivered as model version 0.1, with a volume corresponding to the regional model volume as defined above. The combined model contained all the modelled deformation zones of all sizes. The combined format was selected to facilitate further work by the hydrogeological modelling group who were the primary end users of version 0.1. For version 1.0 separate local and regional deformation zone models as well as a combined model have been delivered. In addition a local rock domain model has been developed. These model formats have been selected to facilitate the work by the various downstream users.

Table 1-1. Coordinates defining the model areas for SFR in metres. RT90 (RAK) system.

Regional model volume		Local model volume	
Easting	**Northing**	**Easting**	**Northing**
1631920.0000	6701550.0000	1632550.0000	6701880.0000
1633111.7827	6702741.1671	1633059.2484	6702388.9854
1634207.5150	6701644.8685	1633667.2031	6701780.7165
1633015.7324	6700453.7014	1633157.9547	6701271.7311

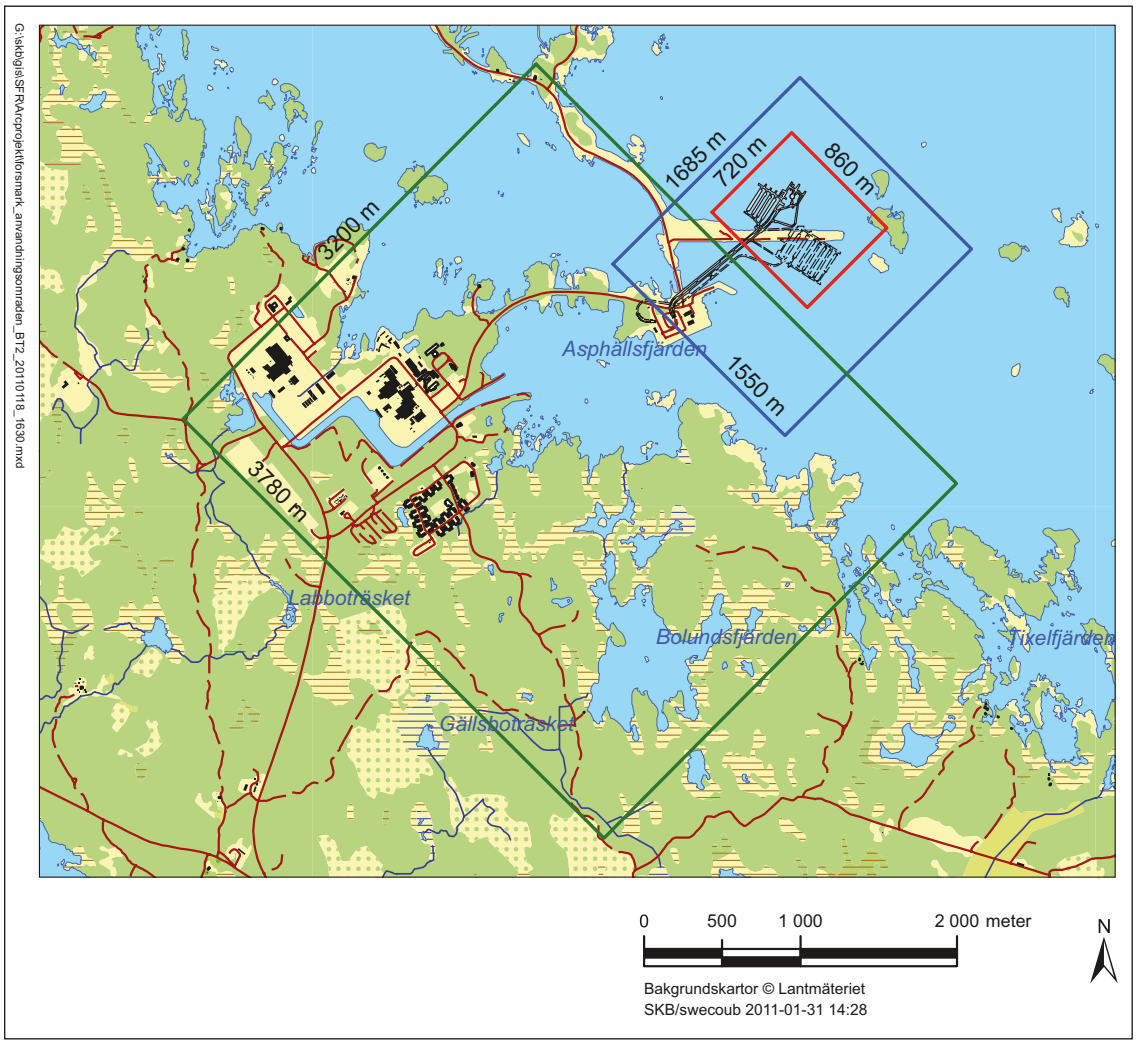

Figure 1-4. *Regional (blue) and local (red) model areas for SFR model version 1.0 relative to the local model area used in the Forsmark site investigation, model stage 2.2 (green).*

2 Previous geological models for SFR

2.1 Previous structural models

Version 0.1 and earlier structural models are reported in /Curtis et al. 2009/ and only a brief summary is provided here. The first conceptual model of the fracture zones around SFR was presented by /Carlsson et al. 1985, 1986/, with the purpose of providing input to a performance assessment study of the facility. The model was based on geological and hydrogeological data, with complementary information from refraction seismic investigations and aerial photographs. The central concept was a number of steeply to moderately dipping deformation zones, dividing the rock mass around SFR into three distinct blocks (Figure 2-1).

The model includes eight steeply dipping zones, exceeding one metre in thickness. It should be noted that there is considerable difference in the assessment of zone thickness used during the SFR construction work compared with that currently used by SKB. Earlier thickness definitions focused on the rock quality from an engineering viewpoint. The existence and width of zone intercepts were generally based on a significant increase in the frequency of broken fractures and, in some cases, an increased hydraulic conductivity (cf. /Carlsson et al. 1985, 1986/). This differs significantly from the methodology used to define possible deformation zones by the geological SHI methodology as currently implemented by SKB. The current SKB methodology generally leads to a greater number of zones with thicknesses that are usually significantly larger (see Section 3.1 for further details).

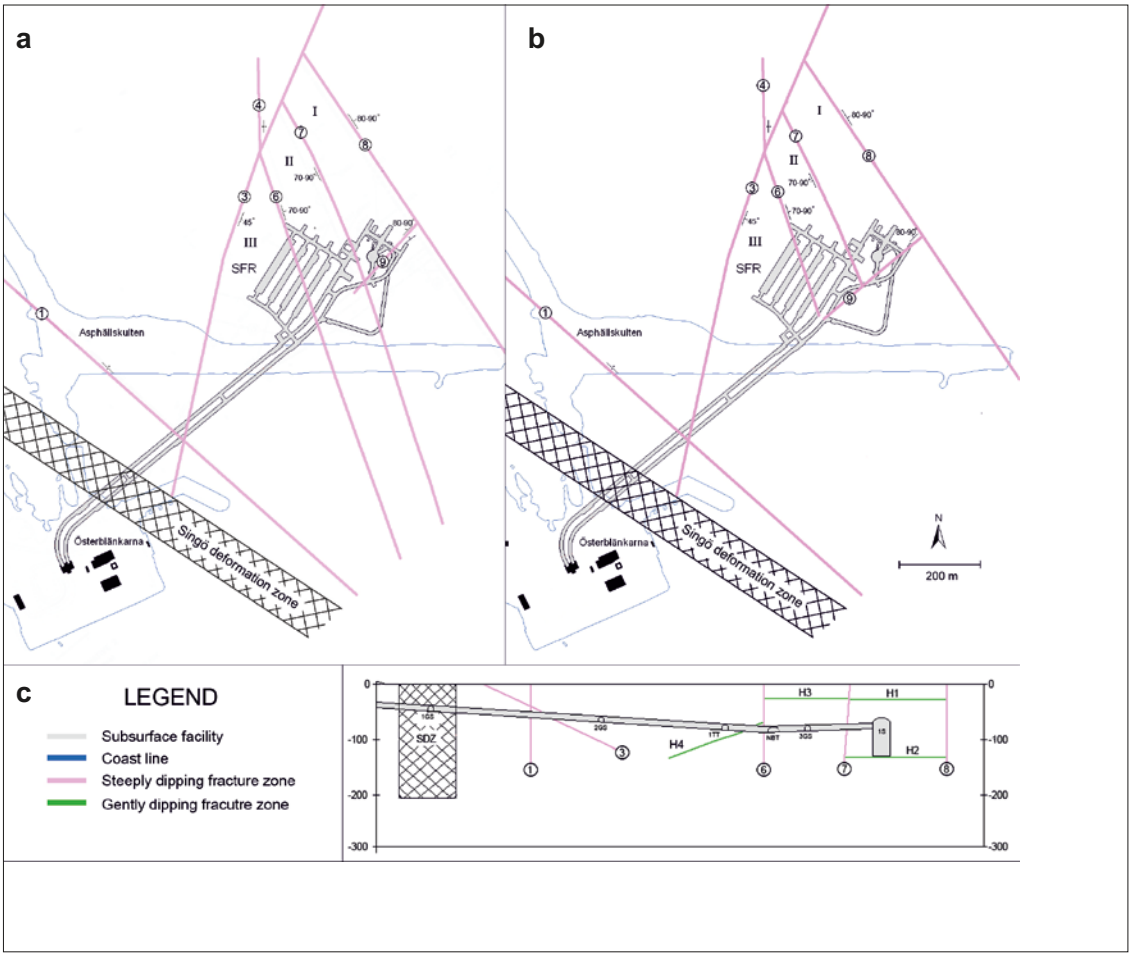

Figure 2-1. a) and b) Two alternative models for the eight most prominent fracture zones at repository depth. Interpretation based on borehole logs and tunnel mapping. c) Vertical profile along one of the access ramps (tunnel BT) to SFR showing the position of gently dipping zones. The three blocks in the rock mass, as discussed in the text, are marked by I, II and III. a), b) and c) are redrawn after /Carlsson et al. 1985/.

The model presented by /Carlsson et al. 1985, 1986/ includes two alternative interpretations, with minor differences for the eight more prominent zones (cf. Figure 2-1a and b). The gently dipping zones (denoted by 'H' followed by a number) are truncated by the more steeply dipping zones that define the three blocks (Figure 2-1). The north-eastern block (Block I) is intersected by two inferred, gently dipping zones between –20 and –40 (H1), and between –90 and –140 (H2) masl, the central block (Block II) by one zone between –15 and –35 masl (H3) and the south-western (block III) by one zone (H4) that strikes N75°E and dips 25° towards the south-east (geometrical control of the involved intercepts indicates a dip to the NNW). The most well-defined of these gently dipping zones, zone H2, is characterised by high hydraulic conductivity, an increased frequency of sub-horizontal fractures and, locally, significant amounts of clay. The other gently dipping zones are mainly manifested by high hydraulic conductivity, whereas their geological character is less significant and described as 'zones of released joints' /Carlsson et al. 1985/. In model version 1.0, H1 and H3 are inferred to be unloading or stress relief structures, due to their orientation and shallow depth.

An evaluation by /Christiansson 1986/, based on additional borehole data, resulted in a more comprehensive characterisation of some of the larger zones close to SFR, as well as an extension of zone H2 through the central block (Block II). It was inferred that H2 (ZFM871 in Stephens et al. 2007 and the current study) terminated against zones 3 (ZFMNNE0869), 6 (ZFMNNW1209), 8 (ZFMNW0805A) and, towards the south-east, against zone 9 (ZFMNE0870) in the model. Moreover, the dip of zone 3 (ZFMNNE0869) was changed from 35–45° to 70–80°, based on borehole intersections.

Seven of the most prominent zones, Singö as well as zones 1, H2, 3, 6, 8 and 9, were included in a performance assessment study for the SFR facility.

A review of the original conceptual model was performed by /Axelsson et al. 1995/. The major findings were that there were uncertainties in the fracture zone model and that other interpretations were possible. An alternative model was therefore presented by /Axelsson and Mærsk Hansen 1997/, based on a review of geophysical, geological and hydrogeological data. The zones affected by this work are H2, 6, 8 and 9, which were revised according to the following (Figure 2-2):

Zone H2 (ZFM871) Extended beyond zones 3, 6, 8 and 9, probably also beyond the Singö fault zone.

Zone 6 (ZFMNNW1209) Shortened and terminated before it reaches the drift tunnel.

Zone 8 (ZFMNW0805A) Reduced to a relatively unimportant zone from a hydraulic viewpoint.

Zone 9 (ZFMNE0870) Extended so as to terminate against zone 3.

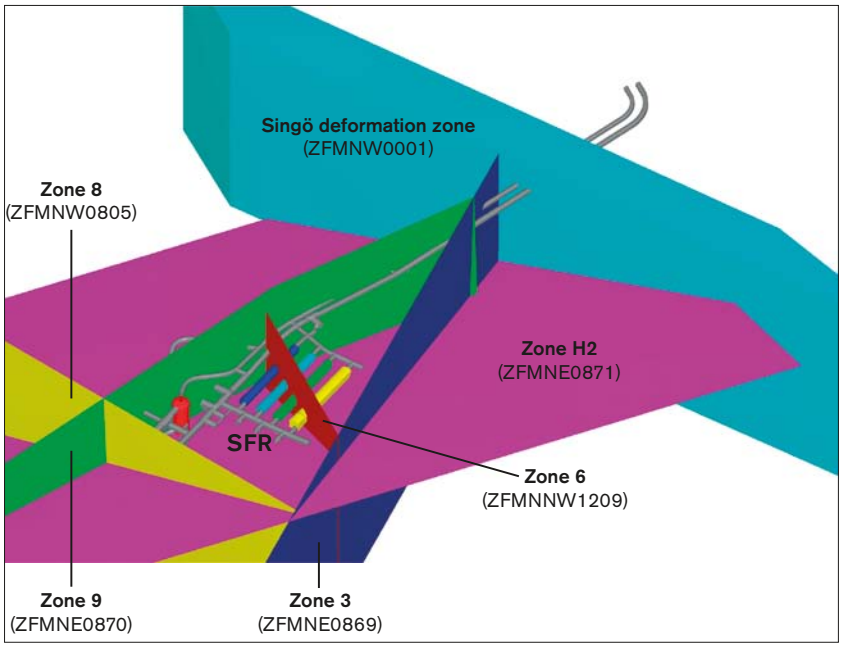

Figure 2-2. *Deformation zones in the local structural model updated by /Axelsson and Mærsk Hansen 1997/. The general layout of the SFR tunnel systems is also shown. The zones are marked both according to the SFR terminology and the system established during the Forsmark site investigation /SKB 2004/. View towards south.*

Thus, the original concept with a modelled termination of the gently dipping zones against the nearest, more steeply dipping zone was abandoned by the extension of zone H2. This interpretation formed the basis for the hydraulic modelling work by /Holmén and Stigsson 2001/ that gave input to the latest performance assessment study for SFR. It must be emphasized that all zone indications given by /Carlsson et al. 1986/ for H2, 3, 6, 8 and 9 were adopted by /Axelsson and Mærsk Hansen 1997/ without any changes in borehole or tunnel positions. However, /Axelsson and Mærsk Hansen 1997/ included additional intercepts and extended some of the earlier defined zones. Hence, the model represents an alternative interpretation, based on the same data, as pointed out by /Axelsson and Mærsk Hansen 1997/.

The most recent interpreted zone intercepts, defined in /Axelsson and Mærsk Hansen 1997/, were taken as providing the starting point for the modelling work in SFR version 0.1 /Curtis et al. 2009/. The interpreted borehole and tunnel interceptions with the zones, as defined in /Axelsson and Mærsk Hansen 1997/, have been logged in Sicada to ensure traceability. For version 1.0, all of the available drill core from the earlier SFR investigation and construction work has been re examined, re-interpreted and photographed (see Section 3.4). This has included the identification of the position and apparent thickness of PDZ's (possible deformation zones) in the core in accordance with current SKB practice. In addition, a further review of all the available relevant documentation from the SFR investigation and construction phase has been performed.

2.2 Previous lithological models

During the construction of SFR, the modelling was mainly focused on brittle structures in terms of their hydraulic properties and the implications for the tunnelling work. The bedrock and its ductile structural character were treated more superficially, with emphasis on individual rock types.

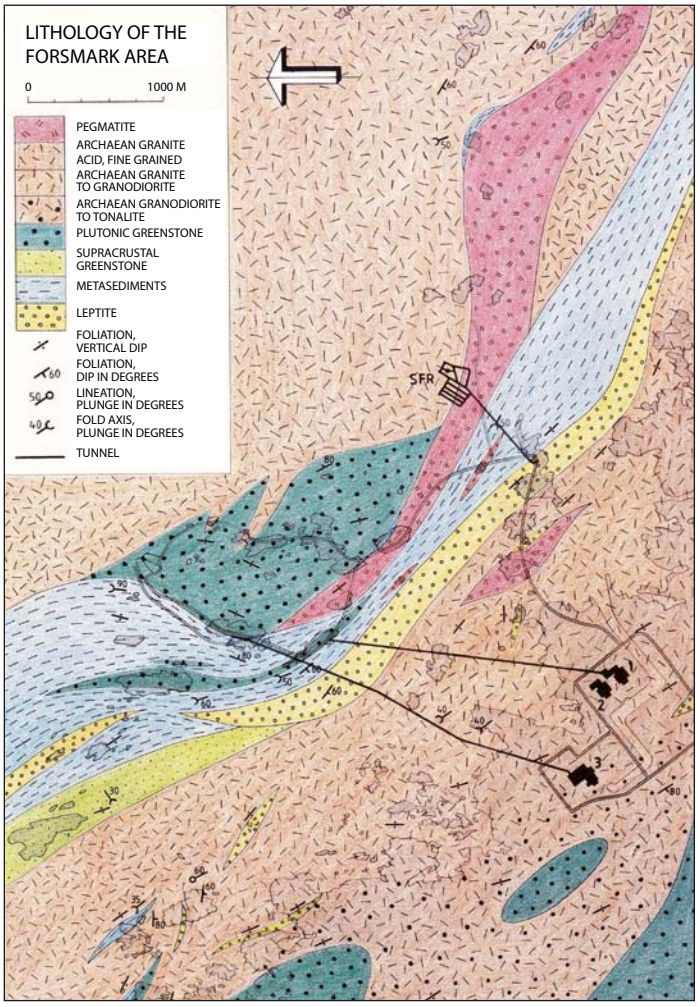

Figure 2-3. *Bedrock geological map of the Forsmark area. After /Hansen 1989/.*

The most detailed descriptions are provided by /Christiansson and Bolvede 1987/, though some information is included in virtually all geological reports from the project. A bedrock geological map with description that covers the archipelago area around SFR was initially compiled by /Hansen 1989/ (Figure 2-3).

2.3 Conceptual understanding of deformation zones and the bedrock structure

A description of the deformation zones and rock domains inside the larger model volumes (local and regional) used in the Forsmark site investigation was presented in the final geological model stage 2.2 during the site investigation work /Stephens et al. 2007/. Complementary stage 2.3 data were evaluated in /Stephens et al. 2008b/. An integrated site descriptive model was presented in /SKB 2008b/. No information or interpretation work in the current study has come to light that contradicts the earlier presented conceptual understanding. No kinematic studies have been included in the current project and direct reference is made to the earlier Forsmark site investigation results.

The oldest discrete structures in the area are the steeply dipping, WNW-ENE and NW-SE zones (e.g. Singö deformation zone), generally referred to as the WNW to NW set. These zones initiated their development in the ductile regime and continued to be active as faults in the brittle regime. Together with the broader structural belts with the same orientation, which developed earlier under higher-grade metamorphic conditions, they account for a pronounced structural anisotropy in the bedrock. In addition to the conspicuous WNW to NW zones, there are three distinctive sets of brittle deformation zones (fracture zones) in the area:

- Vertical to steeply dipping fracture zones that strike ENE-WSW (NE-SW) and NNE-SSW, generally referred to as the ENE to NNE set including ENE(NE) and NNE sub-sets.
- Vertical and steeply dipping fracture zones that strike NNW-SSE, generally referred to as the NNW set.
- Gently dipping ($\leq 45°$) fracture zones that, relative to all the other sets, contain a higher frequency of open fractures and non-cohesive fault rocks.

This basic orientation set division has been maintained in the current modelling work and reporting. Kinematic data along major zones of the WNW to NW set shows that these zones have been affected by brittle deformation under different stress regimes. Also the ENE to NNE set is inferred to have developed under different stress regimes with evidence of both sinistral and dextral movement along minor, steeply dipping faults that strike ENE to NE inside the zones and a dominance of sinistral displacement along the NNE minor faults. Subordinate dip-slip movement has also occurred. The NNW set, on the other hand, shows evidence for a predominant sinistral strike-slip displacement, as well as minor dextral strike-slip and dip-slip movements. The gently dipping zones reveal evidence of both reverse dip-slip and subordinate strike-slip senses of movement, suggesting development in one or more compressive regimes. However, fault-slip data are absent along some of them and these structures are possibly joint zones /SKB 2008b/.

A concept where the four different sets of deformation zones formed initially in response to compressive tectonic regimes, during the later part of the Svecokarelian orogeny, was presented already in early model versions /SKB 2005, 2006/, and was further refined in the final geological model /Stephens et al. 2007, SKB 2008b/. This concept involved dextral strike-slip displacement in low-temperature ductile and subsequently brittle regimes along the steeply dipping, WNW to NW set and possibly even the steeply dipping NNW set (Figure 2-4). This was followed by continued dextral strike-slip displacement along these structures in the brittle regime, in combination with sinistral strike-slip displacement along the steeply dipping ENE(NE) and NNE sub-sets (Figure 2-4). Bulk crustal shortening in a NW–SE to N–S direction during the later part of the Svecokarelian orogeny was inferred (Figure 2-4). It is inferred that reactivation along the WNW or NW belts continued in the brittle regime (epidote stable) and that some of the smaller zones with WNW or NW strike could have formed more or less simultaneously with zones with ENE, NE or NNE strike.

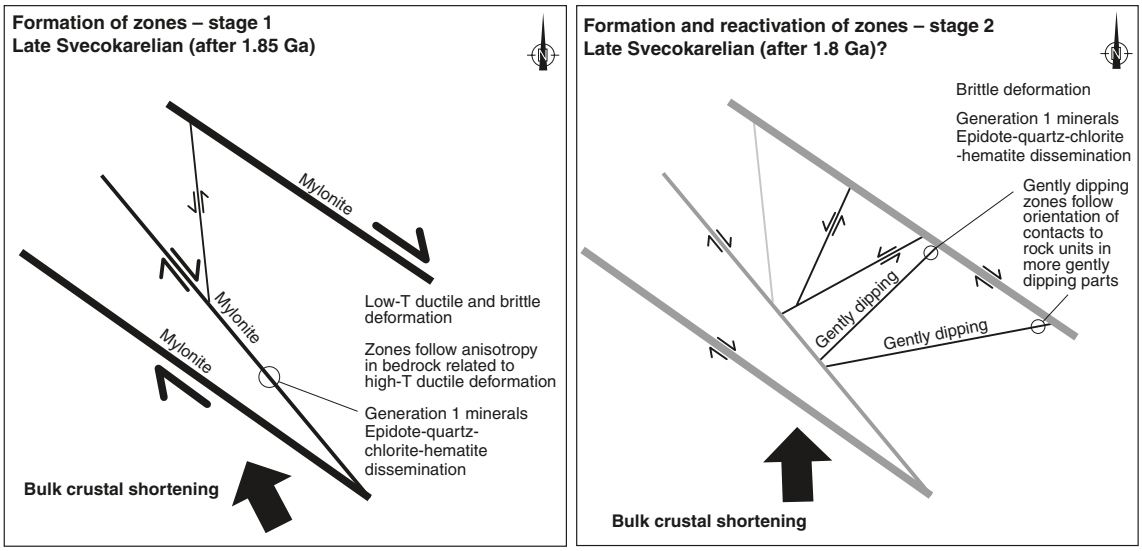

Figure 2-4. *Two-dimensional cartoon illustrating the regional-scale geodynamics during the initial development of the steeply dipping WNW-ESE and NW-SE zones and the subordinate sets of brittle deformation zones in response to late stage Svecokarelian tectonic activity. After /SKB 2008b/.*

The modelled truncation of the gently dipping zones is based on the conceptual hypothesis that these structures formed after the steeply dipping set of WNW to NW regional zones, and more or less at the same time as the steeply dipping ENE(NE) sub-set, NNE sub-set and at least some of the steeply dipping NNW set in the brittle regime (Figure 2-4). For this reason, the gently dipping zones were extended in space as far as the nearest steeply dipping zone in the 3D modelling work /Stephens et al. 2007/. It was proposed that the gently dipping zones, at least in the south-eastern part of the Forsmark candidate area, followed arrays of amphibolite boudins in the predominant metagranite. Furthermore, the markedly lower frequency of these hydrogeologically important structures in the target area (north-western part of the candidate area) was related to the steeper dips of the ductile structures in this area, i.e. the structural anisotropy in the bedrock /Stephens et al. 2007/.

All the four sets of deformation zones underwent reactivation in the brittle regime during the subsequent geological evolution. For example, sinistral strike-slip displacement has been documented along the zones in the WNW to NW set (see review in /Stephens et al. 2008b/). Furthermore, reactivation due to the effects of stress release at the later part of loading and unloading cycles during the Proterozoic and Phanerozoic time periods has been recognised /Stephens et al. 2007/. This type of reactivation in the form of extensional failure and the development of dilatational joints is most conspicuous along the gently dipping zones in the near-surface realm. The stress release also formed sheet joints.

Four major groups of rock types (A to D) were distinguished in the Forsmark site investigation area on the basis of their relative age, whereas individual rock types were distinguished on the basis of their modal composition, grain-size and relative age /Stephens et al. 2007/. All rocks were affected by brittle deformation. Groups A and B were affected by penetrative ductile deformation under amphibolite-facies metamorphic conditions, group C by penetrative ductile deformation under lower amphibolite-facies metamorphic conditions and group D only partly by ductile deformation and metamorphism.

The rock domain model developed during the Forsmark site investigation is based on a concept where high-strain belts with more oblate ductile strain anastomose around tectonic lenses in which the bedrock is typically affected by somewhat lower and more prolate ductile strain /Stephens et al. 2007/. One such lens of considerable extent is the Forsmark tectonic lens, which is rather homogeneous in terms of bedrock composition and deformation style. The more highly deformed rocks surrounding the Forsmark lens show a conspicuous WNW-ESE to NW-SE structural trend.

The SFR model volume is situated within the costal deformation belt north-east of the Forsmark lens, where older rocks that belong to groups A and B are generally strongly deformed and exhibit a foliation and/or lineation, locally in combination with tectonic banding, to form heterogeneous BSL-tectonites. The foliation and mineral lineation correspond to grain-shape fabrics, which in the dominant felsic rocks are defined by the orientation of biotite and, if present, muscovite and hornblende, as well as elongate aggregates of recrystallized quartz and feldspar. Tectonic banding is largely restricted to occurrences of metavolcanic rock, such as in the upper part of borehole KFM11A, or high-strain varieties of the fine- to medium-grained metagranodiorite (to granite). The Group C rocks also show a penetrative, linear grain-shape fabric in the Forsmark site investigation area. In a broader regional perspective, /Stephens et al. 2009/ inferred that the fabric developed during strong, progressive, non-coaxial deformation under amphibolite-facies metamorphic conditions.

Evidence for a subsequent folding at different scales is conspicuous both in the immediate surroundings of SFR (Figure 2-5) and in the Forsmark area as a whole. The folding has primarily affected older rocks that belong to groups A and B, but also group C and older members of group D, such as some of the pegmatitic granites. It deforms the tectonic foliation, but evidence for folding of the mineral stretching lineation is lacking in the Forsmark area. Consequently, it is inferred that linear fabric was established prior to, but continued to develop during, the folding phase. It has been suggested that the folding developed initially with a normal cylindrical shape and was progressively drawn out, to a variable extent, into the stretching direction into sheath folds (Figure 2-6), so that the orientation of the folds follows the stretching lineation /Stephens et al. 2009/.

Existing kinematic data from the Forsmark site investigation suggest a dextral strike-slip component of displacement, both along the folded, high-strain fabric and the younger ductile fabric inside the high-strain belt that hosts the Singö deformation zone and its splays to the north /SKB 2005, Stephens et al. 2007/.

The relevant reports for the previous structural models for SFR and the modelling work during the Forsmark site investigation, including the final document of the site investigation referred to as SDM-Site Forsmark, are listed in Appendix 1.

Figure 2-5. *Intense folding of an inferred felsic to intermediate metavolcanic rock veined by pegmatitic material at Rönngrundet, situated just east of the regional SFR model area.*

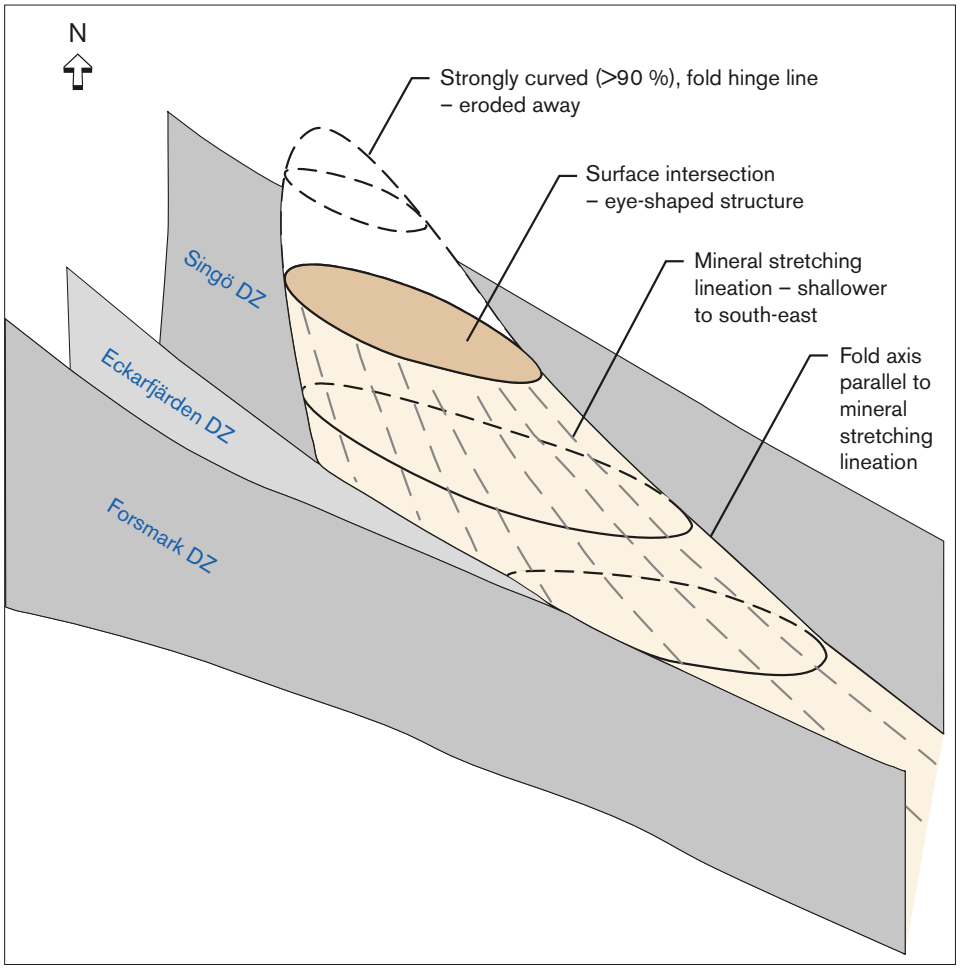

Figure 2-6. *Conceptual model for the development of major, sheath folds inside the Forsmark tectonic lens, with fold axis parallel to the mineral stretching lineation. After /Stephens et al. 2007/.*

3 Overview of available geological and geophysical data

3.1 Data quality

Although there is a considerable quantity of geological documentation from the construction of SFR, the quality of the data is highly variable, and there are, moreover, uncertainties in the methodology used to obtain the data as well as differences in the methodology used to define, for example, zones (see below). The basis for the modelling methodology established by SKB is quality-assured data available in the SKB databases Sicada and GIS. However, there are also data from the construction of SFR, used in this modelling work, which lack this quality-assurance.

There is a restricted quality and less control of the data from the old boreholes drilled during the construction of SFR. Similarly, there is also an inherently lower quality of data from the percussion boreholes compared with cored boreholes in the current drilling campaign. For this reason, cored borehole data from the later SFR and Forsmark site investigations have been given precedence over data from percussion boreholes and older cored boreholes.

In general, tunnel data are of greater quality than borehole data, simply because the 'observation window' is so much greater. However, the older tunnel data does not allow the full application of currently accepted SKB methodology. For this reason, the tunnel mapping has been considered key data to define the position, orientation and basic character of a part of a zone while the SHI intercepts of the same zone are used to provide details concerning zone thickness, fracture frequencies and orientations, rock types, mineralogy, etc in accordance with current SKB methodology.

In order of descending data quality, even after the further review and processing as described in Section 3.4, the input data for the version 1.0 modelling work can be summarised as follows for the three data categories:

Borehole data

- Results from the recent Forsmark and SFR site investigations, in particular the borehole SHI results.
- SHI results from selected older SFR boreholes subjected to standard SHI remapping, performed during version 0.1.
- Simplified SHI results from the re-inspection and review of remaining available drill core from the older boreholes from the SFR investigation and construction phases.

Tunnel data

- Tunnel mapping results based on re-inspection of the lower construction tunnel (NBT).
- Tunnel mapping results from the SFR construction phase.

Construction data

- Input from the results and interpretations included in the various older SFR investigation and construction reports.

A part of the earlier version 0.1 modelling work was to review the older SFR data and to identify which data could be the subject of further processing and quality checks, with the aim of reaching a level where it can be included in the Sicada and GIS databases for use in version 1.0. This process has been performed during the initial stages of version 1.0. As well as the remapping and geological single-hole interpretation (SHI) of selected older SFR boreholes, performed during version 0.1 /Petersson and Andersson 2011, Petersson et al. 2011/ all of the remaining available drill core from the older boreholes from the SFR investigation and construction phases has been re-inspected and reviewed. Details of the methodology and results are included in Section 3.4.

The available tunnel mapping results from the excavation phase /Christiansson and Bolvede 1987/ have been reviewed and processed as described in Section 4.1 and Appendix 2. Although the tunnel itself has been re-inspected, little information can be gained concerning deformation zones due to the

applied rock support, ventilation ducts and other installed facilities. The position of the deformation zones, if they intercept the tunnels, is based on the earlier documented tunnel mapping results, while the zone thickness and character are based on any available SHI results.

The lower construction tunnel (NBT) has been the subject of more detailed studies (/Berglund 2009/ and Section 4.1) but, once again due to the use of rock support and installations, the results have supplied few new data on structures at a scale that is relevant for a significant input to the version 1.0 deformation zone modelling work.

Data from the Forsmark site investigation and the current SFR drilling campaign, followed by data based on remapping and geological single-hole interpretation (SHI) of selected older SFR boreholes, performed during version 0.1, have been given precedence over the older, less controlled data. Thus, where possible, intercepts between boreholes and deformation zones, upon which previous structural models of SFR were built, have been replaced by correlations based on the occurrence of possible deformation zones in the SHI of the same boreholes. However, issues arise particularly with the old tunnel data and their earlier interpretations, which are difficult to review in a meaningful way, yet are, at the same time, a very important source of information and inherently give a valuable indication of the character of a particular deformation zone in a different manner to that indicated by a borehole intercept. In the same way, it is not considered reasonable to discount documented experience from the construction phase of SFR, even if the reporting does not correspond to current SKB methodology and traceability standards.

One important issue that has arisen is the contrast in the methodology used during the SFR construction work and that used currently by SKB for the definition of what constitutes a deformation zone and how a zone's thickness is defined. In contrast to the SKB implemented concept, presented by /Munier et al. 2003/ that forms the basis for the SHI approach, where a typical deformation zone can be divided into a core flanked by damage zones (see Figure 5-3), the earlier thickness definitions generally focused on open fractures and considered only the core or simply the groundwater-bearing part of a zone (cf. /Carlsson et al. 1985, 1986/). The geological SHI provides an integrated synthesis of the geological data from the drill core mapping and geophysical borehole data with the aim of identifying rock units and possible deformation zones. The geological SHI analysis of fracture frequencies is not restricted to broken fractures, but also includes sealed fractures, sealed fracture networks, open and partly open fractures, and crush zones. In addition, current SHI practice gives equal weight to the presence and character of ductile deformation structures when defining deformation zones, in contrast to earlier judgements where such structures were to a certain extent ignored. The significant differences in the methodologies to define the existence and boundaries of possible deformation zones mean that current SKB methodology generally leads to more zones with thicknesses that are usually significantly larger. Consequently, while a particular deformation zone's existence and overall geometry may be based on a mixture of older and newer data, the zone thickness and character is based first and foremost on SHI data.

A summary of the available bedrock geological and geophysical data and their treatment in SFR model version 1.0 is presented in Appendix 1.

3.2 Forsmark bedrock geological map stage 2.3

A bedrock map over the mainland and archipelago at Forsmark, at the scale 1:10,000, was generated during the Forsmark site investigation, primarily on the basis of outcrop data. The description of the map, including the rock type distribution and the ductile structures, was presented initially in /SKB 2005/ and, in more detail, in /Stephens et al. 2008a/.

Both the regional and local SFR model areas are located in a part where the judged quality of the map is defined as 'variable but generally low' (cf. /SKB 2008b/). No outcrops exist in the local SFR model area and the observation points in the regional SFR model are limited to the small island south of Grisselgrundet and outcrops along the road to Biotestsjön (Figure 3-1).

All outcrops within and in proximity to the regional SFR model area were revisited for brief inspection during the SFR site investigation. However, no new surface geological data have been produced since the Forsmark site investigation.

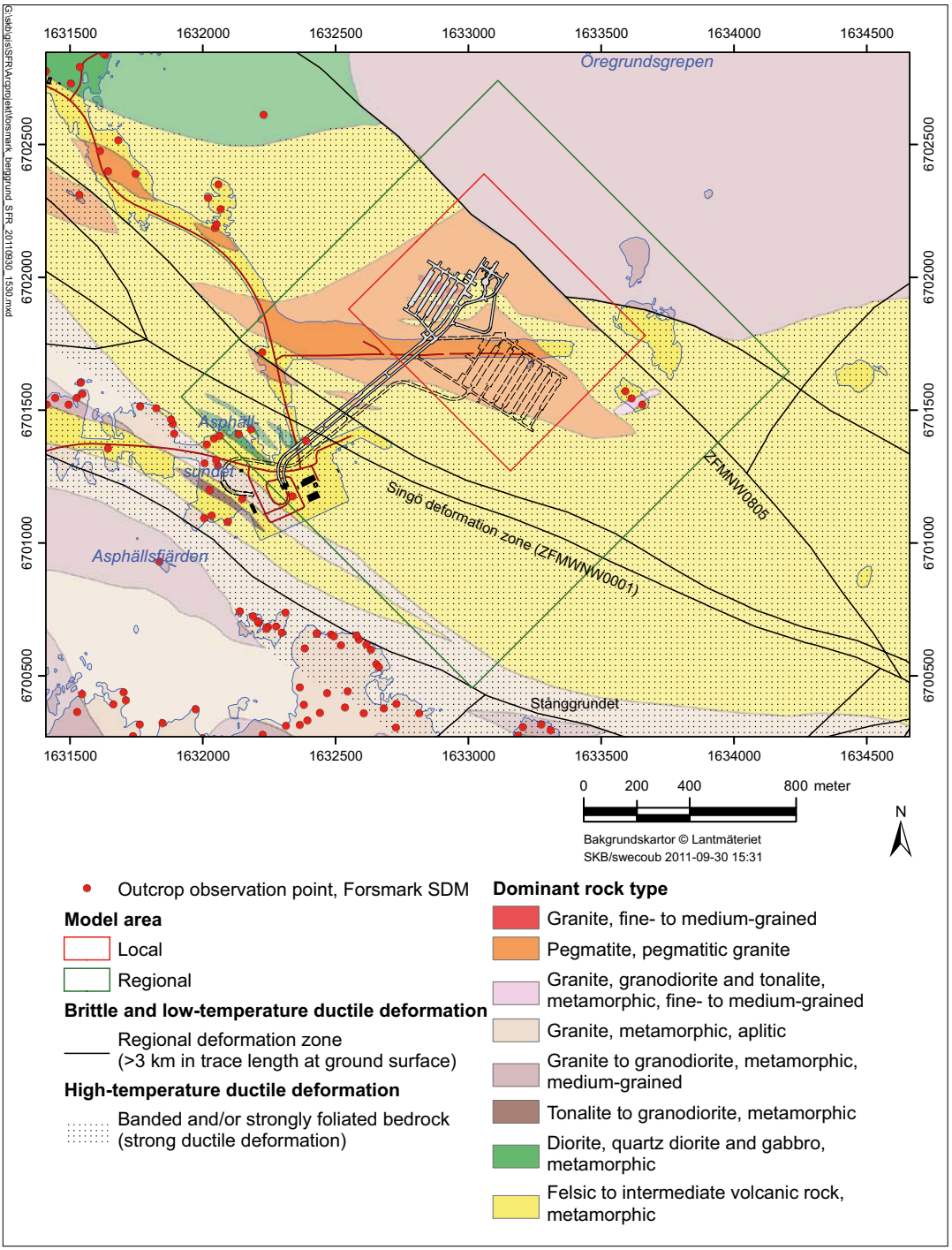

Figure 3-1. *Summary of outcrop observation points relative to the Forsmark bedrock geological map (stage 2.3) in the area around SFR. Paler shades for each colour on the map indicate that the corresponding rock unit is covered by water.*

3.3 Geological tunnel mapping from SFR

Geological maps that provide information on rock type, fractures, other tectonic structures and water seepage for all underground openings were generated during the construction of SFR /Christiansson and Bolvede 1987/. All these drawings have been digitally scanned, geo-referenced in ArcGis and attached to the RVS model (stored in SDE GIS database as Field note SFR 146, with ID olfrgeo8576–8578, olfrgeo8580, olfrgeo8551–8556, olfrgeo8561–8562, olfrgeo8564, olfrgeo8566–8575). These drawings have been used in combination with as-built tunnel centre-line and laser scanned tunnel section survey data to estimate the zone tunnel intersection positions in 3D.

A brief review of the drawings with focus on the structural overview drawing (–103; SDE GIS database ID olfrgeo8551), as a primary input to the version 0.1 DZ modelling, was presented in /Curtis et al. 2009/. Appendix 2 in the current report also includes a compilation of intercept positions and orientations for all brittle structures marked on the overview drawing, which might be of interest for the DZ modelling work. These features are referred to as 'possible tunnel deformation zones' (tDZ).

To facilitate the rock domain modelling, a further integration of earlier SFR tunnel mapping results has been completed as part of version 1.0. This work included a translation of the different rock types defined by /Christiansson and Bolvede 1987/ into the bedrock nomenclature introduced during the Forsmark site investigation (cf. /Stephens et al. 2003b/). The translation was followed by a colour coding of the rock types in all detailed drawings at the scale 1:200 of /Christiansson and Bolvede 1987/, except for drawing –14 of the silo, which had 3D conversion problems (stored in SDE GIS database under Field note SFR 146, with ID SDEADM.GOL_FR_GEO_8486–8492). A compilation of the detailed drawings is presented in Appendix 2 and the purpose with this colouring was to emphasize bedrock information in the somewhat confusing black and white drawings, as illustrated in Figure 3-2.

New geological data for the lower construction tunnel (NBT) of SFR has become available after model version 0.1 by an updated mapping performed by /Berglund 2009/. The mapping was based on a template of the laser scanned tunnel geometry and consists of three-dimensional graphical elements related to a database with properties. Fractures, lithology, rock contacts, minor deformation zones and obvious water seepage have been recorded according to the geological nomenclature used by SKB. The extent of the mapping is illustrated in Figure 3-3. More details regarding the minor deformation zones are presented in Appendix 2.

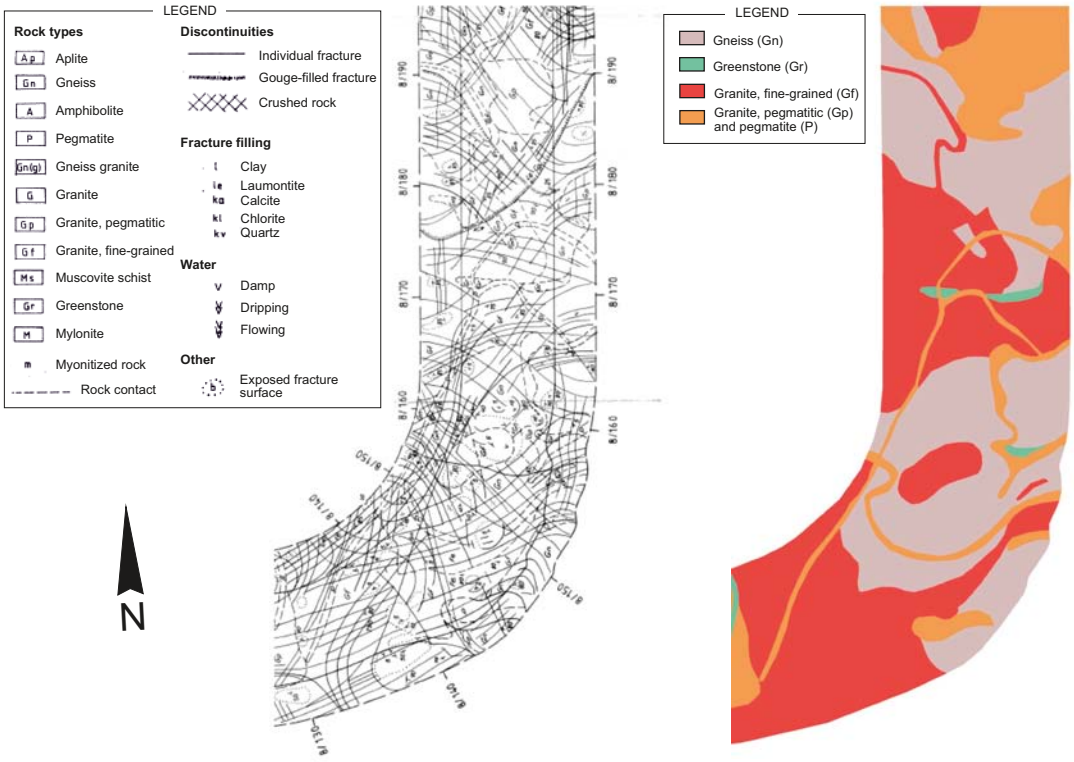

Figure 3-2. *Geological mapping for a section of the lower construction tunnel (NBT) showing the visual difference between the original black and white drawing of /Christiansson and Bolvede 1987/ and the rock type colour coding. The legend is a translation of the original of /Christiansson and Bolvede 1987/ in Swedish. Note that the distinct fault at approximately 8/180 is referred to as tDZ95 in Appendix 2.*

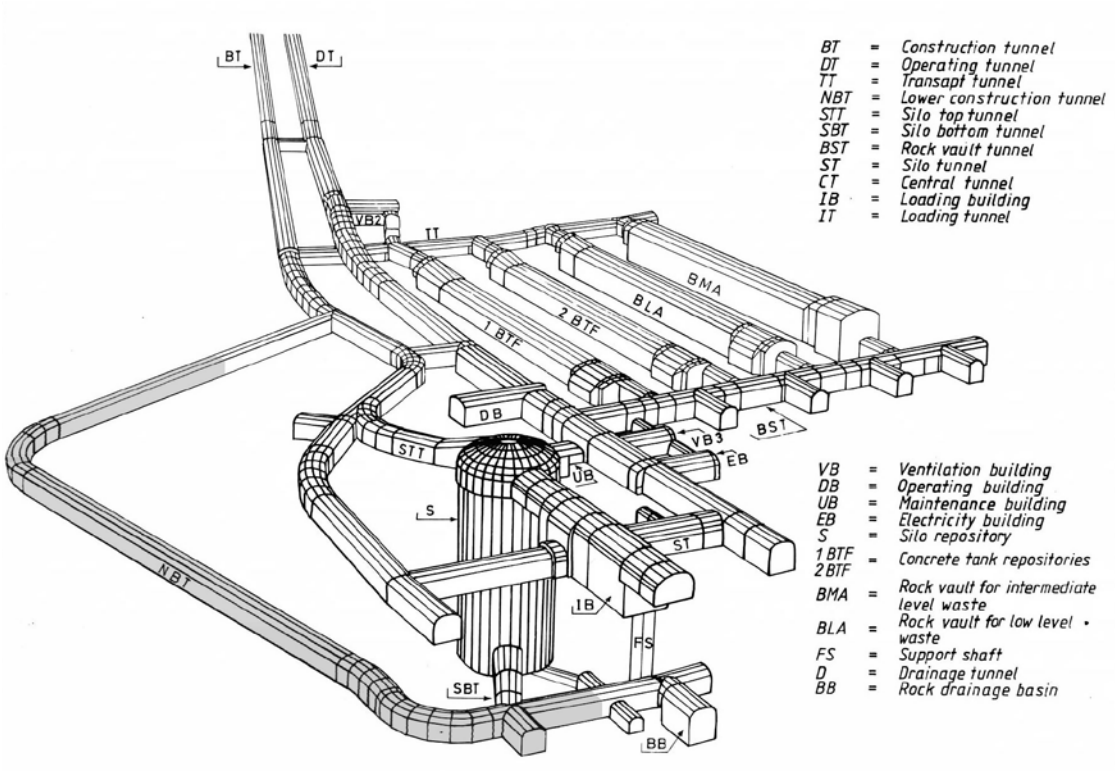

Figure 3-3. *View of SFR from ENE showing the interval covered by updated mapping of /Berglund 2009/ (shaded part of NBT) along with abbreviations used for the different tunnels and caverns. After /Carlsson et al. 1986/.*

3.4 Borehole data

Borehole data from the following three drilling campaigns in the area have been used in the current SFR modelling work:

- The investigation and construction of the SFR facility during the nineteen-eighties, which resulted in a total of 60 cored boreholes drilled both from the surface and within the underground excavations.
- The Forsmark site investigation. The relevant boreholes include one cored borehole (KFM11A) and two percussion boreholes (HFM34 and HFM35) all of which were drilled within or in close proximity to the Singö deformation zone and penetrate the western part of the SFR regional model volume.
- The current site investigation for a future extension of SFR. The drilling campaign yielded seven cored boreholes (KFR101, KFR102A, KFR102B, KFR103, KFR104, KFR105 and KFR106) and four percussion boreholes (HFR101, HFR102, HFR105 and HFR106) situated south to south-east of the SFR facility, predominantly inside the local model volume. The drilling also included an extension of the existing cored borehole KFR27. All drilling, except for that of KFR105, was performed from the ground surface.

Technical data concerning the drilling activities, including the coordinates of the drill sites, the length, bearing and inclination of the boreholes are presented in Appendix 3. Relevant data reports are listed in Appendix 1.

A key input to the geological modelling of borehole data during the SKB site investigations has been the geological single-hole interpretation (SHI), which is an established methodology to provide an integrated synthesis of the geological and geophysical information in a borehole.

The original borehole documentation from the older SFR boreholes is too sparse to allow the full application of the established SHI methodology, due to the lack of BIPS images, obscurities in the lithological classification and the methodology of the original fracture mapping, along with the fact that geophysical logs only exist for seven of the boreholes /Mattsson 2009/. This has required a reassessment of the data together with a renewed examination of all available drill cores from 43 old cored boreholes. However, due to deficiencies in the material, the necessary activities have deviated somewhat from the established SKB methodologies /Petersson et al. 2011, Petersson et al. 2009b/. To allow integration with data from later drilling campaigns, the following activities have been completed for these older cored boreholes:

- All the existing original information on rock type has been translated into the established SKB rock nomenclature. The details of this activity are provided in /Stephens et al. 2008a/ and /Petersson et al. 2011/. The activity was implemented for KFR01, KFR02, KFR03, KFR04, KFR05, KFR08, KR09, KFR10, KFR11, KFR12, KFR13, KFR14, KFR19, KFR20, KFR52, KFR54, KFR55, KFR57, KFR61–KFR68, KFR7B, KFR7C and SFR (Silo1).
- Drill cores for which there is no original mapping have been subjected to overview mapping where rock types exceeding 1 m in drill core length were recorded along with ductile and brittle ductile deformation and alteration. Details are provided in /Petersson et al. 2011/ and the activity comprises KFR31, KFR32, KFR34, KFR37, KFR38, KFR51, KFR69–KFR72 and KFR89.
- Drill cores from eleven boreholes have been subjected to renewed mapping by use of the so-called Boremap-system. The prime criterion for the selection of the boreholes, comprising KFR04, KFR08, KFR09, KFR13, KFR35, KFR36, KFR54, KFR55, KFR7A, KFR7B and KFR7C, was a distinct cross-cutting relationship with inferred deformation zones in the earlier geological model of SFR (cf. /Axelsson and Mærsk Hansen 1997/). Since no BIPS images are available for the boreholes, it has not been possible to obtain absolute orientations. Thus, the mapping is a simplified version of established SKB methodology, generally focused on the location and mineralogy of broken and unbroken fractures, as well as crush zones, breccias and sealed networks. In addition, rock type, alteration and any ductile structures present were documented. The renewed mapping provided input to geological SHI's as presented in /Petersson et al. 2009b/. These data were included in the preceding model version 0.1.
- Remaining boreholes, not selected for renewed mapping by Boremap, have been subjected to a simplified version of the SHI process where identification of possible deformation zones (PDZ) was made by direct visual inspection of the drill cores. Furthermore, the merging of similar rock types into rock units (RU) was based on the rock code translation and the lithological overview mapping. The established criteria and methodology of the geological SHI process have been applied wherever possible and deviations from the standard process were associated with the lack of data or a lack of quality in the available data. Details are given in /Petersson et al. 2011/ and the activity includes 32 boreholes (KFR01, KFR02, KFR03, KFR05, KFR10, KFR11, KFR 12, KFR14, KFR19, KFR20, KFR31, KFR32, KFR34, KFR37, KFR38, KFR51, KFR52, KFR57, KFR61–KFR68, KFR69, KFR70, KFR71, KFR72, KFR89, SFR (Silo1).
- In addition, there are 17 boreholes for which there are no drill cores available and consequently no geological information. These boreholes include KFR06, KFR21–25, KFR27, KFR33, KFR53, KFR56, KFR80 and KFR83–88.

A summary of the activities that have been completed for the old cored boreholes is provided in Table 3-1 along with an illustration of their position in Figure 3-4. Note that boreholes that lack spatial information (i.e. KFR72, KFR89 and SFR (Silo1)) have not been included in the modelling work.

Table 3-1. Data acquired for cored boreholes from the construction of SFR.

BH ID	Old ID	Rock type coding	Overview mapping	Boremap mapping	Geophysics	Simplified SHI	Standard SHI
KFR01	HK1	X	–	–	X	X	–
KFR02	HK2	X	–	–	X	X	–
KFR03	HK3	X	–	–	X	X	–
KFR04	HK4	X	–	X	X	–	X
KFR05	HK5	X	–	–	X	X	–
KFR06	HK6	–	–	–	–	–	–
KFR08	HK8	X	–	X	–	–	X
KFR09	HK9	X	–	X	–	–	X
KFR10	HK10	X	–	–	–	X	–
KFR11	HK11	X	–	–	–	X	–
KFR12	HK12	X	–	–	–	X	–
KFR13	HK13	X	–	X	–	–	X
KFR14	HK14	X	–	–	–	X	–
KFR19	KB19	X	–	–	X	X	–
KFR20	KB20	X	–	–	X	X	–
KFR21	KB1	–	–	–	–	–	–
KFR22	KB2	–	–	–	–	–	–
KFR23	KB3	–	–	–	–	–	–
KFR24	KB4	–	–	–	–	–	–
KFR25	KB5	–	–	–	–	–	–
KFR27	KB7	–	–	–	–	–	–
KFR31	KB11	–	X	–	–	X	–
KFR32	KB12	–	X	–	–	X	–
KFR33	KB13	–	–	–	–	–	–
KFR34	KB14	–	X	–	–	X	–
KFR35	KB15	–	–	X	–	–	X
KFR36	KB16	–	–	X	–	–	X
KFR37	KB17	–	X	–	–	X	–
KFR38	KB18	–	X	–	–	X	–
KFR51	KB21	–	X	–	–	X	–
KFR52	KB22	X	–	–	–	X	–
KFR53	KB23	–	–	–	–	–	–
KFR54	KB24	–	–	X	–	–	X
KFR55	KB25	–	–	X	–	–	X
KFR56	KB26	–	–	–	–	–	–
KFR57	KB27	X	–	–	–	X	–
KFR61	DS1	X	–	–	–	X	–
KFR62	DS2	X	–	–	–	X	–
KFR63	DS3	X	–	–	–	X	–
KFR64	DS4	X	–	–	–	X	–
KFR65	DS5	X	–	–	–	X	–
KFR66	DS6	X	–	–	–	X	–
KFR67	DS7	X	–	–	–	X	–
KFR68	DS8	X	–	–	–	X	–
KFR69	DS9	–	X	–	–	X	–
KFR70	DS10	–	X	–	–	X	–
KFR71	DS101	–	X	–	–	X	–
KFR72	DS102	–	X	–	–	X	–
KFR7A	HK7A	–	–	X	–	–	X
KFR7B	HK7B	X	–	X	–	–	X
KFR7C	HK7C	X	–	X	–	–	X
KFR80	INJ	–	–	–	–	–	–
KFR83	SH3	–	–	–	–	–	–
KFR84	BT 5/241	–	–	–	–	–	–
KFR85	BT 5/247 1	–	–	–	–	–	–
KFR86	BT 5/247 2	–	–	–	–	–	–
KFR87	NBT 1	–	–	–	–	–	–
KFR88	NBT 2	–	–	–	–	–	–
KFR89	SFR1/177	–	X	–	–	X	–
n/a	SFR(Silo1)	X	–	–	–	X	–

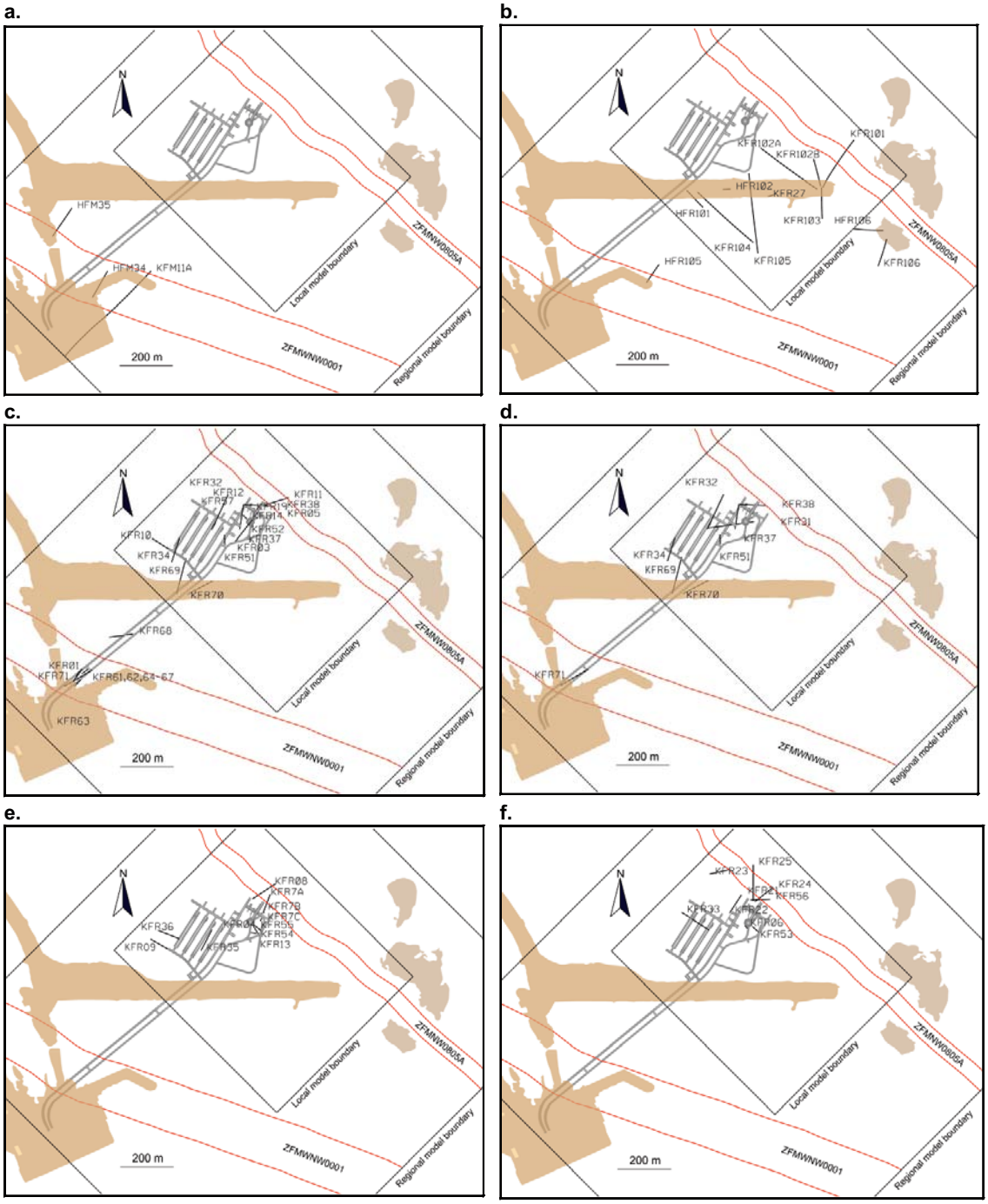

Figure 3-4. *The general position of boreholes within the regional model volume relative to the SFR underground facility, coastline and ground surface trace of ZFMWNW0001 and ZFMNW0805A. a) Forsmark site investigation boreholes, b) boreholes from the current SFR drilling campaign and c– f) old boreholes from the construction of SFR. The latter are divided into c) boreholes where existing lithological logs have been translated into current SKB nomenclature and subjected to a simplified SHI, d) boreholes that were subjected to lithological overview mapping and a simplified SHI e) boreholes that were remapped by the Boremap-system and subjected to SHI and f) boreholes that contain no available drill core and, consequently, no available geological information.*

3.5 Surface geophysics

No new surface based geophysical investigations have been carried out in the current SFR site investigation. Reprocessing and review of earlier produced surface based seismic reflection data, covering the SFR regional model area, has been performed as part of version 1.0 /Juhlin and Zhang 2010/ with a focus on the shallow depth relevant to the SFR storage level. The main results are described in Section 4.6.3 of this report. Earlier geophysical surveys and results are summarised in the following text.

The first detailed geophysical data from the Forsmark area were gathered already during the planning of the nuclear power plants. Since then, geophysical investigations at different scales and for different tasks have been carried out in the area, which have resulted in data of several types with variable spatial resolution and distribution. The intensity in gathering of geophysical data culminated during the Forsmark site investigation, between 2002 and 2007. An overview of the geophysical data used in the Forsmark site investigation is provided in /Stephens et al. 2007/.

During the Forsmark site investigation, the focus was directed on the identification of structural information from magnetic total field data and reflection seismic data. The main source of magnetic data was the dense measurements from the ground survey on land, sea and lakes. However, the helicopter-borne survey also provided information on the magnetic total field, but with lower spatial resolution. At sea, and also quite near the shore, a marine geological survey provided data on the bedrock topography. Campaigns with refraction seismics, both on land and in the sea, resulted in models for the bedrock topography and the P-wave velocity distribution in the bedrock. Only two of the reflection seismic profiles (profiles 5b and 8) cover part of the SFR model areas /Juhlin and Palm 2005/. It is data associated with these two profiles that have been subject to reprocessing and review during version 1.0 /Juhlin and Zhang 2010/.

The characteristics of available magnetic data are presented in Table 3-2 and the surface coverage of all the available geophysical data is presented in Figure 3-5. Relevant data reports for the surface geophysical measurements and lineament interpretation are listed in Appendix 1.

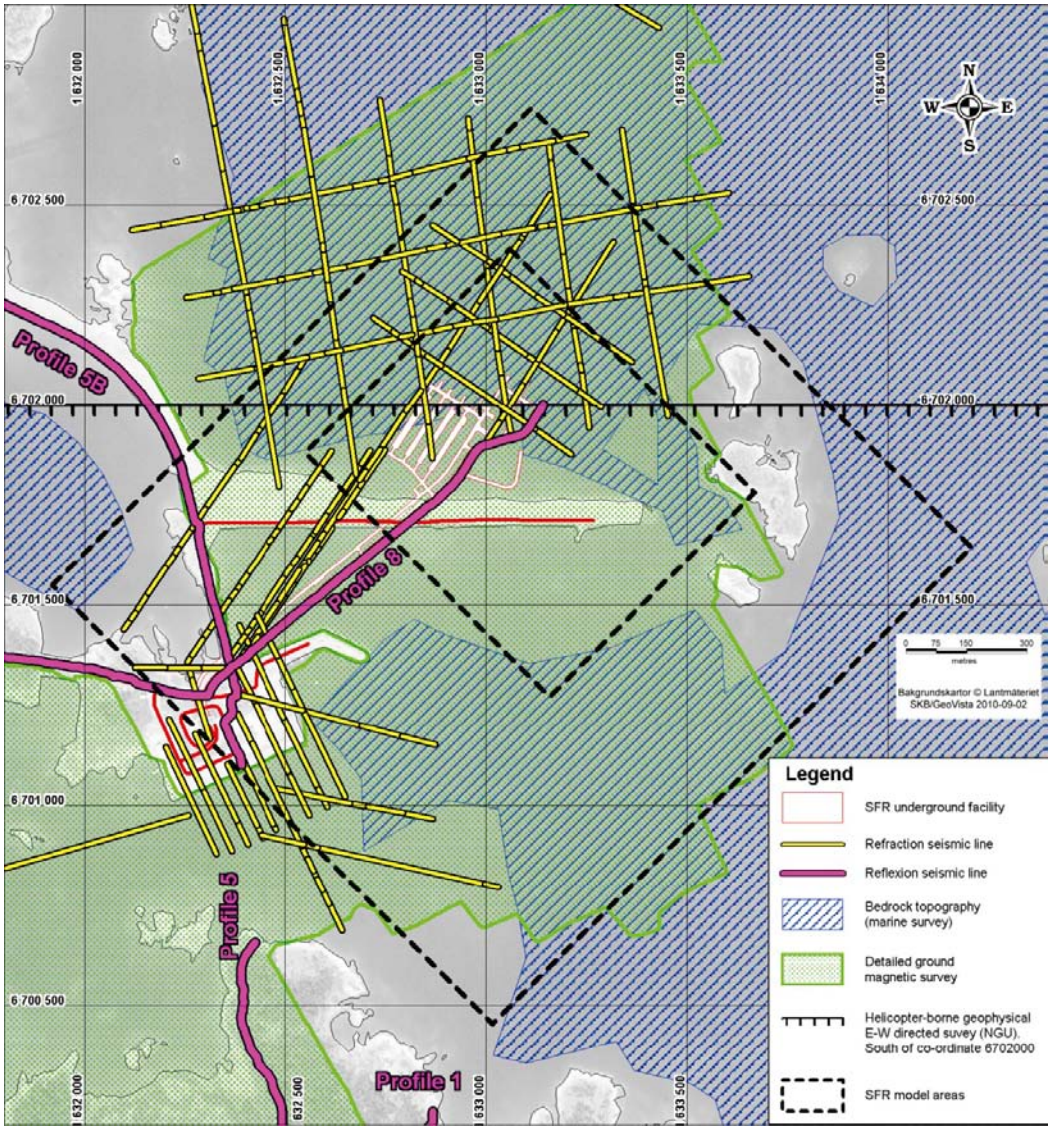

Figure 3-5. *Coverage of available geophysical data around the SFR model areas. The whole area is covered by the SGU fixed-wing airborne survey and the NGU helicopter-borne NS-directed survey (Table 3-1.).*

Table 3-2. Characteristics of magnetic surveys in the Forsmark area. After /Stephens et al. 2007/.

Type of survey	Contractor	Line spacing	Station spacing	Survey direction	Survey elevation	Grid resolution
Airborne, fixed-wing	SGU	200 m	17 or 40 m	EW	60 m (30 m older data)	40×40 m
Airborne, helicopter	NGU	50 m	3 m	NS and EW	45 m	10×10 m
Ground on land, sea and lake	GeoVista AB	10 m	5 m (2–3 m in the marine survey)	150°/330°	ca. 1.5–2 m above ground	4×4 m

4 Evaluation of primary data

4.1 Geological tunnel data from SFR

As part of version 0.1, all the tunnel mapping drawings from /Christiansson 1986/ were digitally scanned, georeferenced in ArcGis and attached to the RVS model /Curtis et al. 2009/. For version 1.0, the overview drawings at the scale 1:2,000 (Appendix 2) have continued to form a primary input to the modelling of deformation zone intersections at the SFR underground facility. During version 0.1, the structural features included in the overview drawings had their character and tunnel chainage positions noted to generate a simplified tunnel log of possible deformation features. The deformation features along with their earlier reported character were noted as 'Tdz's' (possible tunnel deformation zone) in order to follow a systemization very approximately equivalent to the PDZ (possible deformation zones) identified during the borehole SHI process. The tDZ's and tunnel intercept positions corresponding to the deformation zones in the version 1.0 model are included in the property tables in Appendix 11 and the summary tables in Appendix 2. It should be noted that the geometries of all the underground openings presented in the drawings are 'as planned' i.e. they are theoretical rather than 'as built'. This together with deliberate generalizations involved in the mapping methodology /Christiansson and Bolvede 1987/ means that the positions of all recorded features are only approximate. These drawings have been used in combination with as-built tunnel centre-line and laser scanned tunnel section survey data to estimate the zone-tunnel intersection positions in 3D.

4.1.1 Brittle structures

The geological drawings from the construction of SFR are complex, with details regarding rock type, brittle tectonic structures and water seepage superimposed on each other. A general description of the different rock types and the various brittle features is presented in /Christiansson and Bolvede 1987/, along with a description of the mapping methodology. However, there are deficiencies in the nomenclature and several features marked in both the detailed and overview drawings lack any description. Moreover, the correlation between the structures represented in the overview mapping and the results of the fracture mapping presented in the detailed tunnel mapping are often unclear. Clearly identified 'established' fracture zones in the overview drawings are often difficult to identify in the detailed drawings. It has therefore been of importance to obtain updated geological information from SFR.

Most of the underground openings in the SFR facility are covered by shotcrete, which prohibits direct observations of the bedrock, especially in highly fractured tunnel sections. The only part of the facility that is at least to some extent free from shotcrete, is the lower construction tunnel (NBT). An updated geological mapping of NBT was completed by /Berglund 2009/. In addition to lithology, individual fractures and obvious water seepage, /Berglund 2009/ registered 17 deformation zones down to approximately chainage 0+390 along the tunnel. Details for these zones are given in Appendix 2. The criteria used to define these deformation zones are that the fracture frequency is distinctly higher than in the surrounding rock, that the structure shows a high length to width ratio and that the structure is continuous through a large portion of the tunnel perimeter. However, much of the tunnel roof was covered by a ventilation tube during the mapping, and even if a zone was inferred to be continuous across the entire perimeter it was mapped as two separate zones, one in each wall. Most zones were regarded as very minor with a probable local extent and widths of up to 0.6 m (Figure 4-1). The exception is a continuous brittle deformation zone (1D) at 0+120, which has a thickness of approximately 1.5 m in one wall and 0.3 m in the other (here as 5D). This zone does not appear on the overview drawing –103 of /Christiansson and Bolvede 1987/ and it was not possible to link this to a more extensive structure in the current work.

Although several of the brittle structural features marked on the structural overview drawing –103 of /Christiansson and Bolvede 1987/ for the NBT are currently shotcrete covered, it has been possible to gain insights into the complexity by comparing structures defined in the old and updated mapping campaigns. The comparison between the deformation zones defined during the updated geological mapping of NBT by /Berglund 2009/ and the structural overview drawing is presented in Figure 4-2.

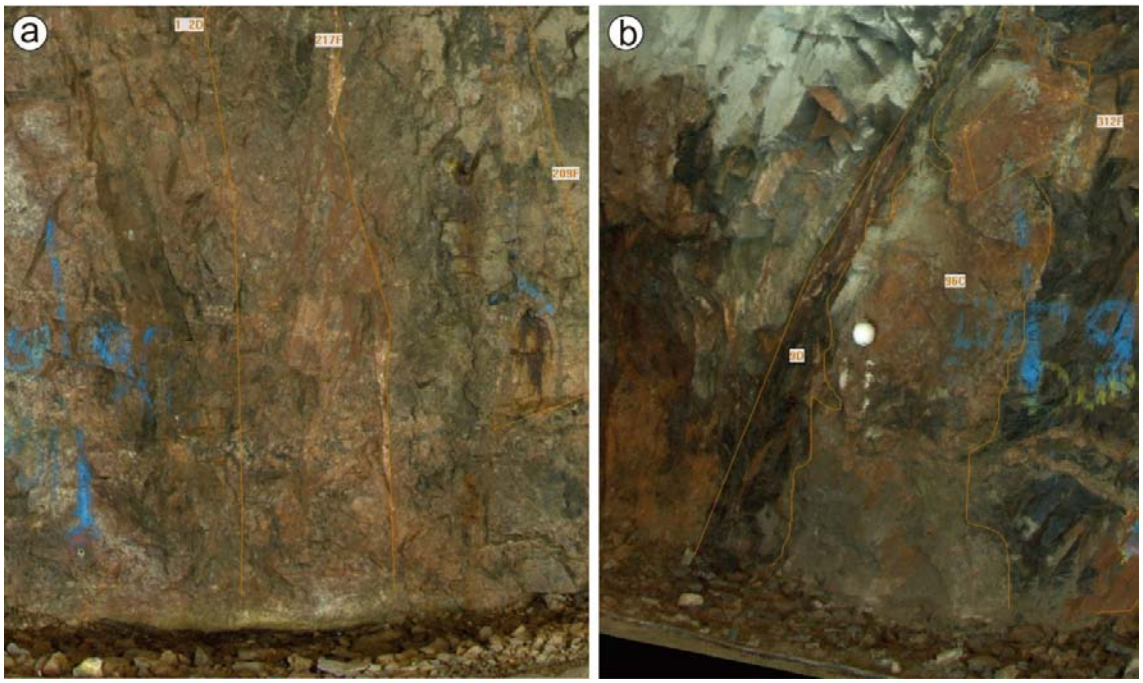

Figure 4-1. *Examples of deformation zones registered during the updated geological mapping of NBT. (a) Deformation zone 1D at 0+120 in the southern tunnel wall. Line 1_2D represent the approximate centre line, which range up to 2 m in width, based on a distinctly increased fracture frequency and associated alteration (oxidation, chloritization and laumontization). (b) Deformation zone 9D, developed in felsic to intermediate metavolcanic rock at 0+190 in the eastern tunnel wall.*

The only deformation zone included in the early structural model of /Carlsson et al. 1985, 1986/ and /Axelsson and Mærsk Hansen 1997/, which occurs along the remapped part of the NBT, is zone 9 (ZFMNE0870). Other, less prominent, brittle structures marked on drawing –103, such as crush zones, brittle shear zones and gouge-filled fractures of varying width, as well as occurrences of closely spaced, parallel fractures and slickensides, were denoted 'possible tunnel deformation zones' (tDZ) during SFR model version 0.1. In total, there are twelve tDZ's in the part covered by the updated mapping of NBT. Information regarding intercept position and orientation for all these features are listed in Appendix 2.

Bearing in mind the uncertainties on the position of recorded structures, it has only been possible to correlate three of the structures marked in drawing –103 with six of the deformation zones registered by /Berglund 2009/. TDZ78, defined as a structure of 'closely spaced, sub-vertical parallel fractures', corresponds to three brittle deformation zones (15D, 17D and 18D) recorded by Berglund between 0+330 to 0+360, of which 15D and 17D include breccias and cataclasites. The two other structures (tDZ95 and tDZ96) in drawing –103 that can be correlated with three deformation zones from the updated mapping are defined as 'fracture zones (gouge filled) < 2 dm'. In the updated mapping, these features (7D, 8D and 9D) are described as brittle-ductile structures and one of them (9D) includes a breccia.

It is noteworthy that several of the deformation zones recorded by /Berglund 2009/, including the most prominent zone (1D) with a width of up to 1.5 m, are not included in drawing –103. Similarly, there are several structural features in drawing –103, which have not been registered as deformation zones by Berglund. The most clear examples are tDZ73, tDZ72 and tDZ80 (ZFMNE0870), defined as 'brittle shear zone, locally crushed and altered rocks'. The most plausible explanation for this is that the structures are currently shotcrete covered. However, there is at least one of the structures (tDZ94), defined as 'closely spaced, gently dipping parallel fractures (dip < 45°)' in drawing –103, which has been registered as a number of separate fractures in the mapping of /Berglund 2009/.

To sum up, the updated mapping of NBT has not yielded sufficient information for a complete translation of the nomenclature used in the drawings of the SFR underground openings presented by /Christiansson and Bolvede 1987/. However, an important outcome of the updated mapping

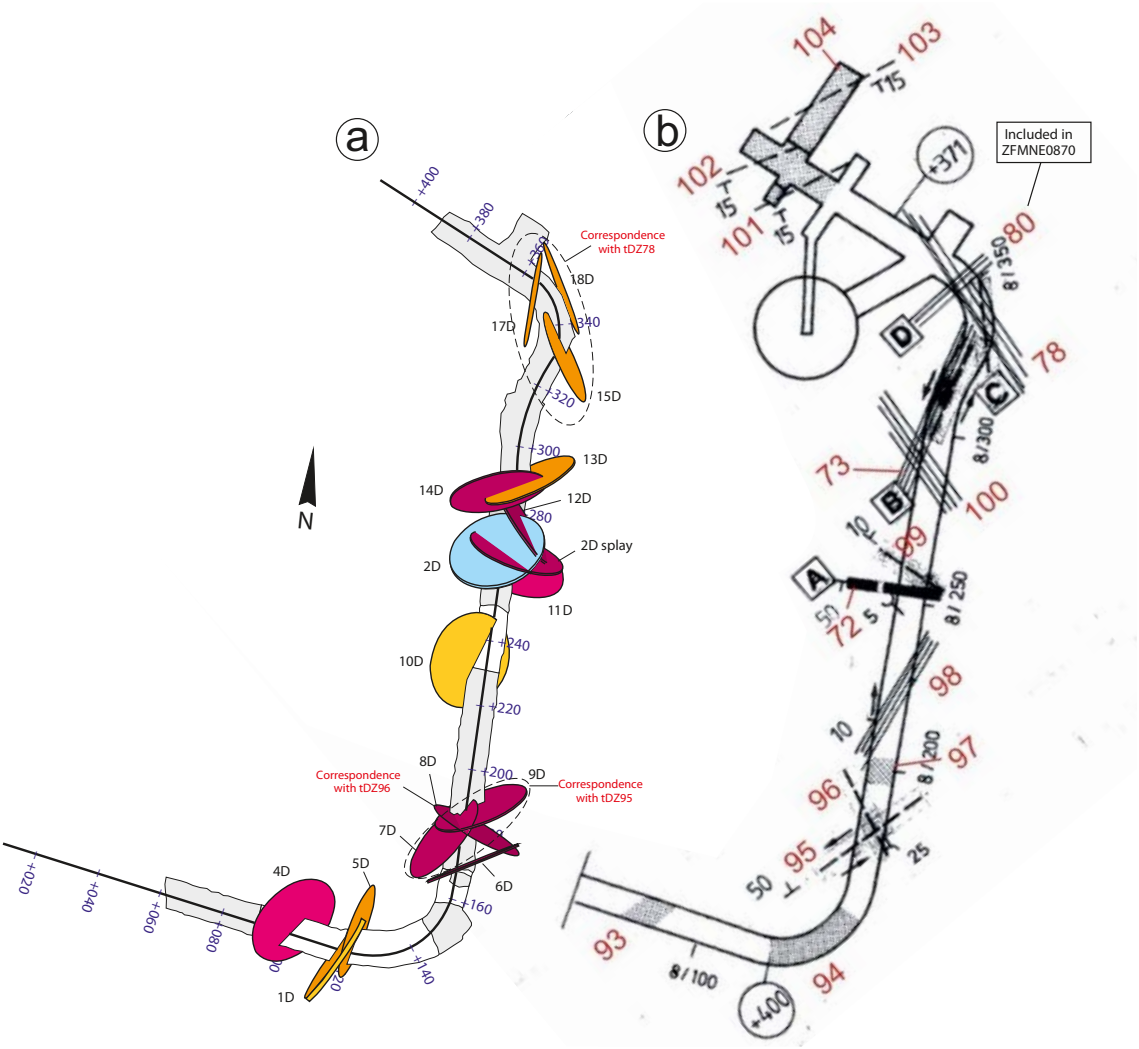

Figure 4-2. *Comparison of deformation zones registered during the updated geological mapping of NBT by /Berglund 2009/ (a) with the overview structural drawing –103 of /Christiansson and Bolvede 1987/ (b). (a) Individual deformation zones are represented by disks (true thickness and default diameter of 30 m) coloured according to the deformation style, where yellow=brittle, violet=brittle-ductile and blue=ductile. Laser scanned cross section of NBT where parts of the roof are covered by shotcrete are shaded in grey. Numbers refers to deformation zones id's listed in Appendix 2. (b) Numbers show tunnel deformation zones (tDZ) listed in Appendix 2. Note the grey areas in (b) mark the mapped location of closely spaced gently dipping fractures in the roof. A complete legend for structural features marked in the drawing (b) is provided in Appendix 2.*

is that many of the structures marked in drawing –103 are minor features without the necessary continuity for deterministic modelling. Another conclusion is that some of the minor structures in the drawing do not qualify as possible deformation zones in terms of the criteria as currently applied by SKB. The primary criteria for defining the structures in the drawings have clearly been an increase in fracture frequency and visual judgements of hydraulic conductivity, i.e. following traditional construction industry practice rather than current SKB criteria focusing also on long term safety.

4.1.2 Rock type

In the main report text, /Christiansson and Bolvede 1987/ describe the bedrock within the SFR area in terms of three main rock types comprising (1) paragneiss with a well-defined planar fabric, (2) red, fine- to medium-grained granite and (3) red or greyish white, coarse-grained, partly pegmatitic granite. Dykes of pegmatite, greenstone and amphibolite occur subordinately. In the geological maps, compiled during the construction of SFR by /Christiansson and Bolvede 1987/, the bedrock has been divided into eleven different rock types (Table 4-1).

Table 4-1. Translation of the rock types defined by /Christiansson and Bolvede 1987/ into the nomenclature introduced during the Forsmark site investigation. Age grouping (A to D) according to the conceptual model of /Stephens et al. 2007/ (cf. Section 2.3).

Original nomenclature		Current SKB nomenclature		
Rock name	Abbrev.	Age group	Code (SKB)	Composition and grain-size
Mylonite	M	–	8004	Very fine-grained rock with distinct deformational fabric
Aplite	Ap	D	1062	Aplite
Granite, pegmatitic	Gp	D	101061	Pegmatitic granite, pegmatite
Granite, fine-grained	Gf	D	111058	Granite, fine- to medium-grained
Granites	G	D	101061	Pegmatitic granite, pegmatite
Pegmatite	P	D	101061	Pegmatitic granite, pegmatite
Greenstone	Gr	B	102017	Amphibolite
Amphibolite	A	B	102017	Amphibolite
Gneiss granite	Gn(g)	B	101057	Granodiorite (to granite), metamorphic, fine- to finely medium-grained
Muscovite schist	Ms	B/A	121057	Orthogneiss, unspecified[1]
Gneiss	Gn	B/A	121057	Orthogneiss, unspecified[1]

[1] The term 'orthogneiss, unspecified' (rock code 121057) may include both the metavolcanic rock (rock code 103076) and the metagranodiorite (rock code 101057).

To be able to use the bedrock mapping in the rock domain modelling work, it was necessary to translate the legend of the drawings into the bedrock nomenclature introduced during the Forsmark site investigation (cf. /Stephens et al. 2003b/). The basis for the translation is primarily a comparison with the updated mapping of NBT by /Berglund 2009/. However, visits were also made to other facility parts with the focus on specific lithological issues. A complete translation of the legend is listed in Table 4-1.

The subordinate rock types, including aplite, pegmatite, amphibolite and mylonite have their analogues in the current SKB nomenclature. They are, moreover, distinctive in terms of grain-size and mineralogy and consequently easy to distinguish. The term 'greenstone' appears to have been used for more altered varieties of amphibolite with a distinguishable tectonic foliation. Greenstone was consequently translated into amphibolite (rock code 102017).

The term 'pegmatitic granite, pegmatite' (rock code 101061), introduced during the Forsmark site investigation, includes all granitic rocks with pegmatitic grain-size, regardless of their relationship to the ductile deformation and textural variability (cf. /Stephens et al. 2005/). Fine- to medium-grained, equigranular granites, in part leucocratic and typically associated with the pegmatitic granite, were defined as a separate rock type with rock code 111058. In the SFR tunnel mapping, these rocks have been mapped as (1) pegmatite, (2) granites, (3) granite, pegmatitic and (4) granite, fine-grained. An ambiguity is the term 'granites', which according to /Christiansson and Bolvede 1987/ includes both fine-grained granite and pegmatitic granite. However, based on the observations during the recent SFR tunnel inspections, it is inferred that the vast majority of the rocks that were mapped as 'granites' are pegmatitic granites. Thus, only 'granite, fine-grained' was translated into fine- to medium-grained granite (rock code 111058), whereas 'pegmatite', 'granites' and 'granite, pegmatitic' were all converted to pegmatitic granite, pegmatite (rock code 101061).

Two different types of gneiss were recognised in the SFR tunnel mapping: (1) gneiss granite and (2) unspecified gneiss used as a 'generic term for undistinguishable, fine-grained, compact dark rocks'. The latter corresponds to the paragneiss as recorded in the description of the tunnels by /Christiansson and Bolvede 1987/. Although somewhat more fine-grained and more granodioritic in composition (see below), the gneiss granite is inferred to correlate with the medium-grained metagranite to granodiorite with rock code 101057 in current SKB nomenclature, the predominate rock type found in the Forsmark tectonic lens (see Section 4.3.1 for a more comprehensive discussion). The ductile deformation and recrystallization are generally more intense than in the lens, but the petrographical similarities are still recognizable. Varieties characterised by more intense ductile deformation appear to have been mapped as 'unspecified gneisses'. Rocks defined as 'felsic to intermediate metavolcanic rocks' with rock code 103076 were also recorded as 'unspecified gneisses'.

The latter are often difficult to distinguish from highly deformed varieties of the metagranodiorite (to granite) (rock code 101057) by ocular inspection. The problem was solved in the current work by the introduction of a more general term, 'orthogneiss, unspecified' (rock code 121057), which may include both the metavolcanic rock (rock code 103076) and the metagranodiorite (to granite) (rock code 101057). Furthermore, the 'muscovite schist', intimately associated in space with the Singö deformation zone, was translated into unspecified orthogneiss, since the rock has been inferred to have a gneissic precursor (cf. /Christiansson and Bolvede 1987/).

Whether a rock type defined by /Christiansson and Bolvede 1987/ exhibits deformational fabric or not is not always obvious in the main report text. The rock types with typically well-defined tectonic foliation include unspecified gneiss, muscovite schist, gneiss granite and greenstone. Also the fine-grained granite displays tectonic foliation locally. For the other rock types, there are no notation of ductile deformation, more than the fact that amphibolite dykes and to some extent pegmatites are largely parallel with the foliation in the wall rock.

To emphasize the bedrock information, the translation was followed by a colour coding of the detailed drawings at the scale 1:200 of /Christiansson and Bolvede 1987/, as included in Appendix 2 (Figure A2-2). Due to difficulties in the three-dimensional conversion, it was decided to exclude drawing –14 of the silo. The colours followed SKB standards for all rock types.

4.2 Borehole data

4.2.1 Deviation measurements and erroneous length adjustments for boreholes from the construction of SFR

Although deviation measurements were carried out for most cored boreholes drilled during the construction of SFR (e.g. /Hagkonsult 1982, 1983/), there are no calculated deviations available in the SKB database Sicada. Instead, the orientations of the boreholes have been defined at the top-of-casing. However, it must be emphasized that the deviations given in /Hagkonsult 1982, 1983/ are all less than one metre from the theoretical orientation.

4.2.2 Borehole mapping including BIPS, radar and geophysical logs

Data from three different drilling campaigns have been used in SFR model version 1.0. All cored and percussion boreholes from the SFR site investigation, as well as KFM11A, HFM34 and HFM35 from the Forsmark site investigation, were characterised by standard SKB methodology, including radar and geophysical logging systems together with geological mapping using the Boremap system. A key input in the mapping procedure is oriented image logs generated along each borehole by the Borehole Image Processing System (BIPS). A combination of some of the geophysical data (e.g. density, natural gamma radiation and single point resistivity) provided support to the geological mapping, especially in the percussion boreholes. The relevant data acquisition reports for all different logs are listed in Appendix 1.

Data acquisition from the cored boreholes drilled during the construction of SFR deviated from the standard SKB procedure, mainly due to the lack of BIPS-images, but also due to the general absence of geophysical logs and a lower quality in available data and drill cores. Drill cores from eleven of these boreholes were selected for renewed mapping by the Boremap system. However, orientation data were restricted to alpha-angles for prevalent fracture sets and individual fractures were separated into broken and unbroken, instead of sealed and open, which is current SKB standard practice. In addition, the mapping included documentation of (1) lithology exceeding 1 m in drill core length, (2) alteration, (3) exact fracture positions along the drill core, (4) fracture mineralogy, (5) crush zones, (6) breccias, (7) sealed fracture networks and (8) ductile and brittle-ductile shear zones. The results of this mapping are presented in /Petersson and Andersson 2011/.

Data acquisition from the remaining 32 boreholes, for which there are drill cores available, was focused on lithological documentation, consisting of (1) translation of original bedrock mapping into established SKB rock nomenclature and (2) if such information does not exist, overview mapping where rock types exceeding 1 m in drill core length were recorded along with ductile and brittle

ductile deformation and alteration. Thus, no primary data for the brittle structures in these drill cores were obtained. Details of the activities are presented in /Stephens et al. 2008a/ and /Petersson et al. 2011/.

The restricted quality and less control of the data from the old boreholes yielded during the construction of SFR remains. Similarly, there is also an inherently lower quality of data from the percussion boreholes. For this reason, cored borehole data from the SFR and Forsmark site investigations have been given precedence over data from percussion and older cored boreholes. Data from the eleven boreholes selected for renewed mapping have been given a similar precedence. Consequently, data from the other old boreholes and the percussion boreholes have primarily been used to support the overall geometry of particular deformation zones and rock domains in the model, though more crucial aspects, such as zone thickness and existence, are based first and foremost on data from the new and eleven remapped cored boreholes.

The geophysical logging methods that have been applied in the boreholes from the latest drilling campaign comprise:

- Density (gamma-gamma).
- Magnetic susceptibility.
- Natural gamma radiation.
- Focused resistivity (300 cm).
- Focused resistivity (128 cm).
- Caliper mean.
- Fluid resistivity.
- Fluid temperature.
- Borehole radar (not used in the percussion drilled boreholes, KFR102B and KFR103).

The analyses of the logging data were made with respect to identifying major variations in physical properties with depth as indicated by the silicate density, the natural gamma radiation and the magnetic susceptibility. A combined interpretation of these parameters, together with petrophysical data for calibration, makes it possible to estimate the physical signature of different rock types. Magnetic data is an important data source in the SFR area, especially due to the general sea cover. Since these three parameters are related to the mineral composition of the rocks in the vicinity of the borehole, they correspond to variations in the primary character and the secondary alteration of rock type. Since alteration can commonly be associated with geologically ancient deformation zones, magnetic susceptibility data can also be used in the identification of zones.

The resistivity and caliper loggings are mainly used for identifying sections with increased fracturing and alteration, in particular sections with an increased frequency of open fractures, i.e fractures with apertures. The vertical gradient of the fluid temperature is used to identify small variations in the fluid temperature, and such anomalies are very often related to water-bearing fractures. Borehole radar reflectors can be related to rock type, fracturing or both these features.

4.2.3 Single-hole interpretation

The geological single-hole interpretation (SHI), which is an interpretation based on an integrated synthesis between geological and geophysical borehole information, provides a key link between the primary borehole data and the modelling work. The procedure includes (1) merging of sections with similar rock types or where one rock type is very dominant into rock units and (2) identification of possible deformation zones. This is made independently for each borehole and the standard SHI is based on geological mapping data using BIPS and the Boremap system, together with geophysical and radar data. The confidence in the interpretation of rock units and possible deformation zones along the borehole is addressed on the following basis: 3 = high, 2 = medium and 1 = low. It needs to be emphasized that neither rock mechanical nor hydrogeological data have been involved in the procedure. Another important point is that no extended SHI, including kinematic data, have been completed for any of the identified possible deformation zones as part of the current project.

Rock units, exceeding a minimum length of 5 m along the borehole, have been defined primarily on the basis of composition, grain-size and inferred relative age (i.e. fundamental criteria of the SKB rock type coding). In a few instances, the following geological features have been of importance for their definition:

- An increased fracture frequency outside possible deformation zones.
- An increased degree of ductile deformation.
- The occurrence of cataclastic overprinting associated with the Singö deformation zone.

The geophysical parameters silicate density, natural gamma radiation and magnetic susceptibility were also used. However, these parameters are mainly employed as an additional check on the rock classification in the Boremap mapping so as to provide a quality assurance for the mapping procedure.

The borehole documentation from the older SFR boreholes is generally too sparse to allow full application of the established SHI methodology to define rock units. In addition, geophysical logs only exist for seven of the boreholes. A summary of the data included in the rock unit interpretation and deviations from the established methodology are presented in Table 4-2. Three sets of geological data, with different degrees of deficiency, are available for the older boreholes:

- Updated geological mapping by the Boremap system for eleven of the boreholes, which includes documentation of lithology, alteration as well as brittle and ductile structures. Except for consistent documentation of rock occurrences (rock types less than 1 m in borehole length), this mapping includes generally all necessary geological data to define rock units by the established SHI methodology.
- Lithological overview mapping by the Boremap system for eleven of the boreholes, which includes documentation of rock type (name, structure, grain-size and texture), ductile shear zones and alteration (except for oxidation). Essential data that are lacking for defining rock units are information on rock occurrences and fracture frequency.
- Rock type coding of the original geological mapping for 20 of the boreholes. These data are limited to rock type name without structural or textural information.

Table 4-2. Basis for interpretation of rock units and deviations from established SHI methodology.

Boreholes	Basis for interpretation	Nonconformities
Forsmark site investigation		
HFM34, HFM35, KFM11A	Generally all necessary data available.	HFM34 was not mapped below 179.0 m length due to poor BIPS-image.
SFR site investigation		
HFR101, HFR102, HFR105, HFR106, KFR27, KFR101, KFR102A, KFR102B, KFR103, KFR104, KFR105, KFR106	Generally all necessary data available.	KFR27 has been mapped as a percussion borehole down to 147.5 m length. Radar data were not available for the percussion boreholes, KFR102B and KFR103.
Older cored SFR boreholes		
KFR04, KFR08, KFR09, KFR13, KFR35, KFR36, KFR54, KFR55, KFR7A, KFR7B, KFR7C	Updated geological mapping by Boremap (includes rock type name, structure, grain-size and texture, along with rock alteration and fracture frequency). Geophysics only for KFR04.	No orientation data due to lack of BIPS-image only a few alpha-angles. No documentation of rock occurrences. Geophysics only for KFR04. No radar data.
KFR31, KFR32, KFR34, KFR37, KFR38, KFR51, KDR69, KFR70, KFR71, KFR72, KFR89	Lithological overview mapping by Boremap (includes rock type name, structure, grain-size and texture, along with ductile shear zones and rock alterations other than oxidation).	No orientation data due to lack of BIPS-image. No documentation of brittle structures and rock occurrences. No geophysics and radar data.
KFR01, KFR02, KFR03, KFR05, KFR10, KFR11, KFR12, KFR14, KFR19, KFR20, KFR52, KFR57, KFR61–KFR68, SFR (Silo1)	Rock type coding of the original geological mapping (includes only rock type name). Geophysics only for KFR01, KFR02, KFR03, KFR05, KFR19, KFR20.	No orientation data due to lack of BIPS-image. No documentation of rock type characteristics, rock alteration, brittle structures and rock occurrences. No radar data.

The subdivision into different rock units was completed for all boreholes both from the newly completed Forsmark and SFR site investigations and the 43 older SFR boreholes by application of the general principles of the SHI methodology, regardless of the data deficiencies. The results of this work are presented in a series of reports listed in Appendix 1.

All identified possible deformation zones are brittle or in a few cases brittle-ductile in character. Some of the zones have a ductile precursor. The identification was primarily carried out on the basis of fracture frequency and rock alteration, together with geophysical data sets. The latter include estimated fracture frequency derived from electric resistivity, caliper anomalies, radar amplitude anomalies and to some extent magnetic susceptibility. Note that the interpretation of geophysical data played a more significant role in the percussion boreholes, where the geological information is more sparse. Open, partly open and sealed fractures, as well as sealed fracture networks and crush zones were differentiated in the analysis of anomalously high fracture frequencies. The most prominent alteration along the possible deformation zones is so-called 'oxidation', manifested by a red staining associated with sub-microscopic hematite dissemination in the feldspars.

Deficiencies in the available geological data, not least the absence of fracture mapping for several boreholes, enforced serious deviations from the established geological SHI methodology for identification of possible deformation zones along the older SFR boreholes. Furthermore, radar data do not exist for any of the older boreholes and geophysics is only available for seven of them. A summary of the data included for the identification of possible deformation zones and deviations from the established methodology is presented in Table 4-3.

The identification of possible deformation zones in the eleven boreholes that were subjected to updated geological mapping by the Boremap system generally followed the established methodology, with the exception that the analysis of anomalously high fracture frequencies differentiated between broken and unbroken fractures, instead of open, partly open and sealed, which is current SKB practice. Geophysical data, in the form of single point resistivity, was only available for KFR04. All remaining boreholes from the construction of SFR were subject to a simplified version of the SHI procedure, where possible deformation zones were identified during direct visual inspection of the drill cores and no preceding inspection and comparison of data logs was involved.

Table 4-3. Basis for identification of possible deformation zones and deviations from established SHI methodology.

Boreholes	Basis for interpretation	Nonconformities
Forsmark site investigation		
HFM34, HFM35, KFM11A	Generally all necessary data available.	HFM34 was not mapped below 179.0 m length due to poor BIPS-image.
SFR site investigation		
HFR101, HFR102, HFR105, HFR106, KFR27, KFR101, KFR102A, KFR102B, KFR103, KFR104, KFR105, KFR106	Generally all necessary data available.	KFR27 has been mapped as a percussion borehole down to 147.5 m length. Radar data were not available for the percussion boreholes, KFR102B and KFR103.
Older cored SFR boreholes		
KFR04, KFR08, KFR09, KFR13, KFR35, KFR36, KFR54, KFR55, KFR7A, KFR7B, KFR7C	Updated geological mapping by Boremap (includes rock alteration and fracture documentation in terms of broken and unbroken fractures, sealed fracture networks, crushes and mineralogy).	No orientation data due to lack of BIPS-image and only a few alpha-angles. No differentiation of open, partly open and sealed fractures. Geophysics only for KFR04. No radar data.
KFR01, KFR02, KFR03, KFR05, KFR10, KFR11, KFR12, KFR14, KFR19, KFR20, KFR31, KFR32, KFR34, KFR37, KFR38, KFR51, KFR52, KFR57, KFR61–KFR72, KFR89, SFR (Silo1)	Identification of PDZ was made on direct drill core observations. Further revision after inspection of drill core photographs and completion with geophysics where available (KFR01, KFR02, KFR03, KFR05, KFR19, KFR20).	No preliminary group inspection of WellCad logs due to the lack of BIPS-image, radar data and documentation of rock alteration and brittle structures.

This process was supplemented by further review of drill core photographs and an input from geophysics in six boreholes (see Table 4-3). In a similar manner as the established SHI standards, the following features were documented:

- The specific geological criteria and, for some boreholes, geophysical criteria used to identify the possible deformation zone.
- The occurrence of crushes, breccias and cataclasites.
- Alpha-angles and mineralogy of fractures inside the possible zone.
- Rock types affected by the possible zone.
- Confidence in the interpretation on the basis of: 3 = high, 2 = medium and 1 = low.

As pointed out earlier (see Section 3.1), there are significant differences in the methodologies to define the existence and boundaries of possible deformation zones in the geological SHI compared with those used to define fracture zones in the early structural models for SFR (cf. /Carlsson et al. 1985, 1986, Christiansson 1986, Axelsson and Mærsk Hansen 1997/). Inferred borehole intercepts for the fracture zones in the previous structural models of SFR, and to some extent model version 0.1 /Curtis et al. 2009/, have therefore been updated in the current model version by the possible deformation zones defined during the SHI work. A detailed comparison between the two data sets was presented by /Curtis et al. 2009/ for the eleven boreholes subjected to updated mapping by the Boremap system.

4.3 Rock type

4.3.1 Character of rock types based on tunnel and borehole data

The general properties and nomenclature of the rock types in the SFR area were initially established during the Forsmark site investigation (see /SKB 2005/). Additional geological and geophysical data generated from the later boreholes in the SFR area conform well to the established rock type nomenclature and do not motivate changes. However, the generally more intense ductile overprinting in the SFR area, compared with the Forsmark lens, provided a strong incentive for upgrading the rock properties.

This compilation primarily makes use of data from cored boreholes drilled during the SFR site investigation, complemented with information from boreholes within the regional SFR model volume and the SFR underground facility. In general, the compilation includes the rock properties needed to allow rock domain modelling work (cf. /Munier et al. 2003/), but there are data deficiencies. The most important is that only three modal analyses from KFM11A exist for rocks in the regional SFR model volume (cf. /Petersson et al. 2007/). As a consequence, all assessment of rock type was based on ocular inspection. It must be emphasized that there exists a considerable number of modal analyses from the local model area of the Forsmark site investigation for all the major rock types found in the SFR area. The decision not to complete modal analyses during the present site investigation was based on experiences from the preceding Forsmark site investigation, where ocular inspection generally turned out to be an adequate method for the distinction of the various rock types /Petersson et al. 2004a/.

The petrophysical laboratory data from the SFR area are limited to 57 drill core samples analysed for density and, only in some cases, magnetic susceptibility /Mattsson and Keisu 2009a, 2010, Mattsson 2009/. Gamma spectrometry measurements to obtain the distribution of K, U and Th do not exist. The purpose with the laboratory analyses was mainly to establish calibration parameters for geophysical logging and also to support the geological rock type classification. Apart from the density data of some rock types, there are too few measurements to enable reliable and complete characterization of the major rock types in the SFR area based on petrophysical data as was used in the Forsmark site investigation /SKB 2005, Stephens et al. 2007/. Instead, the physical properties have been documented by using data from geophysical logging of the cored boreholes in the local model volume from the current drilling campaign (i.e. KFR101, KFR102A, KFR102B, KFR103, KFR104, KFR105 and KFR27, with some exceptions). This compilation integrates borehole measurements of density, magnetic susceptibility and natural gamma radiation with a selection of Boremap data for major rock types and alteration types with adherent intensity.

The previous, upper part of borehole KFR27 was excluded in the compilation, since the drill core supported mapping starts at 147.55 m borehole length. For the new, lower part of KFR27, only magnetic susceptibility and density have been used. The reason for this is that KFR27 was logged twice, before and after the borehole was extended to 501.64 m borehole length. A comparison between the two sets of logging data shows a significant difference in the natural gamma radiation, with an increased radiation level in the later measurement /Mattsson and Keisu 2009b/. However, the anomaly patterns are very similar. The calibration of the logging tool was checked, and there are no indications of any measurement errors. Some of the other boreholes in the SFR area (e.g. KFR104) also show significantly increased natural gamma radiation levels compared, for example, with the data from the boreholes in the Forsmark lens. It should be emphasized that this increase is a general feature and occurs as a constant increase of the radiation level along the entire borehole length. Thus, the increase is shown by all rock types, even rocks such as amphibolites that usually exhibit low radiation levels. A plausible explanation, as proposed by /Mattsson and Keisu 2009b/ would be an increased background radiation, as a result of radon leakage into the water-filled boreholes from rocks and/or fractures at depth. This is further supported by the fact that there is a general increase of U in water samples from the SFR boreholes relative to those from boreholes in the Forsmark lens /Nilsson et al. 2010/. This in turn might well be related to the frequent occurrence of U-bearing fracture minerals /Sandström and Tullborg 2011/ and the large volumes of pegmatitic granites in the SFR area, which both contribute to the increased radiation levels. Gamma spectrometry measurements in boreholes or on outcrops, which could help to elucidate this, have not been performed. The generally increased radiation levels will, of course, affect the compiled natural gamma radiation data in Table 4-4, and must be taken into consideration when comparing the petrophysical data sets from SFR and the Forsmark site investigation.

A summary of the geological and physical properties of the major rock types in the local SFR model area are presented in Table 4-4. Other less frequently occurring rock types have not been included due to data deficiency. The compilation includes rock type name/code, grain-size, density, magnetic susceptibility and natural gamma radiation. Details and noteworthy features for individual rock types are given below in separate sections.

Table 4-4. Grain-size and physical properties of the major rock types in the local SFR model volume. The age grouping (A to D) according to the conceptual model of /Stephens et al. 2007/ (cf. Section 2.3). Sections affected by alteration, such as hematite staining or quartz dissolution, have been omitted in the compilation of physical properties. The physical properties have been estimated on the basis of the geophysical logging data (cf. /SKB 2005, Stephens et al. 2007/).

Code	Name	Grain-size	Density [kg/m^3] (min/max/mean/std)	Magnetic susceptibility [×10^{-5} SI] (min/max/mean/std below/std above)	Natural gamma radiation [µR/h] (min/max/mean/std)
Group D					
111058	Granite	Fine- to medium-grained	2,623/2,838/2,671/19	4/1,560/181/144/695	22/91/56/13
101061	Pegmatite, pegmatitic granite	Coarse-grained (pegmatitic)	2,434/2,818/2,643/29	0/9,281/15/12/62	20/334/76/32
Group B					
101057	Granodiorite (to granite), metamorphic	Fine- to finely medium-grained	2,595/2,880/2,702/25	0/10,617/110/91/509	17/260/39/15
102017	Amphibolite	Fine- to finely medium-grained	2,623/3,027/2,867/71	1/19,243/1,493/1,248/7,610	12/212/24/13
Group A					
103076	Felsic to intermediate volcanic rock, metamorphic	Fine- to finely medium-grained	2,520/2,893/2,746/42	3/8,331/796/655/3,696	12/366/35/27

Granite (111058)

The granites coded 111058 are equigranular and fine- to medium-grained, with a generally low content of ferromagnesian minerals (< 5 vol.%). Typically, they occur as dykes up to a few meters in thickness, with sealed contacts to the host rocks, though more extensive bodies of at least 10–20 m thickness have been recorded in KFR27 and KFR102A, as well as in the SFR underground facility. A spatial association with pegmatitic granite is noted locally. The majority of the granites in the SFR facility have been affected by penetrative ductile deformation under lower amphibolite-facies conditions, with weakly developed linear mineral fabric, and locally a planar mineral fabric. However, similar to the corresponding granites in the Forsmark tectonic lens, there are occurrences of granite that are strongly discordant to the structural trend in their host rocks.

The density, magnetic susceptibility and natural gamma radiation of the granites are summarised in Table 4-4 and Figure 4-3. The density is typical for rocks of monzogranitic composition, with a mean value of 2,671 kg/m^3. The magnetic susceptibility in the local SFR model area shows a distinct bimodal distribution, which resembles the pattern for the metagranodiorite (to granite) (101057). The susceptibility range is largely identical to that of outcrop data from the regional model area, defined during the preceding Forsmark site investigation, though the bimodal pattern cannot be distinguished in the latter case /Isaksson et al. 2004b/, possibly due to the smaller data set. The granites show an increased natural gamma radiation with an average of 56 μR/h.

Pegmatitic granite, pegmatite (101061)

The term pegmatitic granite includes rocks with highly variable grain-size, typically ranging from pegmatite to aplitic granite, often over a short distance within a single occurrence. Pegmatites and pegmatitic granites occur as segregation veins or pods, irregular bodies and dykes, with highly variable relationship to the ductile deformation. Some occurrences are tightly folded and concordant to the banding and mineral fabric in their host rocks, whereas others are distinctly discordant. In the SFR underground facility, it appears from folding and the structural relations with the wall rock that most exposed bodies of pegmatitic granite have been affected at least to some degree by ductile deformation, but it is rarely revealed by ocular inspection of the mineral fabric (i.e. at hand specimen or drill core scale).

The density, magnetic susceptibility and natural gamma radiation of the granites are summarised in Table 4-4 and Figure 4-3. The low density, with an average of 2,643 kg/m³, confirms their predominantly granitic composition with locally high feldspar contents and very low amounts of ferromagnesian minerals. The rocks exhibit a highly variable, but generally distinctly lower, magnetic susceptibility than the other major rock types in the SFR area, with a geometric mean of 15×10^{-5} SI. In contrast to the granites (111058), the magnetic susceptibility data of the pegmatitic granites and pegmatites show a well-defined normal distribution. The pegmatite and pegmatitic granite also show high natural gamma radiation both with a high average, 77 μR/h, and a skewed high end spectra with many readings between 100–200 μR/h.

Granodiorite (to granite), metamorphic (101057)

The rock type is equigranular and fine- to medium-grained, with a moderately to strongly developed planar, and to some extent linear, mineral fabric. Macroscopically, these rocks are distinguished from the younger granites (111058) by a texture of stretched, monomineralic domains and the higher content of ferromagnesian minerals, as estimated by ocular inspection, ranging up to approximately 10 vol.%. They are consistently more fine-grained than the corresponding metagranite (to granodiorite) in the Forsmark tectonic lens. An almost 200 m length interval of a fine- to finely medium-grained variety that strongly resembles the metagranodiorite (to granite) in the SFR area, in terms of texture and grain-size, occurs in KFM05A /Petersson et al. 2004b/, situated within the central part of the Forsmark lens. More strongly deformed varieties (BSL-tectonites) of the metagranodiorite (to granite) are locally difficult to distinguish from the felsic to intermediate metavolcanic rocks (103076) in the area. To some extent, it is possible to separate the metagranodiorite (to granite) from the metavolcanic rocks by density, since the content of ferromagnesian minerals appears generally to be lower in the metagranodiorite (to granite).

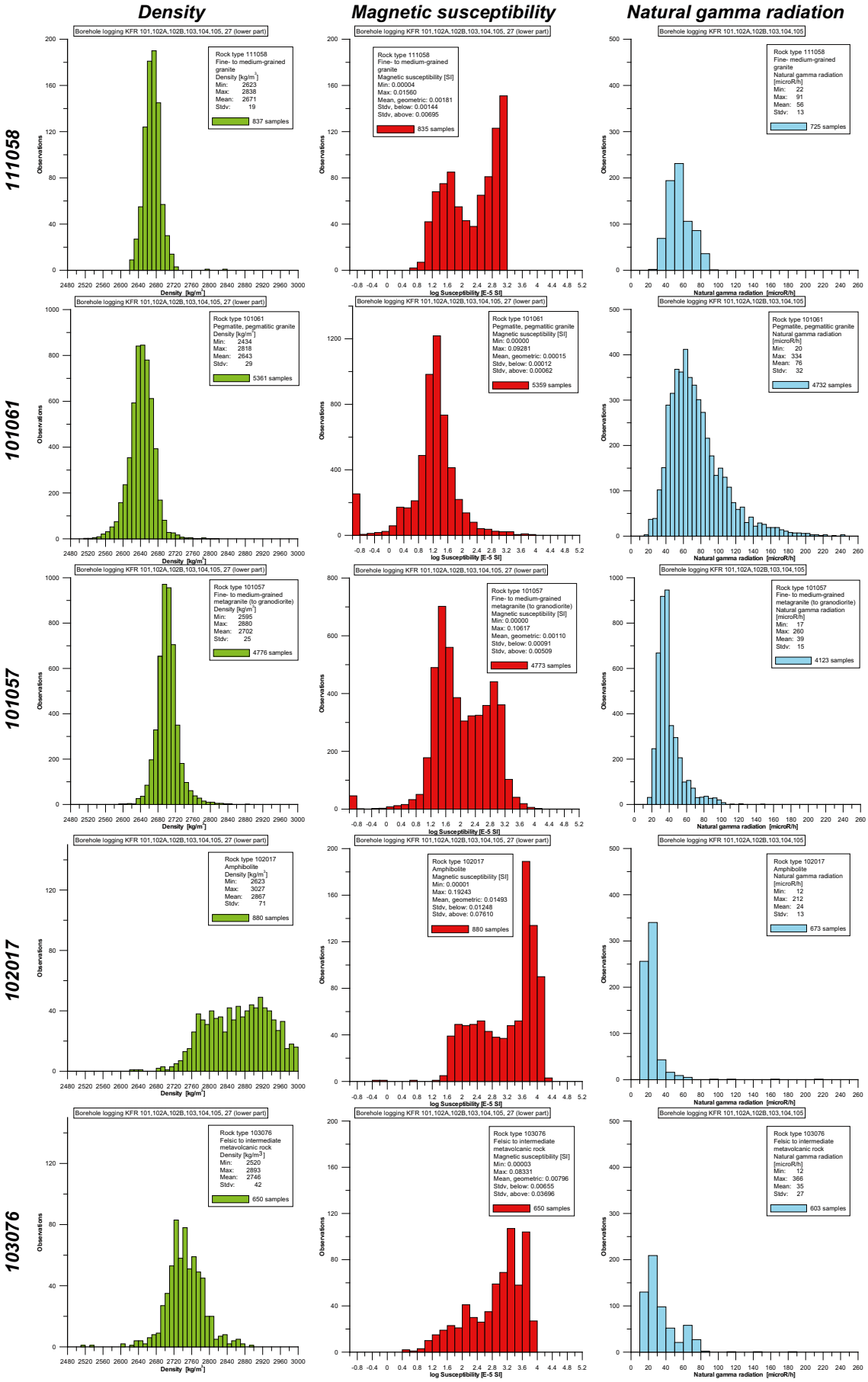

Figure 4-3. *Physical properties of the major rock types in the local SFR model area. Sections affected by alteration, such as hematite staining or quartz dissolution, have been omitted in the diagrams. Compilations on a borehole by borehole basis as well as for individual rock domains (see Chapter 6) are provided in Appendix 4.*

The density, magnetic susceptibility and natural gamma radiation of the metagranodiorite (to granite) are summarised in Table 4-4 and Figure 4-3. An arithmetic mean of 2,702 kg/m^3 for the density reflects the general granodioritic composition with subordinate, granitic varieties. The magnetic susceptibility distribution for the rock type is very similar to that of the younger granites (111058), with a bimodal pattern and a geometric mean of 110×10^{-5} SI. The metagranodiorite (to granite) shows an increased natural gamma radiation with an average of 39 μR/h.

Judging from the density, it would have been more correct to denote the rock as a metagranodiorite (101056), which is frequent in the more intensely deformed belt along the south-western margin of the Forsmark lens, according to the bedrock geological map of /Stephens et al. 2008a/. However, there are borehole intervals with a typical granitic density (< 2,680 kg/m^3), especially in sections of less intense ductile deformation, where the precursor is more obvious. Consequently, it was decided to keep the rock type name metagranite to granodiorite (101057) and accentuate the prevailing granodioritic composition by putting the term 'granite' in brackets.

A comparison between the density distribution for this rock type and samples from the Forsmark site investigation (cf. Table 5-3 in /SKB 2005/), reveals a close similarity to the fine- to medium-grained metagranodiorite, tonalite and granite (101051), which belongs to rock group C. Also the general grain-size of the two rock types is comparable. Several occurrences of the fine- to medium-grained metagranodiorite, tonalite and granite have been recorded at islets south-east of the SFR area (e.g. Rönngrundet), within the high-strain belt that corresponds to RFM021 in the Forsmark rock domain model /SKB 2005/. At these localities, the fine- to medium-grained metagranodiorite, tonalite and granite typically occurs as lenses or bands, which are distinguishable from their hosts of group A and B rocks, by local cross-cutting relationships and a general less intense ductile deformation (cf. /Bergman et al. 2004/). The fact that the group C rock is distinguishable in outcrops further towards east to south-east within RFM021, excludes that the rock type inferred to be fine- to finely medium-grained metagranodiorite (to granite) actually is a group C metagranodiorite. This is further supported by distinct differences in the macroscopic texture of varieties with lower degree of ductile strain, although it cannot be excluded that some intensely deformed occurrences of group C metagranodiorite were misinterpreted as fine- to finely medium-grained metagranodiorite (to granite).

Amphibolite (102017)

Amphibolites form irregular shaped as well as dyke-like bodies that are elongate following the mineral fabric and the structural trend of the host rocks. It is inferred that they intruded originally as dykes. The rock type includes virtually all mafic rocks in the SFR area, regardless of their structural and textural character. The majority are fine-grained with a high content of plagioclase and hornblende. Minor occurrences and the margins of larger bodies display a distinct mineral fabric, whereas the more central parts of larger bodies are typically massive.

The density, magnetic susceptibility and natural gamma radiation of the amphibolites are summarised in Table 4-4 and Figure 4-3. The most distinctive physical property of the amphibolites is the density with an arithmetic mean of 2,867 kg/m^3. There is a large scatter in the density data and the data do not form a clear normal distribution as for the other rock types in Figure 4-3. However, the mean density of the logging data is well in accordance with the mean density of 2,898 kg/m^3 established from petrophysical sample measurements (std. dev. = 81 kg/m^3, n = 14). The petrophysical data also show a fairly wide distribution of the density, ranging from 2,742 kg/m^3 to 3,070 kg/m^3. The results possibly indicate that the amphibolites vary greatly in mineral composition, but this is not consistent with the rather narrow distribution in the natural gamma radiation data. However, there is a slight overlap in density with the more intermediate varieties of the metavolcanic rocks. The metavolcanic rocks are also low in natural gamma radiation and they are sometimes difficult to visually distinguish from the amphibolites. Therefore, it is possible that the wide density distribution of the amphibolites is, to some extent, a result of a mix up in the rock type classification.

A majority of the amphibolites in the SFR area have an anomalously high magnetic susceptibility with a geometric mean of $1{,}493\times10^{-5}$ SI. This feature merits attention, since the outcrop data for amphibolites in the Forsmark regional model volume are consistently low, in the range $51–86\times10^{-5}$ SI /Isaksson et al. 2004b/. It is clear that this can be explained, at least partly, by a high content of magnetite, which locally occurs as separate crystals up to several millimetres in size. The amphibolite shows an increased natural gamma radiation with an average of 24 μR/h.

Felsic to intermediate metavolcanic rock (103076)

The metavolcanic rocks are fine-grained and locally show a compositional banding. Since the metavolcanic rocks are all affected by intense ductile deformation and recrystallization under amphibolite-facies metamorphic conditions, they are distinguished from the spatially associated metagranodiorite (to granite) by their grain-size, higher content of ferromagnesian minerals and banding, rather than by volcanic structures or textures.

The density, magnetic susceptibility and natural gamma radiation of the metavolcanic rocks are summarised in Table 4-4 and Figure 4-3. Their dacitic composition is reflected in the arithmetic mean density of 2,746 kg/m^3. The distribution of the magnetic susceptibility data is similar to that of the amphibolites in the SFR area. Moreover, the magnetic susceptibility is generally higher than for equivalent metavolcanic rocks exposed in the Forsmark regional model area /Isaksson et al. 2004b/. The natural gamma radiation of the metavolcanic rocks show a bimodal character, with mode values between 20–30 µR/h and 60–70 µR/h, respectively.

4.3.2 Proportions of different rock types

The proportions of the different rock types in the local SFR model volume, as well as KFR106 and HFR106 data outside this volume, have been estimated on a borehole by borehole basis by merging the data sets for rock type (> 1 m in borehole length) and rock occurrence (< 1 m in borehole length) in the Sicada database. The working procedure also involved the removal of rock type intervals that overlap with inserted rock occurrences. Apart from the latter adjustment, the procedure is identical to that used in the Forsmark site investigation /Stephens et al. 2007/. The results of the analysis for each borehole at SFR are summarised in Table 4-5. Separate histograms for the new cored boreholes, the cored boreholes from the construction of SFR and the percussion boreholes are presented in Figure 4-4.

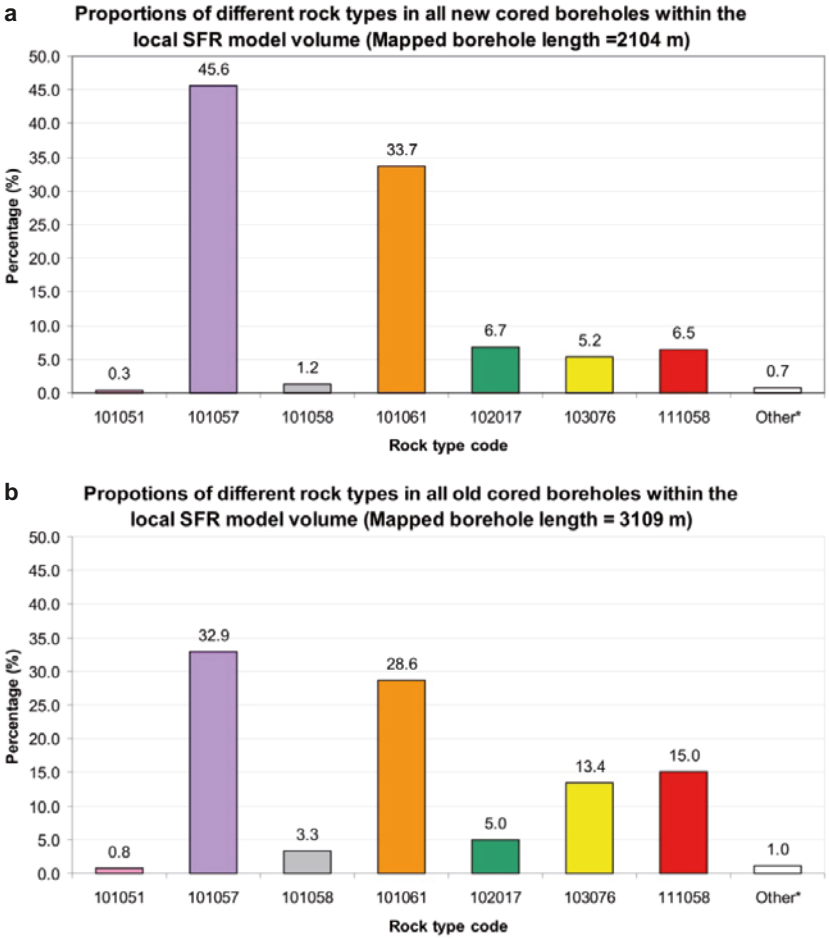

Figure 4-4. *Histograms showing the proportions of different rock types in (a) the cored boreholes from the drilling campaign for the extension of SFR and (b) old cored boreholes from the construction of SFR. Only data from the local SFR model volume as well as KFR106 and HFR106 outside this volume are included. Data are presented in Table 4-5 and the translation of codes for rock names is provided in Table 4-4.*

Table 4-5. Quantitative estimates in length % of the proportions of different rock types in boreholes located within the local SFR model volume.

Borehole	Length	Rock type code (SKB)[1]							
	[m]	101051	101057	101058	101061	102017	103076	111058	Other[2]
HFR101	200.29	–	21	–	60	1	7	10	–
HFR102	45.96	–	36	–	46	2	–	–	16
HFR106	181.07	–	56	–	36	1	6	1	–
Total	**427.32**	**0**	**38**	**0**	**47**	**1**	**4**	**4**	**5**
KFR02	170.33	–	35	–	57	–	5	2	–
KFR03	101.60	8	12	30	34	5	11	–	–
KFR04	100.50	–	25	–	1	8	25	39	2
KFR05	130.08	–	0	–	11	4	48	36	1
KFR08	104.40	–	19	–	44	–	1	30	5
KFR09	80.24	–	5	–	24	1	63	8	–
KFR10	107.28	5	2	–	19	3	44	27	–
KFR11	98.07	–	19	–	24	3	2	40	13
KFR12	50.26	4	44	–	33	–	2	17	–
KFR13	76.60	5	57	–	21	2	–	15	–
KFR14	28.67	–	0	–	11	47	32	10	–
KFR19	110.17	–	8	–	28	2	38	24	1
KFR20	109.70	–	18	1	24	12	27	18	–
KFR31	225.50	–	34	7	29	5	6	19	–
KFR32	193.15	–	50	3	26	10	–	11	–
KFR34	128.45	–	37	–	40	2	19	2	–
KFR35	122.17	3	33	–	36	7	14	6	2
KFR36	107.80	–	33	8	14	4	10	28	2
KFR37	192.67	–	37	18	12	4	–	29	1
KFR38	171.95	–	38	15	22	9	–	16	–
KFR51	46.28	–	44	–	43	3	10	0	–
KFR52	29.95	–	13	–	68	1	–	16	1
KFR54	53.30	–	79	–	7	5	–	9	1
KFR55	61.89	–	85	–	8	–	3	4	–
KFR57	25.38	–	10	–	25	8	42	15	–
KFR69	189.52	–	40	–	53	1	1	5	1
KFR70	163.26	–	15	–	83	2	–	–	–
KFR7A	74.45	–	55	18	23	1	–	3	–
KFR7B	21.10	–	81	–	19	–	–	–	–
KFR7C	34.00	–	57	–	20	–	–	23	–
Total	**3,108.72**	**1**	**33**	**3**	**29**	**5**	**13**	**15**	**1**
KFR27[3]	291.59[4]	–	39	–	46	5	4	6	1
KFR101	328.04	1	48	6	26	6	2	10	2
KFR102A	262.84[4]	–	53	–	24	8	2	13	1
KFR102B	166.13	–	49	–	18	18	8	5	–
KFR103	187.16	0	46	0	28	10	12	2	1
KFR104	376.42[4]	0	32	4	56	2	4	2	0
KFR105	201.38	0	38	0	46	1	6	8	0
KFR106	290.86	2	60	0	26	3	3	5	1
Total	**2,104.42**	**0**	**46**	**1**	**34**	**7**	**5**	**6**	**1**

1 Translation of codes for rock names is provided in Table 4-4.

2 Other includes 1051, 1058, 1062, 5105, 6005, 8003, 8004, 8020, 8021, 101004, 101054, 108019.

3 Upper part of KFR27 (11.82–147.48 m borehole length) is mapped without drill core. The drill core supported mapping starts at 147.55 m borehole length.

4 The borehole penetrates the local SFR model volume (KFR27 at 303.41 m, KFR102A at 333.28 m and KFR104 at 385.15 m borehole length).

The predominant rock types in most boreholes are metagranodiorite (to granite) (101057) together with the pegmatitic granite and pegmatite (101061). Other frequently occurring rock types are fine- to medium-grained granite (111058), felsic to intermediate volcanic rock (103076) and amphibolite (102017). Additional, subordinate rock types occupy less than 3% of the total borehole length and include aplitic metagranite (101058), fine- to medium-grained metagranodiorite to tonalite (101051), fine- to finely medium-grained metatonalite to granodiorite (101054), ultramafic rock (101004), skarn-like rock (108019) and undifferentiated granitoid (1051), granite (1058) and aplite (1062), as well as breccia (6005), cataclastic rock (8003), mylonite (8004), hydrothermal vein (8020) and quartz-dominated hydrothermal vein (8021).

Compared with the Forsmark tectonic lens further south, the SFR area is highly variable and heterogeneous in terms of the distribution of different rock types. There are typically two or more predominant rock types in a single borehole regardless of where in the rock mass the borehole is located, even if there is a slight dominance of the metagranodiorite (to granite), especially in the boreholes from the latest drilling campaign. It is generally the amount of pegmatitic granite, felsic to metavolcanic rock and younger granite that is higher in the SFR area, at the expense of the metagranodiorite (to granite). The proportion of amphibolite is approximately the same in both areas, whereas fine- to medium-grained metagranodiorite, tonalite and granite (101051) is more scarce in the SFR area (cf. /Stephens et al. 2007/ and Section 4.3.1).

It should be noted that the boreholes are located in two spatial clusters, where the old boreholes occur in the northern part of the local SFR model volume, within or close to the SFR underground facility, and the boreholes from the new drilling campaign are generally located within the southern part of the local SFR model volume. The most conspicuous differences in the rock type distribution between the two groups are the relative amount of metagranodiorite (to granite), felsic to intermediate metavolcanic rock and younger granite. As mentioned in the preceding section, the intense ductile deformation and recrystallization in the SFR area have given rise to a high-strain variety of the metagranodiorite (to granite), which is locally indistinguishable from the felsic to intermediate metavolcanic rock. For the SFR tunnel mapping this problem was solved by the introduction of a more general term, 'orthogneiss, unspecified' (rock code 121057), which may include both the metavolcanic rock and the metagranodiorite (to granite). In the boreholes, the separation between the two rock types has been facilitated by their physical properties. However, such data are only available in seven, old boreholes. In addition, some of the sections recorded as felsic to intermediate metavolcanic rock during the rock type coding carried out during an early stage of the Forsmark site investigation /Stephens et al. 2008a/ have been re-interpreted in this study as highly deformed varieties of the metagranodiorite (to granite). Thus, there is an uncertainty in the estimates of the proportions of the two rock types in the older boreholes, and this may explain some of the differences between the two borehole groups.

The relatively high proportion of younger granites in the northern part of the local SFR model area, as shown by the borehole data, is further supported by SFR tunnel mapping. Although their distribution is heterogeneous in the rock volume, a concentration tends to occur in the SFR underground facilities. The distribution appears, moreover, independent of the ductile structural trend in the rock mass. Their occurrence resembles that of the pegmatitic granite, which also shows a largely random distribution. However, there is a concentration of pegmatitic material in the western part of the local SFR model area (e.g. KFR104 and the south-western part of the SFR underground facility included in the local model volume).

4.3.3 Rock alteration

Alteration can affect both the thermal and mechanical properties of rock and therefore needs to be assessed. Furthermore, the relationship between alteration and deformation zones needs to be evaluated since rock alteration is one of the primary data sets by which possible deformation zones are identified during the geological SHI.

An assessment has been made by investigating the proportion of the bedrock affected by each type of alteration, both inside and outside modelled deformation zones (ZFM), along with a general description of each major alteration type. Whether a section belongs to a deformation zone or not is defined by the so-called target intercept, as described in Chapter 5. Quality controlled data concerning type and degree of rock alteration are available from the Sicada database for KFM11A, all cored boreholes from the new drilling campaign and the eleven old SFR boreholes selected for renewed mapping by Boremap. Alteration data from the percussion boreholes are of lower confidence and data from the remaining old SFR boreholes show generally varying degrees of deficiency. For these reasons, the data from these boreholes have been excluded in the analytical work. In this context, the upper part of KFM27, down to 147.48 m length, which has been mapped essentially as a percussion borehole, and is hence omitted from the compilation. Another noteworthy feature is that some of the alteration types overlap each other, even if this is rather rare.

The results are presented in tabular format both as borehole lengths (Table 4-6) and as proportions of the borehole lengths (Table 4-7). A comparison between the total borehole lengths that were affected by alteration inside and outside modelled deformation zones is illustrated in Figure 4-5. Details for the most widespread and important alteration types are given below.

Table 4-6. Occurrences of rock alteration in meters (m) inside/outside modelled deformation zones (ZFM) on a borehole by borehole basis.

Borehole ID	Length inside/outside ZFM	Argillization	Albitization	Oxidation	Chloritization	Qtz dissolution	Sericitization	Other[1]	Total length
Inside deformation zones (ZFM)									
KFM11A	579.0	1.1	5.3	141.1	14.7	–	113.6	38.5	314.3
KFR04	58.0	0.1	–	36.0	–	–	–	–	36.1
KFR08	79.4	–	1.5	59.2	1.3	2.3	–	1.9	66.3
KFR09	58.7	–	–	48.2	1.1	–	–	–	49.4
KFR13	20.5	–	–	13.4	0.7	–	–	–	14.1
KFR27	146.0	13.8	0.3	82.9	12.9	20.8	–	2.4	133.2
KFR35	37.3	–	–	14.9	–	–	–	–	14.9
KFR36	70.5	–	–	52.9	2.6	–	–	1.6	57.1
KFR54	15.5	0.1	–	8.4	–	–	–	–	8.5
KFR55	30.0	–	–	22.8	–	–	–	–	22.8
KFR101	193.0	1.0	1.8	90.8	0.5	0.1	2.5	8.0	104.6
KFR102A	116.0	1.0	–	44.5	–	11.5	1.1	1.1	59.3
KFR102B	12.0	–	0.1	1.0	–	–	–	–	1.1
KFR103	2.5	–	–	1.7	–	–	–	–	1.7
KFR104	99.1	4.0	–	23.4	0.6	2.5	–	9.1	39.4
KFR105	59.2	0.3	–	9.8	0.8	–	–	0.9	11.8
KFR106	16.0	2.4	0.5	2.6	–	–	2.5	2.5	10.5
KFR7A	71.0	1.8	3.0	30.8	–	–	–	0.4	36.0
KFR7B	17.0	–	–	–	–	–	–	–	–
KFR7C	26.0	1.0	1.6	8.0	–	–	–	–	10.5
Total	1,706.7	26.5	14.2	692.3	35.4	37.3	119.7	66.3	991.6
Outside deformation zones (ZFM)									
KFM11A	200.3	–	12.9	6.7	13.5	–	2.4	13.2	48.8
KFR04	42.5	–	–	2.3	–	–	–	–	2.3
KFR08	25.0	–	–	5.4	–	–	–	–	5.4
KFR09	21.5	–	–	10.1	–	–	–	–	10.1
KFR13	56.1	–	–	14.6	–	–	–	0.6	15.2
KFR27	208.1	–	1.6	18.5	–	–	6.3	2.0	28.4
KFR35	84.9	–	–	7.0	–	–	–	0.2	7.2
KFR36	37.3	–	–	31.7	–	–	–	–	31.7
KFR54	37.8	–	–	6.0	–	–	–	–	6.0
KFR55	31.9	–	–	3.0	–	–	–	–	3.0
KFR101	135.0	–	1.3	23.9	0.1	–	–	0.5	25.8
KFR102A	414.4	–	17.2	19.7	–	–	21.5	0.2	58.6
KFR102B	154.1	–	3.4	28.3	–	–	–	0.8	32.5
KFR103	184.7	0.0	0.3	19.4	1.3	–	34.8	0.6	56.4
KFR104	346.8	–	17.2	42.7	2.7	2.5	25.1	2.2	92.4
KFR105	247.6	–	–	7.6	0.5	–	6.5	–	14.7
KFR106	274.9	0.7	2.6	43.9	0.4	4.1	89.4	0.9	142.0
KFR7A	3.5	–	–	–	–	–	–	–	–
KFR7B	4.1	–	–	–	–	–	–	–	–
KFR7C	8.0	–	0.2	–	–	–	–	–	0.2
Total	2,518.4	0.7	56.7	290.8	18.4	6.6	186.1	21.3	580.8

[1] Other includes silicification, carbonatization, epidotization, sassuritization, steatitization and laumontization.

Table 4-7. Occurrences of rock alteration in percentage (%) inside/outside modelled deformation zones (ZFM) on a borehole by borehole basis.

Borehole ID	Argillza-tion	Albitiza-tion	Oxida-tion	Chloriti-zation	Qtz dis-solution	Sericiti-zation	Other[1]	Total length
Inside deformation zones (ZFM)								
KFM11A	0.2	0.9	24.4	2.5	–	19.6	6.6	54.3
KFR04	0.1	–	62.1	–	–	–	–	62.2
KFR08	–	1.9	74.6	1.7	3.0	–	2.4	83.5
KFR09	–	–	82.2	2.0	–	–	–	84.1
KFR13	–	–	65.3	3.5	–	–	–	68.8
KFR27	9.4	0.2	56.8	8.9	14.3	–	1.6	91.2
KFR35	–	–	39.8	–	–	–	–	39.8
KFR36	–	–	75.0	3.7	–	–	2.3	81.0
KFR54	0.6	–	54.0	–	–	–	–	54.6
KFR55	–	–	76.0	–	–	–	–	76.0
KFR101	0.5	0.9	47.0	0.3	0.1	1.3	4.1	54.2
KFR102A	0.9	–	38.4	–	9.9	1.0	1.0	51.1
KFR102B	–	0.8	8.3	–	–	–	–	9.1
KFR103	–	–	68.3	–	–	–	–	68.3
KFR104	4.0	–	23.6	0.6	2.5	–	9.2	39.8
KFR105	0.6	–	16.5	1.4	–	–	1.5	20.0
KFR106	15.2	2.9	16.0	–	–	15.8	15.9	65.8
KFR7A	2.5	4.3	43.4	–	–	–	0.5	50.7
KFR7B	–	–	–	–	–	–	–	–
KFR7C	3.7	6.2	30.6	–	–	–	–	40.6
Total	1.6	0.8	40.6	2.1	2.2	7.0	3.9	58.1
Outside deformation zones (ZFM)								
KFM11A	–	6.5	3.3	6.8	–	1.2	6.6	24.4
KFR04	–	–	5.4	–	–	–	–	5.4
KFR08	–	–	21.4	–	–	–	–	21.4
KFR09	–	–	47.0	–	–	–	–	47.0
KFR13	–	–	26.1	–	–	–	1.1	27.2
KFR27	–	0.8	8.9	–	–	3.0	1.0	13.7
KFR35	–	–	8.2	–	–	–	0.2	8.5
KFR36	–	–	85.0	–	–	–	–	85.0
KFR54	–	–	16.0	–	–	–	–	16.0
KFR55	–	–	9.4	–	–	–	–	9.4
KFR101	–	1.0	17.7	0.1	–	–	0.4	19.1
KFR102A	–	4.1	4.7	–	–	5.2	0.1	14.1
KFR102B	–	2.2	18.3	–	–	–	0.6	21.1
KFR103	–	0.2	10.5	0.7	–	18.8	0.3	30.6
KFR104	0.0	5.0	12.3	0.8	0.7	7.2	0.6	26.6
KFR105	–	–	3.1	0.2	–	2.6	–	5.9
KFR106	0.2	1.0	16.0	0.1	1.5	32.5	0.3	51.7
KFR7A	–	–	–	–	–	–	–	–
KFR7B	–	–	–	–	–	–	–	–
KFR7C	–	1.9	–	–	–	–	–	–
Total	0.0	2.2	11.6	0.7	0.3	7.4	0.8	23.1

[1] Other includes silicification, carbonatization, epidotization, sassuritization, steatitization and laumontization.

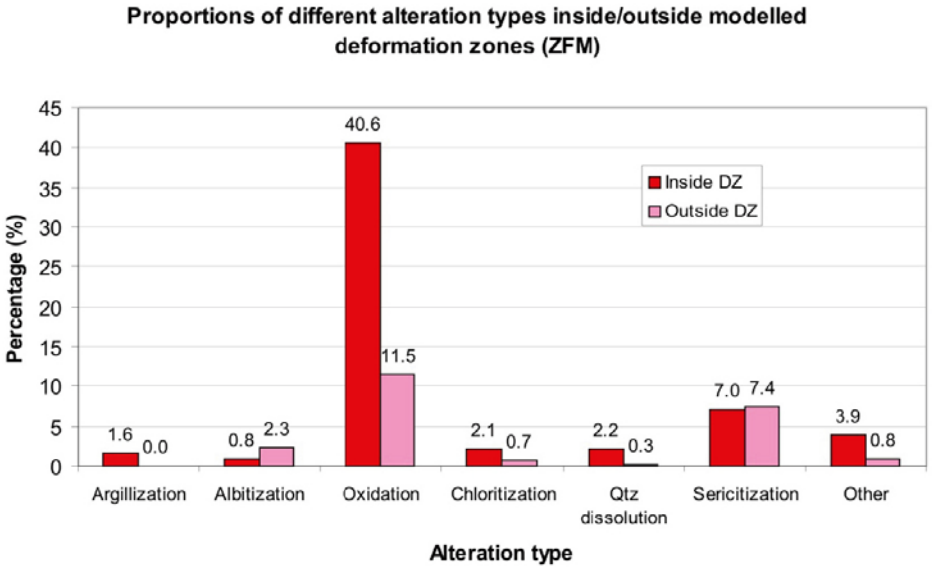

Figure 4-5. *Histogram showing the proportion of borehole length affected by different alteration types inside/outside modelled deformation zones in the regional SFR model volume.*

Hematite dissemination, which is mapped and referred to as oxidation in Sicada, is by far the most abundant type of alteration within the boreholes. The second most frequent alteration type is muscovitization, which is mapped and referred to as sericitization in Sicada. All alteration types, except sericitization and albitization, show an affinity to the modelled deformation zones. Indeed, more than 40% of the total borehole length inside modelled deformation zones was affected by oxidation. The proportion of bedrock affected by muscovitization is more or less identical inside and outside the modelled deformation zones, which reflects its inferred metamorphic origin (e.g. /Döse et al. 2009b/), rather than being related to the brittle deformation in the area. In addition, albitization is inferred to have been formed by processes that predate the brittle regime /Petersson et al. 2005, Stephens et al. 2005, 2007/. The alteration types included by the term 'other' are silicification, carbonatization, epidotization, sassuritization, steatitization and laumontization. The most abundant of these alterations is epidotization and laumontization, which occur in several of the boreholes, but rarely exceed a few decimetres in borehole length. The remaining alteration types included in 'other' are restricted to one or a few of the boreholes.

Argillization

Rock sections with clay alteration are mapped and referred to as argillization in Sicada. The alteration is generally restricted to highly fractured intervals with clay-bearing fractures, which is reflected in the fact that all but three minor occurrences lie inside modelled deformation zones.

Albitization

Rock sections characterised by a general bleaching or whitening, which is imparted by the feldspars in the rock, has been mapped and referred to as albitization in Sicada. Geochemical analyses conducted during the Forsmark site investigation /Petersson et al. 2005/ suggest that the alteration is a form of albitization resulting from alkali redistribution. The alteration has preferentially affected granitic rocks that belong to rock group B, prior to regional deformation and metamorphism (see also /Stephens et al. 2005, 2007/). Large volumes of this alteration type occur along the coast close to Asphällsfjärden and along Klubbudden /Stephens et al. 2003b/, south-west of the regional SFR model area. However, in the SFR boreholes, the presence of albitization is limited to scattered occurrences, which rarely exceed a few meters in borehole length. The most extensive occurrence occurs at 349.4–334.6 m length in KFR104. Albitization is also locally conspicuous along contacts to amphibolite (see also /Stephens et al. 2005, 2007/).

Oxidation

Oxidation or hematite dissemination is manifested by a red-staining. The major mineralogical changes during this type of alteration have been described by /Sandström et al. 2010/ and include saussuritization of plagioclase, chloritization of biotite and a sub-microscopic hematite dissemination within plagioclase together with an increase in porosity and redox capacity. The alteration is intimately associated with fractures at all levels in the boreholes considered. It must be emphasized that it is inferred to be an ancient geological phenomenon formed at temperatures > 150°C, and is consequently not related to recent surficial processes /Sandström et al. 2010/.

Chloritization

The alteration type is largely bound to amphibolites. The major mineralogical change in such altered amphibolites is the conversion of biotite and hornblende into chlorite. Generally, there appears to be an association between the presence of hematite dissemination in the granitic wall rock and chloritization of amphibolites. Note that 75% of the affected intervals occur in KFM11A and KFR27.

Quartz dissolution

Quartz dissolution is one of the more spectacular alteration phenomena in the SFR boreholes. The most extensive occurrences are found in KFR27 and KFR102A, where the total affected borehole length amounts to 20.8 and 11.5 m, respectively. Minor occurrences, ranging up to a few meters in length, were also recorded in KFR08, KFR101, KFR104 and KFR106. In addition, quartz dissolution occurs within KFR11 (66.58–67.15 and 70.45–70.60 m borehole length). The alteration type was also recognised in some of the cored boreholes drilled during the Forsmark site investigation. The most extensive of these occurrences was the focus of a special study by /Möller et al. 2003/.

The dissolution of quartz has mainly affected granitic rocks. Although the void left from the dissolved quartz is generally refilled by new, hydrothermal minerals, such as chlorite, albite, quartz and hematite, the result of the process is a vuggy rock with syenitic composition (Figure 4-6). The alteration is virtually always accompanied by intense red-staining due to oxidation.

The vast majority of these occurrences have been included within possible deformation zones in the single-hole interpretation. However, these features have themselves, along with raised fracture frequency, been taken to be indicative features of a zone. Moreover, there is no simple correlation between the occurrence of quartz dissolution and deformation zone orientation. Except for the affected intervals in KFR106 and some of the intervals in KFR104, all occurrences have been included in four modelled deformation zones, ZFMENE3115, ZFMNE3118, ZFMNW0805A and ZFMWNW0835. In addition, there is one minor occurrence within the modelled zone ZFMNNE0725, which occurs in KFM06A DZ7.

Sericitization

Intervals mapped and recorded in Sicada as sericitization are characterised by an anomalous amount of muscovite with an inferred metamorphic origin. Muscovitization is generally restricted to the fine- to medium-grained metagranodiorite (to granite), and is typically accentuated by the grain-shape fabric. Thus, the occurrence of muscovitization is not confined to deformation zones, as shown in Figure 4-5.

Figure 4-6. *Photograph showing the vuggy, red-stained rock, which is the result of quartz dissolution in combination with oxidation. Upper drill core Section 452.1–452.7 m and lower 453.2–453.8 m from KFR102A.*

4.4 Ductile deformation

Surface data

Structural data from the high-strain belt in which SFR is situated, defined as rock domain RFM021 during the Forsmark site investigation /SKB 2005, Stephens et al. 2007/, are limited to a few islets, none of which are located within the SFR local model area. A stereographic well-exposed summary of these data from RFM021, including fold axes, foliation/banding and mineral stretching lineations, was presented by /Stephens and Forssberg 2006/. From their compilation, it is evident that both fold axes and mineral stretching lineations consistently plunge towards south-east (Figure 4-7). However, linear structures measured south-east of the SFR underground facility plunge more gently (Fisher mean for fold axes 136°/37° and stretching lineations 127°/30°) than those measured north-west of SFR (Fisher mean for fold axes 134°/58°). Poles to the tectonic foliation/banding north-west of SFR tend to plot along a great circle with a pole at 124°/64°. This provides additional support for the existence of major folding in RFM021.

In addition, there exist measurements of the anisotropy of magnetic susceptibility (AMS) from four samples taken on the islets close to the local SFR model volume (PFM001640, PFM001729, PFM001904 and PFM005204). The measurements permit calculations of the mean direction and shape of the anisotropy, which provide some quantitative estimates of the orientation and character of the ductile strain at the sample site. Figure 4-8 shows a stereographic projection of the magnetic lineation from the four sample sites. Each axis is a mean value of four measurements of the same rock type at each locality. The axes shows a well-defined NW–SE trend, but with a highly variable plunge, similar to that observed in the structural measurements (cf. Figure 4-7). The two sample sites closest to the SFR facility, PFM001640 and PFM005204, show a moderate plunge towards the north-west (212°/65°) and south-east (112°/68°), respectively.

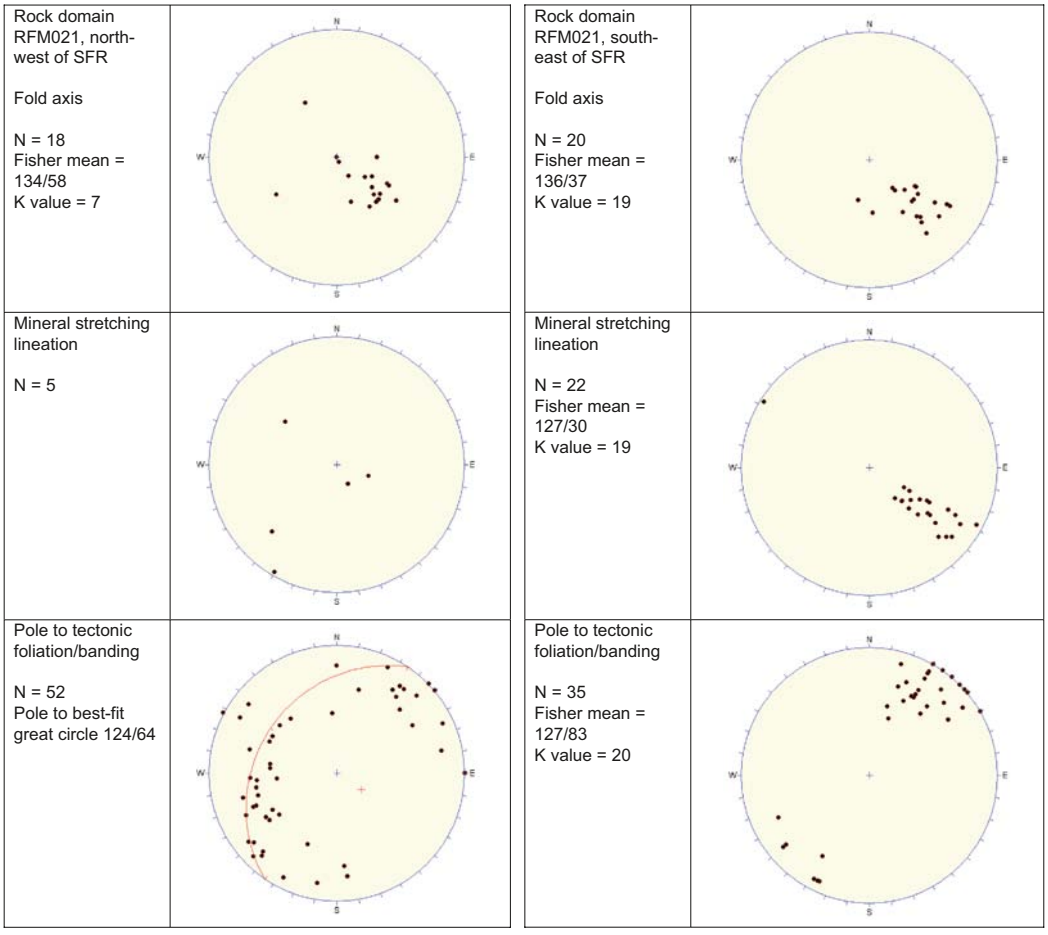

Figure 4-7. *Stereographic presentation of structural data from the north-western and south-eastern part of RFM021, including fold axes, mineral stretching lineation and tectonic foliation/banding. All structures have been plotted on the lower hemisphere of an equal-area projection. After /Stephens and Forssberg 2006/.*

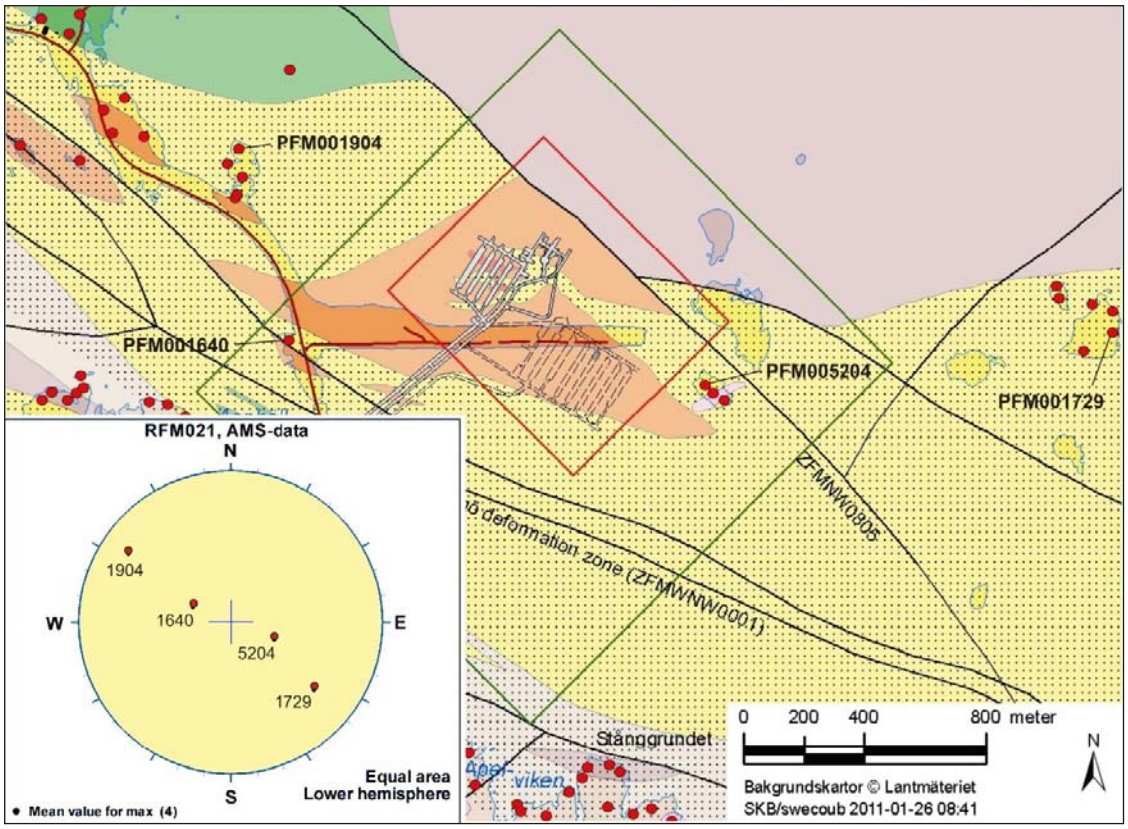

Figure 4-8. *Forsmark bedrock geological map (stage 2.3) in the area around SFR, showing the location of sample sites for AMS measurements. Paler shades for each colour on the map indicate that the corresponding rock unit is covered by water. For legend see Figure 1-2. The inset shows the magnetic lineation in a lower hemisphere, equal-area stereographic projection as inferred from the AMS data.*

Tunnel data from SFR

Ductile structures are treated very briefly, often in relation to brittle tectonics, in the original documentation from the construction of SFR. The tunnel drawings of /Christiansson and Bolvede 1987/ reveal scattered measurements of fold axes, but no other ductile structural data. In general terms, the foliation is steeply to vertically dipping in all parts of the underground facility, except north of and in close proximity to the silo, where it becomes more moderately dipping (60–70°) towards south-west, locally down to 15° under the silo /Christiansson and Bolvede 1987/. From the entrance of the access tunnels, through the Singö belt and towards the SFR depositional area with the rock vaults, the strike of the foliation shifts from 135–150° to 145–160°. Within the depositional area, on the other hand, it ranges between 120 and 140°. The fold axes are typically oriented parallel or, more rarely, perpendicular to the foliation with gentle to moderate plunges towards the south-east or north-east /Christiansson and Bolvede 1987/.

The ductile structural data from the updated geological mapping of NBT by /Berglund 2009/ includes mainly measurements of tectonic foliation and banding, together with a few orientations for fold axes and gneissosity. Tectonic banding is a genetic term that includes all forms of deformational banding, whereas gneissosity is descriptive and defined as bands of felsic minerals with granoblastic texture alternating with more mafic, biotite-rich bands. Measurements of mineral stretching lineation are lacking. A structural variability characterise the data set, though it agrees largely with the general picture presented by /Christiansson and Bolvede 1987/, where planar structures are NW-SE trending with steep dips, but tend to dip more gently in the lower levels of NBT, close to the silo (Figure 4-9). Both the metagranodiorite (to granodiorite) and felsic to intermediate metavolcanic rock exhibit predominantly well-developed foliation of moderate or locally strong intensity. Four of the fold axes are gently plunging (< 30°) and three of them plot in the south-western quadrant. To some extent, the scatter may be the result of rheological differences between the heterogeneously distributed rock types in NBT. The vast majority of the registered measurements of ductile structures are for the foliated metagranodiorite (to granite), even in tunnel sections dominated by pegmatitic granite. In the latter case, the metagranodiorite (to granite) forms less competent occurrences or ‘islands’ within the pegmatitic granite.

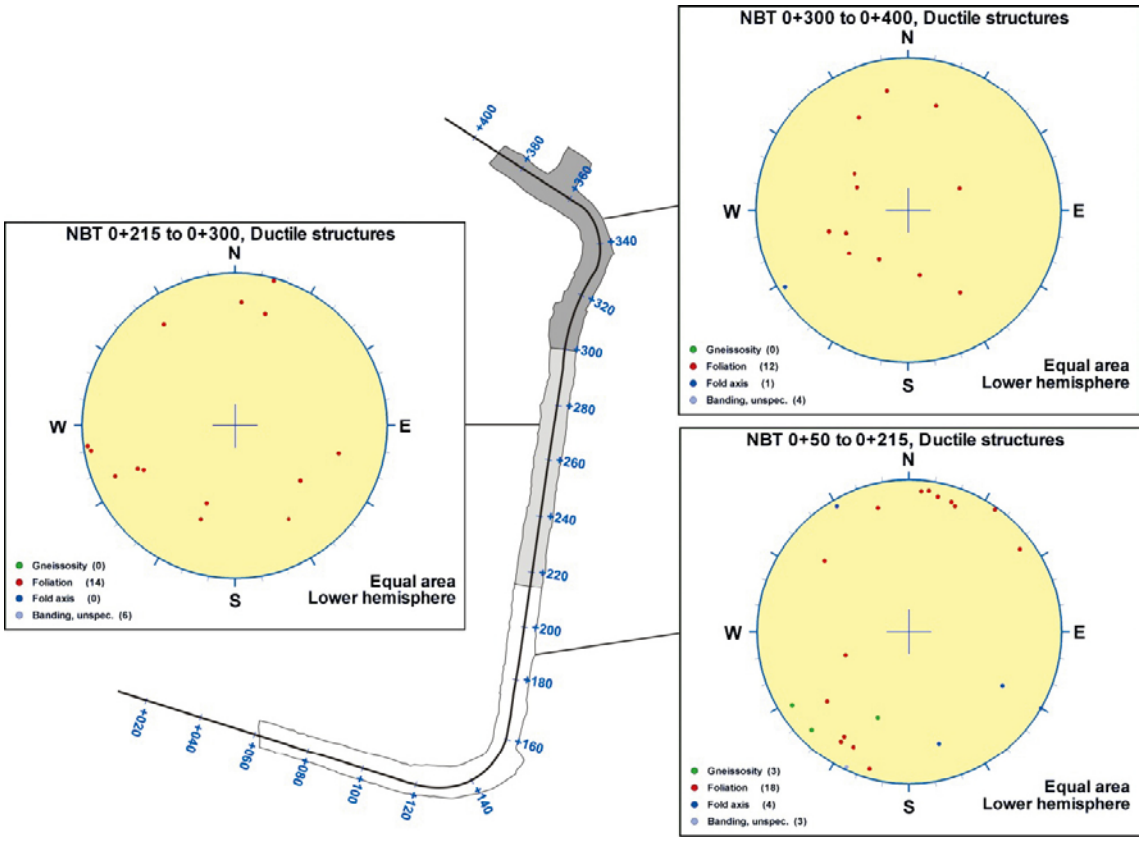

Figure 4-9. *Fold axes and poles to planar structural data from the updated geological mapping of NBT plotted on the lower hemisphere of an equal-area stereographic projection. The data are divided into three separate stereograms to enhance the change in orientation along the tunnel. Note that all but one of the poles to the unspecified banding are hidden behind foliation poles with identical orientations. Moreover, three of the foliation poles are hidden behind gneissosity poles. Data from /Berglund 2009/.*

Cored borehole data

The evaluation of ductile structural data in boreholes is restricted to the cored boreholes from the latest drilling campaign in the SFR area, in order to avoid the low confidence data from percussion boreholes. The ductile structures registered during the geological mapping of the boreholes comprise tectonic foliation and mineral stretching lineation, as well as ductile and brittle-ductile shear zones and mylonite. Figure 4-10 presents the data on a borehole by borehole basis. In a manner similar to the structural data from the updated mapping of NBT, the borehole data show a highly variable orientation in most boreholes, especially in KFR27 and KFR104. However, the general pattern of NBT and all boreholes, as shown in Figure 4-11, is that the tectonic foliation follows the regional trend of the high-strain belt with a WNW–ESE strike and a steep dip, whereas the mineral lineation is variable but mostly moderately plunging towards ESE. A crude, but yet distinguishable girdle pattern, with a best-fit pole of 110°/24°, confirm the existence of regional folding. Local deviations are considerable and thereby the discrepancy between the linear data and the inferred fold axis from the best-fit great circle to the planar ductile structures. This uncertainty in the structural statistics has implications for the use in the modelling work.

It is noteworthy that the most variable structural orientation occurs in KFR27 and KFR104, which have highest contents of pegmatitic granite. This gives further support to the proposed hypothesis, where at least some of the variability is the result of rheological differences between the metagranodiorite (to granite) and pegmatitic granite. Another contributory cause might be the lack of spatial control in the boreholes; the fine-scale folding imparts variability in the planar fabric that normally can be avoided in outcrop measurements, but is very difficult to distinguish in a borehole. Note that data from the uppermost part of KFR27, down to 147.48 m borehole length, which has been mapped without drill core, is included in Figure 4-10.

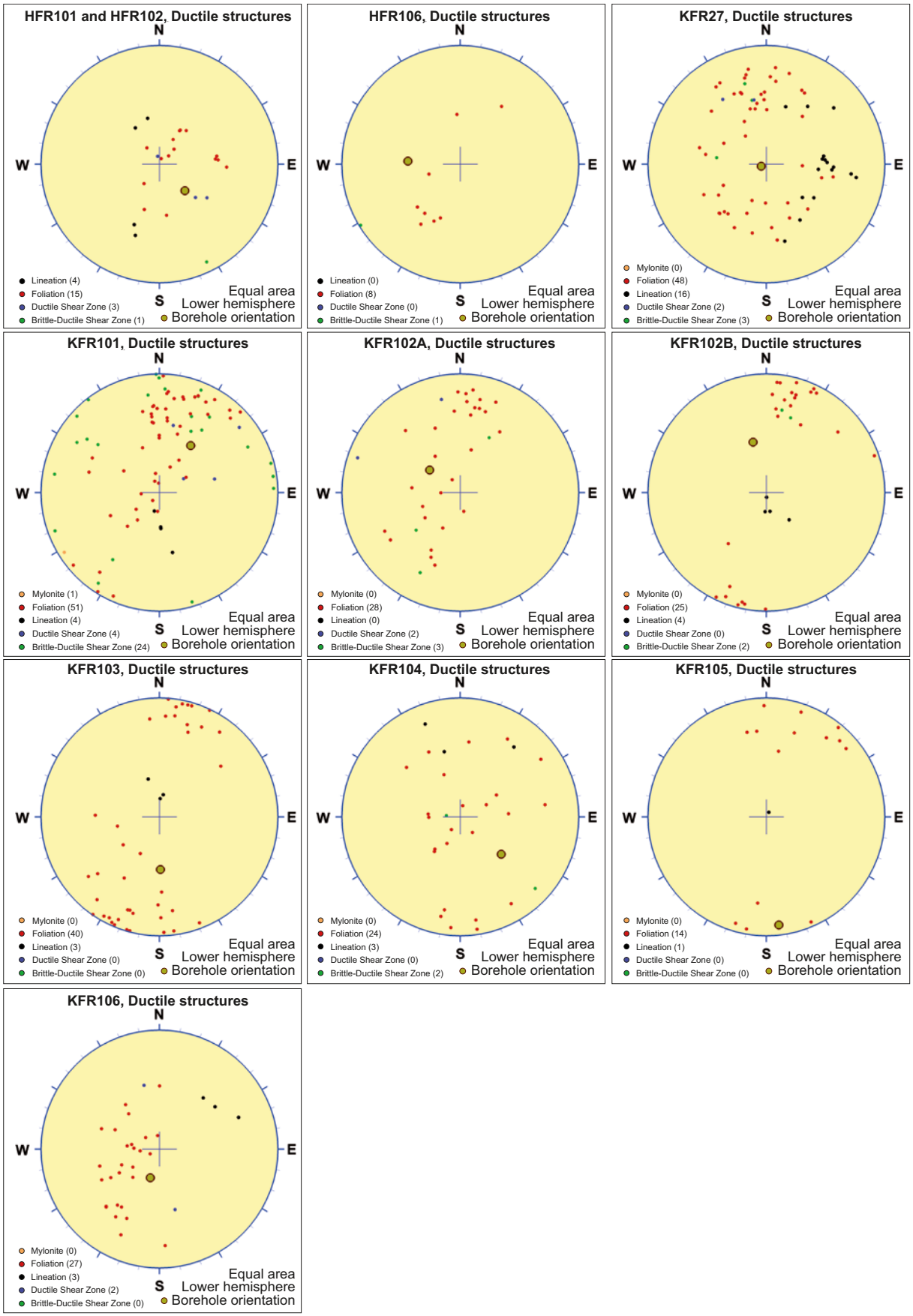

Figure 4-10. *Orientation of ductile structures registered in percussion and cored boreholes from the latest drilling campaign in the SFR area (i.e. HFR101, HFR102, HFR106, KFR27, KFR101, KFR102A, KFR102B, KFR103, KFR104, KFR105 and KFR106). Linear data and poles to planar structures have been plotted on the lower hemisphere of equal-area stereographic projections.*

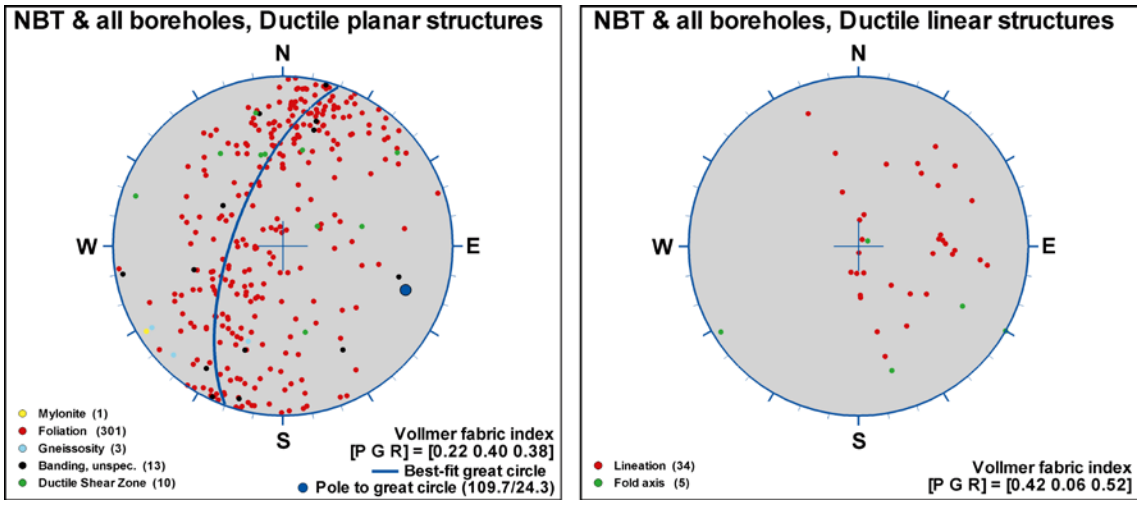

Figure 4-11. *Orientation of ductile structures from the updated geological mapping of NBT and in all cored boreholes from latest drilling campaign in the SFR area (i.e. KFR27, KFR101, KFR102A, KFR102B, KFR103, KFR104, KFR105 and KFR106). Linear data and poles to planar structures have been plotted on the lower hemisphere of equal-area stereographic projections. Note that data from the percussion drilled boreholes are not included in the compilation.*

4.5 Brittle deformation and fracture statistics

Due to the lack of suitable outcrops in the SFR regional model area, no detailed mapping of fractures has been performed at the ground surface. Detailed fracture mapping data is restricted to the new boreholes with BIPS data and to some extent to the NBT.

4.5.1 Fracture orientation from new NBT data

Three different fracture categories, which comprise single, system and en echelon, were used during the updated mapping of NBT. Both the term ‘system’ and ‘en echelon’ were used for groups of sub-parallel fractures, where the distance between individual fractures is less than 3–4 dm. The lower truncation level was approximately 2 m in length and no distinction between ‘open’ and ‘sealed’ fractures was made /Berglund 2009/.

Totally 482 fracture objects (primarily single fractures and fracture systems) were registered along NBT. By dividing the fracture data into five sections along NBT, it is evident that some sets are more intensely developed in certain sections (Figure 4-12). A moderately dipping set with E-W strike is limited to tunnel a chainage less 0+215 and is most intense in the bend at about 0+140. Also a well-defined sub-horizontal set is more or less limited to tunnel a chainage less 0+215. Sub-vertical to steeply dipping fractures with NW-SE or NE-SW strikes, on the other hand, occur throughout the mapped part of NBT.

4.5.2 Fracture orientation from cored borehole data

Orientation data based on BIPS information is only available from the recent Forsmark site investigation and SFR drilling campaigns. For each of the possible deformation zones identified in the single-hole interpretation of boreholes an analysis of the orientation of fractures has been undertaken. Data from the drill core sections that help to define individual modelled deformation zones, so-called target intercepts (see Chapter 5), are presented in the zone descriptions and property tables in Appendix 11. Fractures that are not visible in BIPS have been excluded from the analysis. Orientation data for open and partly open fractures are distinguished from data for sealed fractures. This analysis forms one of the components that has been used in the deterministic modelling of deformation zones (see Chapter 5). In addition to the interpreted individual deformation zone/borehole intercepts, summary plots have also been collated for each modelled deformation zone and for each deformation zone orientation group. Data concerning fracture orientation, more generally inside and outside of deformation zones within the SFR regional model volume, are presented below.

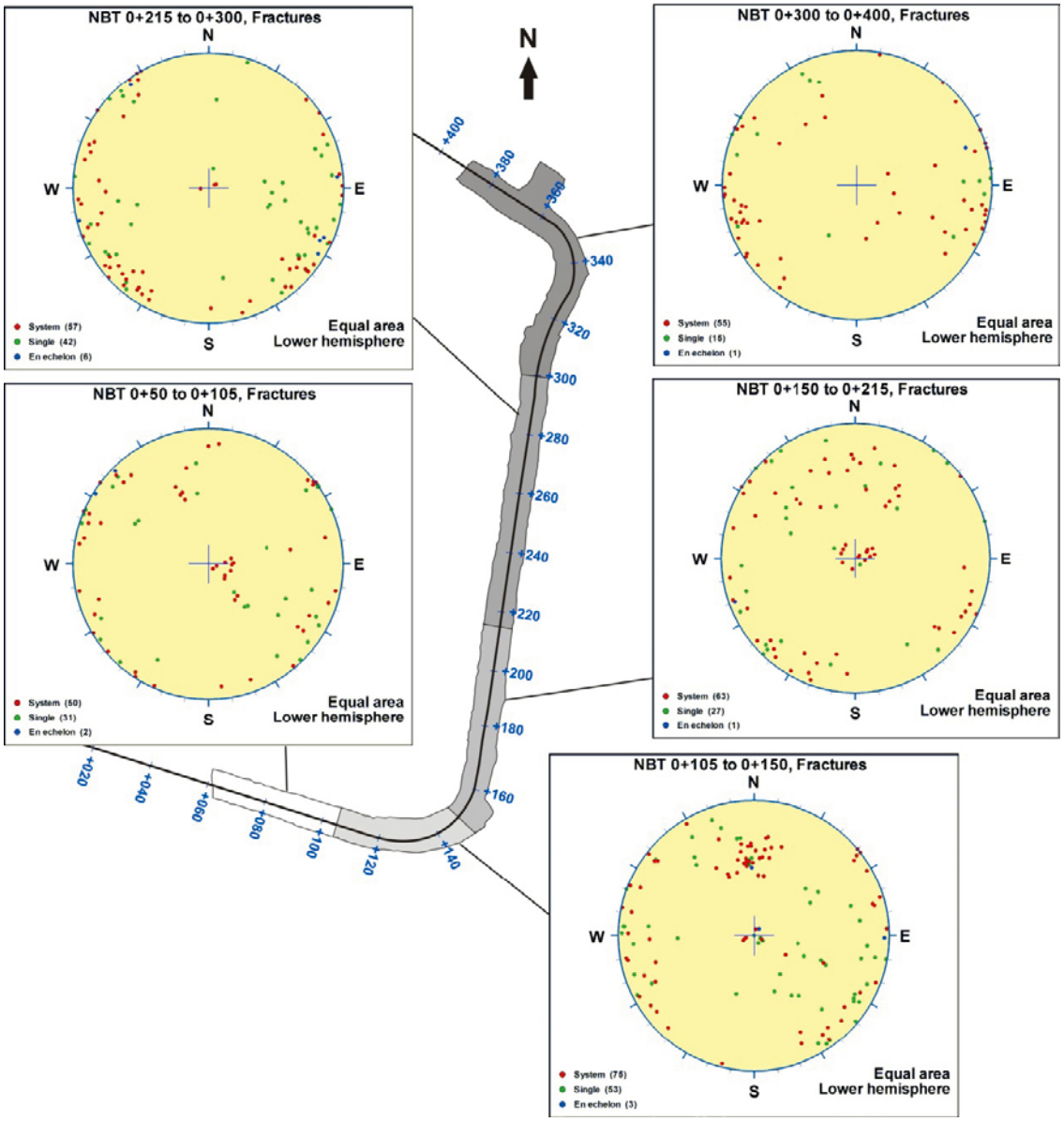

Figure 4-12. *Fractures data from the updated geological mapping of NBT plotted on the lower hemisphere of an equal-area stereographic projection. The data are divided into five separate stereograms to enhance changes in the orientation patterns along the tunnel. Data from /Berglund 2009/.*

There is a clear difference in intensity of the orientation patterns between open and sealed fractures (Figure 4-13). Taking the rock mass as a whole (A1–A4 in Figure 4-13), the horizontal orientation group dominates the open fractures, while sealed fractures are predominantly sub-vertical to steeply dipping and strike WNW-ESE to NW-SE or NE-SW. If the rock mass lying within the modelled deformation zones is considered in isolation (B1–B3 in Figure 4-13), it is the steep WNW-ESE to NW-SE set that dominates the open fractures. For sealed fractures, a comparison of the pattern for the rock mass as a whole with that inside and outside of the modelled deformation zones is more stable and shows no great contrasts (C1–C4 in Figure 4-13). The sealed fractures are predominantly steep and strike NW-SE but there is also a clear steep NE-SW set, along with a weaker sub-horizontal set. There is also a subordinate, moderately dipping set with an E-W strike that is seen most clearly outside the deformation zones (note especially C2 in Figure 4-13).

There are several possible combined explanations for the observations above, relating to different mechanisms for the generation of fracturing in the bedrock, the timing of fracturing and the current anisotropic stress regime (see /Stephens et al. 2007/). Some of the shallower, open, horizontal fractures possibly formed in connection with unloading, for example during a deglaciation, and general stress release. However, it has been inferred that the different sets of fractures, in particular the different steeply and gently dipping fracture sets, are genetically related and formed closely in time during

geologically ancient tectonic events /Stephens et al. 2007/. Thus, many open fractures could have formed in connection with these ancient tectonic events but these planes of weakness have been exploited and closed or opened during one or more later loading and unloading cycles or by jostling of the intervening rock blocks during strike-slip movements along the bounding steeply dipping zones. The current stress regime ($\sigma_1 = \sigma_H$ at a bearing of 145°, and $\sigma_3 = \sigma_v$ /SKB 2008b/) would tend to open horizontal fractures at shallow depths, maintain the openness of steep fractures with WNW-ESE to NW-SE strike and close steep fractures with NE-SW strike.

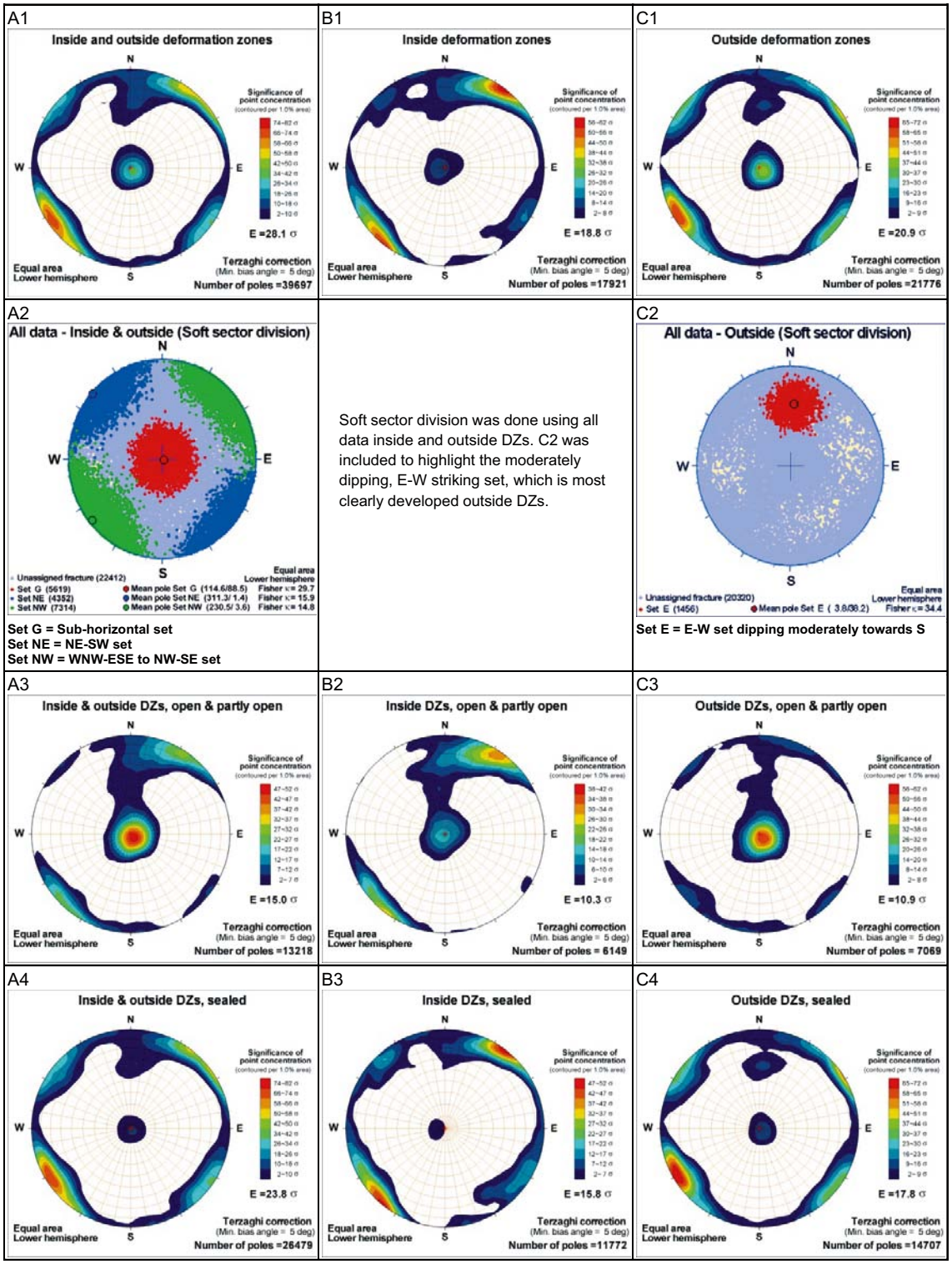

Figure 4-13. *Fracture orientation clustering based on data from KFM11A and the cored boreholes in the current SFR drilling campaign (i.e. KFR27, KFR101, KFR102A, KFR102B, KFR103, KFR104, KFR105 and KFR106): A1–A4 all fractures; B1–B3 fractures within deformation zone target intercepts; C1–C4 fractures outside deformation zone target intercepts.*

4.5.3 Fracture frequency from cored borehole data

Moving average plots of fracture frequencies, identical to those used in the SHI procedure, are presented in Figures 4-14 and 4-15. The data come from cored boreholes in the current SFR drilling campaign along with KFM11A. Terzaghi weighted fracture frequency plots have been produced for each of the deformation zone target intercepts identified in the boreholes. Open fractures, sealed fractures, sealed networks and crush are treated separately and in combination. Details of how the frequencies of the different types of fractures are calculated along with the actual plots are included in the property tables for deformation zones (see Chapter 5). Summary fracture frequencies per meter of mapped drill core are also presented in Chapter 5.

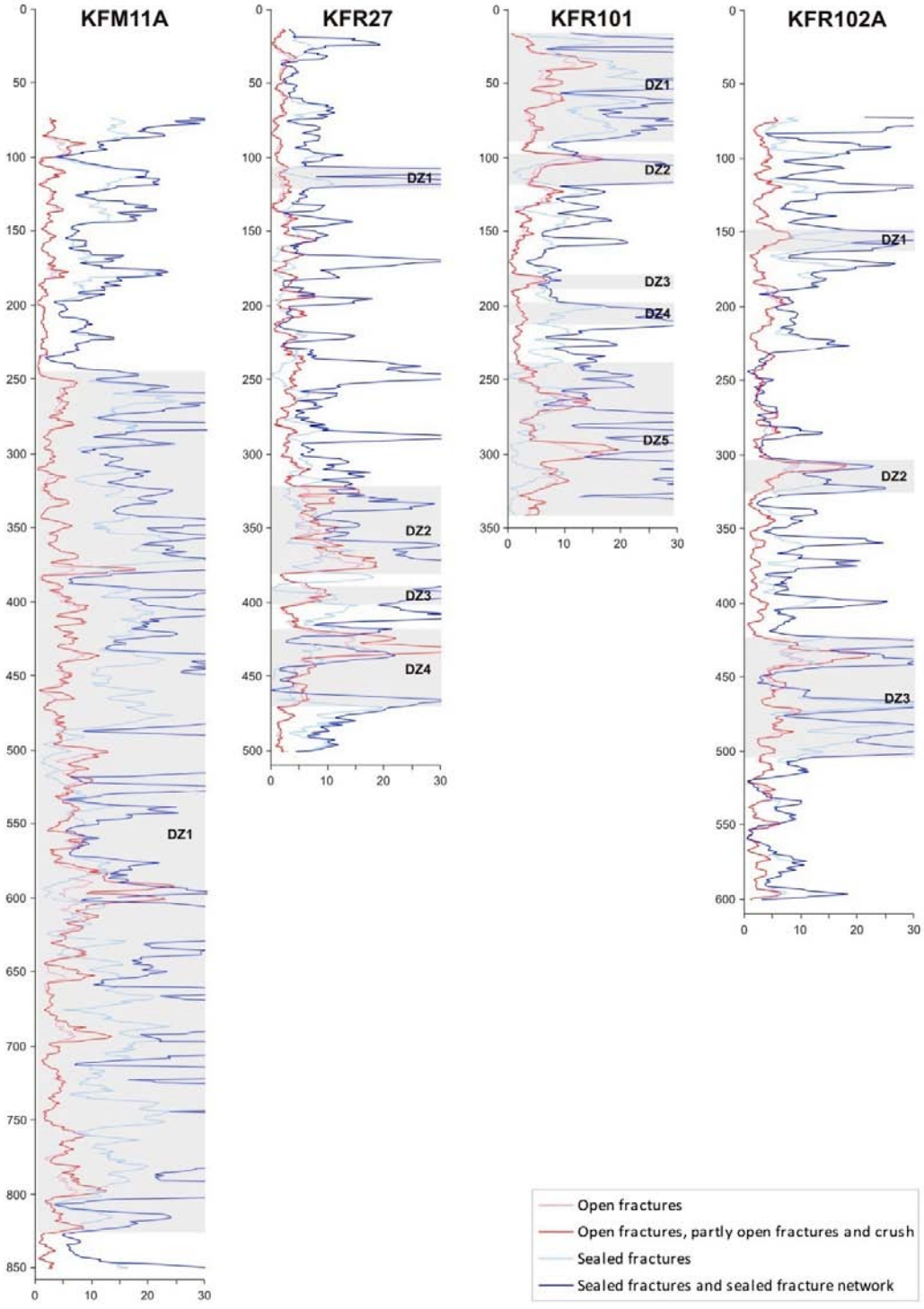

Figure 4-14. *Borehole length (m) versus fracture frequency (fractures per m) plots for KFM11A, KFR27, KFR101 and KFR102A, showing possible deformation zones (DZ) defined during geological SHI. Moving average with a 5 m window and 1 m step length.*

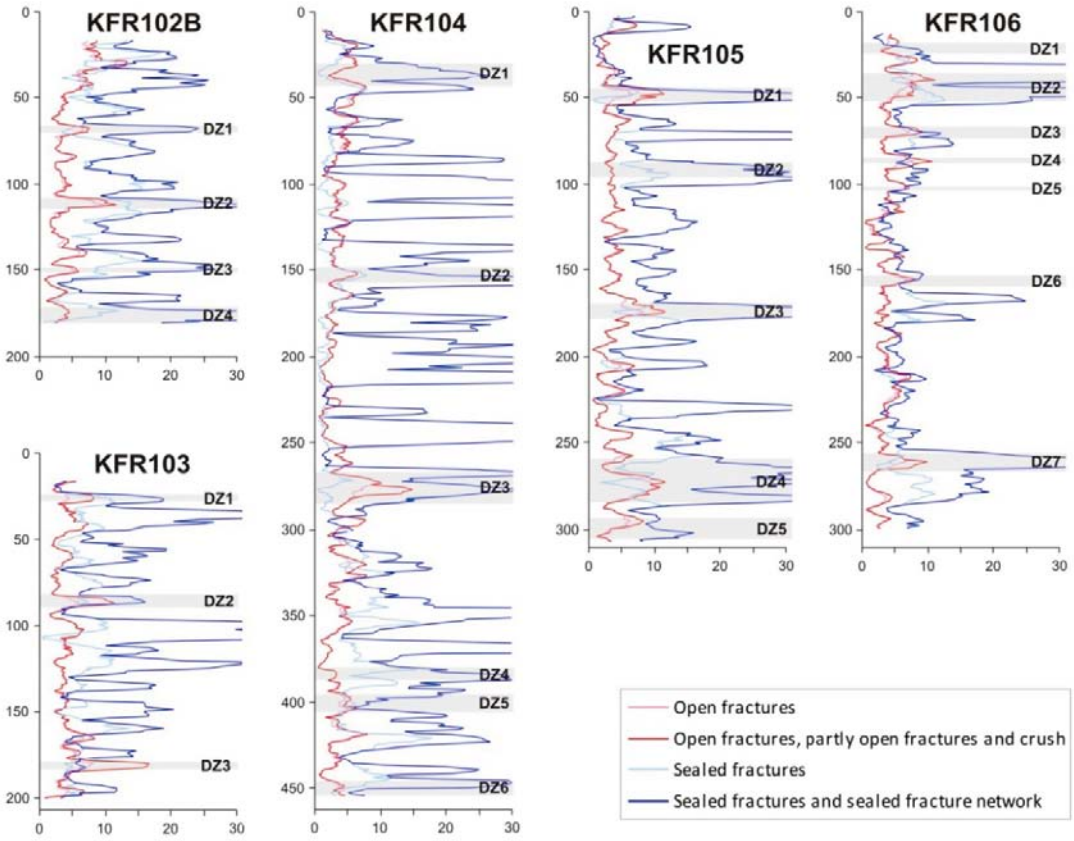

Figure 4-15. *Borehole length (m) versus fracture frequency (fractures per m) plots for KFR102B, KFR103, KFR104, KFR105 and KFR106, showing possible deformation zones (DZ) defined during geological SHI. Moving average with a 5 m window and 1 m step length.*

A plot of RQD (Rock Quality Designation) for each borehole target intercept is included in the property tables for deformation zones as an extremely simplistic indicator of rock quality within the zone. It is hoped that this familiar parameter will assist in the assessment of the significance of the other fracture frequency descriptors, especially those for sealed fractures and sealed fracture networks.

Vertical trends in the intensity of open fractures in the rock mass lying outside the deformation zones recognised in the single hole interpretations have been analyzed in detail by /Öhman and Follin 2010/. The results indicate that the intensity of gently dipping and steeply to vertically dipping fractures in the shallower rock (c. < 200 m) is equally strong regardless of elevation. However, there is a decrease in the frequency of open transmissive fractures with increasing depth.

4.5.4 Fracture mineralogy from cored borehole data

Detailed studies of fracture mineralogy, involving the identification of different families of minerals, i.e. mineral parageneses, and the establishment of the relative age relationship between them, were performed in connection with the Forsmark site investigation /Sandström et al. 2008, 2009/. The basic findings are expected to be applicable to the SFR regional model volume since all the modelled Forsmark fracture domains /Olofsson et al. 2007/, except for domain FFM02 (near-surface realm), have essentially the same fracture mineralogy /Sandström et al. 2008/. In fracture domain FFM02, younger generations of minerals are more conspicuous relative to the other domains, especially along gently dipping to sub-horizontal fractures (SKB 2008b). No detailed fracture mineralogy studies have been performed as part of the SFR extension project. However, simplistic distributions and frequencies are provided in this section as well as in Chapter 5 and in the property tables to the deformation zones. A short summary of the main sequence of fracture mineralisation and other data, based on /Sandström et al. 2008, 2009/, is outlined below.

Four generations of fracture mineralisation have been distinguished and are presented below with decreasing age:

Generation 1 consists of epidote, quartz and chlorite; brittle-ductile cataclasite is sealed with these minerals (T > 200°C). They are conspicuous in sub-horizontal and gently dipping fractures or in steep fractures that strike WNW-ESE to NW-SE. However, they are also present along fractures in other steeply dipping sets. Generation 1 formed between 1.8 and 1.1 Ga and is possibly related to the late Svecokarelian and/or Gothian tectonothermal events.

Generation 2 consists of a sequence of hydrothermal fracture minerals (T ~ 150–280°C) dominated by adularia, albite, prehnite, laumontite, calcite, chlorite and hematite. Generation 2 minerals are particularly common along steep fractures that strike ENE-WSW to NNE-SSW and NNW-SSE. $^{40}Ar/^{39}Ar$ ages from adularia indicate that this mineral probably formed, or the isotope system was reset, in connection with early Sveconorwegian tectonothermal activity at 1.1 to 1.0 Ga. Both reactivation of older fractures and formation of new fractures and breccias are inferred during this period.

A red-staining (oxidation) of the wall rock due to hydrothermal alteration, involving almost complete saussuritisation of plagioclase accompanied by total chloritisation of biotite, is associated with the fractures coated or filled with generation 1 and 2 minerals. Magnetite has been partly replaced by hematite whereas quartz and K-feldspar were relatively unaffected during the hydrothermal alteration. Dissolution of fracture minerals occurred before the formation of generation 3 minerals.

Generation 3 consists of minerals precipitated under low to moderate temperature conditions (60–190°C). Precipitation occurred at several events intermittently during the Palaeozoic. The most abundant minerals are calcite, quartz, pyrite, corrensite (clay) and asphaltite. The orientation of fractures characterised by generation 3 minerals suggests reactivation of older fractures (with generation 1 and 2 minerals). However, formation of new fractures is also indicated by the presence of generation 3 minerals in fractures without the wall rock alteration (red-staining) associated with generation 1 and 2 minerals.

Generation 4 is dominated by chlorite/clay minerals and thin precipitates of calcite in predominantly hydraulically conductive fractures and fracture zones. These minerals are prominent along sub-horizontal and gently dipping fractures, but also in different sets of steeply dipping fractures. It is important to keep in mind that the differentiation of generation 3 and generation 4 minerals can be difficult since many fractures carry minerals from both generations. It is inferred that the hydraulically conductive fractures are ancient structures (Proterozoic to Palaeozoic) and that precipitation of generation 4 minerals most likely occurred during a long period of time (after the Palaeozoic). However, some of the near-surface, sub-horizontal to gently dipping fractures, which include sheet joints formed in connection with stress release, may be Quaternary in age.

Ocular inspection has shown that 2.6% of all of the logged fractures in KFM11A, KFR101, KFR102A, KFR102B, KFR103, KFR104, KFR105 and KFR106 lack mineral filling and wall rock alteration. Detailed micro-analysis, including SEM-EDS work, on similar non-mineralised fractures from the Forsmark lens has revealed that most such fractures actually are mineral coated /Claesson Liljedahl et al. 2011/. Nevertheless, it was further confirmed that a very small number of the studied fractures were non-mineralised. The most likely explanations for this are reactivation of existing fractures due to denudation/glacial rebound, i.e. release of stress during unloading after loading by ice and glacial material, and/or patchy mineral coating in fractures with channelled flow /Claesson Liljedahl et al. 2011/.

Relationship between fracture orientation and mineral infillings

The plots in this section show the orientation of fractures containing specific mineral infillings, regardless of the fracture relationship with deformation zones and rock domains. Open, partly open and sealed fractures are differentiated in the pole plots while the clustering is indicated by the paired kamb plots. While individual minerals belong to more than one generation group, the following comments can be made based on an inspection of the various orientation sets.

Generation 1 mineral infilled fractures are generally sealed and are commonly steeply dipping with a WNW-ESE to NW-SE strike and, more rarely, gently dipping (Figure 4-16). In addition to the generation 1 orientations, steeply dipping fractures with NE-SW and subordinate NNE-SSW and ENE-WSW strike are more prominent in the fractures that are coated or filled by generation 2 minerals (Figure 4-17). There is also a subordinate E-W trending set that has moderate dips to the south. The sample size is smaller and the clustering weaker for the generation 3 minerals (Figure 4-18).

It should also be noted that different clay minerals are not distinguished during the drill core mapping. It is also likely that at least some clay is lost during the drilling and core recovery process so the amount of clay recorded should be considered a minimum.

The relationship between the orientation sets of the modelled deformation zones and the mineral infilling of the fractures lying within them is presented in Chapter 5. The clearest contrast in the distribution of mineral types is between the steeply dipping deformation zones of all orientations and the gently dipping deformation zones. The gently dipping zones are dominated by the generation 3 and 4 minerals chlorite, calcite and clay. The fractures can be inferred to be generally open or partly open. This is also in agreement with both the more general fracture orientation data and the hydrogeological testing results /Öhman and Follin 2010/.

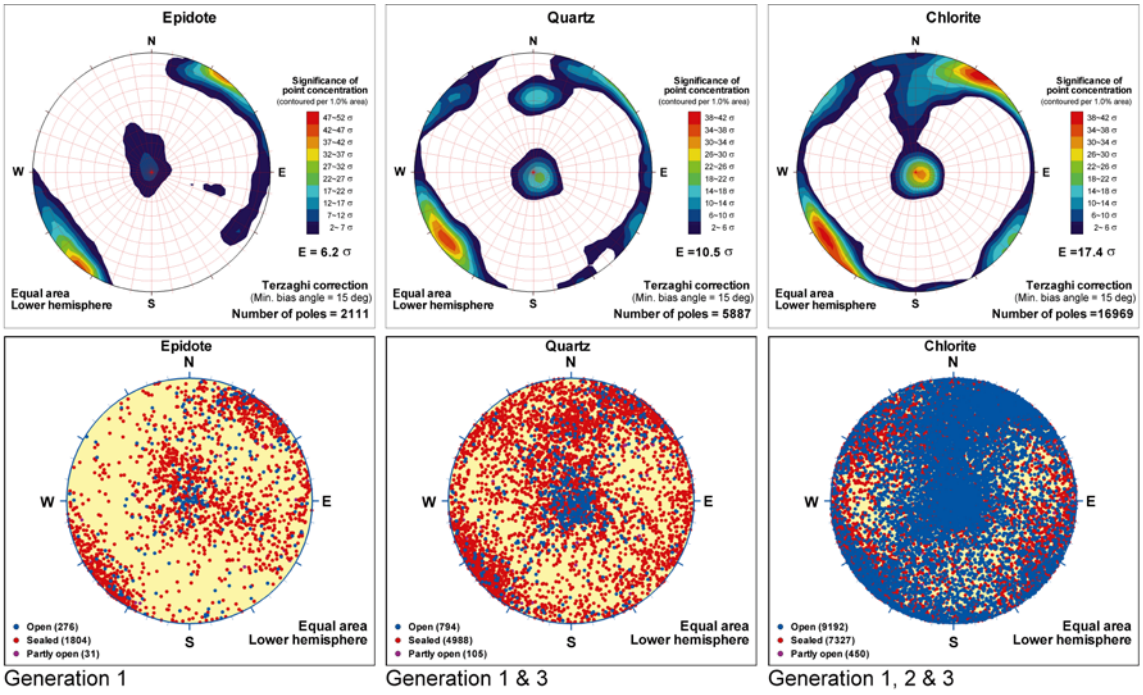

Figure 4-16. *Stereographic projections of generation 1 minerals, including epidote, quartz and chlorite. Data from KFM11A and the cored boreholes in the current SFR drilling campaign (i.e. KFR27, KFR101, KFR102A, KFR102B, KFR103, KFR104, KFR105 and KFR106). All plots utilize a lower-hemisphere, equal-area projection, with a Terzaghi correction of the kamb-plots.*

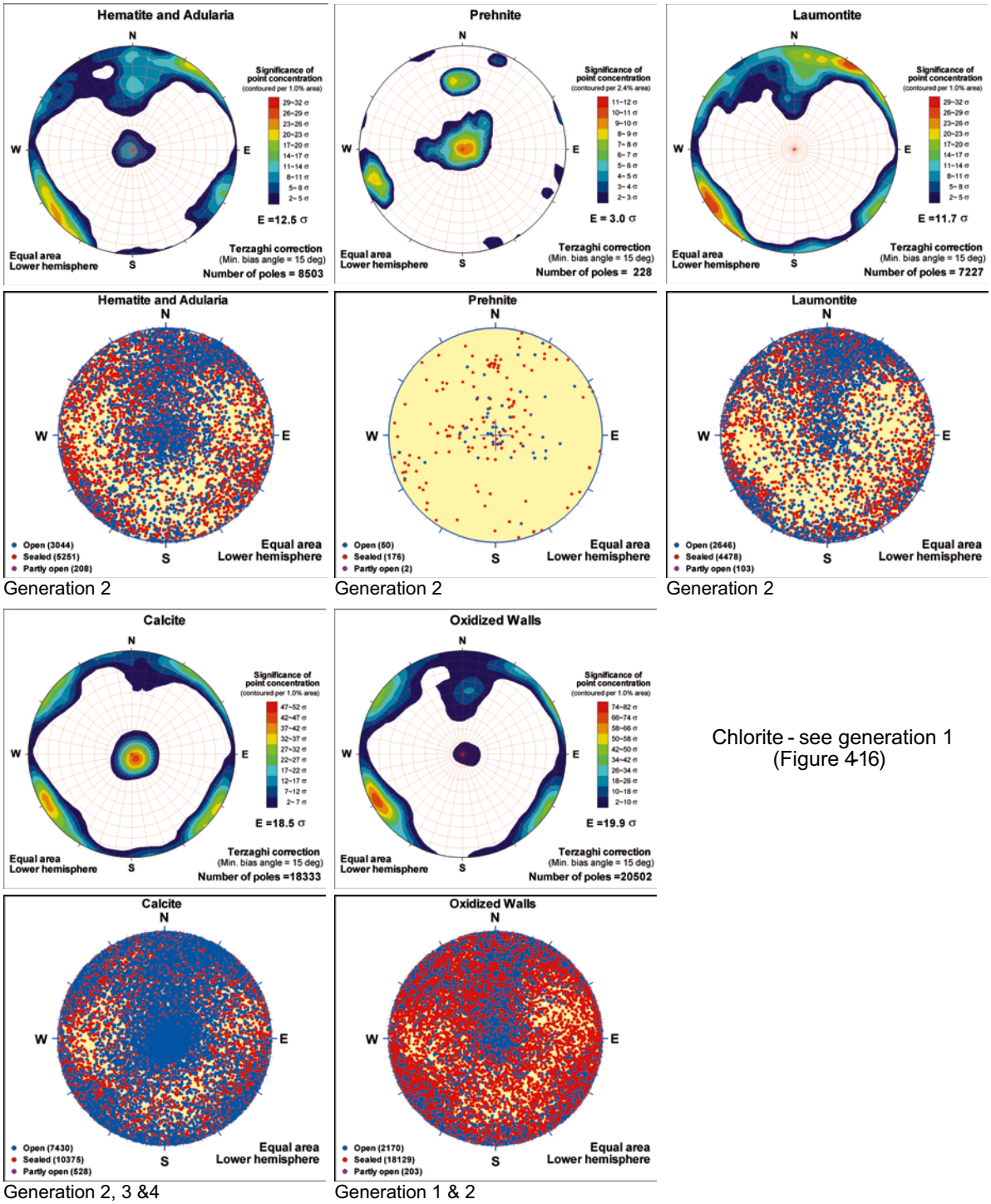

Generation 2

Generation 2

Generation 2

Chlorite - see generation 1 (Figure 4-16)

Generation 2, 3 &4

Generation 1 & 2

Figure 4-17. *Stereographic projections of generation 2 minerals, including adularia, hematite, prehnite, laumontite, calcite, chlorite and oxidized walls. Data from KFM11A and the cored boreholes in the current SFR drilling campaign (i.e. KFR27, KFR101, KFR102A, KFR102B, KFR103, KFR104, KFR105 and KFR106). All plots utilize a lower-hemisphere, equal-area projection, with a Terzaghi correction of the kamb-plots.*

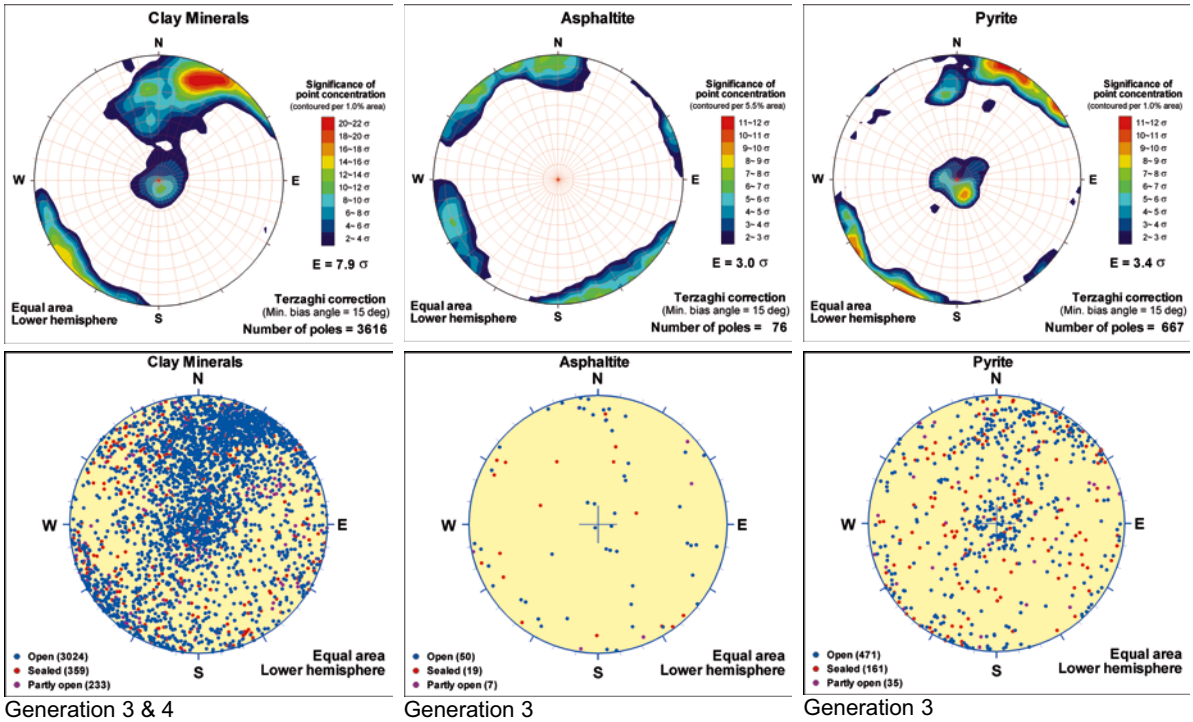

Figure 4-18. *Stereographic projections of generation 3 and generation 4 minerals, including clay minerals, asphaltite and pyrite. For calcite, quartz and chlorite, see generations 1 and 2 (Figure 4-16 and Figure 4-17). Data from KFM11A and the cored boreholes in the current SFR drilling campaign (i.e. KFR27, KFR101, KFR102A, KFR102B, KFR103, KFR104, KFR105 and KFR106). All plots utilize a lower-hemisphere, equal-area projection, with a Terzaghi correction of the kamb-plots.*

4.6 Surface geophysics

4.6.1 Lineaments defined by magnetic minima

Background

The identification of lineaments from different sources of data /Isaksson 2003, Isaksson et al. 2004c, 2006a, b, 2007, Isaksson and Keisu 2005/ has provided an important input for the modelling of steeply dipping deformation zones /SKB 2005, Stephens et al. 2007, 2008b/. However, following the completion of the initial site investigation phase (model version 1.2), uncertainties were recognised in the interpretation of the geological significance of topographic lineaments /SKB 2006/. For this reason, attention was focused on the modelling of steeply dipping deformation zones using lineaments defined by magnetic minima. The detailed surveys of the magnetic total field on land and at sea provided information of very high resolution during the subsequent complete site investigation phase (model stages 2.1, 2.2 and 2.3). This strategic decision to focus on features in the maps of the magnetic field was supported by observations of wall rock alteration associated with zone intersections in boreholes, as well as on the results of excavation work at the site.

As the SFR facility forms part of the Forsmark area, and as the geological setting is comparable, the fundamental conclusions from the preceding site investigation have been implemented in the development work during the SFR model versions 0.1 and 1.0. Hence the primary focus for the modelling of steeply dipping deformation zones is again on the data of the magnetic total field and the identification of lineaments defined by magnetic minima.

However, even though there is nearness in distance and similarity in the general geological setting, there are also differences between the SFR and Forsmark sites. The high frequency content in the magnetic anomalies is obvious when studying the maps of the magnetic field inside the Forsmark lens. This pattern, rich in details, implies an inherent high resolution in all features deduced from the susceptibility variations in the bedrock. The thin moraine layer on the bedrock gives a short distance from the

magnetometer to the anomaly sources. The geology, with an apparently high contrast in the magnetic susceptibility between the low and high susceptibility rock volumes, gives a strong magnetic relief. Civil installations are sparse inside the lens and unwanted disturbances in the magnetic field are uncommon.

Moving out to the SFR area radically changes the situation. The pier and installations on ground and in the bedrock cause distortions visible in the magnetic field mostly as scattered dot-like anomalies. A major part of the SFR model areas are covered by the sea; first there is the water depth, then there are sediments and moraine deposited on the bedrock. Consequently the distance from the sensor in the magnetometer to the sources in the bedrock has increased considerably compared with the measured area inside the lens. This results in a damping of the high frequency content in the anomalies and hence, lowers the spatial resolution. Furthermore, rock volumes of low magnetic character in the SFR model areas are considered not to be related to deformation zones alone, but also to lithological signatures and the nearness to the regionally significant Singö deformation zone (ZFMWNW0001) also plays an important role. All this implies that the possibilities to use the magnetic total field to predict structural and lithological elements in the bedrock inside the lens and in the SFR area are different. In the SFR area, less geometrical detail is possible to achieve compared with the area inside the lens. Hence, difficulties arise in the identification of narrow oxidation zones.

The demand on detail is higher in the current work with the SFR model volumes compared with the site investigation at Forsmark. In the process of mastering the complex balance between the demands on information for detail on the one hand, and the site specific potential to reveal such detail on the other, the two-step working process including a version 0.1 preceding the final version 1.0 has been beneficial. This has allowed a matured interplay between the different data sources which has promoted an increased level of prognosis in the modelling.

The latest interpretation of lineaments from the Forsmark site investigation, stage 2.3, was reported in /Isaksson et al. 2007/. This interpretation was presented after the use of lineaments in the final geological models for Forsmark in the stage 2.2 work /Stephens et al. 2007/. However, the implications of the new lineament interpretation for the geological models were addressed in model stage 2.3 /Stephens et al. 2008b/ and in the final descriptive model for the site /SKB 2008b/. In the current geological modelling of the SFR regional and local model volumes, a revision of stage 2.3 lineaments from the Forsmark site investigation has been carried out. The current revision was required due to the different scale and area of focus of the SFR project compared with the Forsmark site investigation project. The revision (see section ‘Revision of lineaments’ and Appendix 5) has resulted in changes to some of the lineaments that were recognised during the earlier work, as well as the addition of entirely new lineaments. Furthermore, many of the magnetic anomalies connected to the lineaments have been modelled using the programme package EncomModelVision Pro version 8.0 (see section ‘Modelling of low magnetic anomalies connected to lineaments’ and Appendix 6). The lineaments of model version 1.0 have been delivered to Sicada (field note number SFR127) and are stored in SDE GIS database (ID number SDEADM.GV_FR_GEO_7864).

Revision of lineaments

While the local model in the Forsmark site investigation has addressed a relatively large area of approximately 12 km^2, the regional model area for SFR model version 1.0 is much smaller (approximately 2.6 km^2). In spite of this difference, the lineaments from the Forsmark site investigation form the natural framework for any revision of SFR regional model area lineaments. The identification of lineaments during the site investigation focused on detailing the area south and south-west of the Singö deformation zone (ZFMWNW0001) inside the local model area, while to the north and north-east of the zone, outside the local model area, only lineaments with trace lengths longer than 3,000 m were included in the final, stage 2.2 geological model /Stephens et al. 2007/. Shorter lineaments in the area around SFR, identified with the help of the ground high-resolution magnetic data, were only identified during stage 2.3 of the investigation /Isaksson et al. 2007/ and evaluated in /Stephens et al. 2008b/.

The modelling of the bedrock surrounding the SFR facility has focused on evaluating the lineaments from the site investigation, at a scale and in an area adapted to the needs for SFR model version 1.0. This change of focus implies that the revision of lineaments is carried out at a more detailed scale in comparison with earlier work. It should be noted that the local and regional model areas of SFR host the FennoSkan HVDC-cable, piers, roads and the underground facility with its stored waste,

all of which cause disturbances in the magnetic field (Figure 4-19). The revision has taken the most severe of these disturbances into account which has resulted in the rejection of a few of the earlier interpreted lineaments in /Isaksson et al. 2007/ that impinge on these disturbed areas.

An explicit aim of the revision work has been to maintain consistency across the boundary between the areas within and outside the SFR regional model area. Hence, lineaments from the Forsmark site investigation entering the SFR regional model area have generally been maintained without any changes outside the SFR regional model area, while inside the SFR regional model area, changes in length, path or locality are allowed; some parts of lineaments may also have been deleted. This conservative approach at the margin is aimed at simplifying future studies on the interaction between both model sets. However, in a few cases, detailed interpretation of data showed the need to slightly adjust former lineaments that were situated directly outside the SFR regional model area.

Based on this approach, the main focus has been to revise lineaments in the magnetic data from the detailed ground survey. To a limited degree, low velocity zones from the refraction seismic profiles and depressions in the bedrock surface have also provided an input to the revision process. The revision activity started in the work with version 0.1 (stored in SDE GIS database with ID SDEADM. GV_FR_GEO_7301) and has now matured to version 1.0 after further evaluation of the available data sources. The lineament map of version 1.0 contains 127 lineaments based on the interpretation of the magnetic total field. The lineaments are found entirely or partly within the SFR regional area and, consequently, even the local model areas (Figure 4-20). The lengths of the lineaments vary between around 50 m to around 11,400 m. The minimum length of around 50 m should be considered as an adaption to the inherent limitations in the data set to resolve shorter linear trends in the actual environment at the site.

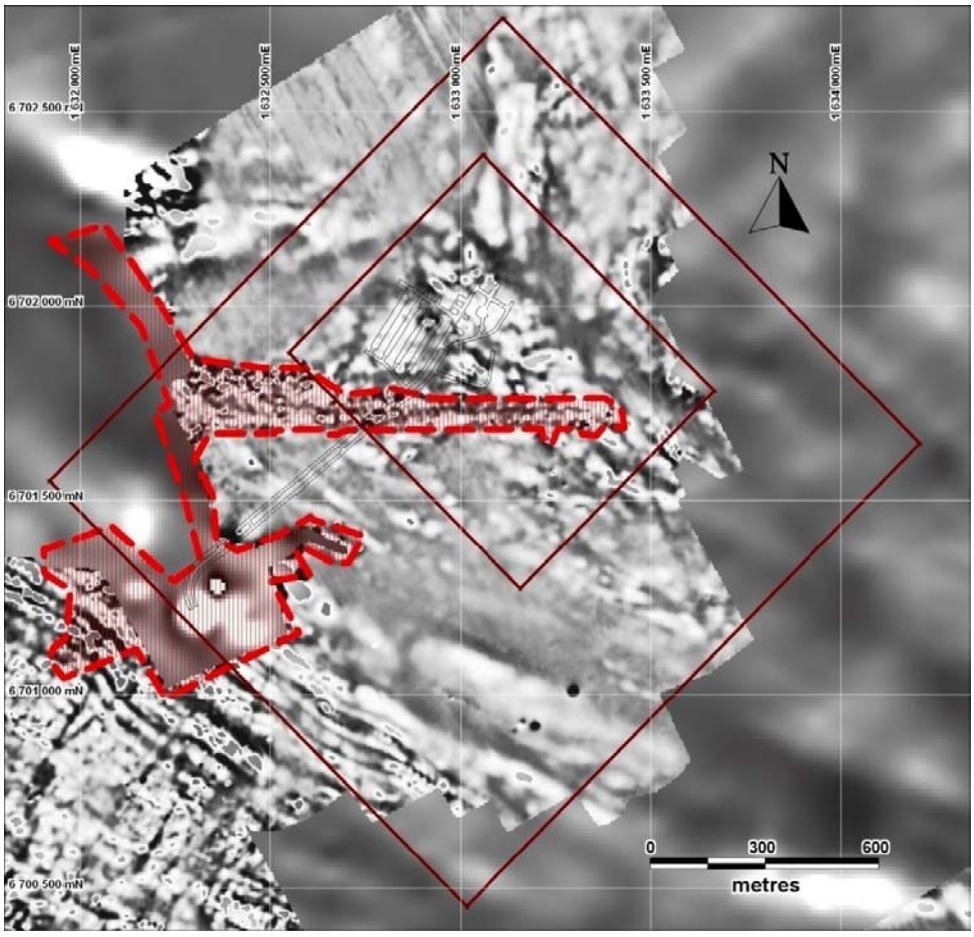

Figure 4-19. *The SFR model areas (regional and local) shown in brown on a map of the first vertical derivative of the magnetic total field from measurements on land, at sea and via helicopter (for details see Section 3.5). Area containing partly severe disturbances on the magnetic total field caused by civil installations is shown in dashed red. Underground constructions are also marked.*

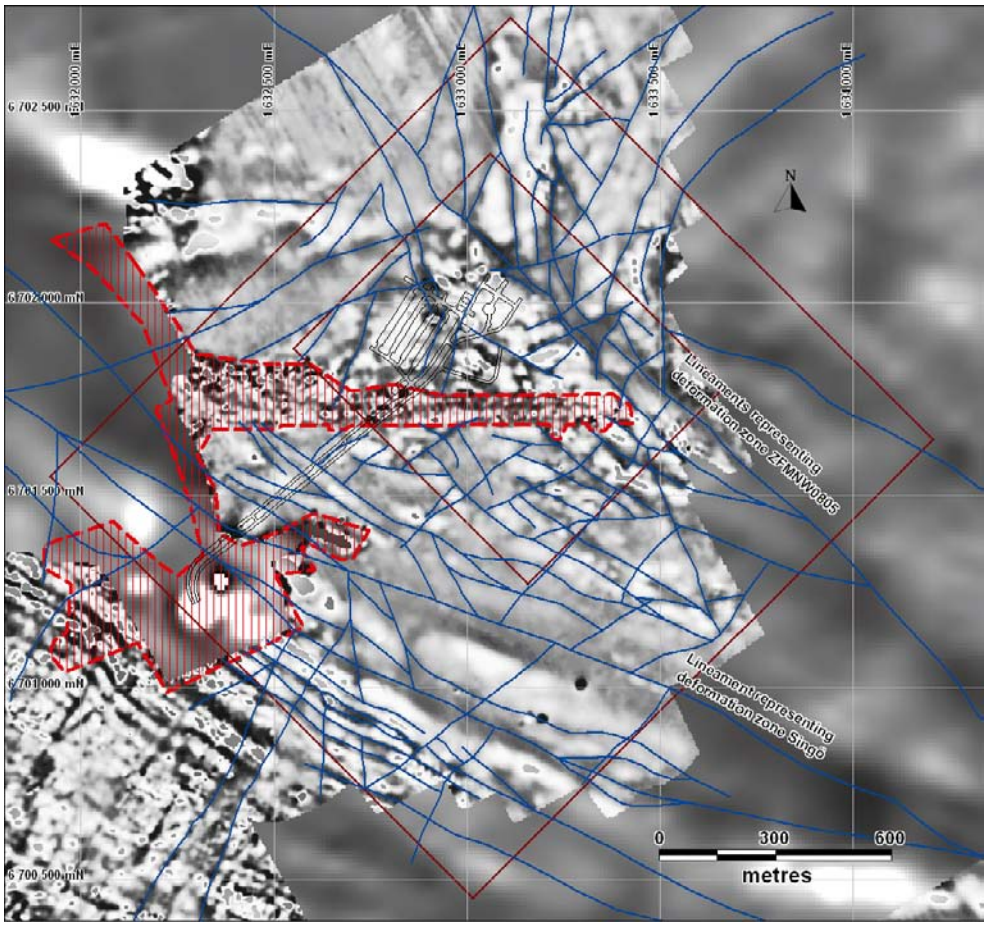

Figure 4-20. *Map of the first vertical derivative of the magnetic total field from measurements on land, at sea, and from helicopter, showing the 127 lineaments that have been identified (blue lines). Only lineaments that are partly or entirely within the SFR regional and local model areas (brown lines) are shown. Prominent low magnetic features in the southern and north-eastern parts of the SFR regional model area correspond to the Singö deformation zone (ZFMWNW0001) and zone ZFMNW0805 in /Stephens et al. 2007/. Area containing partly severe disturbances on the magnetic total field caused by civil installations is shown in dashed red. Underground constructions are also marked.*

In a similar manner as that used during the Forsmark site investigation, a table of attributes connected to each lineament is presented in Appendix 5. The lineaments in SFR version 1.0 consist of two groups. The first group contains lineaments that have been imported directly from the latest version of lineaments in the Forsmark site investigation, stage 2.3 /Isaksson et al. 2007/, while the second group contains lineaments that have been modified from previously identified lineaments in the Forsmark site investigation, or are entirely new lineaments. The names and attributes in the first group are preserved from the site investigation, while the second group has new names (MSFR0800X or MSFR1000X) and also new attributes.

As mentioned above, some parts of the SFR regional and local model areas show disturbances in the magnetic total field data due to the Fenno-Skan HVDC-cable, piers, roads, the underground facility and its stored waste. In the most severely disturbed areas, the density of lineaments is lower due to the high noise level.

In the southern part of the SFR regional model area, a broad significant low magnetic feature is present (see Figure 4-20) that corresponds to the Singö deformation zone /Stephens et al. 2007/. In the revised lineament interpretation, this zone is represented by a thin line drawn close to the centre of the feature. In the north-eastern part of the SFR local model area, a similarly broad but apparently much more complex low magnetic feature is also present and also corresponds to a deformation zone, ZFMNW0805 /Stephens et al. 2007/. Both these features are examples of deformed domains in the bedrock, i.e. rock volumes that could possibly be better represented by volumes rather than by thin sheets.

Comparison between lineaments from SFR version 1.0 and the Forsmark site investigation (stage 2.3)

The relationship between the lineaments in SFR model version 1.0 and the previous lineaments from the Forsmark site investigation stage 2.3 /Isaksson et al. 2007/ is described in Appendix 5 and shown in Figure 4-21. Some of the lineaments from the Forsmark site investigation have not been included in SFR model version 0.1 or version 1.0. The specific motivation behind each decision is presented in Appendix 5.

The lineaments of version 1.0 have been drawn with good correspondence to the features observed in maps of enhanced versions of the magnetic field. Using the terminology applied in the Forsmark site investigation /Isaksson and Keisu 2005/ only the lineaments that have been directly imported from the Forsmark site investigation stage 2.3 are 'linked'. The rest i.e. the majority of the lineaments of SFR model version 1.0 should be considered as 'method-specific' rather than 'co-ordinated' or 'linked'. In order to avoid unnecessary constraints in the process, the lineaments have been drawn without any geological guidance in the work with SFR model version 1.0. For this reason, they should be considered as relatively immature. The termination of the lineaments is a task for the subsequent geological modelling work where the lineaments have been integrated with geological data and used in the identification of steeply dipping deformation zones.

In the southern part of the regional model area, most of the previous lineaments are also considered valid for the SFR model version 1.0. Only minor differences have been observed.

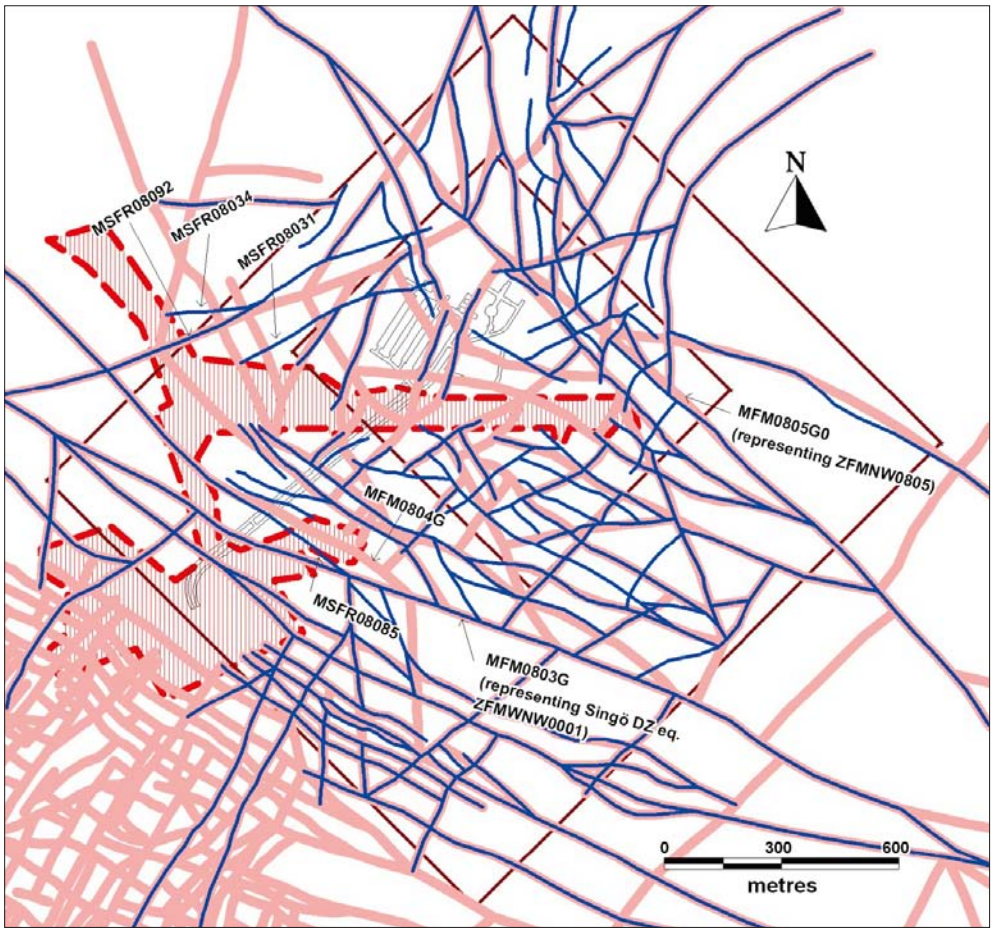

Figure 4-21. *Lineaments from the Forsmark site investigation (pink) compared with the lineaments in connection with SFR version 1.0 (blue). The SFR regional and local model areas are shown in brown. Lineaments that are commented in the text below are labelled. The hatched red area marks disturbances in the magnetic total field from civil installations. Underground constructions are also visible.*

In the central and western parts of the SFR local model area, some of the lineaments from the Forsmark site investigation interpreted during stage 2.3 /Isaksson et al. 2007/ have not been directly inherited into SFR model version 1.0. Instead, their appearance has been modified and, in some cases, they may even have been excluded from the SFR model version 1.0. The main reason for this difference is the disturbance of the magnetic total field caused by civil installations and constructions, which prevent a confident identification of lineaments at the appropriate scale.

One of the prominent low magnetic features found in the SFR model areas is associated with the Singö deformation zone (ZFMWNW0001). During stage 2.3 of the Forsmark site investigation, the identification of lineaments based on dense measurements of the magnetic total field on land and at sea, in the vicinity of the Singö deformation zone, implied changes in some of the former lineaments /Isaksson et al. 2007/. As a consequence, the south-eastern part of lineament MFM0804G replaced lineament MFM1127 /Isaksson et al. 2007/. Furthermore modifications were made with lineament MFM0804, with consideration to the continuation of lineament MFM0804G to the north-west. In SFR model version 1.0, the lineament MFM0804G has been re-evaluated and the south-eastern part of MFM0804G has been redrawn so that it connects to MFM0803G0 at a position about 170 m towards the north-west. The modified version of the former lineament MFM0804G is now called MSFR08085. It is important to keep in mind that the final geological models for Forsmark only had access to the stage 2.2 and earlier interpretations. The implications of the subsequent stage 2.3 lineament interpretation on the Forsmark geological models were evaluated in /Stephens et al. 2008b/. No revised geological models, based on revised lineaments, were produced during stage 2.3.

Lineament MFM0805G0 transects the SFR local model area with a continuous north-westerly trend in the interpretation presented in the Forsmark site investigation /Isaksson et al. 2007/. The detailed revised interpretation of the magnetic data, carried out here, has divided this apparently continuous lineament into a more complex network. A detailed image that demonstrates the complexity introduced here in the lineament version 1.0 is shown in Figure 4-22.

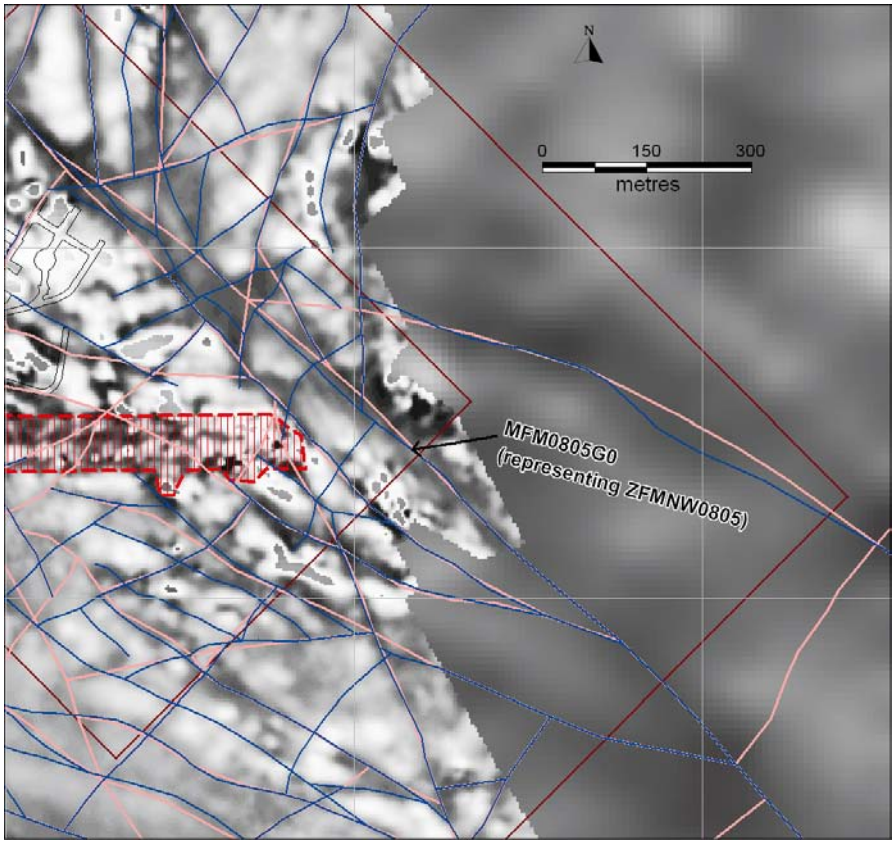

Figure 4-22. *The lineaments from the Forsmark site investigation (pink) compared with the lineaments from SFR model version 1.0 (blue). The SFR regional and local model areas are shown in brown. The lineament MFM0805G0 from the site investigation appears to be fairly continuous in the data if observed in regional scale while the detailed scale shows complexity. The implication is that the possible deformation zone connected with these lineaments probably has a complex geometry, when viewed at a higher degree of resolution.*

Modelling of low magnetic anomalies connected to lineaments

Forward modelling of the magnetic total field data from the detailed ground survey has been performed, in order to estimate the geometries of the sources to the low magnetic anomalies associated with the lineaments, i.e. principally to provide support to judgements on the relative thickness and dip of possible deformation zones connected to the lineaments (Appendix 6). The work is a continuation of the modelling carried out for model version 0.1 /Curtis et al. 2009/. Some of the former results have been re-evaluated and new profiles have been added for modelling.

In total, 44 of the profiles that traverse lineaments were selected for modelling. Forty-one (41) profiles were modelled, while three were abandoned for different reasons. The location of all profiles is shown in Figure 4-23. The profiles are stored in SKBdoc with document ID 1266450–1266491 and 1266493–1266534.

When studying the modelling results, it is important to observe that some of the modelled anomalies are fairly faint. The interplay between a weak anomaly from the source of interest (the possible deformation zone inferred from the lineament) and anomalies caused by 'geological noise', such as an irregular magnetisation in a specific lithological unit, may lead to modelling results with a low level of confidence. Thus, a significant magnetic anomaly in combination with normal variations in the magnetic field over the area can be characterised and modelled with a higher degree of confidence, whereas a small anomaly in the same area introduces a higher degree of uncertainty in the resulting model.

The inversion carried out on the detailed ground magnetic data has provided a model of the 3D distribution of magnetic susceptibility in the bedrock (Section 4.6.5). This 3D model contains geometrical information about the inferred sources to the identified lineaments in the same manner as the source bodies received from the forward modelling. By comparing the results from the 3D inversion with the results from the forward modelling, the interpreter will receive some qualitative information about the level of confidence; this has been completed on most of the forward modelled profiles (Appendix 6).

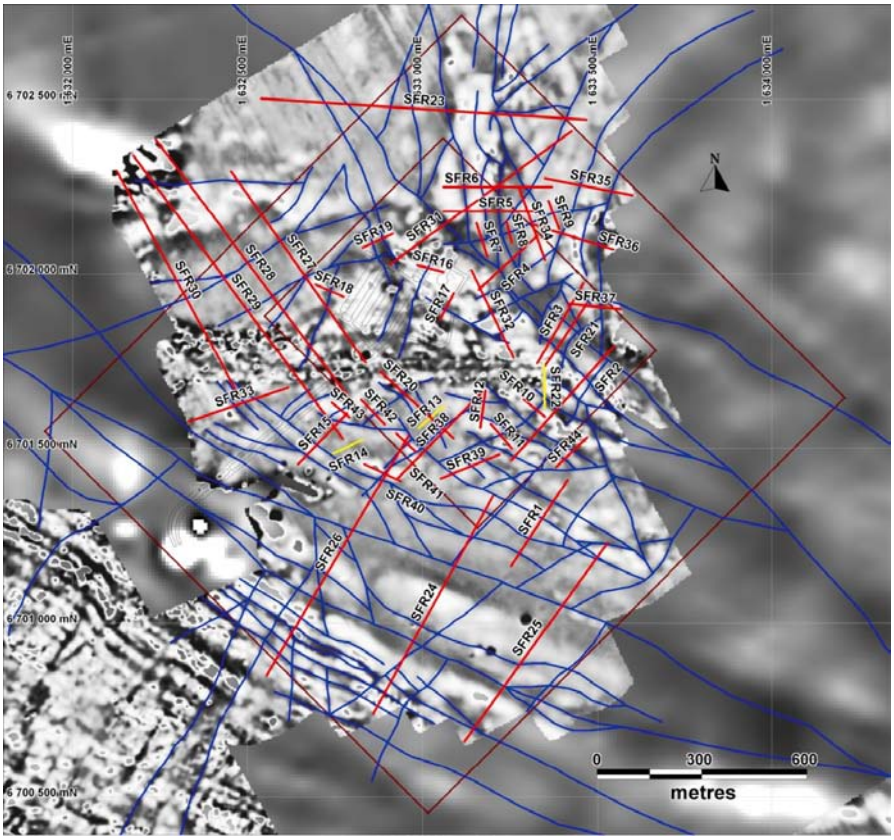

Figure 4-23. *The location of the 41 modelled profiles (red). Profiles omitted from modelling, due to different reasons, are shown in yellow. The lineaments in SFR model version 1.0 are shown in blue. An enhanced version of the magnetic total field image (1st vertical derivative) is shown in the background. Underground constructions are also visible.*

In general, the agreement is good between the results from the two different approaches and, in such cases, the level of confidence should be considered as high in comparison with the few profiles where the results diverge.

The forward modelling of the anomaly complex coinciding with the Singö deformation zone (ZFMWNW0001) was carried out essentially along three profiles (SFR24 to SFR26, see Appendix 6). The results indicate a very low magnetic susceptibility in large volumes of the rock associated with the deformation zone complex. The consequence is that many of the source volumes to the anomalies of interest are buried in these large low susceptibility volumes. Hence, it is difficult to delimit geometries for individual source bodies coupled to specific lineaments. However, the geometry of the whole low susceptibility volume, including the source body of interest, can be used as a guide to estimate the dip of the source to an individual lineament. This method indicates that the dips of the sources to the lineaments identified may be almost vertical or steep towards the south-west.

The lineaments MSFR08031, MSFR08034 and MSFR08092 are located in a low magnetic area in the north-western part of the SFR regional model volume. Four profiles (SFR27 to SFR30, see Appendix 6) have been modelled. The results indicate that several different low susceptibility source body geometries can be used to explain the anomalies. The geometrical alternatives also represent different alternatives in terms of geology. In profile SFR27, a near-surface source body representing a sediment-filled depression in the bedrock surface can be used to explain the anomaly coupled to the lineament MSFR08092. The broad, weak anomaly also indicates the possibility that the source may be coupled to changes in lithology or to a deformational structure that dips gently or moderately. In profile SFR29 (see Appendix 6), the anomaly from the lineament complex including MSFR08034 and MSFR08092 is too weak for modelling. The anomaly associated with the lineament MSFR08031 indicates a steep dip towards the south-east of the sheet-like source body to the lineament. The sheet-like two-dimensional geometry indicates that the inferred source could represent a deformational structure. The modelling of profile SFR30 (see Appendix 6) yields two moderately south-east dipping source bodies to the lineaments MSFR08034 and MSFR08092. Regarding this whole area covered by the profiles SFR27 to SFR30, it is important to observe that the modelled low magnetic anomalies have very low amplitudes which yield models of low confidence. The large variety in the source bodies presented is another expression of the large uncertainty.

Modelling of many of the 41 profiles have resulted in source bodies with steep dips (Appendix 6). Most commonly the 3D inversion has yielded similar results as the forward modelling. Hence, the steep dips in the models are considered to reflect the actual situation in most cases. Regarding the uncertainty in the modelled geometries, it is difficult to quantify in metres and degrees as it depends on several factors that vary from profile to profile. What can be stated, in general, is that the modelling results from areas with low magnetic relief have lower confidence compared with those from areas with high relief in the magnetic pattern. The profiles with expected low confidence in the models have, in general, been commented explicitly in the presentation of the modelling results (Appendix 6).

Geological significance of lineaments

Excavation work and drilling activities inside the Forsmark tectonic lens have addressed a number of lineaments detected as low magnetic features /Stephens et al. 2007/. The work has led to several conclusions of which some are summarised below.

- Lineaments defined by discordant magnetic minima primarily represent fracture zones.
- Lineaments defined by discordant magnetic minima could also represent dykes of granite and pegmatite.
- Lineaments defined by concordant minima connections are related primarily to lithological contrasts that are aligned parallel to the ductile foliation in the bedrock. However, the occurrence of minor fracture zones along the tectonic foliation cannot be excluded as a contributory factor to these lineaments.

These conclusions are principally applicable inside the Forsmark tectonic lens /Stephens et al. 2007/. The character of concordant minima connections inside the ductile high-strain belts outside the lens, including a large part of the SFR regional model area, is uncertain. Some of these lineaments are known to be and many have been modelled as regionally significant deformation zones /Stephens

et al. 2007/. The Singö deformation zone (ZFMWNW0001), for example, is a prominent feature that intersects the southern part of the SFR regional model volume. It intersects tunnels and boreholes and is consequently relatively well studied and characterised. According to the parameter setting of lineaments from the site investigation, more than half of its length is detected in topographical data (bedrock topography), while the whole structure is easily observed in the magnetic total field data as lineament MFM0803G (see Figure 4-21). The deformation zone is intersected by refraction seismic profiles that show decreased P-wave velocity over broad sections along the profiles. As it is associated with a prominent low magnetic anomaly, it illustrates the diagnostic strength of magnetic data to predict tectonic structures in the bedrock.

However, the image of the magnetic total field over the SFR area contains some more diffuse semi-linear rather extensive areas with low magnetic relief. In the north-western part of the regional model area one of these areas is clearly visible in the map of the first vertical derivative of the magnetic total field (Figure 4-24). The area hosts three lineaments in the SFR version 1.0 but considering the large extent of the volume, with low magnetic susceptibility, together with the north-eastern strike of the feature, a lithological unit is likely to be at least part of the explanation to the anomaly (cf. Section 6.2.2). Other volumes of similar character are visible also in other parts of the SFR area. Some of these have less linear expressions than in the example presented in Figure 4-24 and, consequently, lithological units with low magnetic susceptibility ought to be considered as possible explanations. The 3D inversion of magnetic total field data carried out within the version 1.0 has resulted in the delineation of such low susceptibility areas with a corresponding impact on the model of the bedrock of the SFR model volumes (see Sections 4.6.5 and 6.2.2).

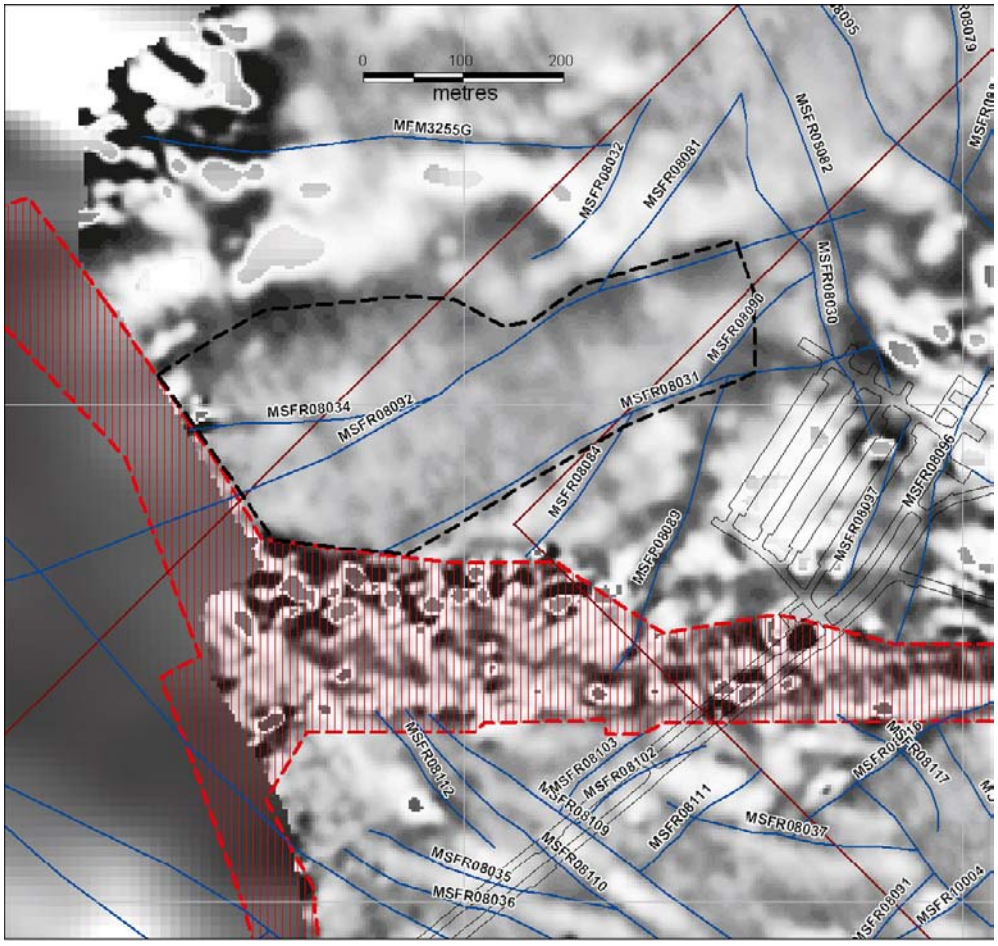

Figure 4-24. *North-west of the SFR facility there is an extensive area with a general low magnetization in the bedrock. The lineaments identified cover only a limited part of the fairly large area indicating a possible lithological unit with a low content of magnetite as being part of the source to the feature. The lineaments in SFR model version 1.0 are shown in blue. An enhanced version of the magnetic total field image (1st vertical derivative) is shown in the background.*

Based on these considerations, a pragmatic interpretation is that lineaments, represented by features with high length/width ratios in the magnetic total field data primarily represent deformed rock. With decreasing values in the length/width ratio lithological factors are increasingly likely. The straightforward method to validate a lineament map is to control the lineaments against solid geological observations from outcrops, trenches, boreholes or tunnels. However, the lineament maps themselves, as presented in this chapter, are unvalidated. Validation of the main lineaments is one of the main aims of the site investigation and modelling strategy that has been applied in the project. Borehole positions and orientations have been selected to investigate these lineaments. Correlation between underground geological data (tunnel mapping and boreholes) and the lineaments aims to identify and characterise the inferred deformation zones. The lineaments are a key input, but they may be removed or modified when developing them into deformation zone traces on the ground surface depending on the investigation results and modelling process. The relationship between the lineaments and the deformation zone traces on the ground surface are described in the individual deformation zone property tables. Uncertainties concerning the lineament position and extents are summarised in Chapter 7.

4.6.2 Low velocity anomalies in refraction seismic data

No new seismic refraction surveys have been carried out in connection with the current project. Seismic refraction surveys were carried out in 1981 to support the design work for the original SFR facility. The aim of the surveys was to identify deformation zones and estimate sea bottom sediment thicknesses /Hagkonsult 1982/. The basic precept was that low velocity anomalies in the bedrock may represent steeply dipping, brittle deformation zones that contain an anomalous concentration of open fractures or sections with incohesive rock. The position of the profiles and the measured seismic velocities are presented in Figure 4-25.

As can be seen in Figure 4-25, the seismic velocities in the bedrock are generally greater than 4,000 m/s. /Isaksson 2007/ evaluated the correlation between low velocity anomalies ≤ 4,000 m/s, low magnetic lineaments and deformation zones (Forsmark stage 2.2). The analysis showed that there is only moderate correlation between low velocity anomalies and low magnetic lineaments or modelled deformation zones. However, both survey methodology and geological conditions need to be considered in the assessment of the relatively poor correlation. These two features are reported in more detail in /Isaksson 2007/ and /Stephens et al. 2007/. Of particular note is the fact that the geophone spacing of 5 m limits the resolution for the identification of anomalies. For the SFR local model area, in particular, where the minimum lineament length for consideration is 300 m, it is unlikely that such short lineaments will have identifiable low velocity anomalies. Thus, it is difficult to resolve individual narrow low velocity sections. The velocity provided in the data is probably an average over longer sections composed of both intact and lower quality bedrock. In addition, it is noteworthy that /Carlsson and Christiansson 2007/ reported that the Quaternary deposits in the area include glacial till some of which is, at least locally, very compact and even required blasting during excavation. Seismic investigations made during the geophysical explorations showed a seismic velocity of around 4,500 m/s in some cases that would possibly mask any underlying lower velocity anomaly associated with a narrow deformation zone.

For these reasons and based on the results of the evaluation presented in /Isaksson 2007/ and /Stephens et al. 2007/, it can be stated that the presence of a well-defined low velocity anomaly can only be expected to be associated with larger, steeply dipping, brittle deformation zones and, even then, there are various reasons to explain the absence of such an anomaly. The low velocity anomalies that do not match lineaments defined by magnetic minima and/or deformation zones and that are, as yet, not explained may represent unidentified fracture zones. Alternatively, they may be related to local, narrow depressions in the bedrock surface that correlate with fractured near-surface bedrock or are simply filled with less compact Quaternary cover material. This is supported by the pattern of anomalies seen across the SFR regional model area, where generally clearly defined low velocity anomalies are lacking.

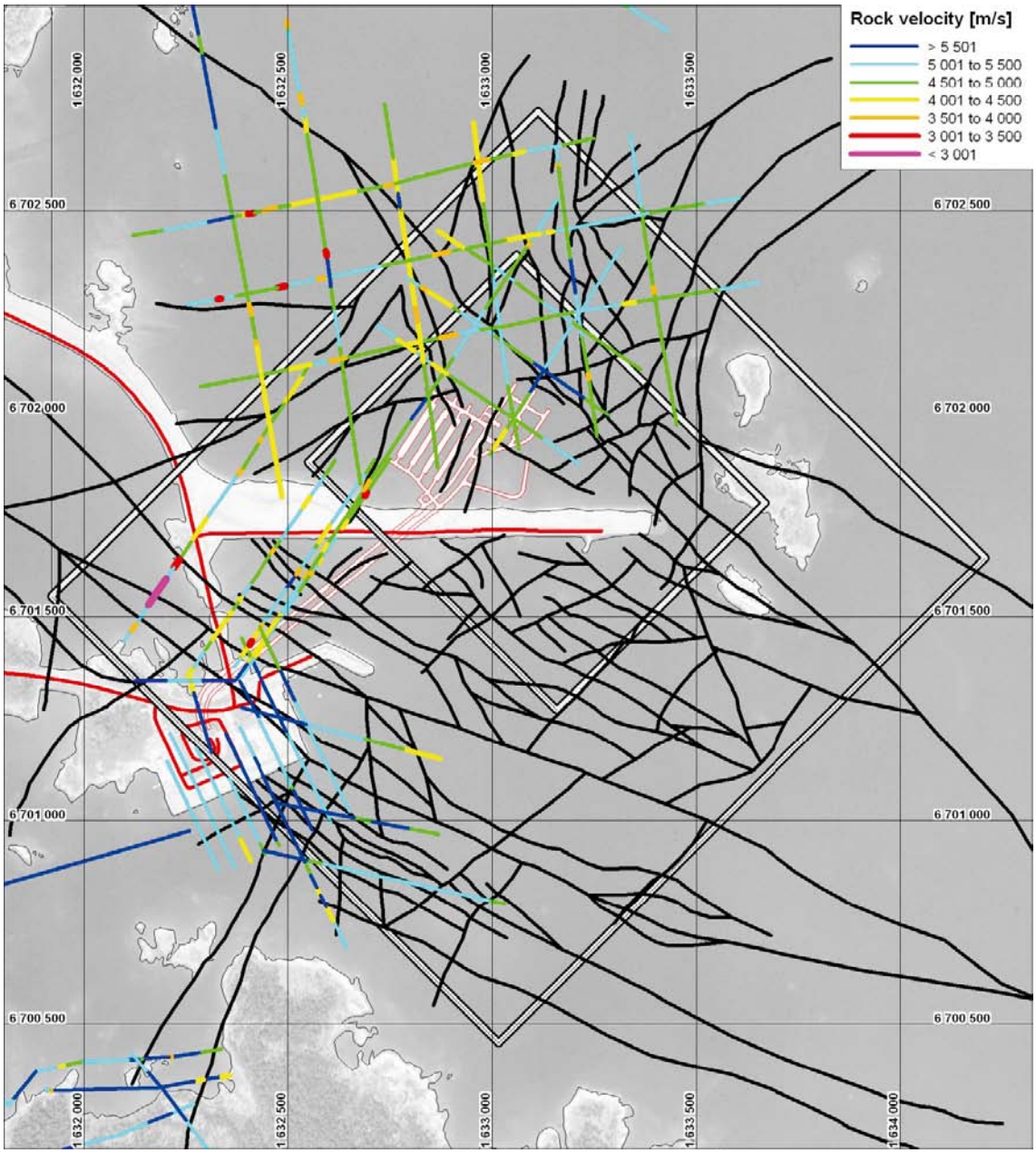

Figure 4-25. *Profiles from seismic refraction surveys partly performed in 1981 to support the design work for the original SFR facility /Hagkonsult 1982/ in relation to the SFR version 1.0 lineaments.*

4.6.3 Reflectors in reflection seismic data

Surface reflection seismics provided a very useful and complementary tool to the surveys of the magnetic total field in the Forsmark site investigation /Stephens et al. 2007/. While data on the magnetic field effectively revealed the low magnetic feature connected to many steeply dipping deformation zones, it had only limited success in detecting gently dipping structural features. In contrast, surface reflection seismic data /Juhlin et al. 2002, Juhlin and Bergman 2004, Juhlin and Palm 2005/ proved to be an important tool in the modelling of gently dipping, brittle deformation zones at the Forsmark site and such data were obtained and evaluated during two separate stages in connection with Forsmark model version 1.2 and model stage 2.1 /SKB 2005, 2006/. The location of the reflectors in 3D space for use in RVS was completed by /Cosma et al. 2003, Balu and Cosma 2005, Cosma et al. 2006/.

No new seismic reflection surveys have been carried out in connection with the current project. Some of the reflectors identified in earlier work coupled to the Forsmark site appeared also to impinge on the SFR regional model volume. Since the current modelling efforts are concentrated on the SFR site, it was judged to be of importance to review the seismic reflection data in and around the SFR area /Juhlin and Zhang 2010/. The results from the Forsmark site investigation also provided background input into the SFR version 0.1 modelling work and are summarised in /Curtis et al. 2009/.

Approximately 40 km of high-resolution (10 m shot and receiver spacing) reflection seismic data were shot during the Forsmark site investigation. The positions of the profiles 5b (LFM000817) and 8 (LFM000818) that lie in and around the SFR regional model area are shown in Figure 4-26. Since the primary focus of the original activities was on the central parts of the Forsmark site investigation area, the potential to extract more focused information on the data in the SFR area was investigated through reprocessing and re-interpretation of data along these two profiles /Juhlin and Zhang 2010/. The principal aim with the re-examination of the data from profiles 5b and 8 was to improve the images in the uppermost 500 m of the bedrock in the SFR model areas. The activity resulted in an update of the formerly identified reflectors adjacent to the SFR model volumes as well as in the identification of some entirely new reflectors. A summary of the reflectors most relevant to the SFR modelling work are presented below while full details are reported in /Juhlin and Zhang 2010/.

Five new reflectors were identified in connection with the reprocessing and re-interpretation of the earlier data, including reflector B10 (confidence class 2 – medium) and reflector A13 (confidence class 3 – low).

The reflector B10 may extend below the SFR site (Figure 4-27). It has a strike of approximately 025° and dips 35° to the south-east. Even though the reprocessing work indicates an uncertainty regarding its dip, the reflector is clearly observed in the data and consequently its presence below the SFR model area is judged as highly probable. There is no correspondence with any lineaments observed in the interpretations related to either the Forsmark site investigation or the SFR modelling. The fairly gentle dip of the reflector excludes a probable correlation with features represented by lineaments.

The existence and geometry of reflector A13 (Figure 4-28) is very speculative but, if it exists, it is expected to intersect the surface within the SFR model area. This reflector is further discussed in Section 5.5.5 – moderately dipping structures.

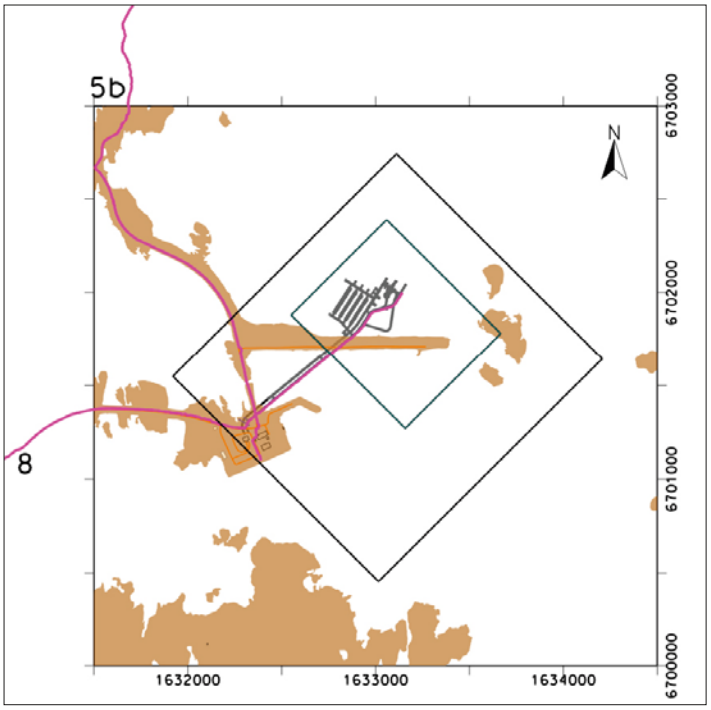

Figure 4-26. *Seismic reflection profile 5b (on land) and profile 8 (on land and along the tunnel).*

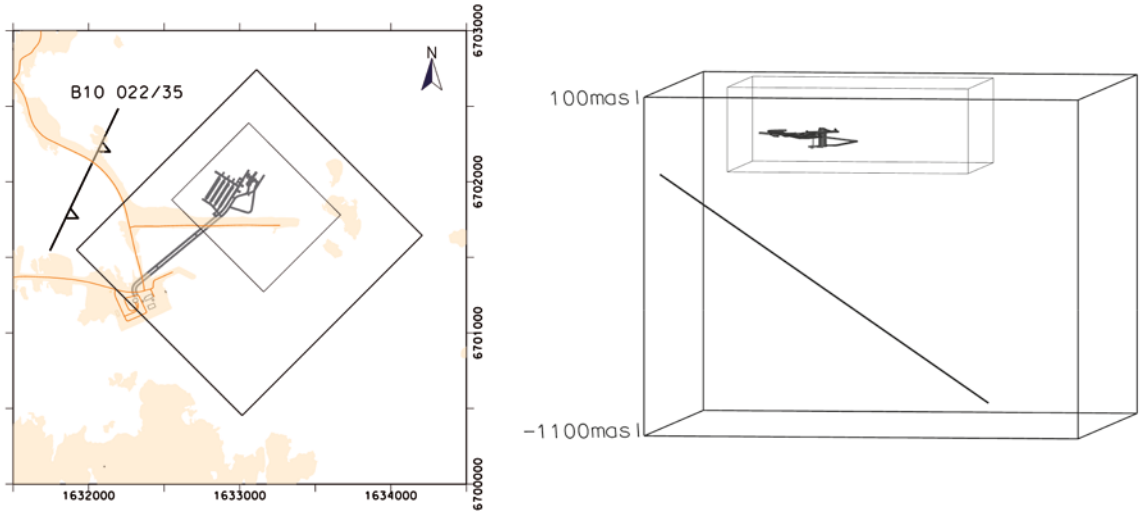

Figure 4-27. *Reflector B10 projected intercept with the ground surface (left) and position, looking along the strike, within the regional model volume (right).*

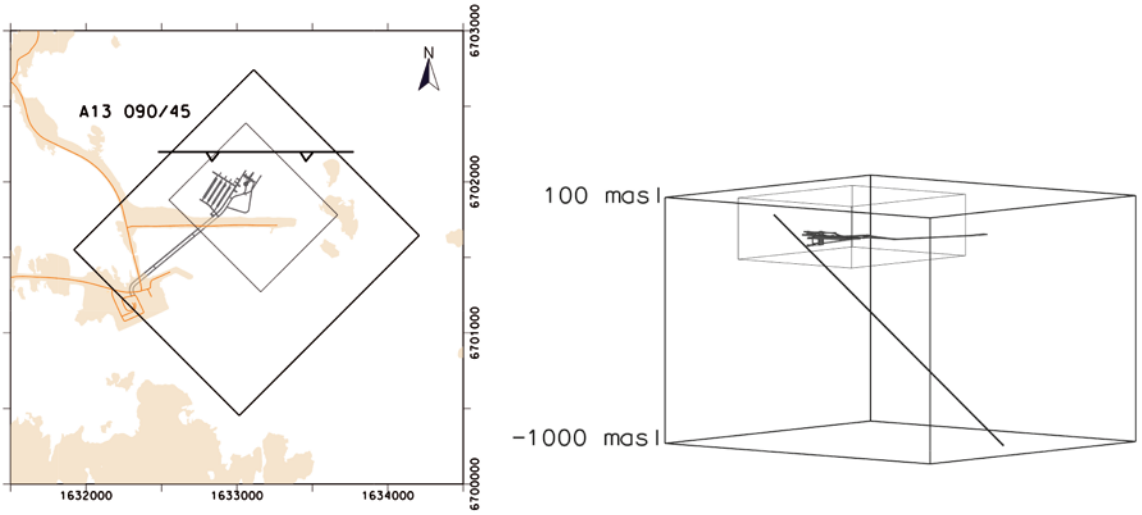

Figure 4-28. *Reflector A13 projected intercept with the ground surface (left) and position, looking along the strike, within the regional model volume (right).*

4.6.4 Qualitative interpretation of detailed, ground magnetic data and correlation with geological features

The detailed ground magnetic data covering the SFR area has been processed and interpreted to provide information on the distribution of magnetic sources in the bedrock, projected to and represented in 2D at the ground surface. This information has been used in the modelling of rock domains and deformation zones.

Processing

The processing and interpretation have been performed sequentially and, in principle, the work has been carried out in the same way as reported earlier during the Forsmark site investigation /Isaksson et al. 2007/. The magnetic data have been processed and filtered to better enhance geological structural patterns in the data. Of particular note in the regional SFR model area is the extent of man-made disturbances to the magnetic field, mainly high frequency noise from scrap-metal in the pier construction but also long wave anomalies from iron objects in the SFR underground storage facility. The area close to the Fenno-Skan HVDC-cable also shows an artificial banding along the magnetic survey lines.

A major magnetic source in the SFR storage is the silo repository but also the waste containers in the caverns contain iron. For this reason, the extent of the storage in each deposit vault was documented during a field visit in May 2009. By forward magnetic modelling, the magnetic response from SFR was roughly reproduced. Subtracting this response from the original survey data minimized the influence from the repository. The high frequency noise along the pier was minimized in two different ways. In one method, the original grid data was filtered with a 60 m, low-pass filter and, in a second method, an inversion technique has been used (see Section 4.6.5).

Figure 4-29 shows the model response from the silo and the deposit vaults. The total anomaly from the model at the ground surface spans from –25 nT to 125 nT. Figure 4-30 shows the magnetic total field with the SFR response subtracted, a low-pass anomaly merged at the pier and an inset map of the inversion transformation along the pier (stored in SDE GIS database with ID SDEADM. GV_FR_GEO_8274 and SDEADM.GV_FR_GEO_8275). The magnetic anomaly span within the whole SFR area is around 400 nT.

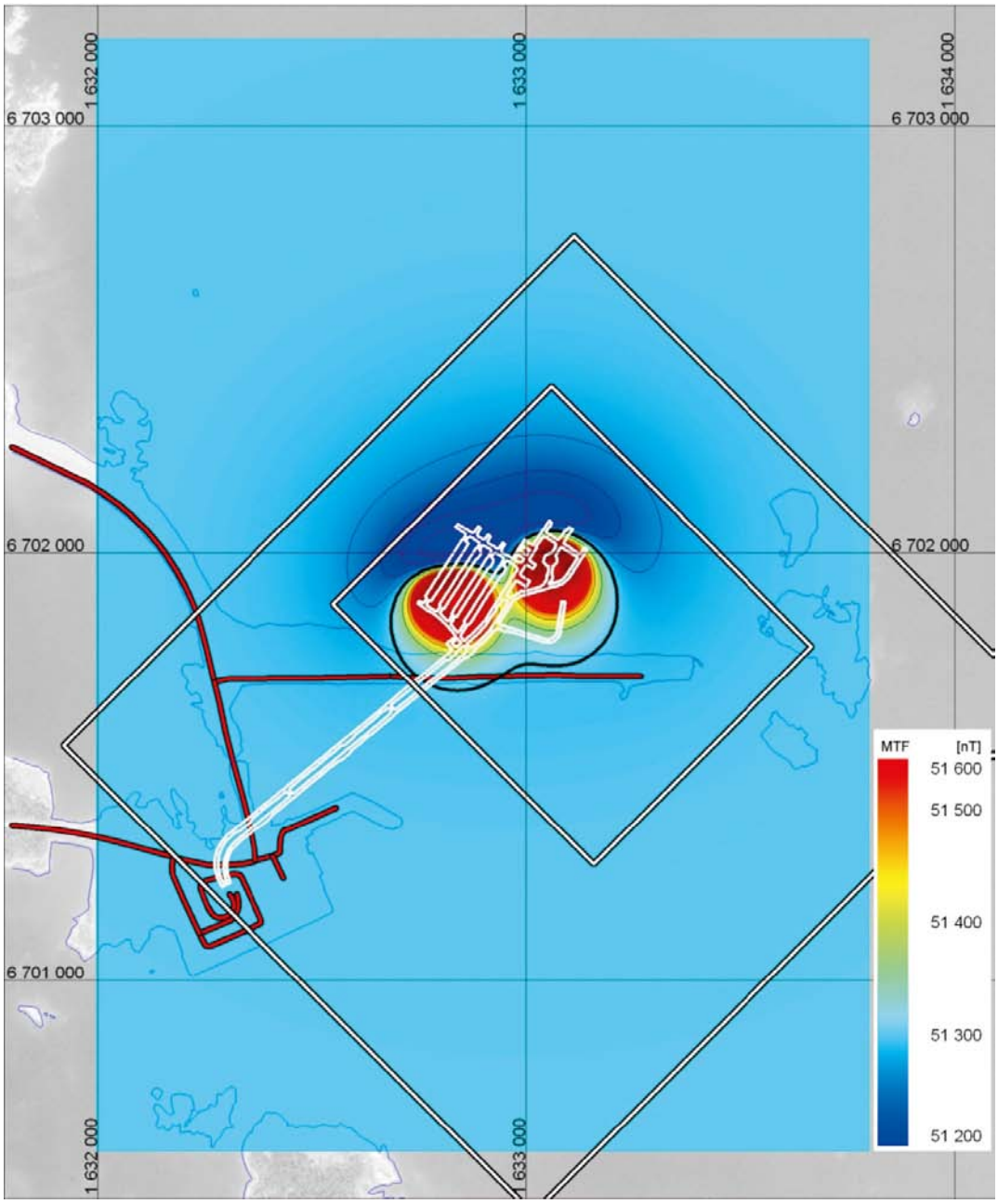

Figure 4-29. *The modelled magnetic field response from the silo repository and the deposit caverns at SFR. The local and regional model areas are marked. The response has been subtracted in Figure 4-30.*

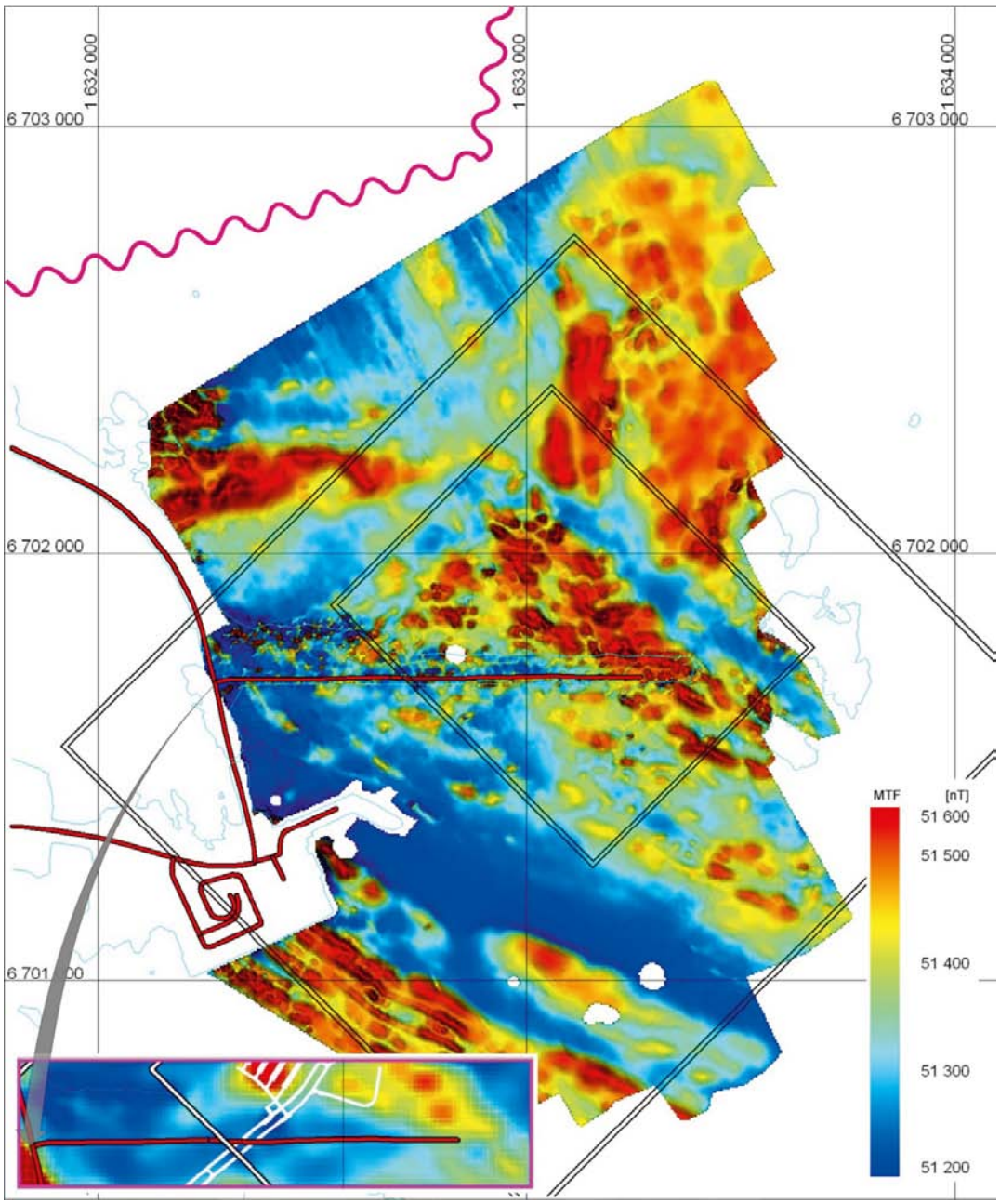

Figure 4-30. *The detailed magnetic total field at SFR, enhanced with a vertical illumination. The local and regional model areas are marked. The model response from the SFR repository, Figure 4-29, has been subtracted and a 60 m low-pass filter has been applied along the pier. An inset map of the pier area with the magnetic total field using inversion as noise reduction is presented in the lower left corner. View the pier road as a scale reference between inset map and full map. The artificial magnetic banding along the survey lines, caused by the Fenno-Skan HVDC cable (magenta wavy line), is clearly seen in the north-western part of the area.*

Interpretation of magnetic patterns

A qualitative interpretation comprises identification and segmentation of the magnetic pattern into 'banded' and 'irregular' patterns. The former usually constitute supracrustal rock units, bedrock that is strongly deformed or both these possibilities. The latter commonly constitute intrusive rocks. The magnetic pattern is then accordingly divided into low, moderate, high and very high intensity. Areas with very low intensity yield little information on the pattern and, hence, these units are kept separate. Apart from the surface pattern, linear features are also identified. Magnetic connections, or magnetic bands, further enhance the structural pattern and discordant magnetic lineaments, which

usually indicate a deformation zone or a break in the bedrock units, are included (stored in SDE GIS database with ID SDEADM.GV_FR_GEO_7821). However, identification of these linear features is generally carried out as a separate, more focused contribution (see Section 4.6.1 in this study). The qualitative interpretation is presented in Figure 4-31 (stored in SDE GIS database with ID SDEADM.GV_FR_GEO_7825). A deviation from the normal procedure is that the magnetic low, probably representing the Singö deformation zone, is represented as a separate unit. Furthermore, the north-westernmost area, close to the DC-cable is disturbed and the pattern received is probably, to a large extent, related to survey line errors, giving uncertainties in the interpretation.

Correlation between geological features and the magnetic field

In order to make use of the high resolution magnetic total field data for geological modelling, it was necessary to evaluate the significance of the possible correlation between rock type and magnetic intensity. A compilation of the magnetic susceptibility for each of the major rock types in the area was conducted from the geophysical borehole loggings to enable this correlation (Section 4.3.1). Only sections apparently unaffected by rock alteration were included in the compilation.

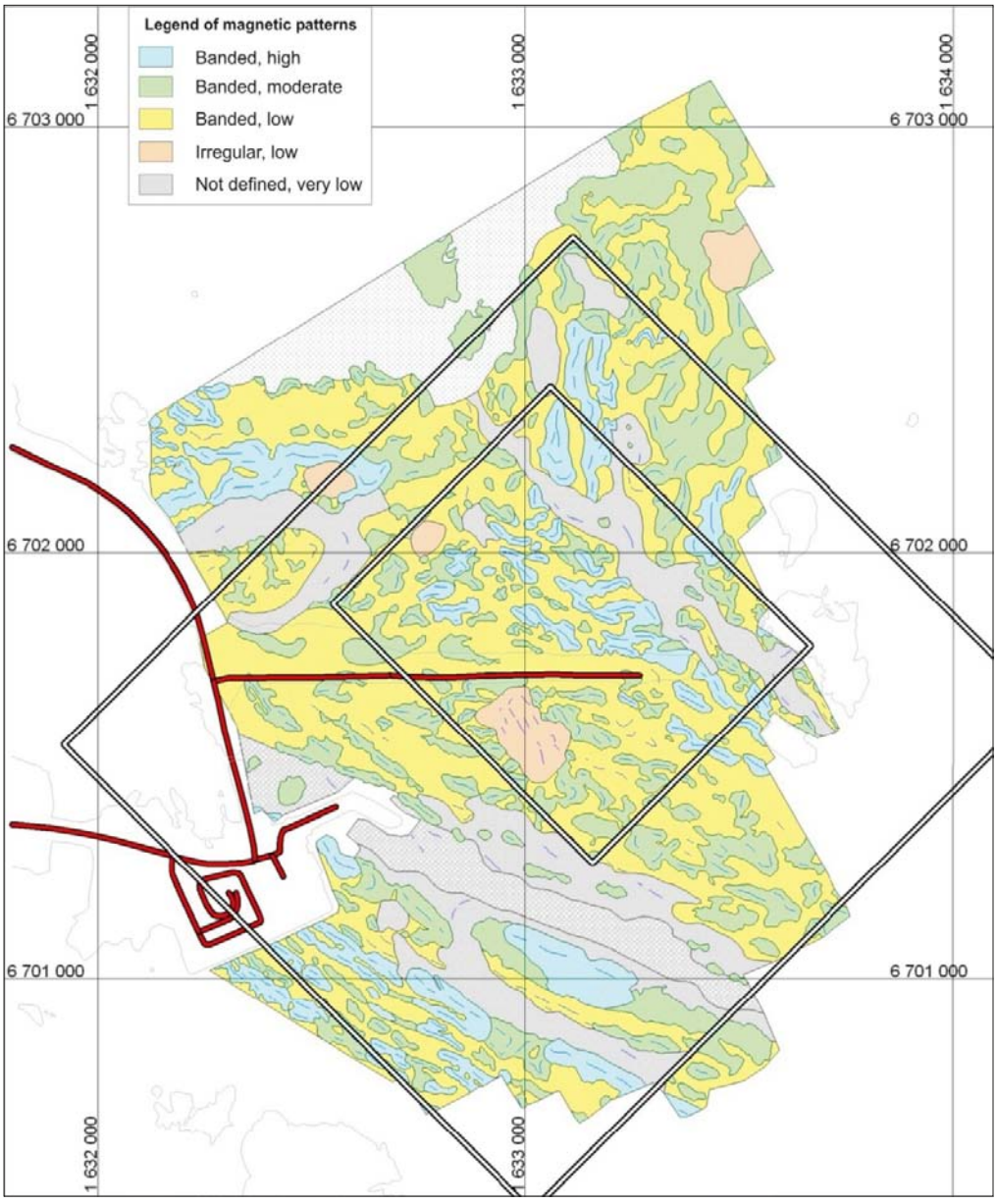

Figure 4-31. *Qualitative interpretation of detailed ground magnetic data. The local and regional model areas are marked. A very low-magnetic unit, possibly outlining the central part of the Singö deformation belt, is marked by a separate grey tone raster.*

Inspection of the graphical presentation of the magnetic susceptibility data in Figure 4-3 shows that there is considerable overlap for all five rock types and it is obviously not simple to distinguish between rock types based on magnetic susceptibility alone. The metagranodiorite (to granite) and the younger granites show a virtually identical bimodal data distribution for magnetic susceptibility, and they are consequently indistinguishable from each other. Similarly, there is an identical data distribution for the amphibolites and felsic to intermediate metavolcanic rocks, which both display a positive bias with a maximum at approximately $10{,}000\times10^{-5}$ SI. The only rock type with potential to be separated in terms of magnetic susceptibility is pegmatitic granite. It has a geometric mean of magnetic susceptibility of 15×10^{-5} SI, which is one order of magnitude less than those for the other rock types. On this basis, the following can be concluded regarding the correlation between rock type in the SFR area and magnetic susceptibility:

- Pegmatitic granite and pegmatite tend to have the lowest magnetic susceptibility of the major rock types that exist in the SFR area.
- Susceptibility values that exceed $1{,}500\times10^{-5}$ SI are generally restricted to amphibolite and felsic to intermediate metavolcanic rock.
- All major rock types in the SFR area are well-represented in the intermediate susceptibility range, including pegmatitic granite and pegmatite.

When assessing the relationship between these conclusions for magnetic susceptibility and patterns in the magnetic total field, it is essential to also consider the geometric context and other supporting data. The magnetic susceptibility of a rock can be strongly reduced by hydrothermal alteration, where magnetite is converted to hematite. This is a common feature along brittle deformation zones in the area, and the basis for the use of lineaments defined by magnetic minima (see Section 4.6.1) in the deformation zone model (see Chapter 5). In conclusion, low intensity in the magnetic total field can either be related to oxidation associated with brittle deformation or volumes dominated by rock types with low magnetic susceptibility (e.g. pegmatitic granite, pegmatite).

4.6.5 Inversion of detailed, ground magnetic data

Inversion of the detailed ground magnetic data has been carried out to provide information on the 3D distribution of magnetic susceptibility in the bedrock as support to the modelling of rock domains and deformation zones. The susceptibility inversion model is built up by volumetric box elements, so-called voxels, that cover the SFR local model volume with a size of 1,200×1,200 m horizontally and 500 m vertically. The voxel resolution is 10 m in all directions, except for the uppermost 50 m which has a higher vertical resolution of 5 m.

The inversion methodology uses a mathematical technique whereby changing a physical property, in this case magnetic susceptibility, in each individual cell sequentially aims to generate a theoretical magnetic response that fits both the actual recorded geophysical survey data and is consistent with the known and inferred geological data. The physical property models recovered via inversion follow an established industrial technique and are an important source of information for understanding subsurface geology as it applies to engineering geology, mineral exploration and rock mechanics. However, there are an infinite number of models that can fit the geophysical data to a desired degree. For this reason, the presented models are typically non-unique. The inversion of detailed magnetic data has also been used for noise reduction along the pier at SFR.

Noise reduction

In the pier area, a high frequency magnetic noise was obtained from the scrap-metal filling material. Inversion has been used to filter out this noise by creating a high resolution voxel model, covering the pier area (see inset map in Figure 4-30). The resolution was 4 m horizontally and 2 m vertically in the uppermost 20 m, followed by sequentially 4 m, 8 m and 20 m resolution, down to a total depth of 200 m. A subset of the magnetic grid and topography, covering the pier area and its immediate surroundings, was created. During the inversion, high frequency anomalies were tied to susceptibility variations in the uppermost cells, while susceptibility distributions in deeper cells were described in terms of bedrock anomalies. After inversion, the voxel susceptibilities were cleared down to a depth of 20 m. From the remaining model, a forward calculation was carried out, resulting in a magnetic anomaly field more related to the bedrock susceptibility composition (inset map in Figure 4-30). Clearing the uppermost 20 m from magnetic susceptibility has the same effect as elevating the magnetic sensor 20 m above ground surface and, hence, the resultant anomaly field is also smoothed.

Bedrock inversion model

The magnetic inversion is based on processed data (see Section 4.6.4), which, in addition, has been transformed to avoid, as much as possible, magnetic sources outside and below the actual model. Hence, an inferred regional trend has been subtracted.

From the inversion, two models were selected for further work. Both are isotropic, which means that no tension or preference has been applied in any x-, y- or z-direction. The difference between the models is that the sea-bottom and ground topography has been used in one model, while the other model has a flat surface providing a lower and smoother resolution in the uppermost part of the model. Principally, the model including topography has been used (stored in SKBdoc with document ID 1267670–1267673).

The 3D inversion of magnetic data has been used in several ways during the modelling of rock domains and deformation zones. From the 3D volume of magnetic susceptibility, a sequence of vertical and horizontal sections, as well as iso-surfaces (stored in SKBdoc with document ID 1243885–1243898), representing susceptibility boundaries, have been transferred to RVS format where they have been used as support in the modelling work. Figure 4-32 shows horizontal sections

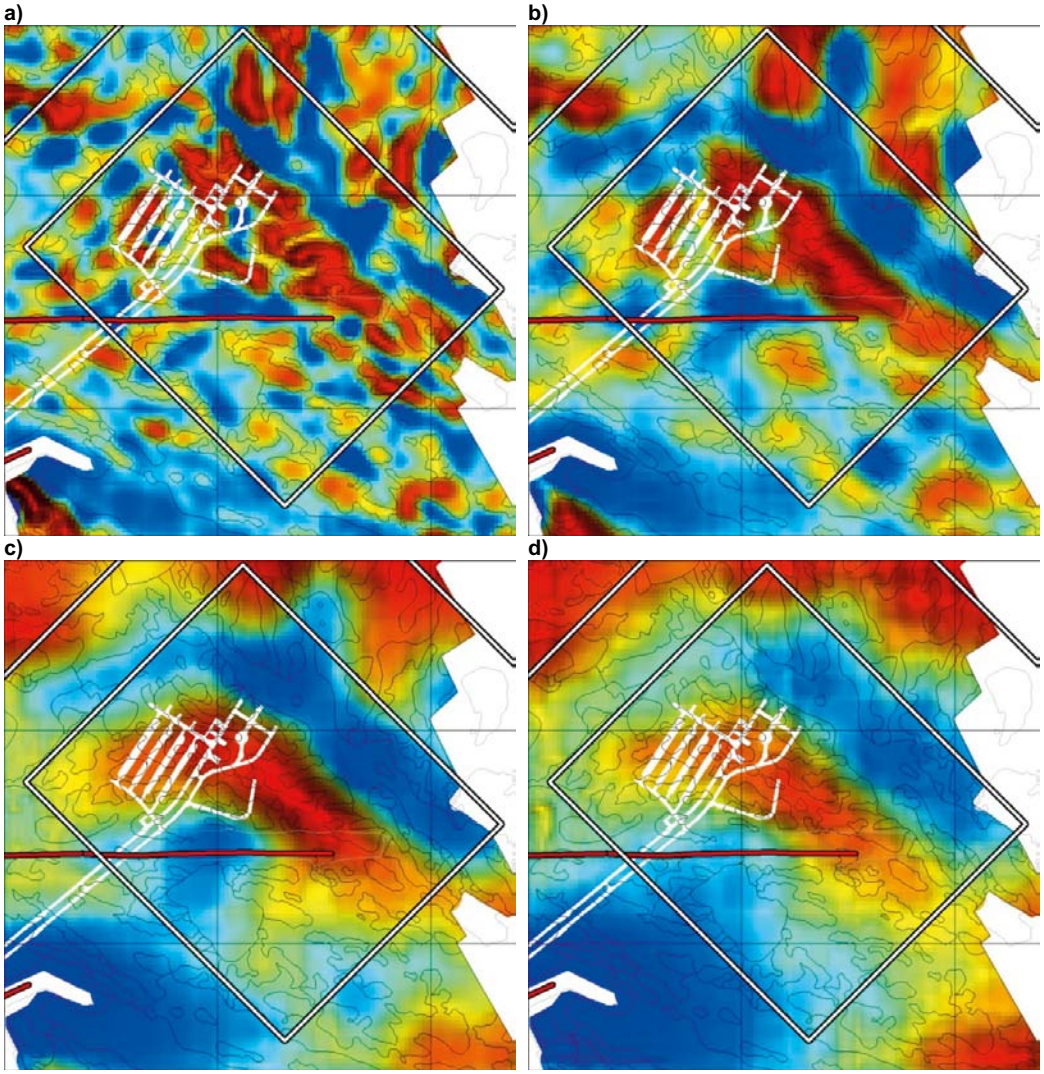

Figure 4-32. *Magnetic susceptibility from inversion model. Susceptibility from 0–0.01 SI, from blue to red colours, respectively. Horizontal sections at a) –50 m elevation b) –100 m elevation c) –200 m elevation and d) –300 m elevation. The local and regional model areas, the current SFR storage and the pier road are all shown. Black contours represent a magnetic pattern skeleton from the qualitative interpretation (Figure 4-31), valid at the ground surface. Area: 1632500–1633700, 6701200–6702400, grid mesh: 500 m.*

of magnetic susceptibility from the elevations –50, –100, –200 and –300 m (stored in SDE GIS database with ID SDEADM.GV_FR_GEO_8266 to SDEADM.GV_FR_GEO_8272). Note the change in spatial resolution with increasing depth. Furthermore, the modelled rock domain elements have been checked against the inversion model for inconsistencies (Figure 4-33). Finally, a 3D volume representing a low magnetic unit has been constructed to provide assistance in the development of the boundary between rock domains RFR02 and RFR03 (stored in SKBdoc with document ID 1267676 and 1270072; see Chapter 6).

The magnetic inversion models have also been used in the verification of possible deformation zones, mainly by superimposing magnetic lineaments and independently forwarding modelled profiles of the magnetic field on vertical and horizontal sections of the magnetic inversion models (see Appendix 6 and Section 4.6.1).

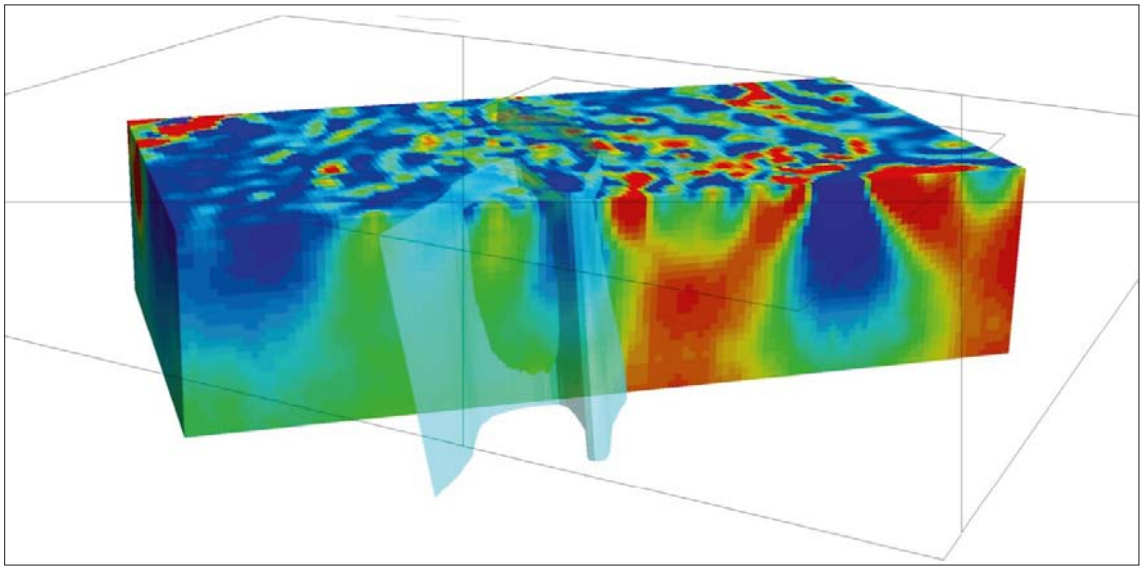

Figure 4-33. *Example of support to the rock domain modelling work. South-north vertical section along the line 1633100E with a view from the east, showing the magnetic inversion model and an early version of the boundary between rock domains RFR01 and RFR02 (see Chapter 6). The boundary was adjusted in a later model version below the deepest geological fix point at –205 m to avoid conflict with the inversion model. Colour spectrum from 0–0.01 SI in blue and red, respectively. Depth of magnetic inversion down to –300 m elevation.*

5 Deformation zone model

5.1 Introduction

This chapter describes the applied deformation zone modelling methodology, the overall results, along with a confidence assessment and key uncertainties. For detailed descriptions of the individual modelled deformation zones the reader is referred to Appendix 11. The geological modelling work during version 1.0 follows SKB's established methodology using the Rock Visualisation System (RVS). The deformation zone model version 1.0 is a further development of the previous version 0.1 /Curtis et al. 2009/.

5.2 Modelling assumptions, input data and general methodology

5.2.1 Modelling assumptions

In contrast to model version 0.1, where only a single combined model of the local and regional volumes was produced, separate local and regional deformation zone models have been produced in model version 1.0 (Figures 5-1 and 5-2). The local and regional model volumes are defined in Section 1.4. The local model contains all modelled deformation zones that have a size corresponding to a trace length on the ground surface of ≥ 300 m. The regional model contains only local major and larger zones, i.e. zones with a trace length on the ground surface of ≥ 1,000 m.

The conceptual understanding of the deformation zones and the bedrock structure at Forsmark, described in /Stephens et al. 2007/ and presented in Section 2.3 was adopted in the SFR study. The current SKB definition of a deformation zone differs considerably from that applied in the previous structural models of SFR, where brittle deformation zones (fracture zones), for example, were identified on the basis of the frequency of open fractures and hydrogeological information (cf. /Carlsson et al. 1985, 1986/ and Section 3.1). Zone thicknesses have currently been estimated on the basis of the SHI borehole intercepts that take into account other features such as the frequency of sealed fractures and hydrothermal rock alteration. In general, this geological methodology generates much larger estimates of zone thickness compared with the earlier construction/engineering geological methodology. The geological methodology used here is in accordance with that used in the Forsmark site investigation (see especially Section 5.2.1 in /Stephens et al. 2007/).

The concept of deformation zone core and damage zones for brittle deformation zones is well established and has been presented earlier (/Munier et al. 2003/ and Figure 5-3). In contrast to the original representation, the use of absolute fracture frequencies to define a damage zone or zone core boundary position has not been applied. Elevated fracture frequencies in a relative sense are implied in the definition of such brittle deformation zones, but the strict application of fixed threshold values is considered unhelpful since there are a number of additional parameters, such as alteration, fracture character, and borehole geophysics, which are of importance to define a deformation zone and its boundaries. The prime criterion used to define a zone core is a highly increased fracture frequency relative to the damage zone, often together with the occurrence of crushes, breccias, sealed networks and/or cataclasites. It should also be noted that deformation zone geometries are often complex, discontinuous and asymmetrical.

The basic assumptions underlying the current deformation zone modelling are outlined below.

- Deformation zones can be interpreted through direct data from surface field observations, tunnels and boreholes. The confidence in geological character and possible extent (length and thickness) of deformation zones inferred from direct data sources is higher than that for deformation zones identified from indirect observations (see bullets 2 and 3 below).
- Deformation zones can be interpreted through indirect sources of data such as geophysical maps (magnetics, VLF, slingram, gravimetric), topography, seismic reflections and seismic refractions.
- Lineaments, in the case of the Forsmark area particularly magnetic lineaments, provide information about the location and trace length at the ground surface of possible deformation zones (see Section 4.6.1 for details).

- Different sources of data can complement each other and increase the confidence in the interpreted deformation zone. Several types of observations, both direct and indirect, also increase the degree of detail in which the deformation zone can be described.
- Interpreted deformation zones can be interpolated between points of observation, if there are reasonable data to suggest the validity of such interpolation.
- Deformation zones are variable in their thickness and although they may in reality have a very complex architecture they can be modelled honouring an inferred generalised thickness.
- Within the limits of the regional or local model volumes, deformation zones interpreted at the ground surface can be extended downwards to a depth equal to the interpreted length of the mapped surface trace. This means, for example, that deformation zones longer than 1,000 m at the ground surface are extended to the bottom of the regional model volume (–1,100 masl). Simplified zone length-depth classes have been implemented in the modelling work (see 5.3.4 for further details).
- Each interpreted deformation zone has been ranked according to the confidence in its existence as being high, medium or low. Deformation zones that have high confidence ratings are based on direct data sources from boreholes and tunnels, complemented by indirect data sources mostly in the form of lineament indications. In addition to this simplistic classification, it is important that the reader considers the spread of the supporting evidence, details of which are provided in a property table for each zone (see Appendix 11). Some high confidence zones may be well supported by a number of data sources spread out over a considerable area, whereas some zones may have a high confidence level based on a single borehole intercept.
- Deformation zones ranked with medium confidence are based solely on indirect information, for example magnetic surface geophysical anomalies that cannot be disregarded as being other linear structures in the landscape, such as power lines or other man-made features.
- Interpreted deformation zones with assigned low confidence are only supported by indirect sources of information with weaker associations to deformation such as deeper lying seismic reflectors.

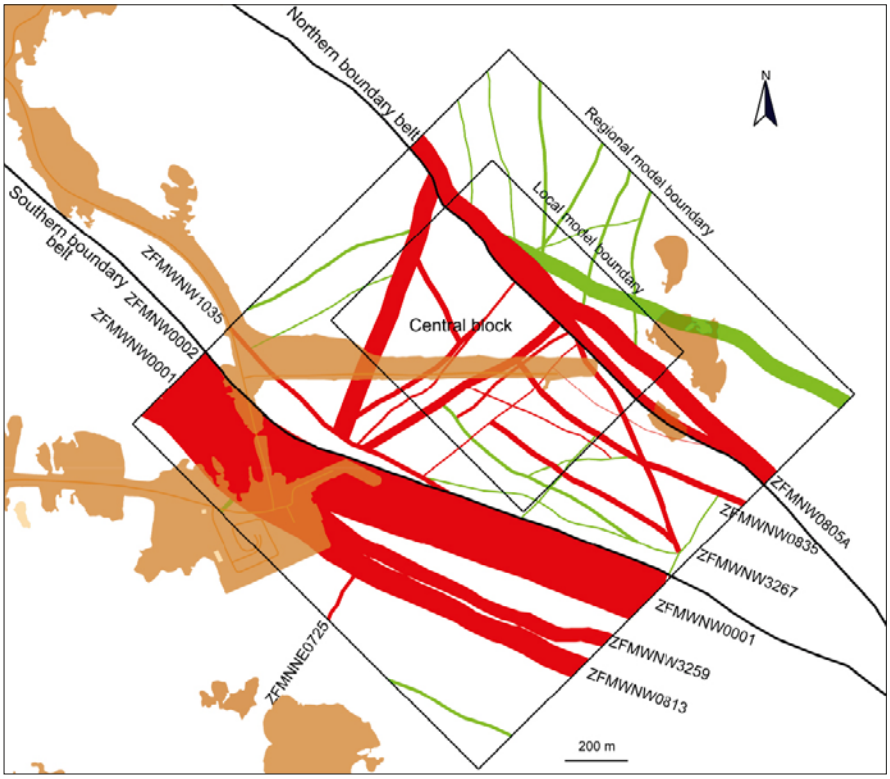

Figure 5-1. *Intersection at the current ground surface of deformation zone traces of all sizes inside the regional model area i.e. a combined model version. The regional deformation zones ZFMWNW0001 and ZFMNW0805A, along with their major splays, form the general southern and northern boundaries of the central SFR tectonic block. Confidence in existence: high=red, medium=green.*

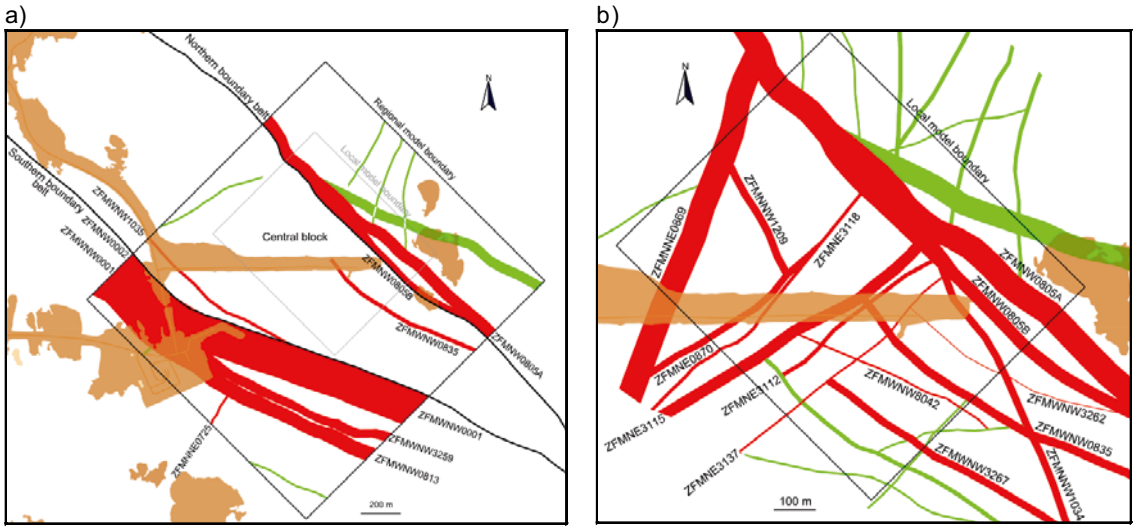

Figure 5-2. *Intersection at the current ground surface of deformation zone traces within a) the regional model and b) the local model. The different colours refer to confidence in existence: high=red, medium=green.*

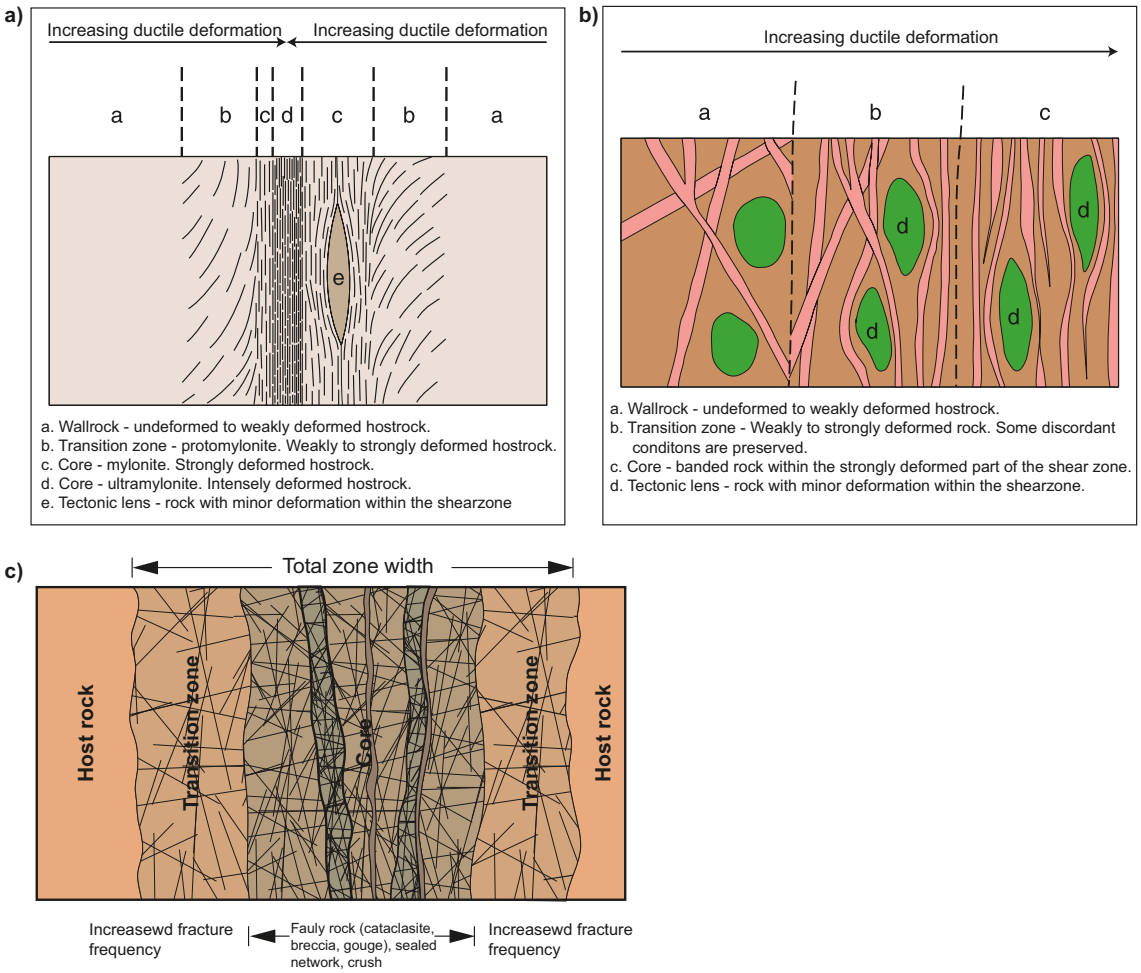

Figure 5-3. *Schematic example of a ductile shear zone in homogeneous rock, which is deformed under low- to medium-grade metamorphic conditions. The increasing degree of deformation is reflected in the formation of protomylonite, mylonite and ultramylonite. The zone may contain less deformed rock volumes, often shaped as lenses. The example shows sinistral shear. (b) Schematic example of a ductile shear zone (or belt) in heterogeneous rock, which is deformed under low- to high-grade metamorphic conditions. The host rock consists of e.g. tonalite (brown) intruded by an ultramafic rock (green) and a swarm of granitic dykes (pink). (c) Schematic illustration of a brittle deformation zone (after /Munier et al. 2003/).*

5.2.2 Input data and general methodological approach

Geological tunnel data from SFR (see Section 4.1) and the geological SHI of borehole KFM11A, the boreholes drilled during the current investigations at SFR and the eleven remapped boreholes from earlier investigations at SFR (see Section 4.2) all provide an important input to the geological modelling work. Modelled deformation zones (ZFM) and their relationship to inferred, so-called possible deformation zones in the respective SHI are presented in Appendix 7 for all boreholes except the old cored boreholes subjected to a simplified SHI. For SFR modelling version 1.0, all the available drill cores from earlier SFR boreholes have been inspected and the findings have been reported in /Petersson et al. 2011/. This exercise included the identification of the existence, apparent thickness and character of possible deformation zone intercepts, in accordance with a simplified variant of SKB's current methodology (see Section 4.2). The process allowed a review of the earlier interpretations that had been made and an update in accordance with SKB current practice. This was not possible during model version 0.1, since, at that stage in the work, only about a quarter of the old SFR boreholes had been subject to a geological SHI.

The lineament map used in SFR model version 1.0, modified after the model stage 2.3 version in the Forsmark site investigation /Isaksson et al. 2007/ (see Section 4.6.1), forms the starting point for the surface interpretation of steeply dipping deformation zones. However, all earlier versions of lineament interpretations have also been considered. During the deformation zone modelling work, the lineaments, particularly their overall continuity, have been continually reviewed and the background data re-examined. Alternative alignments and extents for individual lineaments have been considered, often driven by geological information from boreholes or tunnel mapping and some have been implemented after a joint review by both the geologists and geophysicists.

In the cases where a deformation zone can be correlated with a lineament and borehole data, the strike of the deformation zone is assumed to be the same as the trend of the matching lineament. The dip is inferred by matching the lineament to the borehole intercept(s) and is documented as the average dip angle of the deformation zone, along its entire extent. The matching process is largely geometrical, since any borehole position and orientation is generally sited with the aim of intercepting a particular lineament that is initially assumed to be a steeply dipping deformation zone. However, earlier experience from the Forsmark site investigation has shown that certain attributes can be used to further support SHI borehole PDZ and lineament correlation, for example the orientation of the most significant set of fractures. Deformation zones observed only at the surface, which lack information on their sub-surface extents and geometry, are assumed to be vertical.

The steeply dipping deformation zones are assumed to terminate, along their strike direction, against deformation zones as indicated by the lineament map and in accordance with the conceptual understanding (see Section 2.3). Thus, generally the length of such zones at the ground surface is represented by the length of the corresponding lineament. In certain cases, due to scale issues, the version 1.0 lineament study has clearly represented a lineament included in the Forsmark stage 2.3 work /Isaksson et al. 2007/ by an assembly of much shorter lineaments. Where both lineament sets have been interpreted to correspond to the same structure, but at different scales, a compromise has been made and the overall length quoted for a deformation zone corresponds to the entire longer lineament length, including those parts lying outside the local or regional model boundaries. An example involving deformation zone ZFMNW0805A and its associated lineaments has earlier been reported in /Curtis et al. 2009/ (see Section 4.6.1).

During the Forsmark site investigation, gently dipping deformation zones have been detected by an integration of data from boreholes with the interpretation of seismic reflectors /Stephens et al. 2007/. No new seismic investigations have been performed in conjunction with the current project. However, relevant existing seismic reflection data has been reprocessed and reassessed with a focus on the SFR regional model volume. Details are reported in /Juhlin and Zhang 2010/ and summarised in Section 4.6.3. The conceptual tectonic history described in /Stephens et al. 2007/ suggests that the gently dipping deformation zones in the Forsmark area terminate, both along their strike and in the down-dip direction, against regional or local major, vertical and steeply dipping deformation zones. The SFR version 1.0 modelling work has followed this concept and the modelled extent of the gently dipping zones is constrained on the basis of the lateral extent of the supporting investigation evidence and the subsequent termination against the nearest steeply dipping zone outside the volume where this evidence exists.

Two specific borehole related terms are quoted in the deformation zone descriptions and accompanying property tables, namely *Target borehole intercept* and *Geometrical borehole intercept* (Figure 5-4). These two parameters underlie much of the resulting modelled 3D deformation zone geometries.

A *target borehole intercept* is the interpreted position of a deformation zone in an individual borehole and is described by an upper and lower borehole length (sec_up/sec_low). In general, target intercepts conform to the geological SHI possible deformation zone intercepts but, in certain cases, adjustments have been made on the basis of other information or interpretation, related to information away from the specific borehole. These positions correspond to the top and bottom of the violet cylinders in the boreholes as shown in Figure 5-4. A *target tunnel intercept* is defined in the same manner, but by chainage intervals along a tunnel centre line rather than borehole length.

A *geometrical borehole intercept* is the intercept between a modelled zone and an individual borehole as they exist in the RVS model. In the case of a zone modelled with thickness, any such intercept is described by the intercept positions of the outer surfaces of the modelled structure and specifically by an upper and lower borehole length (sec_up/sec_low). These positions correspond to where the pink modelled zone boundary crosses the boreholes, as shown in Figure 5-4, and are of importance for the estimation of modelled thickness. A *geometrical tunnel intercept* is defined in the same manner, but by chainage intervals along a tunnel centre line rather than borehole length. This method to estimate model thickness differs somewhat from that used in the Forsmark site investigation (/Stephens et al. 2007/ and Chapter 7 of this report). The method used here has a tendency to provide a slightly higher estimate of the thickness of a zone.

As described earlier, the modelled thickness of a particular deformation zone is generally based on information from a number of sources from both the surface and at depth and sometimes includes more than one borehole. At SFR, due to the offshore location, the amount of direct surface data is minimal and zone thickness is estimated primarily from SHI PDZ borehole data. Where multiple borehole intercepts are involved, the modelled zone thickness is generally taken to equal the thickest inferred PDZ intercept, as shown in Figure 5-4. The modelled thickness aims to contain at least the majority of the core(s), damage zone(s) and possible splays of each deformation zone. It is this envelope thickness that defines the deformation zone in the 3D RVS deterministic deformation zone model along with a generally centrally located middle plane with zero thickness. The geometrical intercepts in boreholes or tunnels relate to where the deformation zone envelope surfaces intercept the various boreholes or tunnels. They are described by an upper and lower borehole length (sec_up/sec_low) for each borehole or start and end chainage for each tunnel. A tabular summary of all deformation zone intercepts on a borehole by borehole and tunnel by tunnel basis are presented in Appendices 8 and 9.

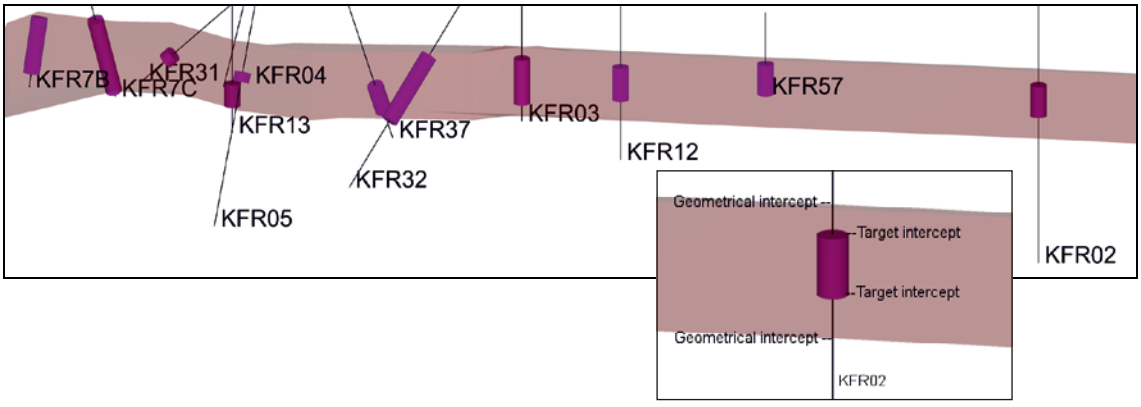

Figure 5-4. *Section view of ZFM871 looking down dip to the south (modelled thickness of 20 m). SHI PDZ sections shown in violet – these equate to the target intercepts in the individual boreholes. The pink box shows the modelled zone thickness (based on the maximum SHI indicated thickness from KFR7C and KFR37). The intercepts between the box outer limits and any individual borehole equate to the geometrical intercepts in that borehole.*

5.3 Geometric modelling

In this section, some of the basic geometrical methods used in the modelling work are described, in order to assist the end users in understanding how the SFR model version 1.0 has been constructed.

5.3.1 Regional and local models

The regional and local model volumes, resolution and scale issues are described in Section 1.4 and Figure 1-4. As discussed in Section 5.1, a minimum deformation zone trace length of 300 m has been applied for zones to be included in the local model. In the case of the regional model a minimum deformation zone trace length of 1,000 m has been applied. In order to assist the Hydrogeology and Design groups and other end users of the model, a supplementary combined deformation zone model, integrating both the regional and local models, has been made available. However, the resulting combined model must be used with caution since it mixes resolutions within a single model boundary and leads to an inhomogeneous data density throughout the modelled volume. In simplistic terms there will be too few small deformation zones outside the local model volume and this will affect any modelling that investigates connectivity or transport within the rock mass. The lack of the deterministically modelled smaller deformation zones can be compensated for by stochastic modelling techniques.

The orientation of each zone is defined by a numerical strike and dip using the right-hand-rule method. However, the letters WNW, NW, NNW, NS, NNE, NE and ENE in the deformation zone name provide a general indication of the strike and they do not follow the right-hand-rule rule procedure. The zones in the different sets (e.g. NE) may dip in both directions (e.g. NW and SE) and can also be described as sub-vertical.

5.3.2 DZ dip classes

To be consistent with earlier terminology used at Forsmark, the following dip terminology has been applied within the SFR project:

Vertical to steeply dipping: ≥ 70°.

Moderately dipping: 45–70°.

Gently dipping: ≤ 45°.

5.3.3 DZ orientation sets as defined in the RVS models

Vertical to steeply dipping deformation zones:

NNW to NS set: strike 325–005° (145–185°).

NNE to ENE set: strike 005–085° (185–265°).

WNW to NW set: strike 095–145° (275–325°).

5.3.4 DZ length/thickness relations

/Stephens et al. 2007/ presented a deformation zone thickness-length correlation chart for modelled zones in the Forsmark site investigation stage 2.2 (Figure 5-5a) and discussed the background and serious limitations in their analysis. This correlation was utilized during the Forsmark stage 2.2 modelling work to define the thickness of deformation zones that were based solely on interpreted lineaments where more direct information was lacking. As part of version 1.0, further efforts were made to investigate possible zone thickness-length relationships with the aim of producing a tool that could be applied in the SFR modelling work. Details are provided in Appendix 10.

While the investigation provided some useful guidelines, for example the need to evaluate deformation zones in separate orientation sets due to their different development history and the importance of truncation effects, no useable relationship could be defined. This failure is considered to be due to the inherent difficulty in the subject as well as the very limited size of the data set. A thickness-length cor-

relation chart is presented in Figure 5-5b for comparison, although no such thickness-length correlation has been applied in the current modelling work. Possible ranges for individual zone thicknesses have been included in the property tables where borehole and tunnel intercept data are available. These ranges are based on a general assessment of all the available data for a particular zone and experienced gained during the modelling work. For inferred zones without any supporting borehole or tunnel data, a simple classification, which is a minor modification of that used in version 0.1, has been applied to estimate thickness.

Deformation zone thickness = 1% of the associated lineament length rounded off to the nearest 5 m.

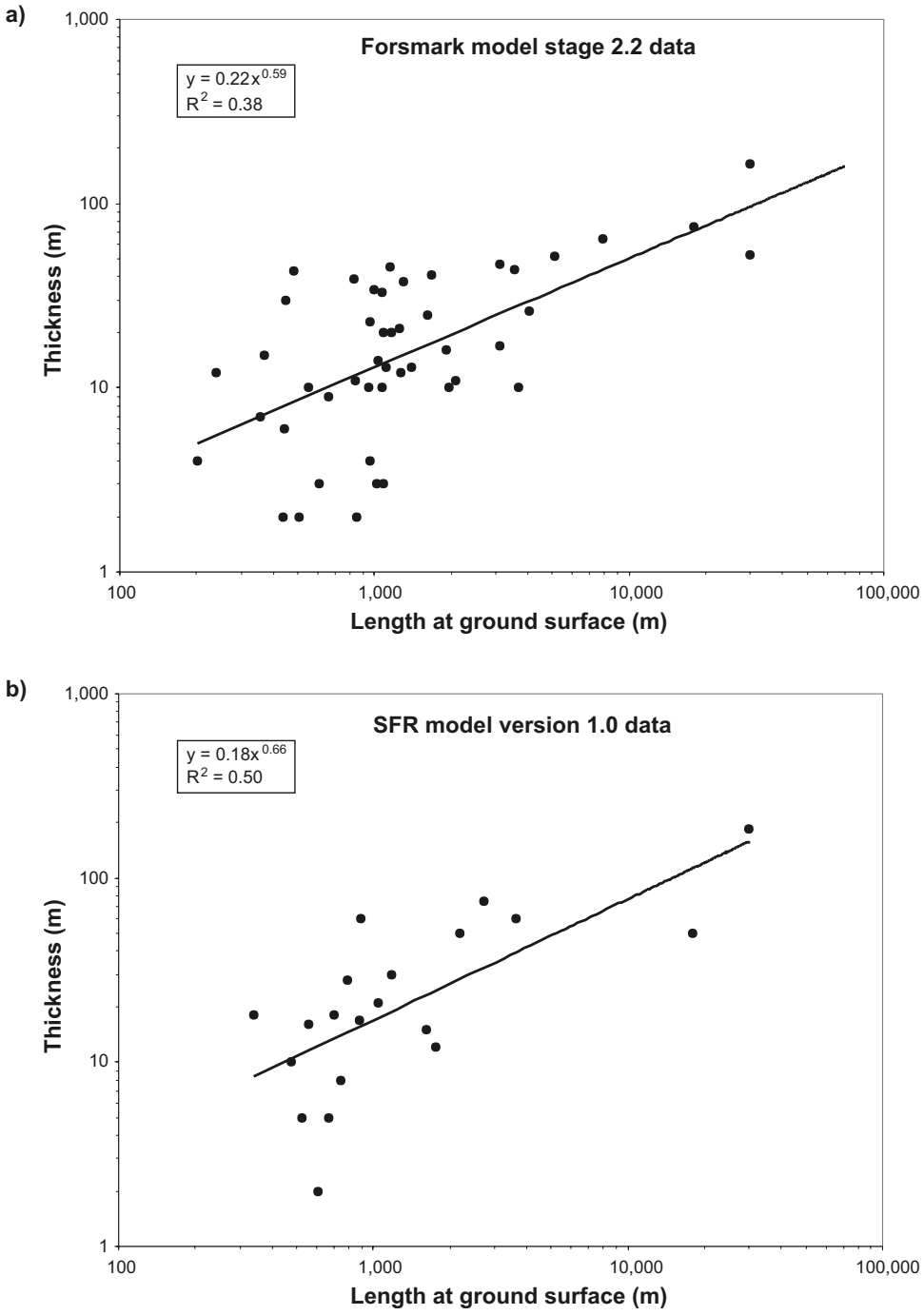

Figure 5-5. *Power law correlation diagrams between thickness and ground surface length of deterministic deformation zones, based on (a) Forsmark model stage 2.2 data /Stephens et al. 2007/ and (b) data for all SFR version 1.0 deformation zones with modelled thicknesses listed in Table 5-1.*

5.3.5 Deformation zone depth cut-off classes

A requirement of the SFR deformation zone modelling has been the application of a deformation zone termination depth versus length classification. Earlier SKB modelling work has followed the general principle that a deformation zone should be modelled to a depth equal to the length of the zone's surface trace. This principle, in combination with the selected local and regional modelling scales and model volume lower boundaries, means in practice that any steeply dipping zone included in the local model terminates at the base of the local model volume and, in the case of the SFR regional model constraints, any steeply dipping zone included in the regional model terminates at the base of the regional model volume. In this way, the systematic division between stochastic and deterministic modelling is maintained. For the combined regional and local deformation zone model the following general classification grouping has been applied:

Zone (lineament) length (m)	Cut-off depth (–masl)
≥ 1,000	1,100
999–500	750
≤ 500	500

Individual deformation zone lengths and cut-off depths for all zones in the model are presented in Table 5-1. As documented in Table 5-1, if a longer zone that belongs to a deeper cut-off depth class terminates against a shorter zone that belongs to a shallower class, then the cut-off depth of the shorter zone has been increased.

5.4 Assignment of properties

A summary of the basic geometrical properties of each of the 40 deformation zones that intercept the regional model volume is presented in Table 5-1. The basis for the interpretation of all these is presented in the property tables in Appendix 11. Some general remarks on the properties of deformation zones that are located inside the local scale model are provided below.

5.4.1 Orientation, length (size) and thickness

The orientation of the deformation zones in the zone descriptions and property tables, i.e. the quoted strike and dip in Table 5-1 and Appendix 11, is the average modelled value provided in RVS based on the input modelling constraints. This means that these values are relevant to the scale of the modelled objects since orientation, like most other parameters, is closely linked to the scale of observation. In practice, the presented strike is an average value of the trend of the associated surface lineament that has been used as input data to RVS and the dip has been constrained by the modeller, or calculated based on the resultant geometry from a series of control points, mostly borehole intercepts.

Any estimate of deformation zone length, like thickness, is closely related to the scale of interpretation. This entity implies the overall traceable length of the surface expression of the interpreted deformation zone. The assessment of geological length is not terminated along, or restricted to, the local or regional scale model boundaries. It is anticipated that such length estimates only give a rough indication of deformation zone size, since such values clearly vary with the elevation of measurement and the interplay with neighbouring (intersecting and truncating) deformation zones. Any estimate of deformation zone or lineament length implicitly involves a judgement of continuity related to the scale of assessment and the realization that deformation zone geometries are not fully continuous in reality. For the local SFR model version 1.0, a minimum deformation zone trace length of 300 m has been applied. Structures with a surface trace length of less than 300 m have not been modelled deterministically. Lineaments with lengths greater than 1,000 m have been taken to represent local major or regional deformation zones, whereas lineaments shorter than 1,000 m have been assumed to represent minor deformation zones, in accordance the terminology of /Andersson et al. 2000/. For the regional model, a minimum deformation zone trace length of 1,000 m has been applied. The length of the deterministic zones is presented in Table 5-1 and Appendix 11. Uncertainties concerning the modelled zone lengths are further discussed in Section 5.6.

Table 5-1. Table showing geometry of deformation zones present inside the regional and local model volumes.

DZ Name	Confidence level	Present in regional model	Present in local model	Strike (°)	Dip (°)	Thick-ness (m)	Length (m) at ground surface	Lower cut off depth (–masl)	Comment
Gently dipping DZs									
ZFM871	H		x	074	19	20	–	–	No surface intersection. Irrespective of its limited modelled extent, it is recommended that this zone should be included in both local and regional modelling studies.
ZFMA1	M	x		082	45	40	–	1,100	No surface intersection.
ZFMB10	L	x		025	35	10	–	1,100	No surface intersection.
Steeply dipping DZs									
NNE to ENE set									
ZFMNNE0725	H	x		201	84	12	1,763	1,100	
ZFMNNE0869	H		x	201	86	60	898	1,100	Depth class increased from 750 m since longer/deeper zones terminate against it.
ZFMNNE2308	M	x		214	80	15	1,250	1,100	
ZFMNNE3130	M	x		030	90	5	411	750	Depth class increased from 500 m since longer/deeper zones terminate against it. Only included in the combined model version as a termination surface. It lies outside the local model volume and has a length of < 1,000 m.
ZFMNNE3264	M	x	x	031	90	10	1,128	1,100	
ZFMNNE3265	M	x	x	032	90	10	1,103	1,100	
ZFMNNE3266	M	x	x	034	90	10	1,015	1,100	
ZFMNE0870	H		x	232	76	16	559	750	
ZFMNE3112	H		x	233	89	10	474	500	
ZFMNE3118	H		x	044	84	8	743	750	
ZFMNE3134	M		x	041	90	5	370	500	
ZFMNE3137	H		x	230	90	5	672	750	
ZFMENE3115	H		x	236	84	28	793	1,100	Depth class increased from 750 m since longer/deeper zones terminate against it.
ZFMENE3135	M		x	081	90	5	368	750	Depth class increased from 500 m since longer/deeper zones terminate against it.
ZFMENE3151	M		x	074	90	5	421	500	
ZFMENE8031	M		x	063	90	5	537	750	
ZFMENE8034	M	x		067	90	10	1,203	1,100	
WNW to NW set									
ZFMWNW0001	H	x		120	90	185	30,000	1,100	
ZFMWNW0813	H	x		115	90	75	2,715	1,100	
ZFMWNW0835	H	x	x	118	88	21	1,044	1,100	
ZFMWNW0836	M	x	x	117	90	50	4,868	1,100	
ZFMWNW1035	H	x		120	80	15	1,622	1,100	
ZFMWNW1056	M	x		110	90	10	2,758	1,100	
ZFMWNW3259	H	x		117	90	50	2,174	1,100	
ZFMWNW3262	H		x	116	86	2	610	750	
ZFMWNW3267	H		x	122	90	18	698	750	
ZFMWNW3268	M		x	109	90	5	861	750	
ZFMWNW8042	H		x	116	89	5	524	750	
ZFMWNW8043	M		x	124	90	10	775	750	
ZFMNW0002	H	x		310	90	50	18,000	1,100	
ZFMNW0805A	H	x	x	312	82	60	3,643	1,100	
ZFMNW0805B	H	x	x	315	75	30	1,181	1,100	
NNW to NS set									
ZFMNNW0999	M		x	170	90	5	692	750	
ZFMNNW1034	H		x	337	78	17	883	750	
ZFMNNW1209	H		x	151	83	18	341	500	
ZFMNNW3113	M		x	173	90	5	376	500	
ZFMNS3154	M		x	180	90	10	757	750	

The estimates of deformation zone thickness presented in Table 5-1 and Appendix 11 refer to true thickness. More specifically, the single thickness values given in the property tables in Appendix 11 refer to modelled true thickness. This means that a value has been assigned that aims to provide a representative overall thickness applicable over the entire length of the zone in the deterministic model. This modelled deformation zone thickness makes use of the geometrical intercepts listed in the property tables and defined in Figure 5-4. It is based on all available data. The thickness estimates include deformation zone cores, damage zones and, to a certain extent, even local splays.

5.4.2 Deformation style

An indication as to whether an individual deformation zone has a ductile, brittle or composite ductile and brittle character is indicated in the property tables and deformation zone descriptions presented in Appendix 11.

5.4.3 Alteration

Red staining caused by a fine-grained dissemination of hematite is associated with a majority of the deformation zones. This type of alteration and the occurrence of other types of alteration, including quartz dissolution, are described in Section 4.3.3 and documented in the property tables in Appendix 11.

5.4.4 Fracture properties

Orientation

Where ever data are available, Terzaghi-corrected fracture stereograms are presented for the individual borehole target intercepts. Only fractures visible in BIPS are included. Open/partly open and sealed fractures are differentiated. Additionally, summary plots of fracture data from all target intercepts included in the individual zone's interpretation have been compiled. If available, data from cored boreholes are presented exclusively and not mixed with data from percussion boreholes. Clustering has been analysed by the definition of both hard and soft sectors (see Appendix 11 for further details).

Frequency

Terzaghi-corrected fracture frequency P10 plots are provided in the property tables where the underlying data is available. Open and sealed fracture frequencies are presented separately in an attempt to provide at least a general indication of fracture condition and character within the deformation zone (see Appendix 11 for further details). A summary of mean fracture frequencies in deformation zones and in the general rock mass is presented in Table 5-2. Further analysis of open and partly open fractures are provided by /Öhman and Follin 2010/.

Crush zones

The position and extent of crush zones are indicated in the borehole P10 fracture plots included in the property tables (Appendix 11) where such data are available i.e. from the interpreted SHI PDZ's of newer cored boreholes completed during the recent drilling program.

Mineralogy

Histograms of fracture fillings identified in the individual borehole target intercepts are included in the property tables. In addition, summary plots of fracture infilling data from all target intercepts included in the individual zone's interpretation, have been compiled. If available, data from cored boreholes are presented exclusively and not mixed with data from percussion or older cored boreholes. The plots differentiate between open/partly open and sealed fracture infillings. In data from older boreholes, this information is plotted as 'broken' or 'unbroken', in accordance with the limitations of the mapping technique applied at that time.

Table 5-2. Summary of mean fracture frequencies per meter of mapped drill core for individual deformation zones, deformation zone sets, total rock mass inside / outside deformation zones, rock domains RFR01 and RFR02 and for the entire rock volume. Mean fracture frequencies for deformation zones are based on multiple borehole target intercepts. For conversion of crushes and sealed networks into fracture frequencies see Appendix 11.

	Open	Partly open	Crush equivalent	Total (open + partly open + crush equiv.)	Sealed	Sealed network	Total (sealed + sealed network)
Deformation zone							
ZFMENE3115	7.66	0.47	1.56	9.69	20.43	10.11	30.54
ZFMNE3112	8.53	0.25	1.39	10.17	13.84	14.50	28.34
ZFMNE3118	7.05	0.59	0.00	7.64	5.69	17.58	23.26
ZFMNE3137	6.44	0.41	0.23	7.08	16.87	14.69	31.56
ZFMNNW1034	6.93	1.62	0.17	8.72	25.35	17.49	42.84
ZFMNW0805A	8.17	1.22	0.51	9.90	7.27	23.40	30.67
ZFMNW0805B	10.56	2.00	0.16	12.72	11.29	45.72	57.01
ZFMWNW0001	8.06	0.34	1.15	9.56	21.00	20.69	41.69
ZFMWNW0813	6.29	0.56	0.35	7.20	30.59	6.94	37.53
ZFMWNW0835	9.49	2.40	1.81	13.70	9.84	10.75	20.59
ZFMWNW3259	6.88	0.55	0.24	7.67	26.38	16.55	42.93
ZFMWNW3262	12.78	0.88	5.11	18.77	19.37	0.91	20.28
ZFMWNW3267	8.25	1.22	0.34	9.81	10.88	15.57	26.45
ZFMWNW8042	11.39	0.00	2.82	14.21	6.05	49.02	55.07
Deformation zone set							
NNE to ENE set	7.62	0.41	1.15	9.18	16.85	12.71	29.56
N-S to NNW set	6.93	1.62	0.17	8.72	25.35	17.49	42.84
WNW to NW set	7.95	0.86	0.91	9.72	19.44	17.03	36.47
Inside / outside deformation zones							
Inside DZs	7.82	0.84	0.90	9.55	19.43	16.32	35.75
Outside DZs	4.39	0.45	0.05	4.89	12.63	5.92	18.55
Rock domains outside DZs							
RFR01	3.32	0.24	0.01	3.57	5.75	7.43	13.18
RFR02	3.44	0.33	0.05	3.82	10.14	3.35	13.50
Entire rock volume including both inside and outside deformation zones							
Inside and outside DZs	5.51	0.58	0.33	6.41	14.85	9.32	24.17

Kinematic properties

Kinematic studies have been performed during the Forsmark site investigation and details are available in /Stephens et al. 2007/ and /Stephens et al. 2008b/. Some of the general conclusions drawn from these studies are considered applicable to the current project and are included in the characterization of the various deformation zone orientation sets presented in Section 5.5.

5.5 Character of different sets of zones

The earlier work associated with the Forsmark site investigation identified four orientation sets of deformation zones based on their geological character /Stephens et al. 2007/. This subdivision has been confirmed and has been maintained in the current report. A generalised summary of the character of each set or sub-set is presented below. Examples of the typical visual appearance of the different sets is indicated by drillcore photographs (Figure 5-6). Details concerning the individual deformation zones are presented in Appendix 11. Possible deformation zones in the SHI work that could not be included in the deterministic model are also described.

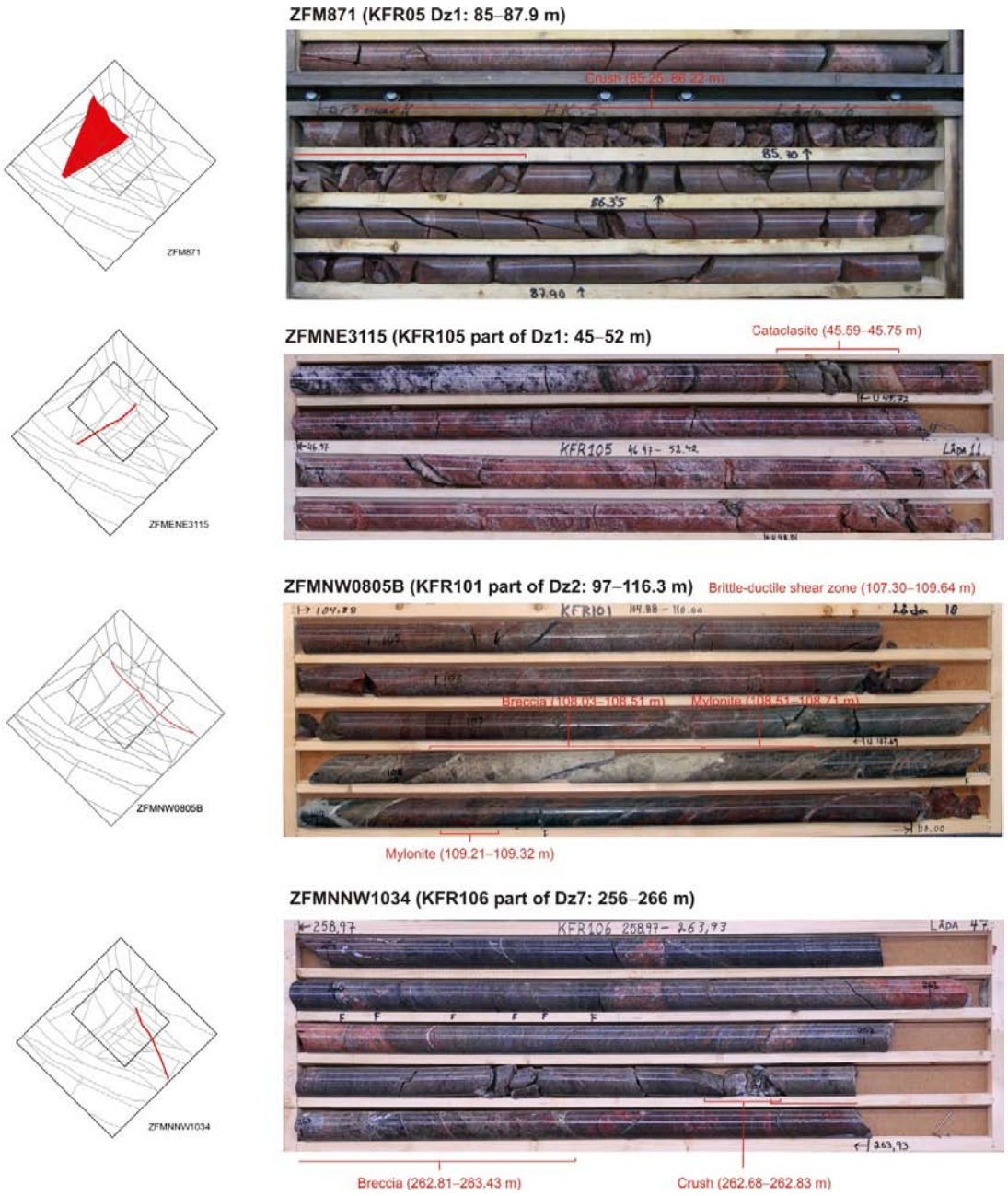

Figure 5-6. *Character of deformation zones in the four orientations in the SFR area, illustrated by drill core photographs of representative zone intersections. The position of each zone relative to the other modelled deformation zones and the SFR model boundaries are also included. ZFM871 (074°/19°): High frequency of open fractures and a crushed interval of almost 1 m length. ZFMNE3115 (236°/84°): Increased frequency of especially sealed fractures and sealed fracture networks, along with cataclasite. Frequent minerals in sealed fractures are calcite and laumontite. ZFMNW0805B (315°/75°): High frequency of both open and sealed fractures and a section of intense brittle-ductile deformation, which includes one interval with breccia and two intervals of mylonitization. ZFMNNW1034 (337°/78°): Increased frequency of sealed and locally open fractures, one crushed interval and one with breccia.*

5.5.1 Vertical to steeply dipping WNW to NW set

Members of this set of zones fall within the local minor to regional deformation zone size ranges, according to the terminology of /Andersson et al. 2000/. The set includes the dominant regional deformation zones that can be said to define the northern and southern boundaries of the SFR central block (Figure 5-7). It also includes the largest and oldest zones in the region and their initial activation is inferred to be related to late-stage Svecokarelian tectonic activity at c. 1.85 Ga /Stephens et al. 2007/. It is this set that has been subject to most reactivation cycles.

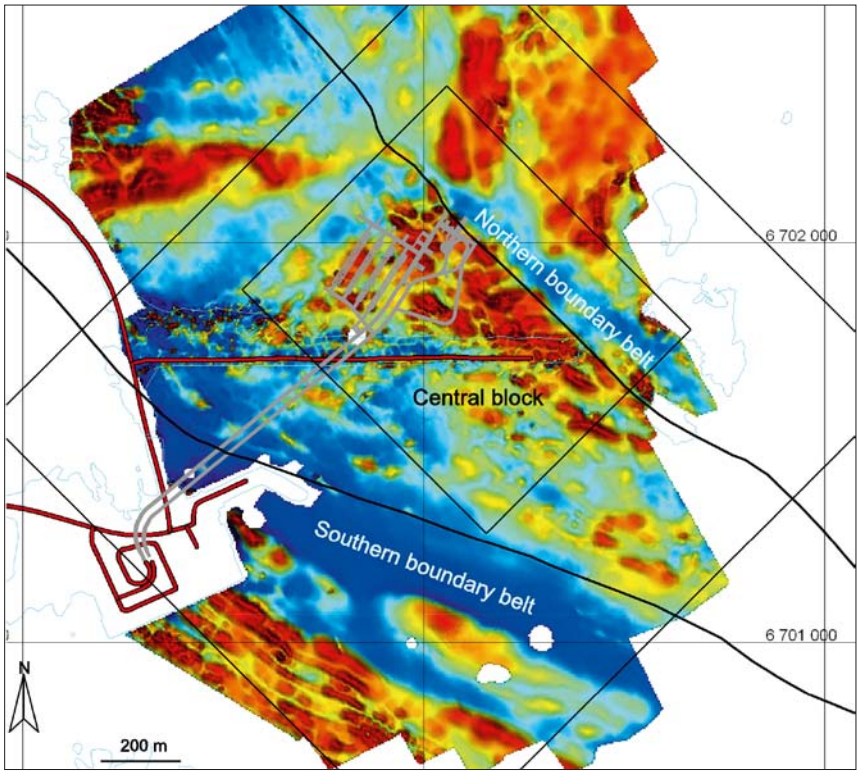

Figure 5-7. *The central SFR block containing the existing SFR storage facility, the northern boundary belt (dominated by ZFMNW0805A) and the southern boundary belt (dominated by ZFMWNW0001), along with the magnetic total field.*

The zones in the vertical to steeply dipping WNW to NW set are generally composite features, characterised by an initial development in the ductile regime followed by brittle reactivation. It is the only set that exhibits ductile deformation. The majority of the fractures are sealed and mylonites, cataclasites and cohesive breccias occur locally, especially in the most prominent zones in the set, i.e. ZFMWNW0001 and ZFMNW0805A. The bedrock within these zones is typically affected by a varying degree of oxidation. Two of the five deformation zones with occurrences of quartz dissolution (vuggy granite) belong to the WNW to NW set: ZFMNW0805A and ZFMWNW0835.

Besides the more common minerals calcite and chlorite, epidote, quartz, adularia, laumontite and clay minerals dominate the mineral fillings and coatings along the fractures in these zones (Figure 5-8). They represent examples of minerals from the oldest generation 1 and the younger mineral generations (see Section 4.5.4).

The kinematic studies completed during the Forsmark site investigation indicate that the brittle deformation along these zones occurred under different compressive stress regimes, including NW-SE to N-S and younger NE-SW and WNW-ESE compressive phases with evidence of both dextral and sinistral strike-slip movement, as well as subordinate reverse and normal dip-slip movement. Details are available in /Stephens et al. 2007, 2008b/.

The zones of this group contain a dominant cluster of steeply dipping fractures that strike WNW-ESE (Figure 5-9). While the majority of these fracture are sealed, a significant proportion are also open (Figure 5-9). There is also a cluster of fractures that are almost exclusively sealed and strike NE-SW with steep dips to the north-west, and a sub-horizontal cluster of mixed open and sealed fractures (Figure 5-9). The mixed sealed and open nature of some of the fracture clusters is inferred to be related to their development throughout geological time and possibly even to the current in situ stress regime. The inferred oldest set, with steep WNW-ESE strike, dominates and has been subject to the most reactivation cycles. This set is now more or less parallel to the maximum horizontal stress, which has a tendency to maintain the openness of these fractures. In contrast, the steep NE-SW set, perpendicular to the current maximum horizontal stress, tends to be sealed. The sub-horizontal set may have developed at the same time as the steeply dipping fracture sets, but their planes of weakness may have been exploited by loading/unloading cycles and, at relatively shallow depths, these fractures will have a tendency to be open.

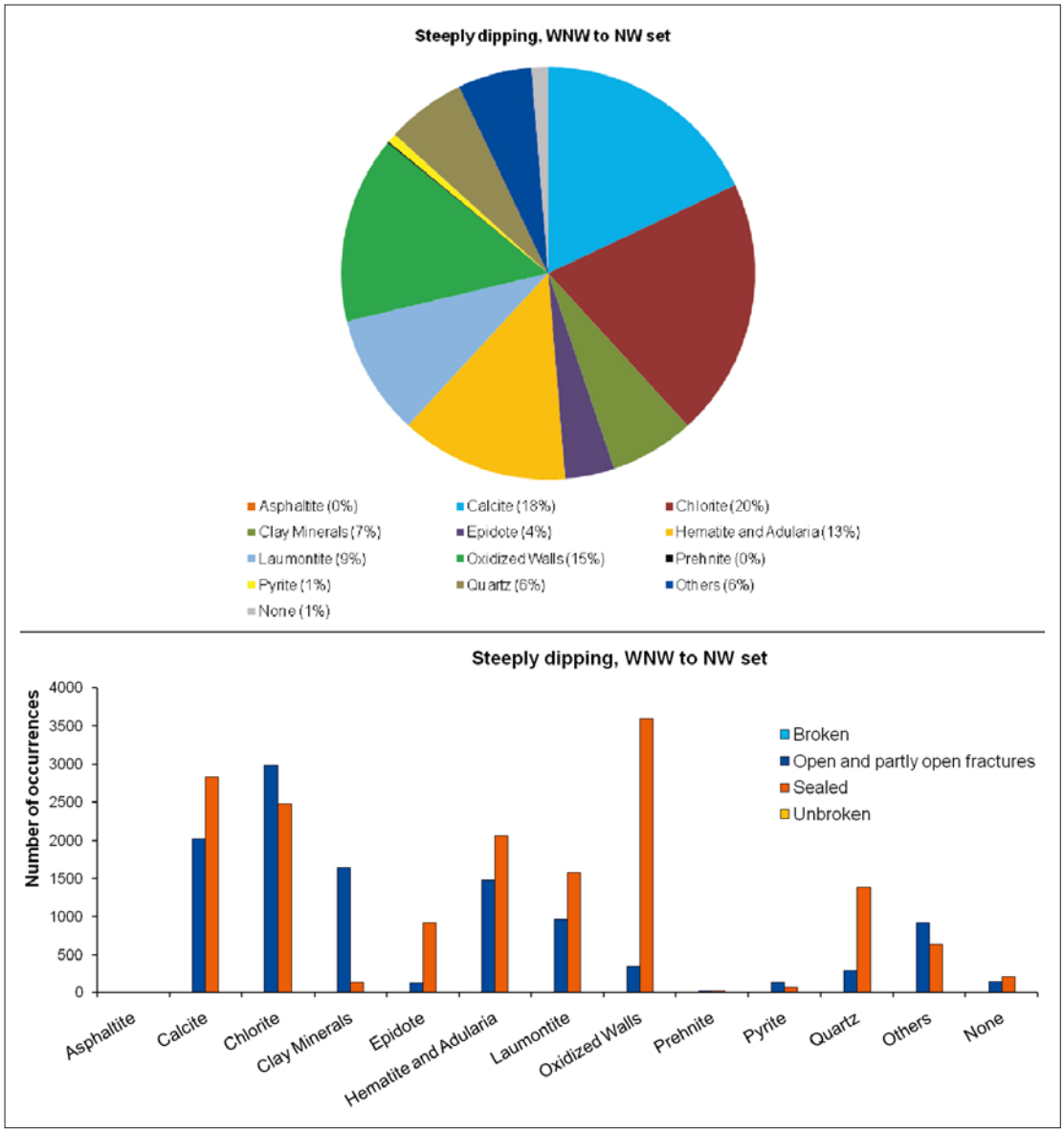

Figure 5-8. *Mineral infillings of fractures lying within the zone boundaries (target intercepts) of the WNW to NW set.*

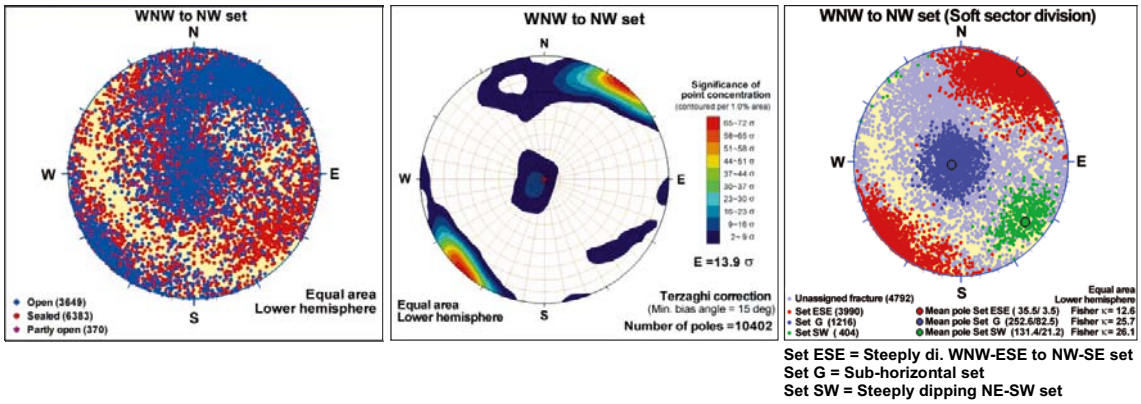

Figure 5-9. *Fracture clustering within the WNW to NW oriented deformation zones. All plots utilize a lower-hemisphere, equal-area projection, with a Terzaghi correction of the kamb-plots.*

Southern belt (ZFMWNW0001 and splays)

In the southern part of the SFR regional model area, in the vicinity of the SFR tunnels, ZFMWNW0001 along with ZFMWNW0813, ZFMWNW3259, ZFMNW0002 and, to a lesser extent, ZFMWNW1035, merge to comprise a complex broad deformation 'belt' (Figure 5-10). This can be seen in the detailed tunnel excavation mapping /Christiansson and Bolvede 1987/ and the SHI results of KFM11A (Figure 5-11). The SHI of KFM11A defined a single extensive PDZ with a borehole length of 579 m. This single PDZ and the corresponding tunnel sections have been the subject of more detailed analysis presented in /Stephens et al. 2008b/ and /Glamheden et al. 2007/, respectively. The results of both these studies have been taken into account in the present modelling and, while adjustments have been made, the essential interpretation remains the same, i.e. ZFMWNW0001 forms the core of the deformation belt while the other zones have lateral positions to the north and south. In the SFR tunnels and along KFM11A, the zones essentially merge and make subdivision difficult and somewhat artificial while, away from the tunnels, the magnetic data and subsequent lineament interpretation suggest the zones diverge somewhat and define more discrete structures.

The dominant zone, ZFMWNW0001, referred to as the Singö deformation zone in earlier SFR models, is a major regional deformation zone interpreted as having a total length of c. 30 km. The version 1.0 interpretation is largely based on that presented in /Stephens et al. 2007/, itself based on earlier work by /Christianson 1986, Axelsson and Mærsk Hansen 1997/. However, the position of the Singö deformation zone and nearby splays have been modified slightly based on the updated interpretation of lineaments during Forsmark stage 2.3 /Isaksson et al. 2007/. Furthermore, very local adjustments have been made to the lineaments to define the zone traces at the ground surface based on the SFR tunnel and KFM11A mapping, in the area where the magnetic field is disturbed by man-made structures. The thicknesses have also been modified with reference to the mapping in the SFR operation (DT) and construction (BT) tunnels and KFM11A. A thickness of 165 m with a thickness span of 53–200 m was indicated by /Stephens et al. 2007/. The thickness of 185 m presented here lies well within the earlier defined span.

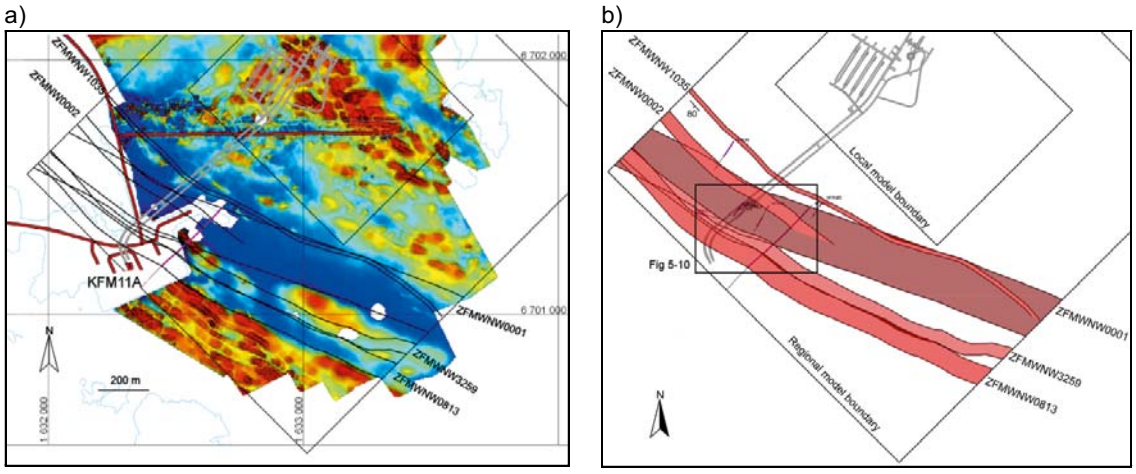

Figure 5-10. *Intersection at the current ground surface of modelled deformation zones of the southern boundary tectonic belt relative to the local and regional model areas; (a)with and (b) without the total magnetic field. Local details along the tunnel section are shown in Figure 5-11.*

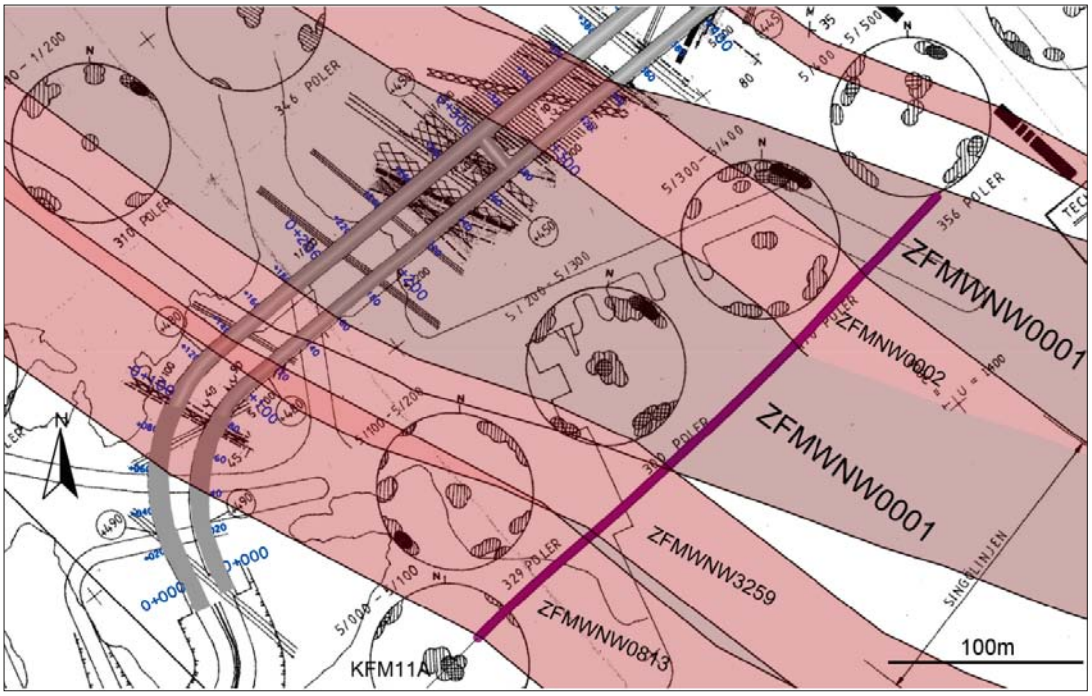

Figure 5-11. *In the southern part of the SFR regional model area, in the vicinity of the SFR tunnels, ZFMWNW0001 along with ZFMWNW0813, ZFMWNW3259, ZFMNW0002 and, to a lesser extent, ZFMWNW1035 merge to comprise a complex broad deformation 'belt' as can be seen in the detailed tunnel excavation mapping /Christiansson and Bolvede 1987/ and the SHI results from KFM11A, marked by a violet cylinder. Note KFM11A has a bearing of 004°, dip of 61° and length of 851m.*

Northern belt (ZFMNW0805A and splays)

A secondary deformation belt that has the same orientation and character as the Singö belt to the south, but is much smaller is situated to the north of the central block around SFR. On a larger regional scale, the magnetic data suggest that it is probably a splay from the main Singö deformation zone or, at least, is a member of the same WNW to NW system of deformation zones.

The northern belt comprises ZFMNW0805A and a smaller splay ZFMNW0805B (Figure 5-12). ZFMNW0805A with a length between 3 and 4 km and a thickness of 60 m, has the same sequence of ductile deformation followed by brittle reactivation that is seen in the southern belt. ZFMNW0805B has the same character as the main zone, and merges with ZFMNW0805A at both its north-western and south-eastern ends. It has also been modelled to merge with the main zone at depth, although this is conceptually based rather than being based on deterministic evidence. As described earlier in /Curtis et al. 2009/, the position of the deformation zone traces at the ground surface have been locally adjusted in comparison to the magnetic lineaments based on the scale of the modelling and conceptual thinking. However, all such adjustments have been made with input and review by the original geophysical lineament interpreters. The complex nature of the surface expression of the northern belt can be inferred from the total magnetic field shown in Figure 5-12. It is reasonable to assume that this complex character is similarly at greater depths.

ZFMNW0805B, as it is included in the present model, intersects both the existing BT and 1B tunnels (see Figure 3-3 for tunnel abbreviations). These tunnel geometrical intercepts are considered to be of very low confidence and are a result of a higher priority being given to borehole SHI information from KFR7A and KFR08. The tunnel mapping itself provides only very weak and partial support for this interpretation. However, the major zones of this set are complex structures characterised by considerable heterogeneity. Thus, well-defined structures in nearby boreholes do not necessarily imply that the structures are of the same dignity in the tunnels. An alternative to the geometry presented in the model is also possible, based on a closer correlation with lineaments and an alternative correlation with borehole data. This alternative model gives rise to a thinner zone without tunnel intercepts.

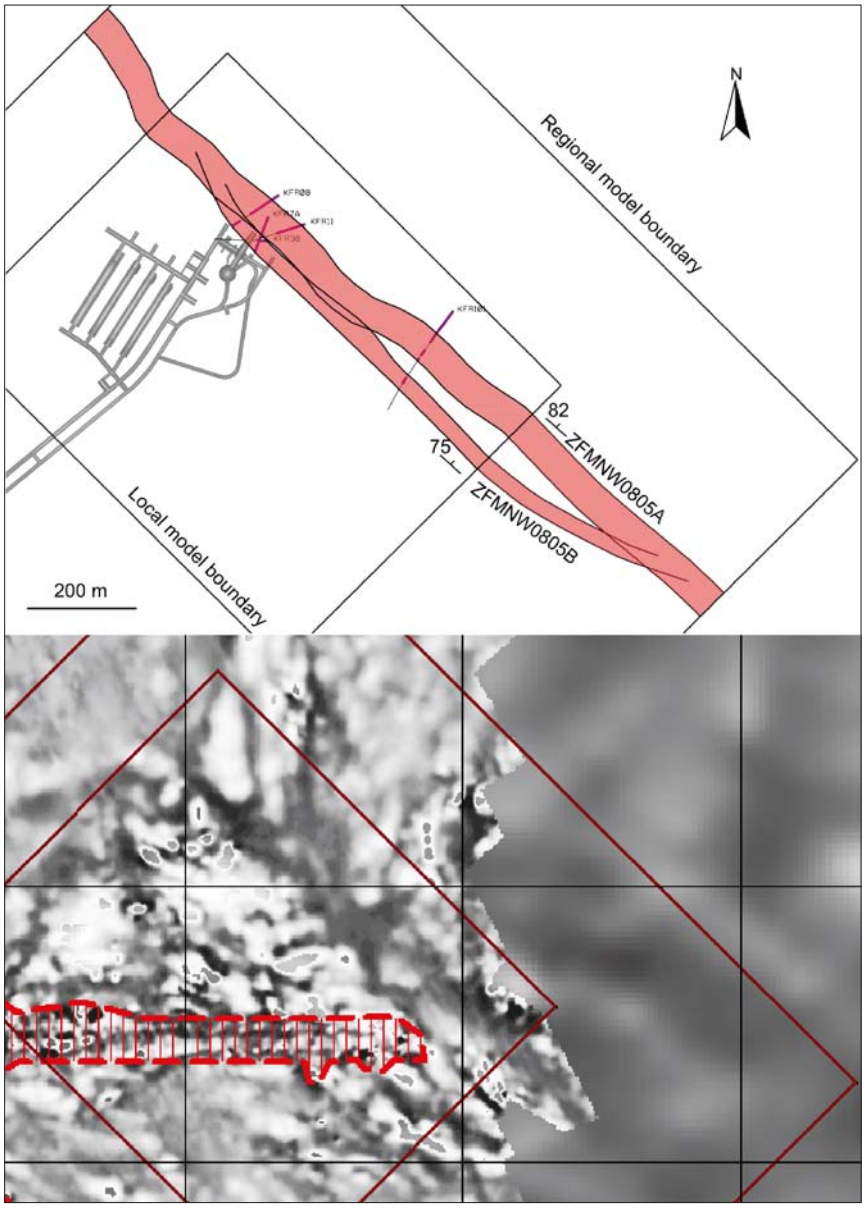

Figure 5-12. *(Top) Intersection at the current ground surface of modelled deformation zones of the northern boundary tectonic belt. (Bottom) A map of the first vertical derivative of the magnetic total field from measurements on land, at sea and via helicopter. Note the complex nature of the surface expression of ZFMNW0805A and B. Area of disturbance caused by the pier, affecting the magnetic total field, is shown in dashed red.*

WNW to NW zones within the central block

There are six zones that belong to the WNW to NW set of structures in the central area, four with high confidence and two with medium confidence in existence. They are relatively short or at least their traceability is restricted with lengths ranging from 524 to 1,044 m (Figure 5-13) and can be considered second order zones in terms of size compared to the regionally dominant northern and southern belts. Zones of this type could have formed more or less simultaneously with zones with ENE, NE or NNE strike according to the conceptual understanding of the development of the deformation zones at the Forsmark site /Stephens et al. 2007/.

None of these brittle zones have been modelled to intersect the existing SFR facility. They occur in the south-eastern part of the local model volume, but are modelled to terminate against various ENE to NE trending structures that are also brittle in character.

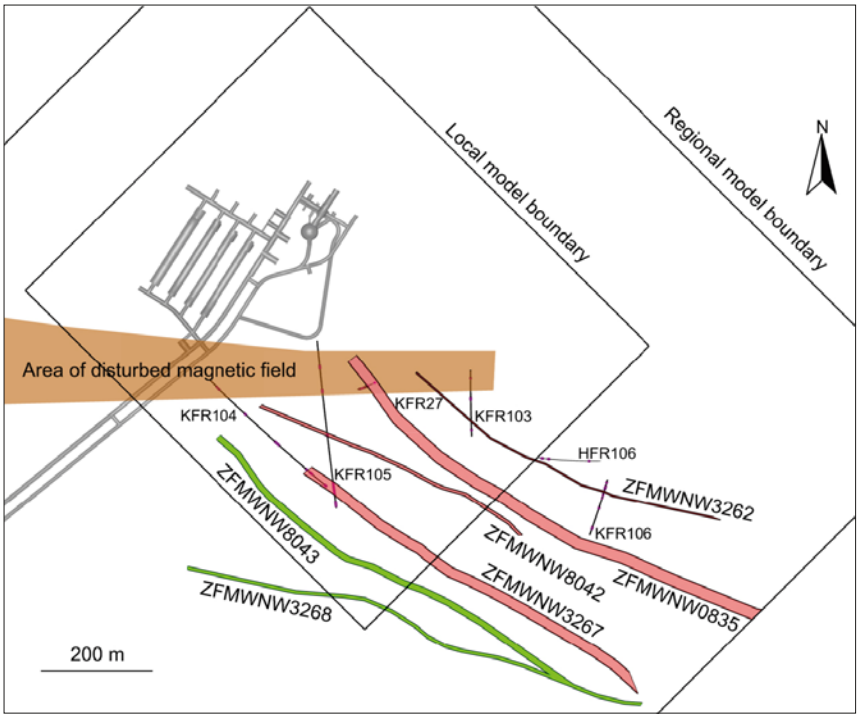

Figure 5-13. *Intersection at the current ground surface of modelled deformation zones of the WNW to NW group lying within the central block (all zone dips are greater than 85°). The different colours refer to confidence in existence: red=high (based on direct observations in boreholes or tunnels, complemented by geophysical data); green=medium (based solely on interpretation of geophysical data).*

Inspection of the map of interpreted lineaments (Figure 4-20) indicates what appears to be a change in character in the rock mass in the general area along zone ZFMENE3115 (Figure 5-2b). To the north-west of this area, above the existing SFR facility, there are virtually no WNW to NW trending lineaments lying within the central block. However, one or more of the zones may indeed extend further to the north-west but this has not been inferred in the current model. Problems of traceability involve the associated magnetic lineaments and anomaly pattern that becomes disrupted by both the man-made pier and changes in the dominant rock types when approaching from the south-east of the pier area. Figure 4-21 compares the lineaments from the earlier Forsmark site investigation and those from the current SFR version. This comparison highlights the uncertainty in the interpretation of lineaments in this area. For this reason the current modelling work has investigated all the lineaments from both interpretations as well as considering further local alternatives when searching for potential correlation with the underlying extensive tunnel mapping and borehole data.

A series of minor structures with similar orientation to those south-east of the pier may well be present in the existing facility and, to a limited extent, are indicated in the mapping as described below. It is possible these extents may have been underestimated in the existing facility, since the zones were of reasonable rock engineering quality and were not judged, at the time, to be very significant for the excavation. Figure 5-14 shows the traces of sub-vertical structures with strikes NNE-ENE and WNW-NW based on tunnel mapping by /Christiansson and Bolvede 1987/. The position, orientation and extents are taken directly from drawing –103 of /Christiansson and Bolvede 1987/, as included in Appendix 2. Inspection of the detailed mapping drawings suggests the figure cannot be used to draw conclusions concerning the relative terminations of the different structures. However, the figure does give an indication of the general frequency and continuity of these sized structures with these general orientations in the existing SFR facility. The mapping indicates a paucity of WNW-NW striking deformation zones and none that penetrate the full width of the central storage area, comprising the four rock caverns and tunnels, and continue in a south-easterly direction into the rock volume intended for the storage facility extension. There are four possible candidate tunnel deformation zones (tDZ's), which were considered for extrapolation and correlation with the modelled structures further to the south east. However, such extrapolation was not considered justified. These tDZ's are labelled 43, 48, 54 and 96 in Figure 5-14 and the detailed drawings for each of them are shown in Figure 5-15.

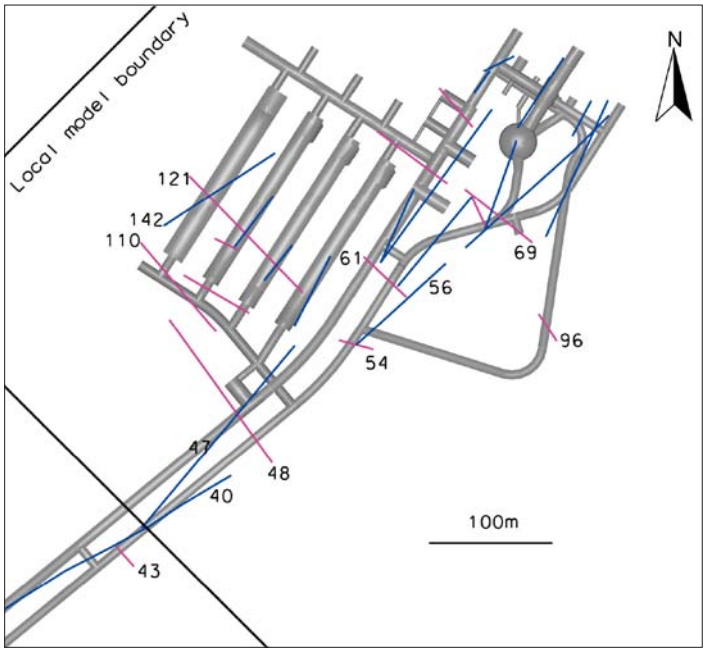

Figure 5-14. *Traces of sub-vertical structures (tDZ's) lying in the so-called central block, striking NNE-ENE (shown in blue) and WNW-NW (shown in pink) based on tunnel mapping by /Christiansson and Bolvede 1987/, as included in Appendix 2. The position, orientation and extents are taken directly from drawing –103 of /Christiansson and Bolvede 1987/. Structures with other dips and orientation have been omitted for clarity.*

TDZ43 is confined to the construction tunnel (BT) and does not extend into the parallel operating tunnel (DT). It is dominated by two short sections of rock (c. 2 m wide) with closely spaced, sub-vertical parallel fractures ('brantstående skivigt berg'). The lack of extension into DT suggests it terminates to the north-west at ZFMNE0870 (tDZ40 in Figure 5-14). TDZ43 is considered a minor structure and there is no borehole or geophysical data to support an extension to the south-east sufficient to warrant its inclusion as a deterministic structure of sufficient size in the model.

TDZ48 is also mapped as a short section (c. 5 m wide) of rock with relatively closely spaced sub-vertical parallel fractures, although the mapping suggests the deformation is less intense compared to tDZ43. It is not considered a very striking feature or a clear deformation zone of sufficient size to warrant inclusion in the model. Borehole data does not support a significant extension of this structure to the south-east, although since borehole coverage is not complete such an extension cannot be ruled out.

TDZ54 is mapped as a relatively broad (c. 12 m) section of rock in the BT with relatively closely spaced sub-vertical parallel fractures. The shotcrete support indicated in the roof of the nearby DT was associated with local sub-horizontal fractures rather than a direct continuation of tDZ54. Attempts were made to model this structure in combination with an overlying geophysical lineament and it was included in version 0.1 of the model /Curtis et al. 2009/. However, subsequent investigation by borehole KFR105 did not support its continuity or existence and consequently it is not included in the current model version.

TDZ96 has been inspected and remapped as part of recent mapping efforts in NBT /Berglund 2009/, and is denoted 8D in Table A2-3, where it is described as a very minor, 0.1 m wide brittle-ductile zone, developed in a narrow amphibolite band. This structure is considered as being below the resolution of the deterministic model and has not been extrapolated and included as a discrete deformation zone.

In summary, it has not been possible, nor is it considered realistic, to correlate the minor structures recorded in the tunnel mapping with the WNW-NW striking deformation zones that occur in the south-eastern part of the model volume. In this context, it should also be emphasized that several of the WNW to NW trending fracture zones registered in the tunnel mapping have dips of 50–60° towards south-west. All four zones in the central block, for which borehole information is available, have inferred dips that exceed 85° and are relatively thin in terms of current SHI methodology.

Figure 5-15. *Sections of the detailed drawings from /Christiansson and Bolvede 1987/, illustrating the structural relationship for tDZ43 (drawing –07), tDZ48 (drawing –08), tDZ54 (drawing –09) and tDZ96 (drawing –16). The general location of the tDZ's of interest lie within the tunnel sections marked by open rhombs. North is up in all four sections and scale is given by the tunnel chainage. For legend see Figure 3-2.*

A more likely alternative interpretation of the frequency and extent of the mapped WNW-NW structures in the central part of the existing SFR facility is that they could be taken to indicate that the continuity of the modelled structures in the central block to the south-east of the existing facility is over emphasized in the current model and that the modelled structures are discontinuous and more like chains with missing links rather than the continuous features included in the model. This is considered possible due to scale issues and the earlier described problems concerning the disruption to the magnetic lineament pattern.

5.5.2 Vertical to steeply dipping NNE to ENE set

The zones in the steep NNE to ENE set that penetrate the SFR central block (Figure 5-16) have the same characteristics as those described by /Stephens et al. 2007/. Compared with the WNW to NW set, the steep NNE to ENE zones penetrating the regional model area are much shorter, with lengths in the range of 368 to 1,763 m, falling within the local minor to local major deformation zone size ranges according to the terminology of /Andersson et al. 2000/.

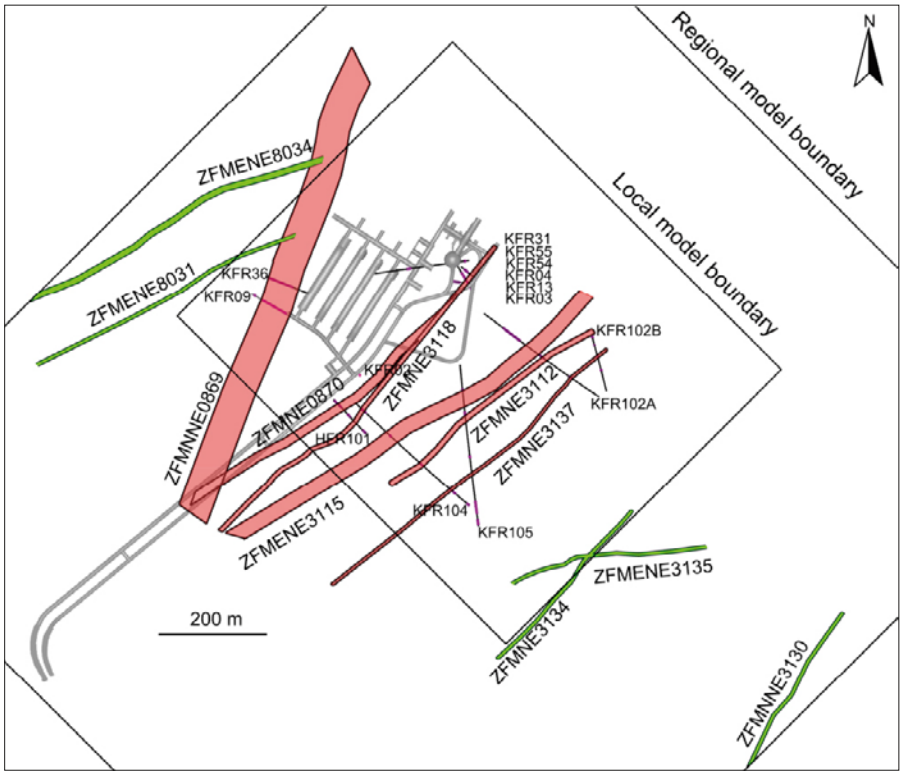

Figure 5-16. *Intersection at the current ground surface of modelled deformation zones of the NNE to ENE group penetrating the central block between ZFMWNW0001 and ZFMNW0805A. The different colours refer to confidence in existence: red=high (based on direct observations in boreholes or tunnels, complemented by geophysical data); green=medium (based solely on interpretation of geophysical data).*

However, their lengths appear to be strongly controlled by existing tectonic structures generally terminating against WNW to NW regional deformation zones (i.e. strong truncation effects). The ENE sub-set additionally shows terminations against the structures in the NNE sub-set and the N-S to NNW set. The steep NNE to ENE zones are generally narrow, with thicknesses of around 5 m to 15 m. There are two clear exceptions of zones with much thicker modelled thicknesses: ZFMNNE0869 with 60 m and ZFMENE3115 with 28 m but, in both cases, the modelled thickness represents more than one structure. They are both interpreted as consisting of a packet or swarm of sub-parallel closely spaced, narrower structures rather than a single discrete zone (see Appendix 11 for details).

The steep NNE to ENE zones formed in the brittle regime and are dominated by sealed fractures. Calcite, chlorite, hematite-stained adularia, laumontite and quartz are conspicuous along the fractures in these zones (mainly generation 2 mineral paragenesis in Section 4.5.4). Younger generation 3 and 4 minerals, for example pyrite and clay minerals, are also present (Figure 5-17). Kinematic studies performed as part of the Forsmark site investigation indicate strike-slip displacement, both sinistral and dextral, consistent with bulk shortening between N-S and NE-SW and approximately WNW-ESE, respectively, as well as subordinate normal and reverse dip-slip movement. Further results and interpretation are presented in /Stephens et al. 2007, 2008b/. Three of the five deformation zones with occurrences of quartz dissolution (vuggy granite) belong to the NNE to ENE set: ZFMENE3115, ZFMNE3118 and ZFMNNE0725.

The steep NNE to ENE zones contain a dominant cluster of steeply dipping, generally sealed fractures that strike NE-SW and a secondary cluster of sealed fractures that are steep and strike NNW-SSE. In addition, more commonly open fracture clusters with sub-horizontal and gentle dips to the south are also present (Figure 5-18).

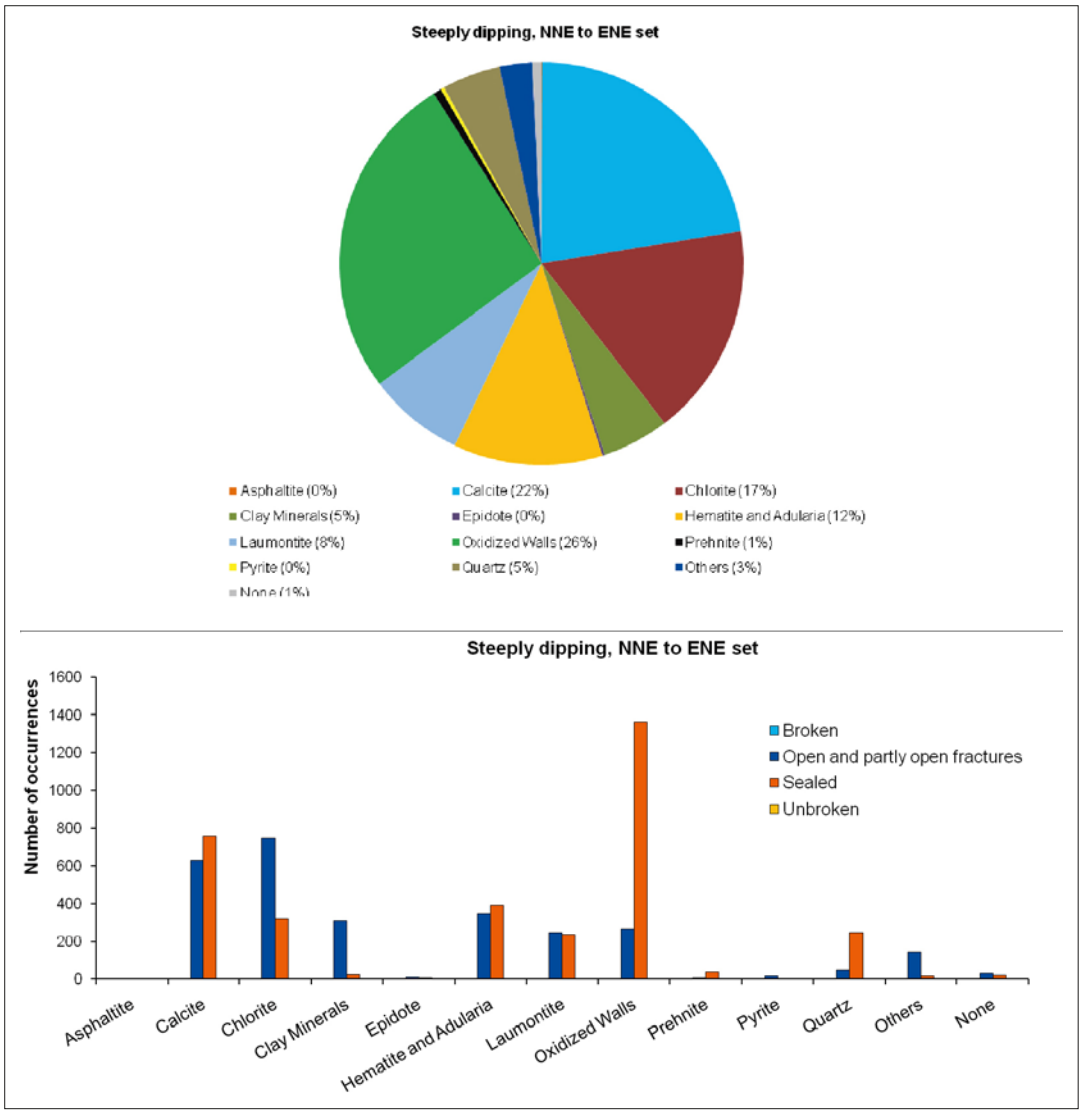

Figure 5-17. *Mineral infillings of fractures lying within the zone boundaries (target intercepts) of the NNE to ENE set.*

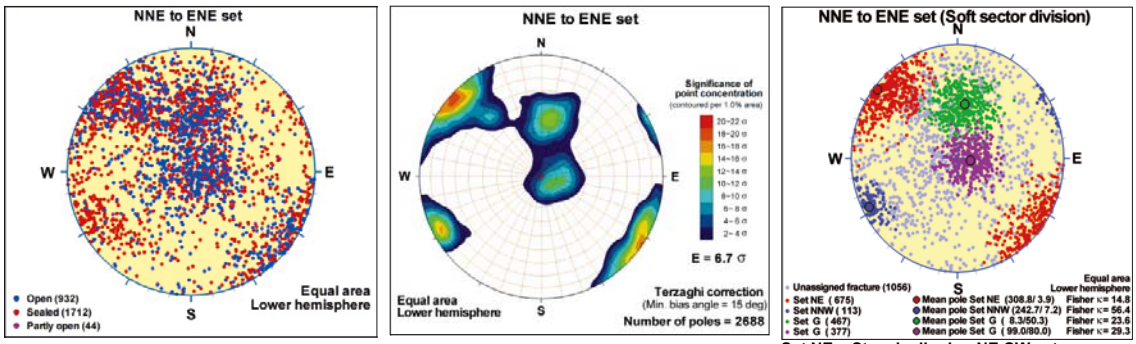

Figure 5-18. *Fracture clustering within the NNE to ENE oriented deformation zones. All plots utilize a lower-hemisphere, equal-area projection, with a Terzaghi correction of the kamb-plots.*

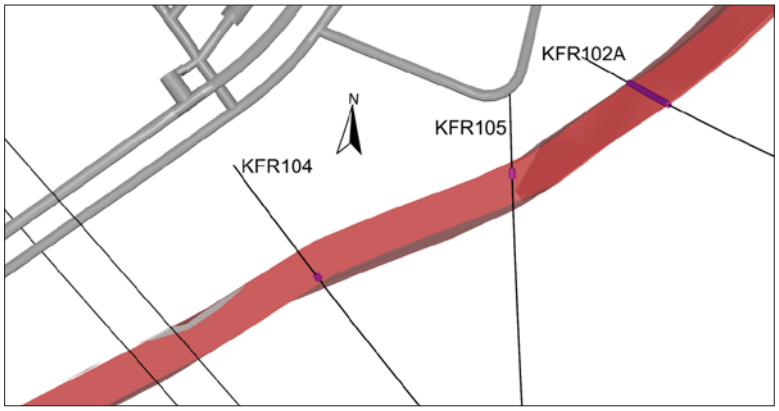

Figure 5-19. *View of ZFMENE3115 (236/84, see Figure 5-16 for zone location) showing the SHI PDZ intercepts (violet cylinders) in KFR102A, KFR104 and KFR105. It should be noted that the modelled zone thickness of 28 m is based on KFR102A DZ3. An alternative interpretation of DZ3 was that it represented more than one zone and this would result in a reduction of ZFMENE3115 thickness to around 10 m.*

Within the central block the ENE sub-set consists of five zones only one of which, ZFMENE3115, has been identified with high confidence with supporting borehole data. This zone is modelled with a steep 84° dip to the NW. The modelled thickness of 28 m is based on the SHI PDZ intercept identified as DZ3 in KFR102A (Figure 5-19). However, an alternative interpretation of DZ3 is possible where it may represent more than one zone and this would result in a reduction of ZFMENE3115 thickness to around 10 m.

The NE sub-set consists of five zones within the central block (Figure 5-16). Four of these zones (ZFMNE0870, ZFMNE3112, ZFMNE3118 and ZFMNE3137) have been identified with high confidence. The zones are relatively thin (5–16 m) and short (370–743 m). They dip steeply both to the north-west and south-east and all terminate against the WNW to NW deformation zone set.

The NNE sub-set consists of six zones, two of which are high confidence and only one, ZFMNNE0869, lies within the central block. Lengths range from 411 to 1,763 m, though the longer values are associated with zones at the edge of the regional model area. The two high confidence zones, ZFMNNE0725 and ZFMNNE0869, have modelled thicknesses of 12 and 60 m, respectively. However, the modelled thickness of ZFMNNE0869 represents a group of thinner, sub-parallel fracture zones, including crushes and alteration, that diverge and converge in a complex pattern rather than a single well-defined zone. Both members of this sub-set dip steeply to the NW and terminate against the NW to WNW deformation zone orientation set.

5.5.3 Vertical to steeply dipping N-S to NNW set

There are five zones in this group, ZFMNNW0999, ZFMNNW1034, ZFMNNW1209, ZFMNNW3113 and ZFMNS3154. Only two of them, ZFMNNW1209 and ZFMNNW1034, lie within the central block and have been identified with high confidence, based on tunnel and borehole data (Figure 5-20). The other three zones lie to the north of zone ZFMNW0805A, the northern boundary belt, and are of medium confidence, being based solely on magnetic lineament interpretation. The members of this group have terminations against all three of the other steeply dipping deformation zone sets.

All the zones in this group that intersect the regional model volume are local minor in size according to the terminology of /Andersson et al. 2000/. The two high confidence zones have similar modelled thicknesses of 17 m and 18 m. However, although the 18 m modelled thickness of ZFMNNW1209 is based on SHI data, evidence for the zone seen in the rock caverns indicates the zone is comprised of a parallel group of thin discontinuous structures rather than a single thick discrete zone with a central core (see Appendix 11 for details).

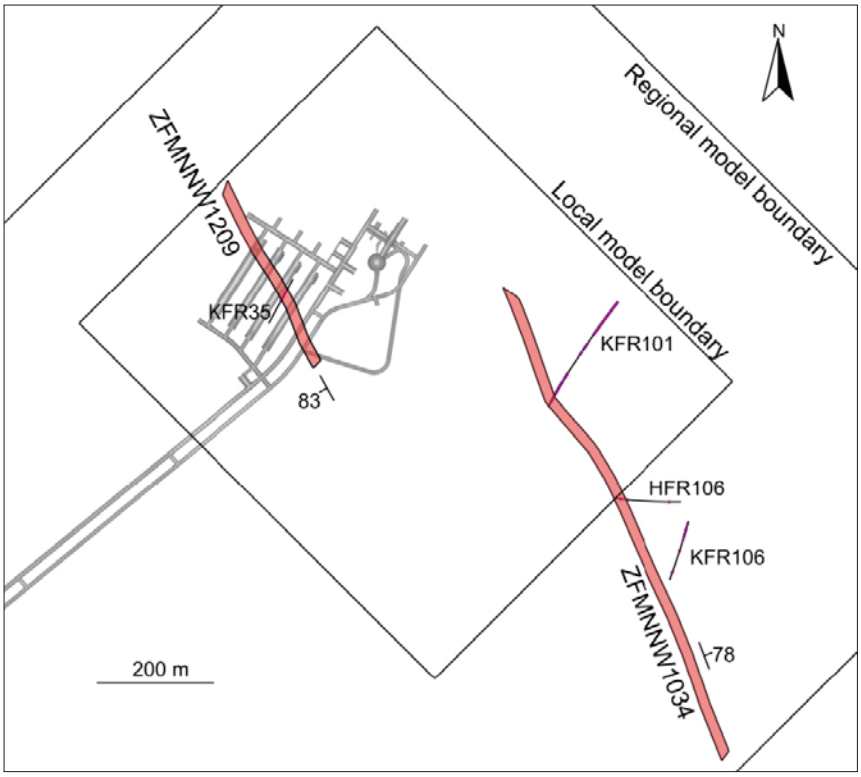

Figure 5-20. *Intersection at the current ground surface of modelled deformation zones of the N-S to NNW deformation zones penetrating the central block between ZFMWNW0001 and ZFMNW0805A.*

These zones are dominated by sealed fractures. Based on the available information, the zones in this group are brittle with minor cohesive breccias, fine-grained hematite dissemination and calcite, chlorite, epidote, adularia and laumontite (generation 1 and 2 mineral parageneses in Section 4.5.4). However, younger generation 3 and 4 minerals, for example, pyrite and clay minerals, also occur (Figure 5-21). A subordinate brittle-ductile component is also locally present. As concluded in /Stephens et al. 2007/ on the basis of their low frequency of occurrence, this orientation set is judged to be of lower significance generally at Forsmark, relative to the other sets.

The kinematic studies performed during the Forsmark site investigation, as reported in /Stephens et al. 2007/, indicate this group of zones has been subject to predominantly sinistral and subordinately dextral strike-slip as well as dip-slip movements.

These zones contain a dominant cluster of steeply dipping, generally sealed fractures with NNW-SSE strike, along with a clear, steeply dipping cluster of dominantly sealed fractures that strike E-W. There is also a more weakly developed cluster of sealed fractures that strike E-W and dip gently to moderately to the south and a cluster of sub-horizontal, predominantly open fractures (Figure 5-22).

5.5.4 Gently dipping zones

Within the regional model area there are three zones within this orientation group, ZFMA1 of medium confidence, lying outside of the central block on the southern side of ZFMWNW0001, ZFMB10 of low confidence, present at significant depth beneath the local model volume, and ZFM871 (old SFR zone H2) of high confidence located within the local model volume (Figure 5-23). None of the zones are interpreted to intercept the ground surface.

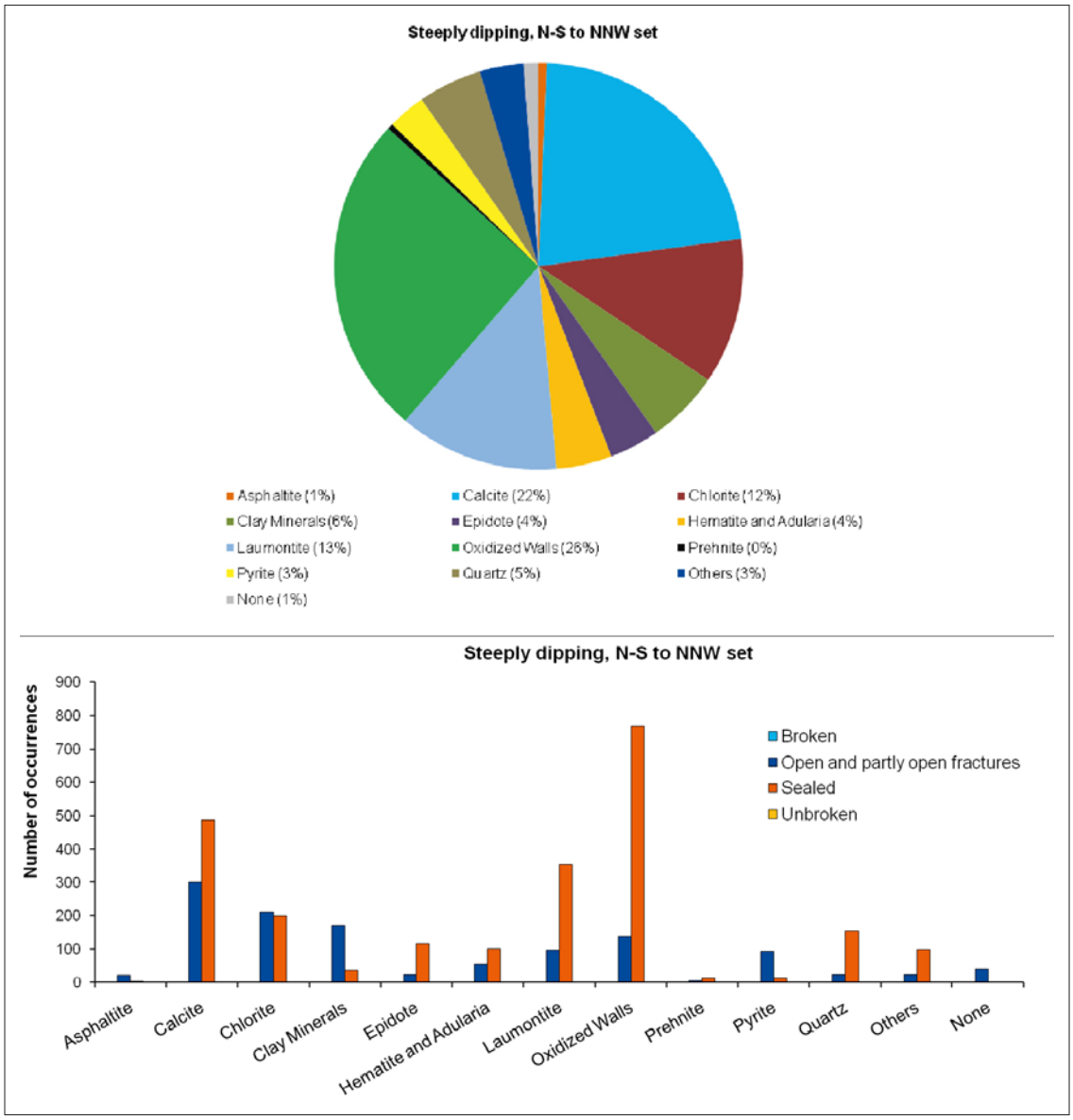

Figure 5-21. *Mineral infillings of fractures lying within the zone boundaries (target intercepts) of the N-S to NNW set.*

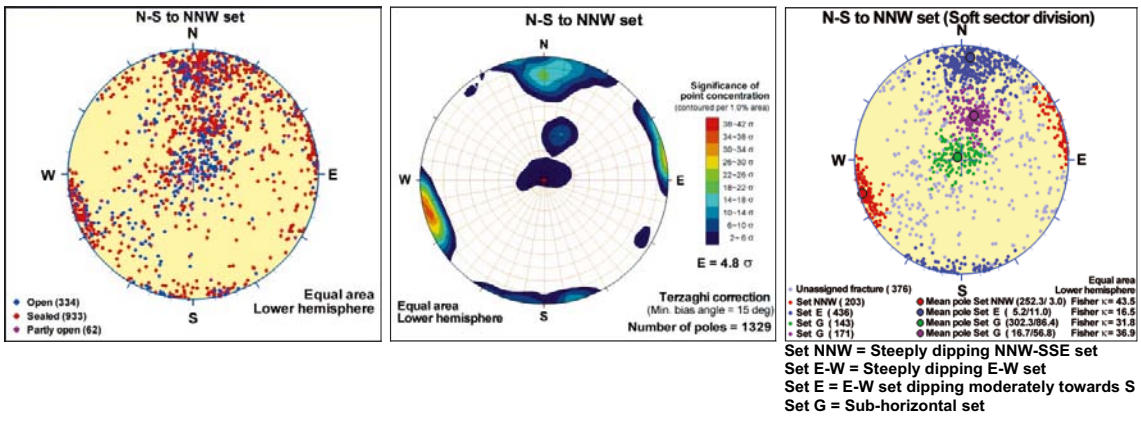

Figure 5-22. *Fracture clustering within the N-S to NNW oriented deformation zones. All plots utilize a lower-hemisphere, equal-area projection, with a Terzaghi correction of the kamb-plots.*

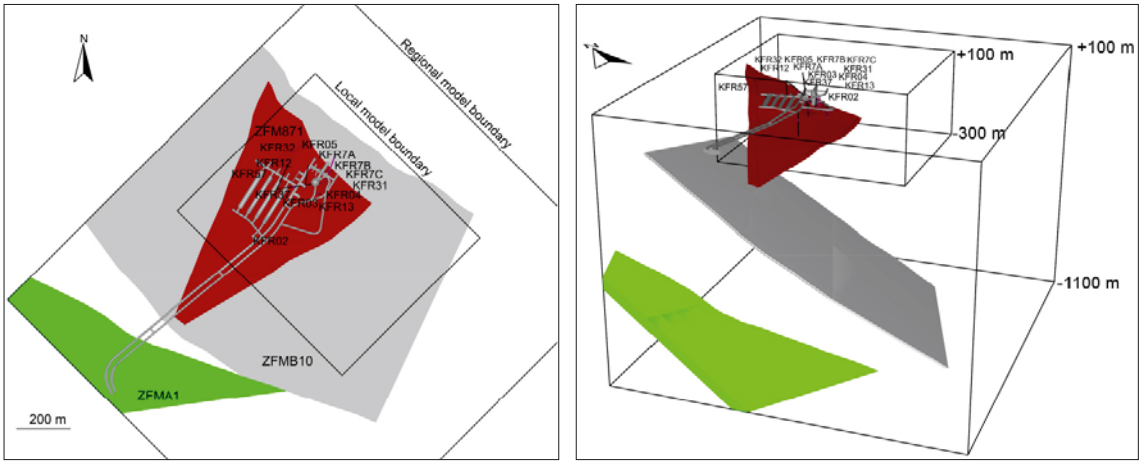

Figure 5-23. *Gently dipping zones penetrating the SFR regional model volume. ZFM871 (red, high confidence), ZFMA1 (green, medium confidence), ZFMB10 (grey, low confidence). Details concerning the zone geometries and terminations at surrounding steeply dipping zones are provided in Appendix 11. Uncertainty concerning the extent of ZFM871 is discussed in Chapter 7.*

ZFMA1 was identified during the Forsmark site investigation and reported in /Stephens et al. 2007/. The inferred zone corresponds to the A1 seismic reflector with an orientation of 082°/45°. However, as earlier reported an alternative interpretation of the seismic reflector is that it is related, wholly or partly, to compositional variations in the bedrock /Stephens et al. 2007/. ZFMB10 also corresponds to a seismic reflector, B10, which was identified during re-processing and reinterpretation of existing seismic data in connection with the current project /Juhlin and Zhang 2010/ (Figures 5-23 and 4-27). The inferred low confidence zone has an orientation of 025°/35°, occurs at significant depth beneath the local model volume and there is no control on its character. In a similar fashion to A1, reflector B10 may be related wholly or partly to compositional variations in the bedrock.

ZFM871, formerly called H2 during the SFR construction phase /Christiansson and Bolvede 1987/, has an orientation of 074°/19°. /Christiansson 1986/ reports the zone's character as being very variable but generally having two to three gently dipping fracture sets, individually recorded zone thicknesses of up to 10 m and a hydraulic thickness varying from 2 to 20 m; the zone is associated with lenses of weathered and highly fractured rock, along with frequent clay-filled joints. The gently dipping fractures, in combination with an increased frequency of steeply dipping fractures, gives rise to the lenses being hydraulically interconnected. Its general character corresponds to the description of the other gently dipping fracture zones identified during the Forsmark site investigation as reported in /Stephens et al. 2007/. Details are available in the property table in Appendix 11. These zones are interpreted as having formed in the brittle regime and, relative to all the other sets, contain a higher frequency of open fractures and incoherent crush material. Chlorite, calcite and clay minerals are conspicuous along the fractures in these zones. However, epidote, quartz, adularia, hematite, prehnite, laumontite, pyrite and asphaltite are also locally present (Figure 5-24).

Zone ZFM871 has been modelled to terminate at zones ZFMENE3115, ZFMNNE0869, ZFMNW0805A, ZFMNW0805B and ZFMWNW1035. The terminations at the surrounding steeply dipping zones and the resulting limited extent means that the zone no longer has an intersection with the sea bottom and no coincidence with a lineament. Details concerning the zone geometries and terminations are provided in Appendix 11.

/Stephens et al. 2007, 2008b/ reported that the kinematic studies carried out during the Forsmark site investigation identified both reverse dip-slip and strike-slip senses of movement as being present along these zones, suggesting movement in one or more compressive tectonic regimes as suggested earlier by /Juhlin and Stephens 2006/.

Due to the open and water-bearing character of ZFM871 identified during the earlier excavation phase and the number of gently dipping zones identified during the Forsmark site investigation, efforts have been made to identify the existence of similar gently dipping structures in the SFR

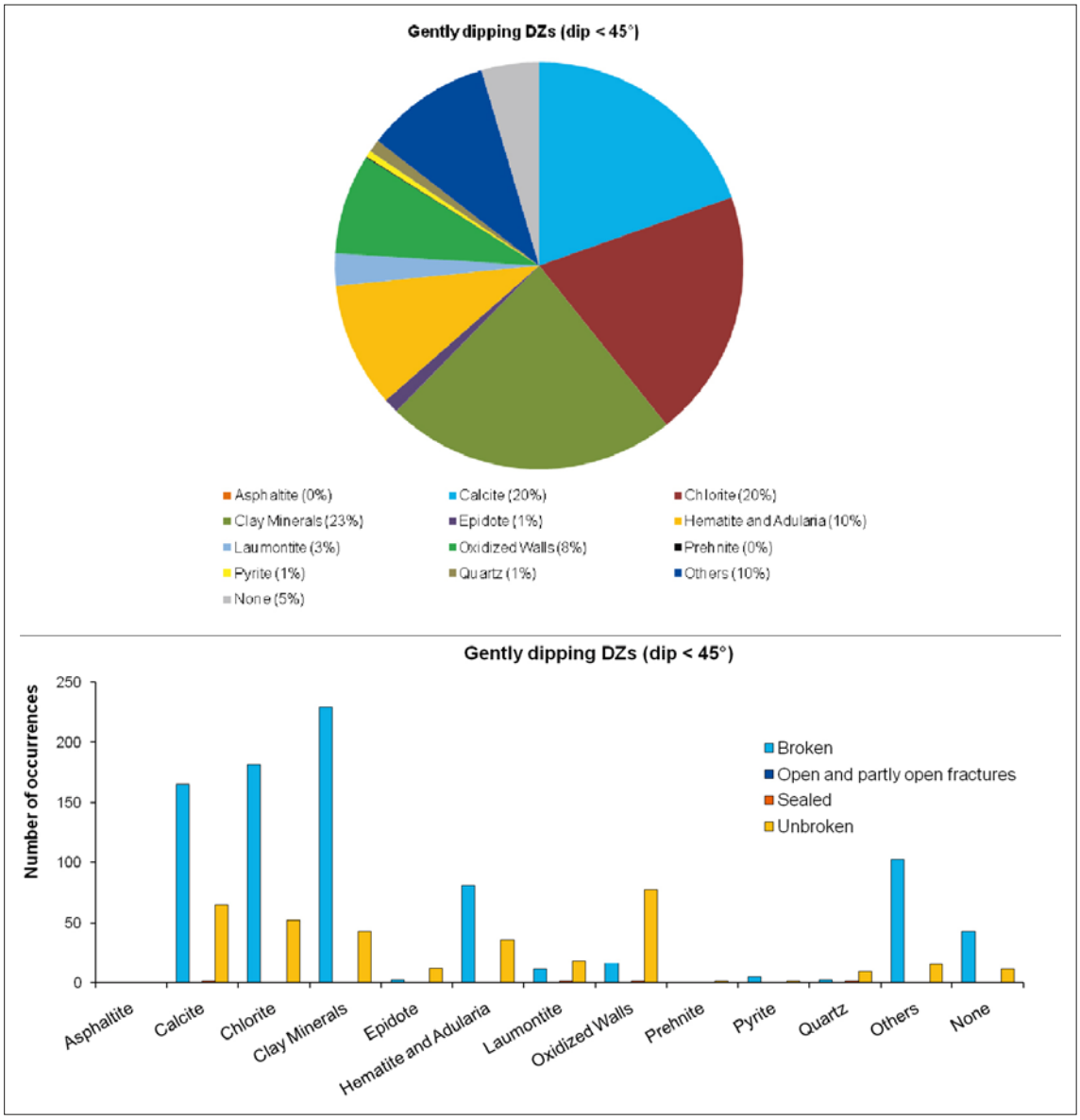

Figure 5-24. *Mineral infillings of fractures lying within the zone boundaries (target intercepts) of the gently dipping set.*

regional model volume. Focus has been placed on lineaments and more diffuse low magnetic anomalies which have a general trend between NNE and ENE. An example of this is the area to the north-west of the existing SFR facility centred on the two lineaments corresponding to the traces of deformation zones ZFMENE8031 and ZFMENE8034 (Figure 5-25).

Attempts were made initially to model these lineaments as deformation zones with a gentle dip to the south-east. The existing borehole and excavation mapping does not allow any connection with the earlier mentioned ZFM871/H2 zone. Any gentle to moderate dip to the south-east would generate intercepts in existing boreholes but, more importantly, even in the existing tunnels, caverns and silo. Whilst sub-horizontal to gently dipping fractures are common in the SFR excavation, no evidence for a corresponding gently dipping zone was identified. Furthermore, the reprocessing of seismic reflection data by /Juhlin and Zhang 2010/ did not identify any gently dipping reflectors in these positions. However, it must be noted that the identification of reflectors at such shallow depths with the data available is difficult and uncertain.

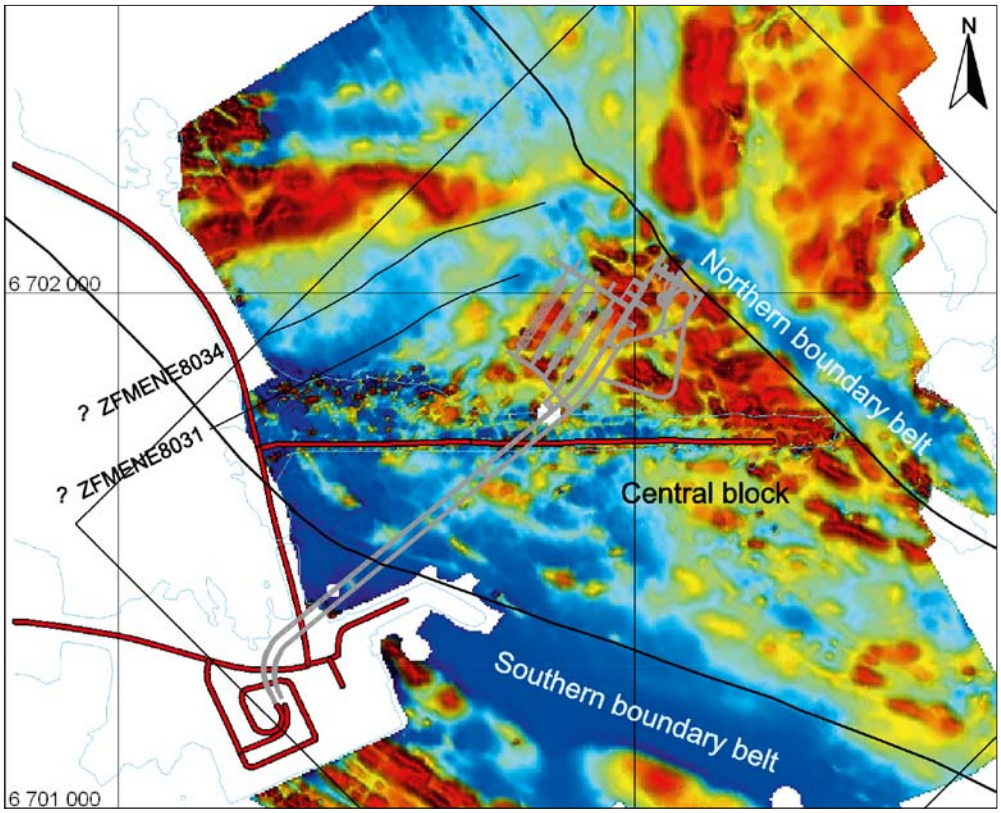

Figure 5-25. *Lineaments/inferred deformation zones ZFMENE8034 and ZFMENE8031 associated with broad diffuse low magnetic anomalies to the west of the existing SFR facility.*

5.5.5 Moderately dipping structures

In accordance with the Forsmark site investigation terminology, gently dipping deformation zones are defined as having a dip of 45° or less, moderately dipping zones as having a dip of greater than 45° but less than 70° while steeply dipping zones are defined as having a dip of 70° or more (see Section 5.2.2).

There are no moderately dipping deformation zones within the Forsmark stage 2.2 local and regional deterministic deformation zone models and this situation is consistent with the well-established conceptual thinking at the Forsmark site. The same conceptual framework has been a guiding principle for the current project and, similarly, no such zones have been identified in the SFR deformation zone models. However, although no local major deformation zones with moderate dips occur within the model, long fractures and minor deformation zones in the general size range of 10 to 50 m that strike E-W and show moderate dips, have been encountered and mapped in the existing SFR excavations (Figure 5-26) and can be expected to be encountered in any new excavations. None of the structures with this general orientation were considered important from a stability or water-in-flow point of view during the construction. At the fracture scale, this orientation is also represented but is only weakly developed (7% of all fractures encountered) compared with the other fracture clusters (Figure 5-27). A possible explanation for the moderately south-dipping structures might be that they represent a conjugate set to gently, north-dipping fractures observed along some of the zones (see, for example, zone ZFMNE3137 in Appendix 11), implying a N-S oriented σ_1 at the time of formation (Figure 2-4).

5.5.6 Structures not included in the deterministic deformation zone model

Possible deformation zones (PDZ) in the single-hole interpretation (SHI)

A total of 31 PDZ's identified during the simplified and standard SHI were not able to be included in the deterministic deformation zone model. Details of these zones are included in Appendix 12. This amounts to c. 28% of all PDZ identified. However, the length of the borehole intersections suggests that most of these structures are minor features, with a size smaller than the resolution level for the deterministic modelling work adopted in version 1.0 and 68% of them are defined as low or medium confidence by SHI.

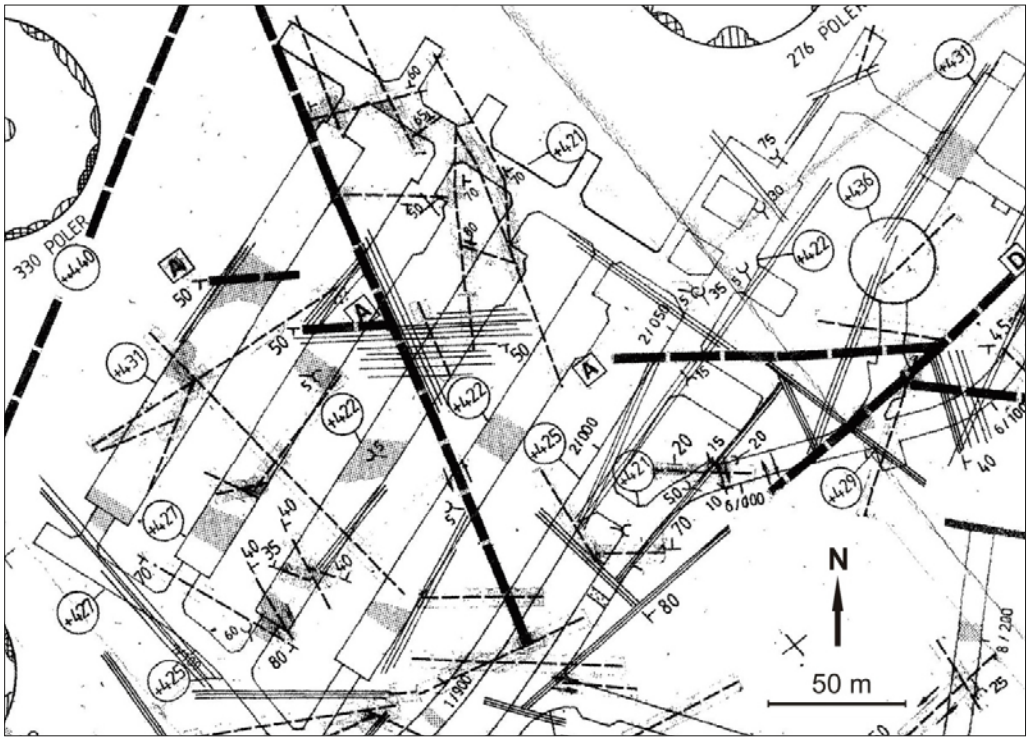

Figure 5-26. *Extract from overview mapping drawing of /Christiansson and Bolvede 1987/ including structures with E-W strike and moderate dips to the south.*

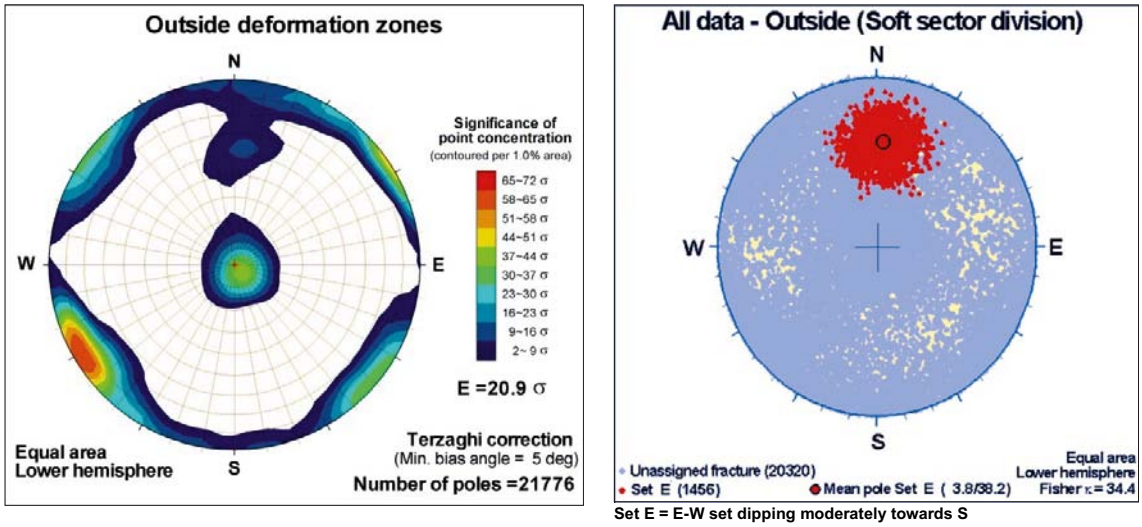

Figure 5-27. *A less well-defined sub-cluster of east west trending fractures with moderate dips to the south. The fracture orientation is possibly associated to the moderately dipping structures shown in Figure 5-26. The data set presented is all fractures; sealed, open and partly open lying outside of deformation zone target intercepts. Both plots utilize a lower-hemisphere, equal-area projection, with a Terzaghi correction of the kamb-plot.*

It should also be noted that there is no lower size limit for defining a PDZ in the SHI process. It has not been possible to correlate such PDZ's with other data in order to define possible estimates of orientation, thickness and extent, fulfilling the model size criteria that can be modelled deterministically.

Seventeen (17) of these PDZ's are from older boreholes lacking BIPS orientation data and it has not been possible to estimate any orientation or true thickness for the structure. The majority have apparent thicknesses of less than 10 m and are not considered to be associated with major structures, since

there would have most likely been evidence in the existing tunnel. There are eight PDZ's judged to be of high confidence from new cored boreholes, all of which have apparent thicknesses of 7 m or less. Low confidence estimates of the orientation and true thickness of six of these isolated PDZ's, using the orientation of fractures, have been calculated in order to assist other modelling disciplines.

Sub-horizontal stress release structures

The planned depth of the facility, –50 to –200 masl, is of particular importance bearing in mind the overall character of the rock volume. In contrast to the planned, deeper lying, neighbouring repository for spent nuclear fuel, the SFR extension will lie wholly within the so-called shallow bedrock aquifer domain (SBA) as described by /Follin 2008/. In this relatively shallow lying rock volume, stress release, associated with the closing stage of sedimentary loading and unloading cycles as well as glacial cycles, has resulted in the development of a high frequency of sub-horizontal open fractures, either by reactivation of older structures or by the development of newly formed sheet joints, it is these structures that dominate the pattern of groundwater flow rather than the steeply dipping deformation zones. Such features are considered to be relatively ubiquitous in the uppermost part of the bedrock, i.e. the near-surface realm, in the Forsmark region /SKB 2008b/. At greater depths, this pattern is likely to be reversed with the brittle deformation zones dominating.

The existence of such horizontal structures, but with a limited lateral extent, lying above the existing silo (Table A12-2 and Figure A12-1) was proposed by /Carlsson et al. 1985/. These particular structures, earlier reported in /Curtis et al. 2009/, are horizontal, lying at an elevation of c. –25 masl, and are similarly interpreted as stress release features rather than deformation zones related to regional-scale tectonic activity. The earlier modelled geometries have not been included in the deformation zone model but have been provided to downstream hydrogeological modellers for further development. A detailed discussion of sub-horizontal stress release structures in the near-surface realm that bear groundwater is available in /Öhman et al. 2011/.

5.6 Confidence assessment, key uncertainties and recommendations

The overall confidence level concerning the deformation history and the broad tectonic framework of the region is judged high, based on the detailed work associated with the Forsmark site investigation and the associated modelling work as reported in /Stephens et al. 2007/ and elsewhere.

The confidence level in existence of each of the deformation zones included in the local model volume is indicated in Table 5.1. As noted earlier, it is important for the reader to consider the nature and spread of supporting evidence for any deformation zone classed with a high confidence of existence. The classification system means that a zone based on a single borehole intercept has the same confidence level as a zone based on multiple borehole and tunnel intercepts. Similarly the spread of evidence needs to be considered; a high confidence zone, coloured red in the model, is shown to have high confidence over its entire length even though supporting borehole evidence may be extremely local.

The overall confidence in the position, character and extent of the so-called southern and northern bounding tectonic 'belts', dominated by ZFMWNW0001 and ZFMNW0805A, respectively, is high. Similarly, confidence is high in the steep to sub-vertical nature of the vast majority of the deformation zones in the SFR area as well as the surrounding Forsmark area, inferred from the underlying conceptual model presented by /Stephens et al. 2007/. This concept has gained independent support from the results of inversion modelling and, in particular, forward modelling of magnetic data carried out as part of the current study. In addition to the extremely local borehole evidence, it is these two geophysical modelling techniques which have given indications, albeit general in character, of the overall dip of larger volumes of rock associated with the structures in the rock mass.

The overall confidence level in the deterministic modelling of the rock volume lying between zones ZFMWNW0001 and ZFMNW0805A is naturally scale-related. In terms of local major zones, confidence is high but, as increasingly smaller structures are considered, so the confidence level drops. As well as being scale-related, the confidence levels in the central SFR block, away from the existing tunnels, are generally lower than within the Forsmark local model area. The reason for this is that the initial basis for much of the modelling of steeply dipping deformation zones at both Forsmark and SFR is the identification and inferred extent of lineaments defined by magnetic minima.

When compared with the Forsmark model area, the SFR regional and particularly the local model areas have a natural magnetic field which is strongly disrupted. As discussed in Section 4.6, the identification of linear low magnetic anomalies, possibly associated with deformation zones, around SFR is made difficult by masking and interference in combination with a heterogeneous lithology. These effects as well as the focus on the detection of smaller-scale structures means that confidence levels are inevitably lower. As discussed in Section 5.5.1, a specific uncertainty remains concerning the continuity and length of the smaller zones in the steeply dipping WNW to NW set lying within the central block. However, it is considered that, even with allowance for these disturbing factors, no local major structure of greater length has been missed.

The site investigations and modelling work have had a focus on locating local major or larger gently dipping deformation zones in the local model volume. Although it was decided not to perform a new seismic reflection survey, which is possibly the best tool to identify such structures, key evidence is supplied by the rock conditions seen in the existing underground SFR facility and, in particular, the silo, extending from c. –60 to –140 m elevation, where no such significant gently dipping structures were identified (note that zone ZFM871 lies beneath the silo). This evidence in combination with the borehole data means there is a high confidence that no, previously unknown, local major or larger gently dipping zone exists in the local model volume.

Uncertainty remains concerning the lateral extent of zone ZFM871, earlier referred to as zone H2, which proved to be of considerable significance from an engineering viewpoint. In version 1.0, the zone is modelled as terminating at ZFMNW0805B (limit to the NE), ZFMNNE0869 (limit to the NW) and ZFMENE3115 (limit to the SE). This interpretation implies a lesser extent to the zone than /Axelsson and Mærsk Hansen 1997/ and closer to the earlier interpretation by /Carlsson et al. 1985/. Clearly, alternative interpretations are possible. The zone's stepped, undulating and heterogeneous character means that, if it does extend further to the north-west so as to intercept the sea bottom, the prediction of the outcrop position is uncertain and that such a structure would generate a clear lineament is considered unlikely. A reasonable alternative is that the zone extends at least beyond ZFMNW0805B to ZFMNW0805A in a north-east direction. Particular focus was placed on identifying a possible greater extent of the zone to the south-east, beyond ZFMENE3115, using the new borehole information. However, no geological evidence to support a further extent in this direction was identified. The earlier SFR investigations demonstrated the heterogeneous character of this zone.

A remaining uncertainty is the existence, frequency and position of very minor, gently dipping fracture zones down to the large single fracture size. This size range is smaller than the resolution level for the deterministic modelling work adopted in version 1.0. These structures may be of little significance from a geological viewpoint but still significant from an engineering viewpoint, due to their potentially open water-bearing character and their intimate interaction with similarly open, sub-horizontal, stress release fractures. There are difficulties to identify such small, gently dipping structures tempered by experience from the existing SFR excavations, including the investigation of zone ZFM871. The correlation of smaller fracture zones between boreholes with similar heterogeneous geological characteristics is clearly not straightforward. The existence and frequency of such structures, along with their interplay with the stress relief features noted below, is best established by hydrogeological investigations and modelling that focuses on the water bearing character that is the parameter of key importance.

The importance of stress release structures in the near-surface realm rather than zones formed in response to tectonic shear stresses that has been advocated in the current study is similar to that proposed in the Forsmark site investigation /Stephens et al. 2007/. There is high confidence that minor sub-horizontal structures do exist but with equivalent trace lengths of a couple of hundred metres or less, down to the single fracture scale. These features are interpreted to occur in, at least, the upper 150 m of the rock mass. At very shallow depths, < 15 m, these features are clearly related to stress release with wide apertures filled with sediment and rock fragments /Carlsson 1979, Leijon 2005, Carlsson and Christiansson 2007/. With increasing depth, the apertures become smaller and more standard mineral infillings including clay minerals occur rather than sediment. The special character of the fracturing in the upper part of the bedrock at Forsmark has been addressed during the Forsmark site investigation /Olofsson et al. 2007, Fox et al. 2007, Stephens et al. 2007/ and, in practical terms, the frequency and persistence of sub-horizontal fractures was noted in the roof during the SFR tunnel excavations. Some of these fractures are open and hydraulically connected with high transmissivities and have been identified down to elevations of c. –200 m.

In addition, some uncertainty remains associated with the PDZ's from the SHI not included in the deterministic model. Details of these zones are included in Appendix 12. However, the length of the borehole intersections suggests that most of these structures are minor features, with a size smaller than the resolution level for the deterministic modelling work adopted in version 1.0.

At the time of writing this report, the design layout for the extension of the storage facility includes the excavation of a completely new access tunnel (see Figure 5-28). The new tunnel lies close to, and runs parallel with, the two existing SFR access tunnels. While the available tunnel geological mapping results from the construction phase of the existing facility have provided a key input to the current modelling work and have provided the basis for the interpretation of all the deformation zones identified along its length, the proximity of the existing and planned tunnels allows for the further utilization of the data at a higher resolution than allowed for in the scope of work for the geological model presented in this report. Due to the proximity of the tunnels simple extrapolation of existing tunnel data from the existing tunnels to the planned tunnel alignment is considered a reasonable approach for the aim of producing a detailed prognosis for rock support, grouting requirements and engineering geological characterization of the rock mass in the new tunnel.

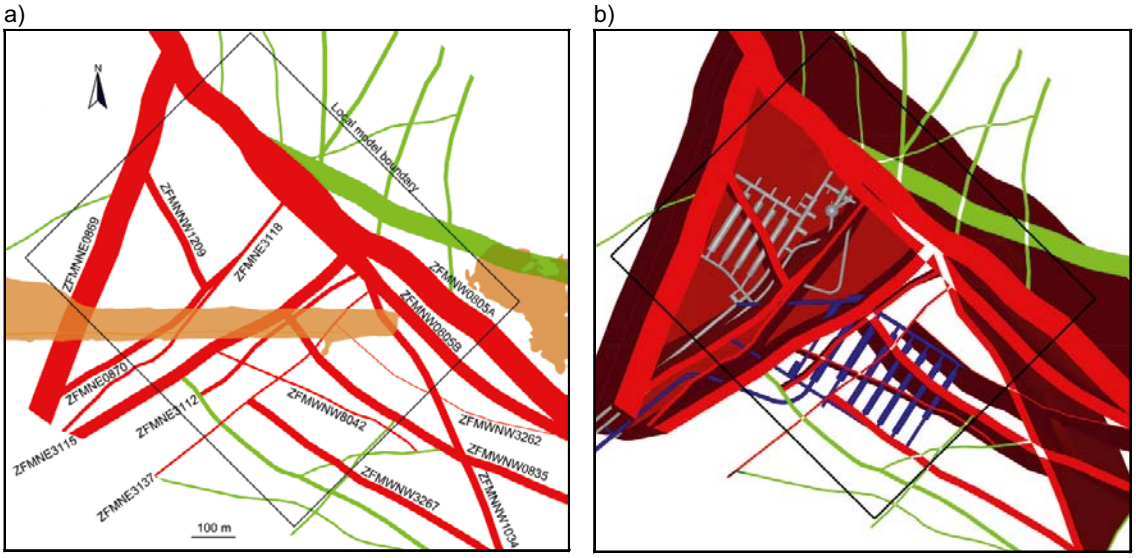

Figure 5-28. *(a) Intersection at the current ground surface of deformation zone traces included in the local model. (b) Top view of the local deformation zone model relative to the existing SFR facility (grey) and the currently planned SFR extension (blue) to the south-east. The different colours of the deformation zones refer to confidence in existence: high=red, medium=green.*

6 Rock domain model

6.1 Input data, methodology and assumptions

A single model for the three-dimensional distribution of rock domains in the local SFR model volume has been established. The term rock domain is used here according to the general guidelines in /Munier et al. 2003/. More specifically, individual domains have been defined on the basis of an integration of the composition, grain-size, heterogeneity and character of ductile deformation in various rock units, as employed in the Forsmark site investigation /Stephens et al. 2007/. However, the importance ascribed to individual parameters differs significantly between the current model and the Forsmark rock domain model. The pronounced lithological and structural heterogeneity in the SFR area practically precludes the detailed structural analysis, which forms the backbone in the Forsmark rock domain model. Instead, there is a greater focus on lithological composition and heterogeneity.

An explicit aim has been, wherever possible, to maintain consistency between the current model and the rock domain model from the Forsmark site investigation /SKB 2008b/, so as to simplify future studies on the interaction between the two models. In practice, this approach was only applicable to the boundary between rock domains RFM021 and RFM033 in the Forsmark regional model stage 2.2, which is the only contact that intersects the local SFR model area. The more detailed modelling scale in the current SFR study has given rise, not unexpectedly, to considerable differences between the SFR local model and the Forsmark regional model stage 2.2 inside the SFR model volume.

Due to the fact that no outcrops exist in the SFR local model area, the SHI of rock units in the boreholes and the tunnel mapping of the SFR underground facility, together with the high resolution magnetic total field data, form the key input data for the establishment of the rock domain model. Rock domains (RFR) and their relationship to rock units in the respective SHI are presented in Appendix 7 for all boreholes except the old cored boreholes subjected to a simplified SHI. A summary of all intercepts of rock domain boundaries in boreholes and tunnels is presented in Appendix 13. The terms *Target borehole/tunnel intercept* and *Geometrical borehole/tunnel intercept*, as defined in Section 5.2.2 for deformation zones, are quoted in Appendix 13. A *target borehole intercept* is the interpreted position of a rock domain boundary in an individual borehole, whereas a *geometrical borehole intercept* is the intercept between a modelled domain boundary and an individual borehole as they exist in the RVS model. Target intercepts conform to the geological SHI rock unit intercepts. A *target/geometrical tunnel intercept* is defined in the same manner, but by chainage intervals along a tunnel centre line rather than borehole length.

The extension of the rock domains at the ground surface was largely defined by using the available high resolution magnetic total field data in the area. This information together with available SHI rock units and SFR tunnel mapping, were used in the projection of the rock domains down to the base of the local model volume at –300 m elevation where geological data are more sparse. Although the ductile structural data exhibit a considerable local heterogeneity, efforts were made to at least follow the general structural NW-SE trend in the region.

Furthermore, projected surfaces were compared with the magnetic inversion model and, if necessary, they were adjusted to avoid conflicts. This was completed by slicing the inversion model into a number of horizontal and vertical sections and then superimposing the domain boundaries on the slices (see Section 4.6.5). It must be emphasized that changes in domain boundaries due to conflicts with the magnetic inversion model were kept to a minimum. Although none of the domain boundaries are inferred to be strictly related to deformation zones, a comparison with the geometrical deformation zone model was also made.

The following assumptions have been adopted in the geometric modelling procedure:

- An initial structural conceptual model where large scale folding has affected the rocks that belong to groups A and B, as well as the major part of the pegmatitic granite that belongs to group D. The fold axes are assumed to plunge downwards in approximately the direction of the mineral stretching lineation. However, the structural heterogeneity is far too great to enable modelling on a purely structural concept.
- Although the mean values of the orientation for planar structures including rock contacts are highly variable, they are assumed to provide a rough estimate of the orientation of the rock domain boundaries.
- All inferred rock domains are related to major geological features. Based on available geological and geophysical data, the domains boundaries are assumed to be steeply dipping and to extend downwards, at least to the base of the local model volume.

The properties of the modelled rock domains in the local model volume were only assigned for two of the domains, due to the lack of geological data in the other domains. Property tables for the two domains with geological information are provided in Appendix 14. Key attributes include the proportions of major rock types, the degree of heterogeneity and the nature of ductile deformation, as well as textural, structural and petrophysical properties of the dominant rock type. In addition, judgements concerning the confidence of existence of a rock domain are provided for each domain. The proportions of different rock types in each rock domain, presented on a borehole by borehole basis, is provided in Appendix 15.

6.2 Conceptual understanding of the rock domains

6.2.1 Heterogeneity and folding

The SFR area is situated within a regional high-strain belt that extends along the Uppland coast and anastomoses around tectonic lenses that are less strongly affected by intense ductile strain. The deformation initiated under amphibolite-facies metamorphic conditions and continued at lower metamorphic grades with the retrograde development of more focused strain along discrete, sub-vertical deformation zones. The rock mass hosting the SFR underground facility, referred to in Chapter 5 as the SFR central block, is bounded by two such regional deformation zones with more focused ductile and brittle strain, zone ZFMWNW0001 (Singö deformation zone) and zone ZFMNW0805A that was referred to as zone 8 in the older SFR work. Relative to the adjacent Forsmark tectonic lens, rocks inside the SFR central block were affected by a generally higher degree of ductile strain and a well-defined WNW-ESE to NW-SE structural trend. In the proximity of the steep WNW to NW zones with more focused deformation, the development of pure S-tectonites continued under lower amphibolites facies metamorphic conditions, whereas there is considerable evidence for a stretching lineation and folding of an older ductile fabric during this phase in the more distal parts of the SFR block.

The most strongly deformed rocks in the area consist of a heterogeneous package of mainly felsic to intermediate metavolcanic rock intercalated with metagranodiorite (to granite) and minor amphibolite. All these rocks display moderate to strong foliation, locally along with banding and/or gneissosity. These rocks have been intruded by considerable amounts of younger granite and pegmatitic granite, which locally forms bodies of significant volume, within which the older rocks occur as xenoliths. Several of these younger rocks display a conspicuous mineral stretching lineation, and locally even a planar tectonic fabric. It should be noted that linear mineral fabric is typically difficult to distinguish in pegmatitic rocks, especially in drill core. Thus, within the SFR area, they intruded after at least some deformation had affected the oldest rocks of group A and B but, in most cases, prior to the later ductile deformation under lower amphibolites-facies metamorphic conditions.

It is evident that folding at different scales has affected most rock types in the SFR area, including a majority of the pegmatitic granites and younger granites that belong to rock group D. However there are group D rocks, such as some pegmatite dykes, that evidently post-date the ductile

deformation in the area. Ductile structural data from both the original tunnel mapping and the updated mapping of NBT (Figure 4-9) reveal a rather irregular folding at tunnel scale, where fold axes trend parallel to the variable foliation and mostly plunge gently to moderately towards the south-east, or locally towards the north-east (cf. /Christiansson and Bolvede 1987/). The mineral stretching lineation data for the boreholes from different parts of the model volume also show an irregular distribution, but are generally oriented towards the south-east or north-east with variable plunge.

Ductile structural data provided by /Stephens and Forssberg 2006/ from outcrops within rock domain RFM021 (Forsmark regional rock domain model, stage 2.2) show, on the other hand, a well-defined and almost identical orientation of mineral stretching lineation and fold axes, with variable plunge towards the south-east (Figure 4-7). These data conform with a process where the linear fabric was established prior to but continued to develop during folding. On this basis, /Stephens et al. 2009/ proposed a folding process, which started with normal cylindrical folds that, to a variable extent, were drawn out in the stretching direction into sheath folds, parallel with the linear grain-shape fabric.

Within the local model volume, it is thus evident that the rheological heterogeneity of the rock mass prior to the folding (see Section 4.4) has resulted in irregular folding at all scales. A structural concept, with the development of major sheath folds, similar to that of the Forsmark tectonic lens, is therefore not fully applicable in the SFR area. Due to this structural uncertainty, the use of borehole and tunnel intercepts marking gross compositional changes, as well as the magnetic anomaly signature have been the primary input to the modelling work, instead of structural measurements. However, where no fixed points are available, projections of the rock domain boundaries were modelled to avoid conflict with the general ductile structural trend, oriented roughly NW-SE in boreholes and along the SFR facility. Due to the structural irregularity, it must be emphasized that all surface projections without supporting geological intercepts are highly uncertain.

6.2.2 Geological significance of areas with contrasting magnetic intensity

The evaluation of the high resolution magnetic data carried out in Section 4.6.4 indicates a highly variable pattern in the magnetic intensity in the local model area. Conspicuous areas with a low magnetic signature are located south of the pier, along the south-western boundary of the local model volume, and along a broad WSW-ENE trending belt that penetrates the north-western part of the local model volume (Figure 4-30).

The southern anomaly, which in part coincides with the pier, has no obvious relationship with any interpreted magnetic lineaments or modelled deformation zones. It should be emphasized that since most of the magnetic contribution from the scrap metal in the pier was removed by low pass filtering of the shallow, high frequency data (see Section 4.6.4), the low magnetic anomaly branch that extends beneath the pier is inferred to have a lithological explanation. Both the SFR tunnel mapping and the boreholes that penetrate the anomaly at depth reveal that the volume is dominated by pegmatitic granite and pegmatite with low magnetic susceptibility.

The WSW-ENE belt of low magnetic intensity, north-west of the SFR underground facility, has a more ambiguous nature. It is associated with a broad ridge of high magnetic intensity, as illustrated in Figure 6-1. /Juhlin and Zhang 2010/ report that there are weak indications of a reflector, A13, which coincides with the ridge, if it is projected to the ground surface (Figure 6-1). Although the existence of the reflector is speculative (rank 3 – possible), it is judged that both the magnetic anomaly and the reflector can be related to lithological changes rather than to a deformation zone. Since the character of the anomaly is highly reminiscent of that of the anomaly south of the SFR underground facility, it is feasible to assume that the rock mass is dominated by pegmatitic granite and pegmatite with low magnetic susceptibility. Lithological data from the volume is limited to the SFR underground openings and a few boreholes situated in the southernmost, peripheral parts of the actual magnetic minima. There are no indications of any extensive volumes of pegmatitic granite and pegmatite in these data. However, these data are restricted to a very small part of the WSW-ENE belt with low magnetic intensity.

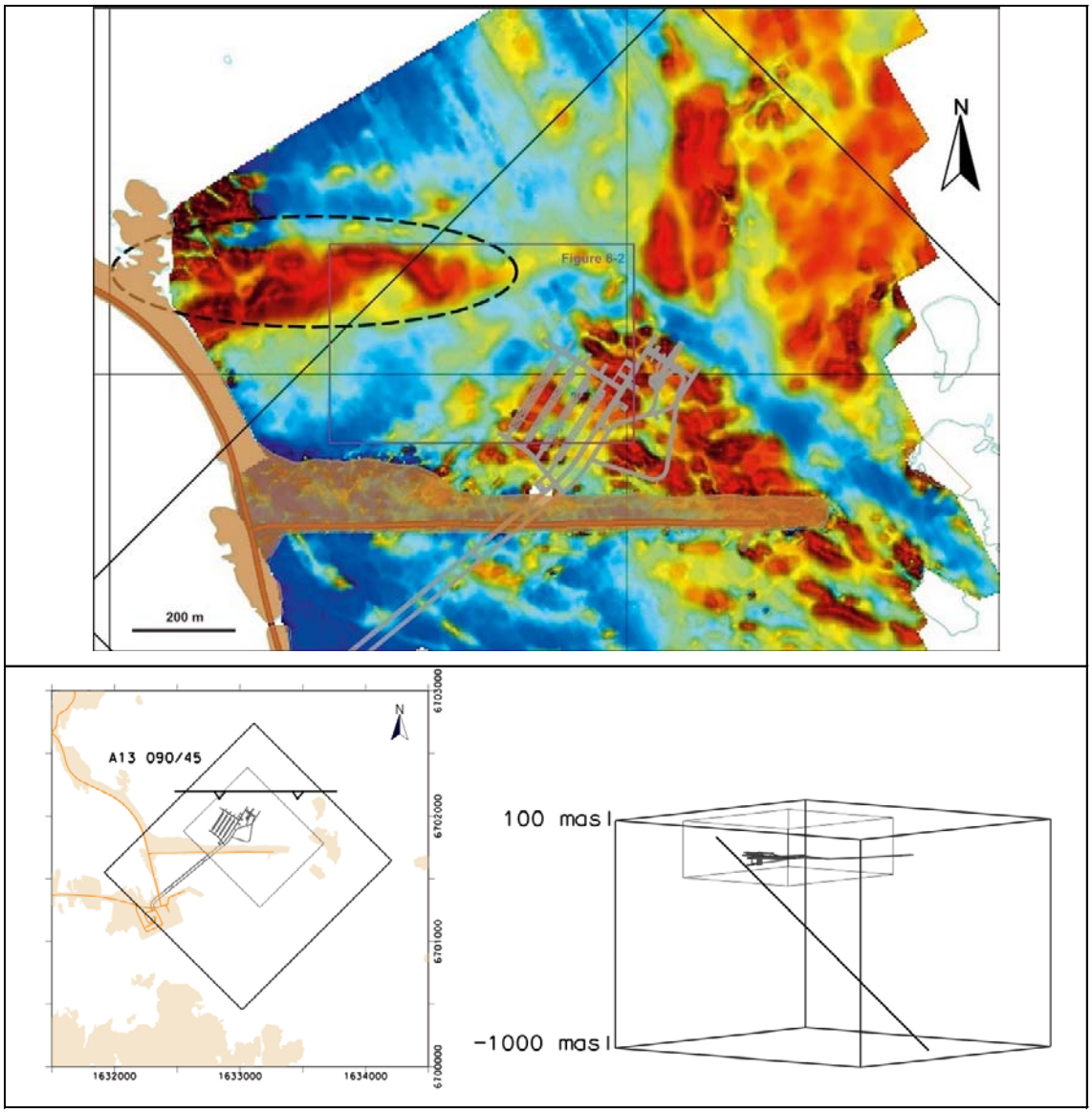

Figure 6-1. *The ellipse on the map of the magnetic total field shows the approximate projected ground surface position of seismic reflector A13. The position of Figure 6-2 is marked by a pink box. The lower left figure is a planar view and the lower right a three-dimensional view of reflector A13, relative to the model volumes and the existing SFR facility.*

The anomaly also coincides with several lineaments defined by magnetic minima and is, at least, locally accentuated by several steeply dipping deformation zones, including the high confidence zones ZFMNNE0869 and ZFMNNW1209 (Figure 6-2). One possible explanation considered was that the broader low magnetic belt is the result of one or a series of deformation zones that dip gently to moderately towards the south. However, no such zone(s) have been identified in boreholes, existing underground facility or available seismic data.

Bearing in mind the considerations above, the WSW-ENE belt of low magnetic intensity, north-west of the SFR underground facility, has been treated in the modelling procedure as a composite result of oxidation related to minor brittle structures and larger volumes dominated by pegmatitic granite and pegmatite.

The remaining part of the local SFR model area, south-west of ZFMNW0805A, consists of a belt with NW-SE trend and a high but variable magnetic intensity that extends from the SFR underground facility to an islet south of Grisselgrundet, just outside the local model area. This feature is related to lithology and the variability in the magnetic intensity conforms to the lithological heterogeneity in the SFR underground openings and boreholes that penetrate the volume.

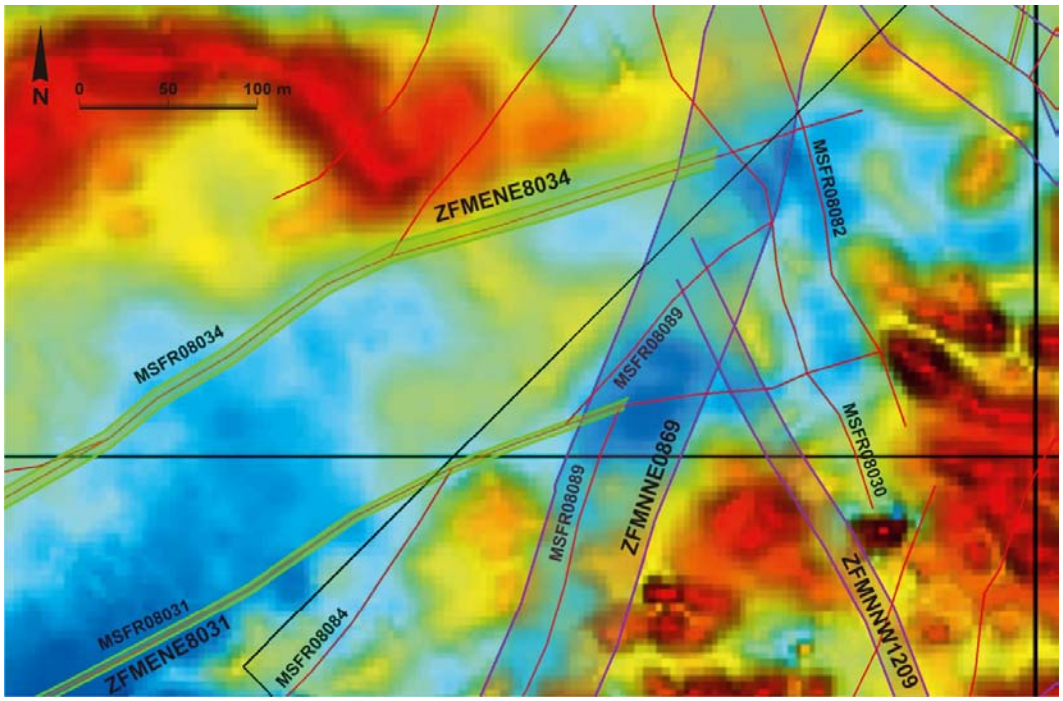

Figure 6-2. *Detail of the WSW-ENE belt with low magnetic intensity north-west of the SFR underground facility and its relationship with magnetic lineaments and modelled deformation zones. The black thin line marks the local SFR model volume and the thicker black lines are RT90 coordinates (6 702 000, 1 633 000). The map position is marked in Figure 6-1.*

The part of the model area located north-east of zone ZFMNW0805A is characterised by a magnetic intensity with NW-SE trend that largely resembles that of the belt of high magnetic intensity that occurs south-west of this deformation zone. The magnetic connections, on the other hand, are generally aligned north-south instead of the NW-SE trending pattern, which is typical south-west of ZFMNW0805A. Since none of the boreholes intersecting ZFMNW0805A penetrate the full thickness of the zone, there exist no lithological data from this part of the local SFR model volume. The closest observation point within this magnetic domain is located on the island Marträd, approximately 1.5 km from the local SFR model area /Stephens et al. 2008a/. The regional rock domain model for Forsmark stage 2.2 /Stephens et al. 2007/ has tentatively indicated that the dominant rock type in this area (rock domain RFM033) is a metamorphosed granite (to granodiorite).

6.3 Geometric model and property assignment

Due to the lack of outcrops in the local SFR model area, a primary step in the modelling procedure has been to correlate the rock units from the borehole SHI results with the high resolution magnetic total field data in the area to support the definition of rock domains (see Section 6.2.2). In combination with the conceptual understanding that involves major, irregular folding and a high degree of ductile strain (see Section 6.2.1), a geometric rock domain model for the local model volume has been constructed.

Four rock domains have been recognised in the local SFR model volume (Figure 6-3). Rock units in the SHI are generally defined on the basis of rock composition and grain-size, along with the style and degree of ductile deformation. Together with heterogeneity, these parameters have been combined so as to correlate with these four domains (Appendix 7). It should be noted that the degree of fracturing has not been considered during the division into rock domains. The four rock domains are arranged in a fashion with a central domain (RFR02) surrounded by three marginal domains (RFR01, RFR03 and RFR04). At the surface, domains RFR01 and RFR03 are recognised by their low intensity in the magnetic total field (Figure 6-4). A conceptual model that involved irregular folding, due to the heterogeneity of the rock mass, is the basis for the modelling of these two marginal domains.

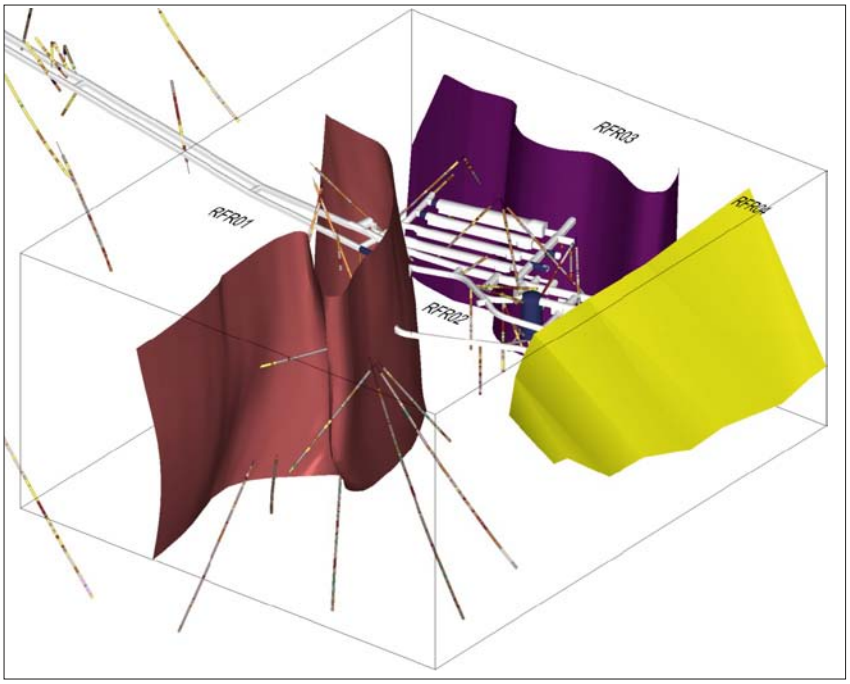

Figure 6-3. *Three dimensional model view from east showing the boundaries between the four rock domains within the local SFR model volume relative to the borehole geology and the geometry of the SFR underground facility. The colour choice is only for legibility, where boundary RFR01–RFR02 is pinkish brown, RFR02–RFR03 violet and RFR02–RFR04 yellow.*

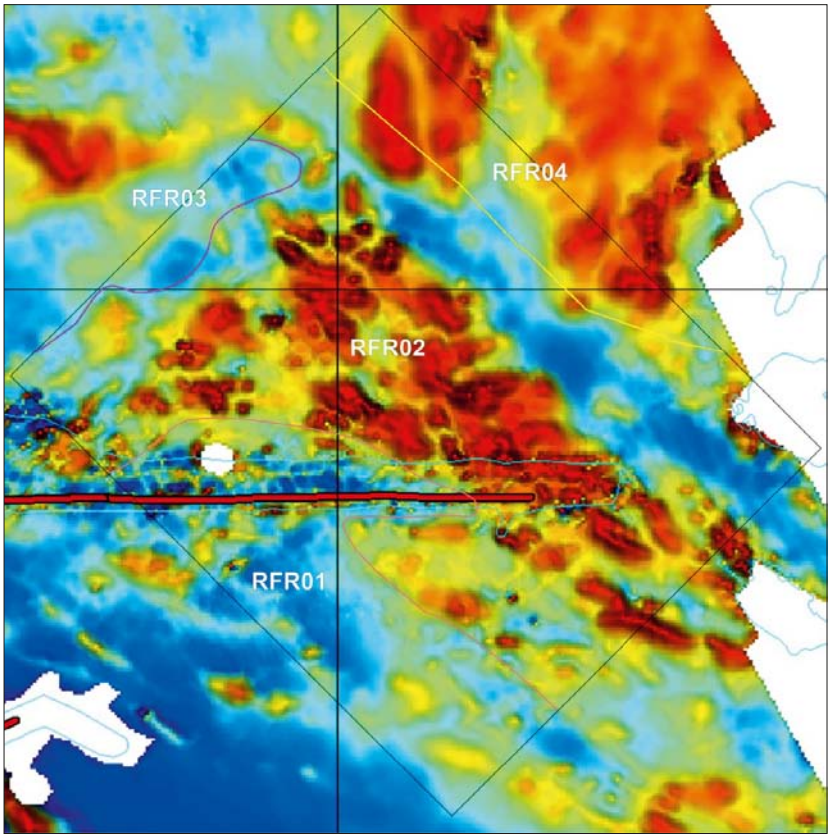

Figure 6-4. *Map of the magnetic total field after low-pass filtering and subtraction of the contribution from the SFR silo and caverns (see Section 4.6.4). The surface trace lines corresponding to the three rock domain boundaries within the local model area are also shown. The colours of the boundaries are identical to those in Figure 6-3.*

Moreover, the boundary of RFR01 was slightly adjusted after reference to the magnetic inversion model to avoid local inconsistencies, whereas the other two domain boundaries remained unchanged (Figure 6-5). The boundary between RFR02 and RFR04 is identical to the contact between RFM021 and RFM033, as defined in the deterministic rock domain model version 2.2 of the preceding Forsmark site investigation /Stephens et al. 2007/. The criteria used to distinguish the four rock domains are summarised in Table 6-1.

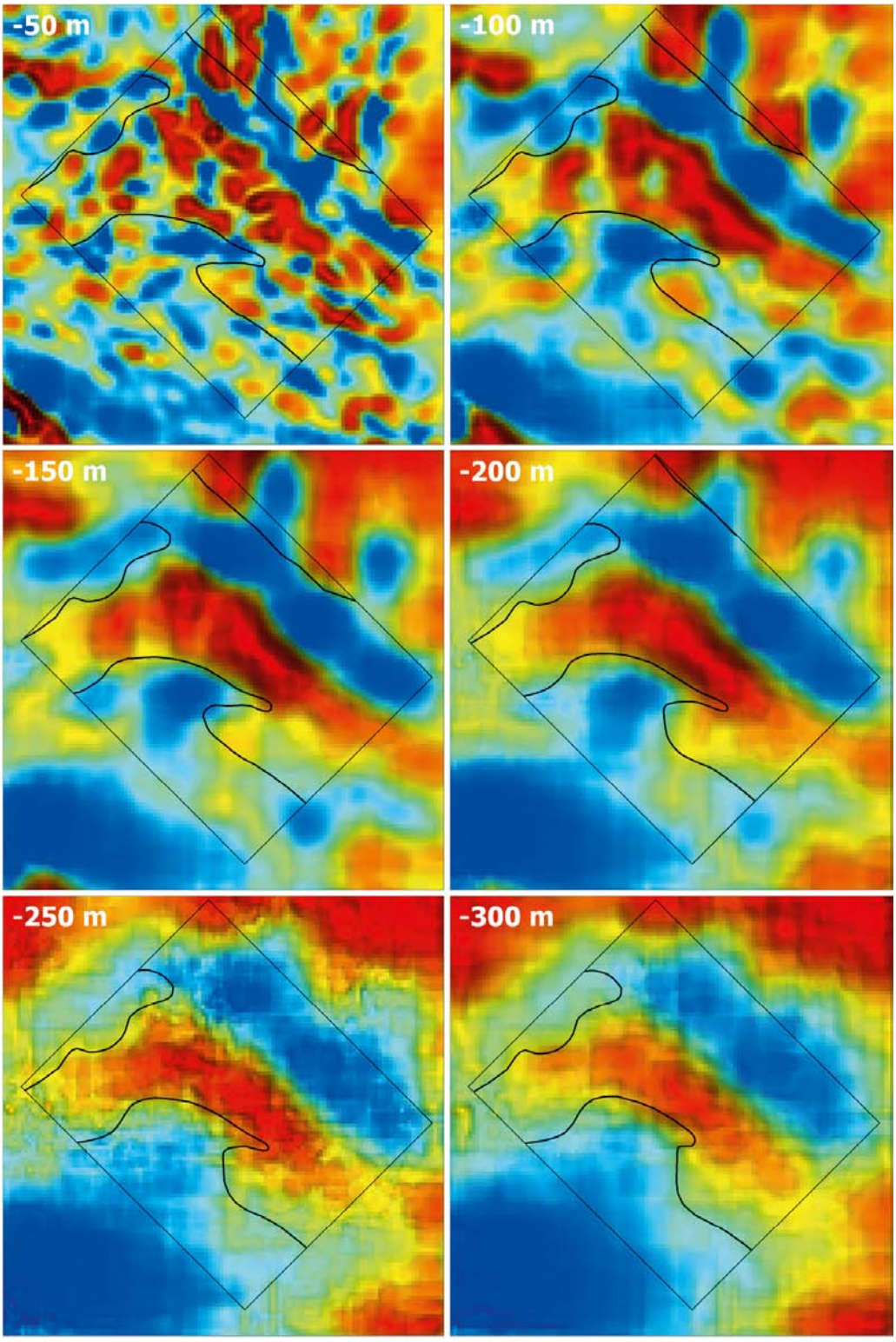

Figure 6-5. *Horizontal slices through the magnetic inversion model every 50 m, down to –300 m elevation, with trace lines of the rock domain boundaries within the local SFR model volume.*

Table 6-1. Summary of criteria used to distinguish the four rock domains in the SFR local model volume.

Rock domain	Borehole data	Tunnel data	Magnetic total field	Comment
RFR01	Rock units dominated by pegmatite, pegmatitic granite.	Sections dominated by pegmatite, pegmatitic granite.	Continuous area of low magnetic intensity.	–
RFR02	Rock units of varying composition, but with a dominance of meta-granodiorite (to granite) and metavolcanic rock.	Heterogeneous sections dominated by bedrock coded as unspecified orthogneiss.	Continuous area of high, but variable magnetic intensity.	–
RFR03	–	–	Continuous area of low magnetic intensity.	Modelled to avoid borehole and tunnel intersections.
RFR04	–	–	Continuous area of moderate magnetic intensity.	Structural trend inferred from magnetic intensity differs from that of RFR02.

The geological borehole and SFR tunnel information is limited to rock domains RFR01 and RFR02, whereas data from the other two domains, RFR03 and RFR04, are lacking. More than 70% (3,767 m) of the mapped borehole length data are from RFR02, which also hosts most of the SFR underground facility. For this reason, property tables have only been constructed for RFR01 and RFR02. A quantitative estimate of the proportion of different rock types was possible for both these domains (Figure 6-6).

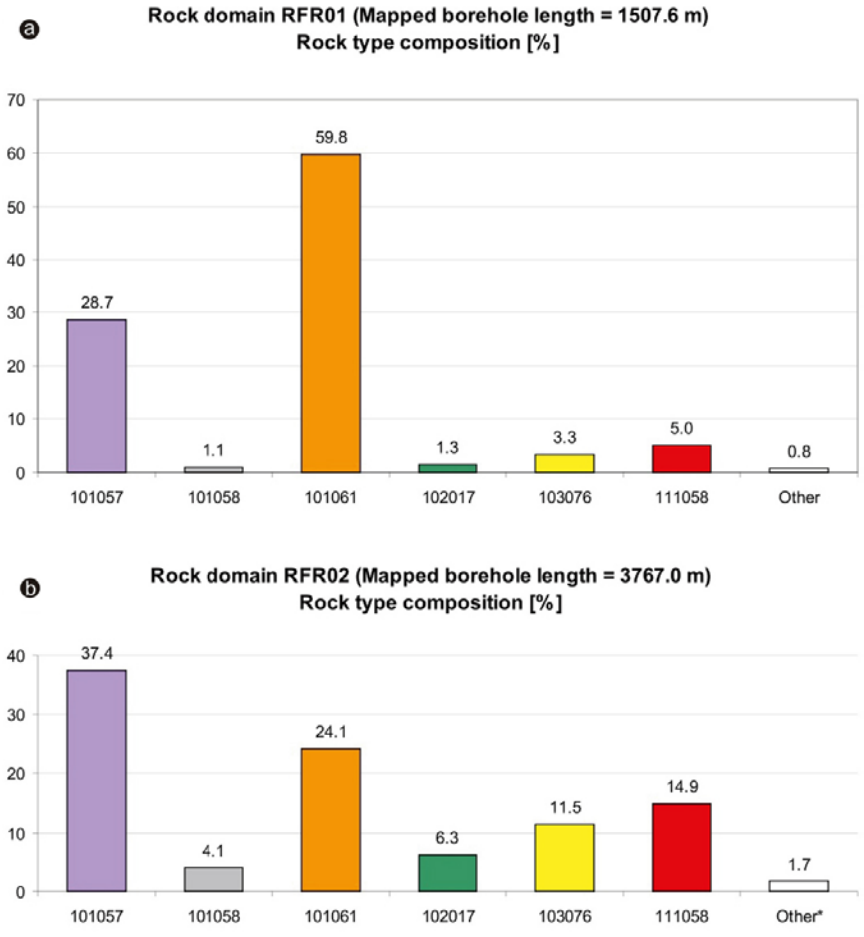

Figure 6-6. *Quantitative estimates in volume % of the proportion of different rock types in rock domains a) RFR01 and b) RFR02. A translation of rock codes to rock names is provided in Table 4-4.*

In general, the intensity of the ductile strain in RFR01 and RFR02 closely follows changes in composition. The oldest rock types, felsic to intermediate metavolcanic rock, metagranodiorite (to granite), amphibolite and aplitic granite, are typically strongly foliated and locally banded. Furthermore, linear ductile fabrics occur, though they are of subordinate importance in these rocks. In the younger rock types, fine- to medium-grained granite, pegmatitic granite and pegmatite, linear ductile mineral fabrics dominate over planar equivalents, if such exist. Trends or variations in the intensity of the ductile strain with respect to distance from regional deformation zones are not obvious within the local SFR model volume.

As mentioned above, no fracture domain modelling or geological DFN were planned during this project, and consequently a detailed analysis of fractures outside the deformation zones is lacking. However, a simple comparison of the mean fracture frequency obtained from borehole data outside modelled deformation zones in RFR01 and RFR02, shows no obvious differences between the two domains with 3.6 open and 13.2 sealed fractures per metre for RFR01 and 3.8 open and 13.5 sealed fractures per metre for RFR02 (Table 5-2). Nevertheless, there are indications of correlations between lithology and the brittle deformation style. Table 5-2 reveals that a majority of the sealed fractures in RFR01, dominated by pegmatitic granite, form fracture networks, whereas most sealed fractures in RFR02 are registered as 'individual' fractures. Turning to the detailed tunnel drawings of /Christiansson and Bolvede 1987/, it is moreover evident that the often well-developed fracture set parallel to the foliation in the metagranodiorite (to granite) and the metavolcanic rock locally terminates or changes character across the contact to rock types with less pronounced ductile fabric, such as the pegmatitic granite (Figure 6-7).

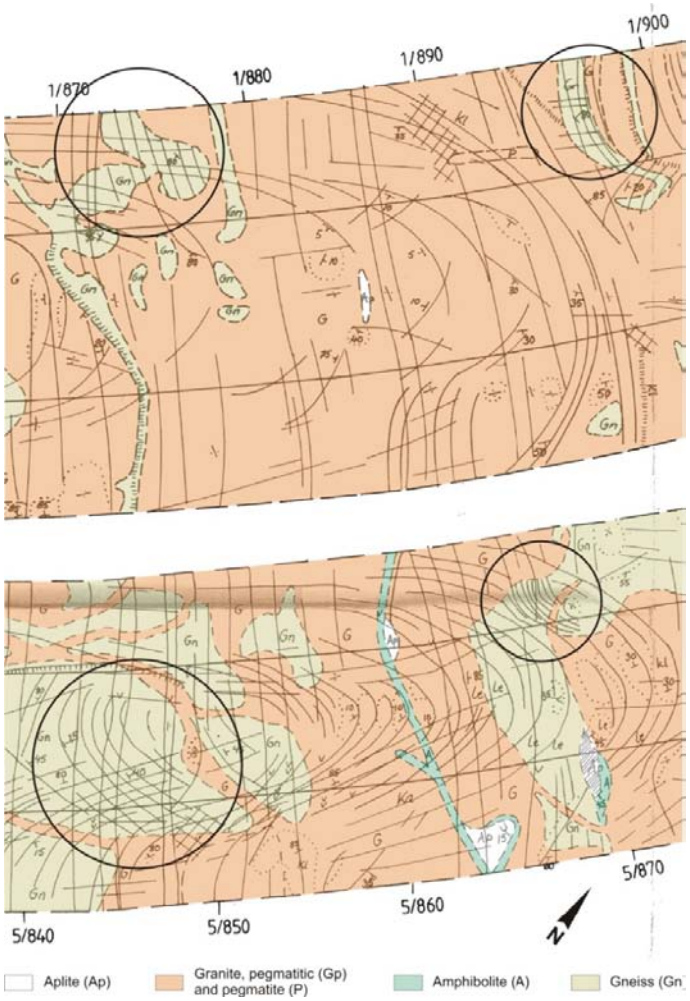

Figure 6-7. *Colour coded sections of the operating (DT) and construction (BT) tunnels from the drawings of /Christiansson and Bolvede 1987/, illustrating how foliation parallel fractures in the unspecified orthogneiss (comprising metagranodiorite (to granite) and felsic to intermediate metavolcanic rock) locally terminate or change character across the contact to the pegmatitic granite (marked by open circles). The tunnel sections are located within RFR01. For legend to the brittle structures, see Figure 3-2.*

6.3.1 Rock domain RFR01

Rock domain RFR01 is modelled as a major fold structure dominated by pegmatitic granite and pegmatite (Figure 6-8). Another important constituent is fine- to finely medium-grained metagranodiorite (to granite), which occupies approximately 30% of the mapped borehole length within RFR01 and is affected by amphibolites-facies metamorphism. The domain is characterised by a relatively high degree of homogeneity compared with domain RFR02 and other, subordinate rock types occupy approximately 10% of the mapped borehole length.

The boundary between RFR01 and RFR02 is defined by four fixed points from three boreholes and five from underground openings in SFR distributed between –71 and –205 m elevation in the model volume (Appendix 13). Although the subsurface projection of the domain boundary is largely unknown, the data conform with rather steeply dipping, fold-like structure, which generally coincides with the structural trend in this part of the model volume. Imaginary fold axes orientations of approximately 090°/70° (Figure 6-8), which neither violate on the surface trace nor the geologically defined tunnel and borehole intersections, were used to project the surface to the model base. Furthermore, the boundary between rock domains RFR01 and RFR02 was slightly adjusted during the modelling work after reference to the magnetic inversion model to avoid local inconsistencies (see Section 4.6.5).

6.3.2 Rock domain RFR02

Rock domain RFR02 was modelled to include all subsurface geological data in the local SFR model volume that is not assigned to RFR01. It is far more heterogeneous relative to rock domain RFR01 (Figure 6-6). The dominant rock type is the fine- to finely medium-grained metagranodiorite (to granite), which is commonly indistinguishable from the felsic to intermediate metavolcanic rock. However, it needs to be emphasized that there is a considerable uncertainty in the exact estimate of the two rock types. According to the mapping, the felsic to intermediate metavolcanic rock is more frequent in boreholes within or associated with SFR than in boreholes further south (see Table 6-2). It is possible that at least some of this difference between the northern and southern part of the domain is related to the difficulties in separating the two rock types macroscopically.

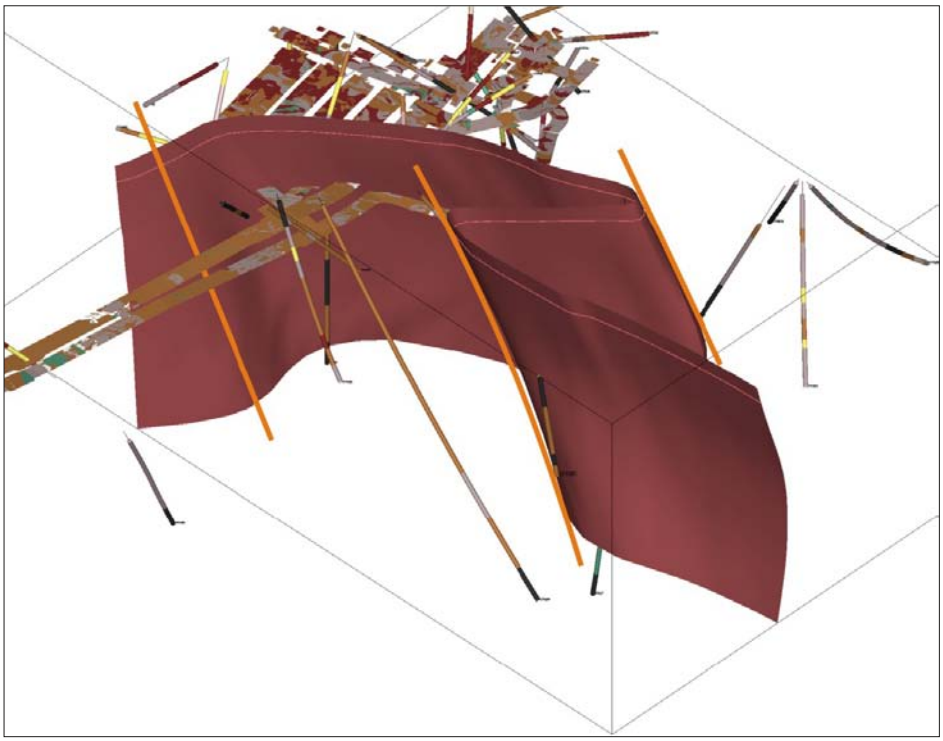

Figure 6-8. *Three dimensional model of the rock domain boundary between RFR01 and RFR02 relative to the borehole geology, the geometry of the SFR underground facility and the local model volume. Also shown are imaginary fold axes in orange for the structure. Note, however, that the folding of the rock mass in the SFR area is characterised by considerable irregularity and that the shape of the boundary primarily is based on geological fixed points and is not a product of a pure structural concept. View from SSW.*

Table 6-2. Quantitative estimates in volume % of the proportions of different rocks in domains RFR01 and RFR02, where the latter has been divided into a northern part, which includes all boreholes from the construction of SFR, and a southern part, which includes all boreholes from the new drilling campaign. Estimates for individual boreholes are provided in Appendix 15.

Rock domain	101057	101058	101061	102017	103076	111058	Other*	Total length
RFR01	28.7	1.1	59.8	1.3	3.3	5.0	0.8	1,507.6
RFR02	37.4	4.1	24.1	6.3	11.5	14.9	1.7	3,767.0
Southern BHs	50.0	1.6	24.8	9.2	5.9	7.4	1.1	1,139.5
Northern BHs	32.0	5.1	23.9	5.0	13.9	18.1	2.0	2,627.5

* Other includes granitoid (1051), granite (1058), aplite (1062), hybrid rock (5105), breccia (6005), cataclastic rock (8003), mylonite (8004), hydrothermal vein/segregation, unspecified (8020), Quartz-dominated hydrothermal vein/segregation (8021), ultramafic rock, metamorphic (101004), granite, granodiorite and tonalite, metamorphic, fine- to medium-grained (101051), tonalite to granodiorite, metamorphic (101054) and calc-silicate rock (skarn) (108019).

The subordinate rock types are dominated by pegmatitic granite and pegmatite, which amounts to 24%, if all boreholes within RFR02 are included. Other volumetrically important rock types are younger granite (15%), amphibolite (6%) and aplitic metagranite (4%). The proportions among the subordinate rock types differ also between the southern and northern parts of the domain, especially for the younger granites, which occupy 18% of the boreholes in northern and 7% in the southern part. In spite of these differences, which also occur among the boreholes within each subarea, RFR02 was modelled as one heterogeneous rock domain.

The heterogeneity and content of rock types with high magnetic susceptibility conform with the belt of high, but variable magnetic intensity that extends with a NW-SE trend from the SFR underground facility to an islet south of Grisselgrundet, just outside the local model area. In the modelling process, this belt was taken as an approximation of the surface extent of RFR02.

6.3.3 Rock domain RFR03

As mentioned above, the low magnetic belt that forms the surface expression of RFR03 has been treated as a composite result of oxidation related to brittle structures and volumes dominated by pegmatitic granite and pegmatite. A considerable part of the SFR underground facility, including the rock vault tunnel (BST) and connecting parts of the caverns (BMA and BLA), lies directly beneath a part of the low magnetic belt (Figure 6-9a). As indicated above, these parts of the facility exhibit no obvious difference in rock composition from the remaining parts of SFR within RFR02. Pegmatitic granite and pegmatite occur but are no more frequent in these parts than in other, proximal parts of SFR.

The overview structural map provided by /Christiansson and Blovede 1987/ reveals several minor fracture zones that strike NNW-SSE in the BST and connecting caverns, as illustrated in Figure 6-9a. These zones can be correlated with two magnetic lineaments (MSFR08030 and MSFR08082), which are parallel with zone ZFMNNW1206 and intersect the caverns further to the west (Figure 6-9b). Bearing in mind these relationships, it is inferred that these minor fractures zones rather than lithological differences contribute to most of the magnetic low. However, the zones are too small to be modelled deterministically. ZFMNNE0869 also contributes to the low magnetic belt, and the surface trace of RFR03 does not correspond exactly to the low magnetic belt.

The character of the boundary between rock domains RFR02 and RFR03 in unknown, but the magnetic signatures inside these two domains are similar. On the basis of this observation, domain RFR03 has also been modelled so as to define the core of a major fold structure. In addition, it is necessary to use steeply plunging axes to avoid those parts of the SFR underground facility included within RFR03. A rather steep boundary is also supported by the magnetic inversion modelling (see Section 4.6.4). Due to the lack of other information, it was decided to use the 13 mineral stretching lineations recorded in boreholes from the latest drilling campaign (Appendix 14) as a very approximate orientation of the fold axes that define the folded boundary between RFR02 and RFR03. The data cluster rather tightly with a mean pole at 151°/84°. It should be emphasized that this inference is associated with a high uncertainty. Note also that with a fold axis orientation of 151°/84°, the associated belt of high magnetic intensity, situated north of the low magnetic belt, will plunge downwards intercepting the deeper part of the local model volume. However, only a minor part of this belt would extend into the local model volume and, considering the general uncertainties in the extent of RFR03, it was decided to disregard this in the modelling procedure.

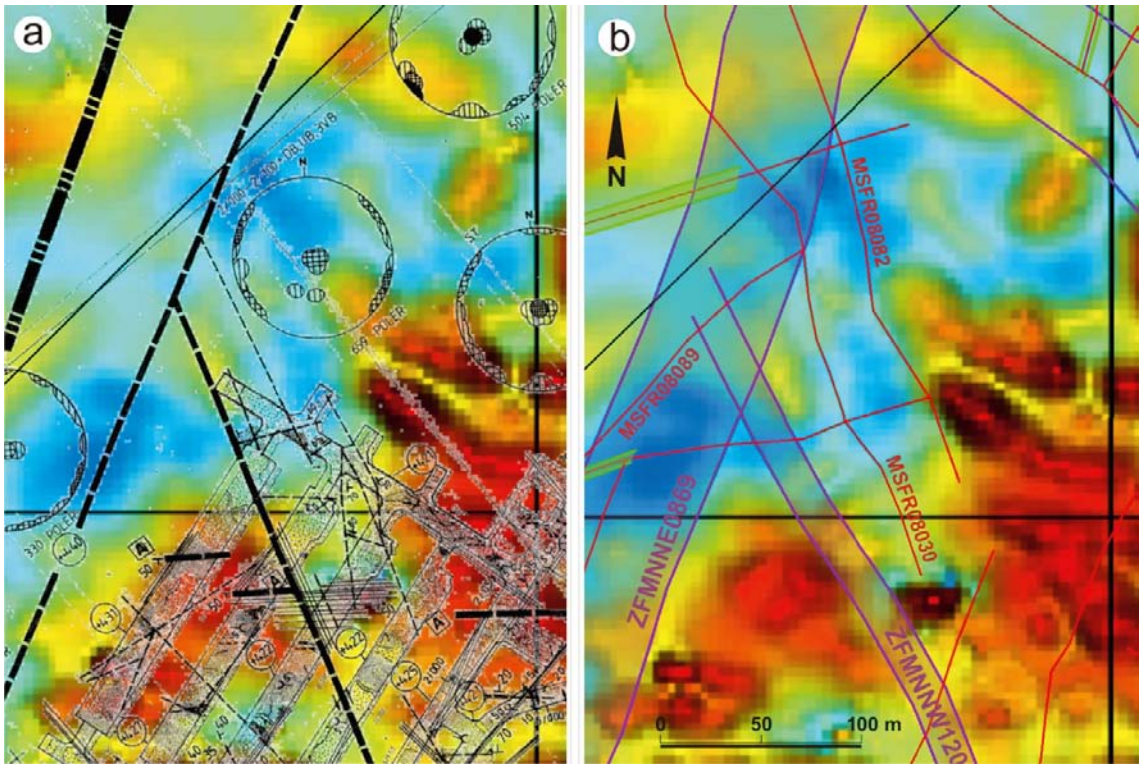

Figure 6-9. *Detail of the WSW-ENE trending belt of low magnetic intensity north-west of the SFR underground facility and its relationship with a) the overview structural map of /Christiansson and Bolvede 1987/ and b) magnetic lineaments and modelled deformation zones. The black thin line marks the local SFR model volume and the thicker black lines are RT90 coordinates (6 702 000, 1 633 000).*

The geometrical extension of this domain towards the east and south-east remains uncertain in the absence of geological data. A connection with rock domain RFR01, outside the local model volume and beneath the pier, cannot be excluded according to the magnetic total field.

6.3.4 Rock domain RFR04

Geological data from RFR04 are completely lacking and there are no other information available than the magnetic total field for the location and orientation of the boundary between RFR02 and RFR04. For this reason and in order to simplify future interaction between both the SFR local model and the regional rock domain model for Forsmark stage 2.2 /Stephens et al. 2007/, it was decided to follow the contact between RFM021 and RFM033 as the boundary between RFR02 and RFR04. On the basis of the magnetic total field data, the boundary is tectonic, at least in its north-western part.

An appropriate boundary to follow is the current north-eastern margin of ZFMNW0805A. In the north-western part of the model volume, this margin corresponds well with the contact between RFM021 and RFM033, as defined in the regional rock domain model stage 2.2 /Stephens et al. 2007/. Indeed, the same conceptual thinking for this rock domain boundary was adopted in the stage 2.2 modelling work. However, in the south-eastern part of the model volume, the boundary strikes more to the E-W away from zone ZFMNW0805A. A possible alternative solution would have been to make use of a combination of zone ZFMNW0805A and zone ZFMWNW0836 to help define the boundary in this part of the model volume. The main difference between these two solutions is a difference in dip between the two alternatives, where the contact between RFM021 and RFM033 is more gently dipping (39°, and in the local SFR model volume 61°) towards the north-east and terminates along the north-eastern model boundary at approximately –200 m elevation in the model adopted here, instead of extending to the base of the model in the alternative solution (Figure 6-10). Deformation zone ZFMNW0805A, on the other hand, has a dip of 82° towards north-east, and consequently intercepts the base of the model volume. It is important to keep in mind that neither a boundary defined completely by deformation zone ZFMNW0805A nor a boundary defined only partly by zone ZFMNW0805A, as presented here, is in conflict with the available geological or geophysical data.

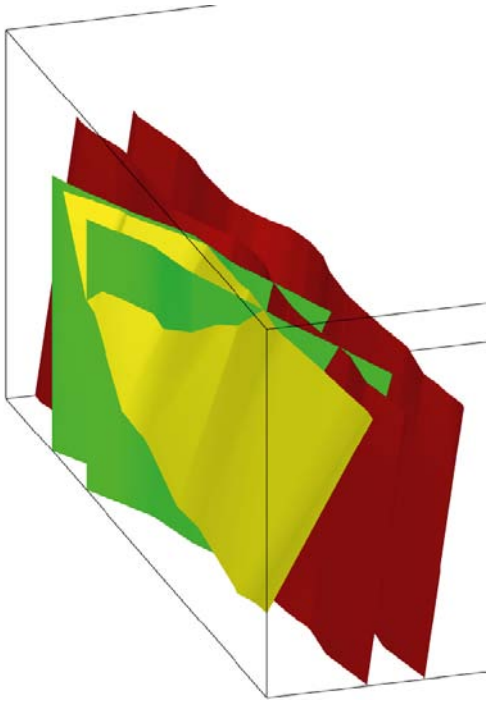

Figure 6-10. *Three dimensional model showing the relationship between the boundary between RFR02 and RFR04 (yellow) and ZFMNW0805A (red) and ZFMWNW0836 (green), relative to the local model volume. View from NNW.*

6.4 Evaluation of key uncertainties

The geometries of the rock domain model rely on the accuracy of the SFR tunnel mapping and the positioning of boreholes at depth. Data from the construction of SFR lack much of the quality-assurance that marks current SKB methodology, not least regarding positioning. It is impossible to quantify these uncertainties, but they need to be considered when using the model. Calculated uncertainties for the spatial position of boreholes from the Forsmark site investigation and the latest drilling campaign in the area are judged to be minor in character, considered in the context of the uncertainties in the position of older data from the construction of SFR. However, there are uncertainties related to the geological mapping that affect the general uncertainty in the rock domains.

Specific uncertainties of importance for the rock domains include the following:

- Deviation measurements were not available in the SKB database Sicada for any of the boreholes from the construction of SFR.
- Geometries of all SFR underground openings in the drawings of /Christiansson and Bolvede 1987/ are theoretical rather than ‘as built’ and involve deliberate mapping generalizations as a result of the unfolding. Laser defined tunnel centre-lines were used for positioning of the drawings in the model volume.
- Translation of the bedrock mapping from /Christiansson and Bolvede 1987/ into the rock type nomenclature introduced during the Forsmark site investigation.
- Orientation of linear structures in boreholes, especially percussion drilled boreholes.
- The separation of the fine- to finely medium-grained metagranodiorite (to granite) and the felsic to intermediate metavolcanic rock by ocular inspection. However, the overlap in the petrophysical and structural properties suggests similar mechanical properties.
- The character of the rock described as fine- to finely medium-grained metagranodiorite (to granite), especially in terms of modal composition and origin.
- The physical properties of the rocks in the SFR area are based on density and magnetic measurements on a fairly small number of samples from drill core. There are few surface-bound petrophysical data and gamma spectrometry measurements on outcrops or in boreholes.

With four fixed points from boreholes and five from underground openings in SFR, distributed between –71 and –205 m elevation in the model volume, the uncertainty in the geometry of the boundary between RFR01 and RFR02 is judged to be low. The use of the high-resolution magnetic total field has refined the modelling of the boundary at levels where direct geological information is lacking. Sufficient data are available to estimate quantitatively the proportions of different rock types in RFR01 and RFR02, and associated uncertainties are judged to be low to moderate.

The geometry of the domain boundary between RFR02 and RFR03 is defined by geological information from RFR02 and the high-resolution magnetic total field, with no fixed points. Uncertainties in the geometry are consequently considered to be moderate to high.

The domain boundary between RFR02 and RFR04 is identical to the contact between RFM021 and RFM033 in the regional rock domain stage 2.2 model for Forsmark, which, in turn, was defined by geological information outside the local SFR model volume and without the use of the high-resolution ground magnetic data currently available inside this volume. Therefore, uncertainties in the geometry are considered to be moderate to high.

Geological data are lacking for both RFR03 and RFR04 and uncertainties in the properties are considered to be high. However, since the rock domains are peripheral to the volume of interest for extension of SFR, this lack of data is not judged to be of any major significance.

7 Comparison of SFR model version 1.0 with Forsmark model stage 2.2

The conceptual model for the geological evolution of the Forsmark area /Stephens et al. 2007/ has been used to supply the basic framework and approach for the SFR modelling work. Indeed, the SFR central block and its bounding shear belts to the south-west and north-east share some similarities to the neighbouring Forsmark lens geometry, albeit on a smaller scale and with a less well-developed contrast in structural anisotropy in the rock mass. The Forsmark geological modelling team has been the primary internal reviewer of the SFR work and have ensured, as far as deemed necessary, that it has been consistent with the earlier developed models. In particular, it was a guiding control that the SFR version 1.0 and Forsmark stage 2.3 lineaments and, as a consequence, the associated inferred deformation zones should have the same surface positions at the interface between the Forsmark local and SFR regional model volumes, which bear the same degree of resolution. At the time of writing the current report, the upgrading of the geological Forsmark stage 2.2 geological models has not yet been completed. Clearly account needs to be taken of the updated structures presented in the SFR version 1.0 regional geological model in this upgrading work. Differences in the details of how zone thickness are modelled, described below, also needs to be noted.

7.1 Deformation zone models

The SFR regional model volume lies wholly within the Forsmark regional model volume. However, as can been seen in Figure 1-4, there is only a partial overlap between the Forsmark local model and SFR regional model volumes. The deformation zone modelling work in these two volumes share the same resolution, in that both models include zones with a minimum trace length of 1,000 m. In comparison, the resolution of the Forsmark regional model is very different and only includes zones with a surface trace length of 3,000 m or more.

In general, the same modelling procedure has been applied in both the Forsmark and SFR projects. However, details of how zone thickness is estimated differ slightly. For Forsmark stage 2.2, on the few occasions where more than one borehole intercept have been correlated with a particular zone, the overall modelled thickness of that zone is a mean value calculated from the individual SHI PDZ's intersected /Stephens et al. 2007/. However, in general, the thickness is based on the data from a single borehole intercept. For SFR version 1.0, where more zones are based on multiple borehole and tunnel intercepts, zone thickness has been modelled using an envelope concept involving the definition of target and geometrical intercepts for included boreholes and tunnels. Details of the methodology and explanations of these terms are presented in Section 5.2.2. However, it essentially relies on using the maximum thickness as indicated by the thickest individual SHI PDZ correlated with the particular modelled deformation zone. It is considered that this slightly more conservative approach is a minor improvement on the earlier applied methodology, since the maximum zone thickness identified by a borehole intercept is highly unlikely to equate to the point of maximum thickness of the zone. Similarly, the minimum thickness of a zone is often in practical terms zero, since experience shows it is possible to drill through a established zone without finding evidence in an individual borehole intercept. Where no borehole intersections are involved, zone thickness for Forsmark stage 2.2 was estimated from a deformation zone length vs. thickness correlation, developed during the project, whereas for SFR version 1.0, a simplistic classification has been applied. The correlation chart and classification are presented in Section 5.3.4.

As well as the differences in coverage and resolution there are key differences in input data. The results from the latest SFR drilling campaign were not available for the Forsmark modelling work. To a certain extent, since all these data are from an area to the north-east of the regional zone ZFMWNW0001, it is of less importance to the focused study at Forsmark to identify a potential site for a deep repository. However, as part of the Forsmark site investigation and its associated model stage 2.3, data produced during Forsmark stage 2.3 were acquired after and were not used in the final stage 2.2 geological models for Forsmark /Stephens et al. 2007/. They were used instead to help verify the existing stage 2.2 models /Stephens et al. 2008b/. These activities included new high-resolution ground magnetic data that lead to an updated lineament map and new borehole data

including widespread kinematic data. Of particular relevance to the shared Forsmark local and SFR regional model volumes was the completion of the 851 m long borehole KFM11A, which penetrates the regional ZFMWNW0001 deformation zone and its neighbouring splays that together constitute the tectonic shear belt north-east of the Forsmark tectonic lens. It is this belt that divides the much larger Forsmark lens from the neighbouring SFR central block.

The additional magnetic and borehole data were analysed and the results reported in /Stephens et al. 2008b/. However, the results of this analytical work remain to be incorporated into upgraded geological models for Forsmark. Thus, although there are minor differences between the SFR version 1.0 deformation zone model and the existing Forsmark stage 2.2 local model, in the treatment of the deformation zones in the overlapping rock volume, including the Singö deformation zone (ZFMWNW0001), its neighbouring splays and sub-parallel structures (ZFMNW0002, ZFMWNW0813, ZFMWNW1056, ZFMWNW1035 and ZFMWNW3259) and the cross-cutting zones in the NNE sub-set (ZFMNNE0725 and ZFMNNE2308), these differences are principally related to the lack of an updated Forsmark model that takes account of stage 2.3 data. There are no interpretations in the SFR model version 1.0 which impact the existing Forsmark models with any significance.

Further to the north-east, inside the SFR central block, there are only three deformation zones from the Forsmark stage 2.2 local model that penetrate the SFR regional model; ZFM871, ZFMNNE0869 and ZFMWNW0835B. Two of these zones, ZFM871 and ZFMNNE0869, correspond to zone H2 and zone 3 in the older SFR models. They were adopted from /Axelsson and Mærsk Hansen 1997/ in the Forsmark stage 2.2 model /Stephens et al. 2007/ and are described in detail here in Chapter 5 and Appendix 11.

In comparison with earlier models, ZFM871 has had its orientation and thickness somewhat modified from 048°/15°, 10 m to 074°/19°, 20 m in model SFR version 1.0. However, the most significant difference is that the extent of the zone has been considerably reduced and is, in fact, much closer to that earlier reported in /Christiansson 1986/. The uncertainty of the extent of ZFM871 is further discussed in Section 5.6. ZFMNNE0869 has essentially the same position and orientation in both models but has had its thickness increased from 10 to 60 m in SFR version 1.0. This apparently dramatic increase, based both on SHI PDZ's and tunnel mapping, is due to the version 1.0 modelled zone geometry representing the thickness of an inferred swarm of sub-parallel smaller structures, rather than the single, simpler structure modelled earlier in /Axelsson and Mærsk Hansen 1997/ that was adopted in Forsmark stage 2.2 /Stephens et al. 2007/. ZFMWNW0835B is represented very differently in the two models. This is simply due to the earlier Forsmark stage 2.2 lineament being no longer supported by the later high-resolution data of Forsmark stage 2.3. The lineament name and number were maintained between the two stages but their positions differ significantly. The stage 2.3 lineament MFM0835BG and the linking of version 1.0 lineaments MSFR08107 and MSFR08106 are the basis for the modelling of zone ZFMWNW0835 in SFR model version 1.0.

In addition to the three deformation zones named above there are three more zones from the Forsmark regional model stage 2.2 that penetrate the SFR regional model volume; ZFMNE0808A, ZFMNW0805 and ZFMWNW0836. Zone ZFMNE0808A is a medium confidence zone and lies outside the SFR regional model volume at the ground surface. It only penetrates the lower part of the SFR regional model volume, based on an assumed dip to the north-west. It has not been included in the SFR regional model. ZFMNW0805 from Forsmark stage 2.2 is represented by ZFMNW0805A and its nearby splay ZFMNW0805B in both the SFR local and regional models. These zones together constitute a similar complex deformation shear belt comparable with ZFMWNW0001 and its neighbouring splays on the south-western side of the SFR central block, albeit on a much smaller scale. Although there are differences in all details concerning how this zone(s) has been modelled by the Forsmark and SFR projects, they are not considered to be of any significance and are based on updated lineament and drilling data coupled to the higher degree of resolution in the SFR modelling work. ZFMNW0836 is a medium confidence zone in both models. There are differences in the zone's alignment within the SFR regional model area that are based on the SFR version 1.0 lineaments and a further review of the magnetic data. However, these differences are not considered significant and the position of this zone on the north-eastern side of the ZFMNW0805A/B shear belt means that this zone is of little importance in both projects.

The initial identification of gently dipping zones in the Forsmark model areas was largely based on the results of the seismic reflection surveys summarised in /Stephens et al. 2007/. At an early stage in the investigations, it was decided that no new seismic reflection survey would be acquired in conjunction with the SFR investigations. The existing seismic survey data only provide a very limited coverage

of the SFR local model area. However, in order to optimize the use of the available data, it was decided to reprocess and reinterpret the data with a focus on SFR and the shallow depth of interest. The results were reported in /Juhlin and Zhang 2010/ and summarised in Section 4.6.3 of this report. Only two gently dipping reflectors, intercepting the SFR regional model volume but lying outside the local model volume, were identified by the reprocessing work; reflector A1, which was the basis for the modelled zone ZFMA1 in the Forsmark stage 2.2 model and a new reflector, B10.

ZFMA1 is located at depth on the south-eastern side of the regional deformation zone ZFMWNW0001. The reprocessing work confirmed that the reflector A1 does not extend to the ground surface and does not occur on the north-eastern side of ZFMWNW0001, which is consistent with how the possible zone ZFMA1 was modelled Forsmark stage 2.2 /Stephens et al. 2007/. A slight adjustment in the orientation was suggested in the reprocessing work, but this adjustment was uncertain and falls within the earlier quoted range by /Stephens et al. 2007/. On this basis, the Forsmark stage 2.2 geometry has been maintained in the SFR version 1.0 model. The uncertainty in the geological character of this reflector is emphasized by its lower confidence of existence as a deformation zone (see property tables of deformation zones in /Stephens et al. 2007/ and in Appendix 11).

Reflector B10 is interpreted as having an orientation of 025°/35° and lies outside and below the SFR local model volume on the north-eastern side of ZFMWNW0001. Its existence as a reflector is judged highly probable but the dip is particularly uncertain. It has been included in the SFR regional model as a low confidence deformation zone, although the reflector could be related wholly or partly to compositional variations in the bedrock. Since this reflector was not identified in the earlier interpretation /Juhlin and Palm 2005/, it was not addressed in the earlier Forsmark models. The reflector geometry is largely limited by the spread of the survey data and, for this reason, its true extent is unknown. Thus, the earlier established Forsmark concept has been applied, i.e. this type of zone has been terminated at the nearest, steeply dipping, major deformation zone with WNW-ESE or NW-SE strike. The reflector appears to extend to the surface although its position is uncertain. The general area of its supposed outcrop is not covered by high resolution magnetic data nor does it coincide with any potential candidate regional lineament.

7.2 Rock domain models

The local SFR model volume is situated at the boundary between rock domains RFM021 and RFM033, as defined in the regional rock domain model stage 2.2 /Stephens et al. 2007/. Rock domain RFM021, which hosts almost the entire local SFR model volume, is inferred to have a high degree of heterogeneity (cf. /Stephens et al. 2007/). A significant difference between the Forsmark and SFR rock domain models is the scale of resolution. The heterogeneity of the model volume accentuates with increasing resolution and becomes crucial for the domain division within a volume that measures 720×860×300 m, compared with the Forsmark regional model volume at 15,000×11,000×2,100 m, especially in the SFR volume where large amounts of younger, group D rocks are present. For these reasons, the current division of the SFR rock domain model is inferred to lie within the scope of the inferred heterogeneity of RFM021. The increased data coverage yielded by the latest SFR drilling programme has mainly contributed to the understanding of the details of individual domains in the SFR model.

Another noteworthy aspect is the occurrence of felsic to intermediate metavolcanic rock, which is the inferred dominant rock type within RFM021 /Stephens et al. 2007/. In the local SFR model volume, this rock type is present but is a subordinate component, being most frequent in RFR02, where it occupies approximately 11% of the total mapped borehole length. The most obvious reason for this difference is the large volume of pegmatitic granite, pegmatite and younger granite in the SFR volume, as mentioned above. However, some of the difference can also be ascribed to the difficulties in the ocular separation of the felsic to intermediate metavolcanic rock from the rock defined as high-strain varieties of the metagranodiorite (to granite). Thus, there is considerable uncertainty in the estimates of the proportions of these two rock types. Some of the sections recorded as felsic to intermediate metavolcanic rock during the rock type coding carried out during an early stage of the Forsmark site investigation /Stephens et al. 2008a/ have been re-interpreted, in this study, as highly deformed varieties of the metagranodiorite (to granite). It must also be emphasized that limited outcrop data distributed along almost 7 km of RFM021 have been the primary input to its characterization. In contrast, there are no outcrops in the local SFR model area and the compositional estimates are largely based on drill core information. It is evident that there are large-scale variations in RFM021, both in terms of rock type and degree of ductile deformation.

8 References

SKB's (Svensk Kärnbränslehantering AB) publications can be found at www.skb.se/publications.

Andersson J, Ström A, Svemar C, Almén K-A, Ericsson L O, 2000. What requirements does the KBS-3 repository make on the host rock? Geoscientific suitability indicators and criteria for siting and site evaluation. SKB TR-00-12, Svensk Kärnbränslehantering AB.

Axelsson C-L, Mærsk Hansen L, 1997. Update of structural models at SFR nuclear waste repository, Forsmark, Sweden. SKB R-98-05, Svensk Kärnbränslehantering AB.

Axelsson C-L, Ekstav A, Lindblad Pässe A, 1995. SFR – Utvärdering av hydrogeology. SKB R-02-14, Svensk Kärnbränslehantering AB. (In Swedish.)

Balu L, Cosma C, 2005. Estimation of 3D positions and orientations of reflectors based on an updated interpretation of Stage 1 reflection seismic data. Preliminary site description Forsmark area – version 1.2. SKB R-05-39, Svensk Kärnbränslehantering AB.

Berglund J, 2009. Site investigation SFR. Geological mapping and laser scanning of the lower construction tunnel. SKB P-09-74, Svensk Kärnbränslehantering AB.

Bergman T, Andersson J, Hermansson T, Zetterström Evins L, Albrecht L, Stephens M B, Petersson J, Nordman C, 2004. Forsmark site investigation. Bedrock mapping. Stage 2 (2003) – bedrock data from outcrops and the basal parts of trenches and shallow boreholes through the Quarternary cover. SKB P-04-91, Svensk Kärnbränslehantering AB.

Carlsson A, 1979. Characteristic features of a superficial rock mass in Southern central Sweden. Horizontal and sub-horizontal fractures and filling material. Striae 11.

Carlsson A, Christiansson R, 1987. Geology and tectonics at Forsmark, Sweden. SKB SFR 87-04, Svensk Kärnbränslehantering AB.

Carlsson A, Christiansson R, 2007. Construction experiences from underground works at Forsmark. Compilation report. SKB R-07-10, Svensk Kärnbränslehantering AB.

Carlsson L, Carlsten S, Sigurdsson T, Winberg A, 1985. Hydraulic modeling of the final repository for reactor waste (SFR). Compilation and conceptualization of available geological and hydrogeological data. Edition 1. SKB SFR 85-06, Svensk Kärnbränslehantering AB.

Carlsson L, Winberg A, Arnefors J, 1986. Hydraulic modeling of the final repository for reactor waste (SFR). Compilation and Conceptualization of Available Geological and Hydrogeological Data. SKB SFR 86-03, Svensk Kärnbränslehantering AB.

Carlsten S, Gustafsson J, Mattsson H, Petersson J, Stephens M, 2005. Forsmark site investigation. Geological single-hole interpretation of KFM06A and KFM06B (DS6). SKB P-05-132, Svensk Kärnbränslehantering AB.

Carlsten S, Döse C, Samuelsson E, Gustafsson J, Petersson J, Stephens M, Thunehed H, 2007. Forsmark site investigation. Geological single-hole interpretation of KFM11A, HFM33, HFM34 and HFM35. SKB P-07-109, Svensk Kärnbränslehantering AB.

Christiansson R, 1986. Geologisk beskrivning av zoner kring slutförvaret. SKB SFR 86-02, Svensk Kärnbränslehantering AB. (In Swedish.)

Christiansson R, Bolvede P, 1987. Byggnadsgeologisk uppföljning. Slutrapport. SKB SFR 87-03, Svensk Kärnbränslehantering AB. (In Swedish.)

Christiansson R, Magnusson K-Å, 1985a. Geologisk miljö kring Silo 1. SKB SFR 85-07, Svensk Kärnbränslehantering AB. (In Swedish.)

Christiansson R, Magnusson K-Å, 1985b. Hydrogeologiskt program. Beskrivning av den geologiska miljön kring kärnborrhålen HK1–4. SKB SFR 85-03, Svensk Kärnbränslehantering AB. (In Swedish.)

Claesson L-Å, Nilsson G, 2007. Forsmark site investigation. Drilling of flushing water well HFM33 and monitoring wells HFM34 and HFM35 at drill site DS11. SKB P-07-11, Svensk Kärnbränslehantering AB.

Claesson L-Å, Nilsson G, Ullberg A, 2007. Forsmark site investigation. Drilling of the telescopic borehole KFM11A at drill site DS11. SKB P-07-45, Svensk Kärnbränslehantering AB.

Claesson Liljedahl L, Munier R, Sandström B, Drake H, Tullborg E-L, 2011. Assessment of fractures classified as non-mineralised in the Sicada database. SKB R-11-02, Svensk Kärnbränslehantering AB.

Cosma C, Balu L, Enescu N, 2003. Estimation of 3D positions and orientations of reflectors identified during the reflection seismic survey at the Forsmark area. SKB R-03-22, Svensk Kärnbränslehantering AB.

Cosma C, Balu L, Enescu N, 2006. Estimation of 3D positions and orientations of reflectors identified during the reflection seismic survey. Site descriptive modelling Forsmark Stage 2.1. SKB R-06-93, Svensk Kärnbränslehantering AB.

Curtis P, Elfström M, Markström I, 2007. Rock Visualization System. Technical description (RVS version 4.0). SKB R-07-44, Svensk Kärnbränslehantering AB.

Curtis P, Petersson J, Triumf C-A, Isaksson H, 2009. Site investigation SFR. Deformation zone modelling. Model version 0.1. SKB P-09-48, Svensk Kärnbränslehantering AB.

Döse C, 2009. Site investigation SFR. Boremap mapping of percussion drilled boreholes HFR101, HFR102, HFR105 and core drilled borehole KFR27 (down to 147.4 m length). SKB P-09-37, Svensk Kärnbränslehantering AB.

Döse C, Samuelsson E, 2007. Forsmark site investigation. Boremap mapping of percussion boreholes HFM33-37. SKB P-07-106, Svensk Kärnbränslehantering AB.

Döse C, Stråhle A, Mattsson K-J, Carlsten S, 2009a. Site investigation SFR. Boremap mapping of core drilled borehole KFR101. SKB P-09-36, Svensk Kärnbränslehantering AB.

Döse C, Winell S, Stråhle A, Carlsten S, 2009b. Site investigation SFR. Boremap mapping of core drilled boreholes KFR102B and KFR103. SKB P-09-38, Svensk Kärnbränslehantering AB.

Follin S, 2008. Bedrock hydrogeology Forsmark. Site descriptive modelling, SDM-Site Forsmark. SKB R-08-95, Svensk Kärnbränslehantering AB.

Fox A, La Pointe P, Hermanson J, Öhman J, 2007. Statistical geological discrete fracture network model. Forsmark modelling stage 2.2. SKB R-07-46, Svensk Kärnbränslehantering AB.

Glamheden R, Maersk Hansen L, Fredriksson A, Bergkvist L, Markström I, Elfström M, 2007. Mechanical modelling of the Singö deformation zone. Site descriptive modelling Forsmark stage 2.1. SKB R-07-06, Svensk Kärnbränslehantering AB.

Gustafsson J, Gustafsson C, 2006a. Forsmark site investigation. RAMAC and BIPS logging in boreholes KFM08C, HFM30, HFM31, HFM33 and HFM34. SKB P-06-178, Svensk Kärnbränslehantering AB.

Gustafsson J, Gustafsson C, 2006b. Forsmark site investigation. RAMAC and BIPS logging in boreholes KFM10A, HFM35 and HFM38. SKB P-06-177, Svensk Kärnbränslehantering AB.

Gustafsson J, Gustafsson C, 2007. Forsmark site investigation. RAMAC and BIPS logging in borehole KFM11A. SKB P-07-10, Svensk Kärnbränslehantering AB.

Gustafsson J, Gustafsson C, 2008. Site investigation SFR. Radar and BIPS loggings in KFR101 and BIPS loggings in KFR27 (0–147 m), HFR101, HFR102 ans HFR105. SKB P-08-71, Svensk Kärnbränslehantering AB.

Gustafsson J, Gustafsson C, 2009a. Site investigation SFR. BIPS-logging in the core drilled boreholes KFR102A, KFR102B, KFR103, KFR104 and KFR27 (140–500 m) and radar logging in KFR27 (0–500 m), KFR102A and KFR104. SKB P-09-11, Svensk Kärnbränslehantering AB.

Gustafsson J, Gustafsson C, 2009b. Site investigation SFR. Radar and BIPS loggings in KFR105, KFR106 and HFR106. SKB P-09-58, Svensk Kärnbränslehantering AB.

Hagkonsult, 1982. Geologiska undersökningar och utvärderingar för lokalisering av SFR till Forsmark. SKBF/KBS SFR 81-13, Svensk Kärnbränsleförsörjning AB. (In Swedish.)

Hagkonsult, 1983. Geologiska undersökningar och utvärderingar för förvarsutrymmen i berg. SKBF/KBS SFR 83-05, Svensk Kärnbränsleförsörjning AB. (In Swedish.)

Hansen L, 1989. Bedrock of the Forsmark area. Technical report, Swedish State Power Board, Stockholm.

Hermansson T, Stephens M B, Corfu F, Andersson J, Page L, 2007. Penetrative ductile deformation and amphibolite-facies metamorphism prior to 1851 Ma in the western part of the Svecofennian orogen, Fennoscandian Shield. Precambrian Research, 153, pp 29–45.

Hermansson T, Stephens M B, Corfu F, Page L M, Andersson J, 2008a. Migratory tectonic switching, western Svecofennian orogen, central Sweden: Constraints from U/Pb zircon and titanite geochronology. Precambrian Research, 161, pp 250–278.

Hermansson T, Stephens M B, Page L M, 2008b. $^{40}Ar/^{39}Ar$ hornblende geochronology from the Forsmark area in central Sweden: Constraints on late Svecofennian cooling, ductile deformation and exhumation. Precambrian Research, 167, pp 303–315.

Holmén J G, Stigsson M, 2001. Modelling of future hydrogeological conditions at SFR. SKB R-01-02, Svensk Kärnbränslehantering AB.

Isaksson H, 2003. Forsmark site investigation. Interpretation of topographic lineaments 2002. SKB P-03-40, Svensk Kärnbränslehantering AB.

Isaksson H, 2007. Correlation between refraction seismic data, low magnetic lineaments and deformation zones (model stage 2.2). In: Stephens M B, Skagius K (eds). Geology – Background complementary studies. Forsmark modelling stage 2.2. SKB R-07-56, Svensk Kärnbränslehantering AB, pp 113–130.

Isaksson H, Keisu M, 2005. Forsmark site investigation. Interpretation of airborne geophysics and integration with topography. Stage 2 (2002–2004). An integration of bathymetry, topography, refraction seismics and airborne geophysics. SKB P-04-282, Svensk Kärnbränslehantering AB.

Isaksson H, Mattsson H, Thunehed H, Keisu M, 2004a. Forsmark site investigation. Interpretation of petrophysical surface data. Stage 1 (2002). SKB P-03-102, Svensk Kärnbränslehantering AB.

Isaksson H, Mattsson H, Thunehed H, Keisu M, 2004b. Forsmark site investigation. Petrophysical surface data. Stage 2 – 2003 (including 2002). SKB P-04-155, Svensk Kärnbränslehantering AB.

Isaksson H, Thunehed H, Keisu M, 2004c. Forsmark site investigation. Interpretation of airborne geophysics and integration with topography. Stage 1 (2002). SKB P-04-29, Svensk Kärnbränslehantering AB.

Isaksson H, Pitkänen T, Thunehed H, 2006a. Forsmark site investigation. Ground magnetic survey and lineament interpretation in an area northwest of Bolundsfjärden. SKB P-06-85, Svensk Kärnbränslehantering AB.

Isaksson H, Thunehed H, Pitkänen T, Keisu M, 2006b. Forsmark site investigation. Detailed ground and marine magnetic survey and lineament interpretation in the Forsmark area – 2006. SKB P-06-261, Svensk Kärnbränslehantering AB.

Isaksson H, Thunehed H, Pitkänen T, Keisu M, 2007. Forsmark site investigation. Detailed ground magnetic survey and lineament interpretation in the Forsmark area, 2006–2007. SKB R-07-62, Svensk Kärnbränslehantering AB.

Juhlin C, Bergman B, 2004. Reflection seismics in the Forsmark area. Updated interpretation of Stage 1 (previous report R-02-43). Updated estimate of bedrock topography (previous report P-04-99). SKB P-04-158, Svensk Kärnbränslehantering AB.

Juhlin C, Palm H, 2005. Forsmark site investigation. Reflection seismic studies in the Forsmark area, 2004: Stage 2. SKB R-05-42, Svensk Kärnbränslehantering AB.

Juhlin C, Stephens M B, 2006. Gently dipping fracture zones in Paleoproterozoic metagranite, Sweden: Evidence from reflection seismic and cored borehole data and implications for the disposal of nuclear waste. Journal of Geophysical Research, 111, B09302.

Juhlin C, Zhang F, 2010. Site investigation SFR. Reprocessing of reflection seismic profiles 5b and 8, Forsmark. SKB P-10-50, Svensk Kärnbränslehantering AB.

Juhlin C, Bergman B, Palm H, 2002. Reflection seismic studies in the Forsmark area – stage 1. SKB R-02-43, Svensk Kärnbränslehantering AB.

Keisu M, Isaksson H, 2004. Forsmark site investigation. Acquistition of geological information from Forsmarksverket. Information from the Vattenfall archive, Råcksta. SKB P-04-81, Svensk Kärnbränslehantering AB.

Leijon B (ed), 2005. Forsmark site investigation. Investigations of superficial fracturing and block displacements at drill site 5. SKB P-05-199, Svensk Kärnbränslehantering AB.

Mattsson H, 2009. Site investigation SFR. Interpretation of geophysical borehole measurements from KFR01, KFR02, KFR03, KFR04, KFR05, KFR19 and KFR20 and petrophysical measurements from KFR04, KFR05 and KFR20. SKB P-09-72, Svensk Kärnbränslehantering AB.

Mattsson H, Keisu M, 2007a. Forsmark site investigation. Interpretation of geophysical borehole measurements from KFM10A, KFM08C, HFM30, HFM31, HFM33, HFM34, HFM35 and HFM38. SKB P-06-258, Svensk Kärnbränslehantering AB.

Mattsson H, Keisu M, 2007b. Forsmark site investigation. Interpretation of geophysical borehole measurements from KFM02B, KFM08D and KFM11A. SKB P-07-125, Svensk Kärnbränslehantering AB.

Mattsson H, Keisu M, 2009a. Site investigation SFR. Interpretation of geophysical borehole measurements and petrophysical data from KFR101, HFR101, HFR102 and HFR105. SKB P-09-02, Svensk Kärnbränslehantering AB.

Mattsson H, Keisu M, 2009b. Site investigation SFR. Interpretation of geophysical borehole measurements from KFR102A, KFR102B, KFR103, KFR104 and KFR27 (0–500 m). SKB P-09-26, Svensk Kärnbränslehantering AB.

Mattsson H, Keisu M, 2010. Site investigation SFR. Interpretation of geophysical borehole measurements and petrophysical data from KFR105, KFR106 and HFR106. SKB P-10-12, Svensk Kärnbränslehantering AB.

Mattsson H, Isaksson H, Thunehed H, 2003. Forsmark site investigation. Petrophysical rock sampling, measurements of petrophysical rock parameters and in situ gamma-ray spectrometry measurements on outcrops carried out 2002. SKB P-03-26, Svensk Kärnbränslehantering AB.

Munier R, Stenberg L, Stanfors R, Milnes A G, Hermansson J, Triumf C-A, 2003. Geological Site Descriptive Model. A strategy for the model development during site investigations. SKB R-03-07, Svensk Kärnbränslehantering AB.

Möller C, Snäll S, Stephens M B, 2003. Forsmark site investigation. Dissolution of quartz, vug formation and new grain growth associated with post-metamorphic hydrothermal alteration in KFM02A. SKB P-03-77, Svensk Kärnbränslehantering AB.

Nielsen U T, Ringgaard J, 2007a. Forsmark site investigation. Geophysical borehole logging in boreholes KFM08C, KFM10A, HFM30, HFM31, HFM33, HFM34, HFM35 and HFM38. SKB P-07-05, Svensk Kärnbränslehantering AB.

Nielsen U T, Ringgaard J, 2007b. Forsmark site investigation. Geophysical borehole logging in boreholes KFM011A and KFM09B. SKB P-07-92, Svensk Kärnbränslehantering AB.

Nielsen U T, Ringgaard J, 2008. Site investigation SFR. Geophysical borehole logging in the boreholes HFR101, HFR102, HFR105, KFR27 (0–148 m), KFR101 and HFM07. SKB P-08-93, Svensk Kärnbränslehantering AB.

Nielsen U T, Ringgaard J, 2009a. Site investigation SFR. Geophysical borehole logging in the boreholes KFR27 (0–500 m), KFR102A, KFR102B, KFR103, KFR104 and HFM07. SKB P-09-16, Svensk Kärnbränslehantering AB.

Nielsen U T, Ringgaard J, 2009b. Site investigation SFR. Geophysical borehole logging in the boreholes KFR105 and HFM07. SKB P-09-76, Svensk Kärnbränslehantering AB.

Nielsen U T, Ringgaard J, 2009c. Site investigation SFR. Geophysical borehole logging in the boreholes KFR106, HFR106 and HFM07. SKB P-09-77, Svensk Kärnbränslehantering AB.

Nilsson A-C, Tullborg E-L, Smellie J, 2010. Preliminary hydrogeochemical site description SFR (version 0.2). SKB R-10-38, Svensk Kärnbränslehantering AB.

Nilsson G, 2009a. Site investigation SFR. Drilling of groundwater monitoring well HFR106. SKB P-09-47, Svensk Kärnbränslehantering AB.

Nilsson G, 2009b. Site investigation SFR. Drilling of the cored borehole KFR105. SKB P-09-41, Svensk Kärnbränslehantering AB.

Nilsson G, 2009c. Site investigation SFR. Drilling of the cored borehole KFR106. SKB P-09-55, Svensk Kärnbränslehantering AB.

Nilsson G, Ullberg A, 2008. Site investigation SFR. Drilling of water well HFR101 and monitoring wells HFR102 and HFR105. SKB P-08-95, Svensk Kärnbränslehantering AB.

Nilsson G, Ullberg A, 2009a. Site investigation SFR. Drilling of the cored boreholes KFR101, KFR102B, KFR103 and KFR104. SKB P-09-13, Svensk Kärnbränslehantering AB.

Nilsson G, Ullberg A, 2009b. Site investigation SFR. Drilling of the telescopic borehole KFR102A. SKB P-09-19, Svensk Kärnbränslehantering AB.

Nilsson G, Ullberg A, 2009c. Site investigation SFR. Drilling of the traditional borehole KFR27. SKB P-09-12, Svensk Kärnbränslehantering AB.

Nordgulen Ø, Saintot A, 2006. Forsmark site investigation. The character and kinematics of deformation zones (ductile shear zones, fault zones and fracture zones) at Forsmark – report from phase 1. SKB P-06-212, Svensk Kärnbränslehantering AB.

Olofsson I, Simeonov A, Stephens M B, Follin S, Nilsson A-C, Röshoff K, Lindberg U, Lanaro F, Fredriksson A, Persson L, 2007. Site descriptive modelling Forsmark, stage 2.2. A fracture domain concept as a basis for the statistical modelling of fractures and minor deformation zones, and interdisciplinary coordination. SKB R-07-15, Svensk Kärnbränslehantering AB.

Petersson J, Andersson U B, 2011. Site investigation SFR. Overview Boremap mapping of drill cores from KFR04, KFR08, KFR09, KFR13, KFR35, KFR36, KFR54, KFR55, KFR7A, KFR7B and KFR7C. SKB P-08-02, Svensk Kärnbränslehantering AB.

Petersson J, Berglund J, Danielsson P, Wängnerud A, Tullborg E-L, Mattsson H, Thunehed H, Isaksson H, Lindroos H, 2004a. Forsmark site investigation. Petrography, geochemistry, geophysics and fracture mineralogy of boreholes KFM01A, KFM02A and KFM03A+B. SKB P-04-103, Svensk Kärnbränslehantering AB.

Petersson J, Berglund J, Wängnerud A, Danielsson P, Stråhle A, 2004b. Forsmark site investigation. Boremap mapping of telescopic drilled borehole KFM05A. SKB P-04-295, Svensk Kärnbränslehantering AB.

Petersson J, Berglund J, Danielsson P, Skogsmo G, 2005. Forsmark site investigation. Petrographic and geochemical characteristics of bedrock samples from boreholes KFM04A–06A, and a whitened alteration rock. SKB P-05-156, Svensk Kärnbränslehantering AB.

Petersson J, Berglund J, Andersson U B, Wängnerud A, Danielsson P, Ehrenborg J, 2007. Forsmark site investigation. Boremap mapping of telescopic drilled borehole KFM11A. SKB P-07-104, Svensk Kärnbränslehantering AB.

Petersson J, Nissen J, Curtis P, Bockgård N, Öhman J, Mattsson H, Stråhle A, Winell S, 2009a. Site investigation SFR. Geological single-hole interpretation of KFR102A. SKB P-09-60, Svensk Kärnbränslehantering AB.

Petersson J, Curtis P, Bockgård N, Simeonov A, 2009b. Site investigation SFR. Geological single-hole interpretation of KFR04, KFR08, KFR09, KFR13, KFR35, KFR36, KFR54, KFR55, KFR7A, KFR7B and KFR7C. SKB P-09-32, Svensk Kärnbränslehantering AB.

Petersson J, Curtis P, Bockgård N, Simeonov A, Mattsson H, Gustafsson J, Stråhle A, 2009c. Site investigation SFR. Geological single-hole interpretation of KFR101, HFR101, HFR102 and HFR105. SKB P-09-34, Svensk Kärnbränslehantering AB.

Petersson J, Curtis P, Bockgård N, Simeonov A, Mattsson H, Döse C, Stråhle A, Winell S, 2009d. Site investigation SFR. Geological single-hole interpretation of KFR102B and KFR103. SKB P-09-33, Svensk Kärnbränslehantering AB.

Petersson J, Nissen J, Bockgård N, Simeonov A, Thunehed H, Döse C, Stråhle A, Winell S, 2009e. Site investigation SFR. Geological single-hole interpretation of KFR104 and KFR27. SKB P-09-35, Svensk Kärnbränslehantering AB.

Petersson J, Nissen J, Curtis P, Bockgård N, Mattsson H, Stråhle A, Winell S, 2010a. Site investigation SFR. Geological single-hole interpretation of KFR106 and HFR106. SKB P-10-08, Svensk Kärnbränslehantering AB.

Petersson J, Nissen J, Curtis P, Bockgård N, Öhman J, Mattsson H, Stråhle A, Winell S, 2010b. Site investigation SFR. Geological single-hole interpretation of KFR105. SKB P-10-06, Svensk Kärnbränslehantering AB.

Petersson J, Curtis P, Bockgård N, Mattsson H, 2011. Site investigation SFR. Rock type coding, overview geological mapping and identification of rock units and possible deformation zones in drill cores from the construction of SFR. SKB P-10-07, Svensk Kärnbränslehantering AB.

Sandström B, Tullborg E-L, 2011. Site investigation SFR. Fracture mineralogy and geochemistry of borehole sections sampled for groundwater chemistry and Eh. Results from boreholes KFR01, KFR08, KFR10, KFR19, KFR7A and KFR105. SKB P-11-01, Svensk Kärnbränslehantering AB.

Sandström B, Tullborg E-L, Smellie J, MacKenzie A, Suksi J, 2008. Fracture mineralogy of the Forsmark site. SDM-Site Forsmark. SKB R-08-102, Svensk Kärnbränslehantering AB.

Sandström B, Tullborg E-L, Larson S Å, Page L, 2009. Brittle tectonothermal evolution in the Forsmark area, central Fennoscandian shield, recorded by paragenesis, orientation and 40Ar/39Ar geochronology of fracture minerals. Tectonophysics, 478, pp 158–174.

Sandström B, Annersten H, Tullborg E-L, 2010. Fracture-related hydrothermal alteration of metagranitic rock and associated changes in mineralogy, geochemistry and degree of oxidation: a case study at Forsmark, central Sweden. International Journal of Earth Sciences, 99, pp 1–25.

SKB, 2002. Forsmark – site descriptive model version 0. SKB R-02-32, Svensk Kärnbränslehantering AB.

SKB, 2004. Preliminary site description. Forsmark area – version 1.1. SKB R-04-15, Svensk Kärnbränslehantering AB.

SKB, 2005. Preliminary site description. Forsmark area – version 1.2. SKB R-05-18, Svensk Kärnbränslehantering AB.

SKB, 2006. Site descriptive modelling Forsmark stage 2.1. Feedback for completion of the site investigation including input from safety assessment and repository engineering. SKB R-06-38, Svensk Kärnbränslehantering AB.

SKB, 2008a. Geovetenskapligt undersökningsprogram för utbyggnad av SFR. SKB R-08-67, Svensk Kärnbränslehantering AB. (In Swedish.)

SKB, 2008b. Site description of Forsmark at completion of the site investigation phase. SDM-Site Forsmark. SKB TR-08-05, Svensk Kärnbränslehantering AB.

Stephens M B, Forssberg O, 2006. Rock types and ductile structures on a rock domain basis, and fracture orientation and mineralogy on a deformation zone basis. Preliminary site description. Forsmark area – version 1.2. SKB R-06-78, Svensk Kärnbränslehantering AB.

Stephens M B, Skagius K (eds), 2007. Geology – background complementary studies. Forsmark modelling stage 2.2. SKB R-07-56, Svensk Kärnbränslehantering AB.

Stephens M B, Bergman T, Andersson J, Hermansson T, Wahlgren C-H, Albrecht L, Mikko H, 2003a. Bedrock mapping. Stage 1 (2002) – outcrop data including fracture data, Forsmark. SKB P-03-09, Svensk Kärnbränslehantering AB.

Stephens M B, Lundqvist S, Bergman T, Andersson J, Ekström M, 2003b. Forsmark site investigation. Bedrock mapping. Rock types, their petrographic and geochemical characteristics, and a structural analysis of the bedrock based on Stage 1 (2002) surface data. SKB P-03-75, Svensk Kärnbränslehantering AB.

Stephens M B, Lundqvist S, Bergman T, Ekström M, 2005. Forsmark site investigation. Bedrock mapping. Petrographic and geochemical characteristics of rock types based on stage 1 (2002) and stage 2 (2003) surface data. SKB P-04-87, Svensk Kärnbränslehantering AB.

Stephens M B, Fox A, La Pointe P R, Simeonov A, Isaksson H, Hermanson J, Öhman J, 2007. Geology Forsmark. Site descriptive modelling Forsmark stage 2.2. SKB R-07-45, Svensk Kärnbränslehantering AB.

Stephens M B, Bergman T, Isaksson H, Petersson J, 2008a. Bedrock geology Forsmark. Modelling stage 2.3. Description of the bedrock geological map at the ground surface. SKB R-08-128, Svensk Kärnbränslehantering AB.

Stephens M B, Simeonov A, Isaksson H, 2008b. Bedrock geology Forsmark. Modelling stage 2.3. Implications for and verification of the deterministic geological models based on complementary data. SKB R-08-64, Svensk Kärnbränslehantering AB.

Stephens M B, Ripa M, Lundström I, Persson L, Bergman T, Ahl M, Wahlgren C-H, Persson P-O, Wickström L, 2009. Synthesis of the bedrock geology in the Bergslagen region, Fennoscandian Shield, south-central Sweden. Uppsala: Geological Survey of Sweden. (Serie Ba 58)

Söderbäck B (ed), 2008. Geological evolution, palaeoclimate and historical development in the Forsmark and Laxemar-Simpevarp areas. Site descriptive modelling, SDM-Site. SKB R-08-19, Svensk Kärnbränslehantering AB.

Söderlund P, Hermansson T, Page L M, Stephens M B, 2009. Biotite and muscovite 40Ar–39Ar geochronological constraints on the post-Svecofennian tectonothermal evolution, Forsmark site, central Sweden. International Journal of Earth Sciences, 98, pp 1835–1851.

Winell S, 2009. Site investigation SFR. Boremap mapping of core drilled borehole KFR105. SKB P-09-59, Svensk Kärnbränslehantering AB.

Winell S, 2010a. Site investigation SFR. Boremap mapping of core drilled borehole KFR106. SKB P-10-09, Svensk Kärnbränslehantering AB.

Winell S, 2010b. Site investigation SFR. Boremap mapping of percussion drilled borehole HFR106. SKB P-10-10, Svensk Kärnbränslehantering AB.

Winell S, Carlsten S, Stråhle A, 2009a. Site investigation SFR. Boremap mapping of core drilled borehole KFR102A. SKB P-09-52, Svensk Kärnbränslehantering AB.

Winell S, Döse C, Stråhle A, Carlsten S, Selnert E, 2009b. Site investigation SFR. Boremap mapping of core drilled boreholes KFR104 and KFR27 (from 147.5 m). SKB P-09-39, Svensk Kärnbränslehantering AB.

Öhman J, Follin S, 2010. Site investigation SFR. Hydrogeological modelling of SFR, model version 0.2. SKB R-10-03, Svensk Kärnbränslehantering AB.

Öhman J, Bockgård N, Follin S, 2011. Site investigation SFR. Hydrogeological modelling of SFR – Data review and parameterisation. SKB R-11-03, Svensk Kärnbränslehantering AB.

Appendix 1

Specification of available data

Available bedrock geological and geophysical data and their treatment in SFR model version 1.0.

Data specification	Reference to data report	Activity plan	Reference in Sicada/SDE/SKBdoc	Usage in version 1.0 analysis/ modelling
Bedrock mapping – outcrop data				
Rock type, rock type distribution and ductile deformation	/Stephens et al. 2003a/	AP PF400-02-011	SICADA-10-125, GIS_request11_03	Input to RD modelling
	/Bergman et al. 2004/	AP PF400-02-011		
	Bedrock geological map, Forsmark version 1.1	AP PF400-02-011		
	Bedrock geological map, Forsmark version 1.2	AP PF400-02-011		
	Revised bedrock geological map, Forsmark version 2.2	AP PF400-02-011		
	Revised bedrock geological map, Forsmark version 2.3	AP PF400-02-011		
	/Stephens et al. 2008a/			
Ground geophysical data and lineament interpretation				
Petrophysical and in situ gamma-ray spectrometric data from rock types	/Mattsson et al. 2003/	AP PF400-02-011	SICADA-11-017	Input to RD modelling
	/Isaksson et al. 2004a/	AP PF400-02-047		
	/Isaksson et al. 2004b/	AP PF400-02-011 AP PF400-02-047		
High-resolution ground magnetic measurements	/Isaksson et al. 2006a/	AP PF400-05-082	GIS_request11_03	Identification of magnetic lineaments and input for RD and DZ modelling
	/Isaksson et al. 2006b/	AP PF400-06-034		
	/Isaksson et al. 2007/	AP PF400-06-034		
Interpretation of topographic, bathymetric and helicopter-borne geophysical data. Lineament assessment	/Isaksson et al. 2004c/	AP PF400-02-047	GIS_request11_03	Identification of magnetic lineaments and input for RD and DZ modelling
	/Isaksson and Keisu 2005/	AP PF400-02-047		
Correlation between refraction seismics, lineaments and DZ's	/Isaksson 2007/		SICADA-11-065	Input to DZ modelling
Reflectors identified during reflection seismic survey	/Balu and Cosma 2005/		SICADA-11-019, GIS_request11_03	Input to DZ modelling
	/Cosma et al. 2006/			
	/Cosma et al. 2003/			
	/Juhlin et al. 2002/	AP PF400-03-84		
	/Juhlin and Bergman 2004/	AP PF400-03-84		
	/Juhlin and Palm 2005/	AP PF400-04-78		
	/Juhlin and Zhang 2010/			
Data from core-drilled boreholes from the construction of SFR				
Technical data	/Hagkonsult 1982/	–	SICADA-11-016	Siting and orientation of the boreholes in the modelling work
	/Hagkonsult 1983/	–		
	/Carlsson et al. 1986/	–		
	/Keisu and Isaksson 2004/	AP PF400-02-048		
Geophysical logging and petrophysical data (KFR01, KFR02, KFR03, KFR04, KFR05, KFR19, KFR20)	/Christiansson and Magnusson 1985a/	–	SICADA-09-061, SICADA-11-014, SICADA-11-021	Data used in geological SHI and input for RD and DZ modelling
	/Christiansson and Magnusson 1985b/	–		
	/Mattsson 2009/	AP SFR-09-009		
Older geological mapping including fracture logging	/Hagkonsult 1983/	–	–	Input to rock type coding according to SKB:s current nomenclature
	/Christiansson and Magnusson 1985a/	–		
	/Christiansson and Magnusson 1985b/	–		
	/Christiansson 1986/	–		

Data specification	Reference to data report	Activity plan	Reference in Sicada/SDE/SKBdoc	Usage in version 1.0 analysis/ modelling
Updated geological mapping and rock type coding	/Petersson and Andersson 2008/	AP SFR-07-004	SICADA-10-031, SICADA-10-051, SICADA-10-066, SICADA-11-011, SICADA-11-013,	Used in geological SHI and as input to RD and DZ modelling
	/Petersson et al. 2009a/	AP SFR-09-014 AP SFR-09-020 AP SFR-09-028		
Geological SHI	/Petersson et al. 2009a/	AP SFR-09-014 AP SFR-09-020 AP SFR-09-028	SICADA-10-082	Input for RD and DZ modelling
	/Petersson et al. 2009b/	AP SFR-07-005		
Data from core- and precussion-drilled boreholes from the period 2006 to 2009				
Technical data (HFM34, HFM35, HFR101, HFR102, HFR105, HFR106, KFM11A, KFR27, KFR101, KFR102A, KFR102B, KFR103, KFR104, KFR105, KFR106)	/Claesson et al. 2007/	AP PF400-06-006 AP PF400-06-025	SICADA-11-016	Siting and orientation of the bore-holes in the modelling work
	/Claesson and Nilsson 2007/	AP PF400-06-027		
	/Nilsson and Ullberg 2008/	AP SFR-08-001		
	/Nilsson and Ullberg 2009a/	AP SFR-08-001 AP SFR-08-002		
	/Nilsson and Ullberg 2009b/	AP SFR-08-011		
	/Nilsson and Ullberg 2009c/	AP SFR-08-002 AP SFR-08-020		
	/Nilsson 2009a/	AP SFR-09-015		
	/Nilsson 2009b/	AP SFR-09-004		
	/Nilsson 2009c/	AP SFR-09-015 AP SRF-09-016		
Radar and BIPS-logging (HFM34, HFM35, HFR101, HFR102, HFR105, HFR106, KFM11A, KFR27, KFR101, KFR102A, KFR102B, KFR103, KFR104, KFR105, KFR106)	/Gustafsson and Gustafsson 2006a/	AP PF400-06-046	SICADA-10-010, SICADA-11-012, SICADA-11-014	Data used in borehole mapping (BIPS) and in geological SHI (radar logging) with focus on the identifica-tion of brittle deformation zones. Input for both RD and DZ modelling.
	/Gustafsson and Gustafsson 2006b/	AP PF400-06-046		
	/Gustafsson and Gustafsson 2007/	AP PF400-06-092		
	/Gustafsson and Gustafsson 2008/	AP SFR-08-003		
	/Gustafsson and Gustafsson 2009a/	AP SFR-08-017		
	/Gustafsson and Gustafsson 2009b/	AP SFR-09-011 AP SFR-09-019		
Geophysical logging, petrophysical data and interpretation of geophysical data (HFM34, HFM35, HFR101, HFR102, HFR105, HFR106, KFM11A, KFR27, KFR101, KFR102A, KFR102B, KFR103, KFR104, KFR105, KFR106)	/Nielsen and Ringgaard 2007a/	AP PF400-06-050	SICADA-11-014, SICADA-11-021	Data used in the borehole mapping and in geological SHI. Input for both RD and DZ modelling.
	/Nielsen and Ringgaard 2007b/	AP PF400-06-103		
	/Nielsen and Ringgaard 2008/	AP SFR-08-004		
	/Nielsen and Ringgaard 2009a/	AP SFR-08-018		
	/Nielsen and Ringgaard 2009b/	AP SFR-09-010		
	/Nielsen and Ringgaard 2009c/	AP SFR-09-018		
	/Mattsson and Keisu 2007a/	AP PF400-06-074		
	/Mattsson and Keisu 2007b/	AP PF400-07-018		
	/Mattsson and Keisu 2009a/	AP SFR-08-010		
	/Mattsson and Keisu 2009b/	AP SFR-08-010 AP SFR-08-019		
	/Mattsson and Keisu 2010/	AP SFR-09-017		

Data specification	Reference to data report	Activity plan	Reference in Sicada/SDE/SKBdoc	Usage in version 1.0 analysis/ modelling
Boremap mapping (HFM34, HFM35, HFR101, HFR102, HFR105, HFR106, KFM11A, KFR27, KFR101, KFR102A, KFR102B, KFR103, KFR104, KFR105, KFR106)	/Döse and Samuelsson 2007/	AP PF400-06-115	SICADA-08-194, SICADA-10-001, SICADA-10-008, SICADA-10-023, SICADA-10-031, SICADA-10-034, SICADA-10-035, SICADA-10-040, SICADA-10-051, SICADA-10-066, SICADA-10-092, SICADA-10-130, SICADA-10-175, SICADA-11-011, SICADA-11-018	Used in geological SHI and as input to RD and DZ modelling.
	/Petersson et al. 2007/	AP PF400-06-094		
	/Döse 2009/	AP SFR-08-006		
	/Döse et al. 2009a/	AP SFR-08-006		
	/Döse et al. 2009b/	AP SFR-08-015		
	/Winell et al. 2009a/	AP SFR-09-001		
	/Winell et al. 2009b/	AP SFR-08-028		
	/Winell 2009/	AP SFR-09-012		
	/Winell 2010a/	AP SFR-09-027		
	/Winell 2010b/	AP SFR-09-027		
Geological SHI (HFM34, HFM35, HFR101, HFR102, HFR105, HFR106, KFM11A, KFR27, KFR101, KFR102A, KFR102B, KFR103, KFR104, KFR105, KFR106)	/Carlsten et al. 2007/	AP PF400-07-016	SICADA-10-082	Input to RD and DZ modelling.
	/Petersson et al. 2009c/	AP SFR-08-009		
	/Petersson et al. 2009f/	AP SFR-08-009		
	/Petersson et al. 2009d/	AP SFR-08-009		
	/Petersson et al. 2009e/	AP SFR-08-009		
	/Petersson et al. 2010b/	AP SFR-09-026		
	/Petersson et al. 2010a/	AP SFR-09-026		
Data from tunnel mapping				
Geological tunnel mapping and interpretation of fracture zones	/Christiansson and Bolvede 1987/	–	SICADA-11-015, GIS_request11_06	Input to modelling in proximity to the SFR facility
	/Berglund 2009/	AP SFR-07-007		
Previous models				
SFR structural models	/Carlsson et al. 1985/	–		Incorporated into SFR SDM version 0 from report form. Input to DZ modelling of zones H2, 3, 6, 8 and 9
	/Carlsson et al. 1986/	–		
	/Christiansson 1986/	–		
	/Axelsson and Hansen 1997/	–		
Forsmark SDM versions and stages 0, 1.1, 1.2, 2.1, 2.2 and 2.3. SDM-Site Forsmark	/SKB 2002/	The approved models are stored in the SKB model database SIMON	Stage 2.2 DZ GEO_MGPGVAPX GEO_IZTKKYIL RD GEO_ZAIWQGYJ GEO_ZSVNDATT	Conceptual understanding and comparison
	/SKB 2004/			
	/SKB 2005/			
	/SKB 2006/			
	/Olofsson et al. 2007/			
	/Fox et al. 2007/			
	/Stephens et al. 2007/			
	/Stephens and Skagius 2007/			
	/Sandström et al. 2008/			
	/Stephens et al. 2008b/			
	/SKB 2008b/			
SFR SDM version 0	/SKB 2008a/	–		Introduction to available data
SFR geological model 0.1	/Curtis et al. 2009/	AP SFR-08-021	RVS model SKBdoc 1224857	Input to the SFR DZ model

Appendix 2

Structural and bedrock mapping of the existing SFR facility

This appendix summarises the brittle structural data along with the colour coded bedrock mapping for the underground openings of SFR, as presented in a series of drawings by /Christiansson and Bolvede 1987/. Also data for the 18 minor deformation zones documented during the updated geological of NBT by /Berglund 2009/ are presented.

The documentation by /Christiansson and Bolvede 1987/ includes two overview drawings (–103 and –104) at the scale 1:2,000 and 23 maps at the scale 1:200 that provide supporting details. There is also a documented methodology for the tunnel mapping work as well as detailed sketches for some of the zones. However, the correlation between the structures represented in the overview mapping and the results presented in the detailed fracture mapping is unclear in some cases.

All the tunnel mapping drawings have been digitally scanned, georeferenced in ArcGis and stored in the SKB SDE GIS database as Field note SFR 146 (ID olfrgeo8576–8578, olfrgeo8580, olfrgeo8551–8556, olfrgeo8561–8562, olfrgeo8564, olfrgeo8566–8575). The drawings have subsequently been attached to the RVS model. Only the two structural overview mappings, which have formed a primary input to the DZ modelling work and a compilation of the colour coded bedrock mapping, are included here. A number of different brittle features have been marked on Drawing –103. The classification system applied includes mapped crush zones, brittle shear zones and gouge-filled fractures of varying width, as well as occurrences of closely spaced, parallel fractures and slickensides, though there is no detailed explanation of the legend in the drawing.

Table A2-1 lists the brittle features marked on Drawing –103, which are judged to be relevant at the scale of the current modelling work. Quantitative information regarding all these features is listed in Table A2-2. Each brittle feature is given an ID that consists of a number accompanied by the abbreviation tDZ (tunnel deformation zone). Numbers are marked in red on Drawing –103. 145 tDZ's have been logged and each is defined by type (cf. Table A2-1), location (facility and chainage) and orientation. The abbreviations used for the various SFR tunnels and caverns are presented in Figure 3-3 that shows a view of SFR from the north-east. In addition, Table A2-2 contains information on whether individual tDZ's were used in the previous structural models for SFR.

The colour coded bedrock map, included along with the structural overview drawings, is a compilation of the detailed drawings at the scale 1:200 of /Christiansson and Bolvede 1987/. All drawings except for drawing –14 of the silo are included and stored in SDE GIS database under Field note SFR 146, with ID SDEADM.GOL_FR_GEO_8486–8492. Both the original and current SKB nomenclatures are presented in the legend (Figure A2-2). The colours followed SKB standards for all rock types.

The new geological mapping of NBT was based on a template of the laser scanned tunnel geometry and consists of three-dimensional graphical elements related to a database with properties. Fractures, lithology, rock contacts, minor deformation zones and obvious water seepage have been recorded according to the geological nomenclature used by SKB. Figure A2-1 illustrates the extent of the 18 minor deformation zones that were registered during the NBT mapping and their relation to individual fractures. The character of individual zones are summarised in Table A2-3.

Contents

TECKENFÖRKLARING
LÄGESPARKERING AVSER TAKNIVÅ
TAKNIVÅ, LOKALT HÖJDSYSTEM (+500 = HAVSYTAN)
STÖRRE KROSSZON (SMÅGÅ)
MINDRE KROSSZON
LOKALT KROSSAT BERG
RÖRELSEZON, DELVIS KROSSAT KROSSAT OCH OMVANDLAT BERG, LAMINLAR
SPRICK - (SKÖLZONER) BREDD >2 DM
SPRICK - (SKÖLZONER) BREDD =< 2 DM
SKIVIGT BERG, BRANTSTÅENDE
SKIVIGT BERG, FLACKT (LUTNING<15°)
LUTNING 15 - 80°
VESKAXEL MED STUPNING
FÖRSKJUTNINGAR
SLICKENSIDE (OLJIDYTA)
KONNEKTION AV ZONER MELLAN OLIKA ANLÄGGNINGSDELAR
SVAGHETSZONER ENLIGT FÖRUNDERSÖKNING
POLFUNKTSDIAGRAM
FÖRSKÄRNING
SJÖSLUSEN
SAMMANSTÄLLNINGEN OMFATTAR
BYGGNADSGEOLOGISK UPPFÖLJNING
DELRAPPORT 1-6 I TOM 1985-03-181
VIAK AB
VATTENFALL
FORSMARKSARBETENA SFRI
BYGGNADSGEOLOGISK UPPFÖLJNING
TEKTONISK ÖVERSIKT
SKALA 1:2000
4920 4326
- 103

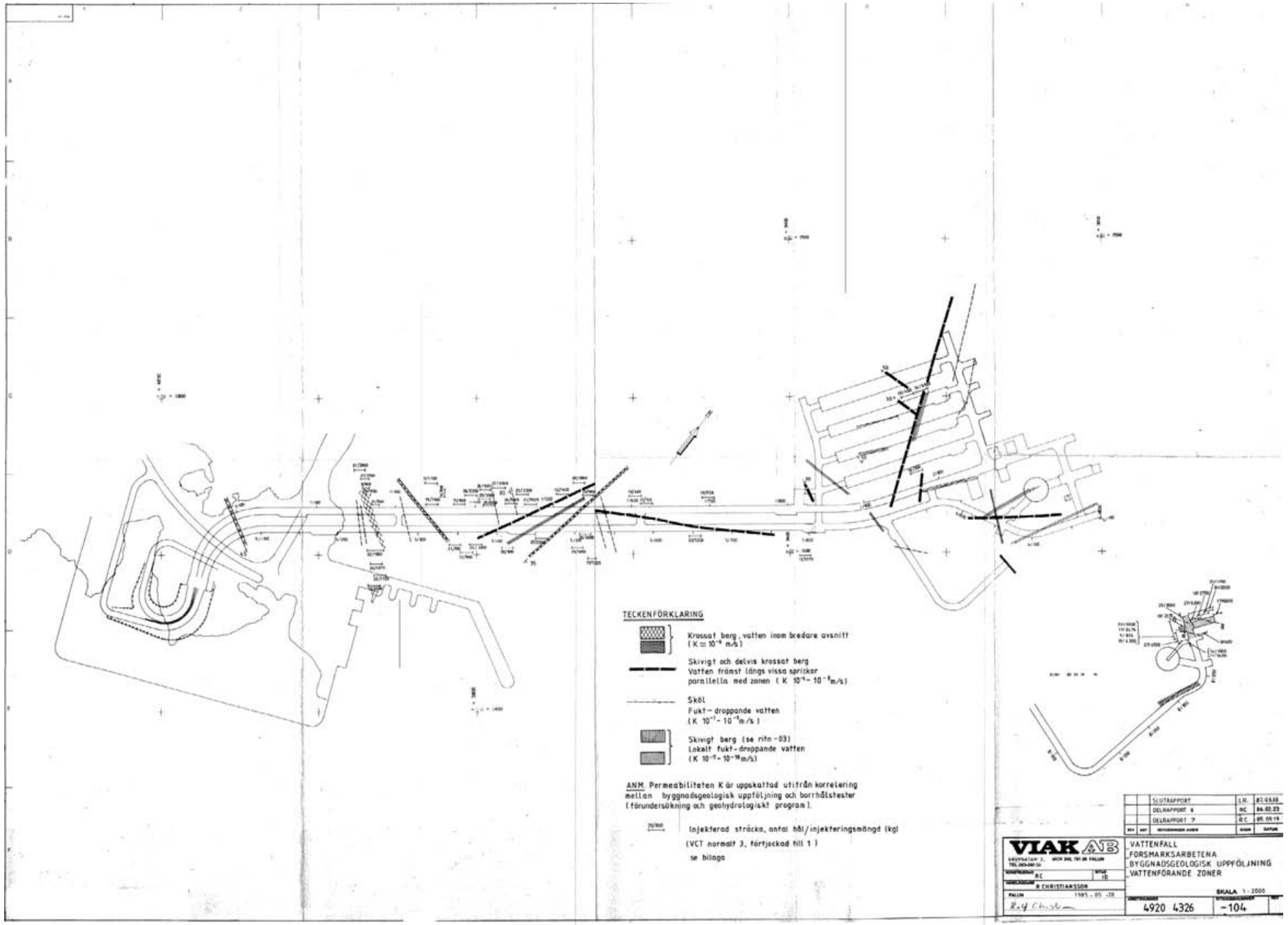
TECKENFÖRKLARING
Krossat berg, vatten inom bredare avsnitt
(K ≈ 10⁻⁶ m/s)
Skivigt och delvis krossat berg
Vatten främst längs vissa sprickor
parallella med zonen (K 10⁻⁶ – 10⁻⁸ m/s)
Sköl
Fukt – droppande vatten
(K 10⁻⁷ – 10⁻⁹ m/s)
Skivigt berg (se rifn - 03)
Lokalt fukt - droppande vatten
(K 10⁻⁷ – 10⁻¹⁰ m/s)
ANM. Permeabiliteten K är uppskattad utifrån korrelering
mellan byggnadsgeologisk uppföljning och borrhålstester
(förundersökning och geohydrologiskt program).
Injekterad sträcka, antal hål/injekteringsmängd (kg)
(VCT normalt 3, förtjockad till 1)
se bilaga
SLUTRAPPORT
DELRAPPORT 8
DELRAPPORT 7
VIAK AB
VATTENFALL
FORSMARKSARBETENA
BYGGNADSGEOLOGISK UPPFÖLJNING
VATTENFÖRANDE ZONER
SKALA 1 : 2000
4920 4326
-104

Table A2-1. Abbreviations for brittle structures listed in Table 2. Translated from legend in overview drawing –103 of /Christiansson and Bolvede 1987/.

Abbreviation	Structure (english)	Struktur (Swedish)
tDZ	Tunnel deformation zone	Tunneldeformationszon
MCZ	Major crush zone (Singö)	Större krosszon (Singö)
mCZ	Minor crush zone	Mindre krosszon
FZ	Brittle shear zone, locally crushed and altered rock, sealings	Rörelsezon, delvis krossat och omvandlat berg, läkningar
GF	Gouge-filled fracture, > 2 dm wide	Sprick – (skölzoner), bredd > 2 dm
gF	Gouge-filled fracture, < 2 dm wide	Sprick – (skölzoner), bredd < 2 dm
SPF	Closely spaced, sub-vertical parallel fractures	Skivigt berg, brantstående
GPF	Closely spaced, gently dipping parallel fractures	Skivigt berg, flackt (lutning < 15°)

Table A2-2. Tunnel intercepts for the more prominent brittle structures included in drawing –103 of /Christiansson and Bolvede 1987/. 'Modelled zone' shows the zones in the structural model of /Carlsson et al. 1985, 1986/. Deformation zone names of the current version 1.0 model are given in brackets. The correlation between the TDS's and the deformation zones in the current model is provided in Appendices 9 and 10.

Zone ID	Zone typ	DT	BT	1 BTF	2 BTF	BLA	BMA	STT	ST	NBT	TT	BST	IB	S	EB	UB	BB	Modelled zone /Carlsson et al. 1985/	Orient.
tDZ1	SPF	1+030–1+044																	296°/90°
tDZ2	SPF	1+065	5+085																050°/90°
tDZ3	gF	S-crete	5+070																120°/90°
tDZ4	mCZ	S-crete	5+076																105°/45°
tDZ5	gF	S-crete	5+072																120°/90°
tDZ6	SPF	1+143	S-crete																118°/90°
tDZ7	SPF	1+212	5+189															Singö zone (ZFM-WNW0001)	105°/80°
tDZ8	SPF	1+243	5+220															Singö zone (ZFM-WNW0001)	115°/90°
tDZ9	gF	1+255	5+228															Singö zone (ZFM-WNW0001)	115°/90°
tDZ10	gF	1+257	5+229															Singö zone (ZFM-WNW0001)	115°/90°
tDZ11	gF		5+231															Singö zone (ZFM-WNW0001)	110°/90°
tDZ12	gF	1+259	5+234															Singö zone (ZFM-WNW0001)	110°/90°

Zone ID	Zone typ	DT	BT	1 BTF	2 BTF	BLA	BMA	STT	ST	NBT	TT	BST	IB	S	EB	UB	BB	Modelled zone /Carlsson et al. 1985/	Orient.
tDZ13	GF	1+260	5+238															Singö zone (ZFM-WNW0001)	105°/90°
tDZ14	MCZ (Singö)	1+258–1+271	5+238–5+249															Singö zone (ZFM-WNW0001)	115°/90°
tDZ15	SPF	1+275	5+248															Singö zone (ZFM-WNW0001)	115°/90°
tDZ16	MCZ (Singö)	1+278–1+295	5+267–5+283															Singö zone (ZFM-WNW0001)	110°/90°
tDZ17	gF	1+291	5+268															Singö zone (ZFM-WNW0001)	125°/90°
tDZ18	gF	?	5+280															Singö zone (ZFM-WNW0001)	125°/90°
tDZ19	SPF	1+309–1+372	5+297–5+347															Singö zone (ZFM-WNW0001)	105°/90°
tDZ20	mCZ	1+322	5+302															Singö zone (ZFM-WNW0001)	100°/90°
tDZ21	gF	1+355	5+339															Singö zone (ZFM-WNW0001)	100°/90°
tDZ22	gF		5+345															Singö zone (ZFM-WNW0001)	115°/90°
tDZ23	SPF	1+395	5+370																120°/90°
tDZ24	gF	1+389	5+370																120°/90°
tDZ25	gF	1+420	?																130°/90°
tDZ26	SPF	1+422	5+398																120°/90°
tDZ27	gF	1+425																	110°/90°
tDZ28	gF	1+433	5+416																120°/90°
tDZ29	gF	1+449																	115°/80°
tDZ30	SPF	1+430	5+355																25°/80°
tDZ31	FZ	1+475	5+400															Zone 3 (ZFMNNE0869)	Dextral 205°/75°
tDZ32	gF	1+478	5+414																150°/75°
tDZ33	SPF	1+490	5+465																125°/70°
tDZ34	SPF	1+525	5+450																195°/80°
tDZ35	mCZ	1+534	5+484																355°/35°
tDZ36	SPF	1+540																	015°/90°

Zone ID	Zone typ	DT	BT	1 BTF	2 BTF	BLA	BMA	STT	ST	NBT	TT	BST	IB	S	EB	UB	BB	Modelled zone /Carlsson et al. 1985/	Orient.
tDZ37	gF		5+505																110°/90°
tDZ38	gF		5+530																110°/55°
tDZ39	gF	1+564	5+545																110°/55°
tDZ40	FZ	1+535– 1+570 1+610*	5+640– 5+690															Zone 9 (ZFMNE0870)	050°/80°
tDZ41	gF	1+594	5+579																100°/55°
tDZ42	GPF		5+600																125°/20°
tDZ43	SPF		5+630																130°/80°
tDZ44	GPF	1+680																	145°/25°
tDZ45	GPF		5+712																130°/50°
tDZ46	GPF		5+750																130°/10°
tDZ47	SPF	1+790	5+690								7+033								210°/85°
tDZ48	SPF	1+800	5+770																135°/85°
tDZ49	GPF		5+785– 5+805																155°/10°
tDZ50	gF		5+795																290°/65°
tDZ51	gF	1+872																	105°/80°
tDZ52	GPF		5+850– 5+872																135°/15°
tDZ53		1+893																	120°/35°
tDZ54	SPF		5+880																140°/85°
tDZ55	gF	1+906	5+921																070°/90°
tDZ56	SPF		5+888– 5+907															Zone 9 (ZFMNE0870)	050°/80°
tDZ57	gF		5+903							8+000– 8+023									Sinistral 285°/75°
tDZ58	gF	1+914	5+907																100°/90°
tDZ59	FZ	1+930		0+100	0+080	0+060	0+030											Zone 6 (ZFMNNW1209)	Sinistral 165°/90°
tDZ60	gF	1+939																	080°/90°
tDZ61	SPF	1+965	5+942																320°/80°
tDZ62	gF	1+970																	340°/50°
tDZ63	gF		5+951																275°/70°
tDZ64	SPF		5+942– 5+990																035°/90°

Zone ID	Zone typ	DT	BT	1 BTF	2 BTF	BLA	BMA	STT	ST	NBT	TT	BST	IB	S	EB	UB	BB	Modelled zone /Carlsson et al. 1985/	Orient.
tDZ65	gF		5+994																295°/20°
tDZ66	FZ		6+020–6+050					6+810–6+820										Zone 9 (ZFMNE0870)	235°/75°
tDZ67	SPF		6+040																320°/85°
tDZ68	SPF		6+040											X					015°/90°
tDZ69	SPF		6+060																140°/90°
tDZ70	gF		6+063																020°/70°
tDZ71	SPF		6+093																340°/40°
tDZ72	FZ	2+045	6+095			0+081	0+085	6+823		8+256									135°/55°
tDZ73	SPF		6+095						4+088	8+295–8+340									020°/90°
tDZ74	gF		6+115																300°/70°
tDZ75	gF		6+129																300°/60°
tDZ76	gF		6+146																225°/80°
tDZ77	gF		6+153																Sinistral 090°/75°
tDZ78	SPF		6+175							8+330–8+373									135°/90°
tDZ79	gF		6+163																045°/85°
tDZ80	SPF								4+088	8+352								Zone 9 (ZFMNE0870)	035°/85°
tDZ81	SPF								4+075										030°/90°
tDZ82	SPF								4+025				X	X					030°/90°
tDZ83	GPF												X						215°/05°
tDZ84	gF							6+831											295°/80°
tDZ85	gF													X					220°/85°
tDZ86	SPF	1+985–2+030																	020°/90°
tDZ87	SPF	2+000–2+050														X			030°/90°
tDZ88	SPF	2+055										3+040*							315°/85°
tDZ89	SPF	2+110													X				140°/90°
tDZ90	SPF	2+134–2+160																	030°/85°
tDZ91	SPF	2+160																	235°/80°

Zone ID	Zone typ	DT	BT	1 BTF	2 BTF	BLA	BMA	STT	ST	NBT	TT	BST	IB	S	EB	UB	BB	Modelled zone /Carlsson et al. 1985/	Orient.
tDZ92	gF	2+165–2+192																	225°/90°
tDZ93	GPF									8+080–8+090									195°/25°
tDZ94	GPF									8+120–8+165									060°/40°
tDZ95	gF									8+178									Sinistral 230°/50°
tDZ96	gF									8+183									310°/80°
tDZ97	GPF									8+193–8+210									090°/05°
tDZ98	SPF									8+222									020°/90°
tDZ99	gF																		
tDZ100	SPF									8+283									125°/90°
tDZ101	gF									X								Zone H2 (ZFM871)	Cf. tDZ60
tDZ102	gF									X							X	Zone H2 (ZFM871)	Cf. tDZ60
tDZ103	gF																X	Zone H2 (ZFM871)	Cf. tDZ60
tDZ104	FZ									8+405–8+435							X	Zone H2 (ZFM871)	040°/20°
tDZ105	FZ										7+045*								300°/20°
tDZ106	gF										7+051								105°/85°
tDZ107	gF			0+200							7+065								265°/85°
tDZ108	SPF			0+185							7+070								260°/80°
tDZ109	gF					0+015	0+003												120°/70°
tDZ110	SPF										7+115–7+155								320°/85°
tDZ111	gF				0+014														000°/75°
tDZ112	gF										3+086								345°/70°
tDZ113	gF				0+017						3+095								330°/70°
tDZ114	gF										3+104								015°/70°
tDZ115	gF										3+113								240°/65°
tDZ116	gF										3+139								270°/40°
tDZ117	gF										3+139								330°/85°
tDZ118	gF										3+177								330°/80°
tDZ119	GPF			0+070–0+090															290°/25°
tDZ120	SPF			0+105–0+165															205°/85°

Zone ID	Zone typ	DT	BT	1 BTF	2 BTF	BLA	BMA	STT	ST	NBT	TT	BST	IB	S	EB	UB	BB	Modelled zone /Carlsson et al. 1985/	Orient.
tDZ121	gF			0+146	0+137	0+129	0+126												320°/80°
tDZ122	GPF			0+135–0+160															000°/00°
tDZ123	gF			0+035															110°/90°
tDZ124	gF			0+102															165°/90°
tDZ125	SPF				0+044–0+077	0+083													105°/50°
tDZ126	SPF				0+078	0+055												Zone 6 (ZFMNNW1209)	165°/90°
tDZ127	GPF				0+118														130°/35°
tDZ128	SPF				0+127–0+157														025°/90°
tDZ129	gF				0+154														330°/50°
tDZ130	gF				0+162														280°/45°
tDZ131	gF				0+175														280°/40°
tDZ132	GPF				0+170–0+190														000°/00°
tDZ133	gF					0+024													100°/50°
tDZ134	SPF					0+052–0+062													035°/90°
tDZ135	GPF					0+100–0+115													080°/40°
tDZ136	gF					0+134													220°/80°
tDZ137	gF					0+148													070°/90°
tDZ138	gF					0+149													120°/40°
tDZ139	GPF					0+150–0+170													000°/00°
tDZ140	SPF						0+075–0+105												035°/80°
tDZ141	GPF						0+075–0+105												000°/00°
tDZ142	gF						0+128												240°/80°
tDZ143	gF						0+132												075°/90°
tDZ144	gF						0+146												105°/90°
tDZ145	GPF						0+170–0+185												000°/00°

* In connecting facility part without notation.

Table A2-3. Character of deformation zones registered during the updated mapping of NBT by /Berglund 2009/.

Zone ID	Deformation style	Kinematic indicators	Width [m]	Orientation	No of fracture sets	Orientation set #1	Orientation set #2	Orientation set #3	Remarks
1D	Brittle	x	2.0	240/85	3	178/67	050/73	235/86	Set #1 continues in 40F. Calcite, laumontite, quartz and chlorite.
2D	Ductile	x	1.0	250/45	1	250/45	–	–	Primarily affects the 101057 along the contact to a pegmatite. Isoclinal folding of pegmatites. Internal narrow (~2–30 mm) brittle-ductile shear zones along the axial planes to isoclinal folding. The zone itself is folded in open folds around gently dipping fold axes. Located in the contact to a 5–10 m wide pegmatite.
4D	Brittle-ductile	x	0.3	046/51	1	046/51	–	–	Zone towards which 182F and 184F ends. Fracture along it contains grout and seem to have aperture.
5D	Brittle	x	0.3	020/80	2	024/78	233/85	–	Probably same zone as 1D.
6D	Brittle-ductile	x	0.5	248/89	2	248/89	060/85	–	Striation in 070/10. Hint: North side down to the NE. The zone does not appear on the western side of the tunnel.
7D	Brittle-ductile	x	0.3	220/70	1	220/70	–	–	Probably the same zone as 9D.
8D	Brittle-ductile	x	0.1	266/80	1	266/80	–	–	Developed in a narrow amphibolite band in a pegmatite. Undulating along the boundary to the pegmatite.
9D	Brittle-ductile	–	0.5	248/72	2	235/70	195/85	–	Striation in 080/10. Partly calcite-laumontite-hematite-sealed breccia.
10D	Brittle	x	0.5	023/40	2	023/40	208/79	–	Ends as single fracture in both ends.
11D	Brittle-ductile	x	0.1	240/60	1	240/60	–	–	Sheared contact between 111058 and 103076.
12D	Brittle-ductile	x	0.5	328/82	1	328/82	–	–	Approximately 10–12 fractures can be related to the zone.
13D	Brittle	–	0.4	245/70	1	245/70	–	–	Breccia and other cataclastic rock.
14D	Brittle-ductile	–	0.6	307/79	2	307/79	102/55	–	Set #2 is partly represented by narrow (~10–50 mm) ductile, rather than brittle-ductile shear zones.
15D	Brittle	–	0.3	156/80	1	156/80	–	–	Brecciated and other cataclastic rock.
16D	Brittle	–	0.3	346/70	1	346/70	–	–	10–15 subparallel fractures, some cuts each other at low angle. Maximum width 2–3 mm. Calcite, laumontite and oxidized walls.
17D	Brittle	–	0.2	190/87	1	190/87	–	–	Brecciated and other cataclastic rock.
18D	Brittle	–	0.1	159/86	2	159/86	150/90	–	–

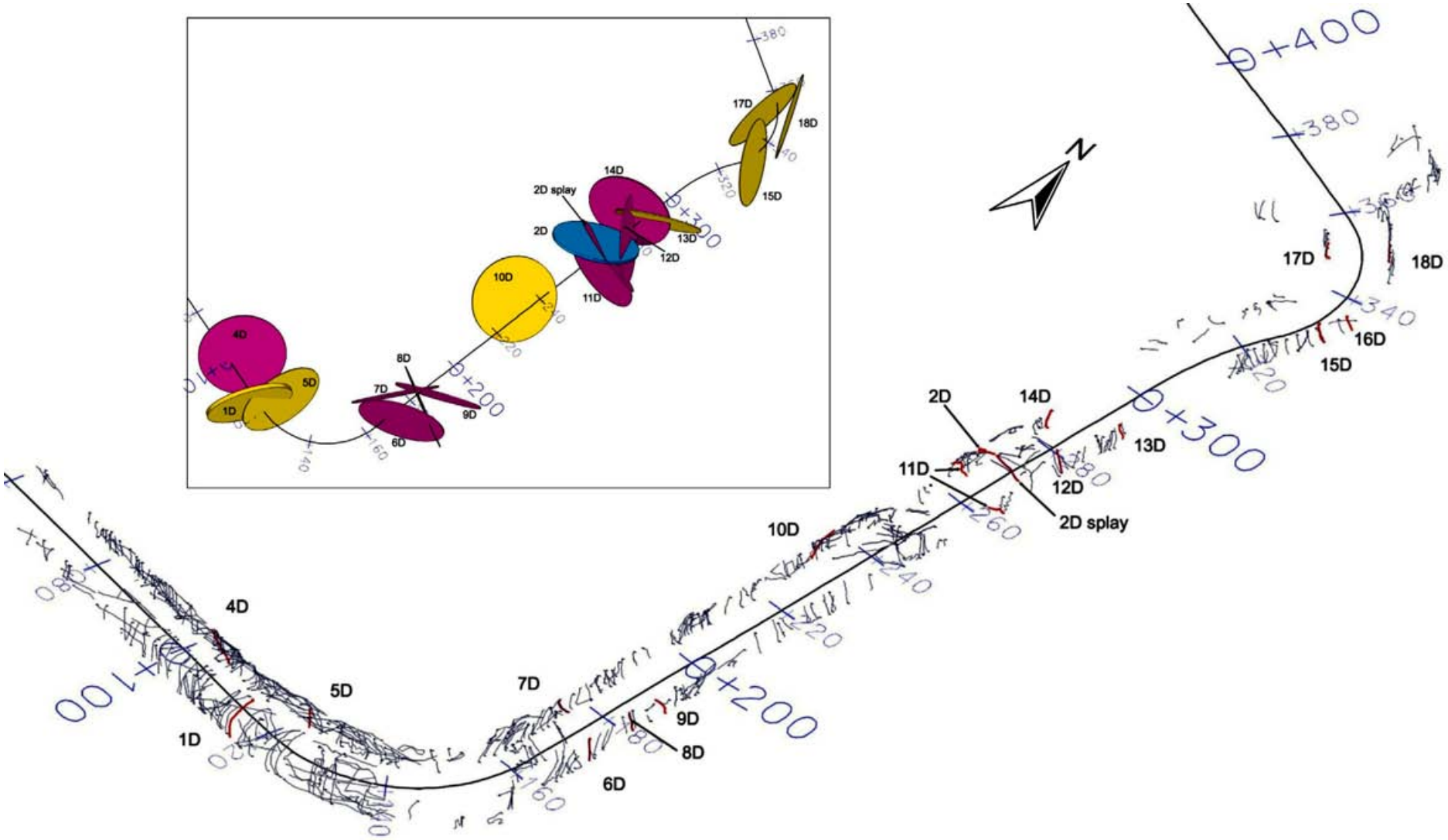

Figure A2-1. *Three-dimensional view showing the spatial distribution of the 18 minor deformation zones (red) recorded during the updated mapping of NBT by /Berglund 2009/, along with registered fractures (black). Individual red lines represent deformation zone centre lines, whereas the black lines represent single fractures, including minor splays. Note the general lack of data in the centre of the roof along the entire tunnel. Inset figure of reduced size shows individual deformation zones as disks (true thickness and default diameter of 30 m) coloured according to the deformation style, where yellow=brittle, violet=brittle-ductile and blue=ductile. Note that deformation zone 16D is not included, due to its limited extent.*

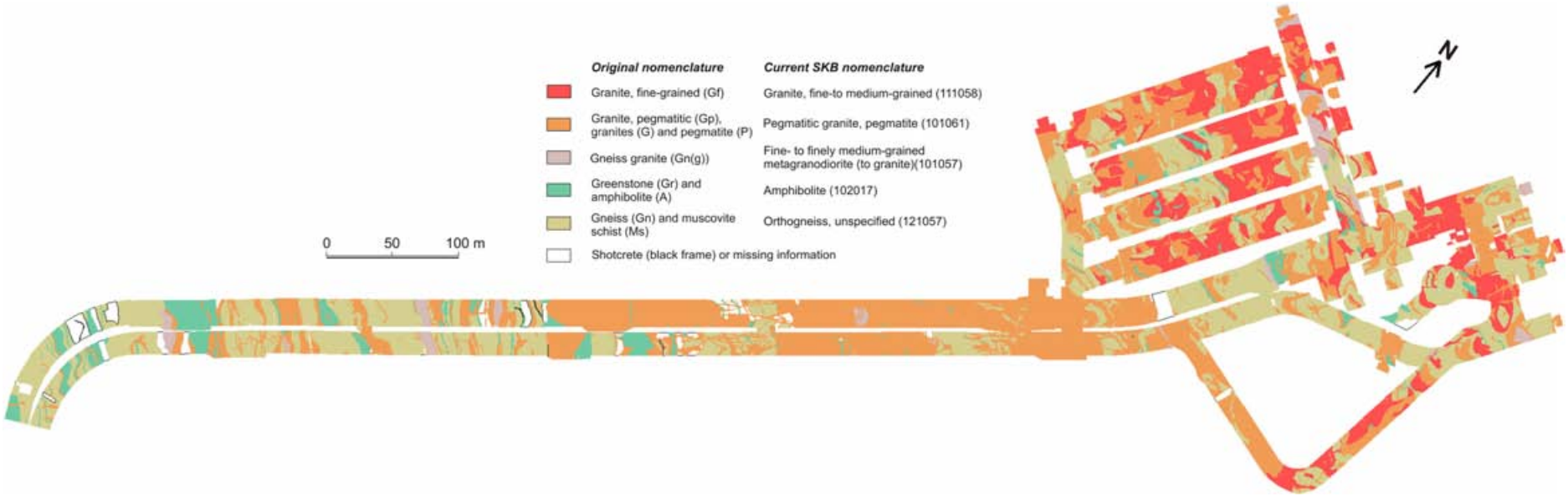

Figure A2-2. *Colour coded bedrock map compiled of the detailed drawings at the scale 1:200 of /Christiansson and Bolvede 1987/. The colours followed SKB standards for all rock types.*

Appendix 3

Technical data for all boreholes within the SFR regional model volume

Table A3-1. Technical borehole data (Coordinate system RT90-RHB70).

BH ID	Old ID	Length (m)	Northing (m)	Easting (m)	Inclination (°)	Bearing (°)
HFM34	n/a	200.75	6,701,325.06	1,632,470.21	–58.6	030.5
HFM35	n/a	200.75	6,701,555.86	1,632,320.51	–59.3	033.0
HFR101	n/a	209.30	6,701,725.15	1,632,838.91	–60.0	150.0
HFR102	n/a	55.04	6,701,728.55	1,632,974.54	–59.1	085.0
HFR105	n/a	200.50	6,701,376.55	1,632,686.82	–63.0	034.5
HFR106	n/a	190.40	6,701,574.11	1,633,579.85	–59.8	269.4
KFM11A	n/a	851.21	6,701,103.82	1,632,366.75	–60.9	040.2
KFR01	HK1	62.30	6,701,434.83	1,632,453.42	–60.0	230.5
KFR02	HK2	116.80	6,701,770.05	1,632,887.78	–90.0	000.0
KFR03	HK3	101.60	6,701,908.96	1,632,997.74	–90.0	000.0
KFR04	HK4	100.50	6,701,946.04	1,633,055.96	–75.0	098.2
KFR05	HK5	131.40	6,701,946.04	1,633,056.58	–70.0	009.1
KFR06	HK6	39.00	6,701,961.50	1,633,059.01	–63.0	315.6
KFR08	HK8	104.40	6,702,071.23	1,633,066.45	–05.0	056.4
KFR09	HK9	80.24	6,701,881.83	1,632,755.38	–05.0	299.9
KFR10	HK10	107.28	6,701,882.58	1,632,755.89	–45.0	302.5
KFR11	HK11	98.07	6,702,046.91	1,633,110.05	–10.0	072.5
KFR12	HK12	50.26	6,702,057.64	1,632,899.87	–90.0	000.0
KFR13	HK13	76.60	6,701,910.29	1,633,092.89	–90.0	000.0
KFR14	HK14	29.10	6,702,010.36	1,633,031.74	–45.0	135.1
KFR19	KB19	110.17	6,701,908.32	1,633,000.46	13.8	038.2
KFR20	KB20	109.70	6,701,909.55	1,632,998.33	10.4	056.4
KFR21	KB1	250.80	6,702,093.30	1,633,037.21	–90.0	230.5
KFR22	KB2	160.10	6,702,087.50	1,633,033.17	–60.0	213.0
KFR23	KB3	160.20	6,702,184.17	1,632,993.04	–60.0	257.0
KFR24	KB4	159.20	6,702,062.95	1,633,083.74	–57.0	051.5
KFR25	KB5	196.50	6,702,065.30	1,633,077.79	–46.0	000.0
KFR27	KB7	501.64	6,701,714.42	1,633,175.52	–87.4	248.2
KFR31	KB11	242.10	6,701,959.66	1,632,915.47	–43.2	082.1
KFR32	KB12	209.70	6,701,956.59	1,632,915.67	–46.5	024.9
KFR33	KB13	167.00	6,701,958.73	1,632,912.61	–43.8	302.5
KFR34	KB14	142.00	6,701,923.75	1,632,794.20	–49.0	198.1
KFR35	KB15	140.20	6,701,956.28	1,632,915.93	–51.5	208.1
KFR36	KB16	123.90	6,701,922.23	1,632,792.99	–46.0	291.7
KFR37	KB17	204.90	6,702,050.31	1,633,033.49	–62.5	188.5
KFR38	KB18	185.40	6,702,048.62	1,633,035.53	–57.6	092.2
KFR51	KB21	46.85	6,701,898.12	1,632,963.47	35.0	358.8
KFR52	KB22	29.95	6,701,963.94	1,633,066.31	10.0	230.5
KFR53	KB23	40.60	6,701,947.78	1,633,100.54	–27.4	312.6
KFR54	KB24	53.30	6,701,949.71	1,633,102.00	–47.7	310.0
KFR55	KB25	61.89	6,701,930.05	1,633,094.49	–11.0	329.0
KFR56	KB26	81.73	6,702,069.46	1,633,067.51	26.0	087.9
KFR57	KB27	25.38	6,702,050.77	1,632,854.91	–90.0	230.5

BH ID	Old ID	Length (m)	Northing (m)	Easting (m)	Inclination (°)	Bearing (°)
KFR61	DS1	70.90	6,701,382.45	1,632,391.99	–44.0	038.4
KFR62	DS2	82.80	6,701,368.43	1,632,401.86	–45.0	042.9
KFR63	DS3	15.08	6,701,226.87	1,632,315.81	–90.0	230.5
KFR64	DS4	54.17	6,701,406.16	1,632,407.71	–60.0	033.9
KFR65	DS5	39.68	6,701,403.62	1,632,406.04	–90.0	230.5
KFR66	DS6	29.17	6,701,420.17	1,632,417.16	–90.0	230.5
KFR67	DS7	48.95	6,701,419.85	1,632,419.75	–65.0	034.6
KFR68	DS8	128.03	6,701,552.67	1,632,530.76	–45.0	082.0
KFR69	DS9	201.20	6,701,713.56	1,632,783.24	–45.4	014.5
KFR70	DS10	172.50	6,701,712.85	1,632,823.74	–51.3	061.8
KFR71	DS101	120.90	6,701,367.83	1,632,363.08	02.0	059.5
KFR72	DS102	100.53	n/a	n/a	n/a	n/a
KFR80	INJ	20.00	6,702,028.08	1,633,056.22	–70.0	196.0
KFR83	SH3	20.00	6,702,061.20	1,632,857.98	–35.0	032.5
KFR84	BT 5/241	29.50	6,701,409.24	1,632,432.52	25.0	308.8
KFR85	BT 5/247 1	12.20	6,701,406.24	1,632,443.03	–05.0	115.3
KFR86	BT 5/247 2	14.70	6,701,406.94	1,632,443.09	–90.0	230.5
KFR87	NBT 1	15.10	6,702,035.75	1,633,042.79	–05.0	212.5
KFR88	NBT 2	30.00	6,702,058.78	1,633,063.72	20.0	338.5
KFR89	SFR1/177	17.00	n/a	n/a	n/a	n/a
KFR101	n/a	341.76	6,701,736.32	1,633,351.40	–55.5	028.8
KFR102A	n/a	600.83	6,701,730.30	1,633,330.21	–65.4	302.3
KFR102B	n/a	180.08	6,701,740.53	1,633,343.91	–54.1	344.9
KFR103	n/a	200.50	6,701,737.13	1,633,347.20	–53.9	179.9
KFR104	n/a	454.57	6,701,719.45	1,632,879.34	–53.8	133.8
KFR105	n/a	306.8	6,701,789.85	1,633,072.96	–10.1	174.5
KFR106	n/a	300.13	6,701,541.19	1,633,592.14	–69.9	195.1
KFR7A	HK7A	74.70	6,702,020.20	1,633,107.36	–02.0	020.8
KFR7B	HK7B	21.10	6,702,017.62	1,633,109.54	–75.0	011.5
KFR7C	HK7C	34.00	6,701,999.29	1,633,100.63	–70.0	196.0
n/a	SFR(Silo1)	45.12	n/a	n/a	n/a	n/a

Appendix 4

Geophysical borehole data and characterization of the major rock types

In contrast to the Forsmark site investigation, where statistical studies were made for comprehensive outcrop and borehole petrophysical laboratory data to investigate the physical signature of different rock types /Isaksson et al. 2004a, 2004b, SKB 2005, Stephens et al. 2007/, the petrophysical laboratory data from the SFR area are limited to 57 drill core samples analysed for density and only, in some cases, magnetic susceptibility /Mattsson 2009, Mattsson and Keisu 2009a, 2010/. Apart from the density data of some rock types, there are too few measurements to enable reliable and complete characterization of the major lithologies in the SFR area. Instead, some physical properties have been assessed with input from geophysical logging data of the cored boreholes from the latest drilling campaign. Since the primary objective was to obtain physical properties for the rock domain modelling, only boreholes situated within, or partly within, the local SFR model volume were included in the assessment (i.e. KFR27, KFR101, KFR102A, KFR102B, KFR103, KFR104 and KFR105).

The compilation presented here integrates geophysical log data with a selection of geological parameters from the mapping with the Boremap-system (Table A4-1) to obtain some physical properties for the major rock types in the area. The following rock types have been addressed in the compilation:

111058 Fine- to medium-grained granite.

101061 Pegmatite, pegmatitic granite.

101057 Fine- to finely medium-grained metagranite (to granodiorite).

102017 Amphibolite.

103076 Felsic to intermediate metavolcanic rock.

Note that the data for the aplitic metagranite (101058) are too few to allow viable evaluation. The rock type is therefore omitted from the histograms and tables in this appendix. The following geophysical log data have been used for the assessment:

- Density (gamma-gamma).
- Magnetic susceptibility.
- Natural gamma radiation.

Table A4-1. Geological parameters selected for integration with geophysical borehole data. The parameter table was created by Martin Stigsson, SKB.

Database field	Explanation/content
SITE	“Forsmark – SFR”
PROJECT	“SFR-utbyggnad”
IDCODE	Borehole identity; KFR101, etc.
SecUp	SecMid –5 cm
SecLow	SecMid +5 cm
SecMid	even dm
NAME_CODE rock/occur	commonly occurring rock code; 101057 etc.
Nof_NAME_CODE_in_interval	number of NAME_CODE occurrences; 1,2,3,…
TYPE_CODE alter	commonly occurring alteration type code
INTENS_CODE alter	adherent alteration intensity code
Nof_TYPE_CODE_in_interval	number of TYPE_CODE occurrences; 1,2,3,…
FEATURE_ID rock/occur	internal database query code
FEATURE_ID alter	internal database query code

New calibration of magnetic susceptibility

A re-levelling and new calibration has been carried out on the magnetic susceptibility data to allow for the statistical treatment of low susceptibility values. For this, a slight difference in the methodology had to be applied compared with that used during the previous geophysical log interpretations and single-hole interpretations. The magnetic susceptibility is very low in large parts of the SFR area and, as a consequence, it is also very low in long sections in many of the boreholes. The previous calibration for magnetic susceptibility uses a zero threshold for low susceptibility values and such thresholds are not applicable for statistical purposes. Hence, the calibration process was carried out again with a fine adjustment valid for the low magnetic susceptibilities. In practice, this involves a more detailed tuning of the zero level of the susceptibility log data. However, it should be observed that estimated noise levels of the susceptibility logging data are in the order of 10^{-4} SI and the residual mean error when fitting logging data to sample measurements is of the order of 10^{-3} SI, so any evaluation of susceptibility logging data smaller than 10^{-3}–10^{-4} SI must be made with caution.

Results

To obtain the characteristics for each occurring rock type, the following two criteria were applied for every single dm section in the selected boreholes:

- Only one rock type is allowed.
- No alteration is allowed.

After removal of sections with alteration and/or overlapping geological rock types, the physical properties for each rock type could be statistically analyzed. A histogram summary for each of the major rock types on a borehole by borehole basis is provided in Figure A4-1 to Figure A4-7. An identical compilation has also been completed for the combined borehole data from two of the modelled rock domains, RFR01 and RFR02 (Figures A4-8 and A4-9). In addition, this compilation describes minimum, maximum, mean and standard deviation values. The geometric mean and the standard deviation above and below this mean are presented for the magnetic susceptibility values. ‘Samples’ shows the number of occurrences which, in practice, corresponds to the number of decimetre sections.

Borehole KFR27 was originally 147.48 m long and it was prolonged to 501.64 m during the current SFR investigation. The older, upper part of borehole KFR27 (11.82–147.48 m borehole length) was excluded in the compilation, since it was mapped without drill core. For the new, lower part of KFR27, where the drill core supported mapping starts at 147.55 m borehole length, only magnetic susceptibility and density have been used. Logging measurements were conducted prior to and after the lengthening of the borehole and, in the later data, the natural gamma radiation level was significantly higher. This increase is believed to be caused by an influx of radon gas /Mattsson and Keisu 2009b/. This fact makes a reliable interpretation of the absolute radiation levels practically impossible, but relative variations are most likely physically reliable as indicated by /Mattsson and Keisu 2009b/.

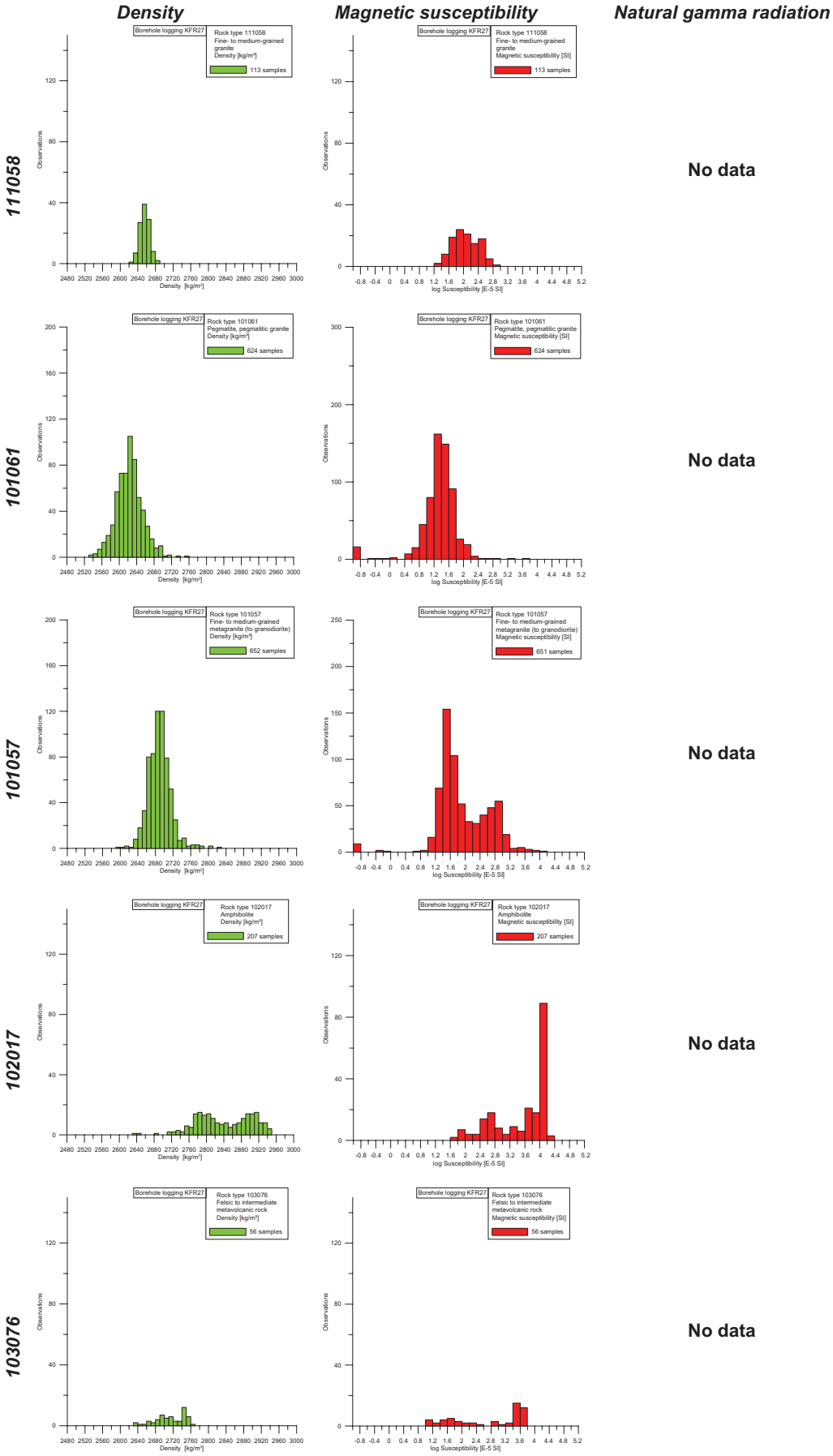

Figure A4-1. *Some physical properties of the major rock types in KFR27, the extended part of the borehole, below 147.55 m. The natural gamma radiation parameter is excluded for the whole borehole.*

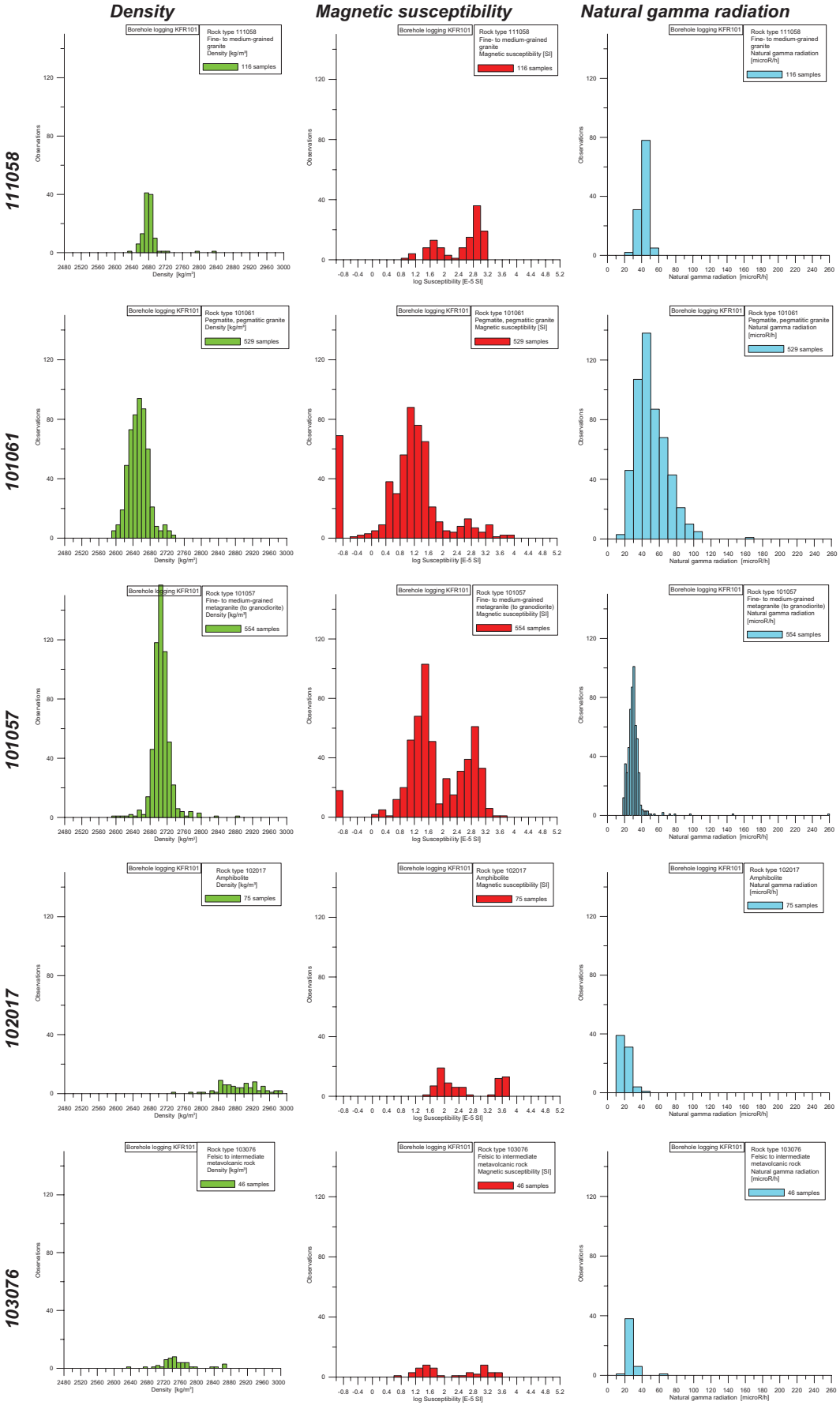

Figure A4-2. *Some physical properties of the major rock types in KFR101.*

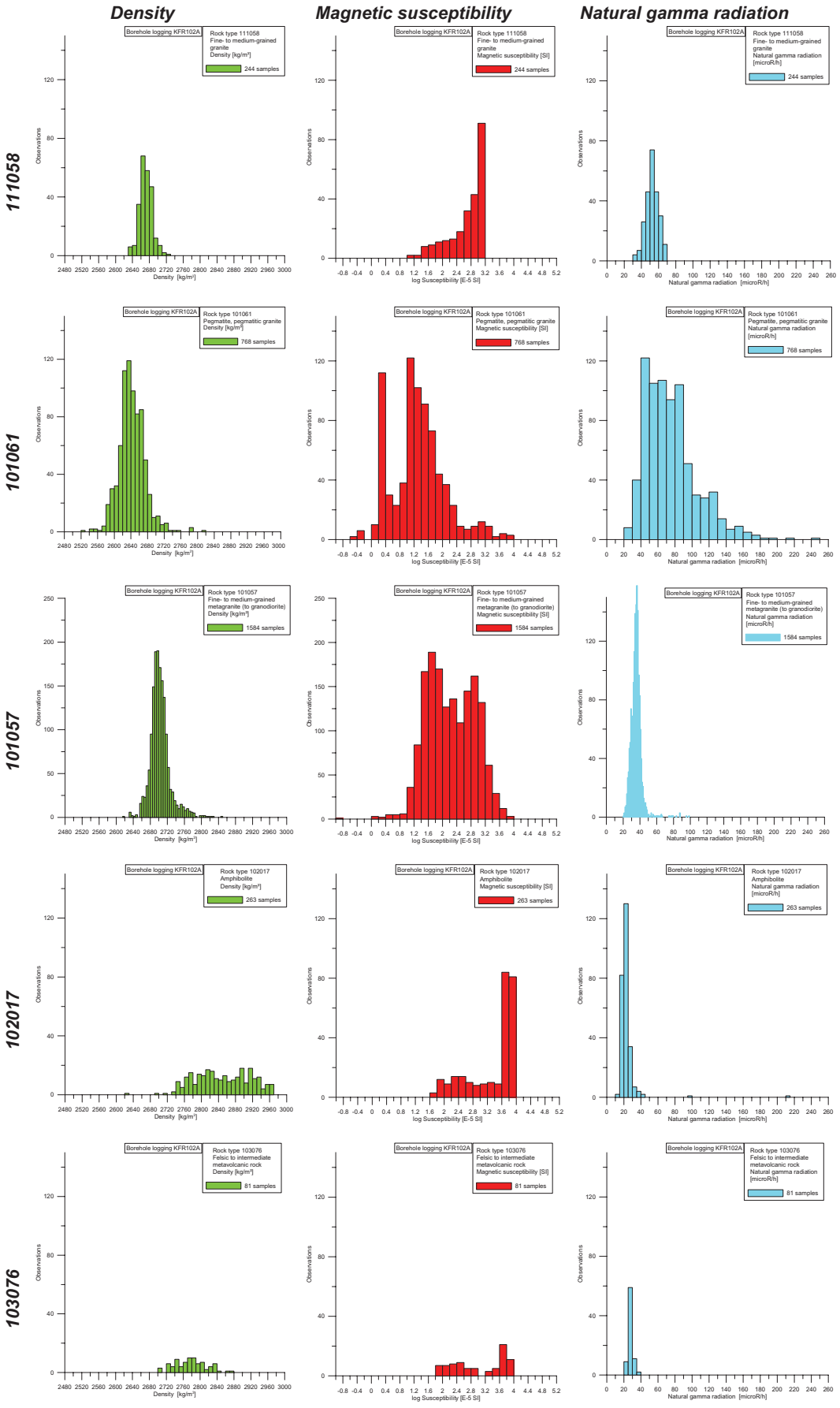

Figure A4-3. *Some physical properties of the major rock types in KFR102A.*

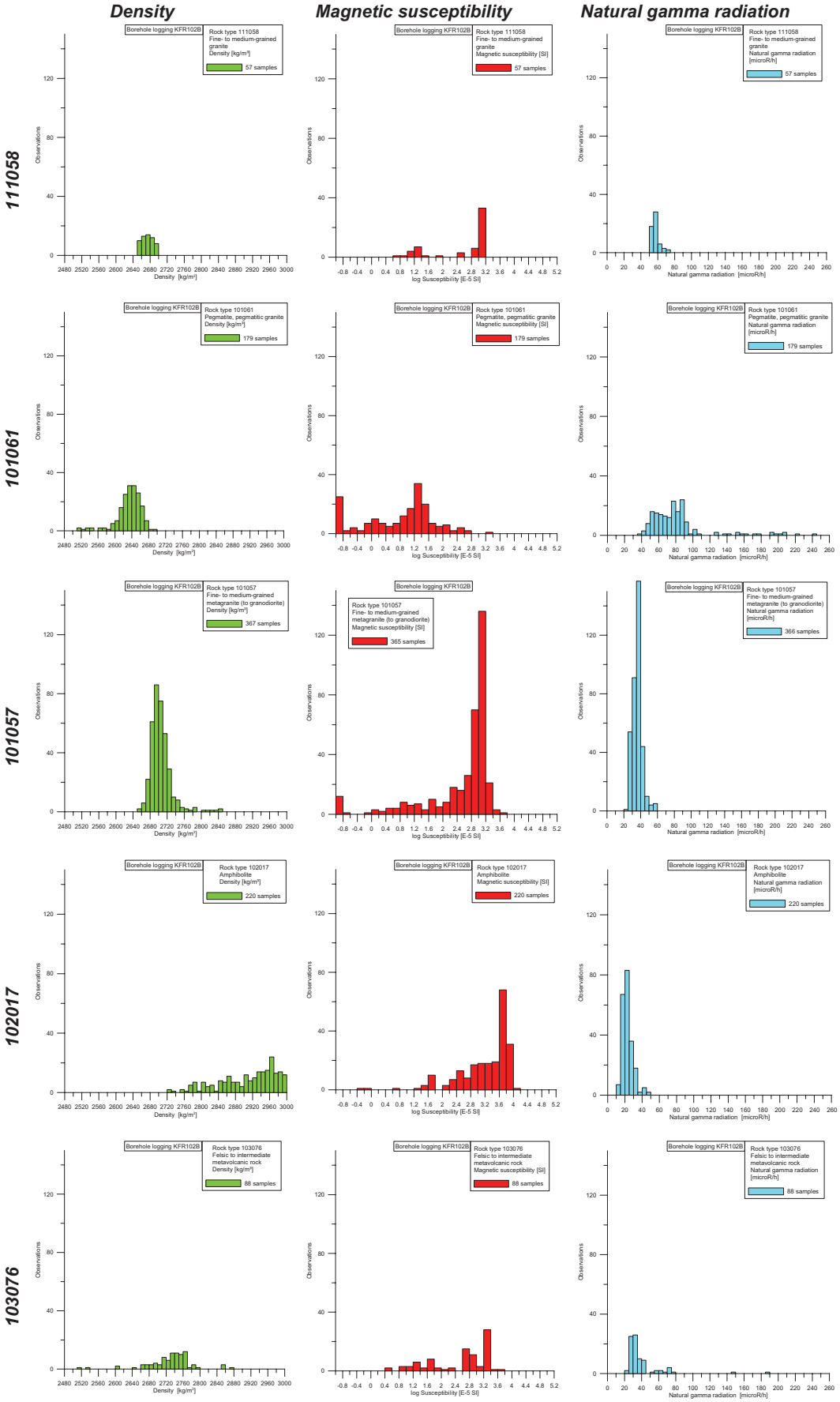

Figure A4-4. *Some physical properties of the major rock types in KFR102B.*

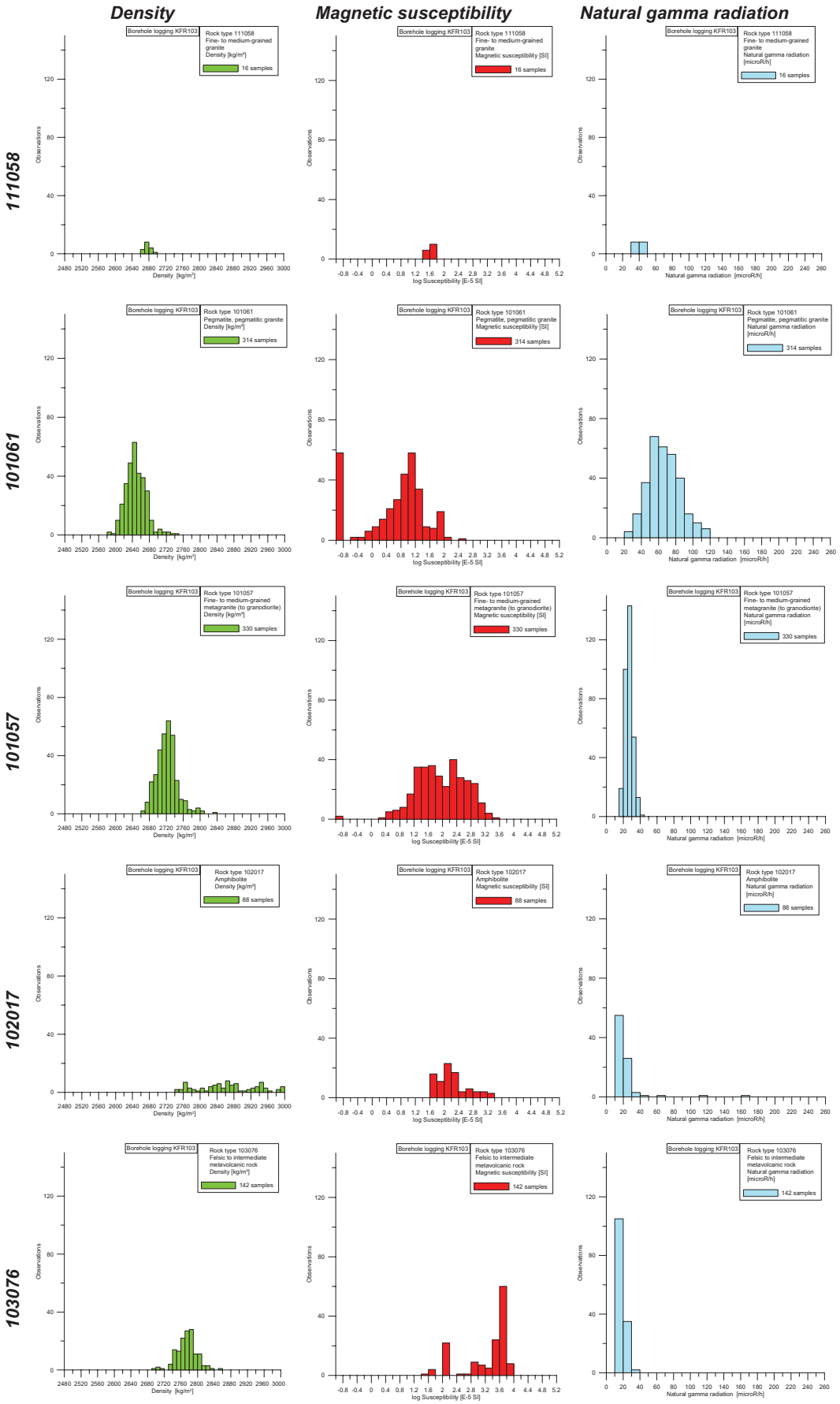

Figure A4-5. *Some physical properties of the major rock types in KFR103.*

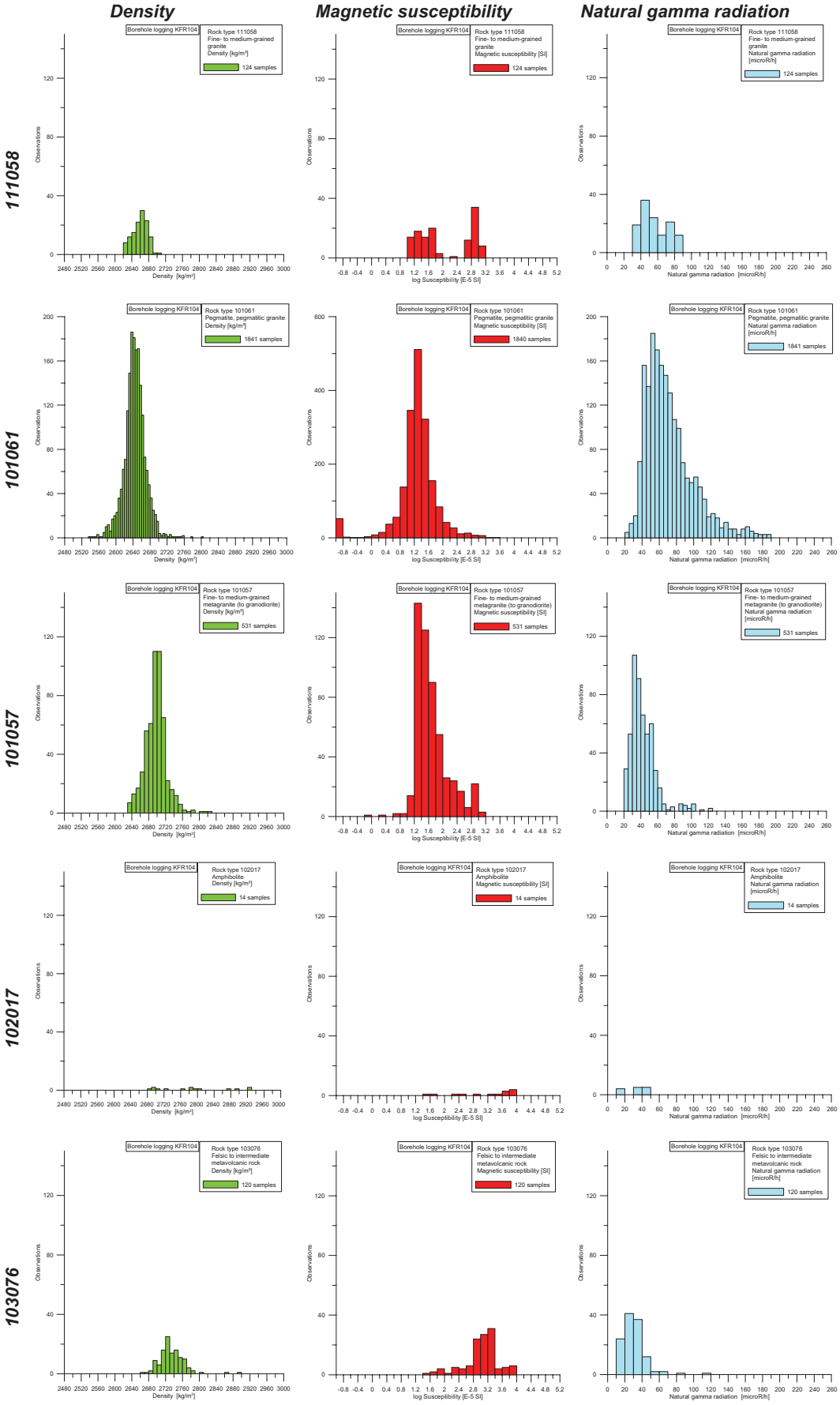

Figure A4-6. *Some physical properties of the major rock types in KFR104.*

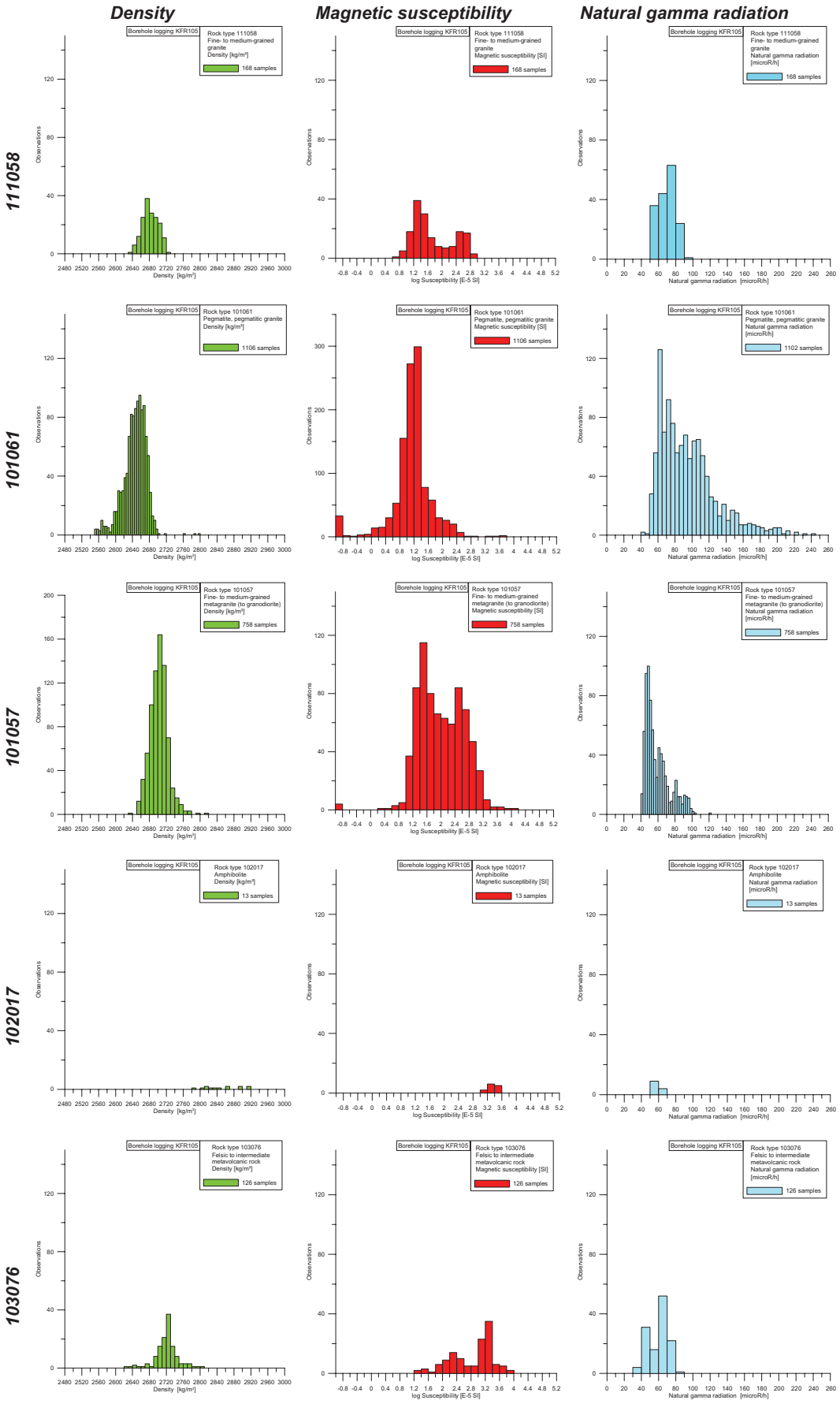

Figure A4-7. *Some physical properties of the major rock types in KFR105.*

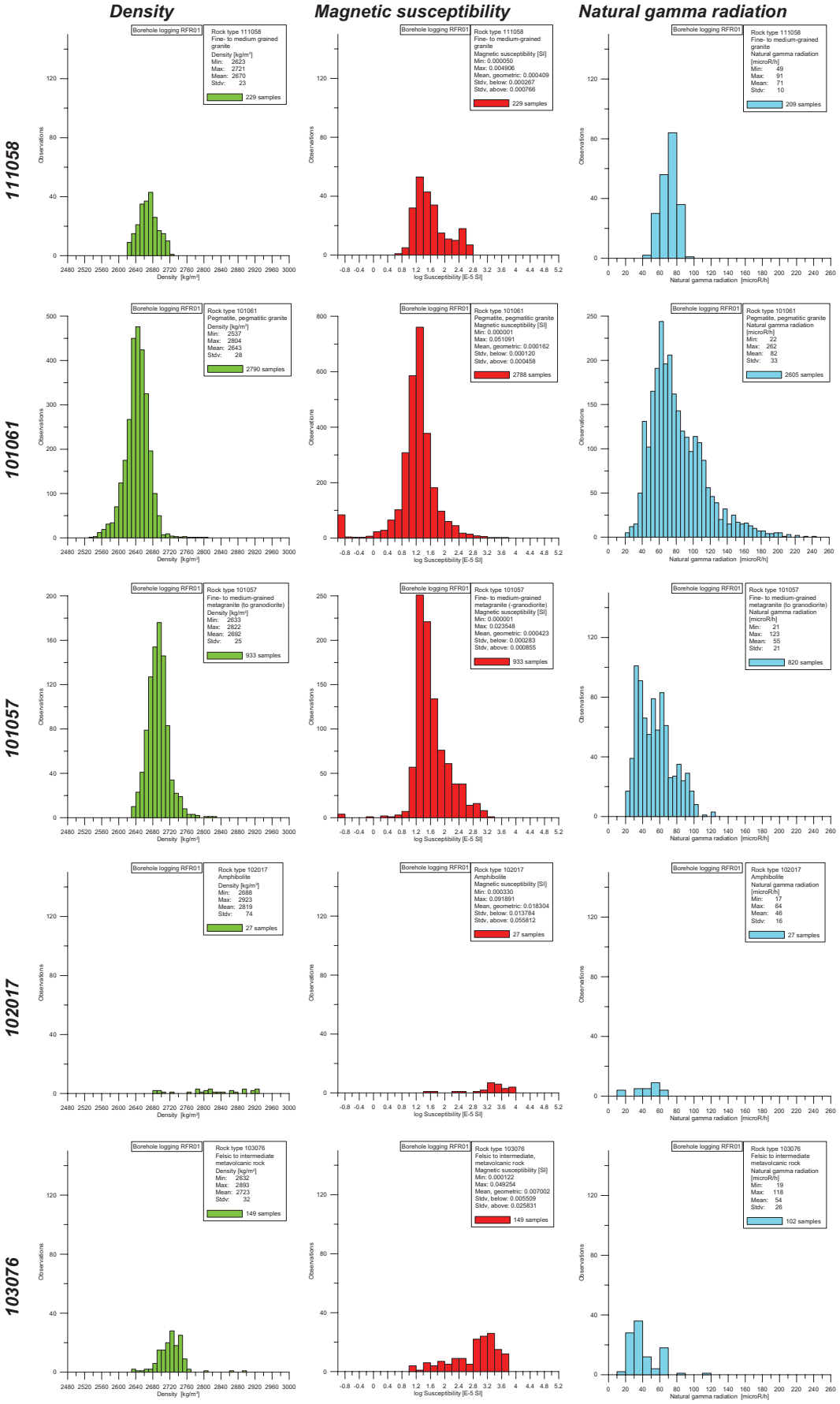

Figure A4-8. *Some physical properties of the major rock types in rock domain RFR01.*

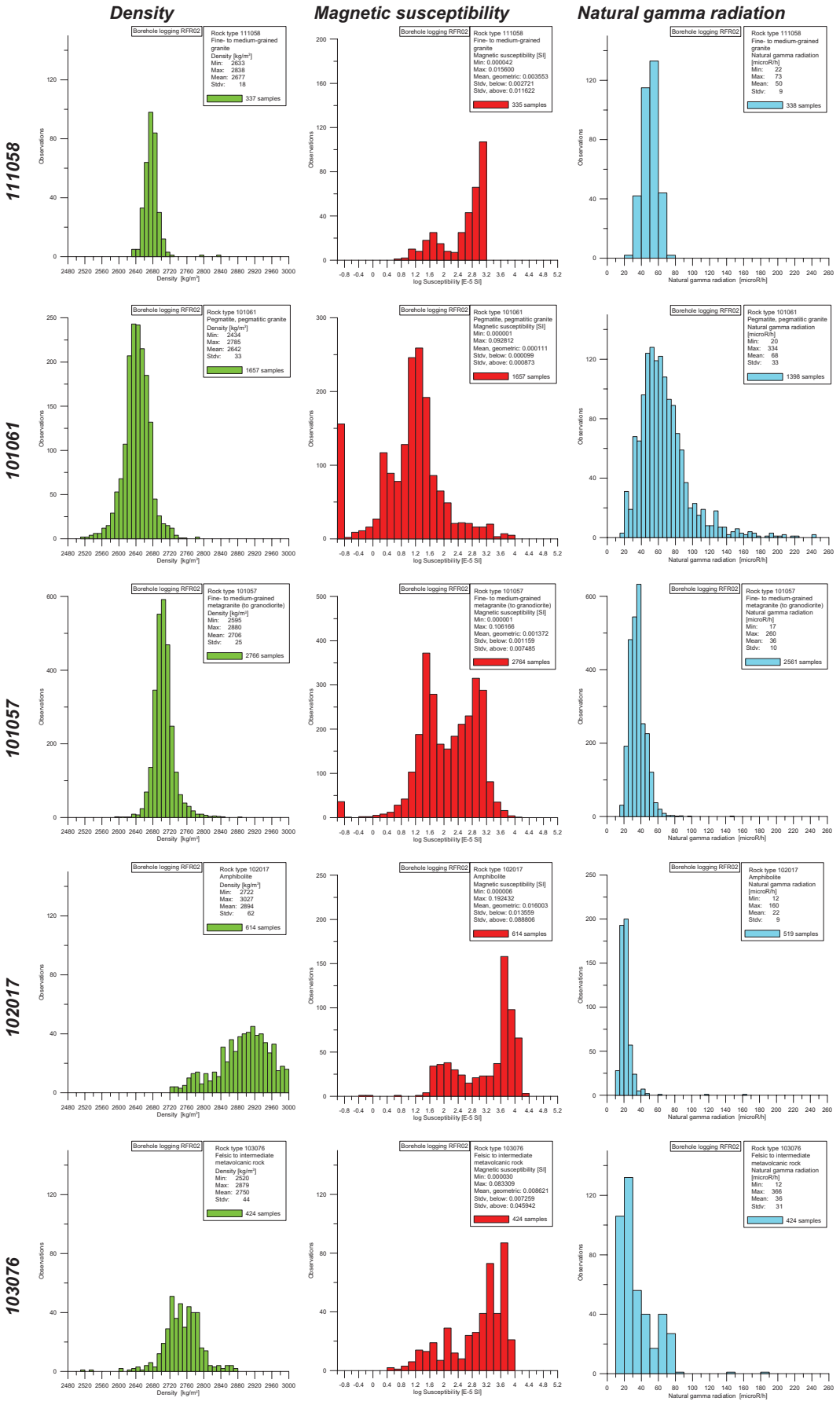

Figure A4-9. *Some physical properties of the major rock types in rock domain RFR02.*

Appendix 5

Lineaments SFR model version 1.0

Contents

Table A5-1. Name of each lineament and the relation to lineaments interpreted during the Forsmark site investigation.

Lineament name in the Forsmark site investigation; wholly or partly connected to a lineament in SFR version 0.1/1.0	Lineament name of lineament in SFR model version 0.1/1.0	Comment version 0.1	Comment version 1.0
MFM3264G	MSFR08001	As MFM3264G, but slightly changed at south	Not changed further in version 1.0
MFM3265G	MSFR08002	MFM3265G has been divided into 3 discontinuous pieces, MSFR08002–MSFR08004, with deviating paths as compared to the original	Slightly changed at south, and connected to MSFR08003
MFM3265G	MSFR08003	MFM3265G has been divided into 3 discontinuous pieces, MSFR08002–MSFR08004, with deviating paths as compared to the original	Straightened at NNE and connected to MSFR08002
MFM3265G	MSFR08004	MFM3265G has been divided into 3 discontinuous pieces, MSFR08002–MSFR08004, with deviating paths as compared to the original	Not changed further in version 1.0
MFM3151G	MSFR08005	MFM3151G has been changed in length and running route	Not changed further in version 1.0
–	MSFR08006	New	Not changed further in version 1.0
MFM0836G	MSFR08007	As MFM0836G but slightly shortened at west and with slightly deviating running	Slightly changed running at west
MFM3153G	MSFR08008	MFM3153G changed at southwest	Not changed further in version 1.0
MFM3266G	MSFR08009	MFM3266G slightly shortened at south	Extended at southwest
–	MSFR08010	New	Not changed further in version 1.0
MFM3152G	MSFR08011	MFM3152G changed at west	Not changed further in version 1.0
MFM3154G	MSFR08012	MFM3154G, divided into three (MSFR08012–MSFR08014) discontinuous pieces with changed running routes	Not changed further in version 1.0
MFM3154G	MSFR08013	MFM3154G, divided into three (MSFR08012–MSFR08014) discontinuous pieces with changed running routes	Not changed further in version 1.0
MFM3154G	MSFR08014	MFM3154G, divided into three (MSFR08012–MSFR08014) discontinuous pieces with changed running routes	Shortened at southeast and connected to MSFR10008

Lineament name in the Forsmark site investigation; wholly or partly connected to a lineament in SFR version 0.1/1.0	Lineament name of lineament in SFR model version 0.1/1.0	Comment version 0.1	Comment version 1.0
MFM3150G, MFM3154G	MSFR08015	coincides partly with MFM3150G and partly also with MFM3154G	Not changed further in version 1.0
–	MSFR08016	New	Not changed further in version 1.0
–	MSFR08017	New	Not changed further in version 1.0
–	MSFR08018	New	Not changed further in version 1.0
–	MSFR08019	New	Not changed further in version 1.0
–	MSFR08020	New	Not changed further in version 1.0
–	MSFR08021	New	Not changed further in version 1.0
–	MSFR08022	New, but part of the complex tectonic structure which is a result of the interplay between MFM0805G0 and MFM0805G1	Deleted
–	MSFR08023	New	Not changed further in version 1.0
–	MSFR08024	New, possibly a dislocated southern continuation of MFM0999G	Deleted
–	MSFR08025	New	Not changed further in version 1.0
–	MSFR08026	New, but possibly part of the complex tectonic structure which is a result of the interplay between MFM0805G0 and MFM0805G1	Not changed further in version 1.0
–	MSFR08027	New	Not changed further in version 1.0
–	MSFR08028	New	Shortened at north-west due to the pier
–	MSFR08029	New	Not changed further in version 1.0
–	MSFR08030	New	Not changed further in version 1.0
–	MSFR08031	New	Not changed further in version 1.0
–	MSFR08032	New	Not changed further in version 1.0
–	MSFR08033	New, but possibly part of the complex tectonic structure which is a result of the interplay between MFM0805G0 and MFM0805G1	Not changed further in version 1.0
–	MSFR08034	New	MSFR08034 is shortened, the shortened section is taken over by MSFR08092
–	MSFR08035	New	Not changed further in version 1.0
–	MSFR08036	New	Not changed further in version 1.0
–	MSFR08037	New	Not changed further in version 1.0
–	MSFR08038	New	Not changed further in version 1.0
–	MSFR08039	New	Not changed further in version 1.0
–	MSFR08040	New	Not changed further in version 1.0
–	MSFR08041	New	Not changed further in version 1.0
–	MSFR08042	New	Slightly straightened
–	MSFR08043	New	Deleted. Replaced by MSFR10002.
–	MSFR08044	New	Not changed further in version 1.0
–	MSFR08045	New	Deleted. Replaced by MSFR10002.
–	MSFR08046	New	Modified due to the introduction of MSFR08046
–	MSFR08047	New	Not changed further in version 1.0
MFM3268G	MSFR08048	Partly coinciding with MFM3268, deviating at north-west.	Deleted. Partially replaced by MSFR10006
MFM1056G	MFM1056G	As original MFM1056G	Not changed in version 1.0
MFM3133G	MFM3133G	As original MFM3133G	Not changed in version 1.0
MFM3108G	MFM3108G	As original MFM3108G	Not changed in version 1.0
MFM2296G	MFM2296G	As original MFM2296G	Not changed in version 1.0
MFM0725G	MFM0725G	As original MFM0725G	Not changed in version 1.0
MFM0812	MFM0812	As original MFM0812	Not changed in version 1.0
MFM2317G	MFM2317G	As original MFM2317G	Not changed in version 1.0

Lineament name in the Forsmark site investigation; wholly or partly connected to a lineament in SFR version 0.1/1.0	Lineament name of lineament in SFR model version 0.1/1.0	Comment version 0.1	Comment version 1.0
MFM1201G	MFM1201G	As original MFM1201G	Not changed in version 1.0
MFM0813G	MFM0813G	As original MFM0813G	Not changed in version 1.0
MFM0803G0	MFM0803G0	As original MFM0803G0	Not changed in version 1.0
MFM2496G	MSFR08059	MFM2496G is divided into two discontinuous parts (MSFR08059, MSFR08060) with slightly changed running	Not changed further in version 1.0
MFM2496G	MSFR08060	MFM2496G is divided into two discontinuous parts (MSFR08059, MSFR08060) with slightly changed running	Not changed further in version 1.0
MFM3261G	MFM3261G	As original MFM3261G	Not changed in version 1.0
MFM3254G	MFM3254G	As original MFM3254G	Not changed in version 1.0
MFM0999G	MFM0999G	As original MFM0999G	Not changed in version 1.0
MFM3131G	MFM3131G	As original MFM3131G	Not changed in version 1.0
MFM3257G	MFM3257G	As original MFM3257G	Not changed in version 1.0
MFM3258G	MFM3258G	As original MFM3258G	Not changed in version 1.0
MFM3140G	MSFR08067	As MFM3140G but slightly changed at north-west	Not changed further in version 1.0
MFM3126G	MFM3126G	As original MFM3126G	Not changed in version 1.0
MFM3253G	MSFR08069	As MFM3253G but extended towards south-east	Not changed further in version 1.0
MFM3127G	MSFR08070	replaces northern part of MFM3127G	Not changed further in version 1.0
MFM0814G	MFM0814G	As original MFM0814G	Not changed in version 1.0
MFM3106G	MSFR08072	As MFM3106G but shortened at north	Not changed further in version 1.0
MFM3259G	MSFR08073	MFM3259G has been divided into three discontinuous pieces MSFR08073–MSFR08075	Not changed further in version 1.0
MFM3259G	MSFR08074	MFM3259G has been divided into three discontinuous pieces MSFR08073	Not changed further in version 1.0
MFM3259G	MSFR08075	MFM3259G has been divided into three discontinuous pieces MSFR08073	Not changed further in version 1.0
MFM3129G	MSFR08076	MFM3129G is divided into two discontinuous pieces (MSFR08076, MSFR08077)	Not changed further in version 1.0
MFM3129G	MSFR08077	MFM3129G is divided into two discontinuous pieces (MSFR08076, MSFR08077)	Not changed further in version 1.0
MFM3149G	MSFR08078	MSFR08078 deviates a bit from its original (MFM3149G) running route at north-east and south-west and is shorter, and forms two discontinuous sub-sections of MFM3149G, together with MSFR08081	Not changed further in version 1.0
MFM3113G	MSFR08079	As MFM3113G but shortened at south and with changed curvature in most of its length	Not changed further in version 1.0
MFM3271G	MSFR08080	As MFM3271G but changed at its north-eastern part	Not changed further in version 1.0
MFM3149G	MSFR08081	Very short discontinuous sub-segment of MFM3149G, the other part is MSFR08078	Not changed further in version 1.0
MFM3119G	MSFR08082	As MFM3119G but shortened at south-east	Not changed further in version 1.0
MFM3255G	MFM3255G	As original MFM3255G	Not changed in version 1.0

Lineament name in the Forsmark site investigation; wholly or partly connected to a lineament in SFR version 0.1/1.0	Lineament name of lineament in SFR model version 0.1/1.0	Comment version 0.1	Comment version 1.0
MFM3146G	MSFR08084	As MFM3146G, but cut at north and slightly deviating from its original route, at south unreliable due to disturbed area	Shortened at southwest due to the disturbing pier
MFM0804G	MSFR08085	As MFM0804G but changed at its south-eastern part where it is moved to another connection point in the Singö line. Earlier it passed more in a severely disturbed area	Not changed further in version 1.0
MFM3252G	MSFR08086	MFM3252G is divided into two discontinuous lineaments MSFR08086–MSFR08087	Not changed further in version 1.0
MFM3252G	MSFR08087	MFM3252G is divided into two discontinuous lineaments MSFR08086–MSFR08087	Not changed further in version 1.0
MFM3142G and partly also MFM3143G	MSFR08088	Partly coinciding with MFM3142G, and partly with the southern part of MFM3143G	North-western part deleted
MFM3143G	MSFR08089	Partly as MFM3143G, but divided into two discontinuous pieces MSFR08089, MSFR08090	Not changed further in version 1.0
MFM3143G	MSFR08090	Partly as MFM3143G, but divided into two discontinuous pieces MSFR08089, MSFR08090	Not changed further in version 1.0
MFM3137G	MSFR08091	As MFM3137G, but shortened	Slightly modified
MFM0137BG	MSFR08092	MFM0137BG has been shortened radically at north-east where MSFR08034 forms an alternative route	Extended and replaces MSFR08034 at its easternmost section
MFM0805G0	MSFR08093	Short sub-section of MFM0805G0	Not changed further in version 1.0
MFM0805G0	MSFR08094	Sub-section of MFM0805G0, with slightly changed running	Not changed further in version 1.0
MFM0805G0	MSFR08095	This is the north-western sub-segment of MFM0805G0, though with slightly changed running	Not changed further in version 1.0
MFM3116G	MSFR08096	Part of MFM3116G but unreliable as it runs through disturbed area, because of that cut at both south and north	Not changed further in version 1.0
MFM3117G	MSFR08097	Part of MFM3117G but unreliable as it runs through disturbed area, because of that cut at south	Not changed further in version 1.0
MFM0805G1	MSFR08098	Discontinuous part of MFM0805G1, together with MSFR08104 and MSFR08095, almost connects to MSFR08014	Slightly changed running
MFM3111G	MSFR08099	As MFM3111G but shortened and with slightly deviating running	Not changed further in version 1.0
MFM1034G	MSFR08100	MFM1034G divided into two discontinuous parts (MSFR08100, MSFR08101). The northernmost part of MFM1034G is entirely removed	Slightly straightened at NNW and connected to MSFR08101
MFM1034G	MSFR08101	MFM1034G divided into two discontinuous parts (MSFR08100, MSFR08101). The northernmost part of MFM1034G is entirely removed	Slightly straightened at NNW
–	MSFR08102	New	Extended towards ENE
MFM3293G	MSFR08103	South-western portion of MFM3293G	Not changed further in version 1.0
MFM0805G1	MSFR08104	SE part of MFM0805G1 though with slightly changed running	Not changed further in version 1.0

Lineament name in the Forsmark site investigation; wholly or partly connected to a lineament in SFR version 0.1/1.0	Lineament name of lineament in SFR model version 0.1/1.0	Comment version 0.1	Comment version 1.0
MFM3262G	MSFR08105	SE part of MFM3262G, slightly deviating from original running	Not changed further in version 1.0
MFM0835BG	MSFR08106	The north-western part of MFM0835BG, which is divided into two discontinuous sections, MSFR08106 and MSFR08107	Slightly modified running
MFM0835BG	MSFR08107	The north-western part of MFM0835BG, which is divided into two discontinuous sections, MSFR08106 and MSFR08107	Not changed further in version 1.0
MFM3109G	MSFR08108	As MFM3109G but prolonged at south-west	Not changed further in version 1.0
MFM3269G	MSFR08109	Partly coinciding with MFM3269G, but changed running route	Slightly changed running to achieve a better connection to MSFR08118
MFM1035G	MSFR08110	Sub-section of MFM1035G but slightly deviating running route	Extended towards southeast
MFM3118G	MSFR08111	Short sub-section of MFM3118G at its south-western part	Not changed further in version 1.0
MFM1035G	MSFR08112	Short and slightly dislocated sub-section of MFM1035G	Not changed further in version 1.0
MFM3135G	MSFR08113	As MFM3135G but shortened at west and slightly bended	Not changed further in version 1.0
–	MSFR08114	New	Deleted
MFM3267G	MSFR08115	Sub-section of MFM3267G, but changed running	Changed running due to weak arguments for the discontinuity towards MSFR08121
MFM3115G	MSFR08116	South-western part of MFM3115G	Not changed further in version 1.0
MFM3155G	MSFR08117	This lineament constitutes a north-western continuation of MFM3155G, and partly coincides with the north-western end of the same	Not changed further in version 1.0
MFM1035G	MSFR08118	Dislocated and short north-western section of MFM1035G	Slightly changed running at west to achieve better connection to MSFR08109, and extended towards southeast
MFM3268G	MSFR08119	Sub-parallel and partly coinciding with MFM3268G	Deleted. Replaced partially by MSFR10006
MFM3132G	MSFR08120	South-western part of MFM3132G	Not changed further in version 1.0
MFM3267G	MSFR08121	As MFM3267G but discontinuous at the entrance to the local model area (where it continues in MSFR08115), shortened, slightly changed at south-east	Not changed further in version 1.0
MFM3130G	MSFR08122	Coinciding with MFM3130G at its northern half, but deviates severely to the south-west	Not changed further in version 1.0
MFM1035G	MSFR08123	Sub-parallel and partly coinciding with MFM1035G, deviating at west	Not changed further in version 1.0
MFM3115G	MSFR10001		New. Partly coinciding with the north-easternmost part of MFM3115G
–	MSFR10002		New. Replaces MSFR08043 and MSFR08045, though with a modified running
–	MSFR10003		New. Replaces part of former MSFR08106 which has been modified

Lineament name in the Forsmark site investigation; wholly or partly connected to a lineament in SFR version 0.1/1.0	Lineament name of lineament in SFR model version 0.1/1.0	Comment version 0.1	Comment version 1.0
–	MSFR10004		New. Replaces former MSFR08091 partly and has another running and increased length
MFM3134G	MSFR10005		New. Partly coinciding with former MFM3134G. MSFR10005 forms the discontinuous southern sub-section of it
MFM3268G	MSFR10006		New. Replaces MSFR08048 and MSFR08119 and coincides partly with former MFM3268G
–	MSFR10007		New. Introduced to build a bridge tentatively connecting MSFR10008 and MSFR08033
–	MSFR10008		New. Introduced to bring order into the chaotic distribution of lineaments in this area. Replaces MSFR08022. Connects with MSFR10007
–	MSFR10009		New. Introduced to bring order in the chaotic distribution of lineaments in this area. Partly replaces MSFR08022
–	MSFR10010		New
MFM3134G	MSFR10011		New. Partly coinciding with former MFM3134G. MSFR10011 forms the discontinuous northern sub-section of it

Table A5-2. Lineaments from the Forsmark site investigation not included in the SFR model version 0.1/1.0, along with the name of each lineament and the reason for exclusion. Comments concerning attribute "uncertainty" refer to the classification made by /Isaksson et al. 2007/.

Lineament name in the Forsmark site investigation	Comment
MFM3155G	This lineament is positioned in a broad and short minimum with a signature indicating a possible low magnetic lithological unit and hence, should possibly be considered having a minima connection character. At its south-eastern part it is of high uncertainty and difficult to trace in data
MFM3141G	This high uncertainty lineament is located in an area with a fairly complex anomaly pattern, which combined with its short length has implied exclusion
MFM3115G	More than half of this high uncertainty lineament is excluded at its north-eastern part due to interference from disturbances created by the installations in the area. The south-western part of MFM3115G is associated with MSFR08116
MFM3112G	This high uncertainty lineament is difficult to follow at south-west; at north-east the lineament is excluded due to interference from disturbances created by the installations in the area
MFM3148G	This lineament has a low-moderate uncertainty north-west of the SFR regional model boundary. However, the south-easternmost third of this lineament inside the model area of SFR, has a high uncertainty. It is located in a low-relief area and furthermore disturbed by the installations in the area
MFM3147G	This high uncertainty lineament is only very faintly and discontinuously observed in data, it occurs in a low-relief area and furthermore its strike is semi-parallel with the magnetic survey lines
MFM3144G	This high uncertainty lineament is only very faintly and discontinuously observed in data and furthermore its strike is semi-parallel with the magnetic survey lines
MFM3114G	This high uncertainty lineament is short and deviating at north-east from the magnetic minimum supposedly used as its indicator
MFM3262G	At south-east this lineament is coinciding with MSFR08105, but for more than half of its length it is not accepted as its trace runs through the area with disturbances from civil installations

Table A5-3. Attribute table for the lineaments in SFR version 0.1/1.0. The table is based on Table 4-2 in /Isaksson et al. 2007/.

Field name	Name	Description	Further comments on attributes used to describe lineaments
Id_t	Identity	Identity of a lineament.	All lineaments within SFR version 1.0 are given new identities, MSFR08001-MSFR08XXX or MSFR10001-MSFR10XXX, with the exception of the lineaments that were directly imported from the latest version of lineaments within the FSI work /Isaksson et al. 2007/; their original names are preserved. The relation between lineaments in this SFR version 0.1/1.0 and lineaments from earlier work within the FSI is partly commented in the attribute "Comment_t" (see below in this attribute table) and in more detail in Tables A5-1 and A5-2.
Origin_t	Origin	Major type of basic data.	Basic data used or Method specific or Coordinated lineaments from the latest version within the FSI work /Isaksson et al. 2007/. With exception for the directly imported lineaments from the FSI work, all lineaments in SFR version 0.1/1.0 were identified almost uniquely in data describing the magnetic total field (magnetics). In the case of lineaments directly imported from the latest version of the FSI work /Isaksson et al. 2007/, their original values have been left without change.
Class_t	Classification	Classification of a lineament based on length.	Regional (> 10 km), local major (1-10 km) and local minor (< 1 km). In the case of lineaments directly imported from the latest version of the FSI work /Isaksson et al. 2007/, their original values have been left without change.
Method_t	Method	The type of data in which the lineament is observed.	Magnetics mostly (see also comments related to "Origin_t" above). The principal data sources used are measurements of the magnetic total field, from helicopter, on land and at sea. In the case of lineaments directly imported from the latest version of the FSI work /Isaksson et al. 2007/, their original values have been left without change.
Weight_n	Weight	A combination of uncertainty and number of properties (methods). An overall assessment of the confidence of the lineament. This assessment is based on both the number of properties upon which the lineament has been identified and the degree of uncertainty.	This attribute is not assigned to the lineaments within SFR version 0.1/1.0 with exception for the value inherited at the direct import of a lineament from the FSI work /Isaksson et al. 2007/.
Char_t	Character	Character of the lineament in letters	Characteristics of the anomaly representing the lineament, like minima, edge, minima connection, dislocation, or characteristics of the lineament itself. In the case of lineaments directly imported from the latest version of the FSI work /Isaksson et al. 2007/, their original values have been left without change.
Char_n	Character	Character of the lineament translated into an integer.	0 = minima connection, 1 = minima, 2 = edge, 3 = dislocation. In the case of lineaments directly imported from the latest version of the FSI work /Isaksson et al. 2007/, their original values have been left without change.
Uncert_t	Uncertainty	Gradation of the lineament in terms of uncertainty. In effect, this attribute involves both the degree of clarity of the lineament as well as a judgement regarding the possible cause of the lineament	1 = low, 2 = medium, 3 = high. In the case of lineaments directly imported from the latest version of the FSI work /Isaksson et al. 2007/, their original values have been left without change. Further explanation can be found in /Isaksson et al. 2007/.
Comment_t	Comment	Specific comments regarding the lineament	
Process_t	Processing	Data processing performed	Grid, image analysis, GIS.
Date_t	Date	Date for the identification	Date.
Scale_t	Scale	Scale of the image used in the identification	In SFR version 0.1/1.0 the scale used has varied, the value presented is a rough estimate of the average. In the case of lineaments directly imported from the latest version of the FSI work /Isaksson et al. 2007/, their original values have been left without change.

Field name	Name	Description	Further comments on attributes used to describe lineaments
Width_t	Width	Width on average	Not assigned in SFR version 0.1/1.0. In the case of lineaments directly imported from the latest version of the FSI work /Isaksson et al. 2007/, their original values have been left without change.
Precis_t	Precision	Spatial uncertainty of position. An estimate of how well the lineament is defined in horizontal position.	In SFR version 0.1/1.0 the value is estimated and dependent on scale. In the case of lineaments directly imported from the latest version of the FSI work /Isaksson et al. 2007/, their original values have been left without change.
Count_n	Count	The number of original segments along the lineament.	In SFR version 0.1/1.0 the value is always 1. In the case of lineaments directly imported from the latest version of the FSI work /Isaksson et al. 2007/, their original values have been left without change.
Cond_n	Conductivity	Shows how much of the lineament that has been identified by EM and/or VLF.	In SFR version 0.1/1.0 no conductivity data have been interpreted, the value is set to 0. In the case of lineaments directly imported from the latest version of the FSI work /Isaksson et al. 2007/, their original values have been left without change.
Magn_n	Magnetic	Shows how much of the lineament that has been identified by magnetics	In SFR version 0.1/1.0 the value is 1. In the case of lineaments directly imported from the latest version of the FSI work /Isaksson et al. 2007/, their original values have been left without change.
Topo_n	Topography	Shows how much of the lineament that has been identified by topography, either on the ground surface, sea bottom surface or in the rock surface.	Topography data have only aided to a very limited extent in the identification of lineaments in the work with SFR version 0.1/1.0, as a consequence this attribute has been set to 0. In the case of lineaments directly imported from the latest version of the FSI work /Isaksson et al. 2007/, their original values have been left without change.
Topog_n	Ground surface	Shows how much of the lineament that has been identified by topography in the ground surface.	Topography data have only aided to a very limited extent in the identification of lineaments in the work with SFR version 0.1/1.0, as a consequence this attribute has been set to 0. In the case of lineaments directly imported from the latest version of the FSI work /Isaksson et al. 2007/, their original values have been left without change.
Topor_n	Rock surface	Shows how much of the lineament that has been identified by topography in the bedrock surface.	Topography data have only aided to a very limited extent in the identification of lineaments in the work with SFR version 0.1/1.0, as a consequence this attribute has been set to 0. In the case of lineaments directly imported from the latest version of the FSI work /Isaksson et al. 2007/, their original values have been left without change.
Prop_n	Property	Shows in average, how many properties (complementary investigation methods) that have been identifying the lineament.	In SFR version 0.1/1.0 the value is 1 (referring to magnetics). In the case of lineaments directly imported from the latest version of the FSI work, their original values have been left without change. Isaksson et al. 2007 explain this attribute further.
Length_n	Length	The length of the lineament	In metres.
Direct_n	Direction	The average trend of the lineament.	In degrees.
Platform_t	Platform	Measuring platform for basic data.	Ground survey grid.
Sign_t	Signature	Work performed by.	In the work of SFR version 0.1/1.0, C-A Triumf GeoVista AB. In the case of lineaments directly imported from the latest version of the FSI work, their original values have been left without change.

Appendix 6

Modelling of anomalies in the magnetic total field interpreted as lineaments in the SFR regional and local model areas – version 1.0

General comments

Modelling of the magnetic total field has been carried out over selected lineaments. The profile locations were chosen in order to study the anomalies that could be coupled directly to the inferred source rock of the lineament, i.e. with a minimum of interference from other nearby irrelevant features. The preceding modelling of magnetic total field data from seventeen profiles (SFR1–SFR12 and SFR15–SFR19; profiles SFR13 and SFR14 were abandoned), within the framework of version 0.1, was reported in /Curtis et al. 2009/. In the modelling within version 1.0, profiles SFR20–SFR44 were added, of these, profile SFR22 was abandoned due to problems with interference from the inferred source rock to a nearby lineament. The profiles SFR1 and SFR 15, modelled during version 0.1, were slightly revised during the work with version 1.0. Basic data about the profiles are summarized in Table A6-1.

In the current work with model version 1.0, a comparison was made of the modelling results presented here with the results of the distribution of the magnetic susceptibility as inferred from a 3D inversion study (see Chapter 4 of the main report). In general, similarities and discrepancies between the two studies are commented in the text below.

The modelling was carried out using Encom Technology ModelVision PRO, version 8.00.37. A background magnetic susceptibility value of 500×10^{-5} SI was used. The starting model for the low susceptibility body representing the source to the lineament involved a magnetic susceptibility of 130×10^{-5} SI. This value commonly changed during the modelling work. Even though the low susceptibility rock volumes have been the primary target for the modelling, high susceptibility source bodies have also been introduced in some of the profiles. This was carried out in order to compensate for local field variations instead of creating very peculiar background fields in ModelVision. In the modelling some of the source bodies have peculiar geometries, especially near the surface. In many of the source bodies, the near-surface parts are broader than at depth.

Many of the magnetic anomalies associated with the lineaments are vague. Modelling of anomalies with low amplitude may give a rather low level of confidence in the resulting models. In the results presented below, the source bodies often end at a depth between 100 and 300 m. However, in modelling of faint anomalies, the results are uncertain already below 50 m. By contrast, modelling of strong anomalies associated with prominent lineaments is expected to yield more diagnostic results even down to depths considerably below 50 m.

The modelling of anomalies in the magnetic field has resulted in three-dimensional source bodies. The bodies have been exported to the RVS system, and have been used as an aid in the modelling of the deformation zones at SFR. In this manner, the exact geometries of the source bodies were possible to study in the RVS system.

The modelling results from forty-one profiles are presented below. As indicated above, profiles SFR13, SFR14 and SFR22 were not possible to model with any significant results and are omitted from the presentation. The location of the profiles is shown in Figure A6-1 to A6-4. The names of the lineaments are also shown.

The modelling has involved lineaments with trends that are either concordant or discordant to the expected main strike of the rock units in the bedrock. This general relationship between lineaments, rock composition and deformation in the Forsmark area is discussed in detail in /Stephens et al. 2007/. A lineament with a trend concordant to the main strike may represent a rock with low magnetic susceptibility. However, where the modelling results are commented upon in each profile below, the general approach has been to assume that the lineaments represent rocks affected by alteration in connection with deformational processes.

Table A6-1. Basic data about the profiles modelled to achieve information regarding the geometry of the inferred source rock to lineaments.

1.1 Profile Id	1.2 Coordinates RT 90	1.3 Comment
SFR1	1633254/6701163–1633414/6701409	Modelled within version 0.1, revised in version 1.0
SFR2	1633253/6701465–1633547/6701793	Modelled within version 0.1
SFR3	1633327/6701743–1633460/6701974	Modelled within version 0.1
SFR4	1633160/6701955–1633327/6702109	Modelled within version 0.1
SFR5	1633060/6702180–1633325/6702180	Modelled within version 0.1
SFR6	1633060/6702250–1633370/6702250	Modelled within version 0.1
SFR7	1633155/6702145–1633185/6702050	Modelled within version 0.1
SFR8	1633240/6702150–1633255/6702090	Modelled within version 0.1
SFR9	1633360/6702210–1633390/6702130	Modelled within version 0.1
SFR10	1633290/6701640–1633350/6701590	Modelled within version 0.1
SFR11	1633195/6701570–1633255/6701500	Modelled within version 0.1
SFR12	1633165/6701560–1633180/6701665	Modelled within version 0.1
SFR13	1632990/6701560–1633060/6701620	Not modelled
SFR14	1632745/6701485–1632830/6701525	Not modelled
SFR15	1632645/6701455–1632785/6701600	Modelled within version 0.1, revised in version 1.0
SFR16	1632985/6702025–1633060/6702005	Modelled within version 0.1
SFR17	1633050/6701870–1633090/6701945	Modelled within version 0.1
SFR18	1632695/6701970–1632775/6701935	Modelled within version 0.1
SFR19	1632830/6702075–1632915/6702115	Modelled within version 0.1
SFR20	1632879/6701719–1633089/6701530	Modelled within version 1.0
SFR21	1633351/6701736–1633470/6701916	Modelled within version 1.0
SFR22	1633347/6701737–1633349/6701618	Not modelled
SFR23	1632540/6702502–1633468/6702442	Modelled within version 1.0
SFR24	1632860/6700740–1633201/6701362	Modelled within version 1.0
SFR25	1633120/6700660–1633528/6701229	Modelled within version 1.0
SFR26	1632555/6700848–1632961/6701537	Modelled within version 1.0
SFR27	1632838/6701746–1632454/6702295	Modelled within version 1.0
SFR28	1632788/6701648–1632237/6702385	Modelled within version 1.0
SFR29	1632773/6701527–1632173/6702339	Modelled within version 1.0
SFR30	1632478/6701646–1632125/6702296	Modelled within version 1.0
SFR31	1632906/6702026–1633427/6702410	Modelled within version 1.0
SFR32	1633260/6701760–1633140/6702010	Modelled within version 1.0
SFR33	1632330/6701576–1632616/6701674	Modelled within version 1.0
SFR34	1633350/6702040–1633275/6702250	Modelled within version 1.0
SFR35	1633600/6702225–1633350/6702275	Modelled within version 1.0
SFR36	1633545/6702070–1633320/6702140	Modelled within version 1.0
SFR37	1633415/6701915–1633565/6701900	Modelled within version 1.0
SFR38	1632930/6701415–1633170/6701660	Modelled within version 1.0
SFR39	1633052/6701414–1633220/6701483	Modelled within version 1.0
SFR40	1632938/6701406–1632834/6701455	Modelled within version 1.0
SFR41	1632981/6701491–1632925/6701542	Modelled within version 1.0
SFR42	1632892/6701569–1632825/6701639	Modelled within version 1.0
SFR43	1632791/6701588–1632741/6701631	Modelled within version 1.0
SFR44	1633382/6701447–1633471/6701532	Modelled within version 1.0

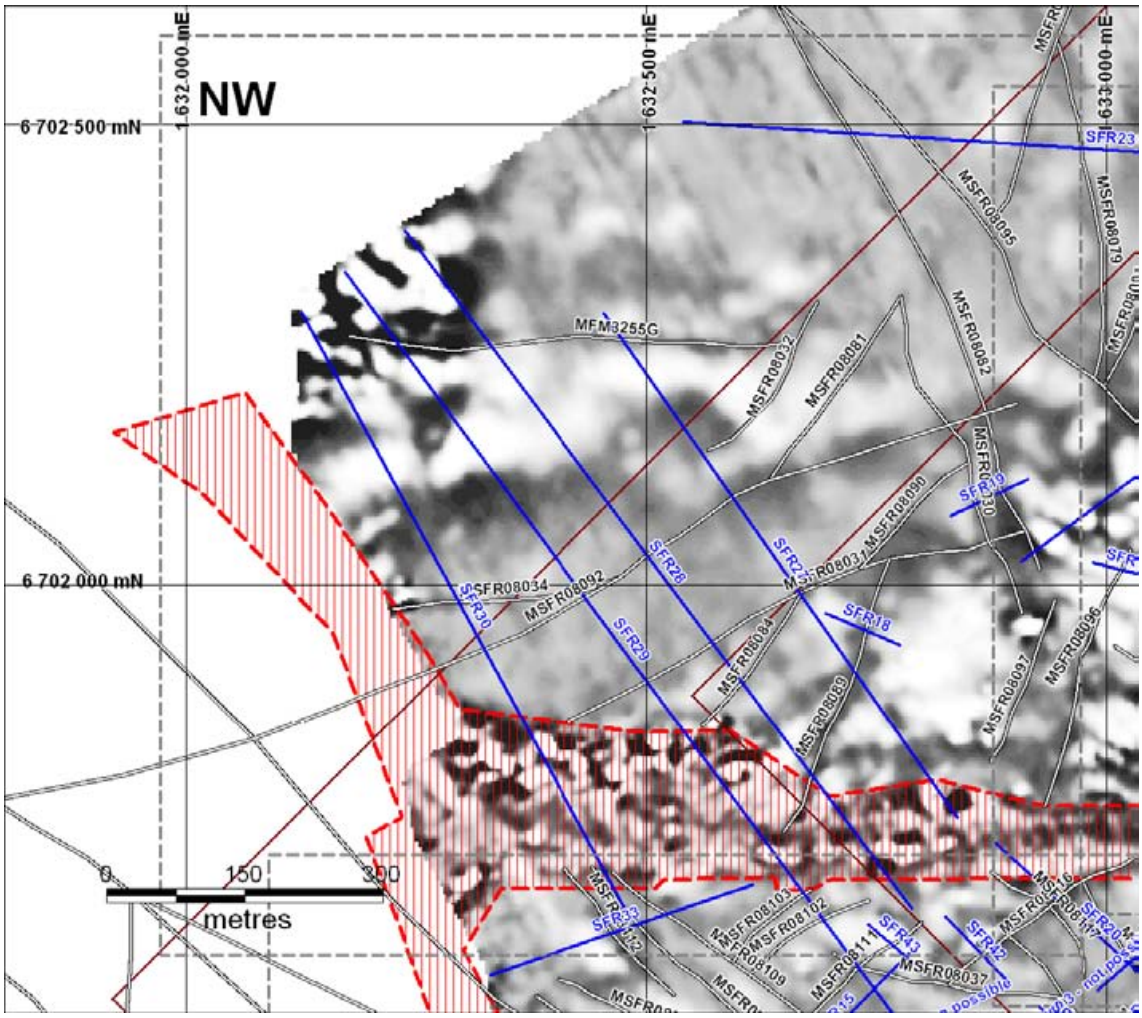

Figure A6-1. *The location of modelled profiles (blue and labelled) in the north-western part of the area. Lineaments of SFR model version 1.0 are marked with thick black-white lines, and labelled. An enhanced version of the magnetic total field image (1st vertical derivative) is shown in the background. The model areas of SFR model version 1.0 are shown as brown rectangles. Red hatching marks the area where the magnetic total field is disturbed.*

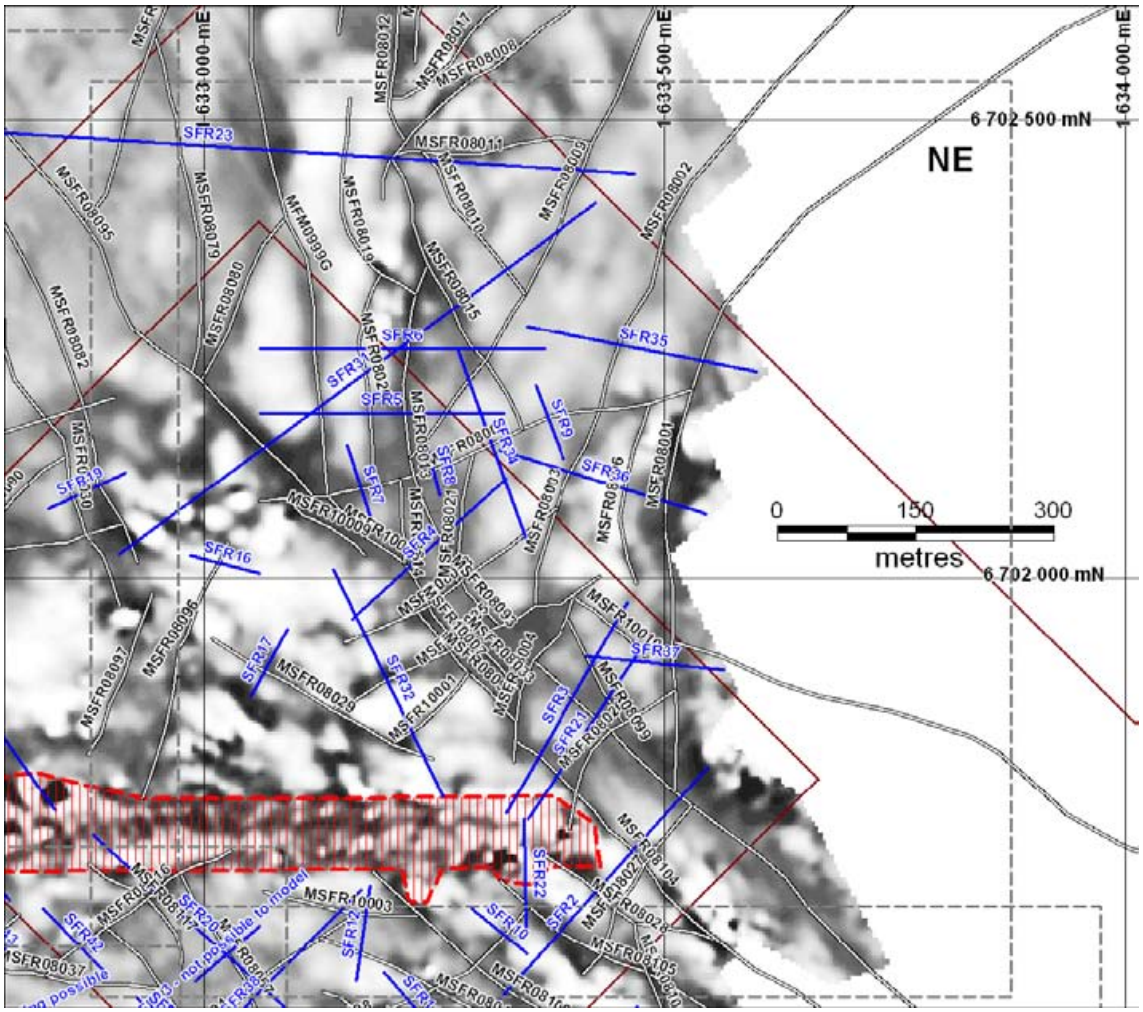

Figure A6-2. *The location of modelled profiles (blue and labelled) in the north-eastern part of the area. Lineaments of SFR model version 1.0 are marked with thick black-white lines, and labelled. An enhanced version of the magnetic total field image (1st vertical derivative) is shown in the background. The model areas of SFR model version 1.0 are shown as brown rectangles. Red hatching marks the area where the magnetic total field is disturbed.*

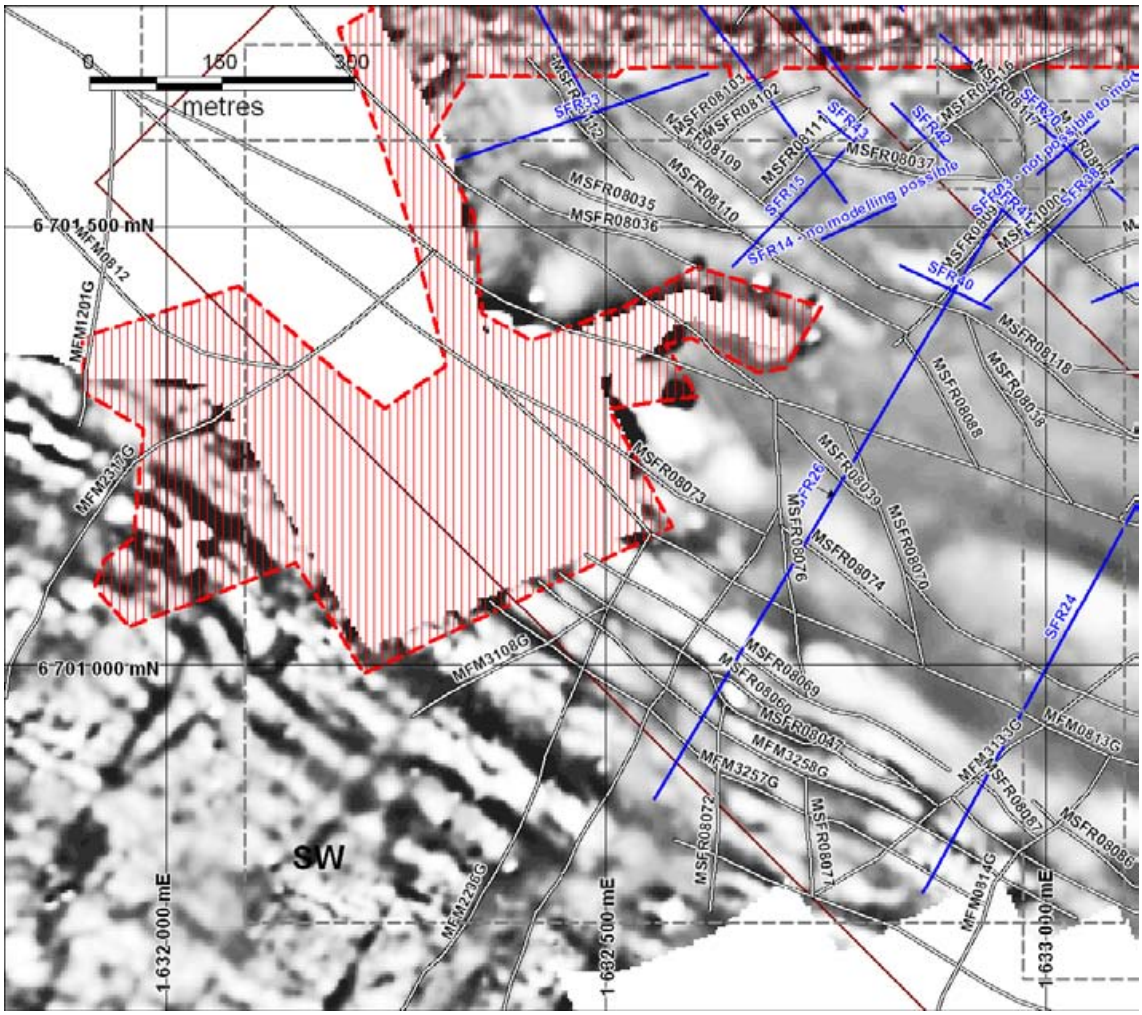

Figure A6-3. *The location of modelled profiles (blue and labelled) in the south-western part of the area. Lineaments of SFR model version 1.0 are marked with thick black-white lines, and labelled. An enhanced version of the magnetic total field image (1st vertical derivative) is shown in the background. The model areas of SFR model version 1.0 are shown as brown rectangles. Red hatching marks the area where the magnetic total field is disturbed.*

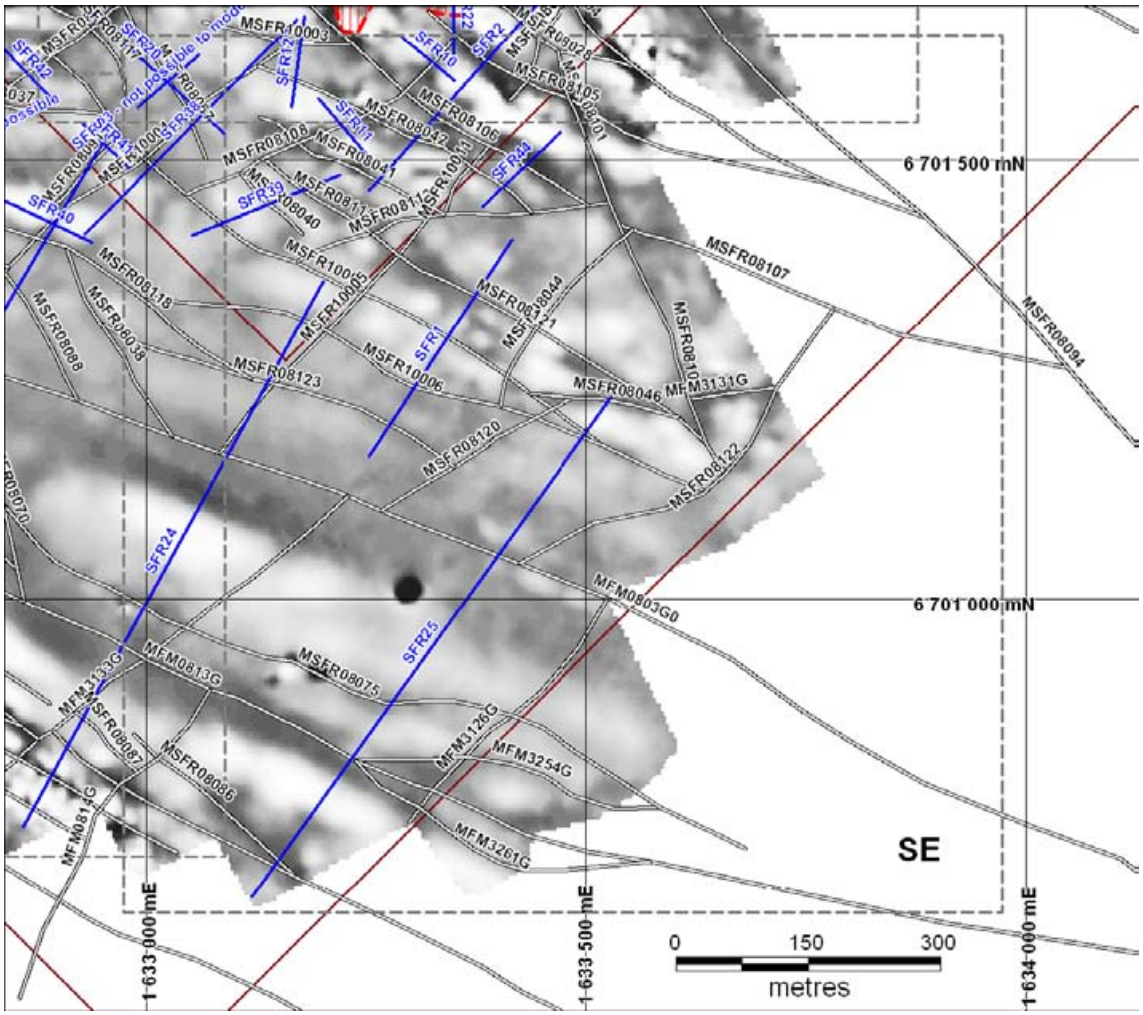

Figure A6-4. *The location of modelled profiles (blue and labelled) in the south-eastern part of the area. Lineaments of SFR model version 1.0 are marked with thick black-white lines, and labelled. An enhanced version of the magnetic total field image (1st vertical derivative) is shown in the background. The model areas of SFR model version 1.0 are shown as brown rectangles. Red hatching marks the area where the magnetic total field is disturbed.*

Profile SFR1, 1633254/6701163 – 1633414/6701409

The profile SFR1 crosses the lineaments MSFR08123, MSFR10006, MSFR10002, and MSFR08121, see Figure A6-5. The low susceptibility bodies in Figure A6-6 represent lineaments MSFR08123, MSFR10006, MSFR08121. The anomaly associated with MSFR10002 is considered difficult to model due to the strong influence of adjacent high magnetic source bodies. The dip of all low susceptibility features is steeply towards the north-east, with the broadest source body representing the lineament MSFR080121.

The results from the inversion of magnetic data in 3D, as presented in the main report, are compared in Figure A6-7. The dips in the forward modelling are comparable with the inversion results though a slight tendency is observed towards more vertical low susceptibility volumes in the 3D inversion.

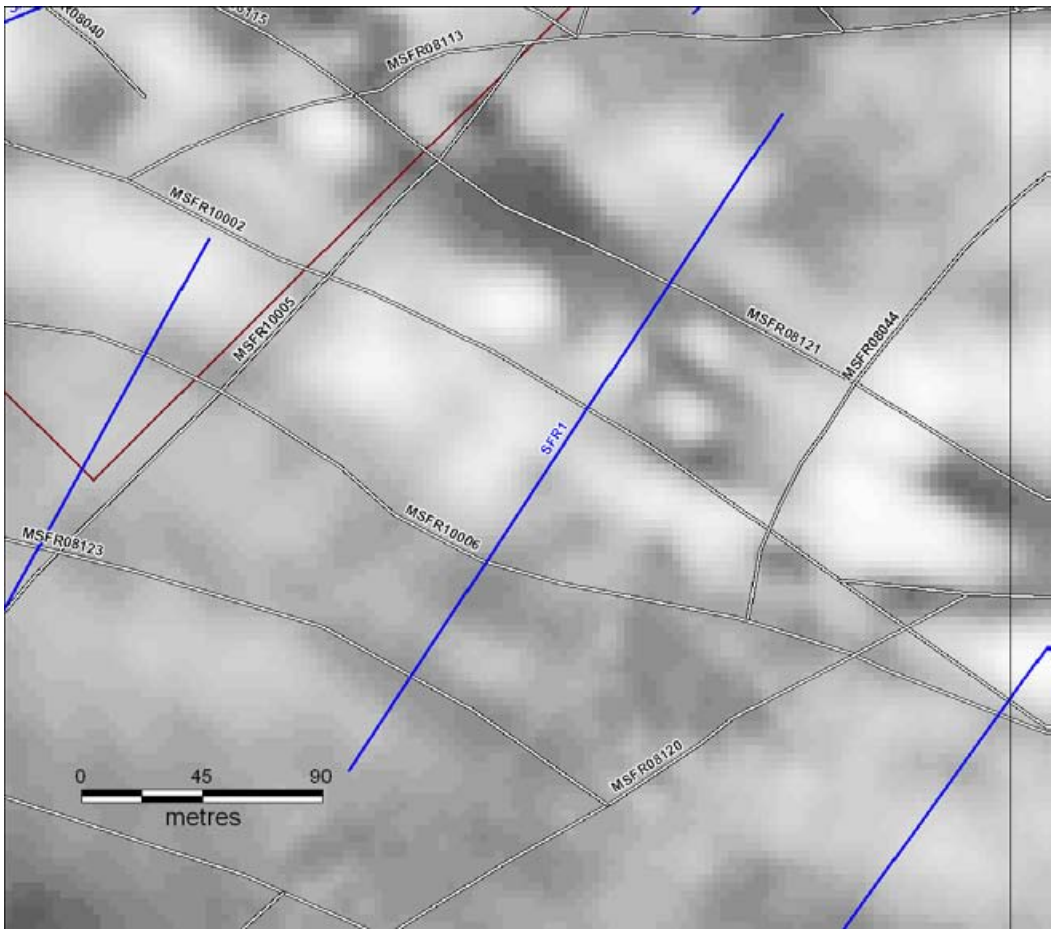

Figure A6-5. *Profile SFR1 with associated lineaments.*

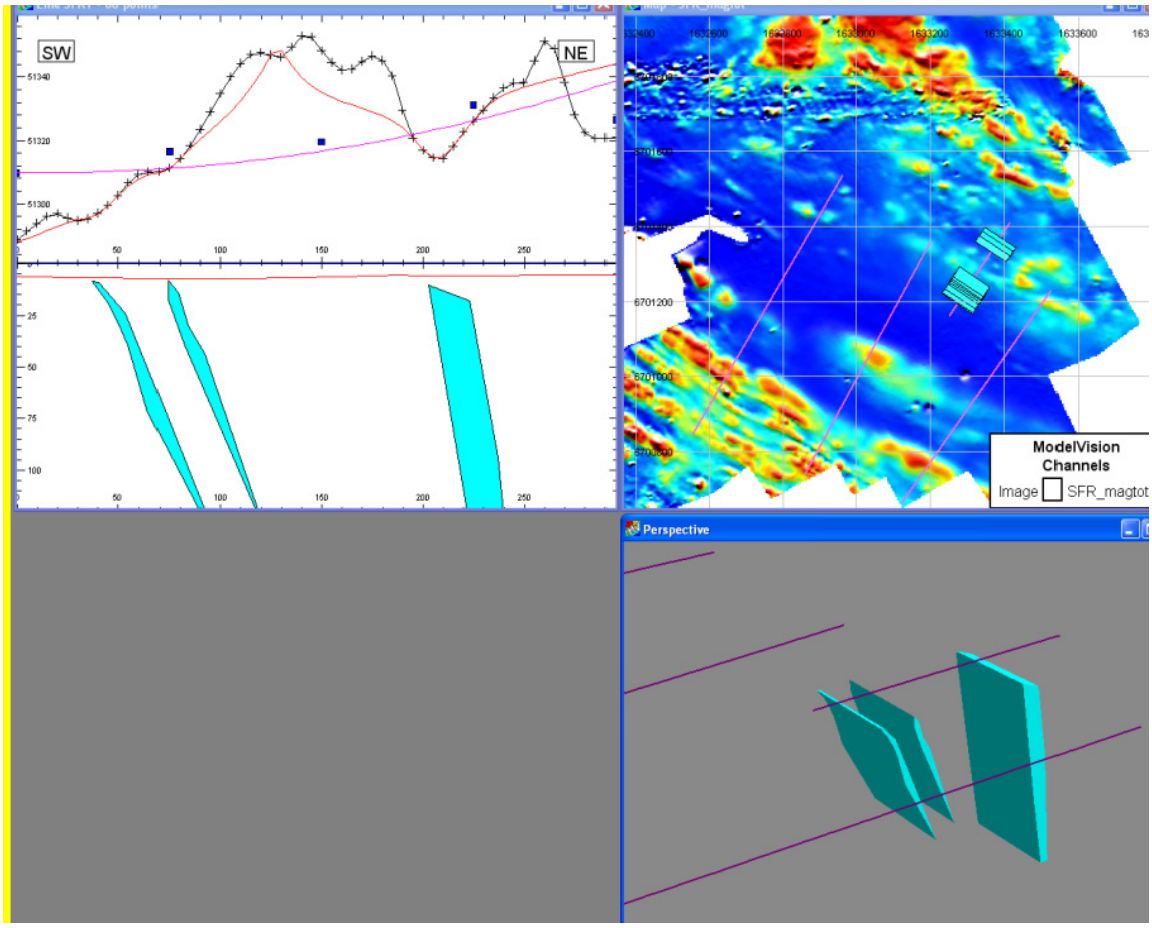

Figure A6-6. *Modelling result from profile SFR1with source bodies representing lineaments MSFR08123, MSFR10006, MSFR08121 (from left to right), all have steep dips towards the north-east. Maximum depth shown in the figure at top left is approximately 120 m.*

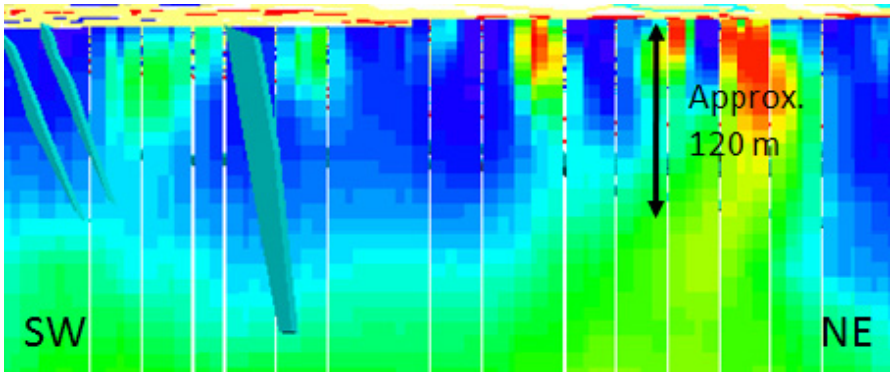

Figure A6-7. *Modelling result from profile SFR1with source bodies representing lineaments MSFR08123, MSFR1006, MSFR08121 (from left to right), all have steep dips towards the north-east and are shown with the inversion result along the same profile in the background.*

Profile SFR2, 1633253/6701465 – 1633547/6701793

The profile SFR2 crosses the lineaments MSFR08041, MSFR08042, MSFR08106, MSFR08105, MSFR08028, MSFR08104 and MSFR08094, see Figure A6-8.

The low susceptibility bodies in Figure A6-9 represent lineaments MSFR08042 and MSFR08106 (the source body at south-west), MSFR08105, MSFR08028, MSFR08104, MSFR08094. The anomaly from MSFR08041 is considered too small for modelling. The geometry of the two lineaments MSFR08042 and MSFR08106 is difficult to distinguish as the source bodies appear to coincide at depth. The uncertainty in the modelling increases where two nearby low susceptibility volumes cause interference. Figure A6-9 also shows the source bodies from the forward modelling on a background displaying the 3D inversion result. A discrepancy can be noted at the south-westernmost part of the profile where the source body representing the lineaments MSFR08042 and MSFR08106, dipping steeply towards north-east in the forward modelling, appears to have an almost vertical dip in the 3D inversion result. The forward modelling indicates a dip of around 45° towards north-east for the source body of lineament MSFR08104; there is a notable difference compared to the 3D inversion result where a rather small low susceptibility volume with a steep dip is the solution. The result for MSFR08104 should be compared with the result from profile SFR3 where the forward modelling gives a steep dip; the difference between the two profiles indicates a large uncertainty in the modelling result for this feature.

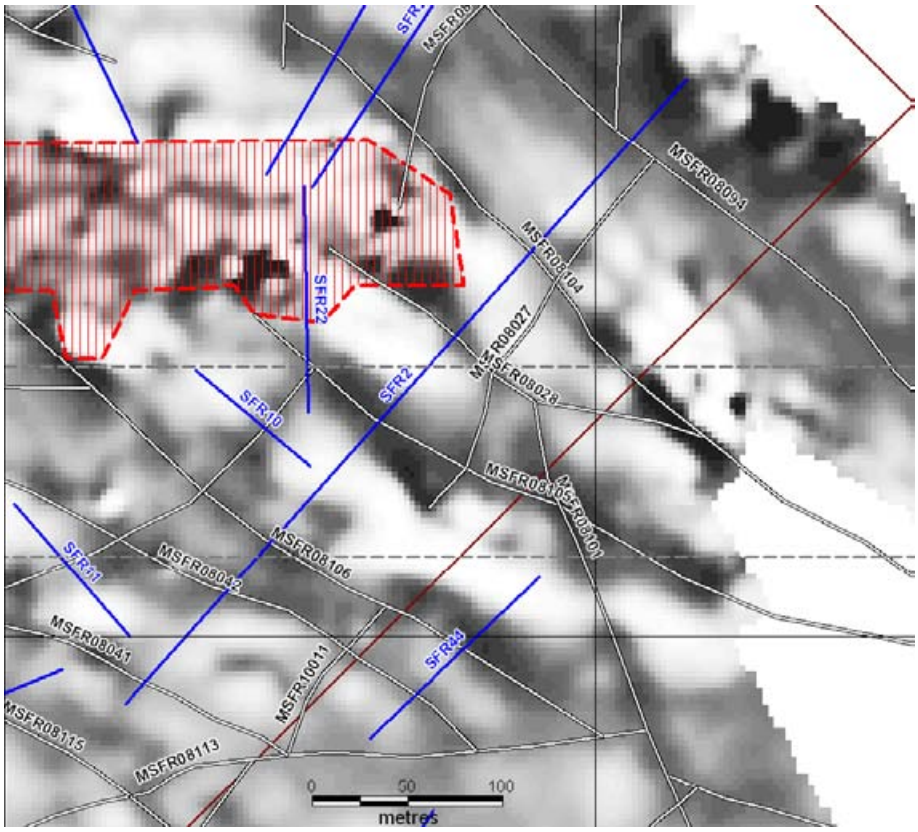

Figure A6-8. *Profile SFR2 with associated lineaments. The border of the local model area of SFR is visible as a brown line.*

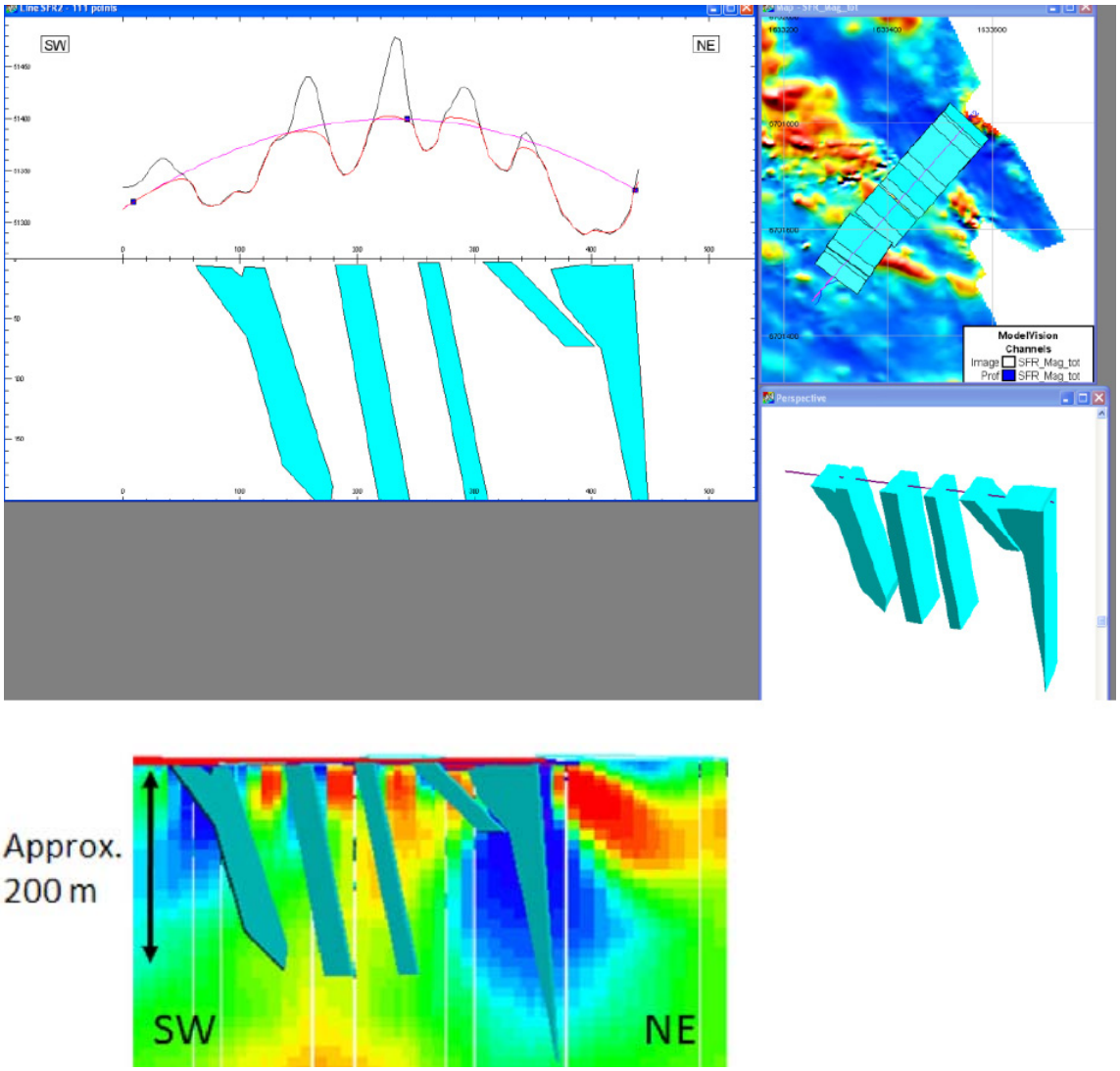

Figure A6-9. *Top: Modelling result from profile SFR2 with source bodies from left to right representing lineaments MSFR08042 and MSFR08106, MSFR08105, MSFR08028, MSFR08104, MSFR08094. Maximum depth shown at the leftmost part of the figure is approximately 200 m. Bottom: comparison between source bodies from the forward modelling and the result from the 3D inversion of magnetic total field.*

Profile SFR3, 1633327/6701743 – 1633460/6701974

The profile SFR3 crosses the lineaments MSFR08104, MSFR08094, MSFR08099 and MSFR10010, see Figure A6-10.

The source bodies representing lineaments MSFR08104, MSFR08094 and MSFR08099 are shown in Figure A6-11. The source to lineament MSFR10010 is not modelled due to a possible interference from a short low magnetic feature sub-parallel with the profile.

The body at north-east in the figure represents two lineaments (MSFR08094 and MSFR08099), indicating that the whole rock volume in association with the lineaments has a low magnetic susceptibility. The reason could be that the whole unit is affected by deformational processes. However, a rock unit with low magnetic susceptibility and without any remarkable deformational overprint, located between the two lineaments, cannot be ruled out. The thinning of the bodies towards depth should not be taken too literally as the uncertainty level becomes rather high in the prediction of geometry at depth. A comparison with the 3D inversion results shows fairly consistent results, both the forward modelling and the 3D inversion indicate a steep dip of the source to the lineament MSFR08104 (Figure A6-11). The results from the forward modelling and the 3D inversion are also consistent regarding the sources to the lineaments MSFR08094 and MSFR08099.

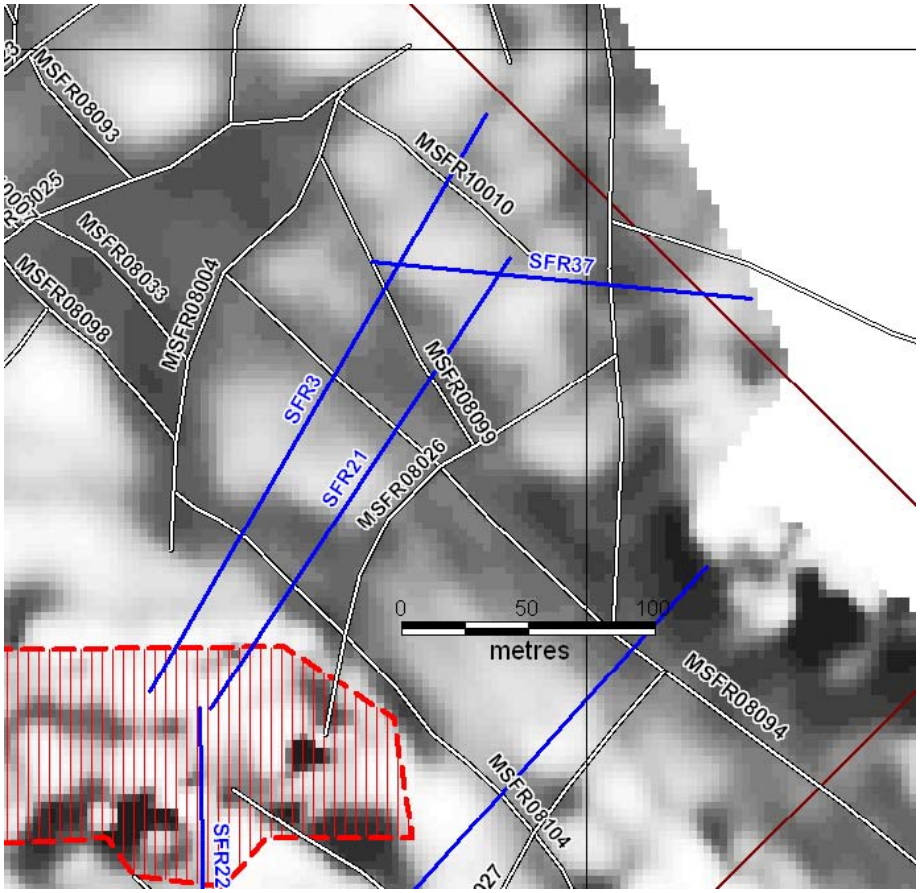

Figure A6-10. *Profile SFR3 with associated lineaments. The local model area of SFR is visible as a brown line.*

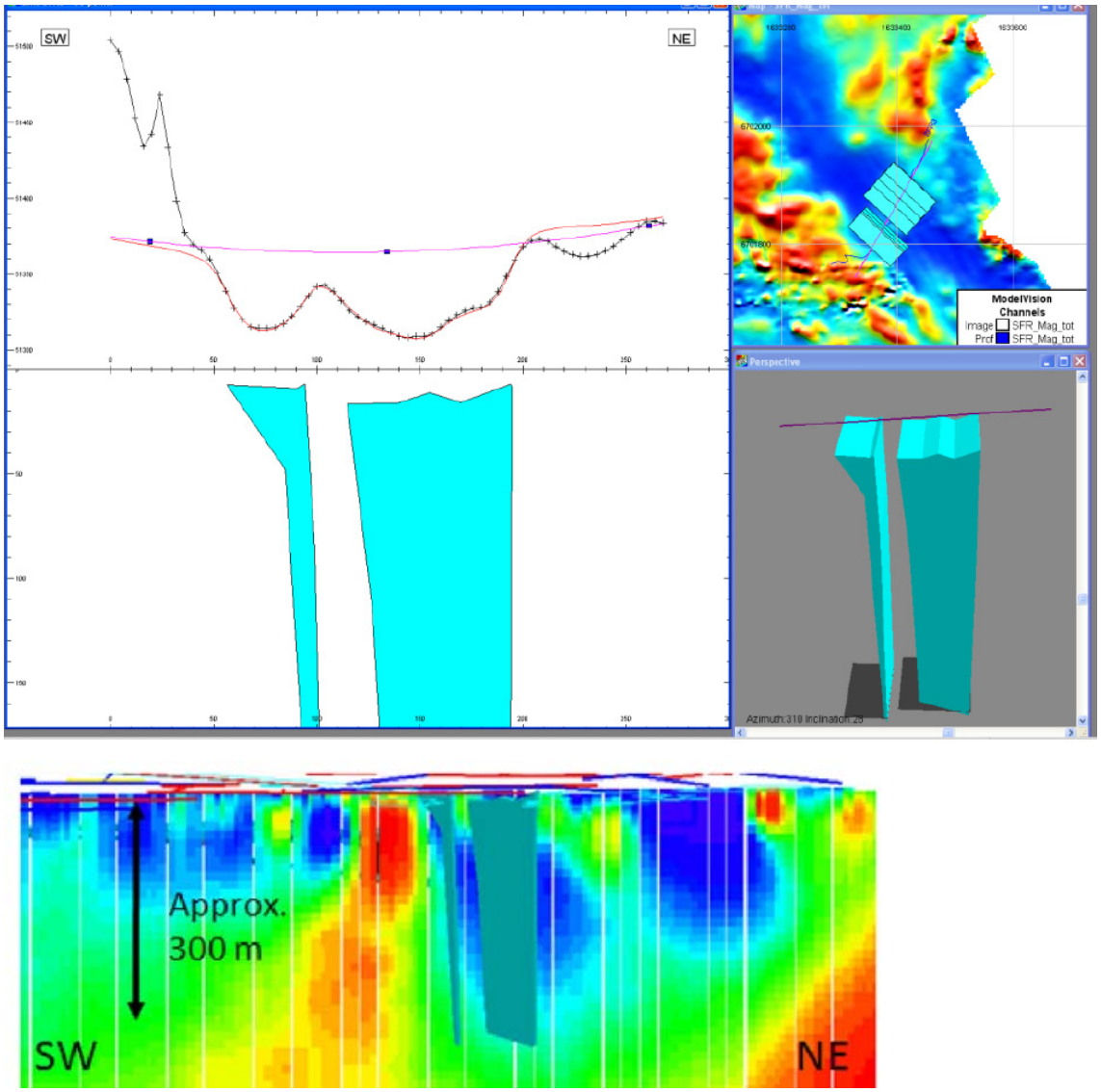

Figure A6-11. *Top: Forward modelling result from profile SFR3 with source bodies from left to right representing lineaments MSFR08104, MSFR08094 and MSFR08099, the two latter lineaments are represented by one source body only. Maximum depth shown in the leftmost part of the figure is approximately 170 m. Bottom: comparison between source bodies from the forward modelling and the result from the 3D inversion of magnetic total field.*

Profile SFR4, 1633160/6701955 – 1633327/6702109

The profile SFR4 crosses the lineaments MSFR10008, MSFR08013 and MSFR08021, see Figure A6-12.

The model used in the forward modelling (see Figure A6-13) consists of three low susceptibility bodies (blue) and two high susceptibility bodies (pink). The three lineaments are represented by the blue source bodies, all three with steep dips. The 3D inversion and the forward modelling give qualitatively the same result (Figure A6-14).

Figure A6-12. *Profile SFR4 with associated lineaments. The local model area of SFR is visible as a brown line.*

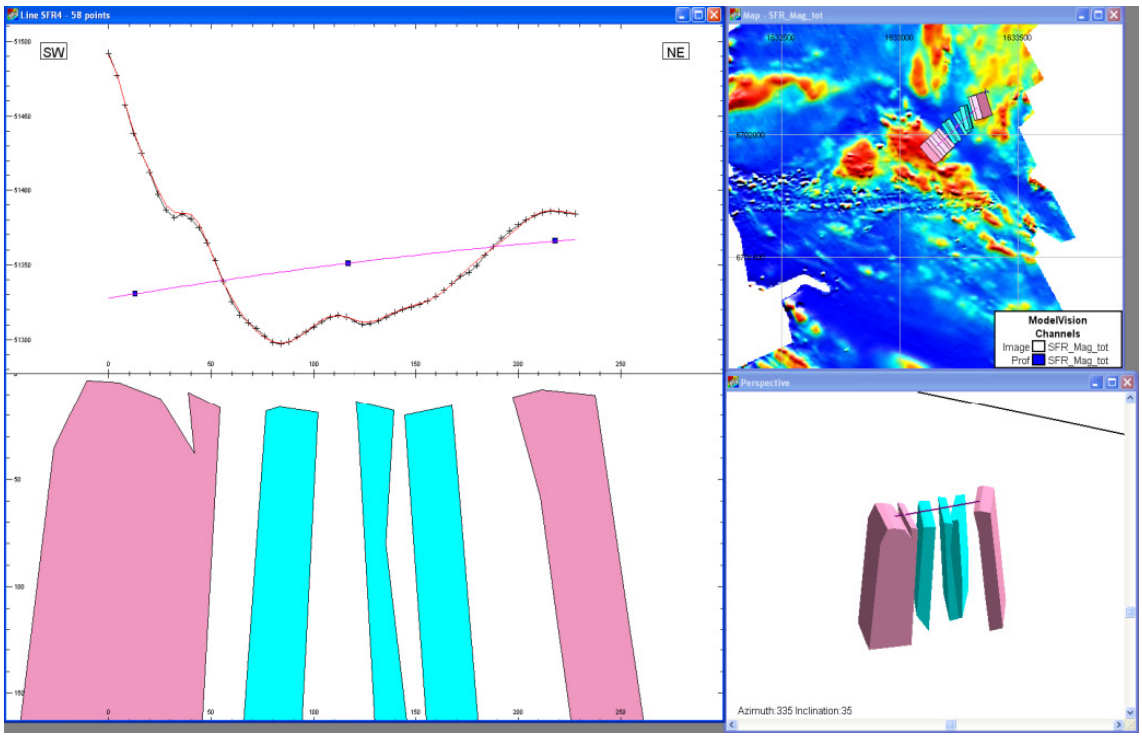

Figure A6-13. *Modelling result from profile SFR4. In this modelling three low susceptibility bodies (blue) have been used, flanked by two high susceptibility rock volumes (pink). The three red source bodies represent the lineaments MSFR10008, MSFR08013 and MSFR08021 (from left to right). Maximum depth shown in the leftmost part of the figure is approximately 160 m.*

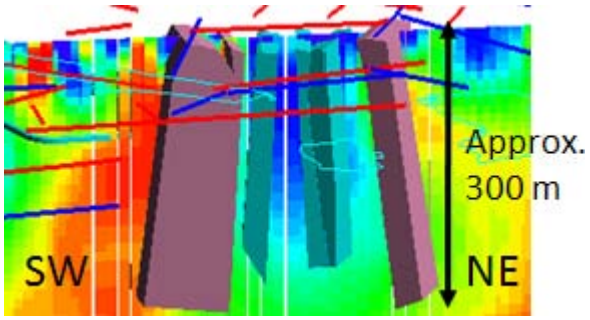

Figure A6-14. *Comparison of the source bodies from the forward modelling with the result from the 3D inversion of magnetic total field data (3D view). Blue colour in the inversion result indicates low relative magnetic susceptibility.*

Profile SFR5, 1633060/6702180 – 1633325/6702180

The profile SFR5 crosses the lineaments MFM0999G, MSFR08020, MSFR08013 and MSFR08009, see Figure A6-15.

The modelling result is shown in Figure A6-16 with the low susceptibility bodies in blue and the high susceptibility bodies in pink. The low susceptibility source bodies represent the three lineaments; all are steeply dipping. The anomaly connected to lineament MSFR08020 is very faint and difficult to model as it is located in a gradient of the magnetic total field, as a consequence the predicted geometry of the source body is of rather low confidence. The anomaly associated with lineament MSFR08009 is located on a gradient in the magnetic field with some overprinting irregularities and, consequently, not modelled. The comparison of the 3D inversion result with the forward modelling (Figure A6-17) shows a fairly good correspondence at surface-near depths. At greater depth the 3D inversion indicates a large low susceptibility rock volume, while the forward modelling indicates that also the high susceptibility source bodies continue towards greater depths. As the sensitivity to variations in susceptibility at depth is rather low, considering the low general magnetization in the area, the difference in the results can be assigned to the general low confidence in both models at depth.

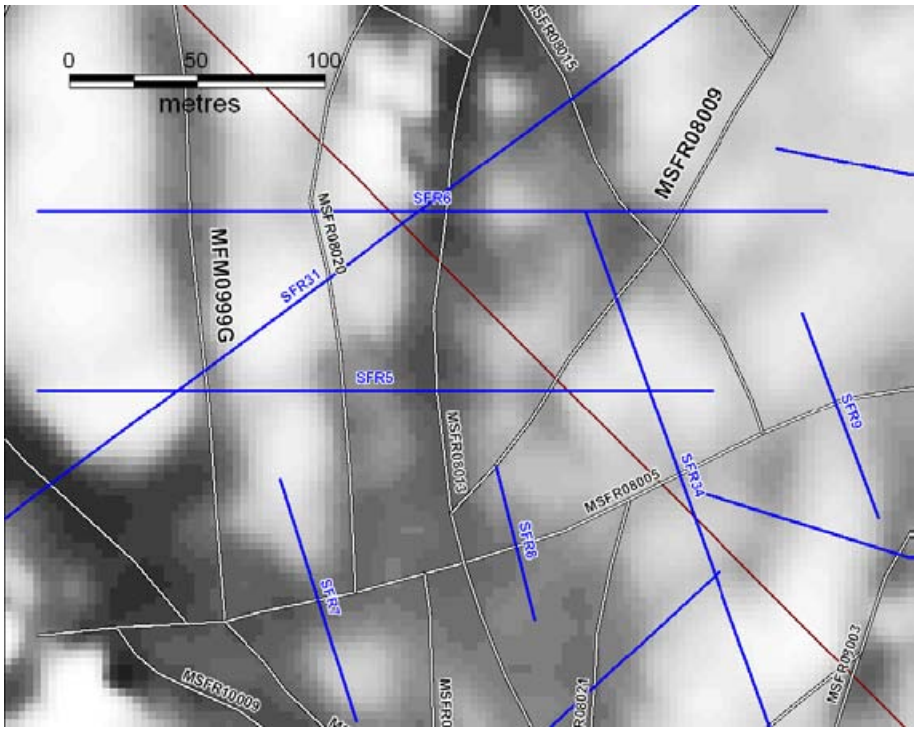

Figure A6-15. *Profile SFR5 with associated lineaments. The local model area of SFR is visible as a brown line.*

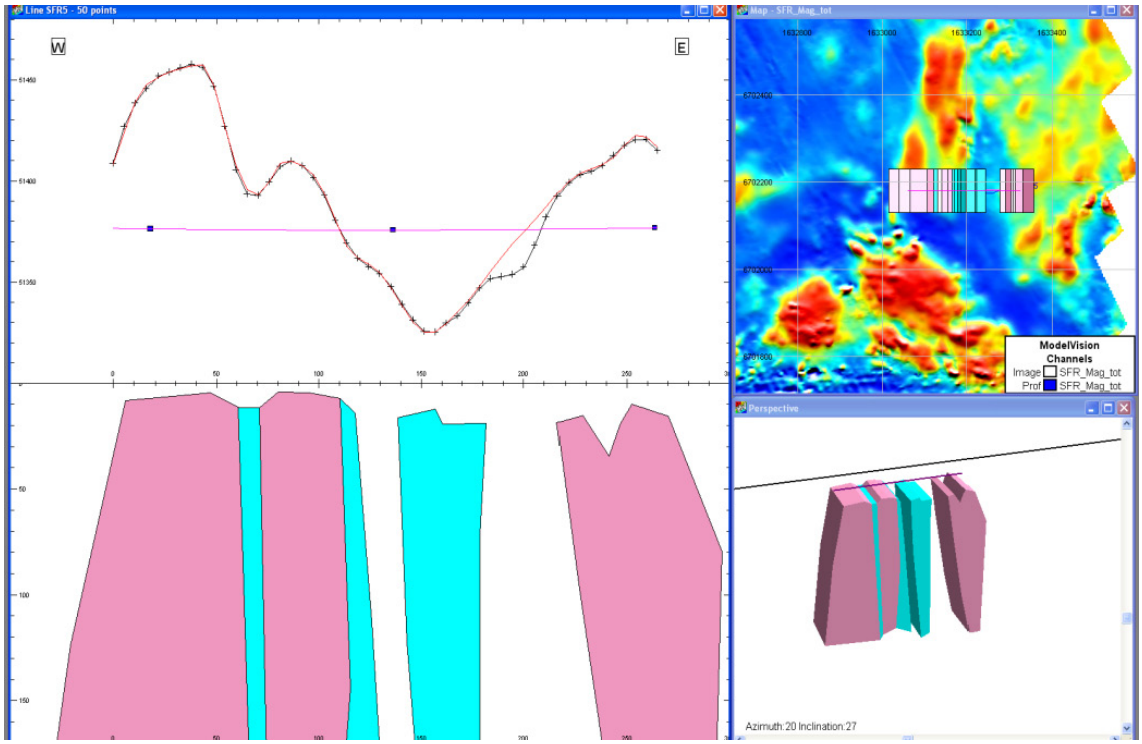

Figure A6-16. *Modelling result from profile SFR5. In this modelling three low susceptibility bodies (blue) have been used, representing the lineaments MFM0999G, MSFR08020, MSFR08013 (from left to right). Maximum depth shown in the figure is approximately 170 m.*

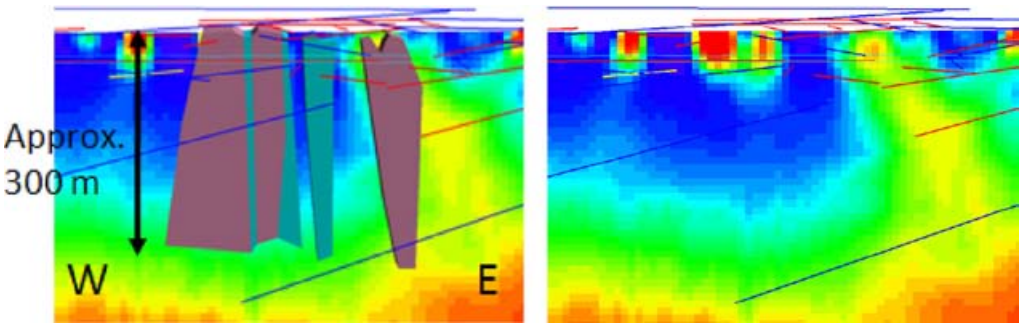

Figure A6-17. *Comparison of the source bodies from the forward modelling with the result from the 3D inversion of magnetic total field data. At left with the source bodies, at right without the source bodies. Blue colour in the inversion result indicates low relative magnetic susceptibility.*

Profile SFR6, 1633060/6702250 – 1633370/6702250

The profile SFR6 crosses the lineaments MFM0999G, MSFR08020, MSFR08013, MSFR08015 and MSFR08009, see Figure A6-15 above. The low and high susceptibility source bodies are shown in Figure A6-18. The lineaments MFM0999G, MSFR08020, MSFR08013 and MSFR08015 are represented by source bodies with steep dips. The anomaly associated with MSFR08009 is too weak to be modelled.

There is a difference in the maximum depth of the two westernmost low susceptibility source bodies when the results from the 3D inversion and the forward modelling of magnetic total field data are compared (Figure A6-19). The 3D inversion suggests a fairly surface-near volume with low magnetic susceptibility surrounded by a high susceptibility volume. The difference is partly dependent on the general decrease in confidence in the models with depth. Otherwise there is a good agreement between the two models.

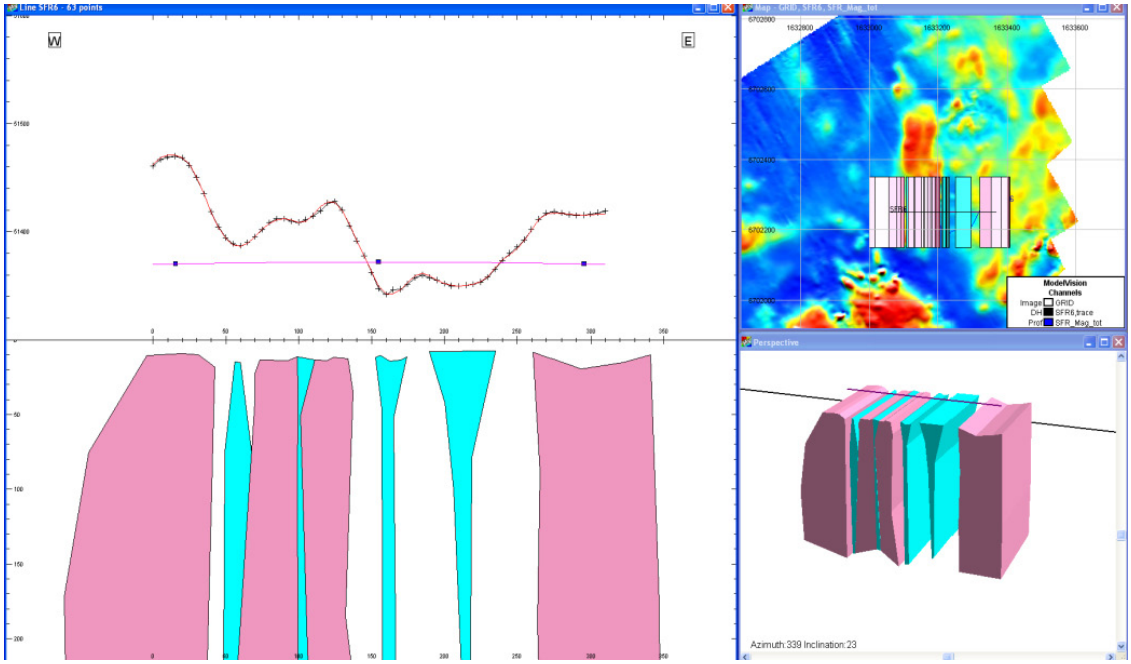

Figure A6-18. *Modelling result from profile SFR6. Four low susceptibility source bodies (blue) have been used together with four high susceptibility bodies (pink). The lineaments MFM0999G, MSFR08020, MSFR08013 and MSFR08015 are represented by the blue bodies (from left to right). Maximum depth shown in the leftmost part of the figure is approximately 220 m.*

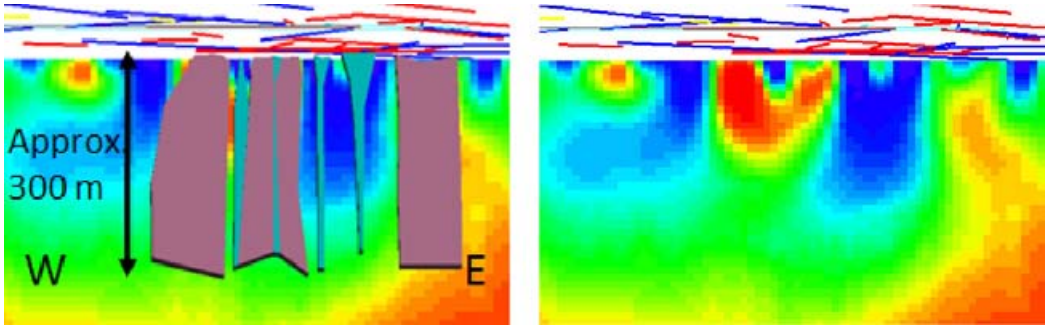

Figure A6-19. *Comparison of the source bodies from the forward modelling with the result from the 3D inversion of magnetic total field data. At left with the source bodies, at right without the source bodies. Blue colour in the inversion result indicates low relative magnetic susceptibility.*

Profile SFR7, 1633155/6702145 – 1633185/6702050

The profile SFR7 crosses the lineament MSFR08005 (see Figure A6-15 above). The model containing a low susceptibility source body representing the anomaly source to lineament MSFR08005 is shown in Figure A6-20. It is flanked by two high susceptibility bodies. The source body to the lineament is steeply dipping towards the north. Furthermore, the 3D inversion (see Figure A6-21) indicates a steep dip of the low susceptibility source body.

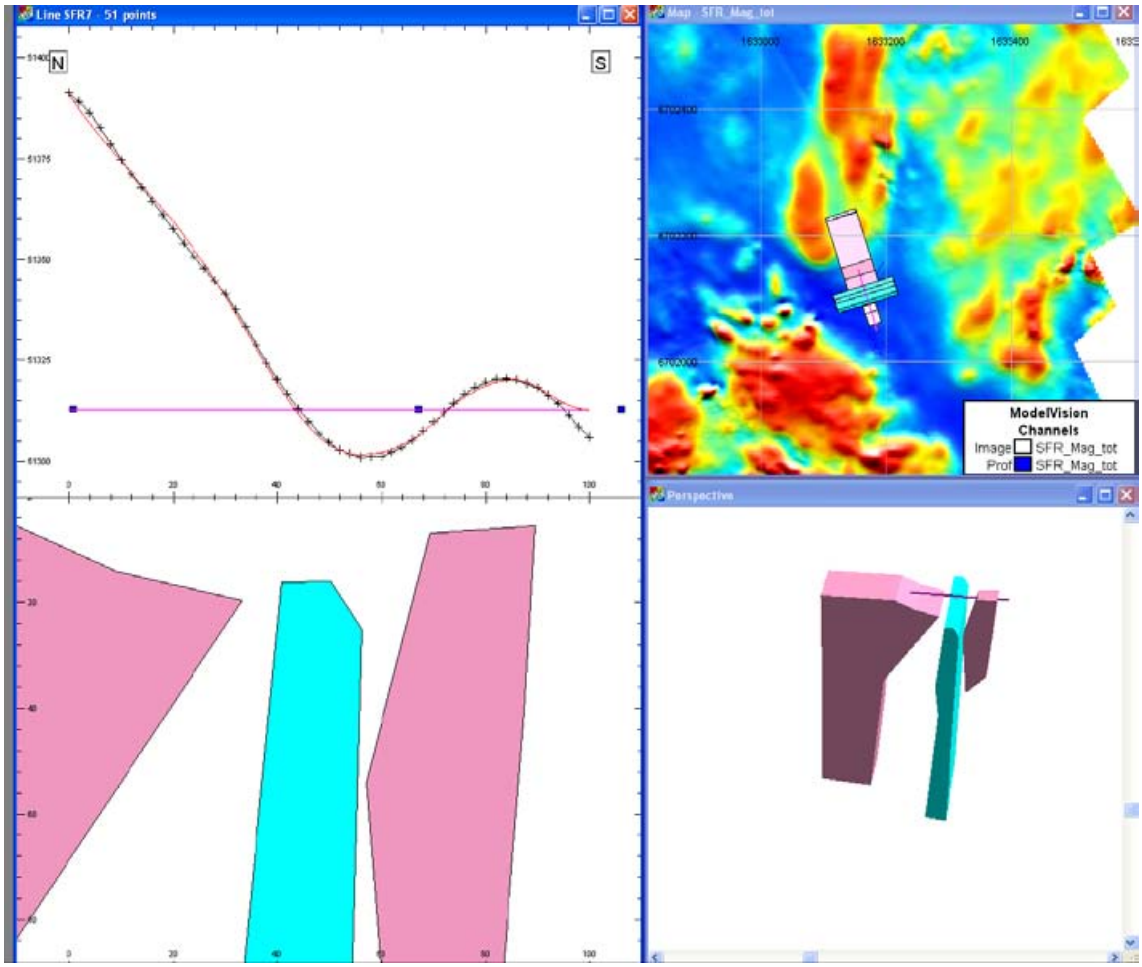

Figure A6-20. *Modelling result from profile SFR7. In this modelling a low susceptibility body (blue), representing lineament MSFR08005, has one high susceptibility body on each side (pink). Maximum depth shown in the leftmost part of the figure is approximately 90 m.*

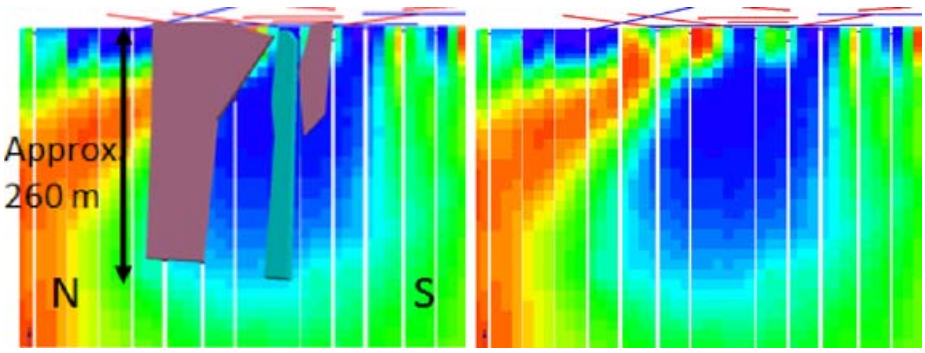

Figure A6-21. *Comparison of the source bodies from the forward modelling with the result from the 3D inversion of magnetic total field data. At left with the source bodies, at right without the source bodies. Blue colour in the inversion result indicates low relative magnetic susceptibility.*

Profile SFR8, 1633240/6702150 – 1633255/6702090

The profile SFR8 crosses the lineament MSFR08005 (see Figure A6-15 above). The model consists of two low susceptibility source bodies and one high susceptibility body (Figure A6-22). The anomaly associated with the lineament MSFR08005 is caused by a source body with a steep dip. The other low susceptibility source body is inserted for reasons of compensation for another zone not involved in this modelling. As seen in Figure A6-21 the anomaly associated with the lineament MSFR08005 is located at a gradient in the magnetic total field, furthermore, the anomaly is quite weak. Due to this the level of uncertainty in the modelling is considered to be rather high.

The comparison between the forward modelling result and the 3D inversion is shown in Figure A6-23. The 3D inversion has classified most of the volume to be of low susceptibility; the low susceptibility source body from the forward modelling is hardly recognisable. In the forward modelling the "high" susceptibility body (0.00570 SI) has a rather low contrast with the background susceptibility (0.00500 SI) which explains the almost total lack of such a solution in the 3D inversion result.

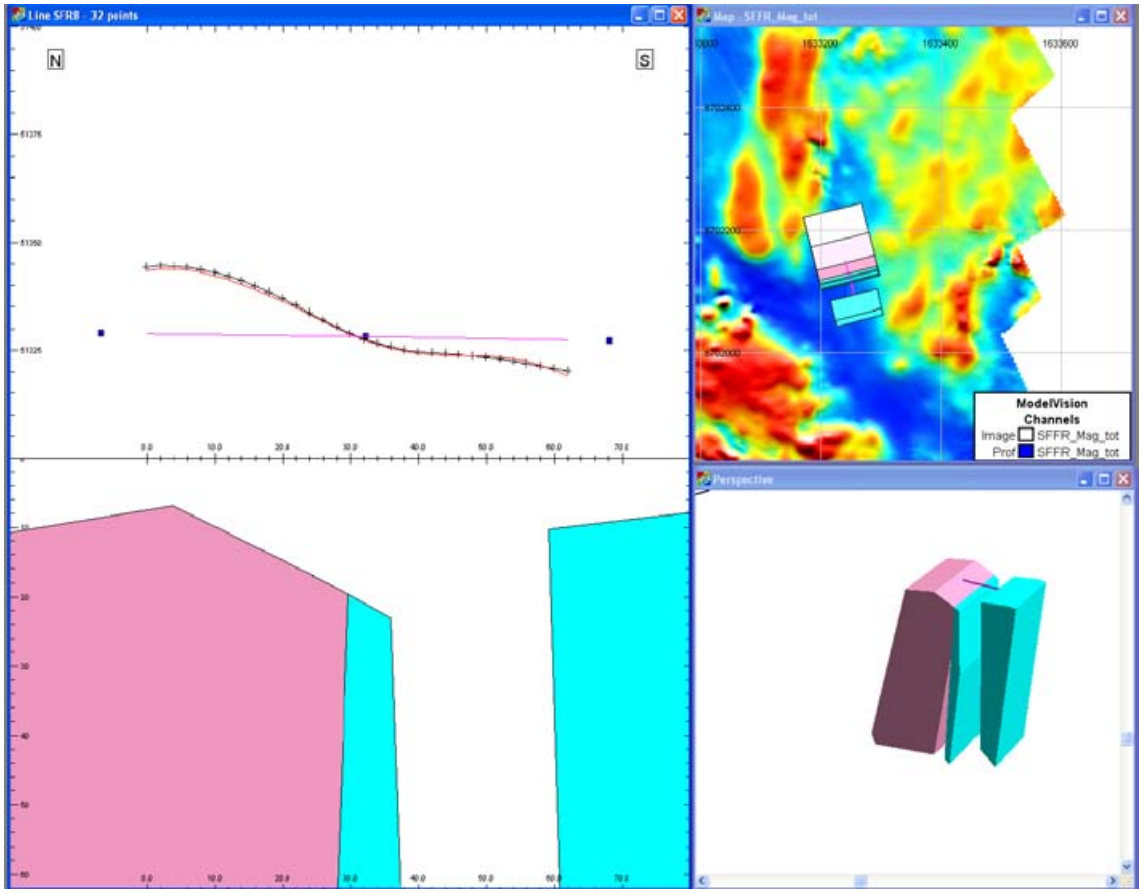

Figure A6-22. *Modelling result from profile SFR8. In this modelling the low susceptibility body (blue) closest to the "high" susceptibility body (pink) is the primary object representing lineament MSFR08005. The blue body at right in the figure is only inserted to compensate for its contribution to the magnetic depression at the side of the step-like lineament anomaly. Maximum depth shown in the leftmost part of the figure is approximately 60 m.*

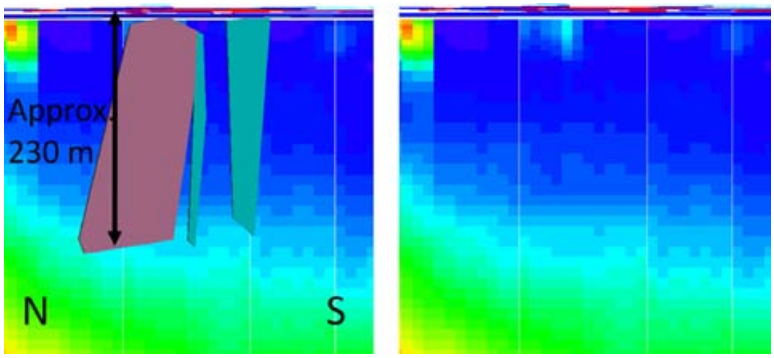

Figure A6-23. *Comparison of the source bodies from the forward modelling with the result from the 3D inversion of magnetic total field data. At left with the source bodies, at right without the source bodies. Blue colour in the inversion result indicates low relative magnetic susceptibility.*

Profile SFR9, 1633360/6702210 – 1633390/6702130

The profile SFR9 crosses the lineament MSFR08005 (Figure A6-15 above). The model contains three low susceptibility bodies and one high susceptibility body (Figure A6-24). The zone representing the lineament MSFR08005 is steeply dipping towards the northwest. The other two low susceptibility bodies are inserted to compensate for other low susceptibility sources not aimed at in this modelling. As seen in Figure A6-24 the anomaly associated with the lineament MSFR08005 is located at a gradient in the magnetic total field. Due to this, the level of uncertainty in the modelling is considered to be high. The result from the forward modelling is in agreement with the 3D inversion (Figure A6-25). The discrepancy between the two models occurs at the southernmost low susceptibility body invoked to compensate for the side minimum outside the modelled part of the profile.

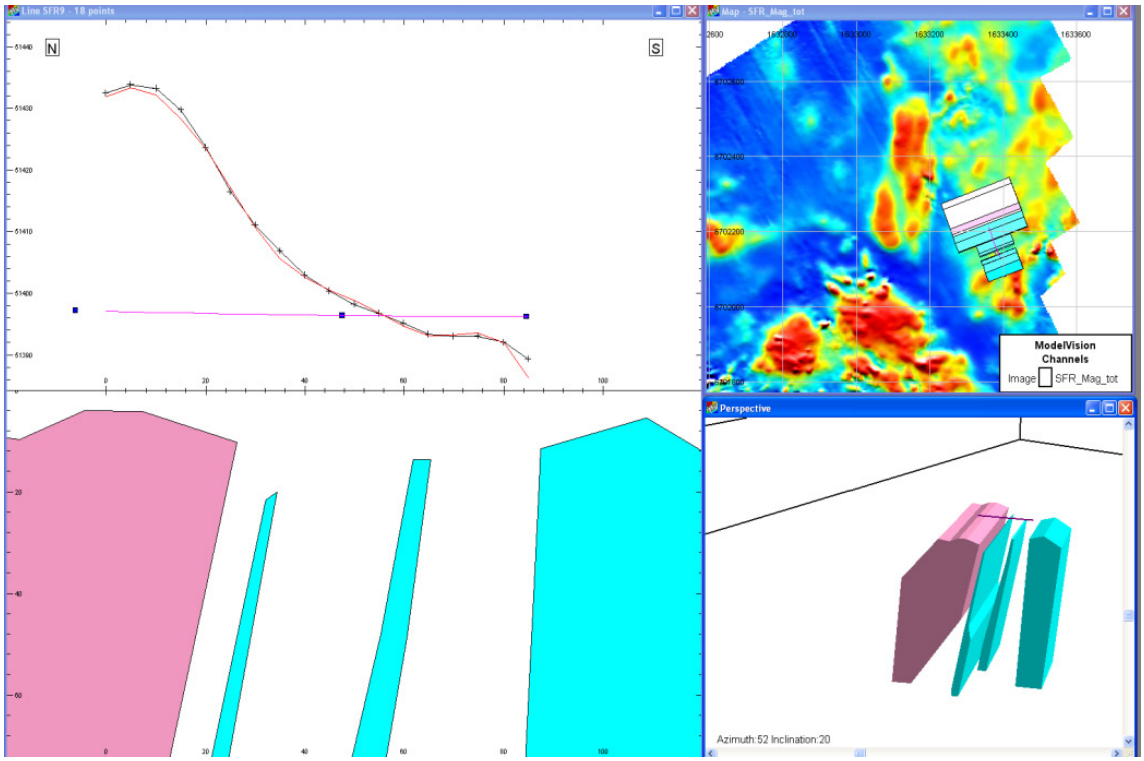

Figure A6-24. *Modelling result from profile SFR9. In this modelling the low susceptibility body (blue) closest to the high susceptibility body (pink) is the source representing the lineament MSFR08005. The two blue source bodies to the right in the figure are only inserted to compensate for their contribution to the magnetic depression at the side of the step-like lineament anomaly. Maximum depth shown in the leftmost part of the figure is approximately 70 m.*

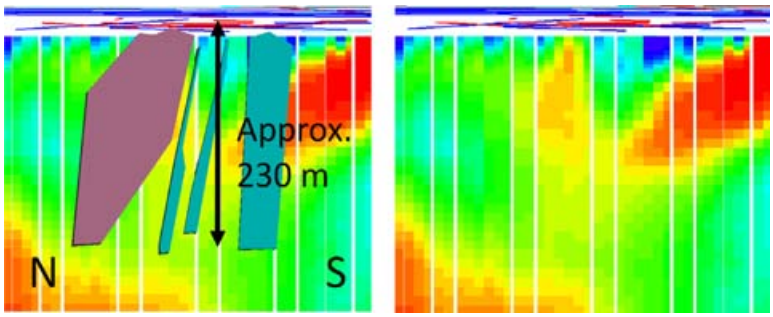

Figure A6-25. *Comparison of the source bodies from the forward modelling with the result from the 3D inversion of magnetic total field data. At left with the source bodies, at right without the source bodies. Blue colour in the inversion result indicates low relative magnetic susceptibility.*

Profile SFR10, 1633290/6701640 – 1633350/6701590

The profile SFR10 crosses the lineament MSFR08108 (Figure A6-26).

The model contains one low susceptibility source body with high susceptibility bodies at each side (Figure A6-27). The source body to the lineament MSFR08108 is almost vertical. Figure A6-28 shows the source bodies from the forward modelling on a susceptibility distribution resulting from the 3D inversion of magnetic total field data; the low susceptibility zone coincides well with the source body at surface-near levels.

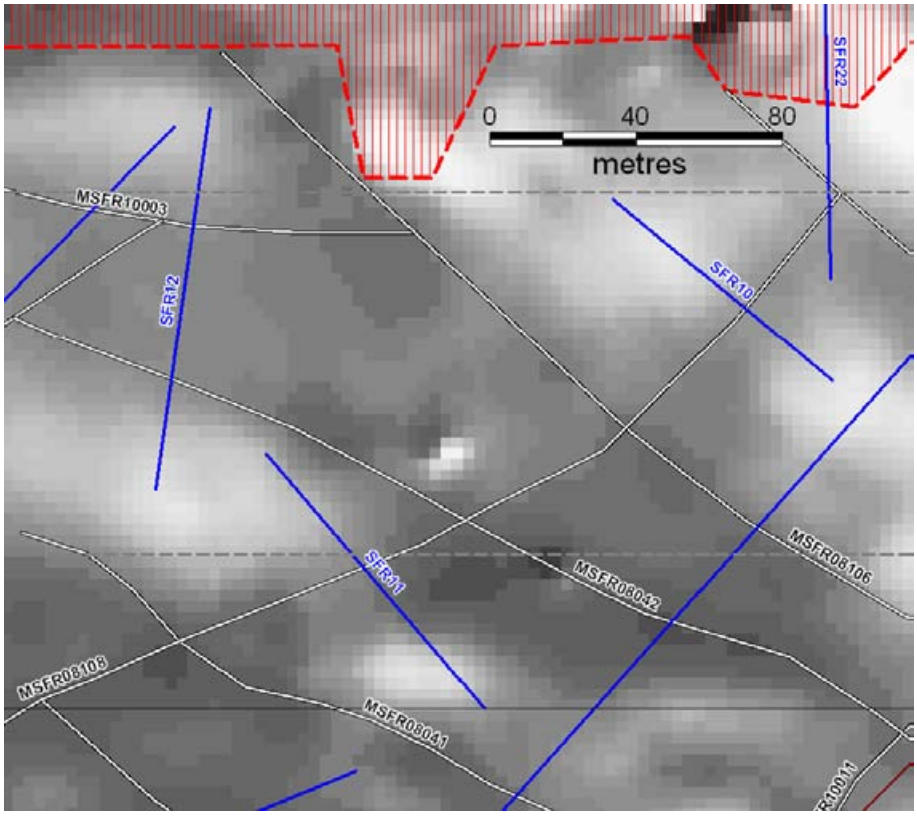

Figure A6-26. *Profiles SFR10, SFR11 and SFR12 with associated lineaments.*

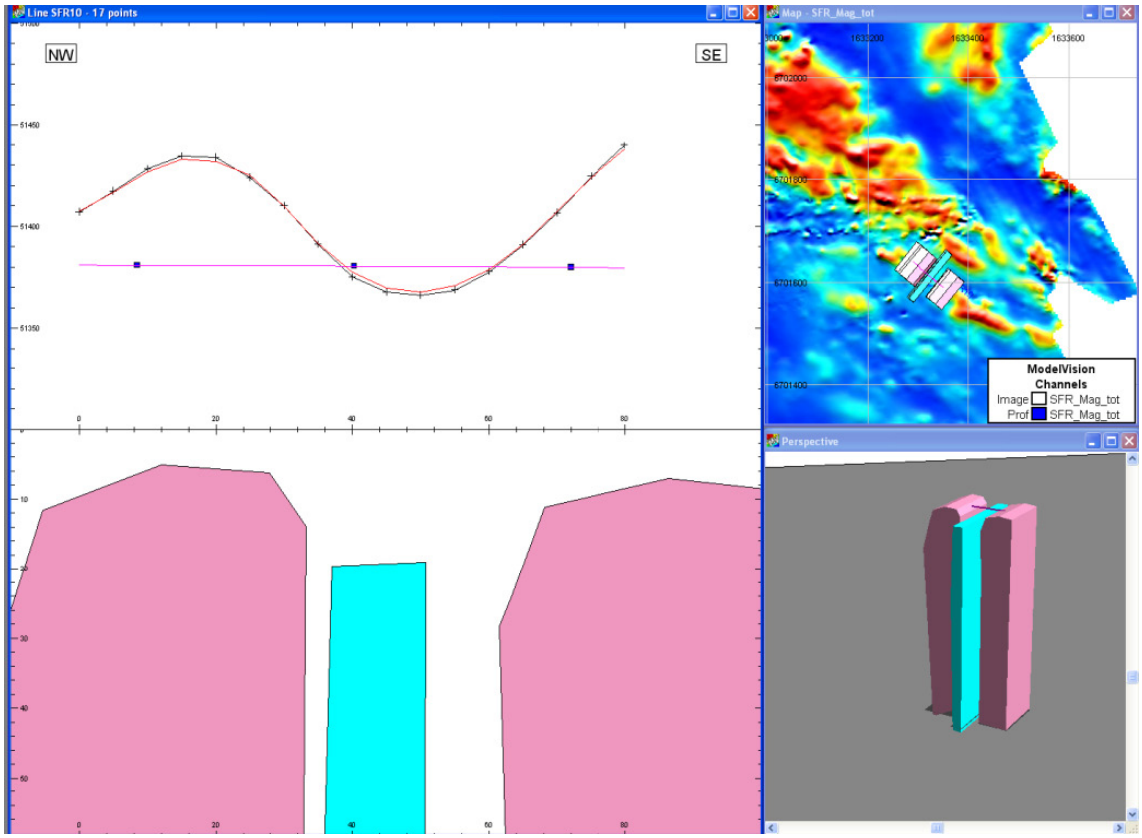

Figure A6-27. *Modelling result from profile SFR10 shows the source body (blue) to lineament MSFR08108. Maximum depth shown in the leftmost part of the figure is approximately 60 m.*

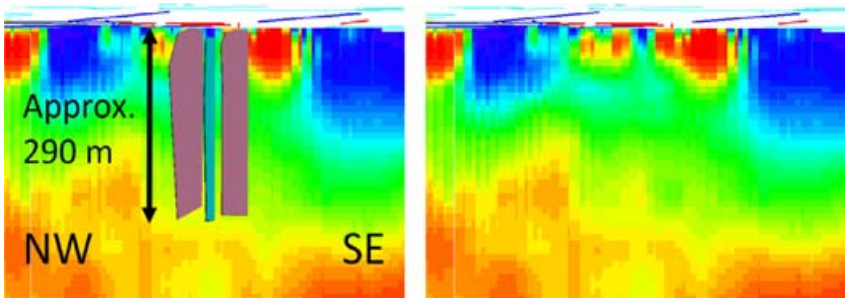

Figure A6-28. *Comparison of the source bodies from the forward modelling with the result from the 3D inversion of magnetic total field data. At left with the source bodies, at right without the source bodies. Blue colour in the inversion result indicates low relative magnetic susceptibility.*

Profile SFR11, 1633195/6701570 – 1633255/6701500

Profile SFR11 crosses the lineament MSFR08108 (see Figure A6-26 above). Figure A6-29 shows the model with a low susceptibility source body flanked by two high susceptibility bodies. The source body representing the lineament MSFR08108 is steeply dipping towards the north-west.

The forward modelling result is compared with the 3D inversion in Figure A6-30. The geometry of the low susceptibility source body from the forward modelling is in good agreement with the distribution of low magnetic susceptibility in the 3D inversion result.

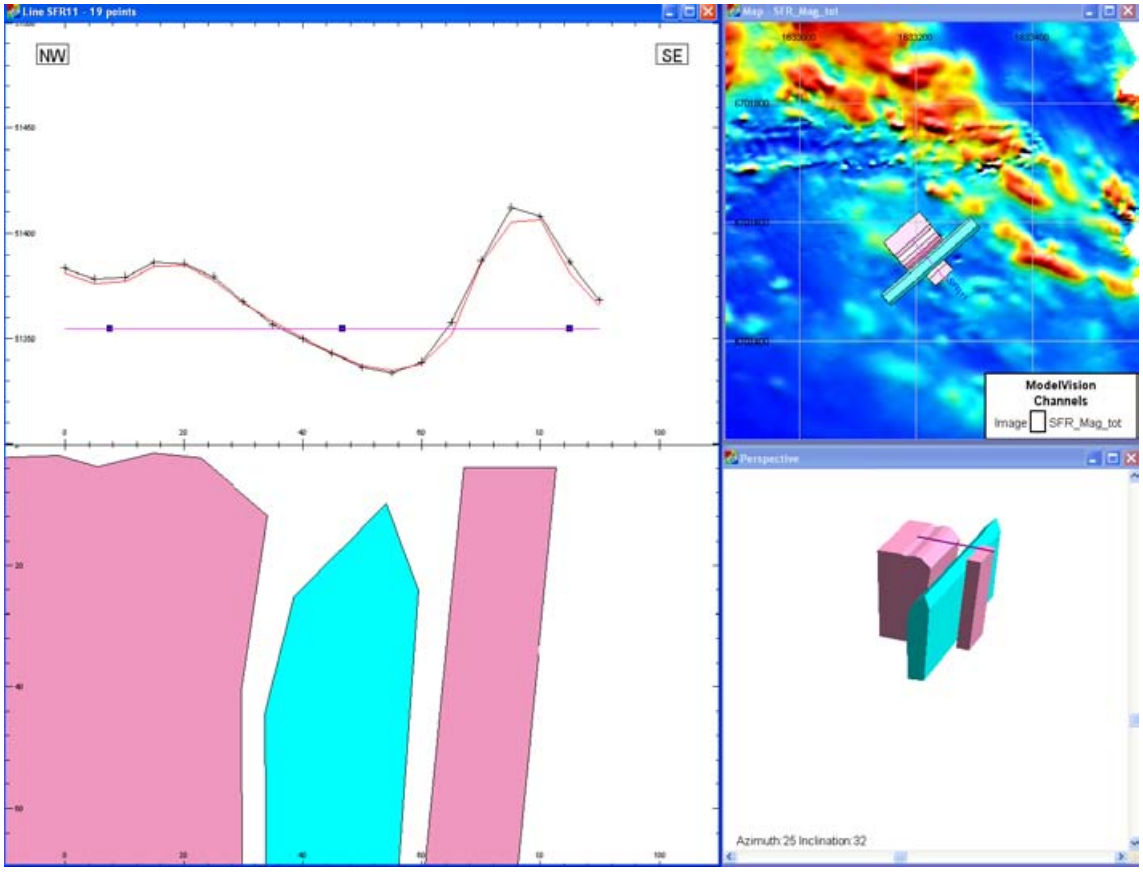

Figure A6-29. *Modelling result from profile SFR11 with a low susceptibility source body (blue) representing the low magnetic anomaly associated with lineament MSFR08108. Maximum depth shown in the leftmost part of the figure is approximately 70 m.*

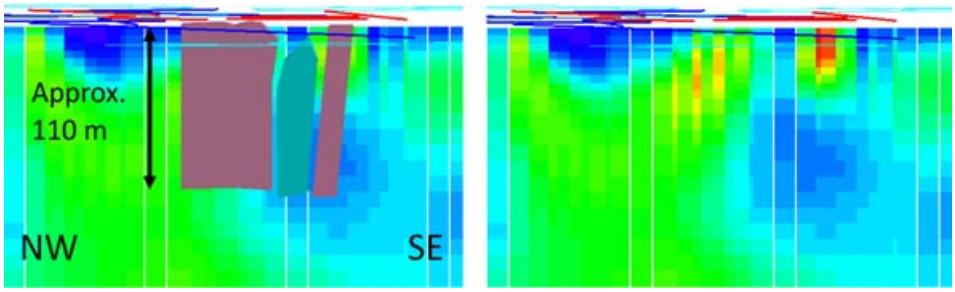

Figure A6-30. *Comparison of the source bodies from the forward modelling with the result from the 3D inversion of magnetic total field data. At left with the source bodies, at right without the source bodies. Blue colour in the inversion result indicates low relative magnetic susceptibility.*

Profile SFR12, 1633165/6701560 – 1633180/6701665

Profile SFR12 crosses the lineaments MSFR08042 and MSFR10003 (see Figure A6-26). Figure A6-31 shows the model with two, steeply dipping, low susceptibility source bodies, bordered by two high susceptibility source bodies.

Figure A6-32 shows a comparison of the forward modelling result with the susceptibility distribution along profile SFR12 as a result from the 3D inversion. The 3D inversion result indicates a possible steep dip towards the north-east while the forward modelling gives almost vertical low susceptibility source bodies.

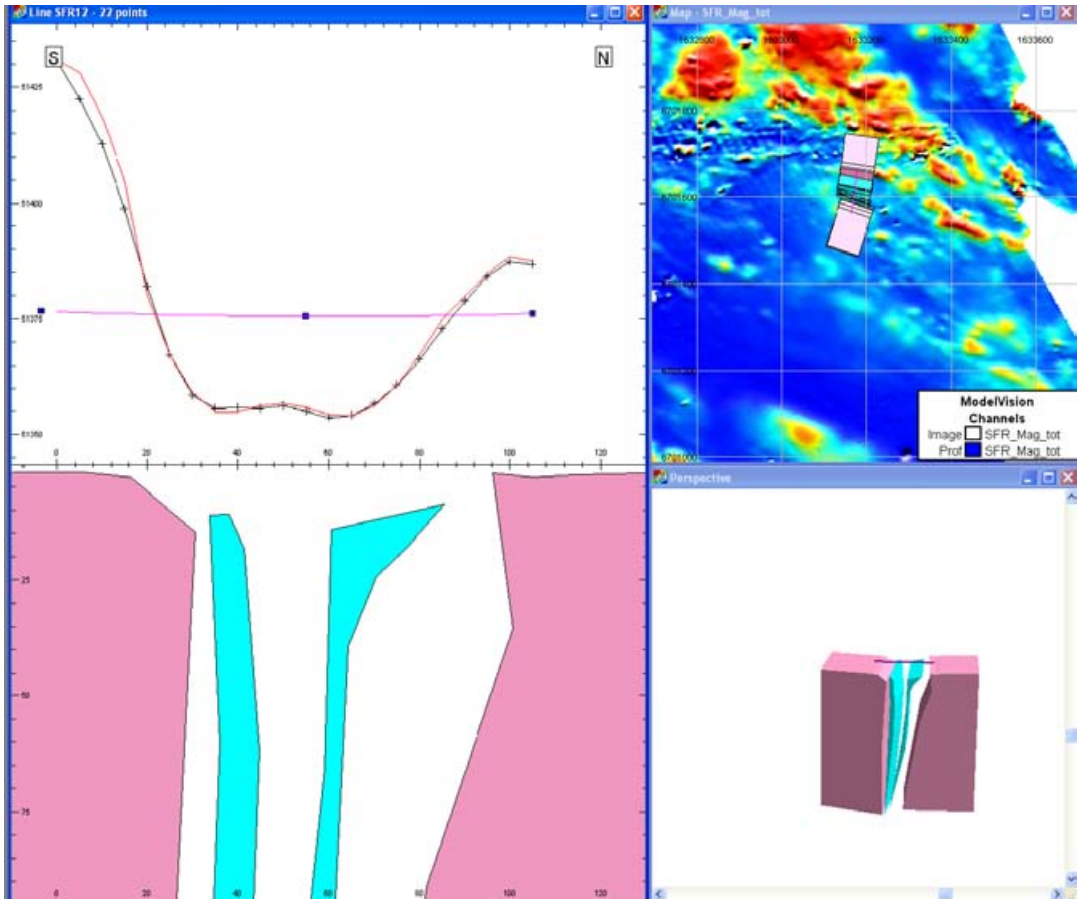

Figure A6-31. *Modelling result from profile SFR12 with two low susceptibility source bodies (blue) representing the lineaments MSFR08042 and MSFR10003 (from left to right). Maximum depth shown in the leftmost part of the figure is approximately 90 m.*

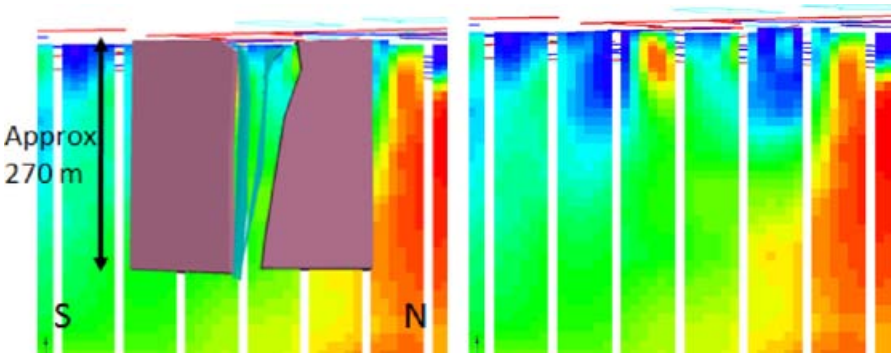

Figure A6-32. *Comparison of the source bodies from the forward modelling with the result from the 3D inversion of magnetic total field data. At left with the source bodies, at right without the source bodies. Blue colour in the inversion result indicates low relative magnetic susceptibility.*

Profile SFR13, 1632990/6701560 – 1633060/6701620

The profile is excluded due to an anomaly too weak for modelling in combination with its position upon a gradient.

Profile SFR14, 1632745/6701485 – 1632830/6701525

The profile is excluded due to an anomaly too weak for modelling in combination with its position upon a gradient.

Profile SFR15, 1632645/6701455 – 1632785/6701600

The profile SFR15 crosses the lineaments MSFR08110, MSFR08109 and MSFR08037, see Figure A6-33.

Figure A6-34 shows a model with low susceptibility bodies (light blue) representing the associated lineaments MSFR08110, MSFR08109 and MSFR08037. Two low susceptibility bodies (dark blue) are also modelled to compensate for local minima though they are not associated with any lineaments. Five high susceptibility bodies (pink) were also included to compensate for local maxima. The low susceptibility source bodies from the forward modelling, representing lineaments (light blue), are all steeply dipping, and in rather good agreement with the 3D inversion results (Figure A6-35).

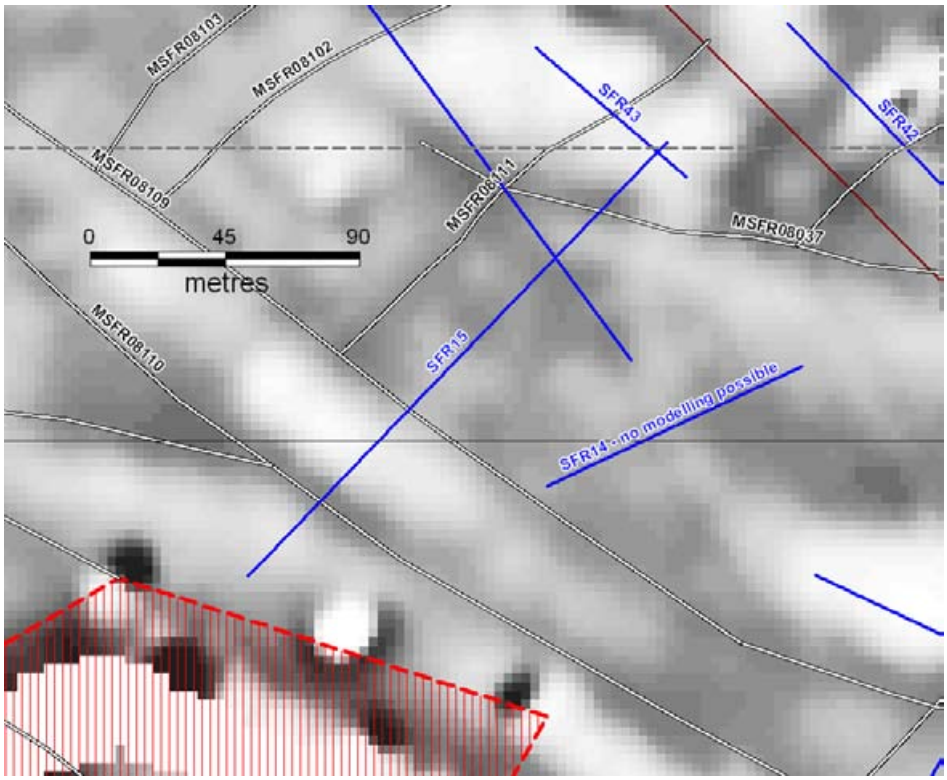

Figure A6-33. *Profile SFR15 with associated lineaments.*

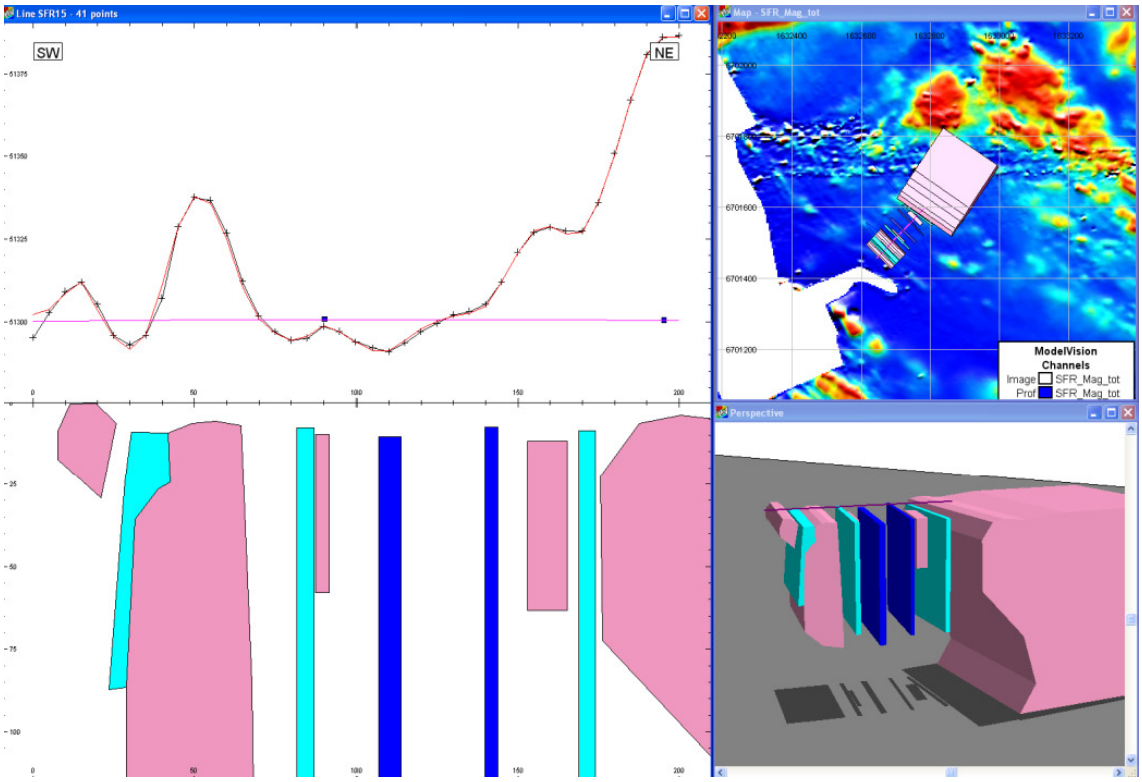

Figure A6-34. *Modelling result from profile SFR15. The light blue source bodies represent the lineaments MSFR08110, MSFR08109 and MSFR08037 (from left to right). The pink bodies are included to compensate for rock volumes with high susceptibilities, the dark blue bodies are included to model two minima, though they are not associated with any lineaments. Maximum depth shown in the leftmost part of the figure is approximately 120 m.*

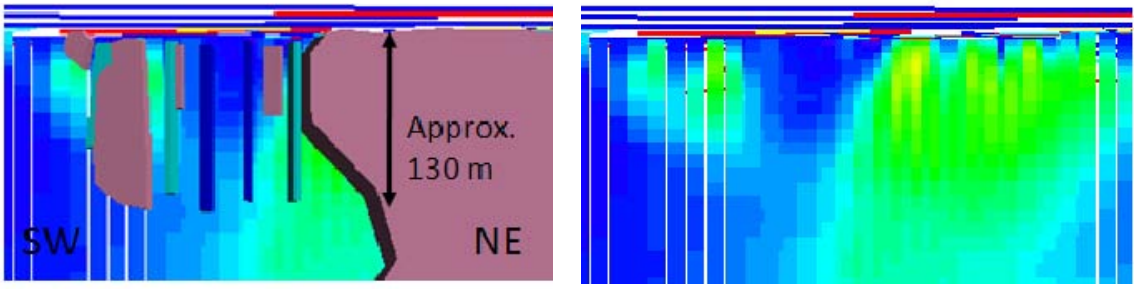

Figure A6-35. *Comparison of the source bodies from the forward modelling with the result from the 3D inversion of magnetic total field data. Left: with the source bodies. Right: without the source bodies. Blue colour in the inversion result indicates low relative magnetic susceptibility.*

Profile SFR16, 1632985/6702025 – 1633060/6702005

The profile SFR16 crosses the lineament MSFR08096 (Figure A6-36).

Figure A6-37 shows the model. The source body inferred to represent the lineament MSFR08096 is steeply dipping according to the forward modelling.

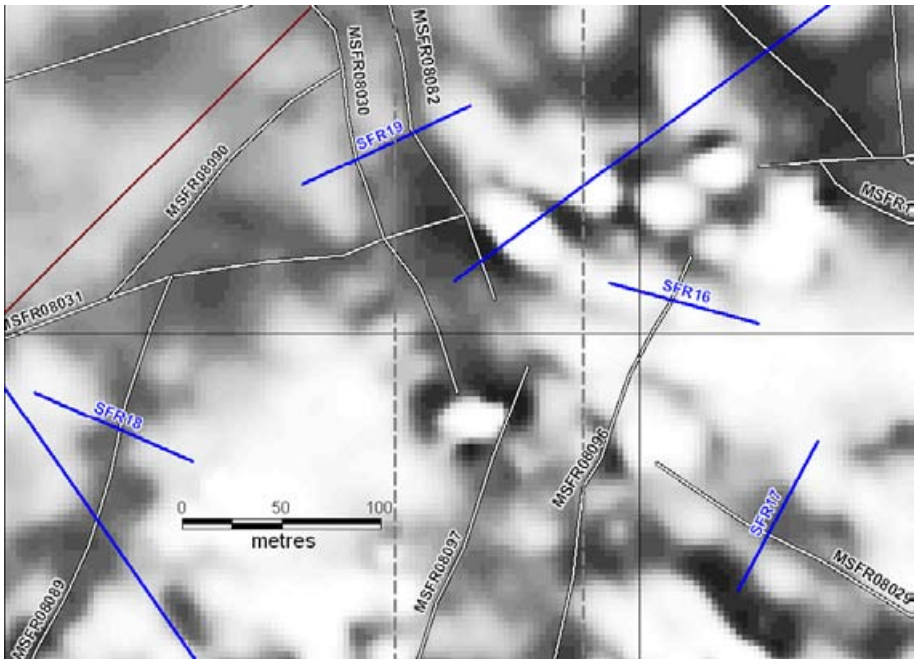

Figure A6-36. *Profiles SFR16, SFR17, SFR18 and SFR19 with associated lineament.*

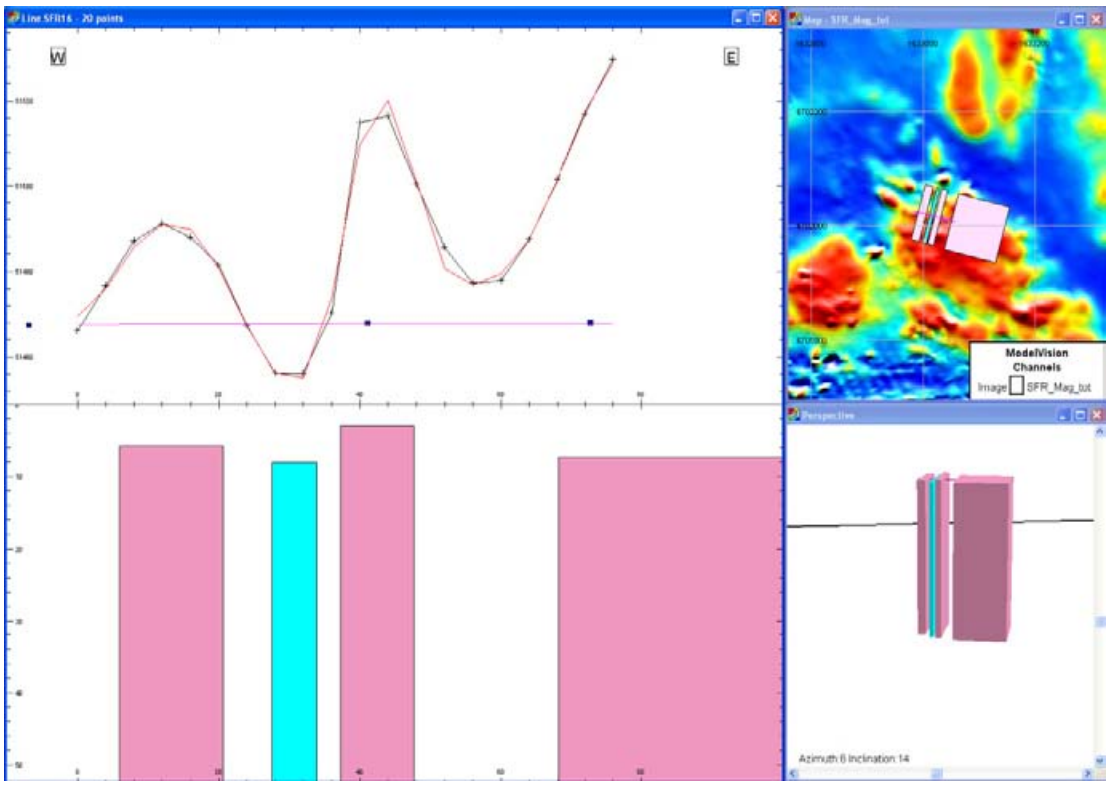

Figure A6-37. *Modelling result from profile SFR16 where the light blue source body represents the source to the lineament MSFR08096. Maximum depth shown in the leftmost part of the figure is approximately 50 m.*

Profile SFR17, 1633050/6701870 – 1633090/6701945

Profile SFR17 crosses lineament MSFR08029 (see Figure A6-36 above). Figure A6-38 shows the model with one low susceptibility source body inferred to represent the lineament MSFR08029. Several high susceptibility bodies and one with low susceptibility have also been introduced to compensate for field variations adjacent to the primary source body. The source body representing lineament MSFR08029 is dipping vertically. The profile is close to the SFR facility which probably raises the degree of uncertainty due to interference from magnetic objects in the installation.

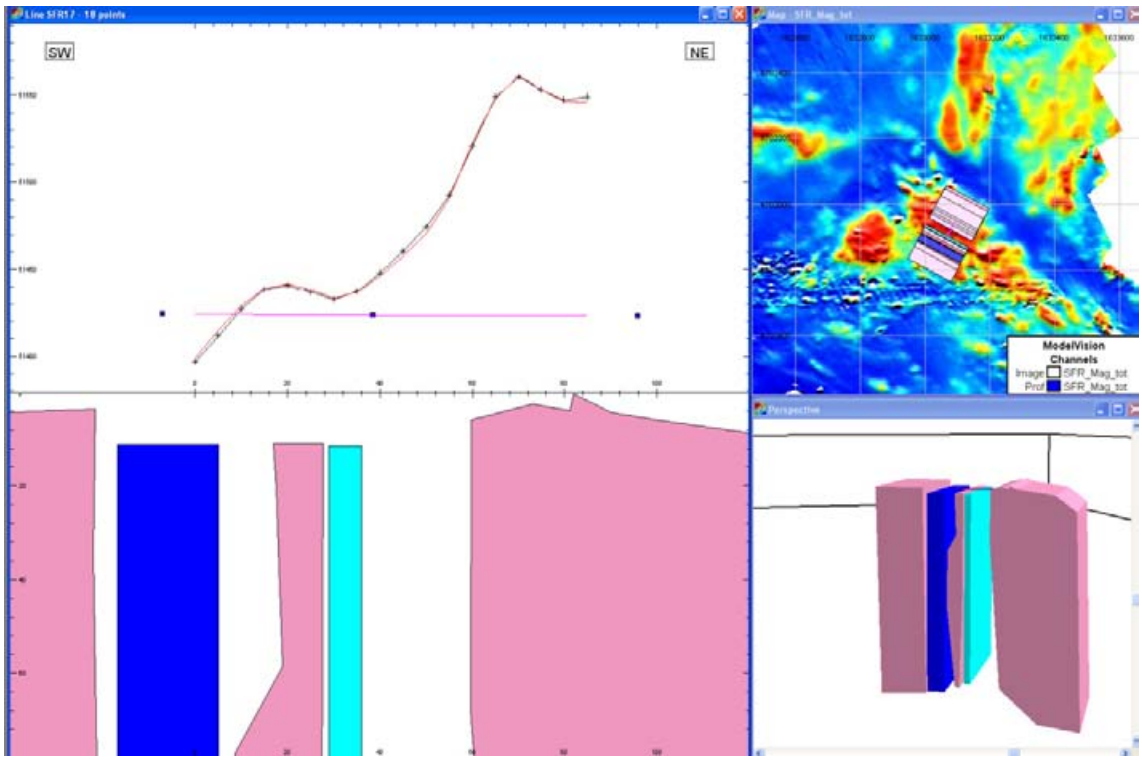

Figure A6-38. *Modelling result from profile SFR17 where the source body in light blue is representing the source to the lineament MSFR080029.Other bodies are introduced to compensate for field variations. Maximum depth shown in the leftmost part of the figure is approximately 80 m.*

Profile SFR18, 1632695/6701970 – 1632775/6701935

Profile SFR18 crosses the lineament MSFR08089 (see Figure A6-36 above). The model used contains a low susceptibility source body and two bordering high susceptibility bodies (Figure A6-39). The source body representing the lineament dips vertically. In the result from the 3D inversion a steep dip towards the east-south-east is observed in the apparent magnetic susceptibility distribution (Figure A6-40).

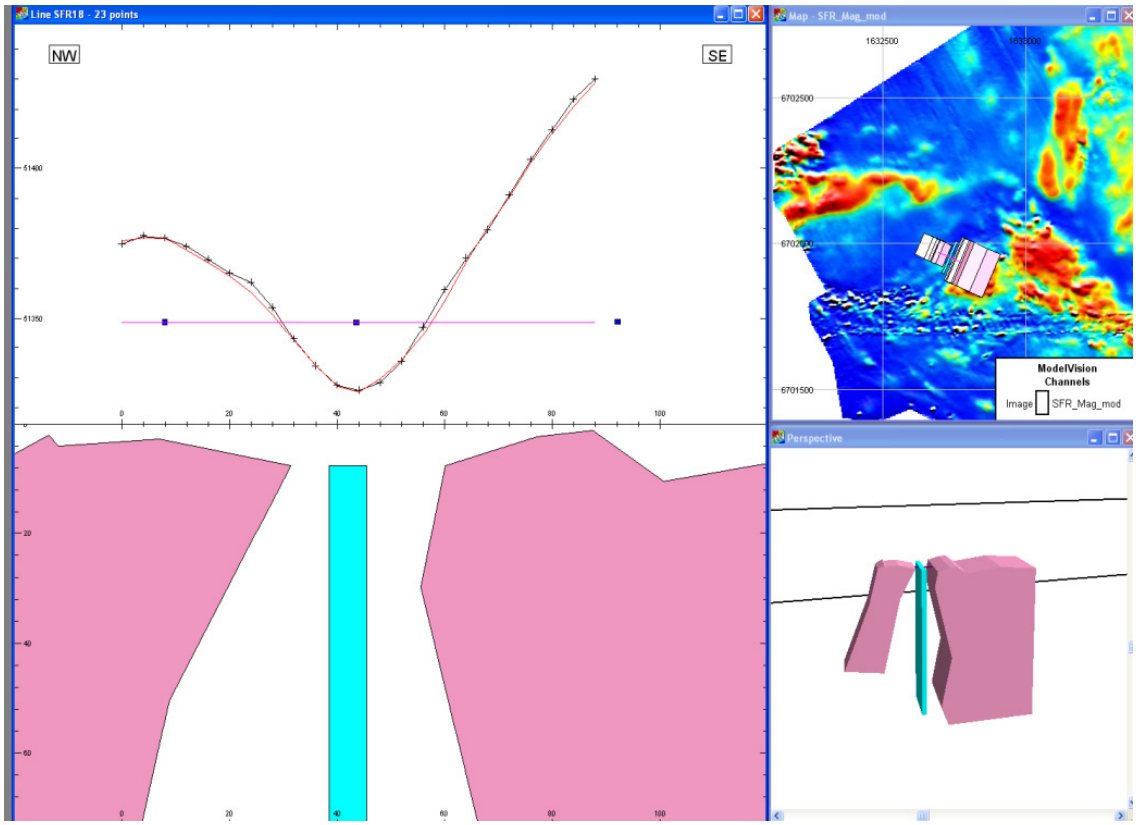

Figure A6-39. *Modelling result from profile SFR18 with the source body in blue representing lineament MSFR08089. Maximum depth shown in the leftmost part of the figure is approximately 70 m.*

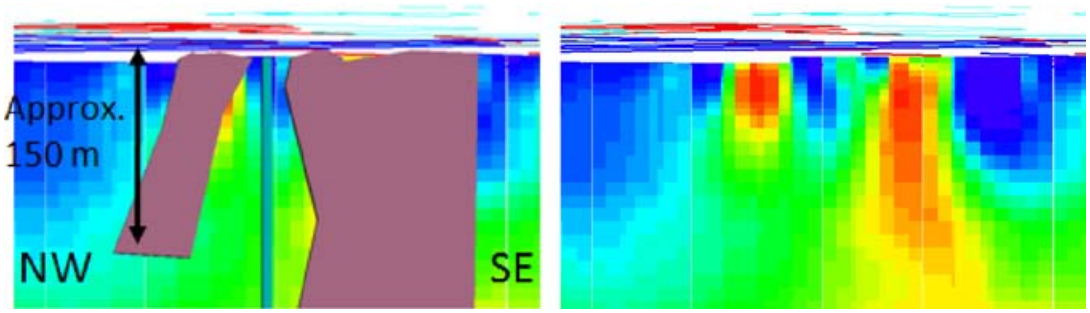

Figure A6-40. *Comparison of the source bodies from the forward modelling with the result from the 3D inversion of magnetic total field data. At left with the source bodies, at right without the source bodies. Blue colour in the inversion result indicates low relative magnetic susceptibility.*

Profile SFR19, 1632830/6702075 – 1632915/6702115

Profile SFR19 crosses the lineaments MSFR08030 and MSFR08082 (see Figure A6-36 above). Figure A6-41 shows the model including both low and high susceptibility source bodies. The source bodies representing the lineaments dip steeply; this is valid both for the forward modelling and the 3D inversion (Figure A6-42).

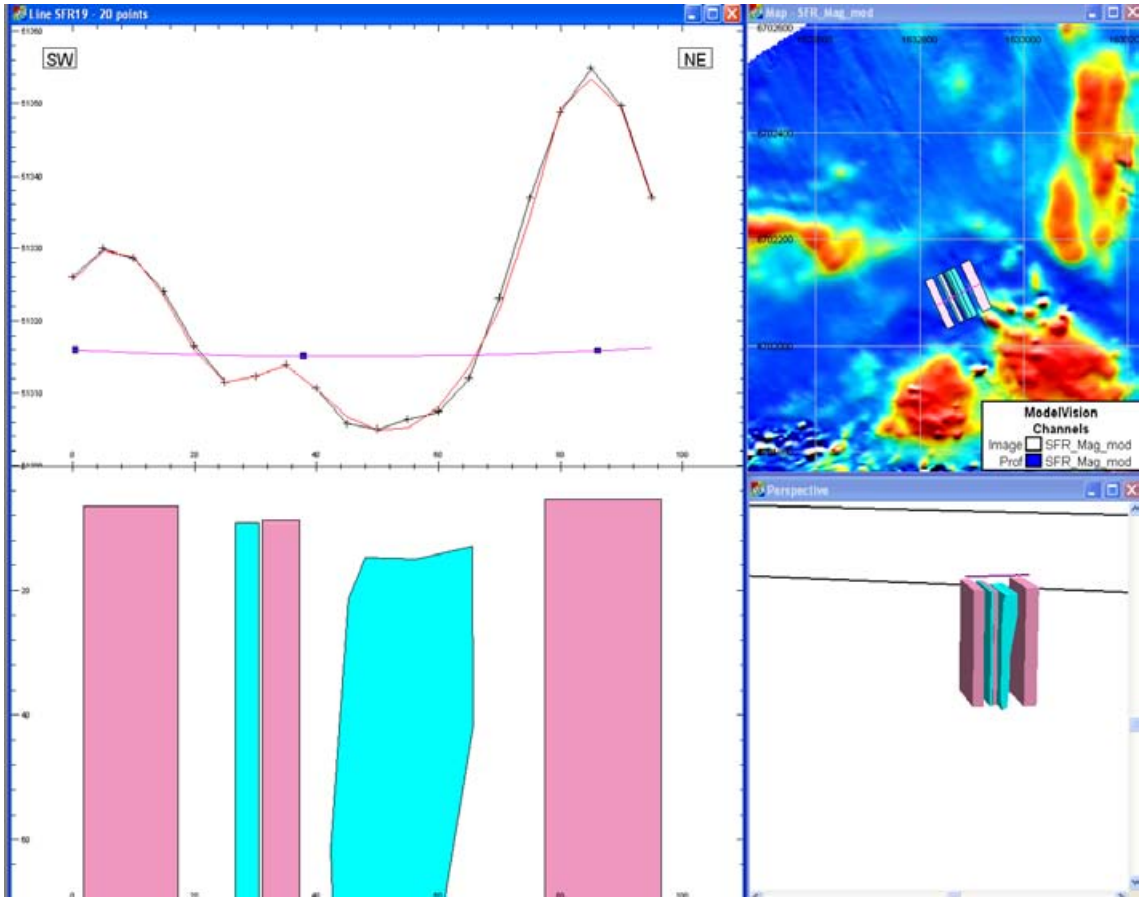

Figure A6-41. *Modelling result from profile SFR19 with the two source bodies in blue representing lineaments MSFR08030 and MSFR08082. Maximum depth shown in the leftmost part of the figure is approximately 70 m.*

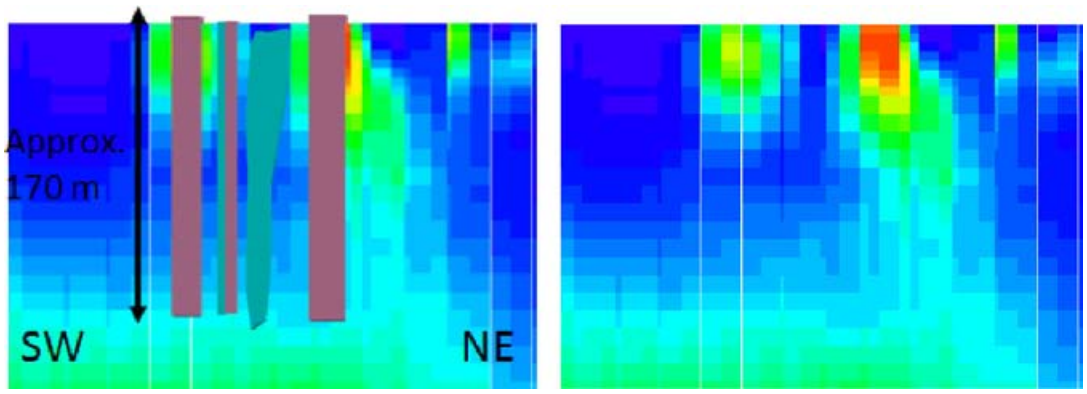

Figure A6-42. *Comparison of the source bodies from the forward modelling with the result from the 3D inversion of magnetic total field data. At left with the source bodies, at right without the source bodies. Blue colour in the inversion result indicates low relative magnetic susceptibility.*

Profile SFR20, 1632879/6701719 – 1633089/6701530

Figure A6-43 shows the location of the profile SFR20. The low susceptibility source body representing lineament MSFR08116 dips steeply towards the north-west (Figure A6-44). Figure A6-44 also shows a comparison of the source body on a background with the apparent magnetic susceptibility distribution according to the 3D inversion. The dip according to the latter is in good agreement with the forward modelling result.

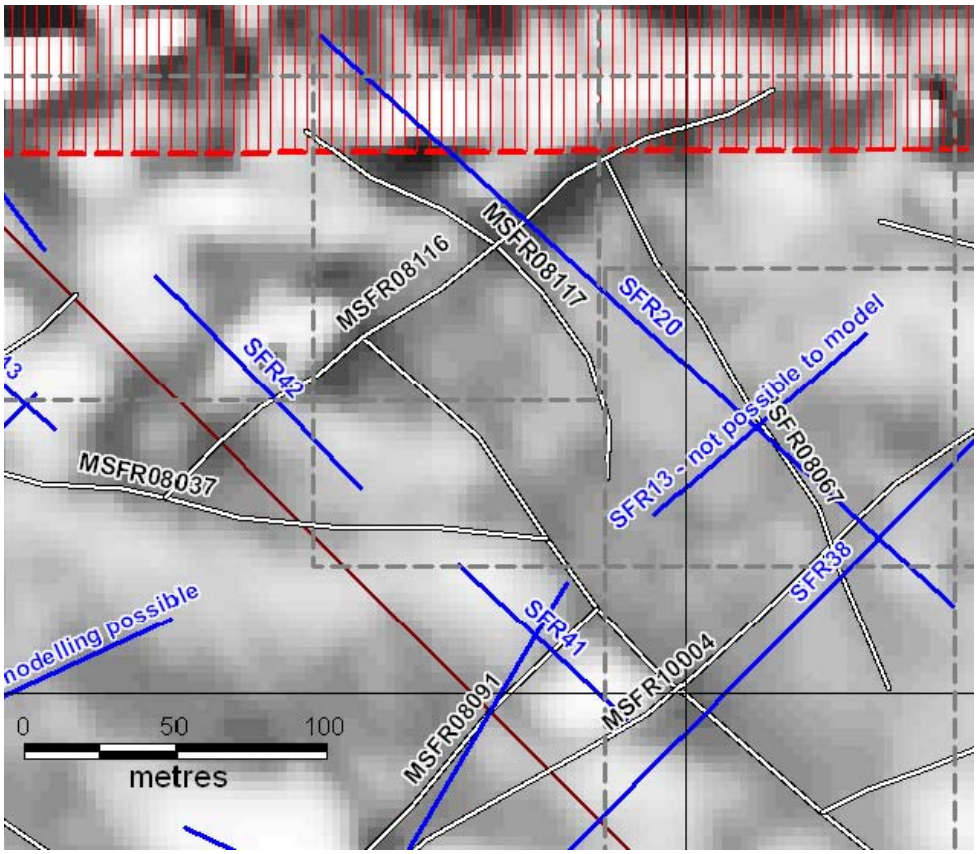

Figure A6-43. *The location of profile SFR20 and the associated lineament MSFR08116.*

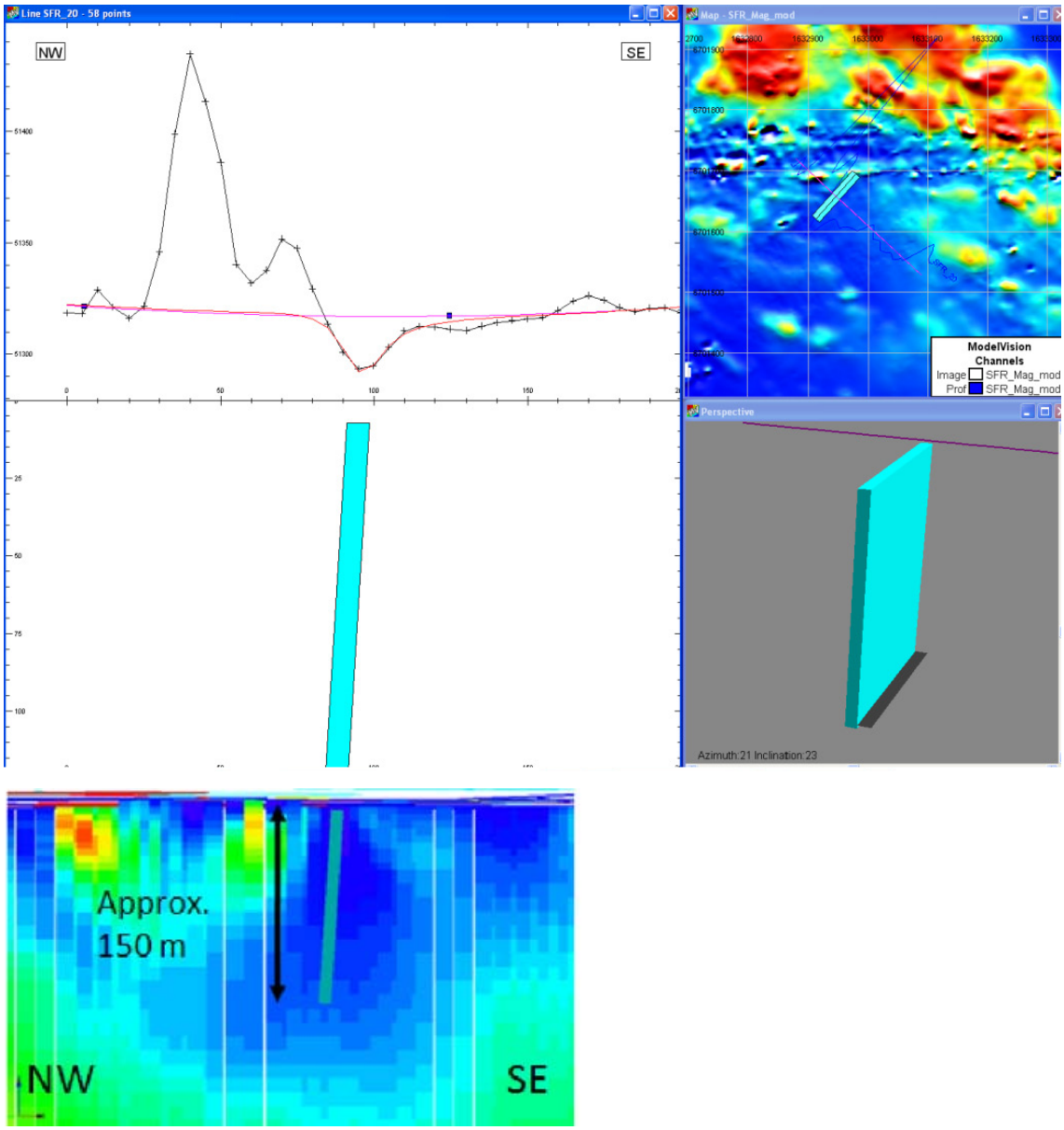

Figure A6-44. *Top: Modelling result from profile SFR20 with the source body representing the lineament MSFR08116. Maximum depth shown in the leftmost part of the figure is approximately 120 m. Bottom: Comparison of the source bodies from the forward modelling of profile SFR20 with the result from the 3D inversion of magnetic total field data.*

Profile SFR21, 1633351/6701736 – 1633470/6701916

Profile SFR21 crosses the lineaments MSFR08104, MSFR08094 and MSFR08099 (Figure A6-45). The forward modelling result (Figure A6-46) discerns only two source bodies although the profile crosses three lineaments; the reason is the interference of anomalies from the two north-easternmost lineaments MSFR08094 and MSFR08099 giving only one source body to represent the two lineaments. Both the source bodies from the forward modelling have steep dips, while the 3D inversion indicates a steep north-eastern dip of the source rock volumes (A6-46).

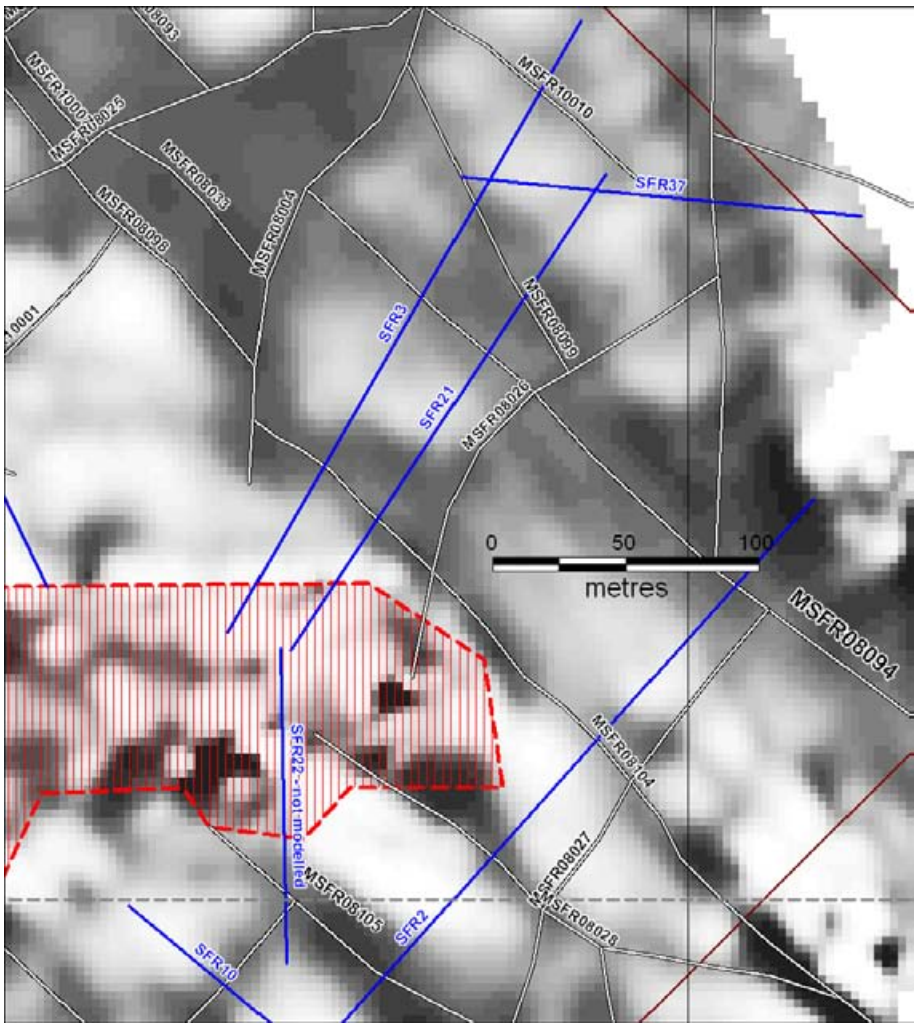

Figure A6-45. *The location of profile SFR21 with its associated lineaments MSFR08104, MSFR08094 and MSFR08099.*

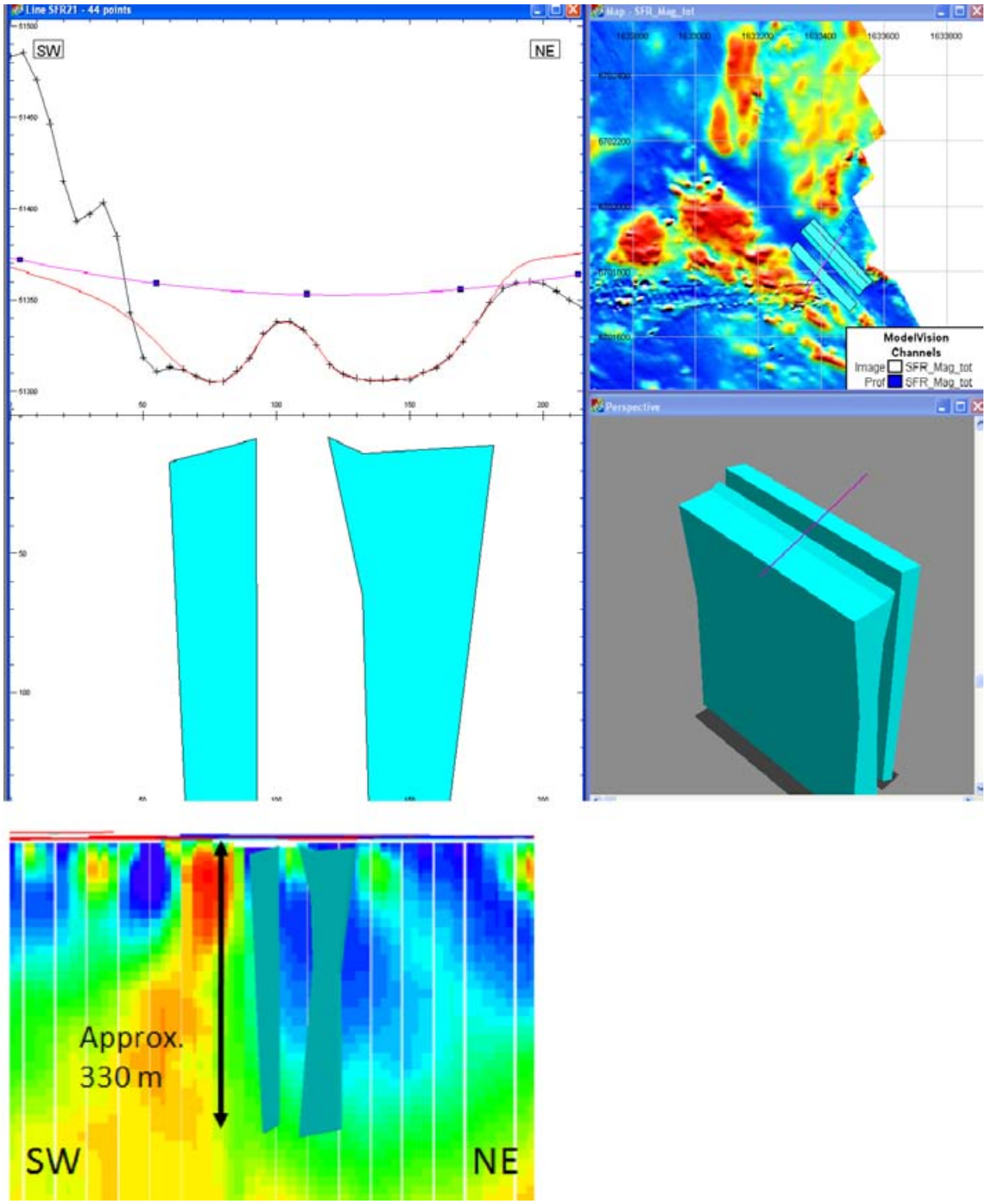

Figure A6-46. *Top: Modelling result from profile SFR21 with the source bodies representing the lineaments MSFR08104, MSFR08094 and MSFR08099. The blue body to the right in the figure coincides with the source rock volumes to the two latter lineaments. Maximum depth shown in the leftmost part of the figure is approximately 140 m. Bottom: Comparison of the source bodies from the forward modelling with the result from the 3D inversion of magnetic total field data.*

Profile SFR22, 1633347/6701737 – 1633349/6701618

Figure A6-45 above shows the location of profile SFR22 and the associated lineament MSFR08105. However, the forward modelling was abandoned as an interference effect from a nearby lineament (MSFR08108) was recognized.

Profile SFR23, 1632540/6702502 – 1633468/6702442

Profile SFR23 crosses the lineament MFM0999G (Figure A6-47). The modelling shows that almost the entire minimum at the western side of the high susceptibility rock volume is explained in the modelling (Figure A6-48). The low susceptibility source rock at the western side of the modelled high susceptibility rock volume contains the source to the lineament MFM0999G. If the source to the lineament is parallel with the contact of the modelled high susceptibility rock then the source rock to the lineament would dip steeply towards the east.

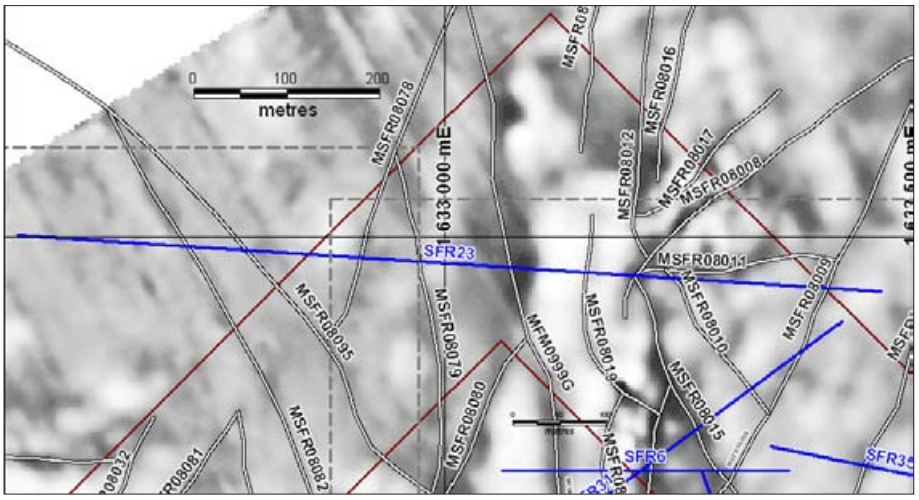

Figure A6-47. *The location of profile SFR23. The modelling aimed to deduce a possible geometry for the high susceptibility rock volume east of the lineament MFM0999G.*

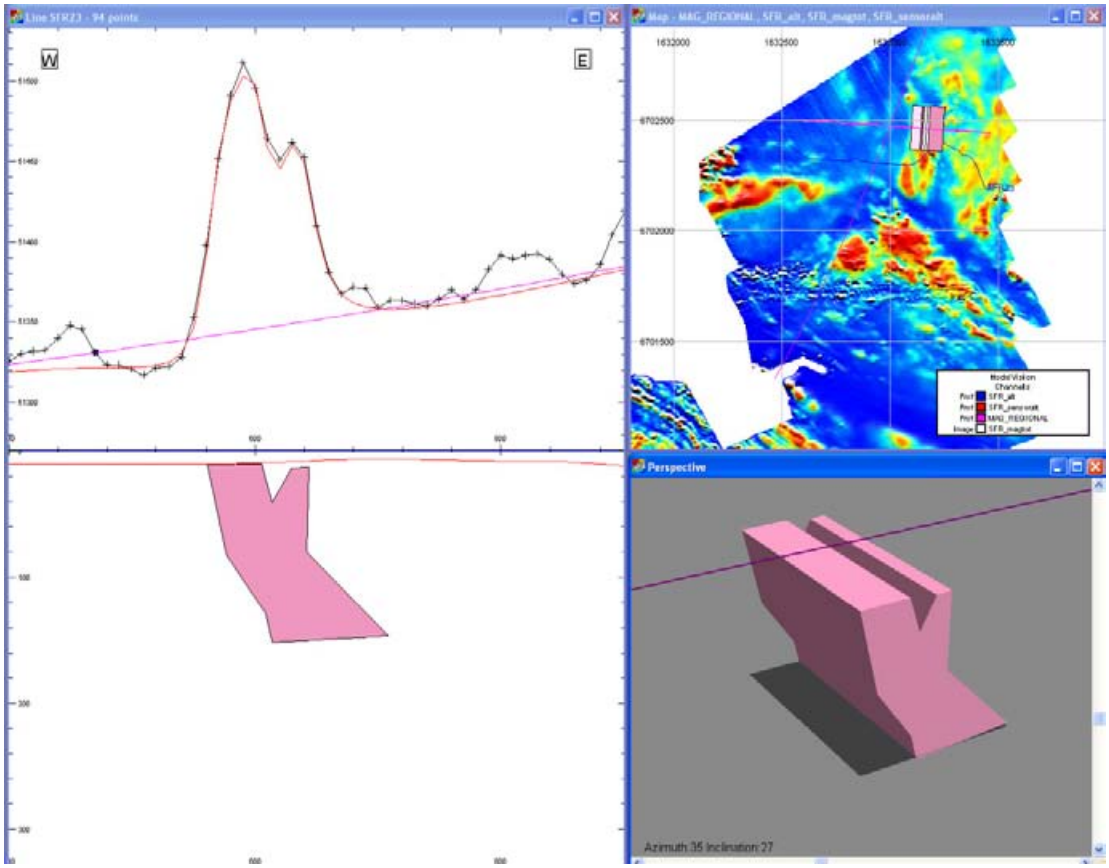

Figure A6-48. *Modelling result from profile SFR23 with the source body representing a high susceptibility rock volume. The lineament MFM0999G is located in the minimum to the left (west) of the source body. Maximum depth shown in the figure is approximately 300 m.*

Profiles SFR24 to SFR26 over the Singö deformation zone complex

The location of the three profiles SFR24, SFR25 and SFR 26 is shown in Figure A6-49.

Profile SFR24, 1632860/6700740 – 1633201/6701362

Profile SFR24 crosses the lineaments MFM0813G, MSFR08075, MFM0803G0, MSFR08123 and MSFR10006 (Figure A6-49).

The lineaments MSFR08123 and MSFR10006 are modelled in profile SFR01 with an alternative approach where thin tabular bodies have been invoked into the modelling program. The result shows how the possible dip of the source bodies is towards the north-east (Figure A6-6). In this alternative modelling of the profile SFR24 the sea bottom topography has been considered. A large source volume with low susceptibility has been invoked to study the possibility to explain the anomalies associated with the lineaments MSFR08123 and MSFR10006. Figure A6-50 shows how undulations in the near-surface part of the north-easternmost body are sufficient to explain much of the comparatively weak anomalies, associated with these two lineaments.

The most pronounced part of the broad low magnetic anomaly at the north-eastern half of the profile coincides with the lineament MFM0803G0. The model shows a steep dip at the southern contact of the large low susceptibility source body.

A high susceptibility source body has been introduced at the centre of the modelled profile (Figure A6-50) to model a local magnetic maximum. The dip of this source body is towards the south-west with the chosen regional field applied.

A low susceptibility source body is modelled at the south-western part of the profile (Figure A6-50). It contains the inferred source volumes to the low magnetic anomalies associated with lineaments MFM0813G and MSFR08075. Neglecting the peculiar geometrical details, which are introduced to achieve a good fit, the main dip of this source body is towards the southwest.

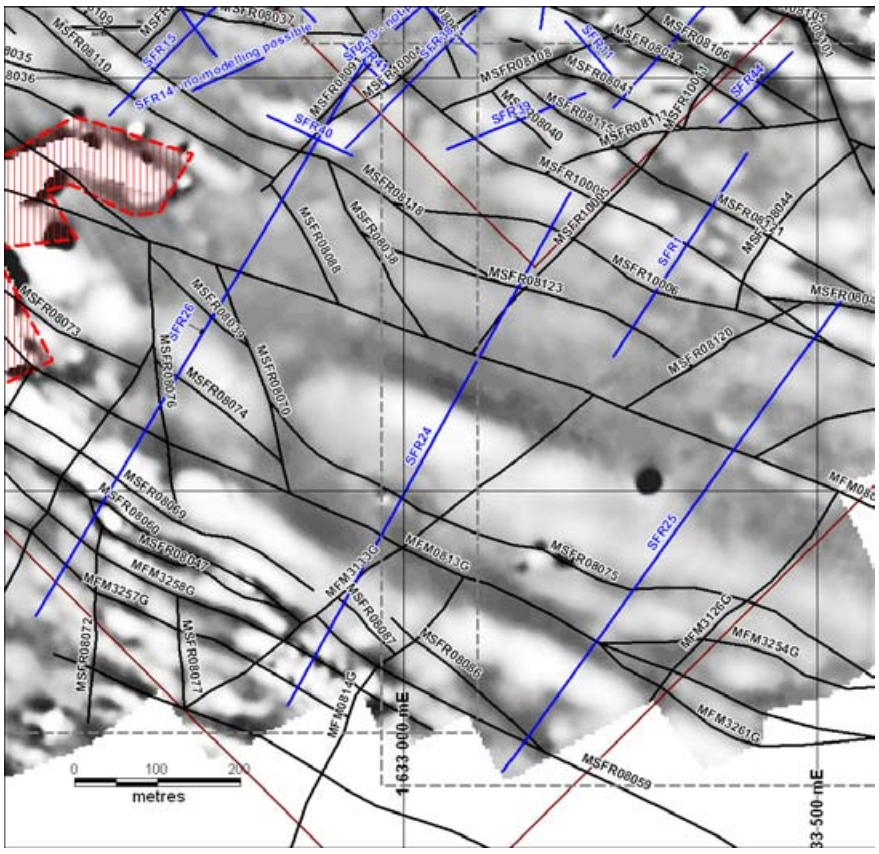

Figure A6-49. *The location of profiles SFR24 to SFR26 (blue lines) selected for modelling of the Singö deformation zone complex.*

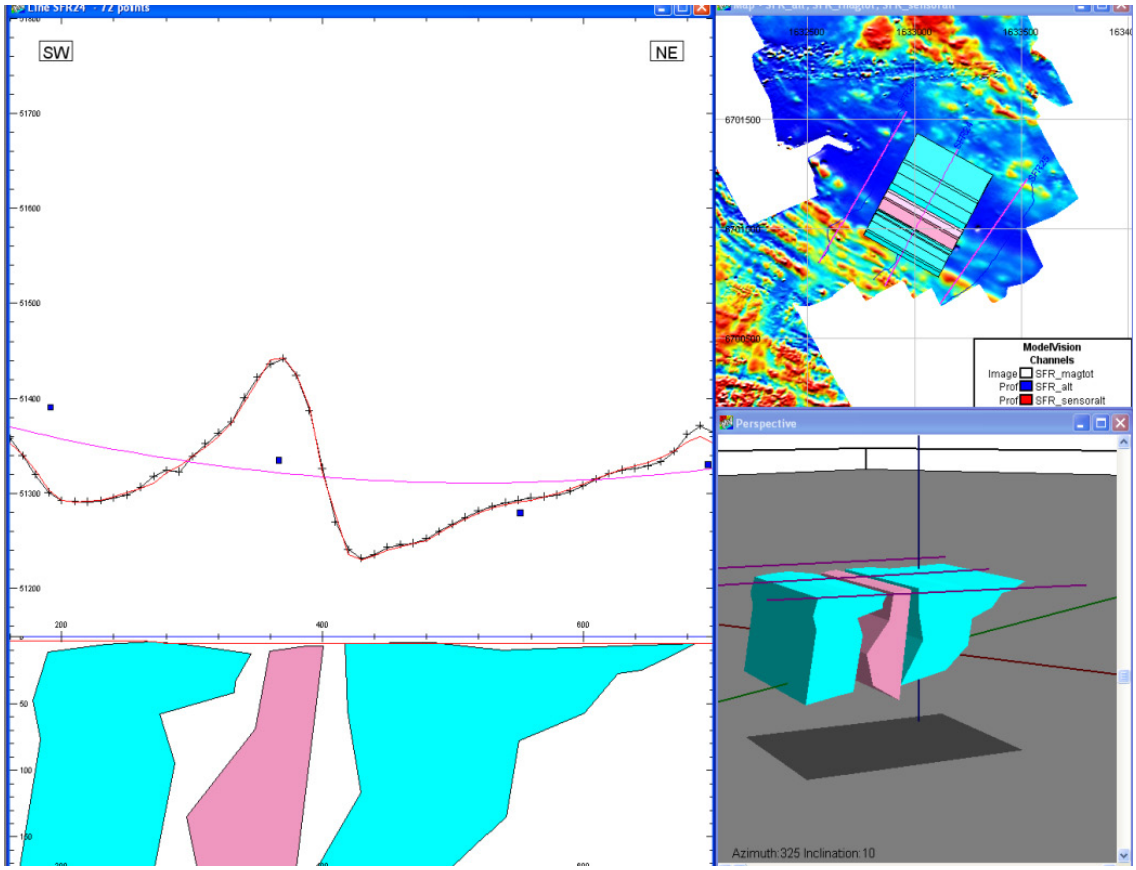

Figure A6-50. *Modelling result from profile SFR24. Two low susceptibility source bodies (blue) are found at each side of a high susceptibility source body (pink). Maximum depth shown in the leftmost part of the figure is approximately 180 m.*

Profile SFR25, 1633120/6700660 – 1633528/6701229

Profile SFR25 crosses the lineaments MFM0813G, MSFR08075, and MFM0803G0 (see Figure A6-49 above). A low susceptibility source body is shown at the south-westernmost part of the profile (Figure A6-51); the body is associated with the two lineaments MSFR08059 and MSFR08086. However, the modelling result is considered to have a high degree of uncertainty as these two lineaments are very close to each other with interfering anomalies. A low susceptibility source body coincides with the lineament MFM0813G (at c. x=195 m in Figure A6-51) and shows a steep dip, but with a peculiar geometry at the surface near parts. The anomaly amplitude is very small and the level of uncertainty in the modelling is consequently high. The low susceptibility source body that coincides with the lineament MSFR08075 (at c. x=270 m in Figure A6-51) dips towards the southwest. The very broad low susceptibility source body at the north-easternmost part of the profile contains the inferred source to the lineament MFM0803G0 (at c. x=480 m in Figure A6-51); the dip is steep at the central part.

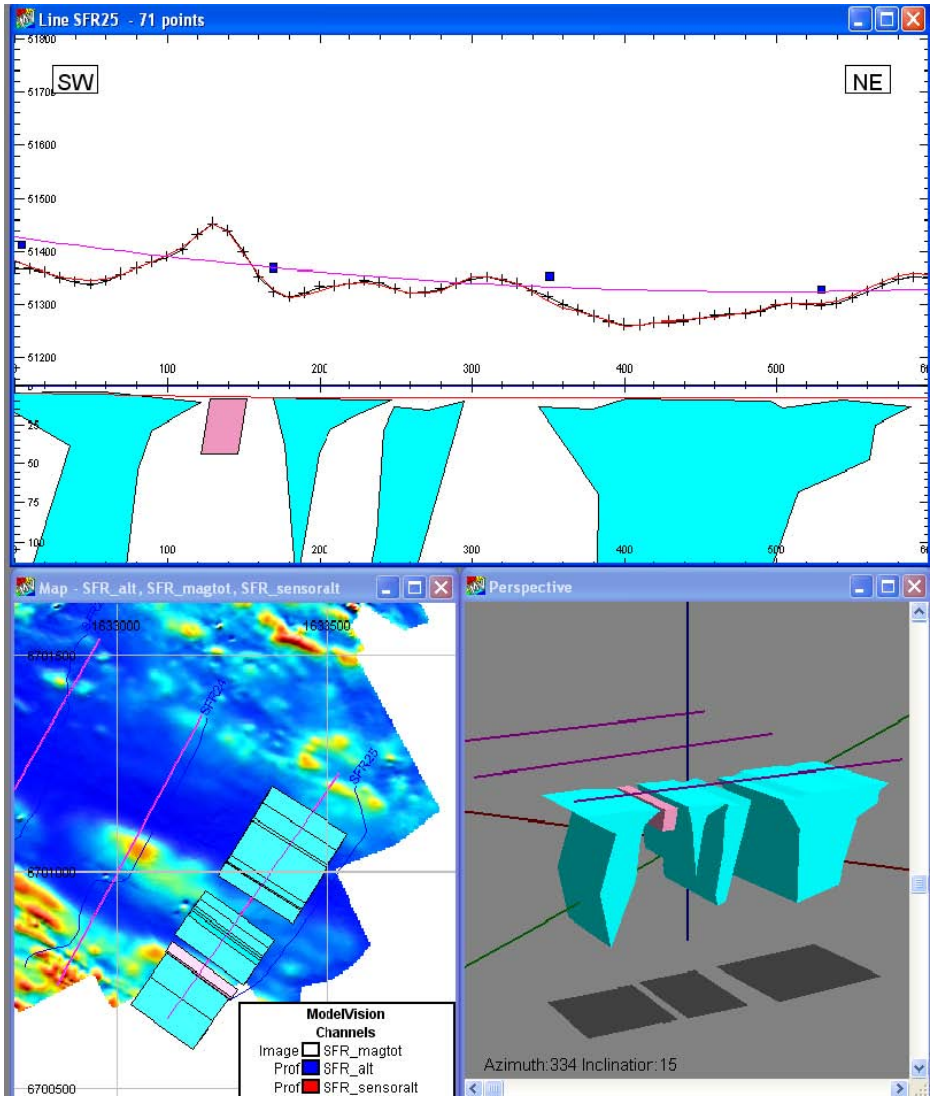

Figure A6-51. *Modelling result from profile SFR25. The south-westernmost low susceptibility source body (blue) is connected to the lineaments MSFR08059 and MSFR08086. At c. x=195 m is a source body connected to the lineament MFM0813G, at c. x=270 is another source body connected to lineament MSFR08075 and at c. x=480 is the low susceptibility source body connected to lineament MFM0803G0. Maximum depth shown in the uppermost part of the figure is approximately 120 m.*

Profile SFR26, 1632555/6700848 – 1632961/6701537

Profile SFR26 crosses several lineaments (see Figure A6-49 above). Many of the lineaments are minor and the primary target for the modelling are the lineaments MFM0813G (c. x=260 m in Figure A6-52) and MFM0803G0 (c. x=485 m in Figure A6-52). At the south-westernmost part of the profile is included a high susceptibility source body to compensate for a magnetic maximum. According to the forward modelling the dip is steep of the large low susceptibility source rock volumes. The sources to the lineaments are buried in these large volumes. Hence, the prediction of the dip and thickness of the lineament source is difficult. One assumption could be to assign the dip of the major body also to the source of the lineament. This is justifiable as these lineaments represent rock volumes connected to the Singö DZ.

Part of the profile SFR26 coincides with the area where 3D inversion of magnetic total field data was performed. Figure A6-53 shows a comparison of the source bodies from the forward modelling and the apparent magnetic susceptibility distribution from the 3D inversion; the results are quite similar.

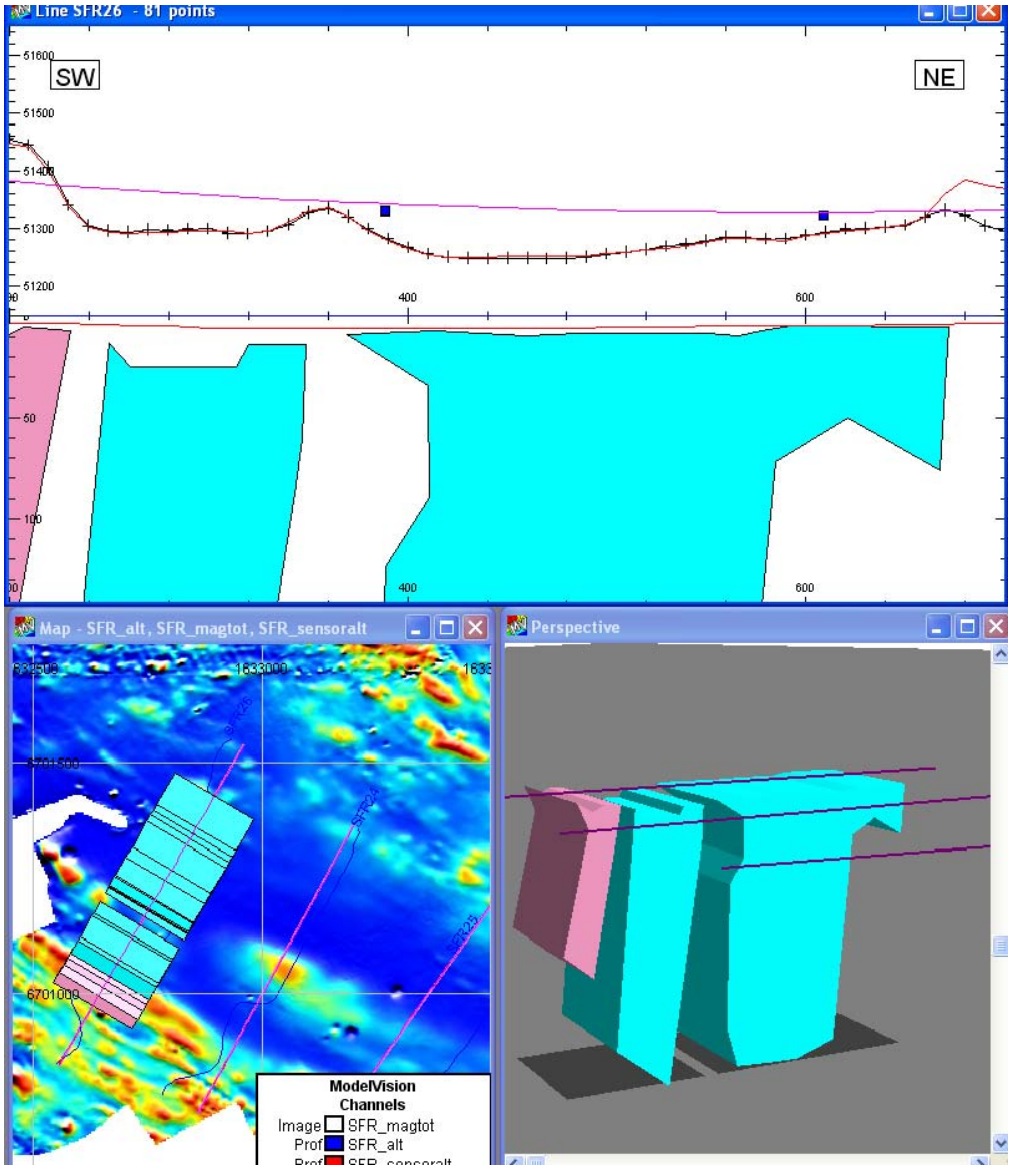

Figure A6-52. *Modelling result from profile SFR26. Maximum depth shown in the uppermost part of the figure is approximately 140 m.*

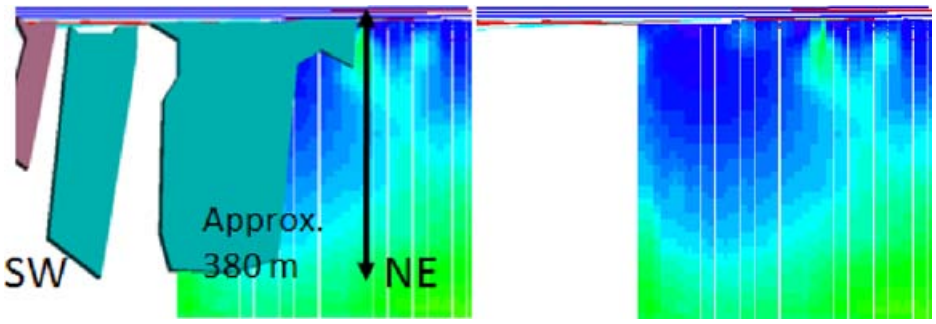

Figure A6-53. *Comparison of the source bodies from the forward modelling with the result from the 3D inversion of magnetic total field data. At left with the source bodies, at right without the source bodies. Blue colour in the inversion result indicates low relative magnetic susceptibility. The south-western part of the profile is not covered by the 3D inversion.*

Summary of the results from profiles SFR24 – SFR26

The modelling of the three profiles over the Singö DZ complex indicates very low magnetic susceptibilities in large volumes of the rock associated with the deformation zone complex. The consequence is that many of the source volumes to the anomalies of interest are buried in these large low susceptibility volumes. Hence, it is difficult to delimit geometries for individual source bodies coupled to specific lineaments. Furthermore, the contrasts are low in the magnetic susceptibility inside these large volumes. The implications are that the geometry of the whole rock volume, including the source body of interest, must be used as a guide to determine the dip of the source to an individual lineament. Modelling of these faint anomalies also implies quite high levels of uncertainty in the predictions.

By using the geometry of the large low susceptibility rock volumes as a general guide, the dips of the sources to the identified lineaments are expected to be steep, mostly to the south-west.

It is important to compare the results from modelling of profiles SFR24 to SFR26 against the results from profile SFR01. In the modelling of the profiles SFR24 to SFR26 the topography of the sea bottom has been included. In the northernmost section of the profile SFR24 it is possible to explain much of the anomalies simply by changing the geometry of the surface-near low susceptibility parts of the sea bottom. They obscure the part of the anomaly that could be considered to emanate from the source bodies to the lineaments MSFR08123 and MSFR10006. But, if such variations are not included it is possible to achieve such a result as displayed in SFR01, i.e. two tabular bodies dipping the north-east.

Profile SFR27, 1632838/6701746 – 1632454/6702295

Figure A6-54 shows the location of profile SFR27 to SFR30 and the associated lineaments.

The forward modelling has concentrated on the lineaments MSFR08092 and MSFR08031. The modelling result (Figure A6-55) displays the possibility to explain the broad and fairly weak anomaly associated with MSFR08092 as a sediment-filled depression in the bedrock surface. The broad, weak anomaly also indicates the possibility that the source may be coupled to changes in lithology or to a deformational structure that dips gently or moderately. Regarding MSFR08031 the modelling indicates an almost vertical dip of the source. However, at the position where the profile SFR27 passes MSFR08031 there is a connection between MSFR08031 and MSFR08084 which may introduce an uncertainty regarding the contribution to the magnetic minimum from the two lineaments.

Figure A6-56 shows a comparison between the forward modelling result and the result from the 3D inversion of the magnetic total field. The 3D inversion suggests a broad low susceptibility rock volume with low magnetic susceptibility associated with MSFR08092, which could support the view that the source is a rock unit rather than a feature reflecting deformation. The dip of the source to MSFR08031 is confirmed by the 3D inversion result.

The source body to the lineament MSFR08089 is not modelled forwardly. However, studying the result from the 3D inversion there is a low susceptibility rock volume associated with the position of this lineament indicating a steep dip.

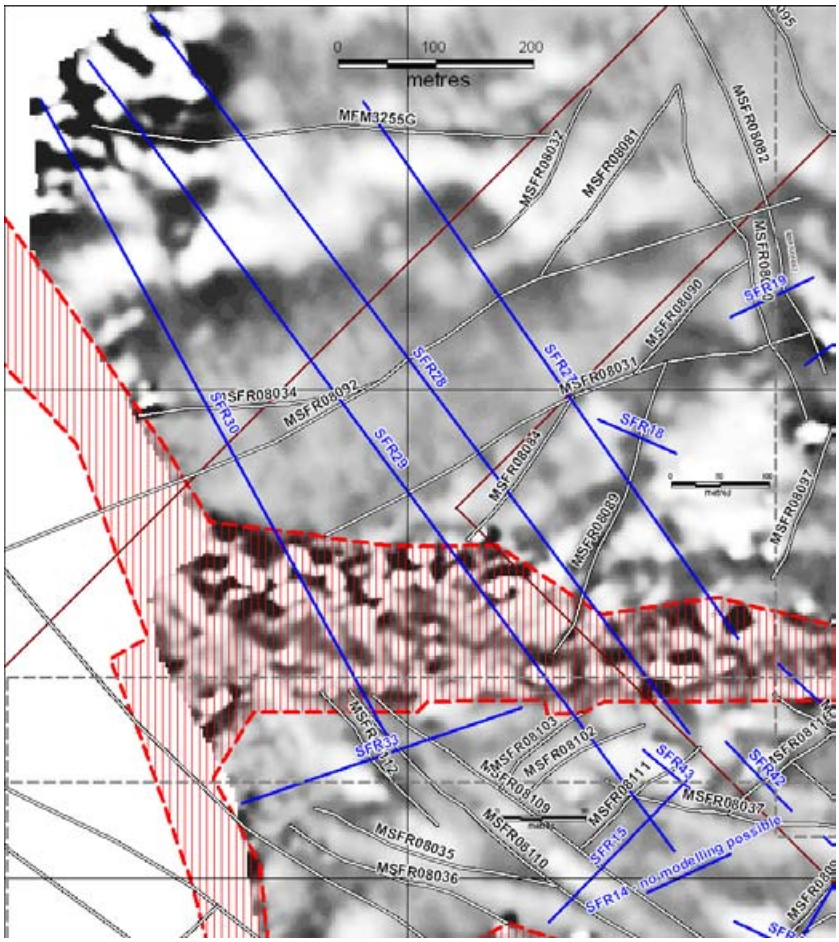

Figure A6-54. *The location of profiles SFR27 to SFR30 and their associated lineaments.*

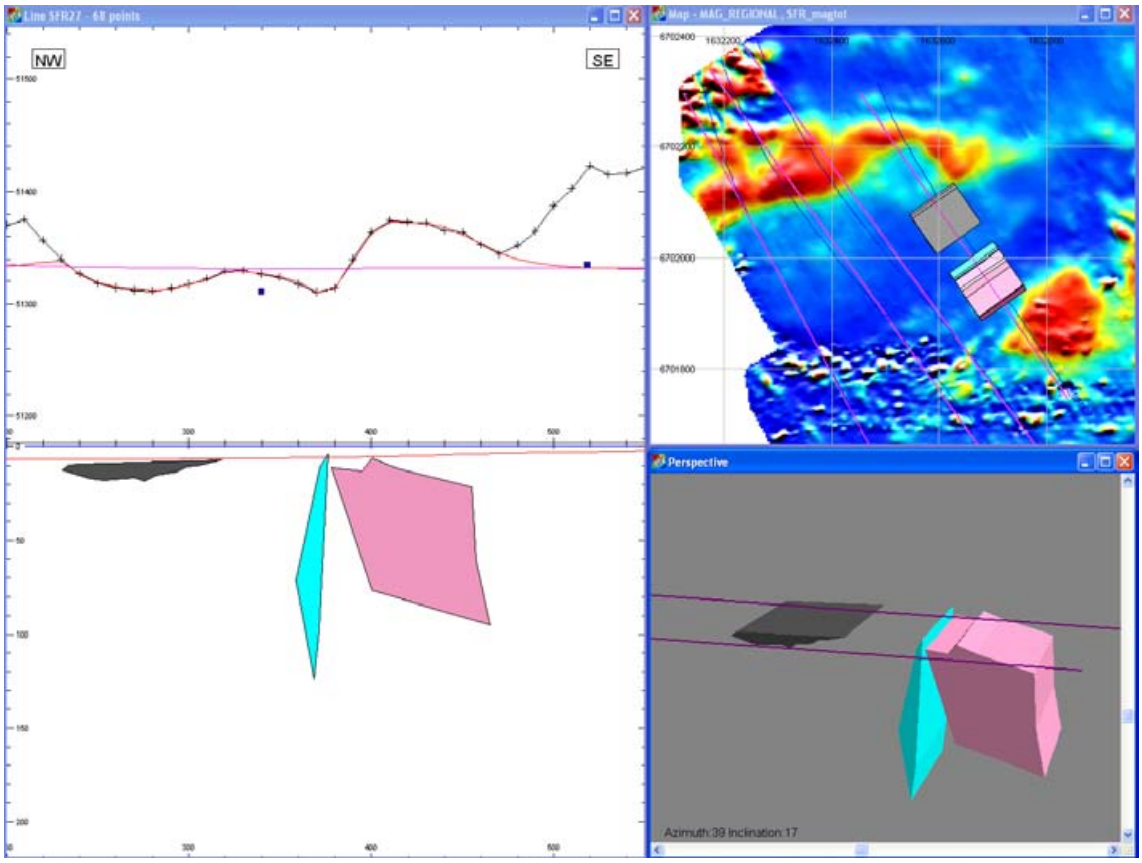

Figure A6-55. *Modelling result from profile SFR27. The almost horizontal source in grey displays a possible depression in the bedrock to the lineament MSFR08092. The blue source body is associated with lineament MSFR08031. The pink source body has a high magnetic susceptibility and is purely introduced to explain a local maximum. Maximum depth shown in the leftmost part of the figure is approximately 220 m.*

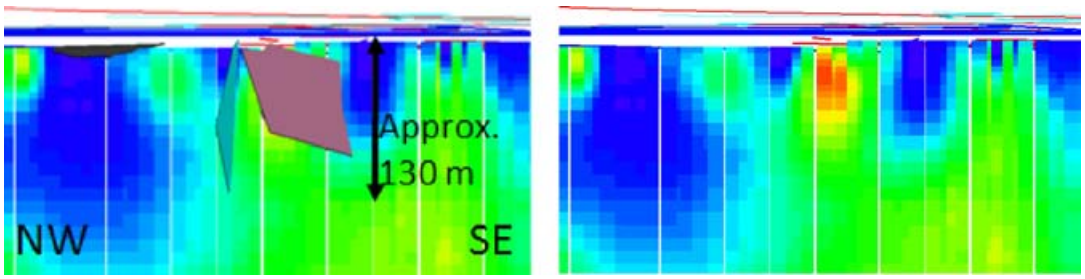

Figure A6-56. *Comparison of the source bodies from the forward modelling with the result from the 3D inversion of magnetic total field data. At left with the source bodies, at right without the source bodies. Blue colour in the inversion result indicates low relative magnetic susceptibility.*

Profile SFR28, 1632788/6701648 – 1632237/6702385

Figure A6-54 above shows the location of profile SFR28 and the associated lineaments. The lineaments are located in a broad low magnetic area where the sources to the individual lineaments are buried in large volumes of rock with expected low magnetic susceptibility. The situation makes modelling of the very faint anomalies coupled to the lineaments highly uncertain. Profiles SFR27 and SFR28 present an alternative which shows that an undulation in the bedrock surface is a possible explanation to the local minima inside the larger low magnetic area. Figure A6-57 shows that the low magnetic depression in the bedrock explains the local magnetic minimum. The high susceptibility source body in the north-west is modelled just to show the dip of the contact, which is steep. In Figure A6-58 the result from the 3D inversion of the magnetic field indicates a broad low susceptibility rock volume associated with the minimum coupled to lineament MSFR08031.

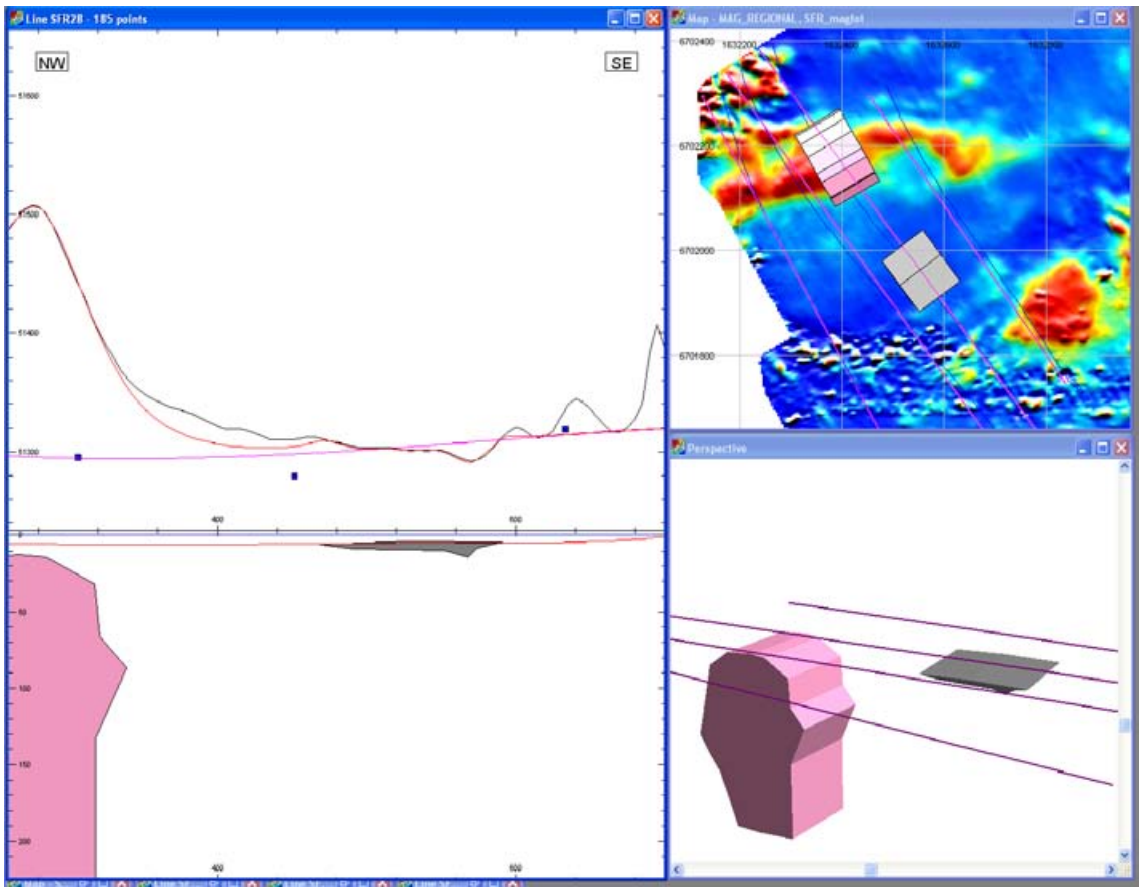

Figure A6-57. *Modelling result from profile SFR28. The grey source body coincides with lineament MSFR08031. Maximum depth shown in the leftmost part of the figure is approximately 220 m.*

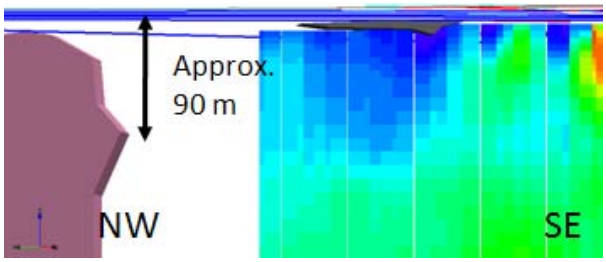

Figure A6-58. *Comparison of the source bodies from the forward modelling with the result from the 3D inversion of magnetic total field data. The north-western part of the profile is not covered by the 3D inversion.*

Profile SFR29, 1632773/6701527 – 1632173/6702339

Figure A6-54 above shows the location of profile SFR29. The anomaly from the lineament complex including MSFR08034 and MSFR08092 is too weak for modelling. The modelling indicates that the source body to lineament MSFR08031 has a moderate dip towards the south-east (Figure A6-59), a result that is partly supported by the 3D inversion (Figure A6-60). The high susceptibility body in the north-west is modelled to have a steeply dipping contact.

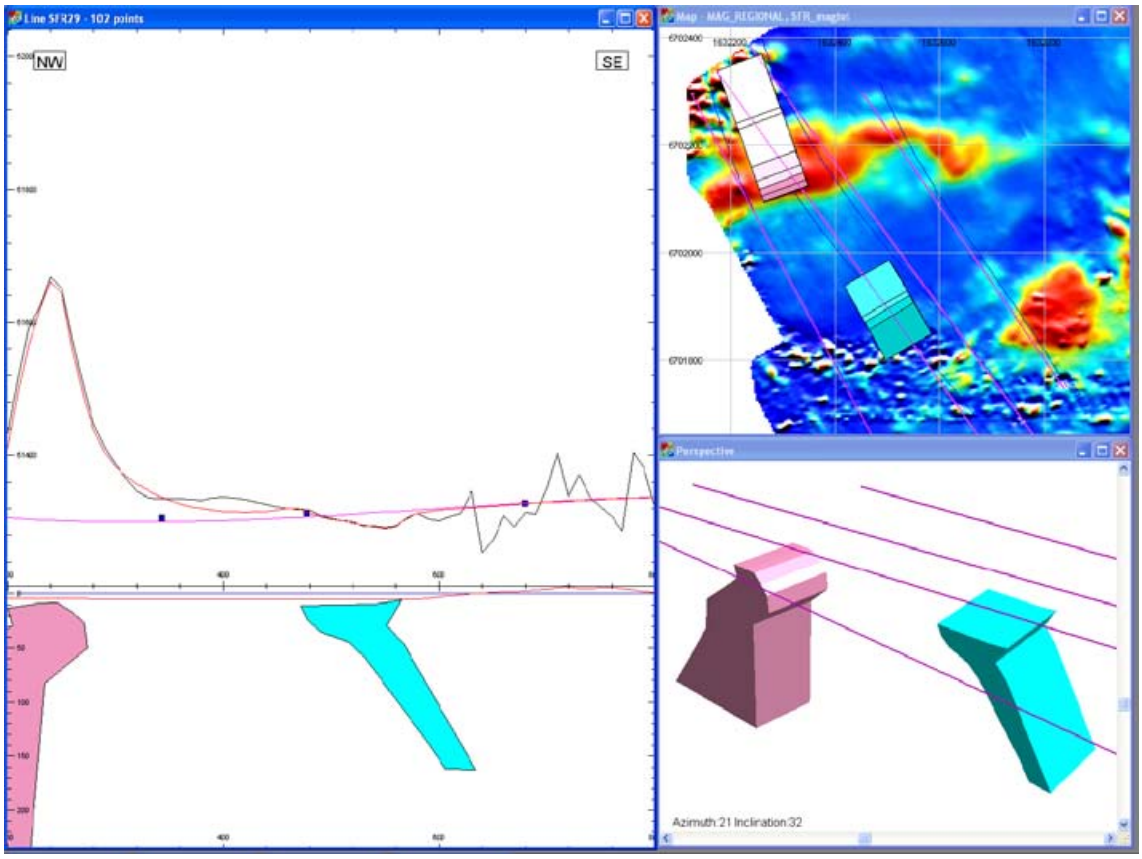

Figure A6-59. *Modelling result from profile SFR29. The blue body is associated with lineament MSFR08031. The pink body is a high susceptibility rock volume with a steep main dip. Maximum depth shown in the leftmost part of the figure is approximately 230 m.*

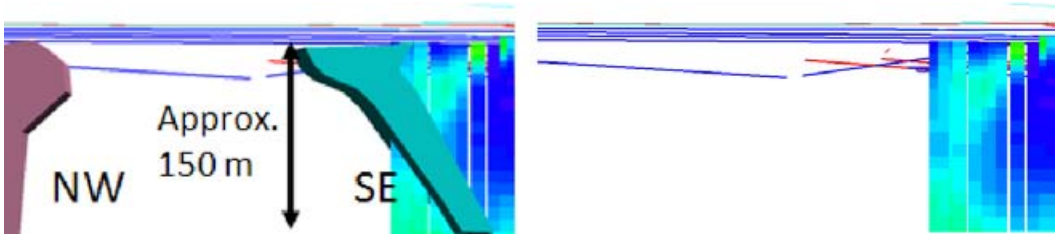

Figure A6-60. *Comparison of the source bodies from the forward modelling with the result from the 3D inversion of magnetic total field data. At left with the source bodies, at right without the source bodies. Blue colour in the inversion result indicates low relative magnetic susceptibility. The north-western part of the profile is not covered by the 3D inversion.*

Profile SFR30, 1632478/6701646 – 1632125/6702296

Figure A6-54 above shows the location of profile SFR30. In this profile two very weak anomalies are modelled which are associated with lineaments MSFR08034 and MSFR08092; the very small anomaly amplitude implies a very low confidence in the prognosis. The modelling suggests a dip that is towards the south-east for both of the low susceptibility source volumes (Figure A6-61). Two low susceptibility source bodies (dark blue) are only included to compensate for local minima.

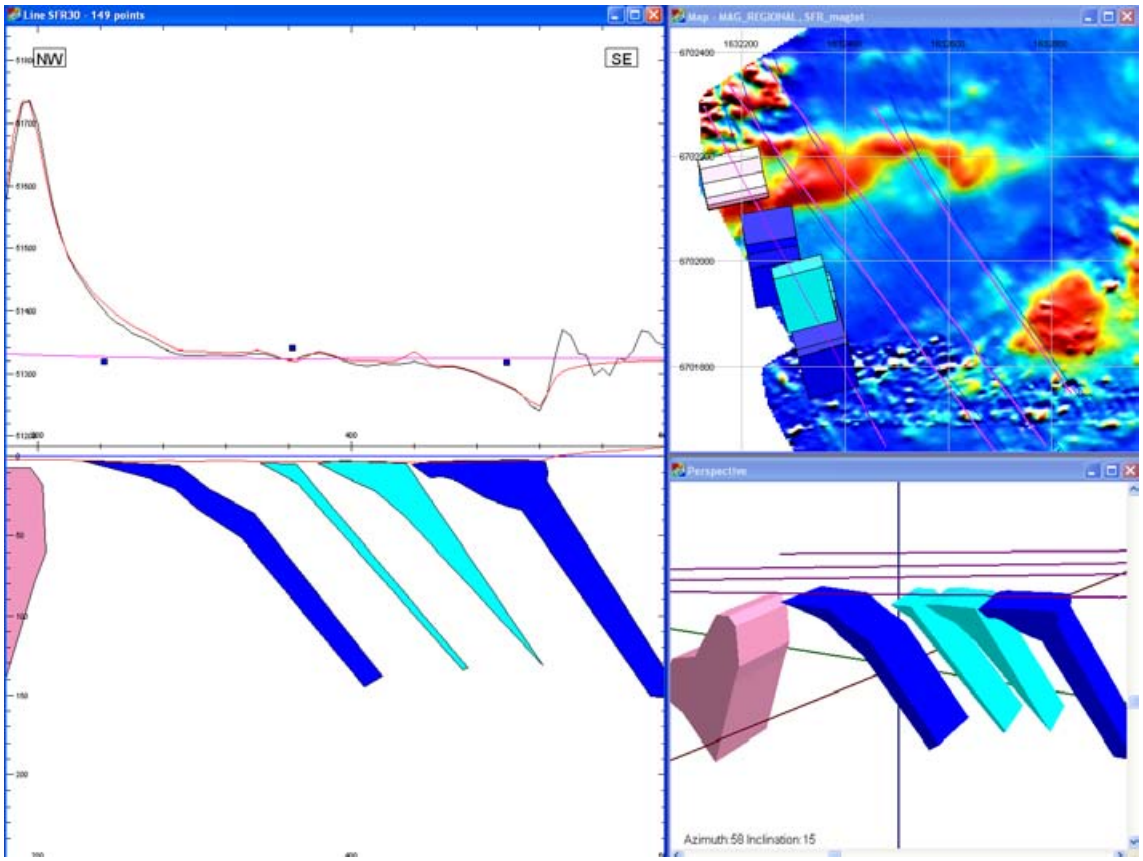

Figure A6-61. *Modelling result from profile SFR30. The light blue source bodies represent lineaments MSFR08034 and MSFR08092 (from left to right in the figure). The pink source body is included to model a high susceptibility lithological unit; the two dark blue bodies are included to model local minima with no connection to any identified lineaments. Maximum depth shown in the leftmost part of the figure is approximately 250 m.*

Profile SFR31, 1632906/6702026 – 1633427/6702410

Figure A6-62 shows the location of the profile SFR31. The primary goal is to model the source body to the lineament MSFR08095 and the result indicates a steep dip (Figure A6-63); the 3D inversion yields similar results (Figure A6-64).

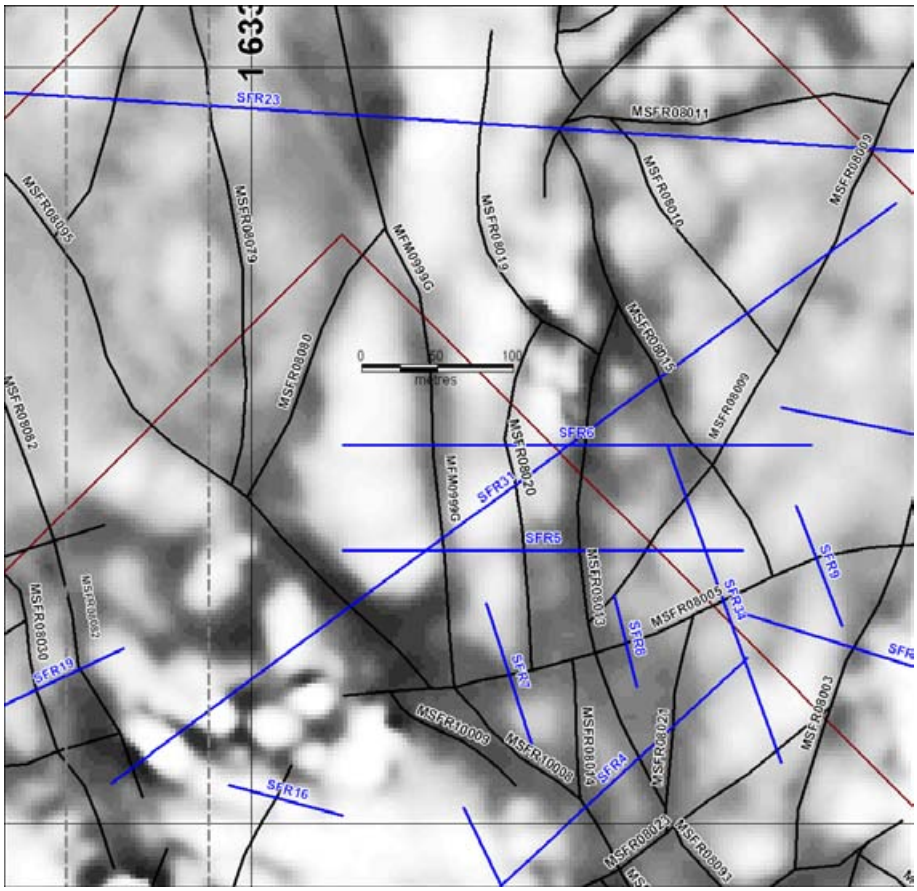

Figure A6-62. *The location of profile SFR31. The model areas of the SFR model are shown as brown rectangles.*

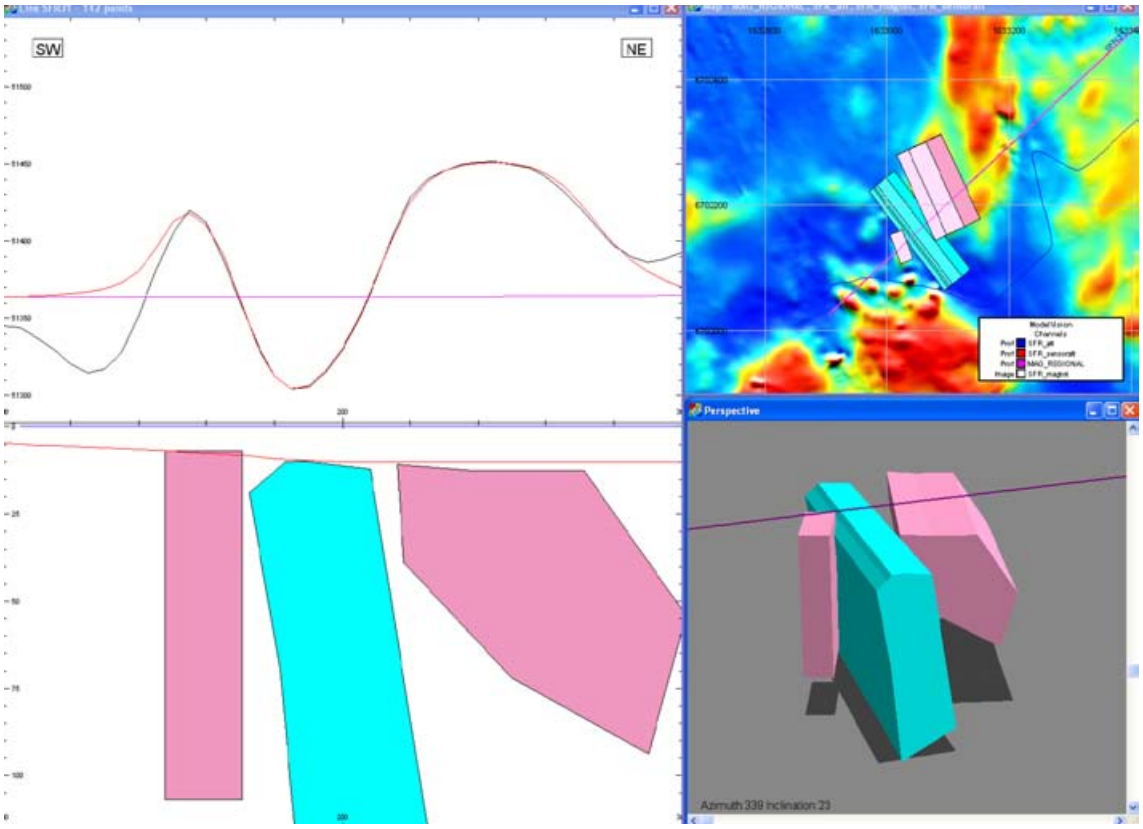

Figure A6-63. *Modelling result from profile SFR31. The blue body represents the inferred source to the lineament MSFR08095. The pink bodies represent high susceptibility volumes. Maximum depth shown in the leftmost part of the figure is approximately 110 m.*

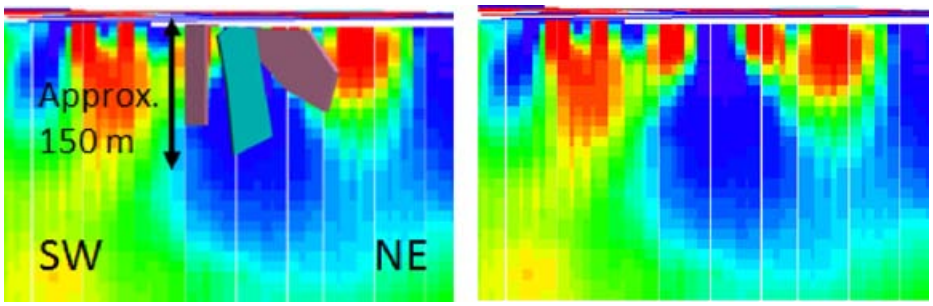

Figure A6-64. *Comparison of the source bodies from the forward modelling with the result from the 3D inversion of magnetic total field data. At left with the source bodies, at right without the source bodies. Blue colour in the inversion result indicates low relative magnetic susceptibility.*

Profile SFR32, 1633260/6701760 – 1633140/6702010

Figure A6-65 shows the location of profile SFR32. The forward modelling result indicates a steep dip (Figure A6-66) of the source to the lineament MSFR08025.

The 3D inversion of the magnetic total field (Figure A6-67) shows much shallower extension for the source volume to the magnetic minimum as compared to the forward modelling result. The discrepancy is due to the increasing insensitivity with depth to narrow low magnetic features buried in a highly magnetized surrounding at depth.

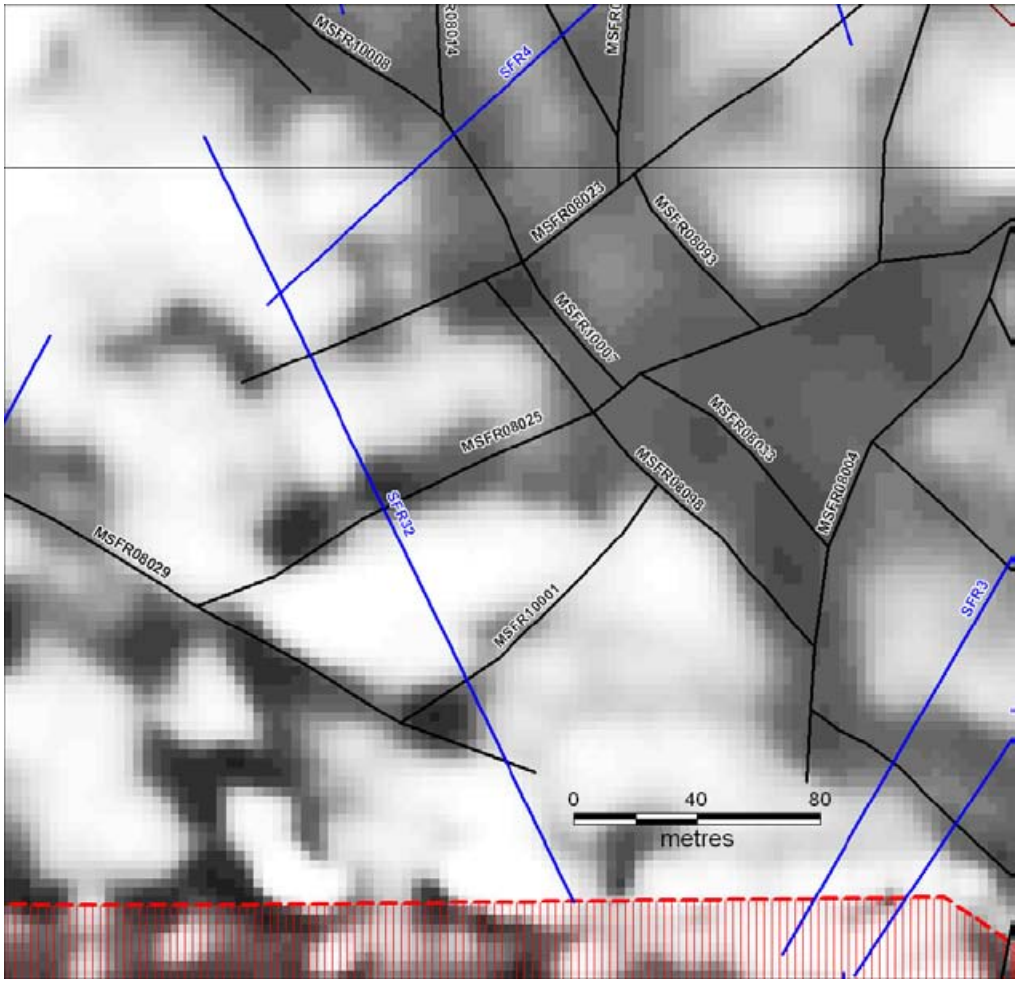

Figure A6-65. *The location of profile SFR32 intended to model the geometry of the lineament MSFR08025.*

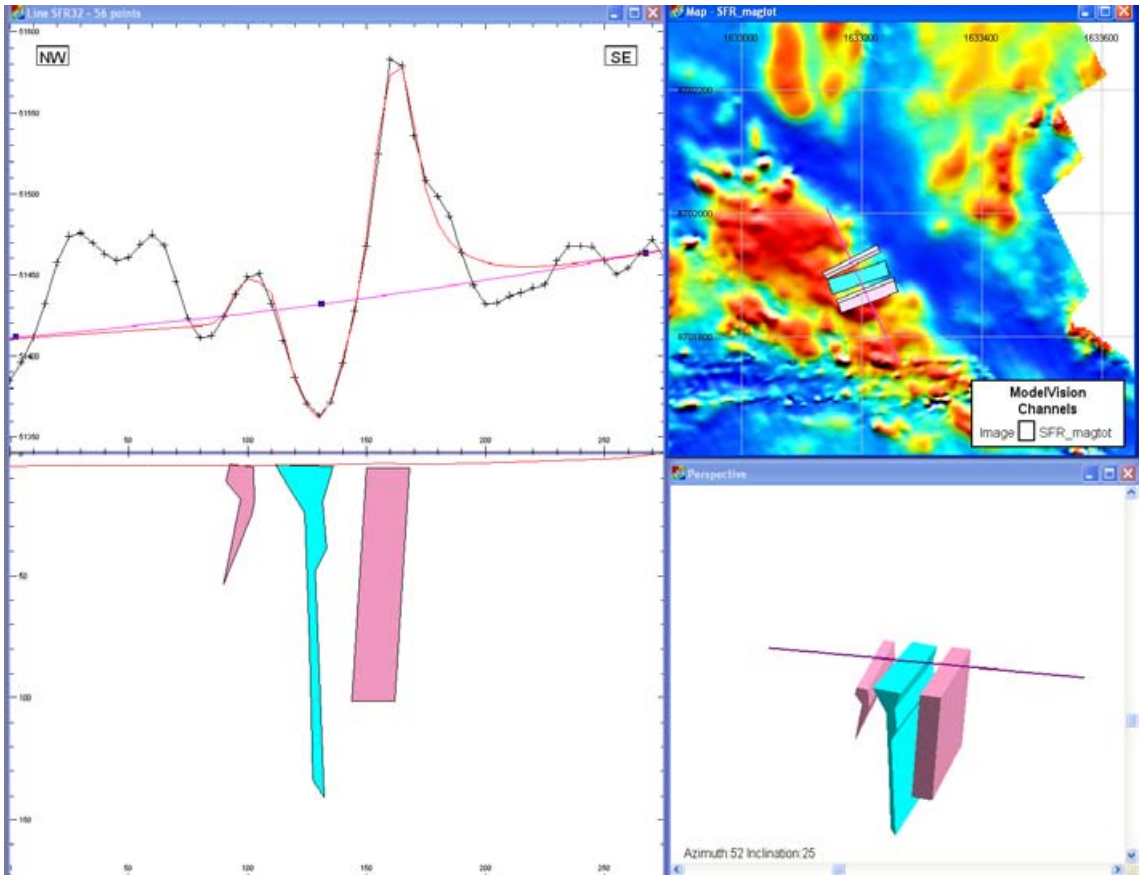

Figure A6-66. *Modelling result from profile SFR32. The blue body represents the possible source to the lineament MSFR08025. Maximum depth shown in the leftmost part of the figure is approximately 170 m.*

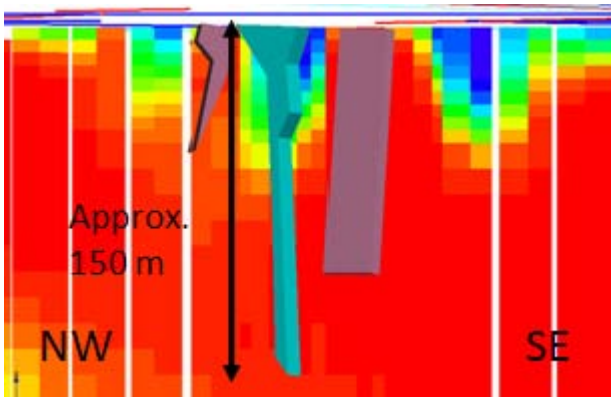

Figure A6-67. *Comparison of the source bodies from the forward modelling with the result from the 3D inversion of magnetic total field data. Blue colour in the inversion result indicates low relative magnetic susceptibility.*

Profile SFR33, 1632330/6701576 – 1632616/6701674

Figure A6-68 shows the location of profiles SFR33 and its connected lineaments MSFR08109, MSFR08110, MSFR008112. Figure A6-69 shows the forward modelling of the broad magnetic minimum with three discernible local minima. In this alternative the three local minima were modelled using three narrow steeply dipping low magnetic sheets connected by an eroded low magnetic near-surface rock volume. It is also possible to achieve a comparable fit between modelled and measured data by instead introducing a broad low magnetic vertically dipping rock volume (Figure A6-70). A comparison between the second forward modelling alternative and the result from the 3D inversion shows a good agreement (Figure A6-71).

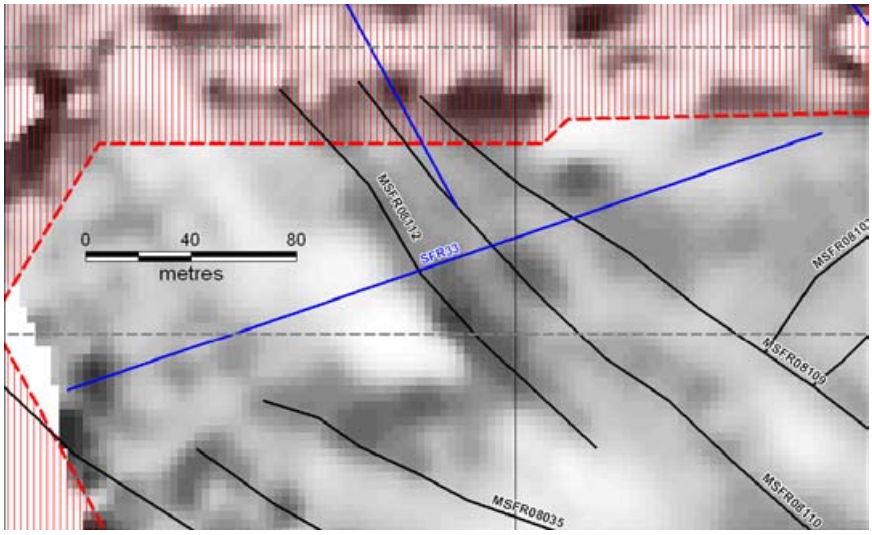

Figure A6-68. *The location of profile SFR33 with its associated lineaments MSFR08109, MSFR08110 and MSFR08112.*

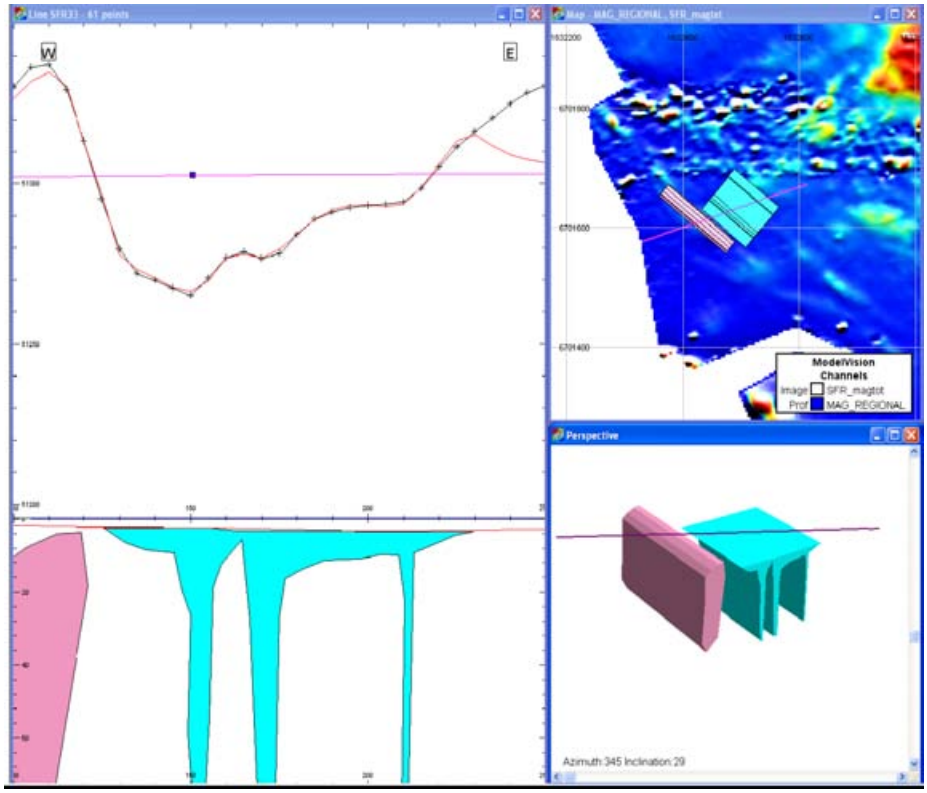

Figure A6-69. *Modelling result from profile SFR33 with a model alternative including an eroded low magnetic depression at top of the bedrock connecting the three low magnetic source volumes representing the lineaments (all in blue). The pink source body is included to compensate for a high magnetic anomaly. Maximum depth shown in the leftmost part of the figure is approximately 70 m.*

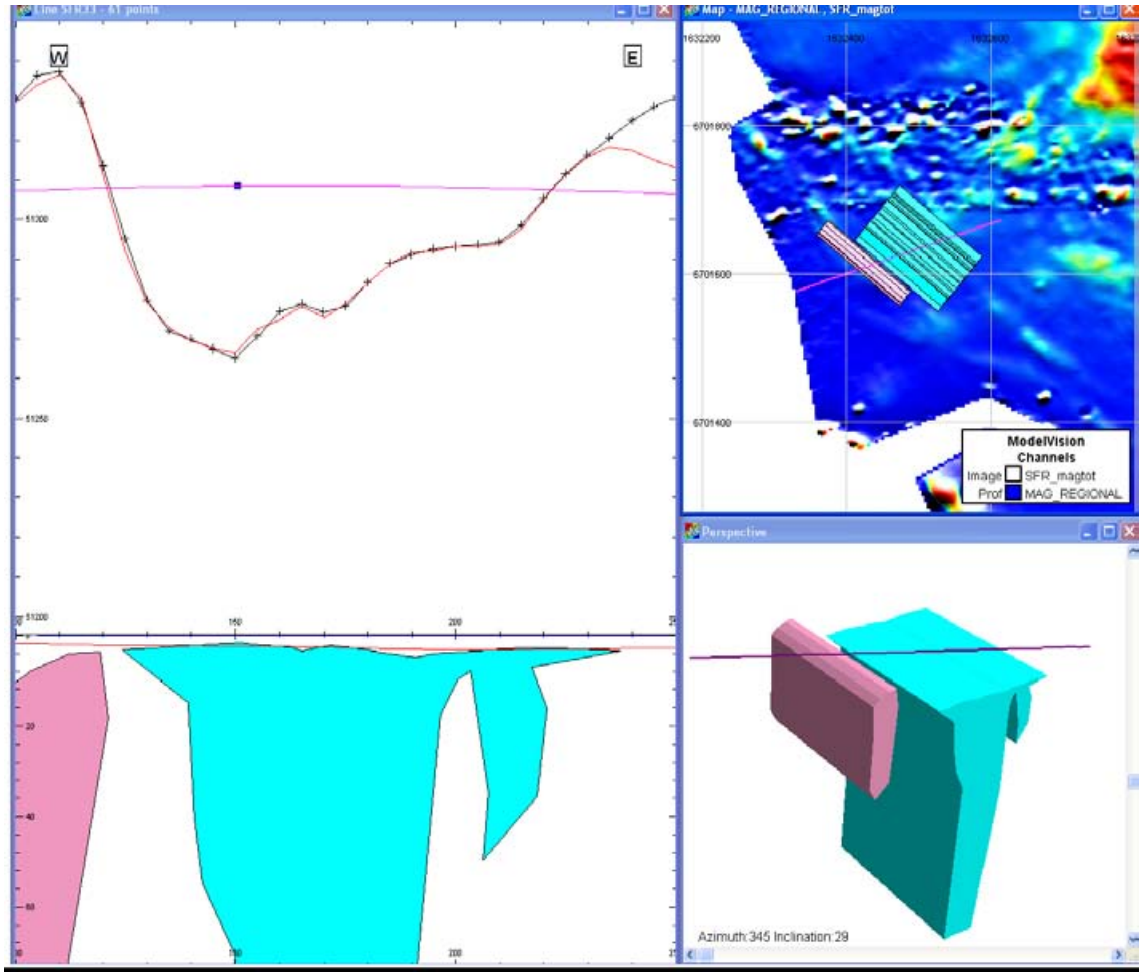

Figure A6-70. *Modelling result from profile SFR33 with a model alternative including a broad low magnetic rock volume (in blue). The pink source body is included to compensate for a high magnetic anomaly. Maximum depth shown in the leftmost part of the figure is approximately 70 m.*

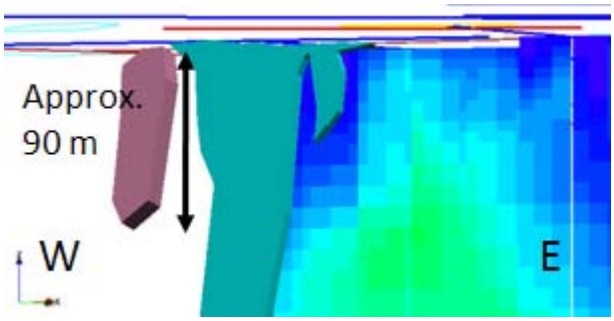

Figure A6-71. *Comparison of the source bodies from the second modelling alternative from the forward modelling with the result from the 3D inversion of magnetic total field data. Blue colour in the inversion result indicates low relative magnetic susceptibility.*

Profile SFR34, 1633350/6702040 – 1633275/6702250

Figure A6-72 shows the location of profiles SFR34–SFR36 and their connected lineaments. Profile SFR34 contains the source body to lineament MSFR08005 with a steep dip (Figure A6-73). The result is in accordance with the profiles modelled earlier (SFR7–SFR9, see above). The result from the 3D inversion shows a near-surface minimum in the magnetic susceptibility at the location of the lineament (Figure A6-74) while the forward modelling has resulted in a feature extending to greater depth.

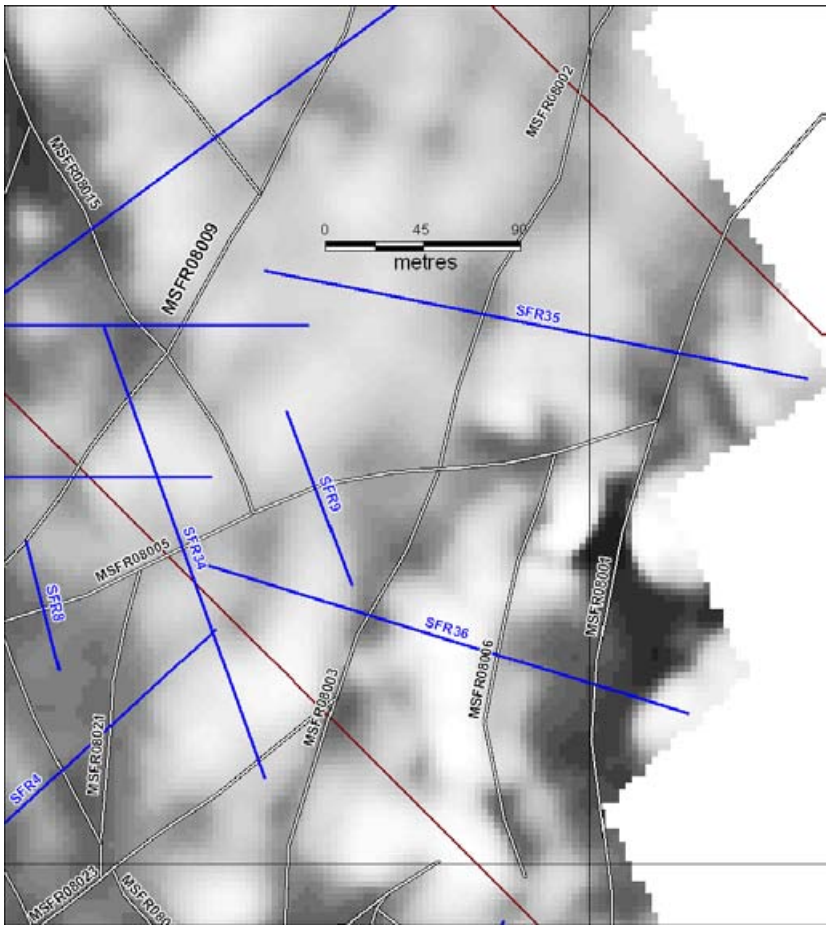

Figure A6-72. *The location of profiles SFR34–SFR36 with their associated lineaments. The model areas of SFR are shown as brown rectangles.*

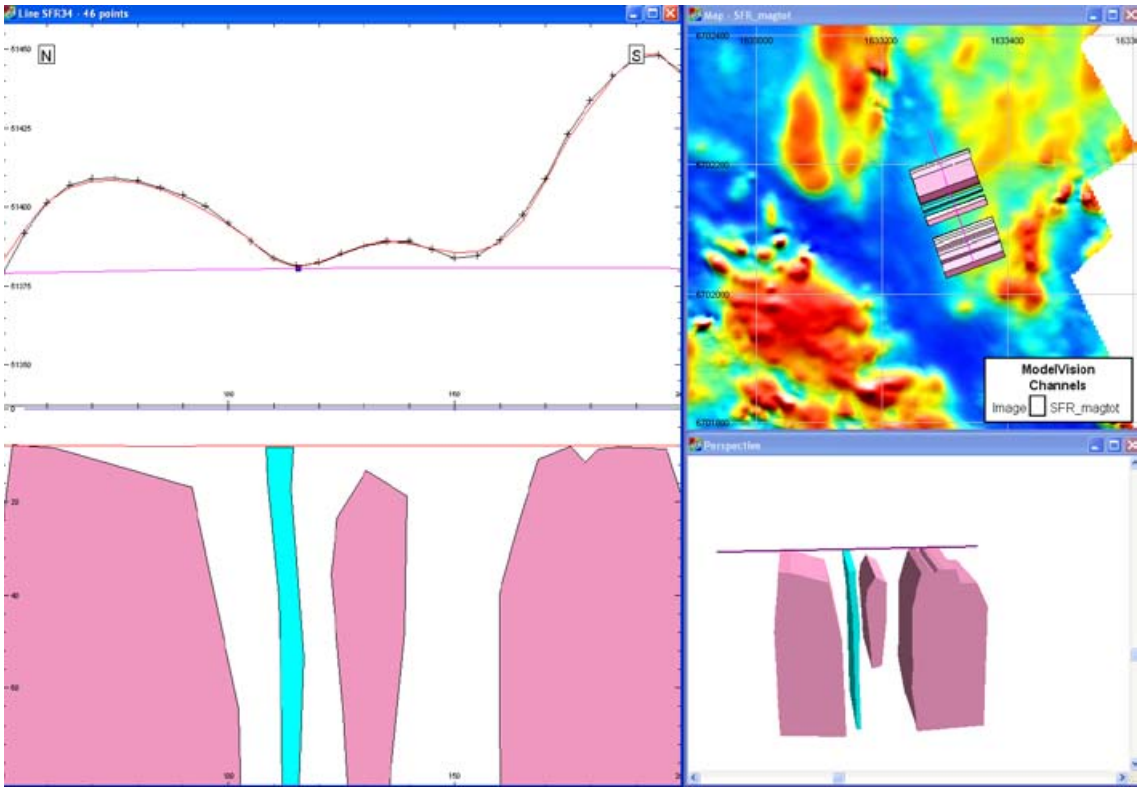

Figure A6-73. *Modelling result from profile SFR34. The modelling of the inferred source body to the lineament MSFR08005 (blue) yields a steep dip. The pink source bodies have high relative susceptibilities and are introduced to compensate the magnetic maxima. Maximum depth shown in the leftmost part of the figure is approximately 80 m.*

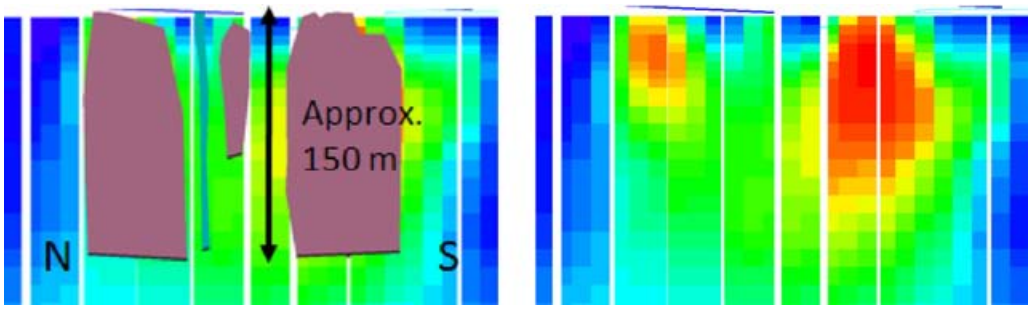

Figure A6-74. *Comparison of the source bodies from the forward modelling with the result from the 3D inversion of magnetic total field data. At left – with source bodies, at right – without source bodies. Blue colour in the inversion result indicates low relative magnetic susceptibility.*

Profile SFR35, 1633600/6702225 – 1633350/6702275

Figure A6-72 above shows the location of profile SFR35 and its associated lineaments MSFR08002 and MSFR08001. Both of the source bodies representing the lineaments are steeply dipping towards the west (Figure A6-75); the result is in good agreement with the distribution of the magnetic susceptibility as obtained by the 3D inversion of magnetic total field data (Figure A6-76).

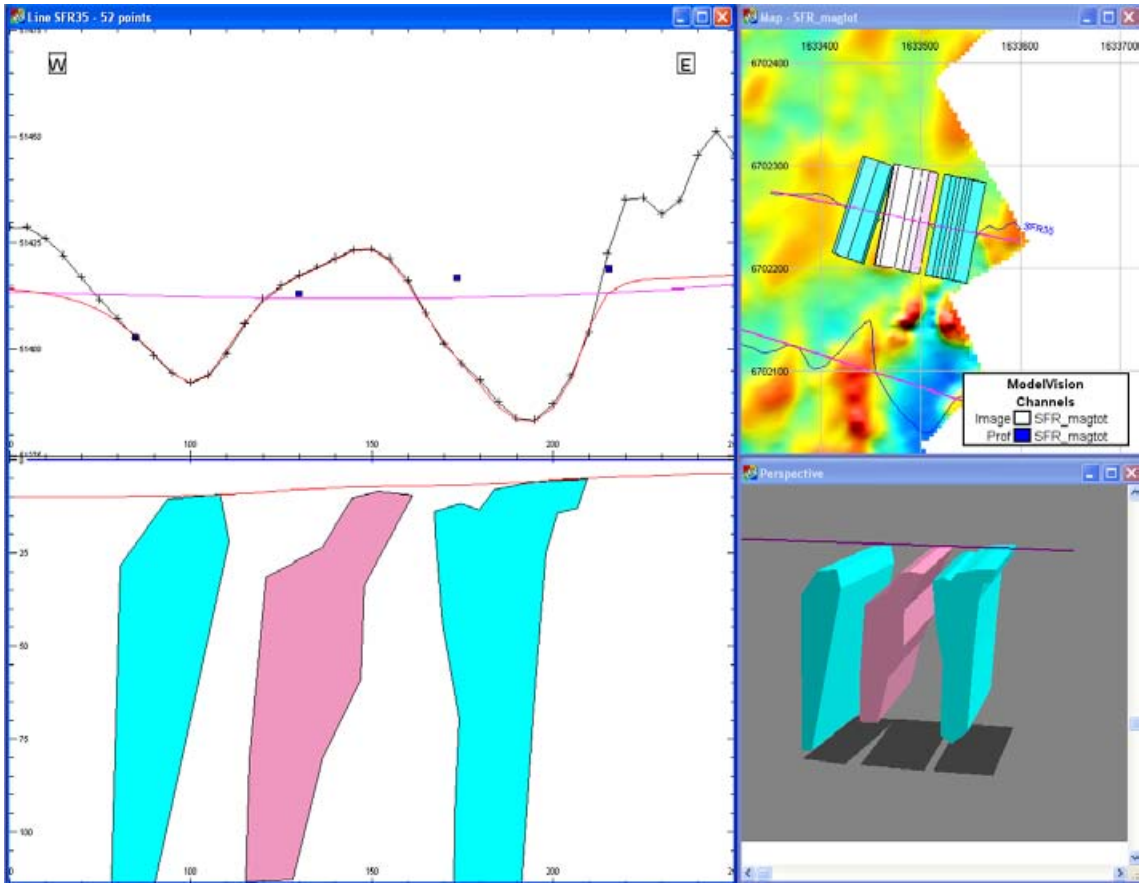

Figure A6-75. *Modelling result from profile SFR35 showing the inferred source bodies to lineaments MSFR08002 (at left in the displayed profile) and MSFR08001 (at right in the displayed profile), both steeply dipping towards west. The pink source body has a high relative susceptibility. Maximum depth shown in the leftmost part of the figure is approximately 110 m.*

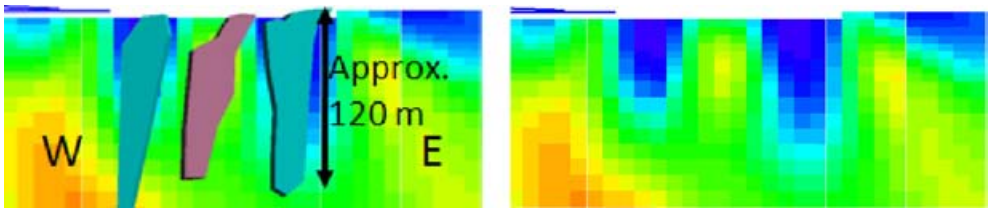

Figure A6-76. *Comparison of the source bodies from the forward modelling with the result from the 3D inversion of magnetic total field data. At left – with source bodies, at right – without source bodies. Blue colour in the inversion result indicates low relative magnetic susceptibility.*

Profile SFR36, 1633545/6702070 – 1633320/6702140

Figure A6-72 above shows the location of profile SFR36 and its associated lineaments MSFR08001 and MSFR08003. The western source body (Figure A6-77) represents lineament MSFR08003; the dip is steep towards west. The pink body has a high susceptibility and is invoked to compensate for the pronounced maximum. The eastern source body represents the source to the lineament MSFR08001. The peculiar geometry is probably due to a change in lithology or alteration in the bedrock to the west of the lineament; this area coincides with the lineament MSFR08006. The 3D inversion yields rather similar results (Figure A6-78).

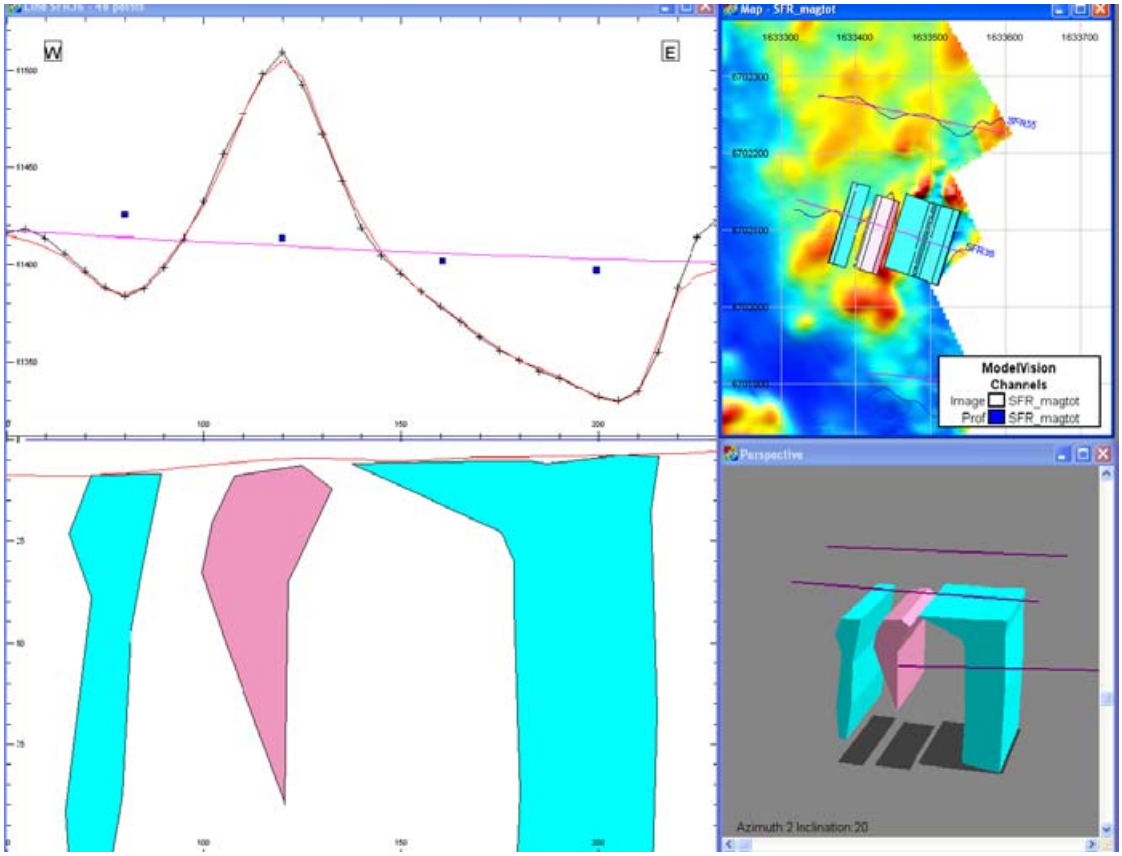

Figure A6-77. *Modelling result from profile SFR36 showing the source bodies to lineaments MSFR08003 (to the left in the displayed profile) and MSFR08001 (to the right in the displayed profile). The pink source body has a high relative susceptibility. Maximum depth shown in the leftmost part of the figure is approximately 100 m.*

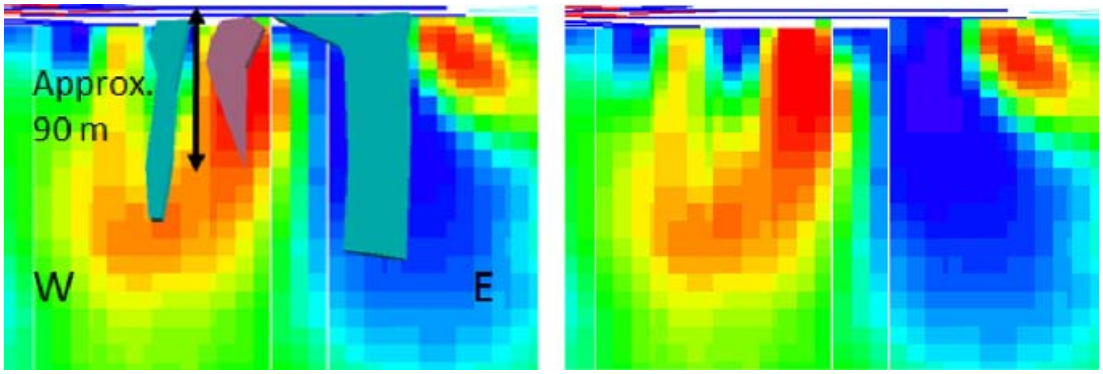

Figure A6-78. *Comparison of the source bodies from the forward modelling with the result from the 3D inversion of magnetic total field data. At left – with source bodies, at right – without source bodies. Blue colour in the inversion result indicates low relative magnetic susceptibility.*

Profile SFR37, 1633415/6701915 – 1633565/6701900

Figure A6-79 shows the location of profile SFR37 and its associated lineament MSFR08001. The modelling result indicates that the source to the lineament dips steeply towards the west (Figure A6-80); the result is in good accordance with the result from the 3D inversion (Figure A6-81).

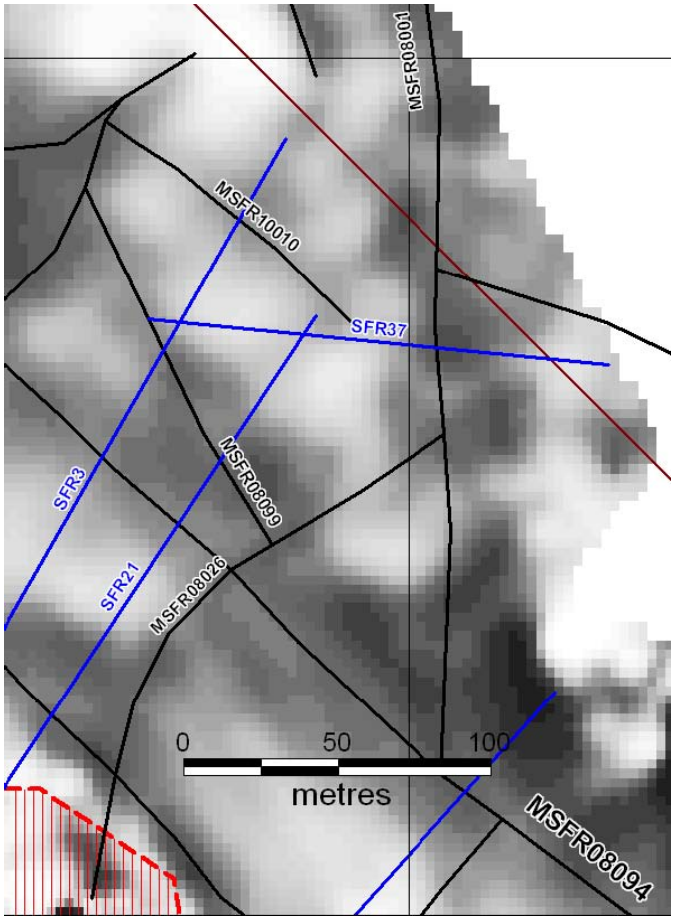

Figure A6-79. *The location of profile SFR37 with its associated lineament MSFR08001.*

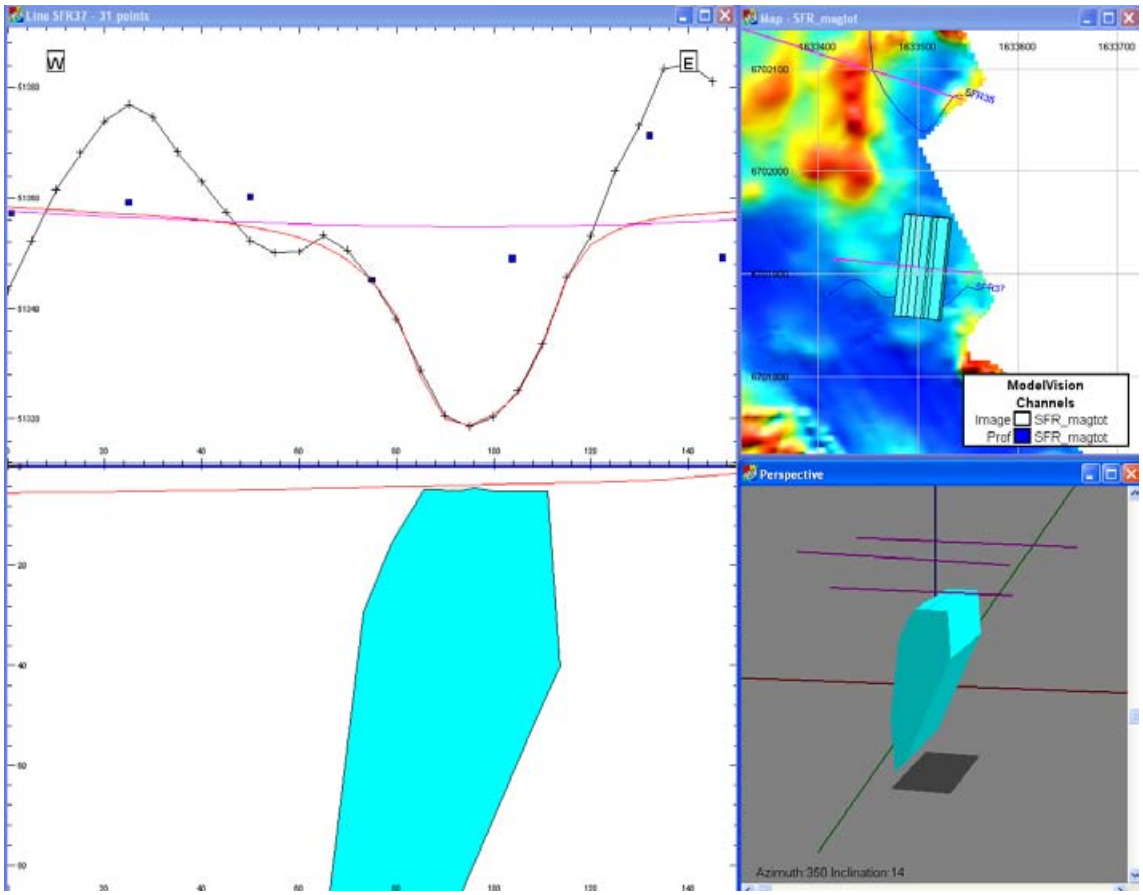

Figure A6-80. *Modelling result from profile SFR37 with the source body to the lineament MSFR08001. Maximum depth shown in the leftmost part of the figure is approximately 80 m.*

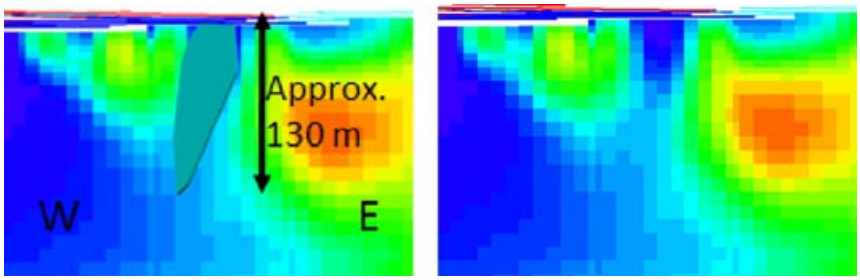

Figure A6-81. *Comparison of the source bodies from the forward modelling with the result from the 3D inversion of magnetic total field data. At left – with source bodies, at right – without source bodies. Blue colour in the inversion result indicates low relative magnetic susceptibility.*

Profile SFR38, 1632930/6701415 – 1633170/6701660

Figure A6-82 shows the location of profile SFR38 and its associated lineaments MSFR08067 and MSFR10002. The modelling result (Figure A6-83) shows that a broad low susceptibility body can be used to explain most of the broad low magnetic anomaly that hosts the source rock to both lineaments. However, the low susceptibility mass hides the geometry of the sources to both of the lineaments due to lack of sufficient contrast in magnetic properties. The broad low magnetic anomaly also indicates that the anomaly could reflect the existence of a lithological unit with low susceptibility. The 3D inversion result supports the forward modelling result i.e. it identifies a broad low susceptibility rock volume. The dip of the low susceptibility rock volume is steep according to the modelling. Whether the inferred sources to the lineaments dip concordantly or not, is not possible to deduce.

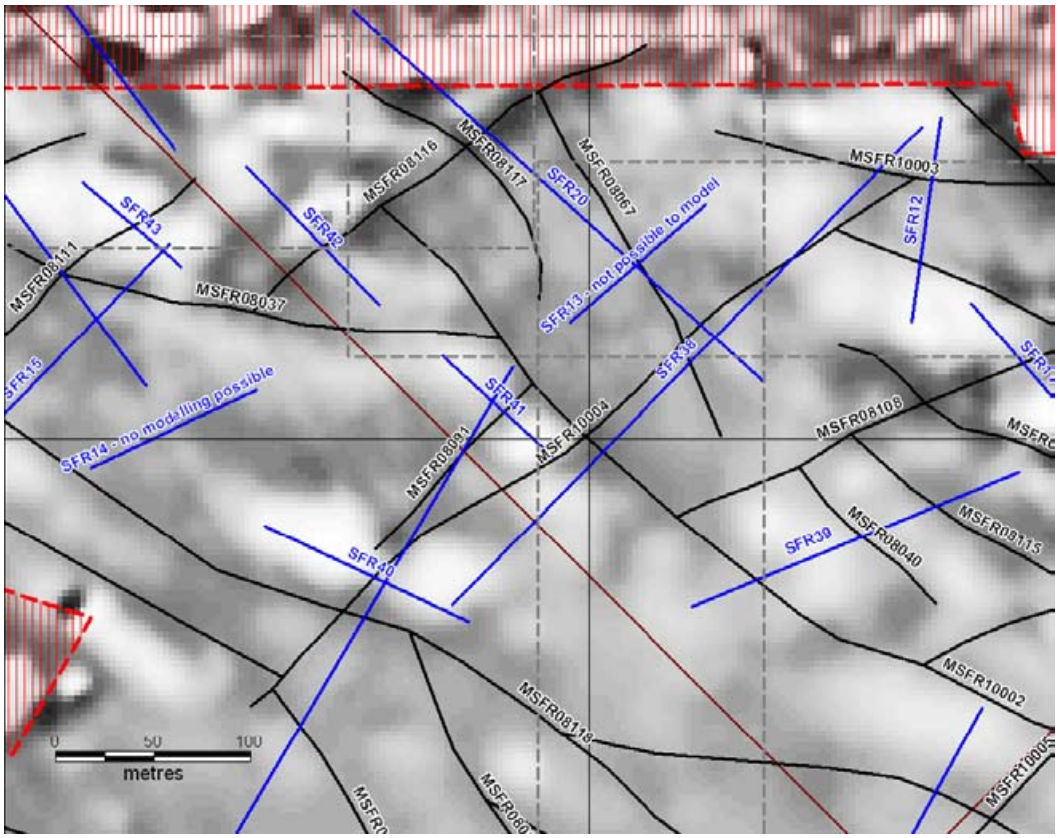

Figure A6-82. *The location of profiles SFR38–SFR43 with their associated lineaments.*

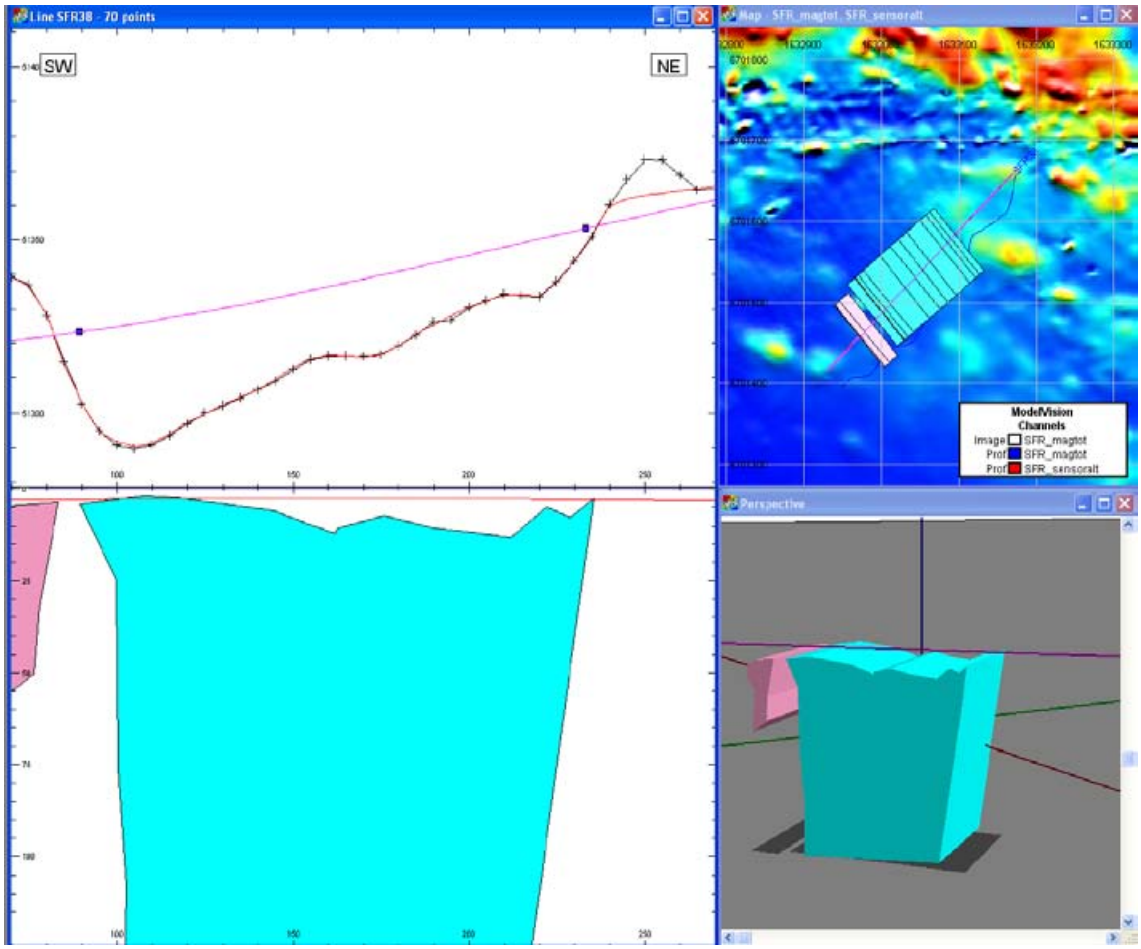

Figure A6-83. *Modelling result from profile SFR38 regarding the source rock volume that includes the lineaments MSFR10002 and MSFR08067. Maximum depth shown in the leftmost part of the figure is approximately 120 m.*

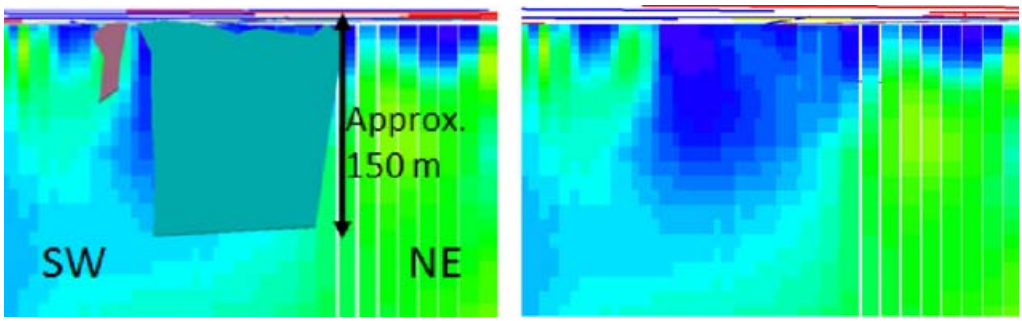

Figure A6-84. *Comparison of the source bodies from the forward modelling with the result from the 3D inversion of magnetic total field data. At left – with source bodies, at right – without source bodies. Blue colour in the inversion result indicates low relative magnetic susceptibility.*

Profile SFR39, 1633052/6701414 – 1633220/6701483

Figure A6-82 above shows the location of profile SFR39 with its associated lineaments MSFR10002, MSFR08040 and MSFR08115. Figure A6-85 shows that the low susceptibility source rock resulting in the lineament MSFR10002 is probably very narrow at the position of this profile as no clear minimum is recognizable. The dips of the source bodies inferred to cause the lineaments MSFR08040 and MSFR08115 are both modelled as steep. The 3D inversion result (Figure A6-86) indicates that the source to the lineament MSFR08040 is very shallow. The difference compared to the forward modelling alternative emanates from the relative insensitivity of the magnetic method to narrow low susceptibility sheet-like bodies at depth. It means that the depth extent of the source body in the forward modelling could have been reduced without any significant loss of fit between modelled and observed data. The source rock geometry for the lineament MSFR08115, from the forward modelling and the 3D inversion, are in good agreement with each other.

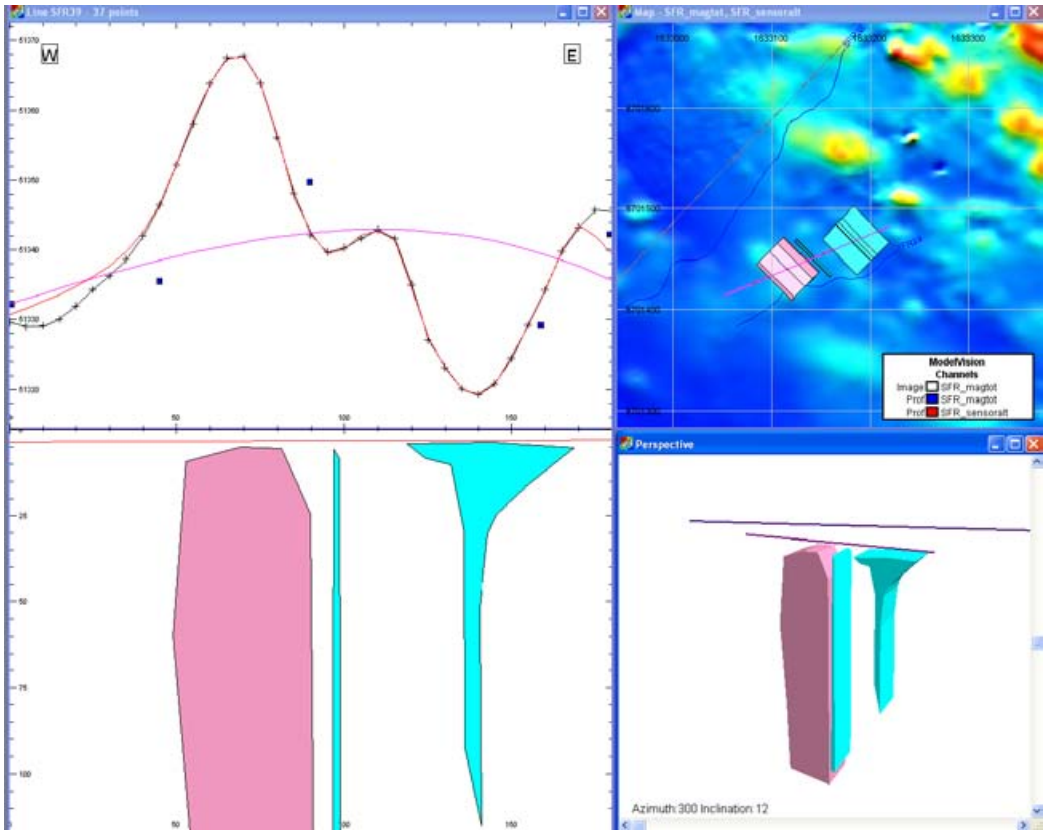

Figure A6-85. *Modelling result from profile SFR39. The blue source body at left corresponds to lineament MSFR08040 and the blue at right to lineament MSFR08115. Regarding the lineaments MSFR10002 no sufficiently pronounced anomaly is recognizable at the position of this profile. The pink source body is invoked to compensate for the local maximum. Maximum depth shown in the leftmost part of the figure is approximately 120 m.*

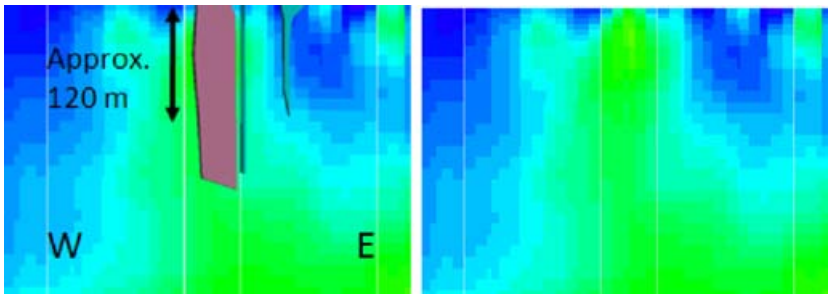

Figure A6-86. *Comparison of the source bodies from the forward modelling with the result from the 3D inversion of magnetic total field data. At left – with source bodies, at right – without source bodies. Blue colour in the inversion result indicates low relative magnetic susceptibility.*

Profile SFR40, 1632938/6701406 – 1632834/6701455

Figure A6-82 above shows the location of profile SFR40 with its associated lineament MSFR10004. Figure A6-87 shows that the dip of the source body inferred to cause the lineament is modelled as steep; the result is supported by the 3D inversion (Figure A6-88).

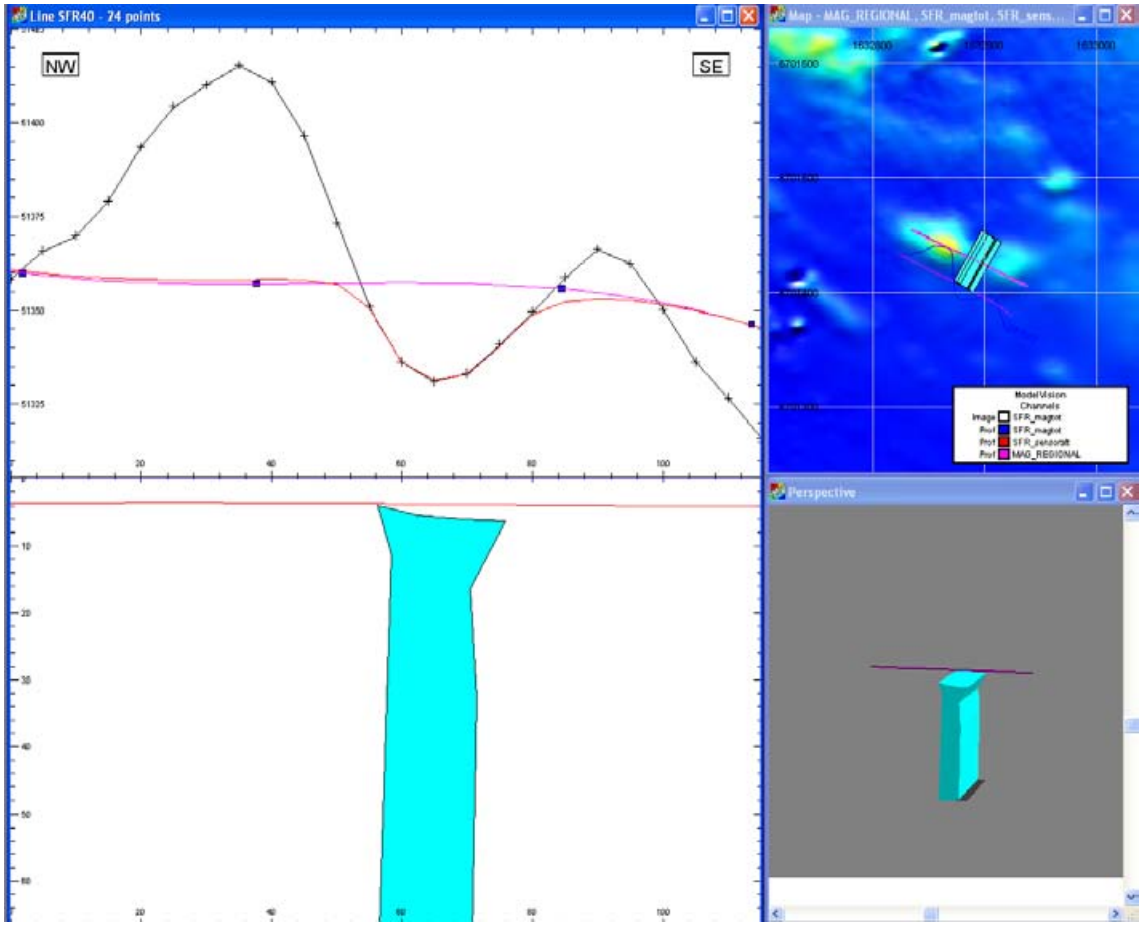

Figure A6-87. *Modelling result from profile SFR40. The blue source body corresponds to lineament MSFR10004. Maximum depth shown in the leftmost part of the figure is approximately 70 m.*

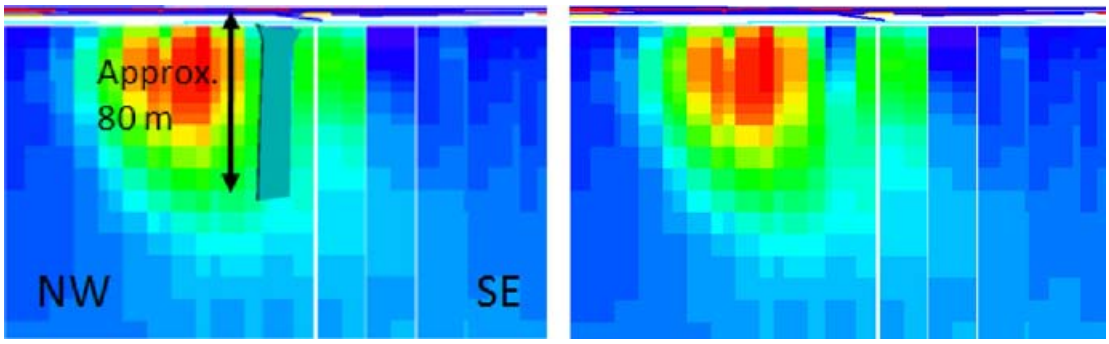

Figure A6-88. *Comparison of the source bodies from the forward modelling with the result from the 3D inversion of magnetic total field data. At left – with source bodies, at right – without source bodies. Blue colour in the inversion result indicates low relative magnetic susceptibility.*

Profile SFR41, 1632981/6701491 – 1632925/6701542

Figure A6-82 above shows the location of profile SFR41 with its associated lineament MSFR08091. Figure A6-89 shows that the source body dips steeply. The 3D inversion gives a similar result but the source body has less depth extent (Figure A6-90).

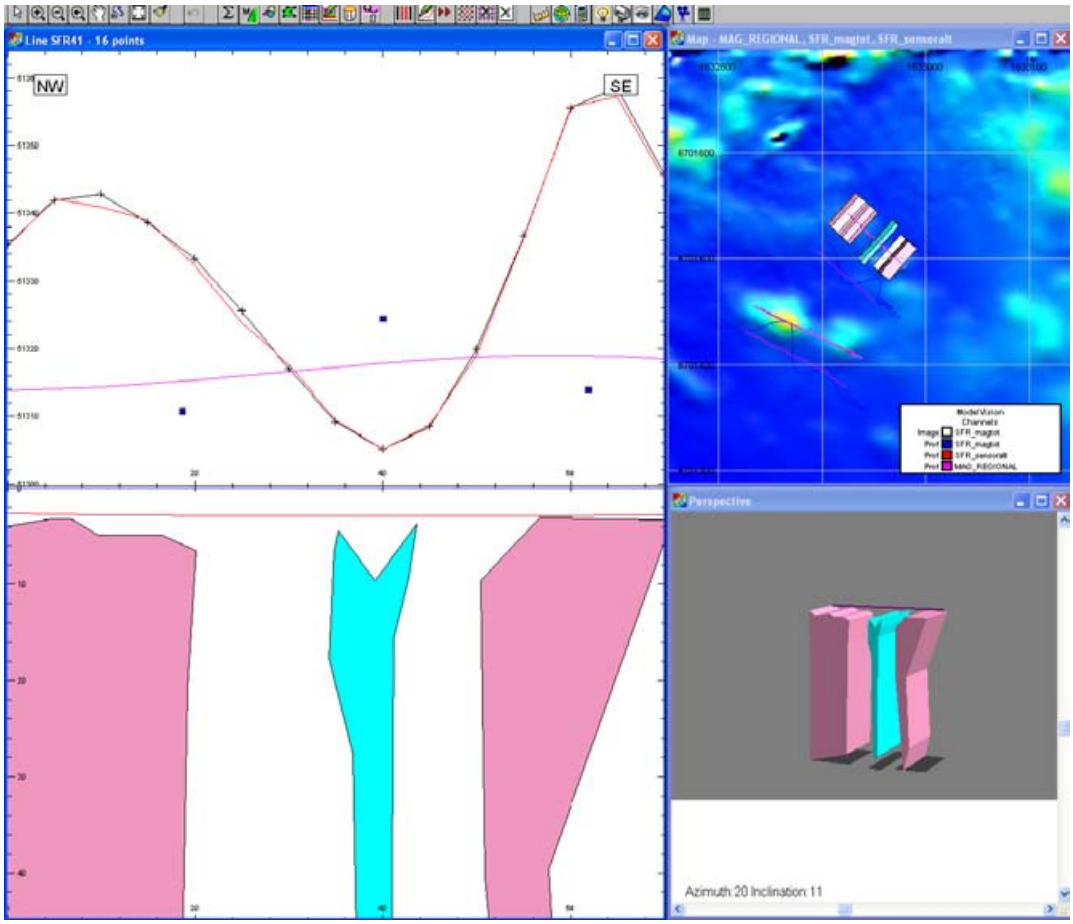

Figure A6-89. *Modelling result from profile SFR41. The blue source body corresponds to lineament MSFR08091. The pink bodies represent high susceptibility rock volumes. Maximum depth shown in the leftmost part of the figure is approximately 40 m.*

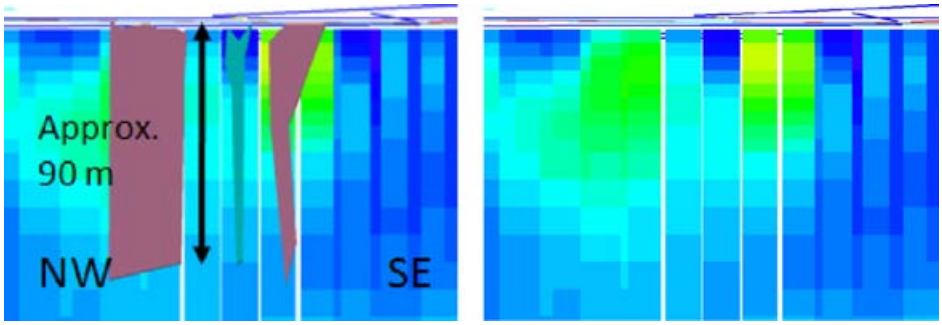

Figure A6-90. *Comparison of the source bodies from the forward modelling with the result from the 3D inversion of magnetic total field data. At left – with source bodies, at right – without source bodies. Blue colour in the inversion result indicates low relative magnetic susceptibility.*

Profile SFR42, 1632892/6701569 – 1632825/6701639

Figure A6-82 shows the location of profile SFR42 with its associated lineament MSFR08116. The two source bodies inferred to cause the lineament MSFR08116 are modelled to dip steeply (Figure A6-91). The confidence level is low in the geometry prediction as the anomaly is weak and the two source bodies interfere. The 3D inversion supports the forward modelling result (Figure A6-91).

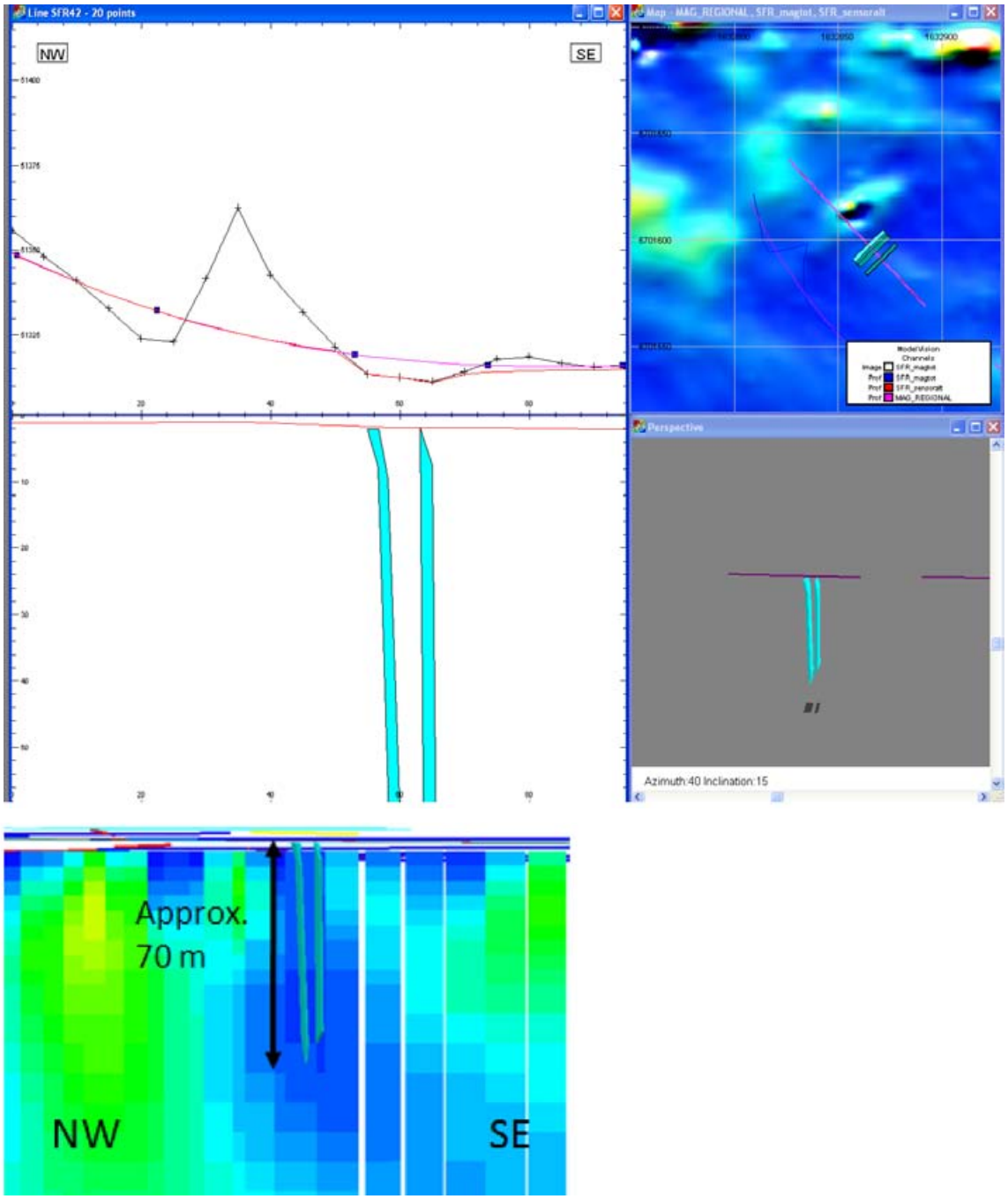

Figure A6-91. *Top: Modelling result from profile SFR42. The two blue source bodies correspond to the lineament MSFR08116. Maximum depth shown in the leftmost part of the figure is approximately 60 m. Bottom: Comparison of the source bodies from the forward modelling with the result from the 3D inversion of magnetic total field data. Blue colour in the inversion result indicates low relative magnetic susceptibility.*

Profile SFR43, 1632791/6701588 – 1632741/6701631

Figure A6-82 shows the location of profile SFR43 with its associated lineament MSFR08111. The dip of the source body inferred to cause the lineament MSFR08111 is forward modelled to have a steep dip towards the south-east (Figure A6-92). The 3D inversion gives a totally different result with a shallow source only. The difference in result may be attributed to the coarseness in the 3D inversion model as compared to the forward modelling (Figure A6-92).

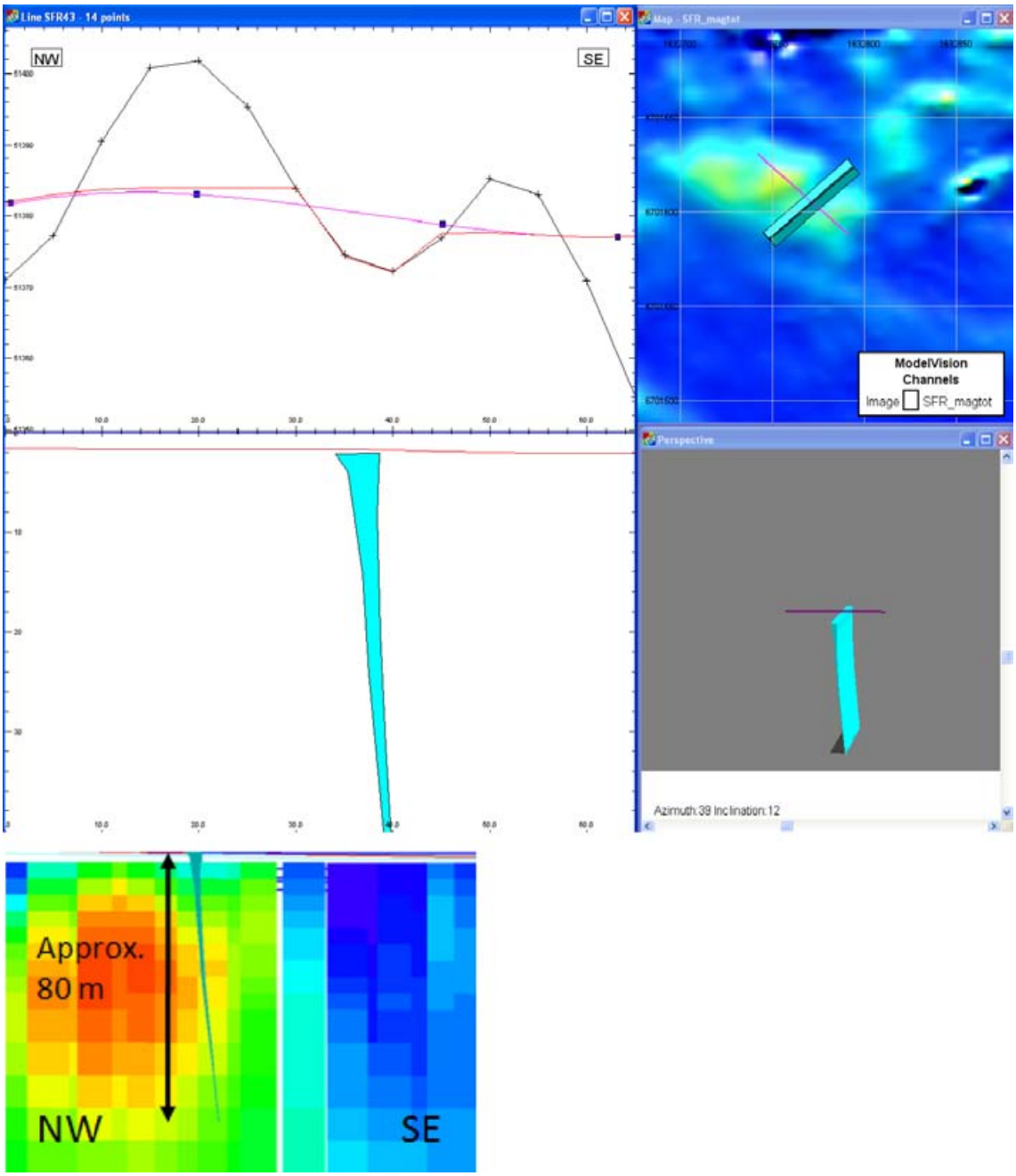

Figure A6-92. *Top: Forward modelling result from profile SFR43. The blue source body corresponds to the lineament MSFR08111. Maximum depth shown in the leftmost part of the figure is approximately 40 m. Bottom: Comparison of the source body from the forward modelling with the result from the 3D inversion of magnetic total field data. Blue colour in the inversion result indicates low relative magnetic susceptibility.*

Profile SFR44, 1633382/6701447 – 1633471/6701532

Figure A6-93 shows the location of profile SFR44 with its associated lineaments MSFR08042 and MSFR08106. The source body inferred to cause the lineament MSFR08042 is forward modelled with a steep dip while the source body to lineament MSFR08106 dips steeply towards the north-east (Figure A6-94). The 3D inversion shows a similar result for lineament MSFR08042 but for the lineament MSFR08106 the 3D inversion indicates a moderate dip towards the south-west (Figure A6-95).

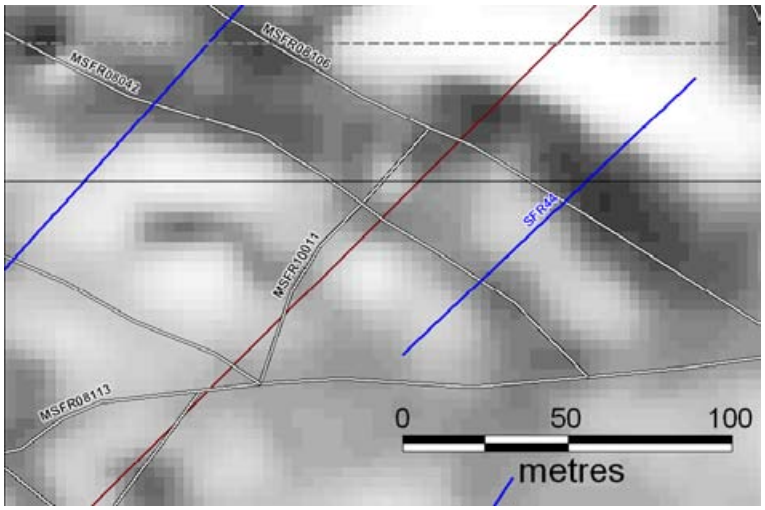

Figure A6-93. *The location of profiles SFR44 with its associated lineaments MSFR08042 and MSFR08106.*

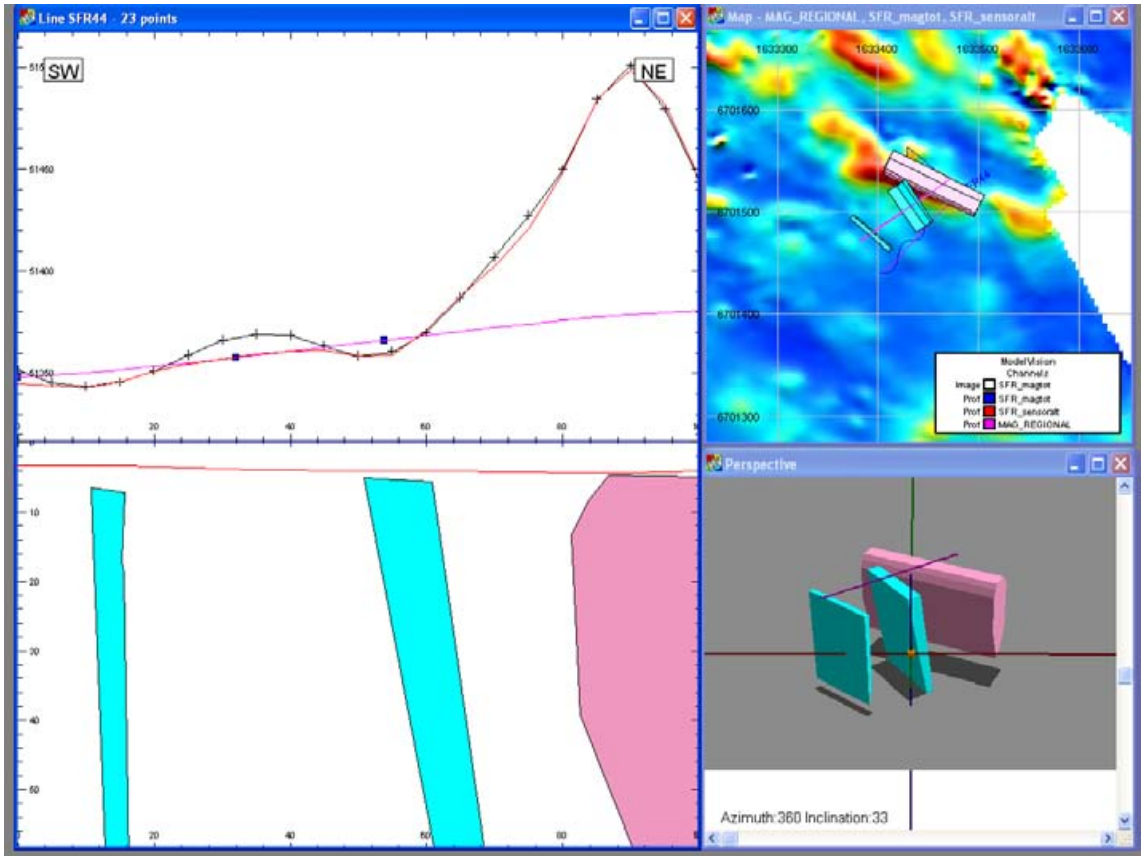

Figure A6-94. *Modelling result from profile SFR44. The blue source at left body corresponds to the lineament MSFR08042 and at right to MSFR08106. The pink body has a high magnetic susceptibility. Maximum depth shown in the leftmost part of the figure is approximately 60 m.*

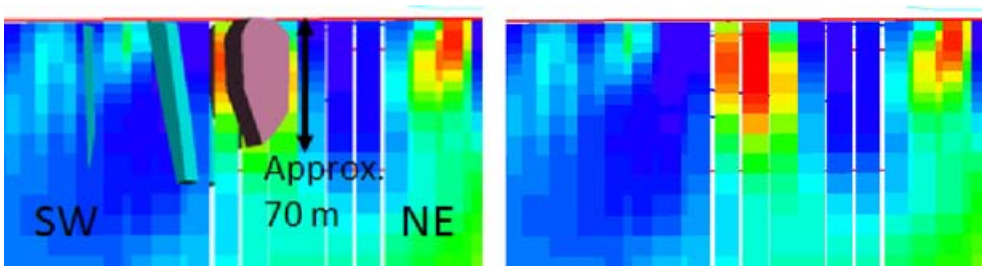

Figure A6-95. *Comparison of the source body from the forward modelling with the result from the 3D inversion of magnetic total field data. At left – with source bodies, at right – without source bodies. Blue colour in the inversion result indicates low relative magnetic susceptibility.*

Appendix 7

Single-hole interpretation (SHI) and correlation with modelled rock domains (RFR) and deformation zones (ZFM) presented on a borehole by borehole basis

An overview of rock units (RU) and possible deformation zones (DZ) from the geological single-hole interpretation (SHI) of the boreholes that penetrate the SFR model volumes and that have been mapped using current SKB methodology (see Sections 3.4 and 4.2.3 in the main text), in combination with the inferred rock domains (RFR) and deformation zones (ZFM) in each borehole, are presented graphically as summary logs for each borehole. The only cored boreholes from the construction of SFR presented as summary logs are the eleven boreholes selected for renewed mapping using the Boremap system. For further discussion of the modelling of deformation zones and rock domains, the reader is referred to Chapters 5 and 6, respectively. The ZFM intervals shown are all target intercepts in the deformation zone model. All negative numbers in the compilation logs refer to model elevation (meters above sea level). Borehole length is measured in relation to the top of the borehole casing (m.f. ToC).

The orientation set, to which each modelled deformation zone is inferred to belong, is shown in each borehole diagram. The different sets of deformation zones at the site are described in the conceptual model for the site. Rock types arranged in the four major groups (A to D) are distinguished in the Forsmark area on the basis of their relative age (see Section 4.3.1 for details).

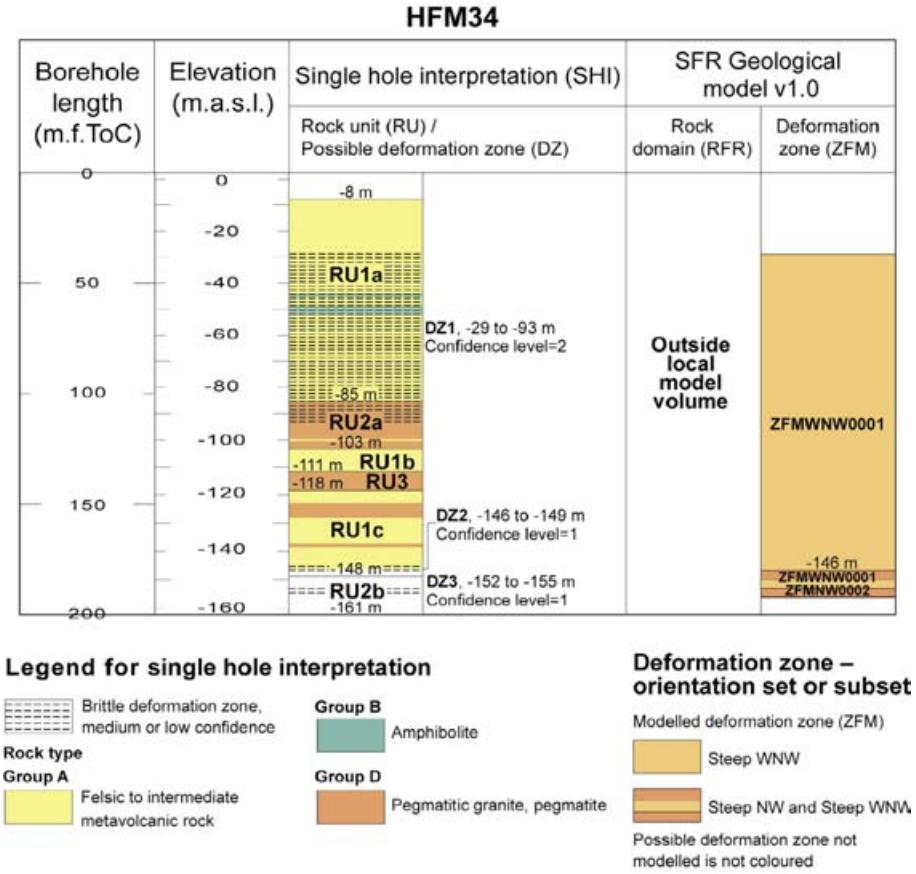

The elevation of a modelled deformation zone is only provided in the cases where the zone boundaries differ from the single hole interpretation.

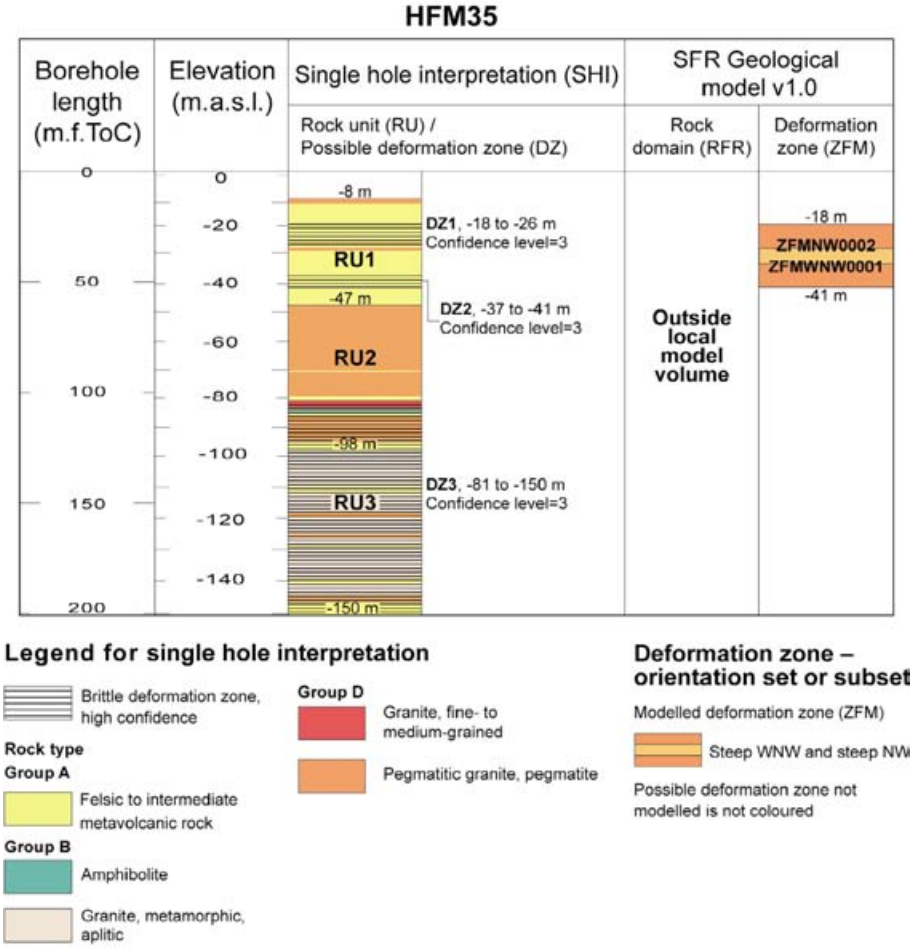

The elevation of a modelled deformation zone is only provided in the cases where the zone boundaries differ from the single hole interpretation.

HFR101

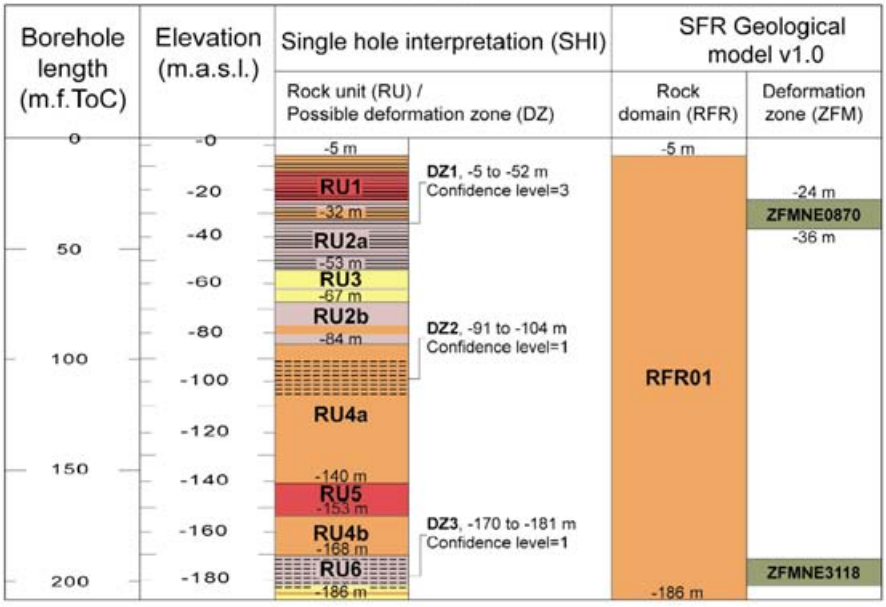

Legend for single hole interpretation

Brittle deformation zone, low confidence

Brittle deformation zone, high confidence

Rock type

Group A

Felsic to intermediate volcanic rock, metamorphic

Group B

Granodiorite (to granite), metamorphic, medium - grained

Group D

Pegmatite, pegmatitic granite

Granite, fine- to medium-grained

Deformation zone – orientation set or subset

Modelled deformation zone (ZFM)

Steep NE

Possible deformation zone not modelled is not coloured

The elevation of a modelled deformation zone is only provided in the cases where the zone boundaries differ from the single hole interpretation.

HFR102

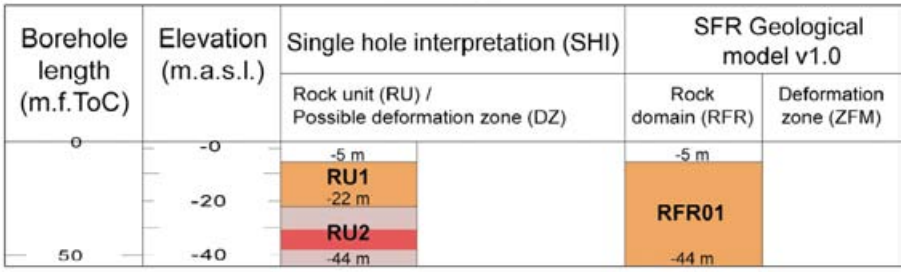

Legend for single hole interpretation

Rock type

Group B

Granodiorite (to granite), metamorphic, medium - grained

Group D

Pegmatite, pegmatitic granite

Granite, fine- to medium-grained

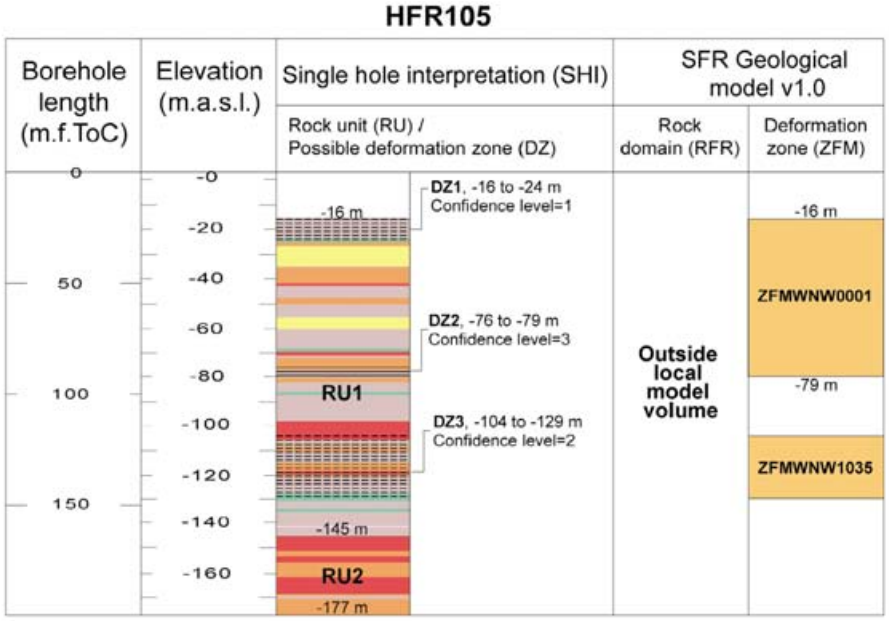

Legend for single hole interpretation

Brittle deformation zone, low to medium confidence

Brittle deformation zone, high confidence

Rock type

Group A

Felsic to intermediate volcanic rock, metamorphic

Group B

Granodiorite (to granite), metamorphic, medium - grained

Amphibolite

Group C

Granodiorite to tonalite, metamorphic, fine- to medium-grained

Group D

Pegmatite, pegmatitic granite

Granite, fine- to medium-grained

Deformation zone – orientation set or subset

Modelled deformation zone (ZFM)

Steep WNW

The elevation of a modelled deformation zone is only provided in the cases where the zone boundaries differ from the single hole interpretation.

HFR106

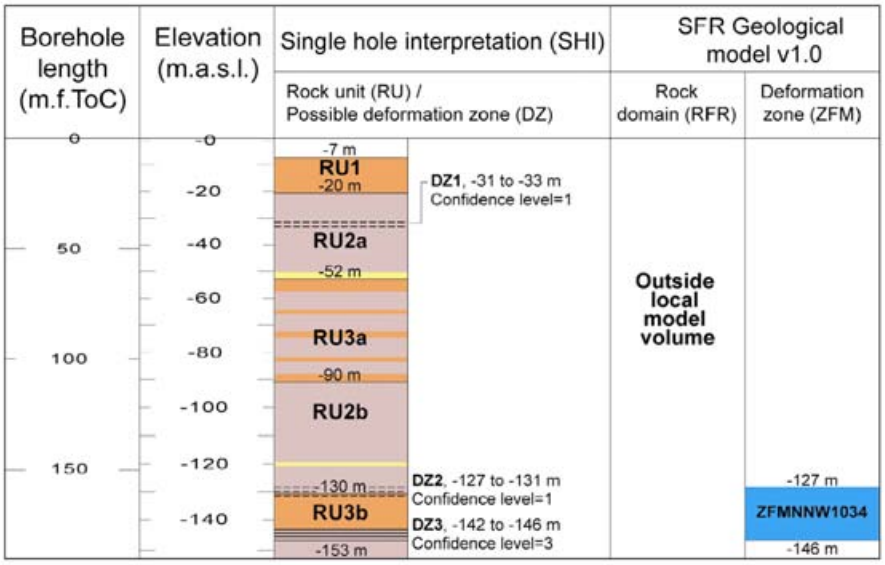

Legend for single hole interpretation

Brittle deformation zone, low confidence

Brittle deformation zone, high confidence

Rock type

Group A

Felsic to intermediate volcanic rock, metamorphic

Group B

Granodiorite (to granite), metamorphic, medium - grained

Group D

Pegmatite, pegmatitic granite

Deformation zone – orientation set or subset

Modelled deformation zone (ZFM)

Steep NNW

Possible deformation zone not modelled is not coloured

The elevation of a modelled deformation zone is only provided in the cases where the zone boundaries differ from the single hole interpretation.

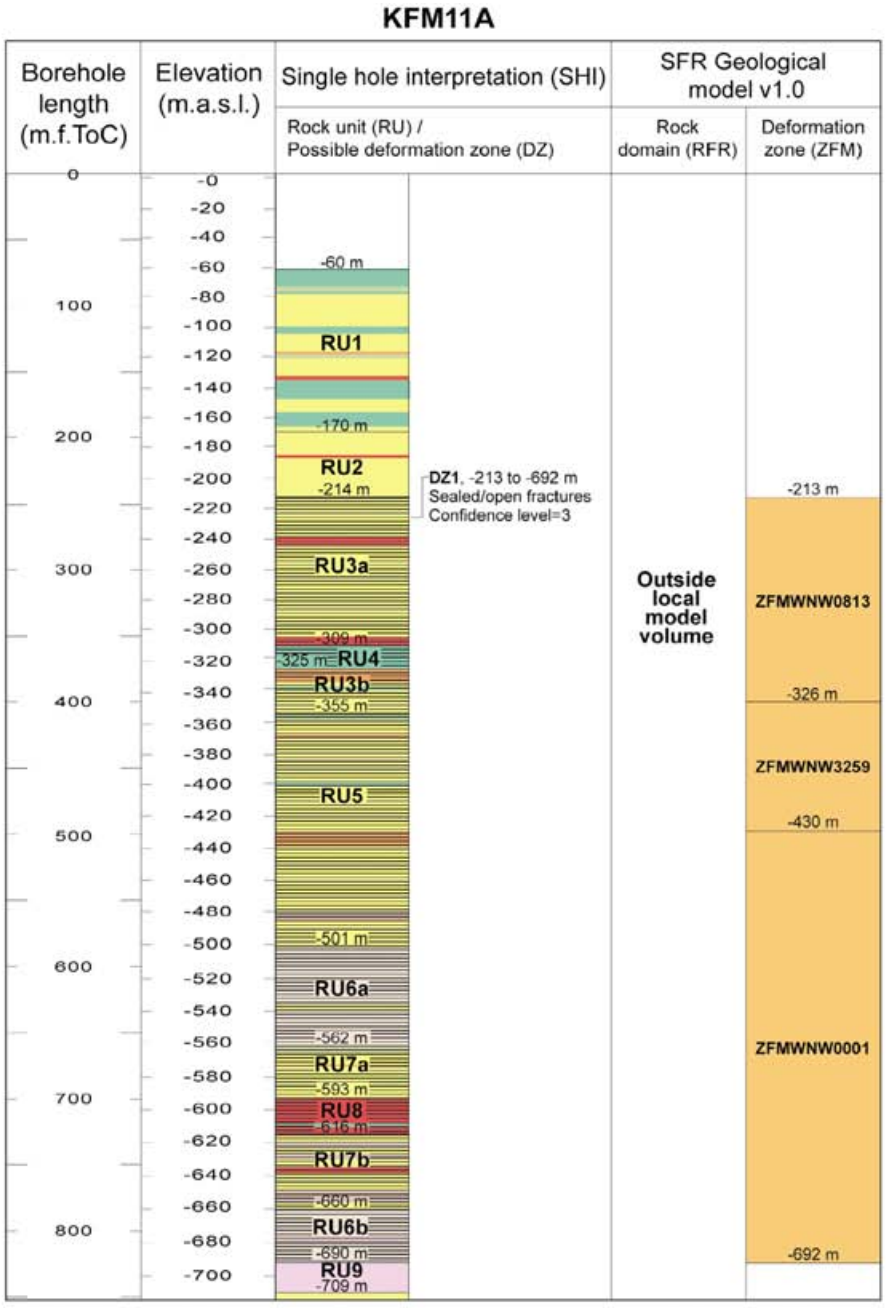

Legend for single hole interpretation

Brittle deformation zone, high confidence

Rock type

Group A

Felsic to intermediate metavolcanic rock

Calc-silicate rock (skarn)

Group B

Granodiorite (to granite), metamorphic, medium - grained

Amphibolite

Granite, metamorphic, aplitic

Group B

Granodiorite, metamorphic

Granitoid, metamorphic

Group C

Granodiorite to tonalite, metamorphic, fine- to medium-grained

Group D

Granite, fine- to medium-grained

Pegmatitic granite, pegmatite

Deformation zone – orientation set or subset

Modelled deformation zone (ZFM)

Steep WNW

The elevation of a modelled deformation zone is only provided in the cases where the zone boundaries differ from the single hole interpretation.

KFR04

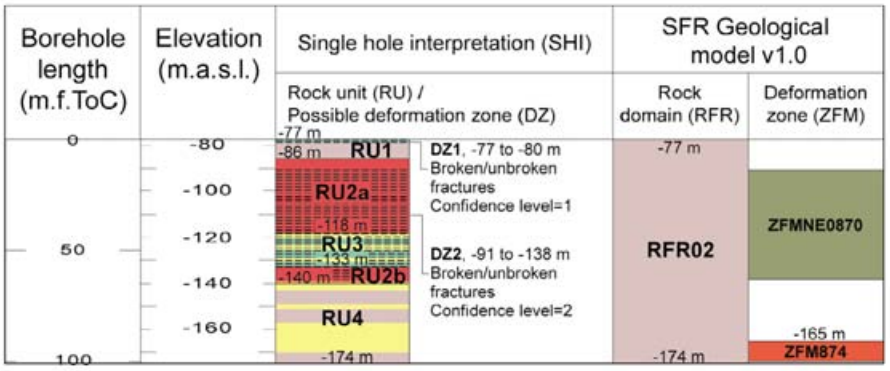

Legend for single hole interpretation

Brittle deformation zone, medium or low confidence

Rock type

Group A

Felsic to intermediate metavolcanic rock

Group B

Granodiorite (to granite), metamorphic, medium - grained

Amphibolite

Group D

Granite, fine- to medium-grained

Pegmatitic granite, pegmatite

Deformation zone – orientation set or subset

Modelled deformation zone (ZFM)

Steep NE

Gentle

Possible deformation zone not modelled is not coloured

The elevation of a modelled deformation zone is only provided in the cases where the zone boundaries differ from the single hole interpretation.

KFR08

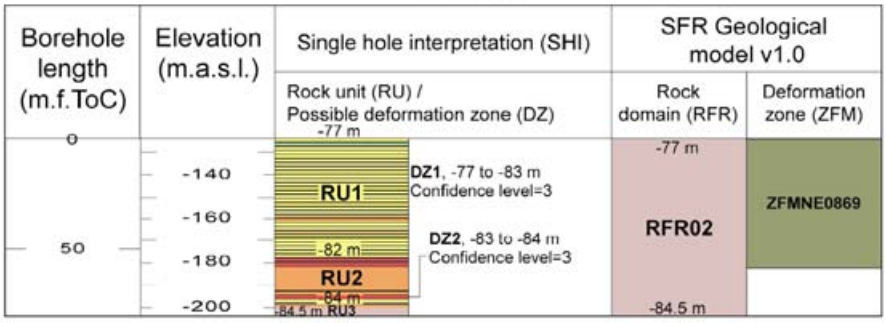

Legend for single hole interpretation

Brittle deformation zone, high confidence

Rock type

Group A

Felsic to intermediate metavolcanic rock

Group B

Granodiorite (to granite), metamorphic, medium - grained

Amphibolite

Group D

Granite, fine- to medium-grained

Pegmatitic granite, pegmatite

Deformation zone – orientation set or subset

Modelled deformation zone (ZFM)

Steep NE

Possible deformation zone not modelled is not coloured

The elevation of a modelled deformation zone is only provided in the cases where the zone boundaries differ from the single hole interpretation.

KFR09

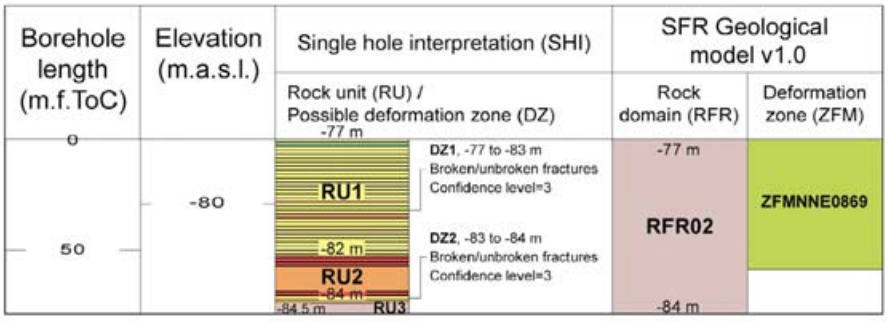

Legend for single hole interpretation

Brittle deformation zone, high confidence

Rock type

Group A

Felsic to intermediate metavolcanic rock

Group B

Granodiorite (to granite), metamorphic, medium - grained

Amphibolite

Group D

Granite, fine- to medium-grained

Pegmatitic granite, pegmatite

Deformation zone – orientation set or subset

Modelled deformation zone (ZFM)

Steep NNE

Possible deformation zone not modelled is not coloured

The elevation of a modelled deformation zone is only provided in the cases where the zone boundaries differ from the single hole interpretation.

KFR13

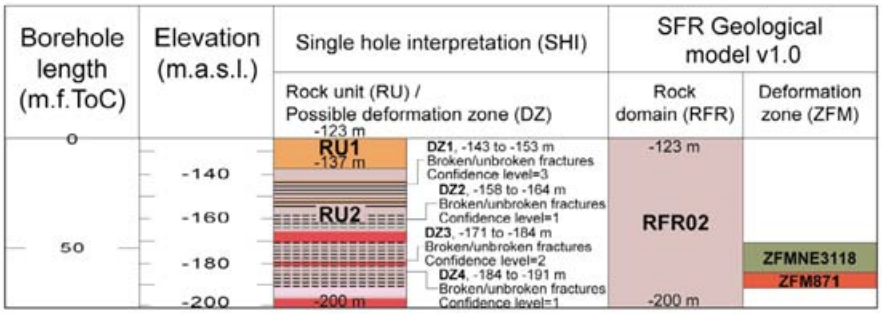

Legend for single hole interpretation

Brittle deformation zone, medium or low confidence

Brittle deformation zone, high confidence

Rock type

Group B

Granodiorite (to granite), metamorphic, medium - grained

Amphibolite

Group C

Granodiorite to tonalite, metamorphic, fine- to medium-grained

Group D

Granite, fine- to medium-grained

Pegmatitic granite, pegmatite

Deformation zone – orientation set or subset

Modelled deformation zone (ZFM)

Steep NE

Gentle

Possible deformation zone not modelled is not coloured

The elevation of a modelled deformation zone is only provided in the cases where the zone boundaries differ from the single hole interpretation.

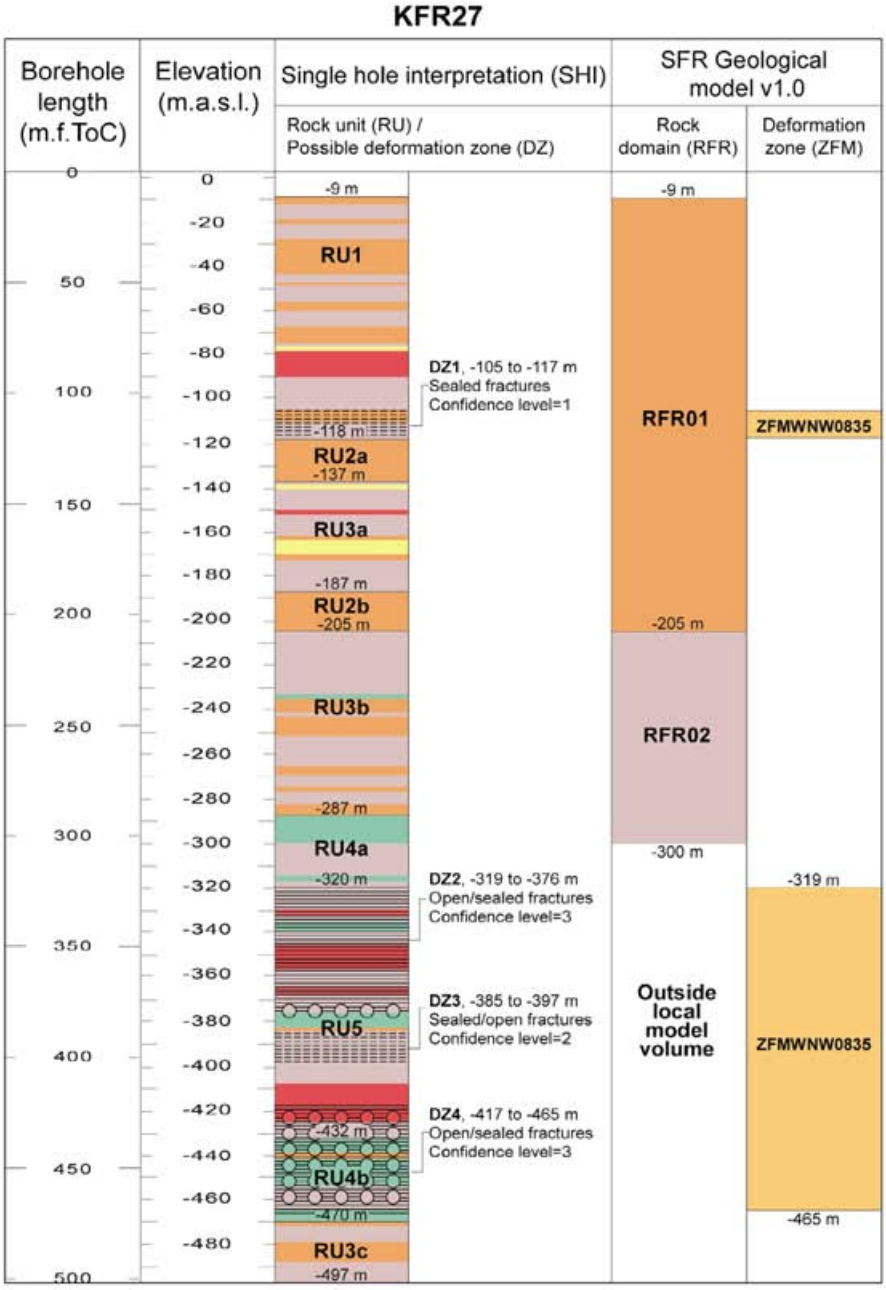

Legend for single hole interpretation

Brittle deformation zone, low to medium confidence

Brittle deformation zone, high confidence

Strongly altered, vuggy rock

Rock type

Group A

Felsic to intermediate metavolcanic rock

Group B

Granodiorite (to granite), metamorphic, medium - grained

Amphibolite

Group D

Granite, fine- to medium-grained

Pegmatitic granite, pegmatite

Deformation zone – orientation set or subset

Modelled deformation zone (ZFM)

Steep WNW

The elevation of a modelled deformation zone is only provided in the cases where the zone boundaries differ from the single hole interpretation.

KFR35

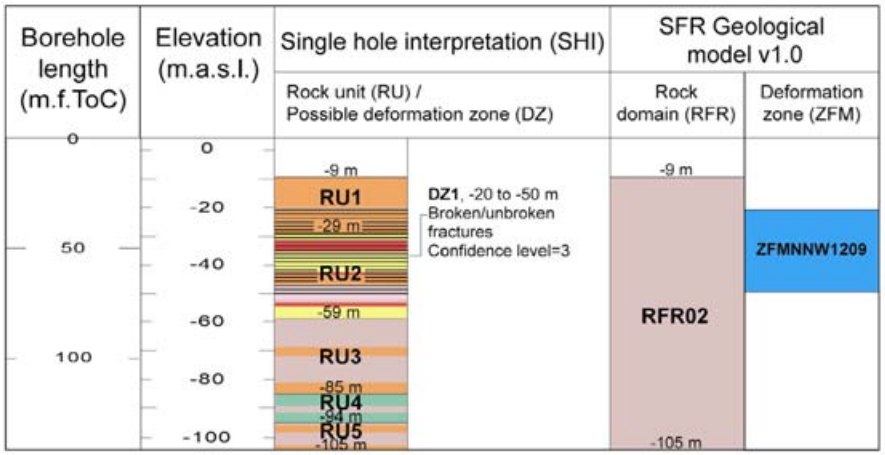

Legend for single hole interpretation

Brittle deformation zone, high confidence

Rock type

Group A

Felsic to intermediate metavolcanic rock

Group B

Granodiorite (to granite), metamorphic, medium - grained

Amphibolite

Group C

Granodiorite to tonalite, metamorphic, fine- to medium-grained

Group D

Granite, fine- to medium-grained

Pegmatitic granite, pegmatite

Deformation zone – orientation set or subset

Modelled deformation zone (ZFM)

Steep NNW

The elevation of a modelled deformation zone is only provided in the cases where the zone boundaries differ from the single hole interpretation.

KFR36

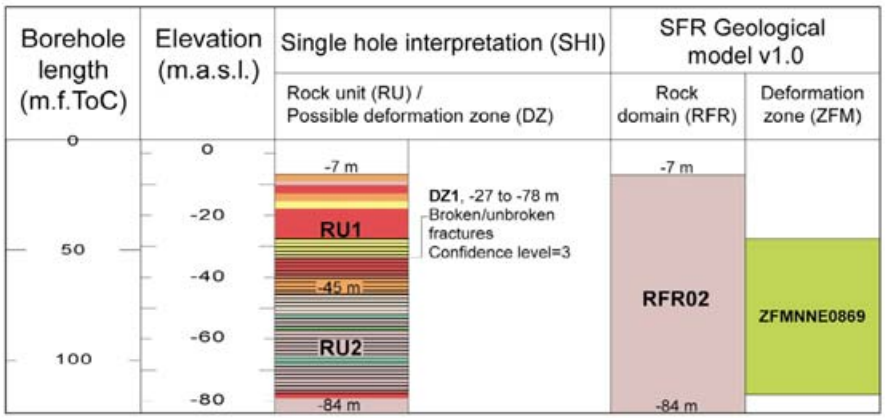

Legend for single hole interpretation

Brittle deformation zone, high confidence

Rock type

Group A

Felsic to intermediate metavolcanic rock

Group B

Granodiorite (to granite), metamorphic, medium - grained

Granite, metamorphic, aplitic

Amphibolite

Diorite, quartz diorite and gabbro, metamorphic

Group D

Granite, fine- to medium-grained

Pegmatitic granite, pegmatite

Deformation zone – orientation set or subset

Modelled deformation zone (ZFM)

Steep NNE

The elevation of a modelled deformation zone is only provided in the cases where the zone boundaries differ from the single hole interpretation.

KFR54

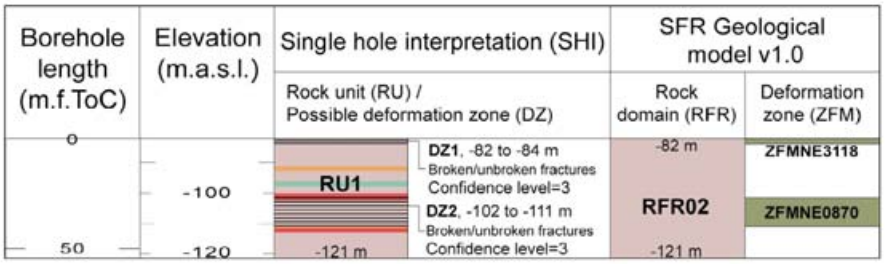

Legend for single hole interpretation

Brittle deformation zone, high confidence

Rock type

Group B

Granodiorite (to granite), metamorphic, medium - grained

Amphibolite

Group D

Granite, fine- to medium-grained

Pegmatitic granite, pegmatite

Deformation zone – orientation set or subset

Modelled deformation zone (ZFM)

Steep NE

The elevation of a modelled deformation zone is only provided in the cases where the zone boundaries differ from the single hole interpretation.

KFR55

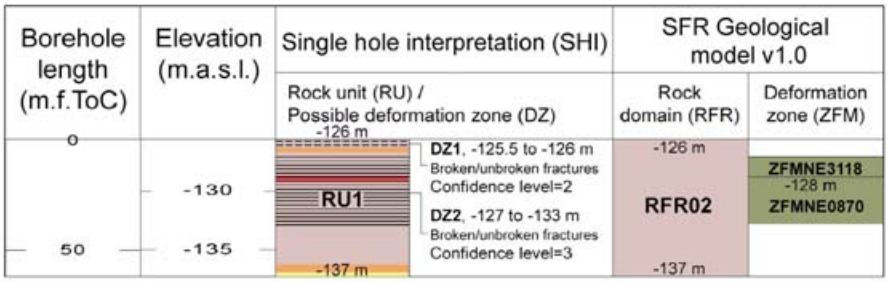

Legend for single hole interpretation

Brittle deformation zone, high confidence

Brittle deformation zone, medium confidence

Rock type

Group A

Felsic to intermediate metavolcanic rock

Group B

Granodiorite (to granite), metamorphic, medium - grained

Group D

Granite, fine- to medium-grained

Pegmatitic granite, pegmatite

Deformation zone – orientation set or subset

Modelled deformation zone (ZFM)

Steep NE

Possible deformation zone not modelled is not coloured

The elevation of a modelled deformation zone is only provided in the cases where the zone boundaries differ from the single hole interpretation.

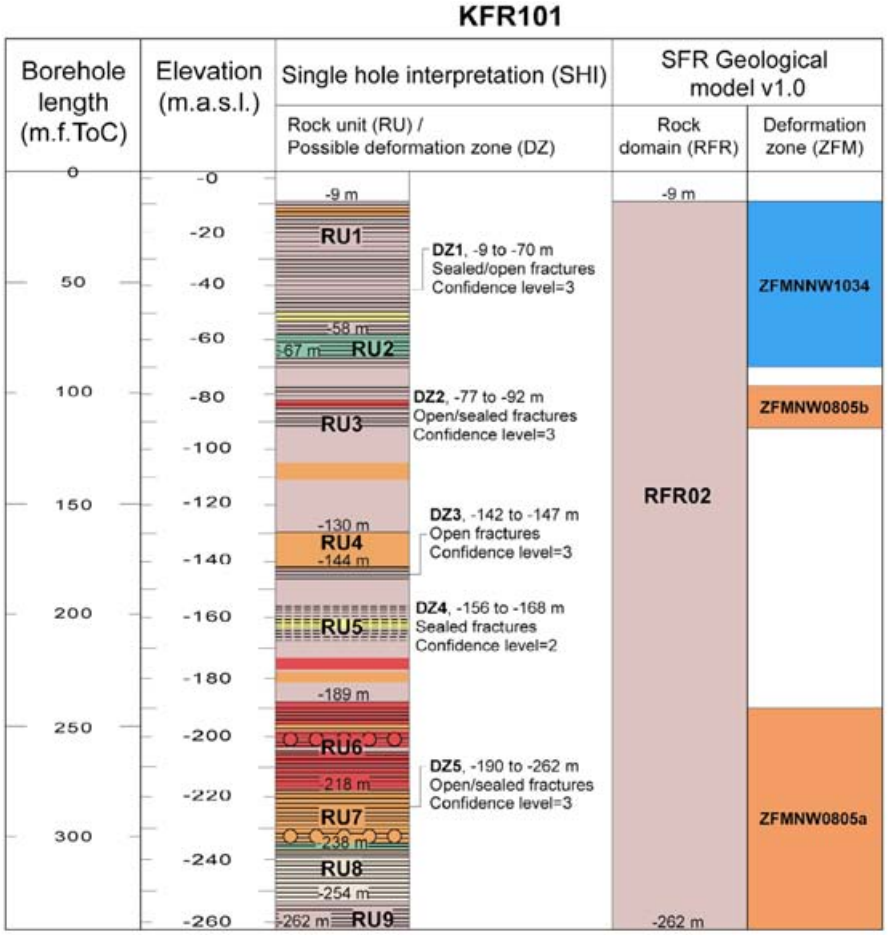

The elevation of a modelled deformation zone is only provided in the cases where the zone boundaries differ from the single hole interpretation.

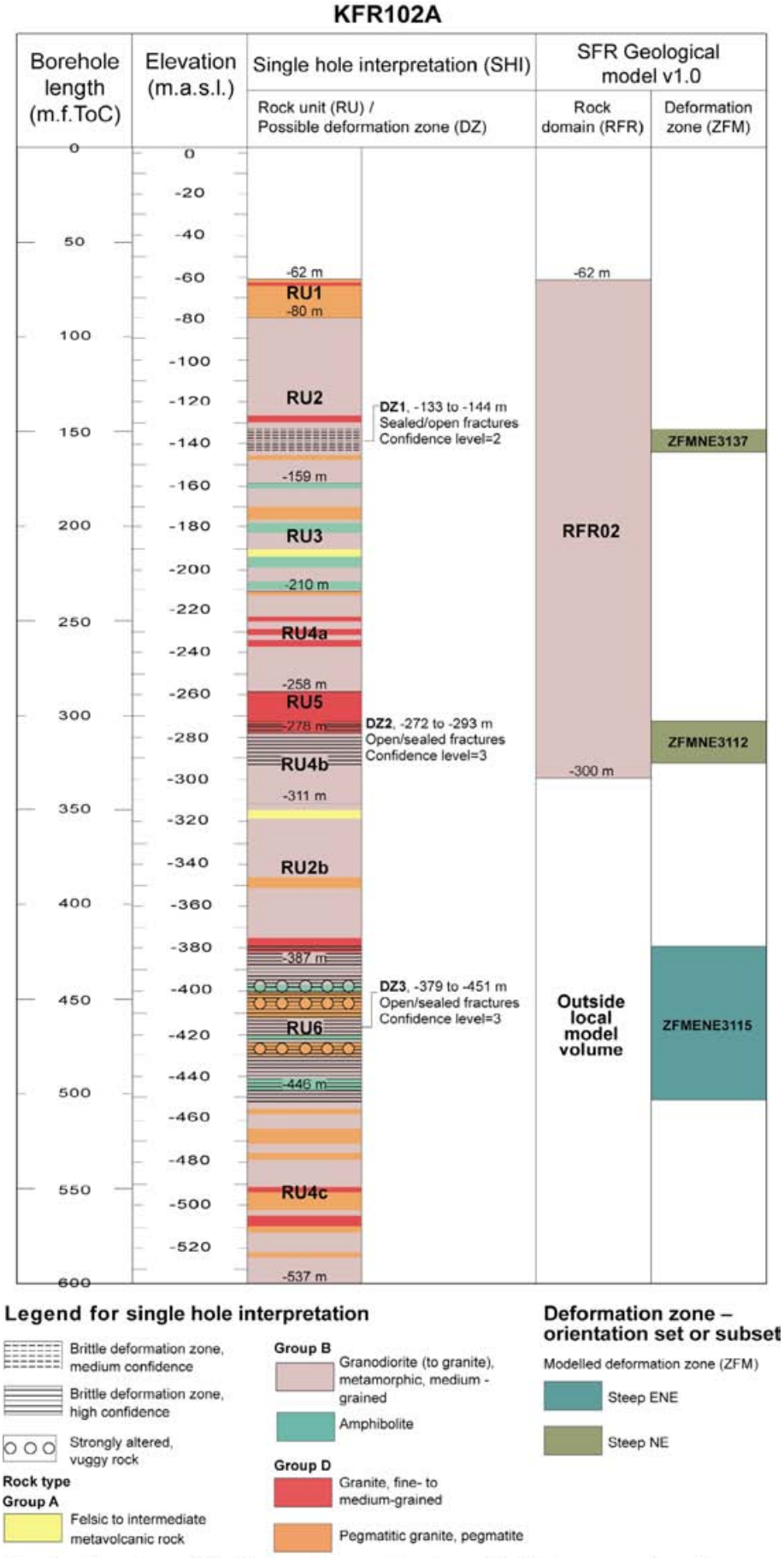

The elevation of a modelled deformation zone is only provided in the cases where the zone boundaries differ from the single hole interpretation.

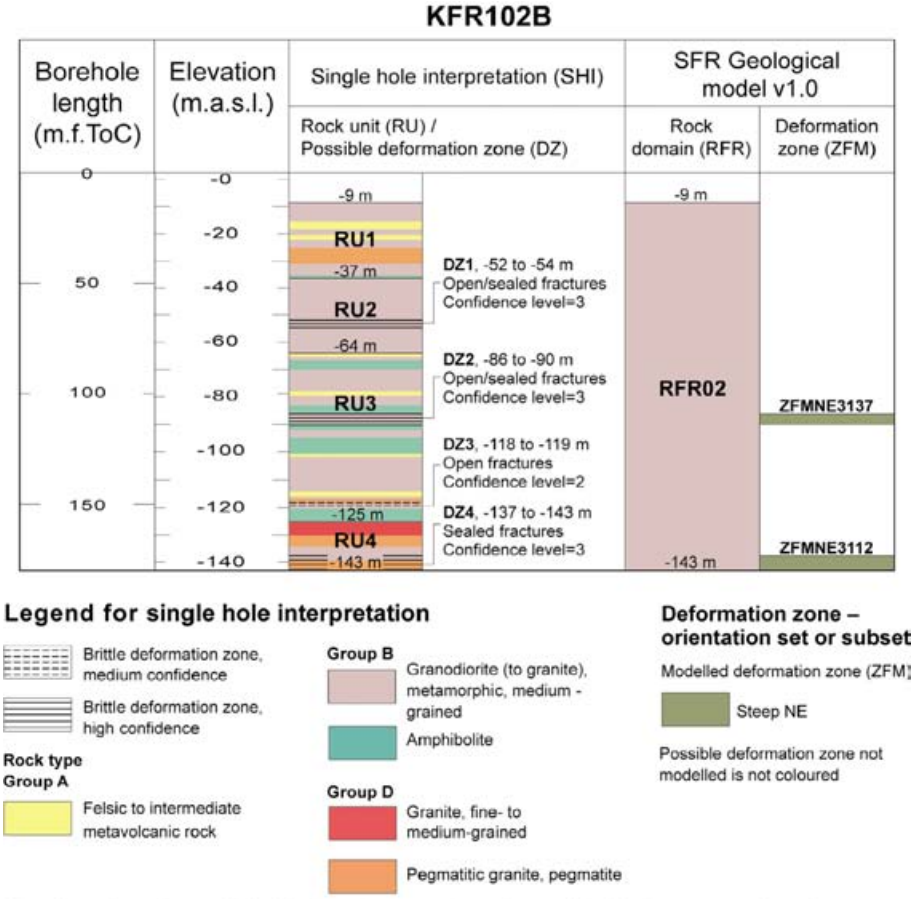

Legend for single hole interpretation

Brittle deformation zone, medium confidence

Brittle deformation zone, high confidence

Rock type

Group A

Felsic to intermediate metavolcanic rock

Group B

Granodiorite (to granite), metamorphic, medium - grained

Amphibolite

Group D

Granite, fine- to medium-grained

Pegmatitic granite, pegmatite

Deformation zone – orientation set or subset

Modelled deformation zone (ZFM)

Steep NE

Possible deformation zone not modelled is not coloured

The elevation of a modelled deformation zone is only provided in the cases where the zone boundaries differ from the single hole interpretation.

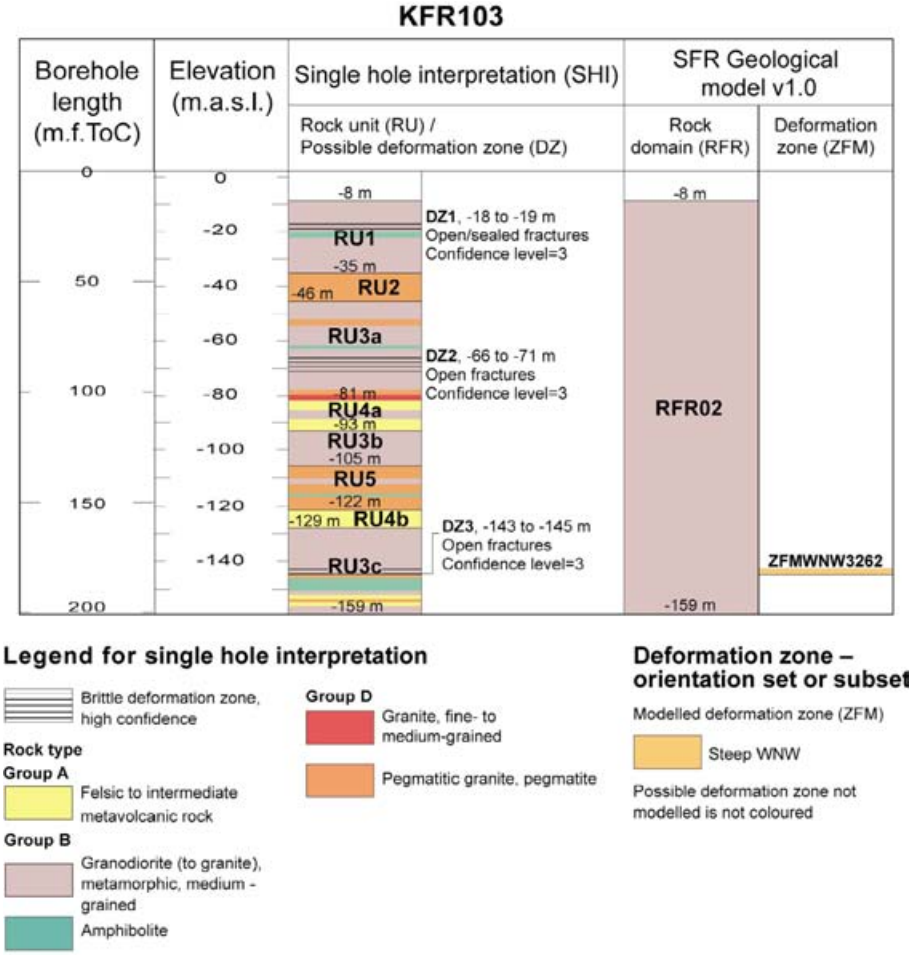

Legend for single hole interpretation

Brittle deformation zone, high confidence

Rock type

Group A

Felsic to intermediate metavolcanic rock

Group B

Granodiorite (to granite), metamorphic, medium - grained

Amphibolite

Group D

Granite, fine- to medium-grained

Pegmatitic granite, pegmatite

Deformation zone – orientation set or subset

Modelled deformation zone (ZFM)

Steep WNW

Possible deformation zone not modelled is not coloured

The elevation of a modelled deformation zone is only provided in the cases where the zone boundaries differ from the single hole interpretation.

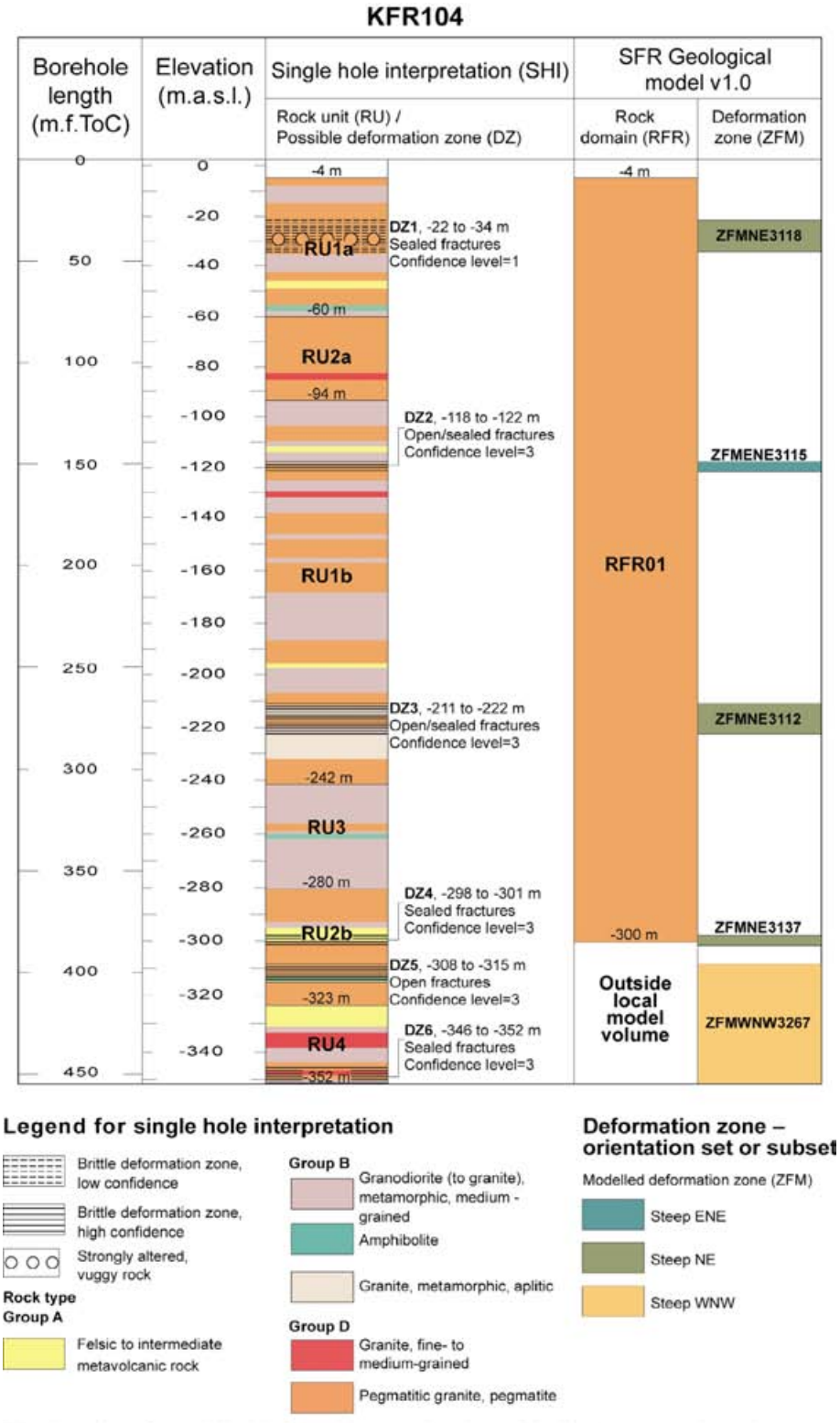

The elevation of a modelled deformation zone is only provided in the cases where the zone boundaries differ from the single hole interpretation.

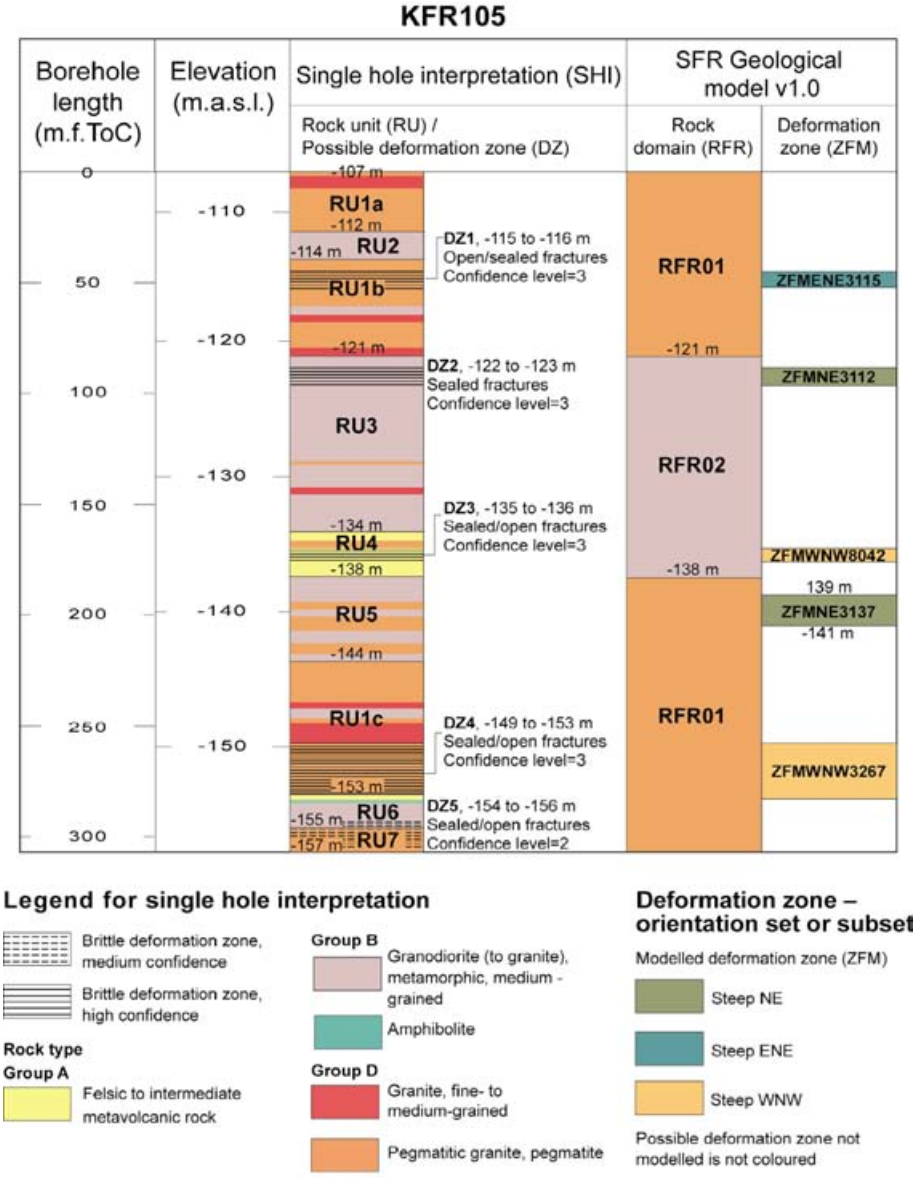

The elevation of a modelled deformation zone is only provided in the cases where the zone boundaries differ from the single hole interpretation.

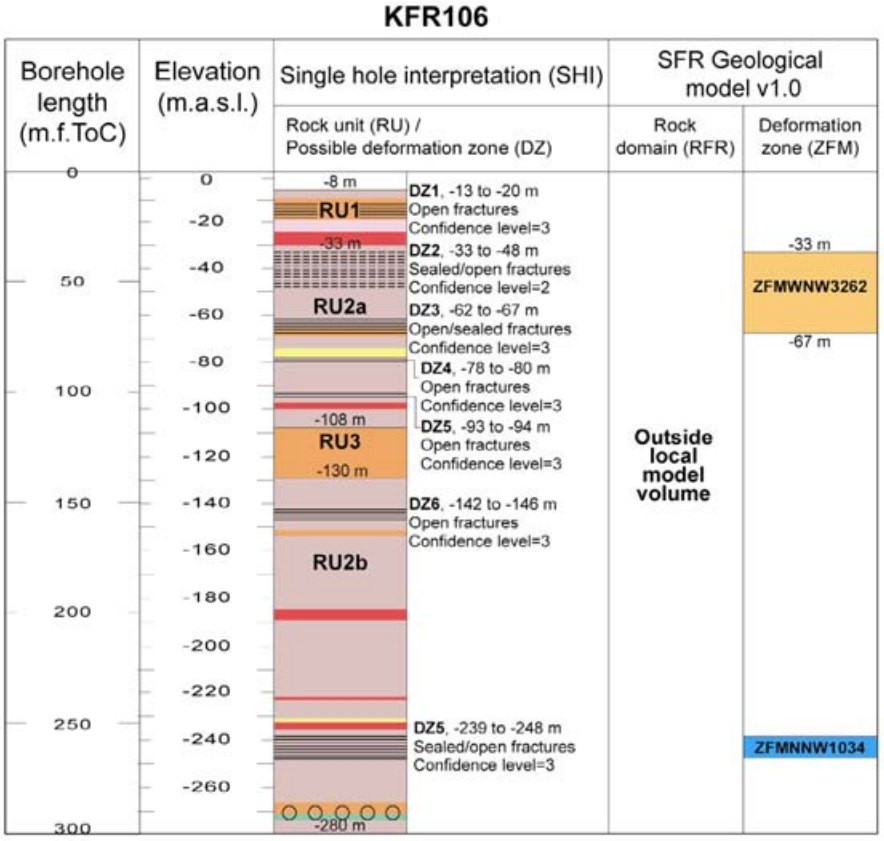

Legend for single hole interpretation

- Brittle deformation zone, medium confidence
- Brittle deformation zone, high confidence
- Strongly altered, vuggy rock

Rock type

Group A
- Felsic to intermediate metavolcanic rock

Group B
- Granodiorite (to granite), metamorphic, medium - grained
- Amphibolite

Group C
- Granodiorite to tonalite, metamorphic, fine- to medium-grained

Group D
- Granite, fine- to medium-grained
- Pegmatitic granite, pegmatite

Deformation zone – orientation set or subset

Modelled deformation zone (ZFM)
- Steep NNW
- Steep WNW

Possible deformation zone not modelled is not coloured

The elevation of a modelled deformation zone is only provided in the cases where the zone boundaries differ from the single hole interpretation.

KFR7A

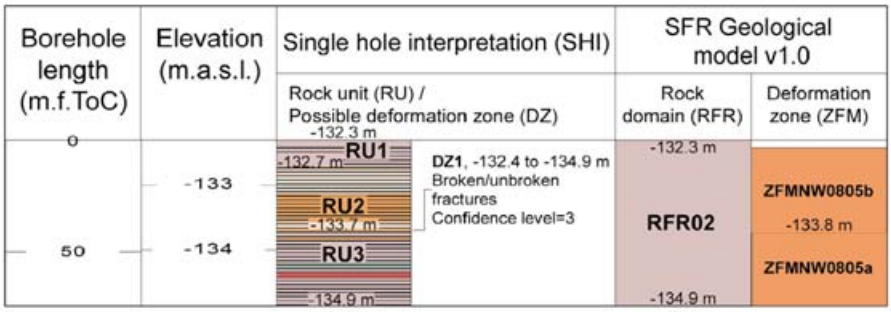

Legend for single hole interpretation

Brittle deformation zone, high confidence

Rock type

Group B

Granodiorite (to granite), metamorphic, medium - grained

Granite, metamorphic, aplitic

Amphibolite

Group D

Granite, fine- to medium-grained

Pegmatitic granite, pegmatite

Deformation zone – orientation set or subset

Modelled deformation zone (ZFM)

Steep NW

The elevation of a modelled deformation zone is only provided in the cases where the zone boundaries differ from the single hole interpretation.

KFR7B

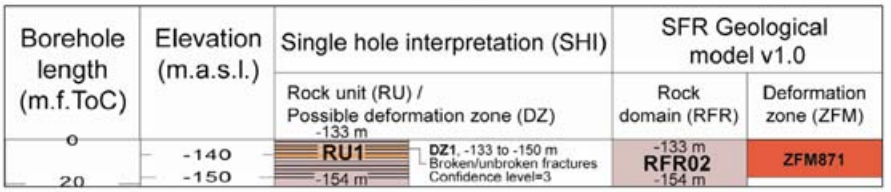

Legend for single hole interpretation

Brittle deformation zone, high confidence

Rock type

Group B

Granodiorite (to granite), metamorphic, medium - grained

Group D

Pegmatitic granite, pegmatite

Deformation zone – orientation set or subset

Modelled deformation zone (ZFM)

Gentle

The elevation of a modelled deformation zone is only provided in the cases where the zone boundaries differ from the single hole interpretation.

KFR7C

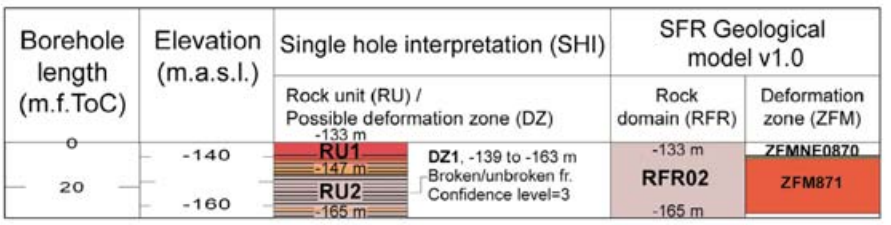

Legend for single hole interpretation

Brittle deformation zone, high confidence

Rock type

Group B

Granodiorite (to granite), metamorphic, medium - grained

Group D

Granite, fine- to medium-grained

Pegmatitic granite, pegmatite

Deformation zone – orientation set or subset

Modelled deformation zone (ZFM)

Steep NE

Gentle

The elevation of a modelled deformation zone is only provided in the cases where the zone boundaries differ from the single hole interpretation.

Appendix 8

Deformation zones in the SFR model version 1.0 on a borehole by borehole and tunnel by tunnel basis

Contents

Table A8-1. Deformation zones on a borehole by borehole basis (SFR model version 1.0). Intercept borehole depths marked in bold indicate the top and bottom levels where multiple SHI sections in the same borehole are taken to represent a single zone; eoh = end of the borehole.

BH	DZ	Geometrical intercept (v1.0) (BH length m)		Target intercept (v1.0) (BH length m)		Intercept defined by geological SHI (BH length m)			Comment
		Sec_up	Sec_low	Sec_up	Sec_low	PDZ	Sec_up	Sec_low	
HFM34	ZFMNW0002	170.32	eoh	**180**	192	DZ2	**180**	184	DZ2 also lies within ZFMWNW0001.
HFM34	ZFMNW0002	170.32	eoh	180	**192**	DZ3	188	**192**	DZ3 also lie within ZFMWNW0001.
HFM34	ZFMWNW0001	0.00	eoh	**37**	192	DZ1	37	133	
HFM34	ZFMWNW0001	0.00	eoh	37	192	DZ2	180	184	DZ2 also lie within ZFMNW0002.
HFM34	ZFMWNW0001	0.00	eoh	37	**192**	DZ3	188	**192**	DZ3 also lies within ZFMNW0002.
HFM35	ZFMNW0002	0.00	54.54	**24**	52.5	DZ1	**24**	33	DZ1 also lies within ZFMWNW0001.
HFM35	ZFMNW0002	0.00	54.54	24	**52.5**	DZ2	47.2	**52.5**	DZ2 also lie within ZFMWNW0001.
HFM35	ZFMWNW0001	0.00	49.27	**24**	52.5	DZ1	**24**	33	DZ1 also lies within ZFMNW0002.
HFM35	ZFMWNW0001	0.00	49.27	24	**52.5**	DZ2	47.2	**52.5**	DZ2 also lie within ZFMNW0002.
HFM35	ZFMWNW1035	180.90	199.19	–	–	DZ3	104	200	DZ3 in HFR105 rather than HFM35 DZ3 has been given a higher priority for defining the ZFMWNW1035 zone geometry. No specific target intercept is defined.
HFR101	ZFMNE0870	19.17	46.17	28	41	DZ1	8.04	58	An interval with slightly increased frequency of steeply dipping (> 65°) fractures, striking SW occurs at approximately 28–41 m length of DZ1. Control point added at 33.02 m, and 28–41 m is taken as target intercept.
HFR101	–	–	–	–	–	DZ2	101	115	See Table A12-1 – PDZ not linked to DZs.
HFR101	ZFMNE3118	183.85	203.09	190	202	DZ3	190	202	
HFR105	ZFMWNW0001	0.00	83.64	**21.12**	31	DZ1	**21.12**	31	
HFR105	ZFMWNW0001	0.00	83.64	88	**92**	DZ2	88	**92**	
HFR105	ZFMWNW1035	117.03	146.16	119	147	DZ3	119	147	
HFR106	–	–	–	–	–	DZ1	38	40	See Table A12-1 – PDZ not linked to DZs.
HFR106	ZFMNNW1034	136.61	179.79	**158**	182	DZ2	**158**	162	
HFR106	ZFMNNW1034	136.61	179.79	158	**182**	DZ3	177	**182**	
KFM06A	ZFMNNE0725	749.14	781.69	740	775	DZ7	740	775	Note: the geometrical intercept comes directly from the DZ_PFM_ Loc_v22_01.rvs model since this intercept is located outside the SFR regional model boundary.
KFM11A	ZFMWNW0001	492.66	831.43	498	824	DZ1	**245**	824	
KFM11A	ZFMWNW0813	247.68	391.95	245	400	DZ1	245	824	

BH	DZ	Geometrical intercept (v1.0) (BH length m)		Target intercept (v1.0) (BH length m)		Intercept defined by geological SHI (BH length m)			Comment
		Sec_up	Sec_low	Sec_up	Sec_low	PDZ	Sec_up	Sec_low	
KFM11A	ZFMWNW1035	714.86	736.38	–	–	DZ1	245	824	The geometrical BH intersection lies within the very extensive SHI DZ1 (245–824 m). BH Section 715–736 m falls within the modelled Singö zone, ZFMWNW0001 itself. The interpreted deformation is attributed to the belt in general without any more specific subdivision. The information from this BH has not been used to define the zone thickness.
KFM11A	ZFMWNW3259	401.86	495.48	400	498	DZ1	245	824	
KFM11A	ZFMNW0002	652.50	735.42	–	–	DZ1	245	**824**	The geometrical BH intersection lies within the very extensive SHI DZ1 (245–824 m). BH Section 653–735 m falls within the modelled Singö zone, ZFMWNW0001 itself. The interpreted deformation is attributed to the belt in general without any more specific subdivision. The information from this BH has not been used to define the zone thickness.
KFR01	ZFMWNW0001	0.00	eoh	0	62.30	DZ1	0	62.30	
KFR02	ZFMNE0870	0	60.99	32.5	37.5	DZ1	32.5	37.5	
KFR02	–	–	–	–	–	DZ2	99.2	100.2	See Table A12-1 – PDZ not linked to DZs.
KFR02	ZFM871	109.18	130.15	114.80	124.45	DZ3	114.80	124.45	
KFR03	–	–	–	–	–	DZ1	6	12	See Table A12-1 – PDZ not linked to DZs.
KFR03	ZFMNE0870	36.39	eoh	**48.00**	95.95	DZ2	**48.00**	53.65	
KFR03	ZFMNE0870	36.39	eoh	48.00	95.95	DZ3	70.42	72.75	
KFR03	ZFMNE0870	36.39	eoh	48.00	**95.95**	DZ4	81.86	**95.95**	
KFR03	ZFM871	78.33	99.73	81.86	95.95	DZ4	81.86	95.95	
KFR04	–	–	–	–	–	DZ1	0	3	See Table A12-1 – PDZ not linked to DZs.
KFR04	ZFMNE0870	2.73	67.69	14	63	DZ2	14	63	
KFR04	ZFM871	84.50	eoh	91	100	–	–	–	Neither of the SHI interpreted possible DZs in KFR04 correlate with ZFM871. However, there are planar chlorite filled fractures from 86 m onwards and some clay filled fractures towards the base of the hole that could be associated with the zone (100.5 m). A target intercept is defined at 91–100 m.
KFR05	ZFM871	76.54	96.27	85	87.90	DZ1	85	87.90	
KFR08	ZFMNW0805B	2.8	32.35	3	19	DZ1	3	19	
KFR08	ZFMNW0805A	40.32	101.46	41	104.4	DZ2	41	104.4	
KFR08	ZFMNNW0999	75.72	81.46	–	–	DZ2	41	104.4	DZ2 is interpreted as being dominated by ZFMNW0805A.
KFR08	ZFMWNW0836	46.04	104.12	–	–	DZ2	41	104.4	DZ2 is interpreted as being dominated by ZFMNW0805A.
KFR09	ZFMNNE0869	0	59.19	0	58.7	DZ1	0	58.7	
KFR09	–	–	–	–	–	DZ2	69	74.3	See Table A12-1 – PDZ not linked to DZs.

BH	DZ	Geometrical intercept (v1.0) (BH length m)		Target intercept (v1.0) (BH length m)		Intercept defined by geological SHI (BH length m)			Comment
		Sec_up	Sec_low	Sec_up	Sec_low	PDZ	Sec_up	Sec_low	
KFR10	ZFMNNE0869	0	97.49	–	–	DZ1	0	5	Judging from the photographs of the drill cores there is a frequency of broken fractures that locally exceeds 10 fractures/m along the target interval. Oxidation of varying degrees occurs frequently throughout the interval 0–97 m. Both the fracture frequency and occurrence of oxidation resembles that for DZ1 in KFR09 DZ1 and KFR36 D1, but is generally slightly lower and less conspicuous, respectively. Thus, ZFMNNE0869 may well have its intersection in this interval, but a specific target intercept cannot be defined.
KFR10	–	–	–	–	–	DZ2	95.65	107.28	See Table A12-1 – PDZ not linked to DZs.
KFR11	ZFMNW0805A	32.63	eoh	41.45	95.65	DZ1	41.45	95.65	
KFR11	ZFMNW0805B	0.00	18.77	–	–	–	–	–	Judging from the photographs of the drill cores there is no obvious indication of a zone with the dignity of ZFMNW0805B along the geometric intercept. The only conspicuous feature is an approximately 2 dm long, intensely fractured interval with moderate oxidation/laumontization at 16 m length. No target intercept is defined.
KFR12	ZFM871	14.73	36.77	21.25	31.50	DZ1	21.25	31.50	
KFR13	–	–	–	–	–	DZ1	20	30	See Table A12-1 – PDZ not linked to DZs.
KFR13	–	–	–	–	–	DZ2	36	41	See Table A12-1 – PDZ not linked to DZs.
KFR13	ZFMNE3118	44.37	eoh	47.5	61	DZ3	47.5	61	
KFR13	ZFM871	53.36	74.99	61	68	DZ4	61	68	
KFR19	–	–	–	–	–	DZ1	38.53	49.32	See Table A12-1 – PDZ not linked to DZs.
KFR20	–	–	–	–	–	DZ1	48.50	52.00	See Table A12-1 – PDZ not linked to DZs.
KFR21	ZFM871	108.57	129.26	–	–	–	–	–	No SHI available.
KFR22	ZFM871	139.98	eoh	–	–	–	–	–	No SHI available.
KFR23	ZFM871	81.75	105.07	–	–	–	–	–	No SHI available.
KFR23	ZFMNW0805A	10.16	11.36	–	–	–	–	–	No SHI available.
KFR24	ZFMNW0805B	0.00	40.81	–	–	–	–	–	No SHI available.
KFR24	ZFMNW0805A	48.99	156.64	–	–	–	–	–	No SHI available.
KFR25	ZFMNW0805B	0.00	62.04	–	–	–	–	–	No SHI available.
KFR25	ZFMNW0805A	50.13	195.09	–	–	–	–	–	No SHI available.
KFR25	ZFMWNW0836	64.07	144.25	–	–	–	–	–	No SHI available.
KFR27	ZFMWNW0835	0.00	153.31	108	120	DZ1	108	120	
KFR27	ZFMWNW0835	195.98	470.56	**323**	469	DZ2	**323**	379.5	
KFR27	ZFMWNW0835	195.98	470.56	323	469	DZ3	389	401	
KFR27	ZFMWNW0835	195.98	470.56	323	**469**	DZ4	421	**469**	

BH	DZ	Geometrical intercept (v1.0) (BH length m)		Target intercept (v1.0) (BH length m)		Intercept defined by geological SHI (BH length m)			Comment
		Sec_up	Sec_low	Sec_up	Sec_low	PDZ	Sec_up	Sec_low	
KFR31	–	–	–	–	–	DZ1	82.05	91.70	See Table A12-1 – PDZ not linked to DZs.
KFR31	ZFM871	217.28	eoh	228.76	232	DZ2	228.76	232	
KFR31	ZFMNE0870	222.79	eoh	228.76	232	DZ2	228.76	232	
KFR32	–	–	–	–	–	DZ1	155.70	159	See Table A12-1 – PDZ not linked to DZs.
KFR32	ZFM871	161.72	186.25	163.10	186.10	DZ2	163.10	186.10	
KFR33	ZFMNNW1209	46.19	114.64	–	–	–	–	–	No SHI available.
KFR33	ZFM871	158.04	eoh	–	–	–	–	–	No SHI available.
KFR35	ZFMNNW1209	32.90	71.04	32.7	70	DZ1	32.7	70	
KFR36	ZFMNNE0869	27.80	118.84	45	115.5	DZ1	45	115.5	
KFR37	–	–	–	–	–	DZ1	36.60	45.60	See Table A12-1 – PDZ not linked to DZs.
KFR37	ZFM871	172.25	200.89	183.43	193.60	DZ2	183.43	193.60	
KFR38	ZFMNW0805B	105.19	eoh	153.60	181.65	DZ1	153.60	181.65	
KFR51	–	–	–	–	–	DZ1	9.84	11.15	See Table A12-1 – PDZ not linked to DZs.
KFR52	–	–	–	–	–	DZ1	19.85	22.40	See Table A12-1 – PDZ not linked to DZs.
KFR53	ZFMNE0870	18.72	37.01	–	–	–	–	–	No SHI available.
KFR54	ZFMNE3118	0.00	7.42	0	2.5	DZ1	0	2.5	
KFR54	ZFMNE0870	25.31	42.18	27	40	DZ2	27	40	
KFR55	–	–	–	–	–	DZ1	0	3.3	See Table A12-1 – PDZ not linked to DZs.
KFR55	ZFMNE3118	8.65	16.80	**8**	17	DZ2	8	38	Division of DZ2 between ZFMNE0870 and ZFMNE3118.
KFR55	ZFMNE0870	17.09	42.69	17	**38**	DZ2	8	38	Division of DZ2 between ZFMNE0870 and ZFMNE3118.
KFR56	ZFMNW0805B	3.92	44.46	–	–	–	–	–	No SHI available.
KFR56	ZFMNW0805A	57.18	eoh	–	–	–	–	–	No SHI available.
KFR57	ZFM871	6.00	eoh	15.85	25.38	DZ1	15.85	25.38	
KFR61	ZFMWNW0001	0.00	eoh	1.40	70.90	DZ1	1.40	70.90	
KFR62	ZFMWNW0001	0.00	eoh	45.64	82.80	DZ1	45.64	82.80	
KFR64	ZFMWNW0001	0.00	eoh	12.79	54.17	DZ1	12.79	54.17	
KFR65	ZFMWNW0001	0.00	eoh	17.63	39.68	DZ1	17.63	39.68	
KFR66	ZFMWNW0001	0.00	eoh	14.99	29.17	DZ1	14.99	29.17	
KFR67	ZFMWNW0001	0.00	eoh	13.74	48.95	DZ1	13.74	48.95	
KFR68	ZFMNNE0869	43.93	eoh	**71.59**	105.13	DZ1	**71.59**	78.11	Note: KFR68 is interpreted as intercepting the meeting point between ZFMNNE0869 and ZFMNE0870. Since the BH lacks fracture orientation data it is impossible to correlate the PDZ with any specific steeply dipping zone. Thus, the PDZ is taken as target intercept for both ZFMNE0870 and ZFMNNE0869.
KFR68	ZFMNNE0869	43.93	eoh	71.59	**105.13**	DZ2	102.83	**105.13**	
KFR68	ZFMNE0870	60.25	93.99	**71.59**	105.13	DZ1	**71.59**	78.11	
KFR68	ZFMNE0870	60.25	93.99	71.59	**105.13**	DZ2	102.83	**105.13**	

BH	DZ	Geometrical intercept (v1.0) (BH length m)		Target intercept (v1.0) (BH length m)		Intercept defined by geological SHI (BH length m)			Comment
		Sec_up	Sec_low	Sec_up	Sec_low	PDZ	Sec_up	Sec_low	
KFR68	ZFMWNW1035	0.00	5.19	–	–	–	–	–	No target intercept defined. Higher priority has been given to tunnel, HFR105 and HFM35 when defining the zone geometry.
KFR69	–	–	–	–	–	DZ1	52.38	79.00	See Table A12-1 – PDZ not linked to DZs.
KFR69	–	–	–	–	–	DZ2	121.60	146.10	See Table A12-1 – PDZ not linked to DZs.
KFR70	ZFMNE0870	34.91	92.80	–	–	–	–	–	Judging from the photographs of the drill cores there is no obvious indication of a possible zone along the geometric intercept. The fracture frequency is generally less than 10 fractures/m and oxidation or other alterations cannot be distinguished. No target intercept has been defined.
KFR71	ZFMWNW0001	0.00	eoh	**65.67**	69.50	DZ1	**65.67**	69.50	The borehole lies wholly within ZFMWNW0001.
KFR71	ZFMWNW0001	0.00	eoh	72.14	**120.90**	DZ2	72.14	**120.90**	The borehole lies wholly within ZFMWNW0001.
KFR80	ZFM871	0.00	13.29	–	–	–	–	–	No SHI available.
KFR83	ZFM871	5.28	eoh	–	–	–	–	–	No SHI available.
KFR101	ZFMNNW1034	8.42	79.85	13.72	88	DZ1	13.72	88	
KFR101	ZFMNW0805B	80.26	131.55	97	116	DZ2	97	116	
KFR101	–	–	–	–	–	DZ3	179	186	See Table A12-1 – PDZ not linked to DZs.
KFR101	–	–	–	–	–	DZ4	197	213	See Table A12-1 – PDZ not linked to DZs.
KFR101	ZFMNW0805A	217.39	334.48	242	341.76	DZ5	242	341.76	
KFR102A	ZFMNE3137	147.83	160.74	149	161	DZ1	149	161	
KFR102A	ZFMNE3112	299.70	323.05	302	325	DZ2	302	325	
KFR102A	ZFMENE3115	423.71	503.36	422	503	DZ3	422	503	
KFR102B	–	–	–	–	–	DZ1	67	70	See Table A12-1 – PDZ not linked to DZs.
KFR102B	ZFMNE3137	106.92	116.23	109	114	DZ2	109	114	
KFR102B	–	–	–	–	–	DZ3	149.5	150.5	See Table A12-1 – PDZ not linked to DZs
KFR102B	ZFMNE3112	170.32	eoh	173	180	DZ4	173	180	
KFR103	–	–	–	–	–	DZ1	24.5	26.5	See Table A12-1 – PDZ not linked to DZs
KFR103	–	–	–	–	–	DZ2	84	91	See Table A12-1 – PDZ not linked to DZs
KFR103	ZFMWNW3262	178.46	183.59	180	182.5	DZ3	180	182.5	
KFR104	ZFMNE0870	0.00	1.88	–	–	–	–	–	The geometrical intercept is at the modelled zone margin. No target intercept is defined.
KFR104	ZFMNE3118	29.73	45.95	30	45.5	DZ1	30	45.5	
KFR104	ZFMENE3115	117.33	168.86	149	154	DZ2	149	154	
KFR104	ZFMNE3112	265.84	282.99	268	283	DZ3	268	283	

BH	DZ	Geometrical intercept (v1.0) (BH length m)		Target intercept (v1.0) (BH length m)		Intercept defined by geological SHI (BH length m)			Comment
		Sec_up	Sec_low	Sec_up	Sec_low	PDZ	Sec_up	Sec_low	
KFR104	ZFMNE3137	380.85	388.50	382	387	DZ4	382	387	
KFR104	ZFMWNW3267	388.50	eoh	**396**	454.57	DZ5	**396**	405	
KFR104	ZFMWNW3267	388.50	eoh	396	**454.57**	DZ6	447	**454.57**	
KFR105	ZFMENE3115	32.87	62.47	45	52	DZ1	45	52	
KFR105	ZFMNE3112	87.69	99.69	88.5	96.5	DZ2	88.5	96.5	
KFR105	ZFMWNW8042	170.49	176.34	170.8	176	DZ3	170.8	176	
KFR105	ZFMWNW3267	257.84	282.99	258	283	DZ4	258	283	
KFR105	–	–	–	–	–	DZ5	293.6	304	See Table A12-1 – PDZ not linked to DZs.
KFR105	ZFMNE3137	203.99	209.71	191	205	–	–	–	There is no SHI DZ interpreted in the position of the target intercept in KFR105. However, the modelled geometry generates an intercept in KFR105 with a section of core that coincides with an interval of increased frequency of steeply dipping fractures that strike NE at 191 to 193 m length. In addition, two NE-striking sealed networks at 202.7–203.8 and 204.2–204.8 m with piece lengths of 30 and 15 mm, respectively, along with NE-striking crush at 205.0–205.05 m.
KFR106	–	–	–	–	–	DZ1	15	20	See Table A12-1 – PDZ not linked to DZs.
KFR106	–	–	–	–	–	DZ2	36.5	52	See Table A12-1 – PDZ not linked to DZs.
KFR106	ZFMWNW3262	67.04	75.34	67	73	DZ3	67	73	
KFR106	–	–	–	–	–	DZ4	84.5	86.0	See Table A12-1 – PDZ not linked to DZs.
KFR106	–	–	–	–	–	DZ5	100.5	101	See Table A12-1 – PDZ not linked to DZs.
KFR106	–	–	–	–	–	DZ6	153	157	See Table A12-1 – PDZ not linked to DZs.
KFR106	ZFMNNW1034	200.93	271.05	256	266	DZ7	256	266	
KFR7A	ZFMNW0805B	11.13	43.20	**3.5**	43.00	DZ1	**3.5**	74.45	Subdivision of DZ1 between ZFMNW0805A and ZFMNW0805B.
KFR7A	ZFMNW0805A	43.61	eoh	43.00	**74.45**	DZ1	3.5	**74.45**	Subdivision of DZ1 between ZFMNW0805A and ZFMNW0805B.
KFR7A	ZFM871	0.00	11.13	–	–	DZ1	3.5	74.45	DZ1 is interpreted as being dominated by ZFMNW0805A and ZFM-NW0805B due to the brittle ductile style of deformation seen in the core. No target intercept for ZFM871 is defined.
KFR7B	ZFM871	0.00	20.39	0	17	DZ1	0	17	
KFR7B	ZFMNE0870	20.27	eoh	–	–	–	–	–	The geometrical intercept is at the modelled zone margin. No target intercept is defined.
KFR7C	ZFMNE0870	0.00	28.72	6.23	7.15	DZ1	6	32	The intercept is considered to be dominated by ZFM871. However, a short section between 6.23–7.15 m contains laumontite filled fractures with low alpha angles that are taken to represent ZFMNE0870.
KFR7C	ZFM871	5.91	32.74	6	32	DZ1	6	32	

Table A8-2. Deformation zones on a tunnel by tunnel basis (SFR model version 1.0). Target intercepts are quoted as tunnel centreline intercepts and are based on the tunnel deformation zones (tDZ) in Appendix 2 complemented by inspection of the detailed geological tunnel mapping results as presented in /Christiansson and Bolvede 1987/.

SFR Facility part	DZ	Geometrical intercept (v1.0) (chainage m)		Target intercept (v1.0) (chainage m)		tDZ given in Appendix 2	Comment and description
DT	ZFMWNW0813	0+062	0+138	0+065	0+128	–	Target intercept mainly based on the shotcrete coverage marked in the detailed tunnel mapping.
DT	ZFMWNW3259	0+128	0+180	0+142	0+170	tDZ6	Target intercept defined from the detailed tunnel mapping of /Christiansson and Bolvede 1987/ and includes tDZ6.
DT	ZFMWNW0001	0+155	0+362	0+212	0+295	tDZ7 to tDZ18	
DT	ZFMNW0002	0+310	0+365	0+309	0+372	tDZ19 to tDZ22	
DT	ZFMWNW1035	0+420	0+435	0+420	0+433	tDZ25 to tDZ28	
DT	ZFMNNE0869	0+430	0+555	0+430	0+530	tDZ30 to tDZ32 and tDZ34	
DT	ZFMNE0870	0+470	0+600	0+535	0+570	tDZ40	
DT	ZFMNE0870	DT-BT connection tunnel at 0+610		DT-BT connection tunnel at 0+610		tDZ40	
DT	ZFMNNW1209	0+920	0+945	0+930	0+930	tDZ59	
BT	ZFMWNW0813	0+042	0+120	0+042	0+082	tDZ3–tDZ5	
BT	ZFMWNW3259	0+108	0+158	0+120	0+150	–	Target intercept mainly based on the shotcrete coverage marked in the detailed tunnel mapping.
BT	ZFMWNW0001	0+140	0+345	0+189	0+283	tDZ7 to tDZ18	
BT	ZFMNW0002	0+292	0+345	0+297	0+347	tDZ19 to tDZ22	
BT	ZFMNNE0869	0+357	0+482	0+355	0+450	tDZ30 to tDZ32 and tDZ34	
BT	ZFMWNW1035	0+398	0+412	0+398	0+416	tDZ25 to tDZ28	
BT	ZFMNE0870	0+620	0+780	0+640	0+690	tDZ40	
BT	ZFMNE0870	0+860	0+925	0+888	0+907	tDZ56	
BT	ZFMNNW1209	0+885	0+907	0+893	0+893	–	Possible low confidence observation based on detailed drawing –09 /Christiansson and Bolvede 1987/.
BT	ZFMNE0870	1+017	1+055	1+020	1+050	tDZ66	
BT	ZFMNE3118	1+075	1+095	1+095	1+095	tDZ73	

SFR Facility part	DZ	Geometrical intercept (v1.0) (chainage m)		Target intercept (v1.0) (chainage m)		tDZ given in Appendix 2	Comment and description
BT	ZFMNW0805B	1+178	1+193	1+182	1+185	–	Several vertical NNW-SSE striking fractures (approximately 160°/90°) that penetrate the entire tunnel perimeter at 6/182–6/185. Some of the fractures are marked as “damp” in the detailed drawing –11 of /Christiansson and Bolvede 1987/. This is taken as a target intercept for ZFMNW0805B.
1B	ZFMNW0805B	0+023	0+044	–	–	–	Generally a high frequency of vertical NW-SE striking fractures (approximately 130°/90°) from the connection with IST and onwards towards north. The fracture set is conspicuous in all parts included in detailed drawing –12 of /Christiansson and Bolvede 1987/ and it is not possible to define a specific target intercept.
BT/ST	ZFMNE3118	1+130	1+166	1+166	–	tDZ73	tDZ73 at 0+088 in ST.
NBT	ZFMNE0870	0+000	0+010	–	–	–	
NBT	ZFMNNW1209	0+000	0+010	–	–	–	
NBT	ZFMNE3118	0+055	0+63	0+055	0+059	–	Target intercept based on shotcrete coverage marked in the detailed tunnel mapping.
NBT	ZFMNE3118	0+295	0+315	0+295	0+340	tDZ73	
NBT	ZFMNE0870	0+350	0+365	0+352	0+352	tDZ80	
NBT	ZFM871	0+382	0+432	0+405	0+432	tDZ101 to tDZ104	
STT	ZFMNE0870	0+800	0+820	0+810	0+820	tDZ66	
IST	ZFMNE0870	0+078	0+095	0+088	0+088	tDZ80	
1 BTF	ZFMNNW1209	0+090	0+117	0+100	0+100	tDZ59	
2 BTF	ZFMNNW1209	0+070	0+090	0+078	0+080	tDZ59 and tDZ126	
BLA	ZFMNNW1209	0+048	0+068	0+055	0+060	tDZ59 and tDZ126	
BMA	ZFMNNW1209	0+030	0+055	0+030	0+030	tDZ59	

Appendix 9

Summary of borehole and tunnel intercepts for each deformation zone in SFR model version 1.0

Contents

Table A9-1. Summary of borehole intercepts for each deformation zone (SFR model version 1.0). Intercept borehole depths marked in bold indicate the top and bottom levels where multiple SHI sections in the same borehole are taken to represent a single zone; eoh = end of the borehole.

DZ	BH	Geometrical intercept (v1.0) (BH length m)		Target intercept (v1.0) (BH length m)		Intercept defined by geological SHI (BH length m)			Comment	Terminated against following DZs
		Sec_up	Sec_low	Sec_up	Sec_low	PDZ	Sec_up	Sec_low		
Gently dipping DZs (dip < 45°)										
ZFM871	KFR02	109.18	130.15	114.80	124.45	DZ3	114.80	124.45		ZFMENE3115, ZFMNNE0869, ZFMNW0805A, ZFMNW0805B, ZFMWNW1035
ZFM871	KFR03	78.33	99.73	81.86	95.95	DZ4	81.86	95.95		
ZFM871	KFR04	84.50	eoh	91	100	–	–	–	Neither of the SHI interpreted possible DZs in KFR04 correlate with ZFM871. However, there are planar chlorite filled fractures from 86 m onwards and some clay filled fractures towards the base of the hole that could be associated with the zone (100.5 m). A target intercept is defined at 91–100 m.	
ZFM871	KFR05	76.54	96.27	85.00	87.90	DZ1	85.00	87.90		
ZFM871	KFR12	14.73	36.77	21.25	31.50	DZ1	21.25	31.50		
ZFM871	KFR13	53.36	74.99	61	68	DZ4	61	68		
ZFM871	KFR21	108.57	129.26	–	–	–	–	–	No SHI available.	
ZFM871	KFR22	139.98	eoh	–	–	–	–	–	No SHI available.	
ZFM871	KFR23	81.75	105.07	–	–	–	–	–	No SHI available.	
ZFM871	KFR31	217.28	eoh	228.76	232.00	DZ2	228.76	232.00		
ZFM871	KFR32	161.72	186.25	163.10	186.10	DZ2	163.10	186.10		
ZFM871	KFR33	158.04	eoh	–	–	–	–	–	No SHI available.	
ZFM871	KFR37	172.25	200.89	183.43	193.60	DZ2	183.43	193.60		
ZFM871	KFR57	6.00	eoh	15.85	25.38	DZ1	15.85	25.38		
ZFM871	KFR80	0.00	13.29	–	–	–	–	–	No SHI available.	
ZFM871	KFR83	5.28	eoh	–	–	–	–	–	No SHI available.	

DZ	BH	Geometrical intercept (v1.0) (BH length m)		Target intercept (v1.0) (BH length m)		Intercept defined by geological SHI (BH length m)			Comment	Terminated against following DZs
		Sec_up	Sec_low	Sec_up	Sec_low	PDZ	Sec_up	Sec_low		
ZFM871	KFR7A	0.00	11.13	–	–	DZ1	3.5	74.45	DZ1 is interpreted as being dominated by ZFMNW0805A and ZFMNW0805B due to the brittle ductile style of deformation seen in the core. No target intercept for ZFM871 is defined.	
ZFM871	KFR7B	0.00	20.39	0	17	DZ1	0	17		
ZFM871	KFR7C	5.91	32.74	6	32	DZ1	6	32		
ZFMA1	–	–	–	–	–	–	–	–	Seismic reflector. The extension of which has been modified in /Juhlin and Zhang 2010/.	ZFMWNW0001
ZFMB10	–	–	–	–	–	–	–	–	Seismic reflector.	ZFMNW0805A, ZFMNW0805B, ZFMWNW0001, ZFMWNW1035
Steeply dipping DZs (dip > 45°)										
NNE to ENE set										
ZFMENE3115	KFR102A	423.71	503.36	422	503	DZ3	422	503		ZFMNW0002, ZFMNW0805A, ZFMWNW1035
ZFMENE3115	KFR104	117.33	168.86	149	154	DZ2	149	154		
ZFMENE3115	KFR105	32.87	62.47	45	52	DZ1	45	52		
ZFMENE3135	–	–	–	–	–	–	–	–	Low magnetic lineament.	ZFMNNW1034, ZFMWNW8043
ZFMENE3151	–	–	–	–	–	–	–	–	Low magnetic lineament.	ZFMNW0805A, ZFMNNE3264
ZFMENE8031	–	–	–	–	–	–	–	–	Low magnetic lineament.	ZFMNNE0869, ZFMWNW1035,
ZFMENE8034	–	–	–	–	–	–	–	–	Low magnetic lineament.	ZFMNNE0869
ZFMNE0870	HFR101	19.17	46.17	28	41	DZ1	8.04	58	An interval with slightly increased frequency of steeply dipping (> 65°) fractures, striking SW occurs at approximately 28–41 m length of DZ1. Control point added at 33.02 m, and 28-41 m is taken as target intercept.	ZFMNE3118, ZFMNNE0869, ZFMNW0805A, ZFMNW0805B, ZFMWNW1035
ZFMNE0870	KFR02	0	60.99	32.5	37.5	DZ1	32.5	37.5		

DZ	BH	Geometrical intercept (v1.0) (BH length m)		Target intercept (v1.0) (BH length m)		Intercept defined by geological SHI (BH length m)			Comment	Terminated against following DZs
		Sec_up	Sec_low	Sec_up	Sec_low	PDZ	Sec_up	Sec_low		
ZFMNE0870	KFR03	36.39	eoh	**48.00**	95.95	DZ2	**48.00**	53.65		
ZFMNE0870	KFR03	36.39	eoh	48.00	95.95	DZ3	70.42	72.75		
ZFMNE0870	KFR03	36.39	eoh	48.00	**95.95**	DZ4	81.86	**95.95**		
ZFMNE0870	KFR04	2.73	67.69	14	63	DZ2	14	63		
ZFMNE0870	KFR31	222.79	eoh	228.76	232	DZ2	228.76	232		
ZFMNE0870	KFR53	18.72	37.01	–	–	–	–	–	No SHI available.	
ZFMNE0870	KFR54	25.31	42.18	27	40	DZ2	27	40		
ZFMNE0870	KFR55	17.09	42.69	17	38	DZ2	8	38	Subdivision of DZ2 between ZFMNE0870 and ZFMNE3118.	
ZFMNE0870	KFR68	60.25	93.99	**71.59**	105.13	DZ1	**71.59**	78.11	Note: KFR68 is interpreted as intercepting the meeting point between ZFMNNE0869 and ZFMNE0870. Since the BH lacks fracture orientation data it is impossible to correlate the PDZ with any specific steeply dipping zone. Thus, the PDZ is taken as target intercept for both ZFMNE0870 and ZFMNNE0869.	
ZFMNE0870	KFR68	60.25	93.99	71.59	**105.13**	DZ2	102.83	**105.13**		
ZFMNE0870	KFR70	34.91	92.80	–	–	–	–	–	Judging from the photographs of the drill cores there is no obvious indication of a possible zone along the geometric intercept. The fracture frequency is generally less than 10 fractures/m and oxidation or other alterations cannot be distinguished. No target intercept has been defined.	
ZFMNE0870	KFR104	0.00	1.88	–	–	–	–	–	The geometrical intercept is at the modelled zone margin. No target intercept is defined.	
ZFMNE0870	KFR7B	20.27	eoh	–	–	–	–	–	The geometrical intercept is at the modelled zone margin. No target intercept is defined.	
ZFMNE0870	KFR7C	0.00	28.72	6.23	7.15	DZ1	6	32	The intercept is considered to be dominated by ZFM871. However, a short section between 6.23–7.15 m contains laumontite filled fractures with low alpha angles that are taken to represent ZFMNE0870.	

DZ	BH	Geometrical intercept (v1.0) (BH length m)		Target intercept (v1.0) (BH length m)		Intercept defined by geological SHI (BH length m)			Comment	Terminated against following DZs
		Sec_up	Sec_low	Sec_up	Sec_low	PDZ	Sec_up	Sec_low		
ZFMNE3112	KFR102A	299.70	323.05	302	325	DZ2	302	325		ZFMNW0805B, ZFMWNW8043
ZFMNE3112	KFR102B	170.32	eoh	173	180	DZ4	173	180		
ZFMNE3112	KFR104	265.84	282.99	268	283	DZ3	268	283		
ZFMNE3112	KFR105	87.69	99.69	88.5	96.5	DZ2	88.5	96.5		
ZFMNE3118	HFR101	183.85	203.09	190	202	DZ3	190	202		ZFMENE3115, ZFMNW0805B, ZFMWNW1035
ZFMNE3118	KFR13	44.37	eoh	47.5	61	DZ3	47.5	61		
ZFMNE3118	KFR54	0.00	7.42	0	2.5	DZ1	0	2.5		
ZFMNE3118	KFR55	8.65	16.80	8	17	DZ2	8	38	Subdivision of DZ2 between ZFMNE0870 and ZFMNE3118.	
ZFMNE3118	KFR104	29.73	45.95	30	45.5	DZ1	30	45.5		
ZFMNE3134	–	–	–	–	–	–	–	–	Low magnetic lineament.	ZFMWNW0835, ZFMWNW1035
ZFMNE3137	KFR102A	147.83	160.74	149	161	DZ1	149	161		ZFMNW0805B, ZFMWNW1035
ZFMNE3137	KFR102B	106.92	116.23	109	114	DZ2	109	114		
ZFMNE3137	KFR104	380.85	388.50	382	387	DZ4	382	387		
ZFMNE3137	KFR105	203.99	209.71	191	205	–	–	–	There is no SHI DZ interpreted in the position of the target intercept in KFR105. However, the modelled geometry generates an intercept in KFR105 with a section of core that coincides with an interval of increased frequency of steeply dipping fractures that strike NE at 191 to 193 m length. In addition, two NE-striking sealed networks at 202.7–203.8 and 204.2–204.8 m with piece lengths of 30 and 15 mm, respectively, along with NE-striking crush at 205.0–205.05 m.	
ZFMNNE0725	KFM06A	749.14	781.69	740	775	DZ7	740	775	Note: the added geometrical intercept comes directly from the DZ_PFM_Loc_v22_01.rvs model since this intercept is located outside the SFR regional model boundary.	ZFMWNW3259

DZ	BH	Geometrical intercept (v1.0) (BH length m)		Target intercept (v1.0) (BH length m)		Intercept defined by geological SHI (BH length m)			Comment	Terminated against following DZs
		Sec_up	Sec_low	Sec_up	Sec_low	PDZ	Sec_up	Sec_low		
ZFMNNE0869	KFR09	0	59.19	0	58.7	DZ1	0	58.7		ZFMNW0002, ZFMNW0805A, ZFMWNW1035
ZFMNNE0869	KFR10	0	97.49	–	–	DZ1	0	5	Judging from the photographs of the drill cores there is a frequency of broken fractures that locally exceeds 10 fractures/m along the target interval. Oxidation of varying degrees occurs frequently throughout the interval 0–97 m. Both the fracture frequency and occurrence of oxidation resembles that for DZ1 in KFR09 DZ1 and KFR36 D1, but is generally slightly lower and less conspicuous, respectively. Thus, ZFMNNE0869 may well have its intersection in this interval, but a specific target intercept cannot be defined.	
ZFMNNE0869	KFR36	27.80	118.84	45	115.5	DZ1	45	115.5		
ZFMNNE0869	KFR68	43.93	eoh	**71.59**	105.13	DZ1	**71.59**	78.11	Note: KFR68 is interpreted as intercepting the meeting point between ZFMNNE0869 and ZFMNE0870. Since the BH lacks fracture orientation data it is impossible to correlate the PDZ with any specific steeply dipping zone. Thus, the PDZ is taken as target intercept for both ZFMNE0870 and ZFMNNE0869	
ZFMNNE0869	KFR68	43.93	eoh	71.59	**105.13**	DZ2	102.83	**105.13**		
ZFMNNE2308	–	–	–	–	–	–	–	–	Low magnetic lineament.	ZFMWNW0813
ZFMNNE3130	–	–	–	–	–	–	–	–	Low magnetic lineament.	ZFMWNW0835
ZFMNNE3264	–	–	–	–	–	–	–	–	Low magnetic lineament.	ZFMNW0805A
ZFMNNE3265	–	–	–	–	–	–	–	–	Low magnetic lineament.	ZFMNW0805A
ZFMNNE3266	–	–	–	–	–	–	–	–	Low magnetic lineament.	ZFMNS3154, ZFMNW0805A
WNW to NW set										
ZFMNW0002	HFM34	170.32	eoh	**180**	192	DZ2	**180**	184	DZ2 also lies within ZFMWNW0001.	ZFMWNW0001
ZFMNW0002	HFM34	170.32	eoh	180	**192**	DZ3	188	**192**	DZ3 also lies within ZFMWNW0001.	
ZFMNW0002	HFM35	0.00	54.54	**24**	52.5	DZ1	**24**	33	DZ1 also lies within ZFMWNW0001.	
ZFMNW0002	HFM35	0.00	54.54	24	**52.5**	DZ2	47.2	**52.5**	DZ2 also lies within ZFMWNW0001.	
ZFMNW0002	KFM11A	652.50	735.42	–	–	DZ1	245	824	The geometrical BH intersection lies within the very extensive SHI DZ1 (245–824 m). BH Section 653–735 m falls within the modelled Singö zone, ZFMWNW0001 itself. The interpreted deformation is attributed to the belt in general without any more specific subdivision. The information from this BH has not been used to define the zone thickness.	

DZ	BH	Geometrical intercept (v1.0) (BH length m)		Target intercept (v1.0) (BH length m)		Intercept defined by geological SHI (BH length m)			Comment	Terminated against following DZs
		Sec_up	Sec_low	Sec_up	Sec_low	PDZ	Sec_up	Sec_low		
ZFMNW0805A	KFR08	40.32	101.46	41	104.4	DZ2	41	104.4		
ZFMNW0805A	KFR11	32.63	eoh	41.45	95.65	DZ1	41.45	95.65		
ZFMNW0805A	KFR23	10.16	11.36	–	–	–	–	–	No SHI available.	
ZFMNW0805A	KFR24	48.99	156.64	–	–	–	–	–	No SHI available.	
ZFMNW0805A	KFR25	50.13	195.09	–	–	–	–	–	No SHI available.	
ZFMNW0805A	KFR56	57.18	eoh	–	–	–	–	–	No SHI available.	
ZFMNW0805A	KFR101	217.39	334.48	242	341.76	DZ5	242	341.76		
ZFMNW0805A	KFR7A	43.61	eoh	43.00	74.45	DZ1	3.5	74.45	Subdivision of DZ1 between ZFMNW0805A and ZFMNW0805B.	
ZFMNW0805B	KFR08	2.8	32.35	3	19	DZ1	3	19		ZFMNW0805A
ZFMNW0805B	KFR11	0.00	18.77	–	–	–	–	–	Judging from the photographs of the drill cores there is no obvious indication of a zone with the dignity of ZFMNW0805B along the geometric intercept. The only conspicuous feature is an approximately 2 dm long, intensely fractured interval with moderate oxidation/laumontization at 16 m length. No target intercept is defined.	
ZFMNW0805B	KFR24	0.00	40.81	–	–	–	–	–	No SHI available.	
ZFMNW0805B	KFR25	0.00	62.04	–	–	–	–	–	No SHI available.	
ZFMNW0805B	KFR38	105.19	eoh	153.60	181.65	DZ1	153.60	181.65		
ZFMNW0805B	KFR56	3.92	44.46	–	–	–	–	–	No SHI available.	
ZFMNW0805B	KFR101	80.26	131.55	97	116	DZ2	97	116		
ZFMNW0805B	KFR7A	11.13	43.20	3.5	43.00	DZ1	3.5	74.45	Subdivision of DZ1 between ZFMNW0805A and ZFMNW0805B.	

DZ	BH	Geometrical intercept (v1.0) (BH length m)		Target intercept (v1.0) (BH length m)		Intercept defined by geological SHI (BH length m)			Comment	Terminated against following DZs
		Sec_up	Sec_low	Sec_up	Sec_low	PDZ	Sec_up	Sec_low		
ZFMWNW0001	HFM34	0.00	eoh	**37**	192	DZ1	**37**	133		
ZFMWNW0001	HFM34	0.00	eoh	37	192	DZ2	180	184	DZ2 also lies within ZFMNW0002.	
ZFMWNW0001	HFM34	0.00	eoh	37	**192**	DZ3	188	**192**	DZ3 also lies within ZFMNW0002.	
ZFMWNW0001	HFM35	0.00	49.27	**24**	33	DZ1	**24**	33	DZ1 also lies within ZFMNW0002.	
ZFMWNW0001	HFM35	0.00	49.27	47.2	**52.5**	DZ2	47.2	**52.5**	DZ2 also lies within ZFMNW0002.	
ZFMWNW0001	HFR105	0.00	83.64	**21.12**	31	DZ1	**21.12**	31		
ZFMWNW0001	HFR105	0.00	83.64	88	**92**	DZ2	88	**92**		
ZFMWNW0001	KFM11A	492.66	831.43	498	824	DZ1	245	824	Geometrical split of DZ1 between ZFMWNW0001, ZFMWNW0813 and ZFMWNW3259.	
ZFMWNW0001	KFR01	0.00	eoh	0	62.30	DZ1	0	62.30		
ZFMWNW0001	KFR61	0.00	eoh	1.40	70.90	DZ1	1.40	70.90		
ZFMWNW0001	KFR62	0.00	eoh	45.64	82.80	DZ1	45.64	82.80		
ZFMWNW0001	KFR64	0.00	eoh	12.79	54.17	DZ1	12.79	54.17		
ZFMWNW0001	KFR65	0.00	eoh	17.63	39.68	DZ1	17.63	39.68		
ZFMWNW0001	KFR66	0.00	eoh	14.99	29.17	DZ1	14.99	29.17		
ZFMWNW0001	KFR67	0.00	eoh	13.74	48.95	DZ1	13.74	48.95		
ZFMWNW0001	KFR71	0.00	eoh	**65.67**	69.50	DZ1	**65.67**	69.50		
ZFMWNW0001	KFR71	0.00	eoh	72.14	**120.90**	DZ2	72.14	**120.90**		
ZFMWNW0813	KFM11A	247.68	391.95	245	400	DZ1	245	824	Geometrical split of DZ1 between ZFMWNW0001, ZFMWNW0813 and ZFMWNW3259.	
ZFMWNW0835	KFR27	0	153.31	108	120	DZ1	108	120		ZFMENE3115
ZFMWNW0835	KFR27	195.98	470.56	**323**	469	DZ2	**323**	379.5		
ZFMWNW0835	KFR27	195.98	470.56	323	469	DZ3	389	401		
ZFMWNW0835	KFR27	195.98	470.56	323	**469**	DZ4	421	**469**		

DZ	BH	Geometrical intercept (v1.0) (BH length m)		Target intercept (v1.0) (BH length m)		Intercept defined by geological SHI (BH length m)			Comment	Terminated against following DZs
		Sec_up	Sec_low	Sec_up	Sec_low	PDZ	Sec_up	Sec_low		
ZFMWNW0836	KFR08	46.04	104.12	–	–	DZ2	41	104.4	DZ2 is interpreted as being dominated by ZFMNW0805A.	ZFMNW0805A
ZFMWNW0836	KFR25	64.07	144.25	–	–	–	–	–	No SHI available.	
ZFMWNW1035	HFM35	180.90	199.19	–	–	DZ3	104	200	DZ3 in HFR105 rather than HFM35 DZ3 has been given a higher priority for defining the ZFMWNW1035 zone geometry. No specific target intercept is defined.	ZFMNW0002, ZFMWNW0001
ZFMWNW1035	HFR105	117.03	146.16	119	147	DZ3	119	147		
ZFMWNW1035	KFM11A	714.86	736.38	–	–	DZ1	245	824	The geometrical BH intersection lies within the very extensive SHI DZ1 (245–824 m). BH Section 715–736 m falls within the modelled Singö zone, ZFMWNW0001 itself. The interpreted deformation is attributed to the belt in general without any more specific subdivision. The information from this BH has not been used to define the zone thickness.	
ZFMWNW1035	KFR68	0.00	5.19	–	–	–	–	–	No target intercept defined. Higher priority given to tunnel, HFR105 and HFM35 when defining the zone geometry.	
ZFMWNW1056	–	–	–	–	–	–	–	–	Low magnetic lineament.	
ZFMWNW3259	KFM11A	401.86	495.48	400	498	DZ1	245	824	Geometrical split of DZ1 between ZFMWNW0001, ZFMWNW0813 and ZFMWNW3259.	
ZFMWNW3262	KFR103	178.46	183.59	180	182.5	DZ3	180	182.5		ZFMNE3137, ZFMNW0805A, ZFMNW0805B
ZFMWNW3262	KFR106	67.04	75.34	67	73	DZ3	67	73		
ZFMWNW3267	KFR104	388.50	eoh	**396**	454.57	DZ5	**396**	405		ZFMNE3137, ZFMNNE3130, ZFMNNW1034
ZFMWNW3267	KFR104	388.50	eoh	396	**454.57**	DZ6	447	**454.57**		
ZFMWNW3267	KFR105	257.84	282.99	258	283	DZ4	258	283		
ZFMWNW3268	–	–	–	–	–	–	–	–	Low magnetic lineament.	ZFMNE3137, ZFMNNE3130, ZFMWNW1035
ZFMWNW8042	KFR105	170.49	176.34	170.8	176	DZ3	170.8	176		ZFMENE3135, ZFMENE3115
ZFMWNW8043	–	–	–	–	–	–	–	–	Low magnetic lineament.	ZFMENE3115, ZFMWNW3268

DZ	BH	Geometrical intercept (v1.0) (BH length m)		Target intercept (v1.0) (BH length m)		Intercept defined by geological SHI (BH length m)			Comment	Terminated against following DZs
		Sec_up	Sec_low	Sec_up	Sec_low	PDZ	Sec_up	Sec_low		
N-S to NNW set										
ZFMNNW0999	KFR08	75.72	81.46	–	–	DZ2	41	104.4	Low magnetic lineament. DZ2 is interpreted as being dominated by ZFMNW0805A.	ZFMNW0805A
ZFMNNW1034	HFR106	136.61	179.79	**158**	182	DZ2	**158**	162		ZFMNNE3130, ZFMNW0805A
ZFMNNW1034	HFR106	136.61	179.79	158	**182**	DZ3	177	**182**		
ZFMNNW1034	KFR101	8.42	79.85	13.72	88	DZ1	13.72	88		
ZFMNNW1034	KFR106	200.93	271.05	256	266	DZ7	256	266		
ZFMNNW1209	KFR33	46.19	114.64	–	–	–	–	–	No SHI available.	ZFMNE0870, ZFMNNE0869
ZFMNNW1209	KFR35	32.90	71.04	32.7	70	DZ1	32.7	70		
ZFMNNW3113	–	–	–	–	–	–	–	–	Low magnetic lineament.	ZFMNW0805A
ZFMNS3154	–	–	–	–	–	–	–	–	Low magnetic lineament.	ZFMNW0805A

Table A9-2. Summary of tunnel intercepts for each deformation zone (SFR model version 1.0). Target intercepts are quoted as tunnel centreline intercepts and are based on the tunnel deformation zones (tDZ) in Appendix 2 of /Curtis et al. 2009/, complemented by inspection of the detailed geological tunnel mapping results as presented in /Christiansson and Bolvede 1987/.

DZ	SFR Facility part	Geometrical intercept (v1.0) (chainage m)		Target intercept (v1.0) (chainage m)		tDZ given in Appendix 2	Comment and description	Terminated against following DZs
Gently dipping DZs (dip < 45°)								
ZFM871	NBT	0+382	0+432	0+405	0+432	tDZ101 to tDZ104		ZFMENE3115, ZFMNNE0869, ZFMNW0002, ZFMNW0805A, ZFMNW0805B, ZFMWNW0001, ZFMWNW1035
Steeply dipping DZs (dip < 45°)								
NNE to ENE set								
ZFMNE0870	DT	0+470	0+600	0+535	0+570	tDZ40		ZFMNE3118, ZFMNNE0869, ZFMNW0002, ZFMNW0805A, ZFMNW0805B, ZFMWNW0001, ZFMWNW1035
ZFMNE0870	DT	DT-BT connection tunnel at 0+610		DT-BT connection tunnel at 0+610		tDZ40		
ZFMNE0870	BT	0+620	0+780	0+640	0+690	tDZ40		
ZFMNE0870	BT	0+860	0+925	0+888	0+907	tDZ56		
ZFMNE0870	BT	1+017	1+055	1+020	1+050	tDZ66		
ZFMNE0870	NBT	0+000	0+010	–	–	–		
ZFMNE0870	NBT	0+350	0+365	0+352	0+352	tDZ80		
ZFMNE0870	STT	0+800	0+820	0+810	0+820	tDZ66		
ZFMNE0870	IST	0+078	0+095	0+088	0+088	tDZ80		
ZFMNE3118	BT	1+075	1+095	1+095	1+095	tDZ73		ZFMENE3115, ZFMNW0805B, ZFMWNW1035
ZFMNE3118	BT/ST	1+130	1+166	1+166	–	tDZ73	tDZ73 at 0+088 in ST.	
ZFMNE3118	NBT	0+055	0+63	0+055	0+059	–	Target intercept based on shotcrete coverage marked in the detailed tunnel mapping.	
ZFMNE3118	NBT	0+295	0+315	0+295	0+340	tDZ73		

DZ	SFR Facility part	Geometrical intercept (v1.0) (chainage m)		Target intercept (v1.0) (chainage m)		tDZ given in Appendix 2	Comment and description	Terminated against following DZs
ZFMNNE0869	DT	0+430	0+555	0+430	0+530	tDZ30 to tDZ32 and tDZ34		ZFMNW0002, ZFMNW0805A, ZFMWNW1035
ZFMNNE0869	BT	0+357	0+482	0+355	0+450	tDZ30 to tDZ32 and tDZ34		
WNW to NW set								
ZFMNW0002	DT	0+310	0+365	0+309	0+372	tDZ19 to tDZ22		ZFMWNW0001
ZFMNW0002	BT	0+292	0+345	0+297	0+347	tDZ19 to tDZ22		
ZFMWNW0001	DT	0+155	0+362	0+212	0+295	tDZ7 to tDZ18		
ZFMWNW0001	BT	0+140	0+345	0+189	0+283	tDZ7 to tDZ18		
ZFMNW0805B	BT	1+178	1+193	1+182	1+185	–	Several vertical NNW-SSE striking fractures (approximately 160°/90°) that penetrate the entire tunnel perimeter at 6/182–6/185. Some of the fractures are marked as ‘damp’ in the detailed drawing –11 of /Christiansson and Bolvede 1987/. This is taken as a target intercept for ZFMNW0805B.	ZFMNW0805A
ZFMNW0805B	1B	0+023	0+044	–	–	–	Generally a high frequency of vertical NW-SE striking fractures (approximately 130°/90°) from the connection with IST and onwards towards north. The fracture set is conspicuous in all parts included in detailed drawing –12 of /Christiansson and Bolvede 1987/ and it is not possible to define a specific target intercept.	
ZFMWNW0813	DT	0+062	0+138	0+065	0+128	–	Target intercept mainly based on the shotcrete coverage marked in the detailed tunnel mapping.	
ZFMWNW0813	BT	0+042	0+120	0+042	0+082	tDZ3 to tDZ5		
ZFMWNW1035	DT	0+420	0+435	0+420	0+433	tDZ25 to tDZ28		ZFMNW0002, ZFMWNW0001
ZFMWNW1035	BT	0+398	0+412	0+398	0+416	tDZ25 to tDZ28		
ZFMWNW3259	DT	0+128	0+180	0+142	0+170	tDZ6	Target intercept defined from the detailed tunnel mapping of /Christiansson and Bolvede 1987/ and includes tDZ6.	
ZFMWNW3259	BT	0+108	0+158	0+120	0+150	–	Target intercept mainly based on the shotcrete coverage marked in the detailed tunnel mapping.	
N-S to NNW set								
ZFMNNW1209	DT	0+920	0+945	0+930	0+930	tDZ59		ZFMNE0870, ZFMNE3118, ZFMNNE0869
ZFMNNW1209	BT	0+885	0+907	0+893	0+893	–	Possible low confidence observation based on detailed drawing –09 /Christiansson and Bolvede 1987/.	
ZFMNNW1209	NBT	0+000	0+010	–	–	–		
ZFMNNW1209	1 BTF	0+090	0+117	0+100	0+100	tDZ59		
ZFMNNW1209	2 BTF	0+070	0+090	0+078	0+080	tDZ59 and tDZ126		
ZFMNNW1209	BLA	0+048	0+068	0+055	0+060	tDZ59 and tDZ126		
ZFMNNW1209	BMA	0+030	0+055	0+030	0+030	tDZ59		

Appendix 10

Investigation of a relationship between deformation zone thickness and length

The question of whether a relationship exists between the interpreted surface trace length of a deformation zone and its modelled thickness has been asked at several points during the site-descriptive model activities at both Forsmark and Laxemar. In general, the answer has been that it is difficult, if not impossible, to develop a relationship between the two parameters with any degree of statistical power. However, a brief analysis was performed using the current (Table 5-1) deformation zone model for the SFR site to determine if any relationships between length and thickness could be determined. On preliminary examination in Excel, both linear (Figure A10-1), power-law and polynomial regressions prove only marginally adequate at describing the aggregate data, with significant data falling outside the 95% confidence interval. Note that the gently-dipping zones are not included in the analysis; since they do not intersect the ground surface they do not have a 'trace length' per se.

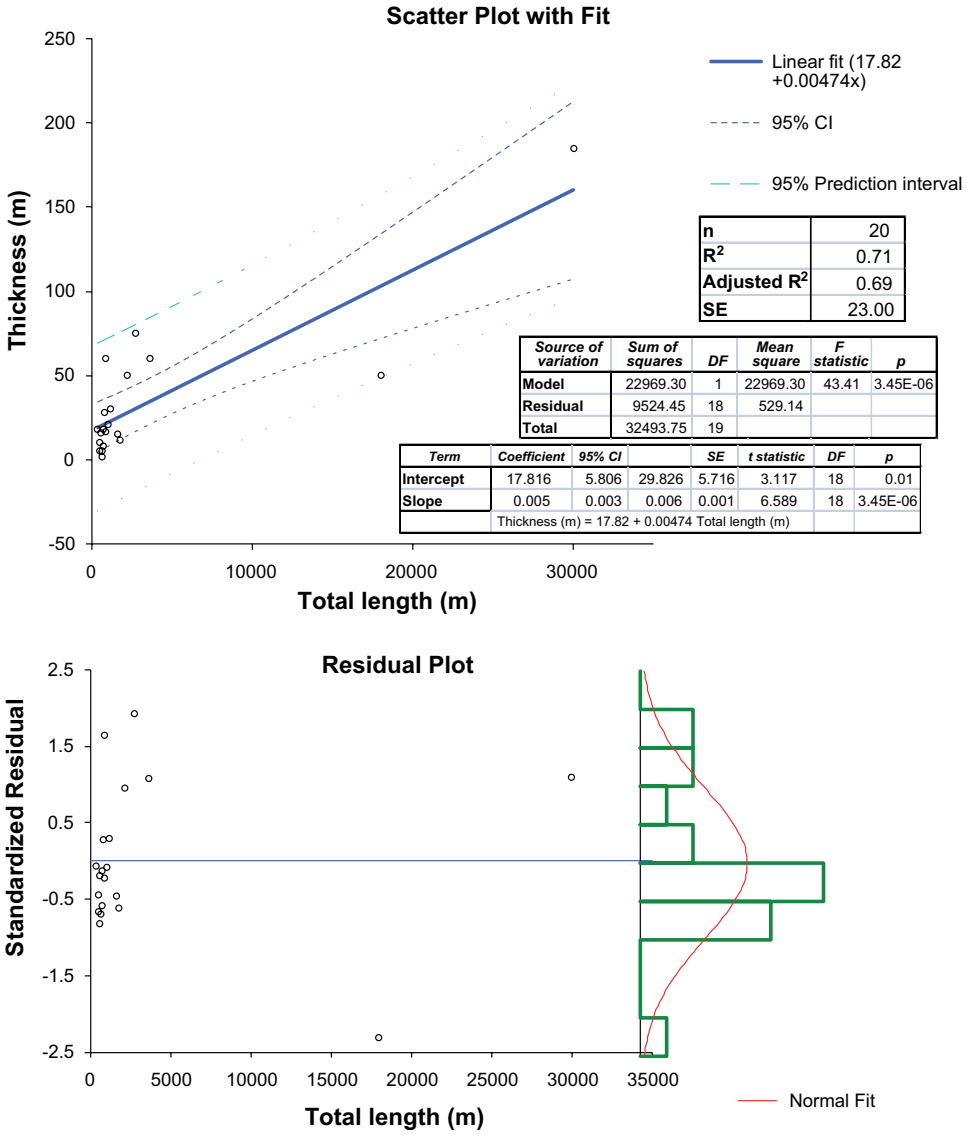

Figure A10-1. *Linear regression between deformation zone surface trace length and interpreted thickness. Data taken from Table 5-1, for all deformation zones with modelled thicknesses. Regression and confidence interval bands calculated using Analyze-It version 2.2.2.*

The deformation zones at SFR fall into several distinct orientation classes, which directly represent the tectonic (both brittle and ductile) history of the site (cf. Chapter 5 or Section 5.2 of /Stephens et al. 2007/). These orientation classes, based largely on the strike orientation, are:

- Steeply dipping NNW to N-S striking zones.
- Steeply dipping NNE to ENE striking zones.
- Steeply dipping WNW to NW striking zones.
- Gently-dipping zones (generally striking NE).

A closer examination of the deformation-zone trace length-thickness data as a function of orientation set (Figure A10-2) shows that there are significant differences in the lengths of the zones between sets. The WNW to NW striking zones are the only ones that show anything approaching a consistent length-thickness relationship, though there is very little data at scales larger than 10 km. Note that the WNW to NW set dominates the regression analysis presented above. Deformation zones in the remaining orientation sets (NNE to ENE and NNW to N-S) show absolutely no relationship between deformation zone length and modelled thickness. The WNW to NW set is the only one for which a reasonable length-thickness regression can be drawn; note that it is this set that is dominating the regression presented in Figure A10-1. Given the significant differences in deformation zone trace length between different orientation sets, it is impossible to draw a single relationship with any real statistical power.

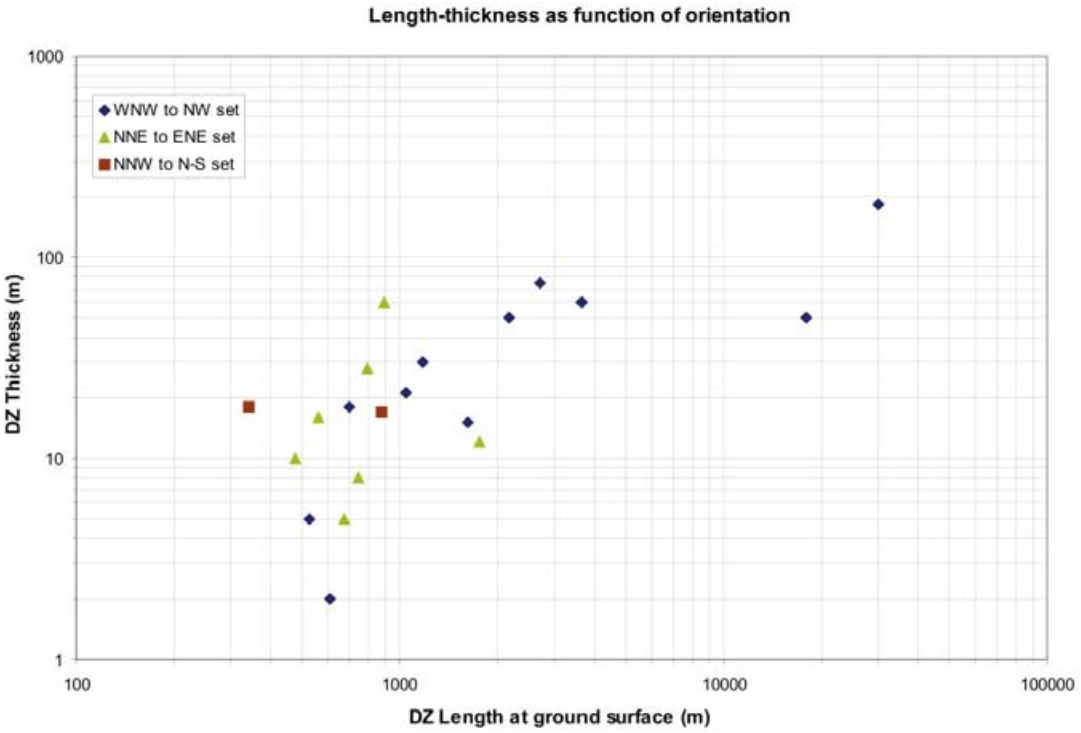

Figure A10-2. *Relationship between deformation zone surface trace length and interpreted thickness as a function of orientation set. Data taken from Table 5-1, for all deformation zones with modelled thicknesses. Note that gently-dipping zones are excluded from this analysis.*

Appendix 11

Deformation zone property tables

Property tables key

Gently dipping deformation zones
ZFM871
ZFMA1
ZFMB10

Steeply dipping NNE to ENE deformation zones
ZFMENE3115
ZFMENE3135
ZFMENE3151
ZFMENE8031
ZFMENE8034

ZFMNE0870
ZFMNE3112
ZFMNE3118
ZFMNE3134
ZFMNE3137

ZFMNNE0725
ZFMNNE0869
ZFMNNE2308
ZFMNNE3130
ZFMNNE3264
ZFMNNE3265
ZFMNNE3266

Steeply dipping WNW to NW deformation zones
ZFMNW0002
ZFMNW0805A
ZFMNW0805B

ZFMWNW0001
ZFMWNW0813
ZFMWNW0835
ZFMWNW0836
ZFMWNW1035
ZFMWNW1056
ZFMWNW3259
ZFMWNW3262
ZFMWNW3267
ZFMWNW3268
ZFMWNW8042
ZFMWNW8043

Steeply dipping NNW to N-S deformation zones
ZFMNNW0999
ZFMNNW1034
ZFMNNW1209
ZFMNNW3113
ZFMNS3154

Properties of deformation zones modelled to intersect the SFR regional model volume, version 1.0

The geological properties of the 40 deformation zones that have been modelled to intersect the SFR regional model volume in version 1.0 are summarized in the tables in this appendix.

Deformation zone –zone name

Borehole and tunnel intersections (metres along borehole/tunnel)

KFRxx: xx–xx m, refers to target interval sec_up and sec_low. (DZxx xx–xx m) refers to corresponding SHI PDZ sec_up and sec_low.

Normally target intervals and SHI PDZ intervals in boreholes are identical but, in certain cases, they may differ due to other factors being involved in the overall zone interpretation.

Deformation style, alteration and geometry

Deformation style: Brittle and/or ductile.

Alteration: Type and degree of alteration.

Strike/dip (span) right-hand-rule: xxx / xx. The quoted span is a judgement based on a general assessment of all the available data and experience gained from the modelling work.

Trace length at ground surface (span): xx m. Total length of the deformation zone trace interception with the ground surface without reference to model boundaries. The span is a judgement based on all the available data, in particular a review of the magnetic data with consideration to the lineament continuity and extent.

Model thickness (span): *x* m. Distance between the two surfaces that have been modelled to envelop the longest intersection in all the borehole target intercepts (see Figure 5-4 in the main report). This is somewhat different from the method used in the Forsmark site investigation /Stephens et al. 2007/ where, in most cases, the modelling was based on a single or only a limited number of borehole intercepts and the true thickness was calculated from a single borehole intersection or the average of more than one borehole intersection if present. The quoted span is a judgement based on a general assessment of all the available data and experience gained from the modelling work.

Confidence in existence: Confidence level rated as high (coloured red in the model) /medium (coloured green in the model) /low (coloured grey in the model).

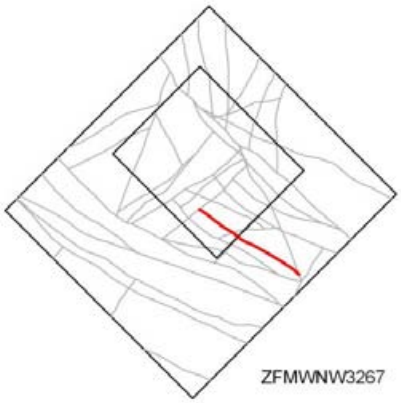

The regional and local SFR model boundaries shown together with the position of the modelled deformation zones at the ground surface. The zone under consideration is shown in colour.

Modelling procedure*:* A short outline of the basis for the modelled geometry representing the deformation zone.

Deformation zone –zone name

Fractures in the deformation zone

General characteristics

Fracture orientation: Terzaghi weighted stereograms of open/partly open and sealed fractures. The summary stereograms show fractures from one or several borehole target intercepts, if such data are available and have been included in the interpretation. The plots show the clusters of fractures identified by a process of hard and soft sectoring as outlined below. Further details describing this process are reported in /Stephens et al. 2007/. A soft-sector division is difficult to carry out manually. For this reason, clusters are initially approximated in terms of hard sectors (manually) and are transformed into soft sectors (numerically) before Fisher parameterization is calculated.

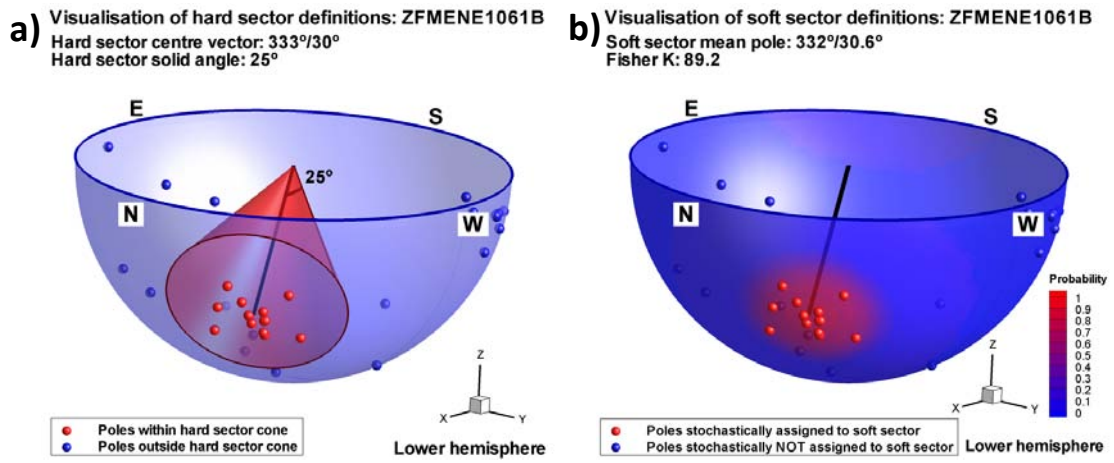

Visualization of principles used; a) a manually hard-sector defined set is transformed into b) a soft sectoring probability field, figure taken from /Stephens et al. 2007/. Note that, for example, the soft sector P=0.5 is defined by the characteristics of the fractures inside the hard sector, and does not necessarily coincide with the initial hard sector solid angle (26°).

Fracture frequency: Mean fracture frequency m^{-1} for the deformation zone based on one or several borehole target intercepts. However, data quality is not mixed. If KFR borehole data from the latest drilling campaign are available, they are used exclusively and are not mixed with lower quality HFR or older KFR borehole data. Open/partly open and sealed fractures are quoted separately.

Fracture mineralogy: A histogram of mineral coating or mineral filling along fractures inside a deformation zone based on one or several borehole target intercepts. If KFR borehole data from the latest drilling campaign are available, they are used exclusively and not mixed with lower quality HFR or older KFR borehole data. Open/partly open and sealed fractures are shown separately. Where Boremap data from older KFR boreholes without BIPS image are available, broken and unbroken fractures are indicated as undifferentiated grey columns.

Photo of drill core from part of the deformation zone. Generally part of a core zone if such has been identified during the single-hole interpretation. The depth numbers shown at the top of each core box are generally unadjusted measurements (not based on detailed borehole geometry survey) since photography was performed at an early stage prior to the down-hole survey. However, the numbers rarely differ more than one decimetre from the adjusted borehole length.

BOREHOLE AND TUNNEL INTERCEPT DETAILS- for the named deformation zone

Borehole intersections for – deformation zone name				
BH	**Geometrical Intercept**		**Target intercept**	
	Sec_up BH length (m) [z (-m)]	**Sec_low BH length (m) [z (-m)]**	**Sec_up BH length (m) [z (-m)]**	**Sec_low BH length (m) [z (-m)]**
KFRxx (BH name)	xx= borehole length m [xx= elevation (-masl)]	xx= borehole length m [xx= elevation (-masl)]	xx= borehole length m [xx= elevation (-masl)]	xx= borehole length m [xx= elevation (-masl)]
	Eoh= end or bottom of borehole	BH= borehole	See section 5.1.2 in the main report for the definition of geometrical and target intercepts. In some cases geometrical intercepts are listed without any corresponding target intercepts. This means that the drill core in a borehole in this interval shows no signs of deformation that can be correlated with the specific modelled deformation zone. This may be due to zone heterogeneity where parts of a zone have similar characteristics to the surrounding rock mass.	

Comment: Infilled, if necessary.

SHI DZx xxx–xxx m: Possible deformation zone (PDZ) in geological single-hole interpretation with a defined sec_up and sec_low borehole length. The text description of the drill core and interpreted PDZ character have been extracted from the published SHI report.

Fracture orientation: Terzaghi weighted stereograms of open/partly open and sealed fractures for the individual specified borehole intercept where oriented fracture data are available).

Fracture mineralogy: A histogram of mineral coating or mineral filling along fractures inside a deformation zone based on the individual specified borehole intercept.

Fracture frequency and RQD plots for the individual specified borehole intercept:

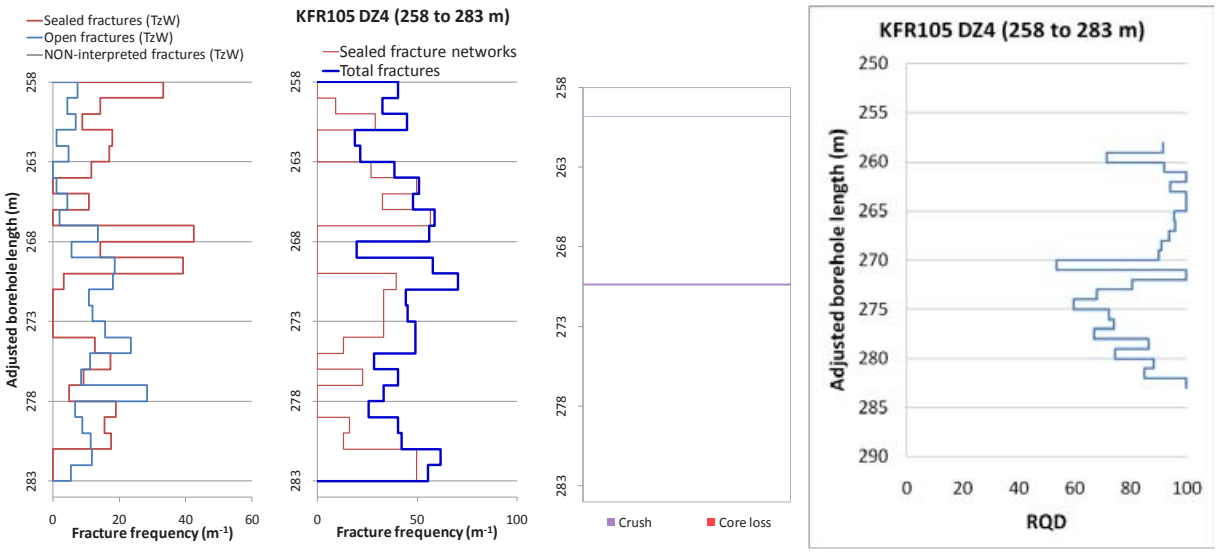

The first figure shows the Terzaghi-corrected (TzW) frequencies of sealed and open (including partly open) fractures, as well as the Terzaghi-corrected frequencies of broken and unbroken fractures in old SFR boreholes, where BIPS information is lacking and a division into open and sealed fractures is not possible, i.e. so-called NON-interpreted fractures, within the modelled deformation zone (DZ) in each borehole. Fracture frequency, P_{10} (number of fractures/m), was calculated for 1 m bins, starting from (adjusted) SEC_UP along the DZ. The lowest bin is constrained by the (adjusted) SEC_LOW and may, therefore, be smaller than 1 m. For example, a DZ defined between 100.5 m to 103.0 m, will be resolved into three bins: 100.5 to 101.5 m, 101.5 to 102.5 m, and 102.5 to 103.0 m. The Terzaghi-weighed P_{10} for each 1 m bin is calculated as:

Borehole intersections for – deformation zone name
$P_{10} = \frac{\sum_n \frac{1}{\sin(\max[\alpha, \alpha_{\min}])}}{L}$, minimum bias angle, $\alpha_{min} = 15\ ^\circ \Leftrightarrow$ Max TzW = 3.86, where L = 1 m, n is the number of fractures inside the bin and α = maximum dip of the fracture relative to the drill core axis. The minimum bias angle is used to avoid artificial weights for small angles, where the effects of non-zero borehole radius are not negligible. The second figure presents fracture frequency information for sealed fracture networks and all the fractures (total fractures), the latter being defined as open (TzW) + sealed (TzW) + sealed network + crush. The third figure shows the occurrence of crush zone and core loss as actual borehole lengths, i.e. not binned. The Terzaghi weighing has not been implemented for sealed fracture networks and crush zones, since TzW concerns geometric bias owing to the orientation of planar features versus scan line (borehole). The orientation of a sealed fracture network or crush zone, itself, is generally unclear, even if the fractures inside such a structure are defined. Fracture frequency, P_{10} (number of fractures/m), for a sealed network or crush zone was calculated using the ratio 1000 [mm/m]/d [mm], where d is the piece-length of rock between fractures in the unit m. It is superimposed onto the DZ 1 m bins, by fractional section length inside each bin. For example, a crush with piece length 10 mm extends from 99.0 m to 102.0 m. The crush has a P_{10} of 100 [1/m]. The first bin in the example above, 100.5 to 101.5 m, will have a crush P_{10} of 100 [1/m], while the second bin, 101.5 to 102.5 m, will have a crush P_{10} of 50 [1/m], as only half of the second bin contains crush. Crush P_{10} is not shown explicitly, but included in the total frequency. The fourth figure is a standard RQD (Rock Quality Designation) plot of the section of drill core.

Tunnel intersections for – deformation zone name					
Tunnel	**Geometrical intercept**		**Target intercept**		**Comment**
	Start ch.(m)	**End ch. (m)**	**Start ch.(m)**	**End ch. (m)**	
Tunnel ID	xxx chainage (x+xxx) Original chainage*	xxx chainage (x+xxx) Original chainage*	xxx chainage (x+xxx) Original chainage*	xxx chainage (x+xxx) Original chainage*	DT = operating tunnel. BT = construction tunnel. See Figure 3-3 for other abbreviations. Chainage refers to tunnel centreline intersections. * The numbering system used during the construction phase /Christiansson and Bolvede 1987/. These chainages are general zone boundary/tunnel wall intersections.

Gently dipping deformation zones

Deformation zone ZFM871

Borehole and tunnel intersections (metres along borehole/tunnel)

KFR02: 114.80–124.45 m (DZ3 114.80–124.45 m)
KFR03: 81.86–95.95 m (DZ4 81.86–95.95 m)
KFR04: 91–100 m
KFR05: 85.00–87.90 m (DZ1 85.00–87.90 m)
KFR7B: 0–17 m (DZ1 0–17 m)
KFR7C: 6–32 m (DZ1 6–32 m)
KFR12: 21.25–31.50 m (DZ1 21.25–31.50 m)
KFR13: 61–68 m (DZ4 61–68 m)
KFR31: 228.76–232.00 m (DZ2 228.76–232.00 m)
KFR32: 163.10–186.10 m (DZ2 163.10–186.10 m)
KFR37: 183.43–193.60 m (DZ2 183.43–193.60 m)
KFR57: 15.85–25.38 m (DZ1 15.85–25.38 m)
NBT: 0+405–0+432 m (tDZ101, tDZ102, tDZ103 and tDZ104 0+405–0+432)

Deformation style, alteration and geometry

Deformation style: Brittle

Alteration: Generally red-stained bedrock with fine-grained hematite dissemination, along with local argillization

Strike/dip (span) right-hand-rule: 074 / 19 (±10 / ±5)

Trace length at ground surface: No intercept with the ground surface (see modelling procedure for comment on terminations)

Model thickness/ model thickness span: 20 m / 1–22 m

Confidence in existence: High

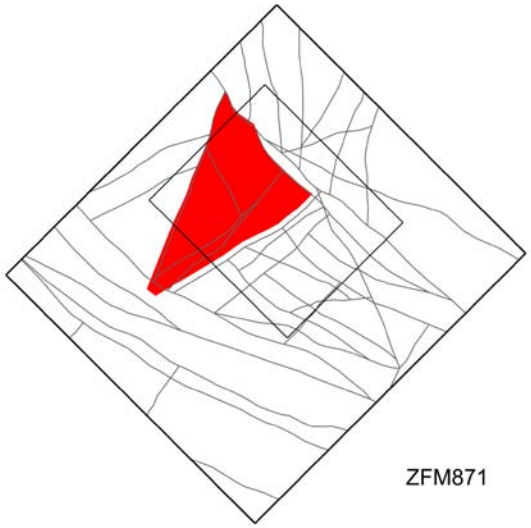

No intersection with the ground surface

Modelling procedure*:* This zone corresponds to zone H2 in earlier SFR models (see, for example, Axelsson and Hansen 1997/). It was renamed ZFM871 in the Forsmark stage 2.2 model /Stephens et al. 2007/. The zone has been modelled in SFR model version 1.0 as an undulating surface passing through a number of borehole control points. There is no corresponding magnetic lineament at the ground surface.

Zone ZFM871 has been modelled to terminate at zones ZFMENE3115, ZFMNNE0869, ZFMNW0805A, ZFMNW0805B and ZFMWNW1035. The terminations at the surrounding steeply dipping zones and the resulting limited extent means that the zone no longer has an intersection with the sea bottom and no coincidence with a lineament. The termination at ZFMNNE0869 is particularly uncertain. A possible extension to the north-west is indicated in KFR10 though since this lies close to the meeting point of ZFM871 and ZFMNE0869 the extension has not been implemented. Similarly possible correlations exist in KFR7A, KFR24, KFR25 and KFR38 indicating an extension further to the all north-east. However, all these points lie within the modelled boundaries of the dominant ZFMNW0805A/B modelled deformation zone belt and consequently ZFM871 has been terminated ZFMNW0805A/B. Particular focus was placed on identifying a possible greater extent of the zone to the south-east, beyond ZFMENE3115, using the new borehole information. However, no geological evidence to support a further extent was identified.

The zone is interpreted as consisting of a group of parallel oriented, smaller hydraulically conductive structures separated by ordinarily fractured rock. The spread of indications suggest that the structure is complex and has a stepped geometry.

/Christiansson 1986/ reports the zone's character is very variable but generally has two to three gently dipping fracture sets, individually recorded zone thicknesses of up to 10 m and a hydraulic thickness varying from 2 to 20 m; the zone is associated with lenses of weathered and highly fractured rock, along with frequent clay-filled joints. The gently dipping fractures, in combination with an increased frequency of steeply dipping fractures, gives rise to the lenses being hydraulically interconnected.

Deformation zone ZFM871

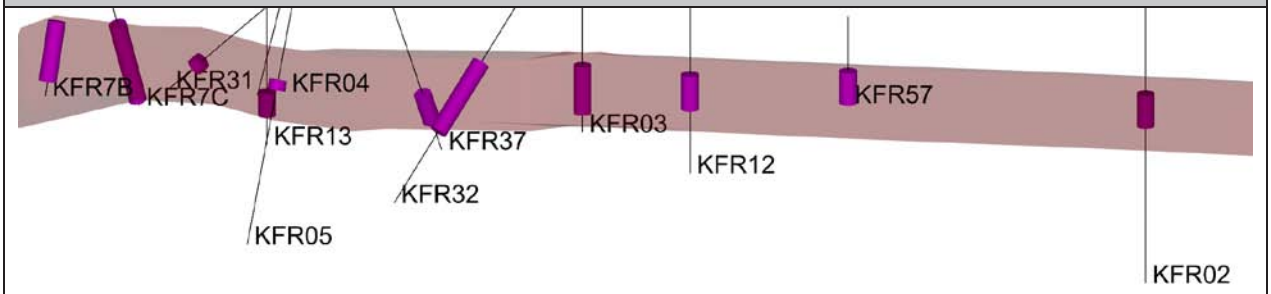

Section view of ZFM871 looking down dip to the south (modelled thickness 20m). SHI PDZ sections shown in pink.

Fractures in the deformation zone

General characteristics

Fracture orientation: No oriented data available. Construction reports generally include the description of two dominantly gently dipping fracture sets as well as an increase in frquency of steeply dipping fractures /Christiansson and Bolvede 1987/.

Fracture frequency: no orientation corrected fracture frequencies are available. See individual older borehole intercepts for a general indication.

Fracture filling mineralogy:

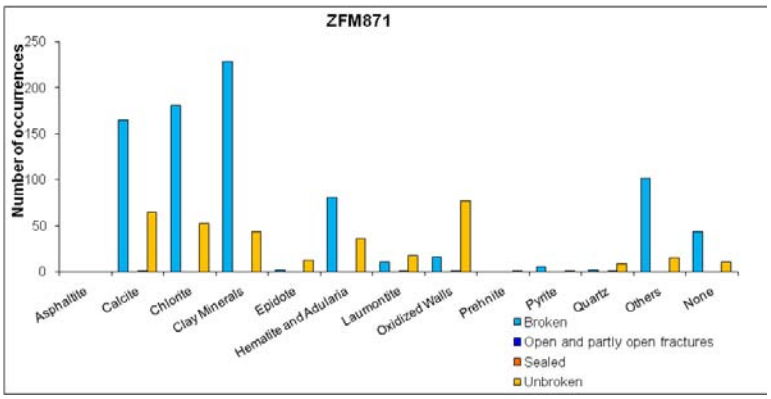

KFR02 DZ3 (114.80–124.45 m)

Deformation zone ZFM871	
	KFR05 DZ1 (85.00–87.90 m) 
	KFR31 DZ2 (228.76–232.00 m) 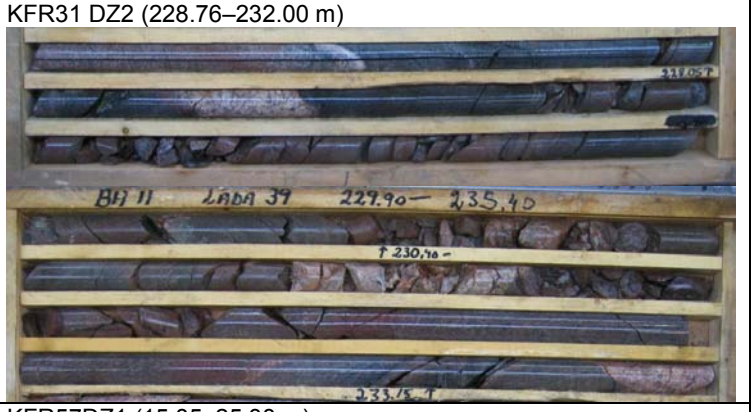
	KFR57DZ1 (15.85–25.38 m) 

BOREHOLE AND TUNNEL INTERCEPT DETAILS

Borehole intersections for ZFM871				
BH	**Geometrical Intercept**		**Target intercept**	
	Sec_up BH length (m) [z (-m)]	**Sec_low BH length (m) [z (-m)]**	**Sec_up BH length (m) [z (-m)]**	**Sec_low BH length (m) [z (-m)]**
KFR02	109.18 [194.61]	130.15 [215.58]	114.80	124.45
Comment:				
SHI DZ3 114.80–124.45 m: Increased frequency of broken fractures, with an average of c. 7 broken fractures/m. Generally high α-angles. Highest frequency of broken fractures in the interval 116.70–117.65 m. Increased frequency of unbroken fractures that form networks in the interval 114.80–116.80 m. Faint to weak oxidation throughout the interval. Predominant minerals in broken fractures are calcite, hematite along with locally minor amounts of clay minerals and in the sealed fracture networks at 114.80–116.80 m adularia, quartz and calcite. Locally vugs in the sealed fracture networks. Pegmatitic granite (101061) and fine- to medium-grained metagranite-granodiorite (101057). Confidence level = 3. Moderate transmissivity of the tested section 81–136 m ($9 \cdot 10^{-8}$ m^2/s).				

Borehole intersections for ZFM871				
BH	**Geometrical Intercept**		**Target intercept**	
	Sec_up BH length (m) [z (-m)]	**Sec_low BH length (m) [z (-m)]**	**Sec_up BH length (m) [z (-m)]**	**Sec_low BH length (m) [z (-m)]**
KFR03	78.33 [160.70]	99.73 [182.10]	81.86	95.95
Comment:				
SHI DZ4 81.86–95.95 m: Increased frequency of broken and unbroken fractures, which locally forms sealed networks. Approximately 9 broken fractures/m outside crushed intervals. Varying α-angles with several conspicuous, clay-dominated fractures at angles < 30°. Four minor crushes. Faint to weak oxidation and minor argillization associated with clay-dominated fractures. Predominant fracture minerals are clay minerals, Fe-hydroxide/hematite, chlorite and calcite, and in unbroken fractures also adularia. Distinct decrease in the SPR logging values along the section 85.0–93.0 m. Fine- to medium-grained granite (111058) and pegmatitic granite (101061). Confidence level = 3. Low transmissivity of the section 81–101.6 m ($2 \cdot 10^{-8}$ m^2/s).				

KFR04	84.50 [158.81]	eoh [174.26]	91	100
Comment: SHI interpreted two possible DZs in KFR04, DZ1 0–3 m and DZ2 14–63 m (BH length) neither of which correlates with ZFM871. However, there are planar chlorite-filled fractures from 86 m onwards and some clay-filled fractures towards the base of the borehole that could be associated with the zone (100.5 m). A target intercept is defined at 91–100 m.				

Borehole intersections for ZFM871

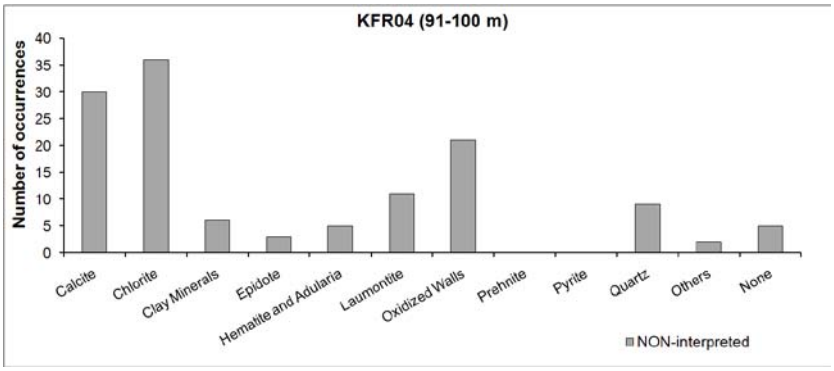

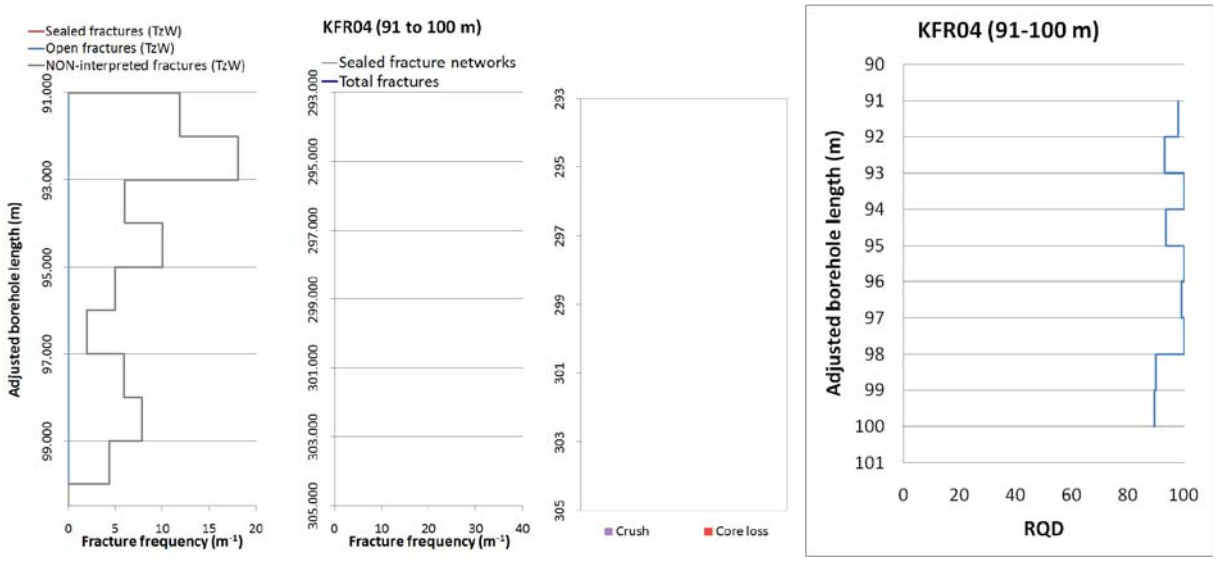

BH	Geometrical Intercept		Target intercept	
	Sec_up BH length (m) [z (-m)]	Sec_low BH length (m) [z (-m)]	Sec_up BH length (m) [z (-m)]	Sec_low BH length (m) [z (-m)]
KFR05	76.54 [149.08]	96.27 [167.63]	85.00	87.90
Comment:				
SHI DZ1 85.00–87.90 m: Increased frequency of broken fractures, most of them with α-angles > 45°. Crushed section at 85.25–86.22 m. Faint to weak oxidation throughout the interval. Predominant fracture minerals are Fe-hydroxide/hematite, calcite, clay minerals and chlorite. Distinct decrease in the SPR logging values along the section 84.2–86.8 m. There is also an anomaly in the fluid temperature data, with its minima at c. 86.6 m, which indicates in or out flow of water. Moderately foliated metagranite-granodiorite (101057). Confidence level = 3. No hydraulic test data from this section of the borehole.				
KFR7B	0.00 [133.25]	20.39 [152.95]	0	17

Borehole intersections for ZFM871

SHI DZ1 0–17 m: Increased frequency of unbroken and especially broken fractures. Four crushed sections at 0.67–1.01, 4.14–4.33, 14.34–14.88 and 15.98–16.25 m and two core losses at 14.48–14.88 and 15.98–16.25 m. Predominant fracture minerals are calcite, chlorite and clay minerals, locally with hematite/Fe-hydroxide staining. α–angles are ranging between 43 and 72°. Moderately foliated metagranite-granodiorite (101057) and pegmatitic granite (101061). Confidence level = 3.

No hydrogeological investigation data from the upper 4 m of the borehole. Moderate hydraulic conductivity of $1 \cdot 10^{-8}$ m/s in the interval 4–7 m. High hydraulic conductivity of $2 \cdot 10^{-6}$ m/s in the interval 8–17 m.

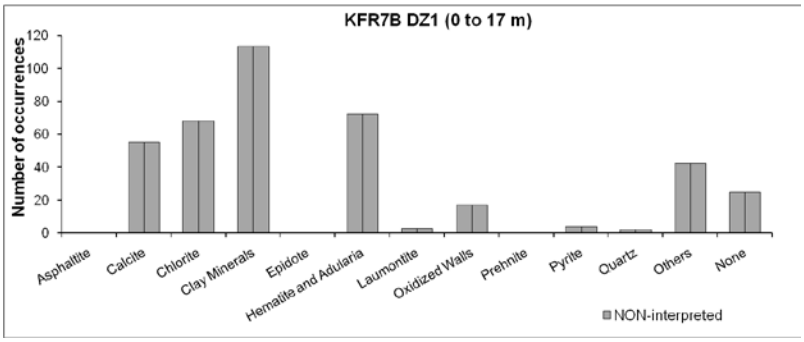

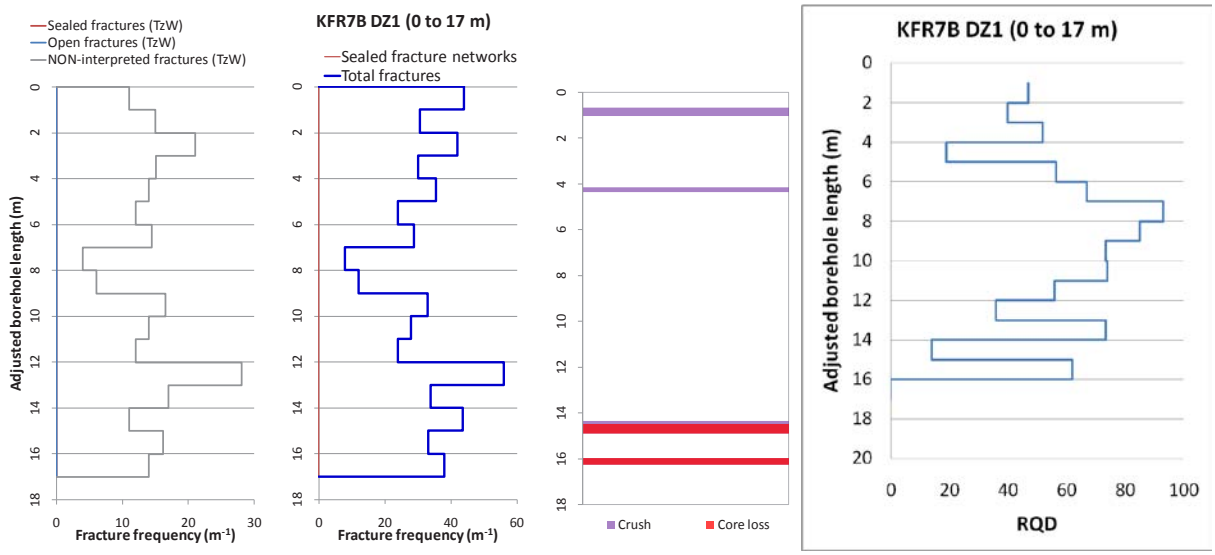

Borehole intersections for ZFM871				
BH	Geometrical Intercept		Target intercept	
	Sec_up BH length (m) [z (-m)]	Sec_low BH length (m) [z (-m)]	Sec_up BH length (m) [z (-m)]	Sec_low BH length (m) [z (-m)]
KFR7C	5.91 [138.96]	32.74 [164.16]	6	32

SHI DZ1 6–32 m: Increased frequency of unbroken and especially broken fractures. Five crushes in the intervals 7.89–7.95, 8.11–8.19, 8.47–8.50, 9.25–9.40 and 14.67–14.77 m. Predominant fracture minerals are clay minerals, locally accompanied by Fe-hydroxide/hematite discolouration, chlorite and calcite. Most fractures have α–angles that are moderate (29–74°). Virtually all laumontite-bearing fractures are concentrated in a zone with low α–angles (9 and 10° for individual fractures) at 6.24–7.15 m length. Locally faint oxidation and minor argillization. Strongly foliated metagranite-granodiorite (101057), fine- to medium-grained granite (111058) and pegmatitic granite (101061). Confidence level = 3.

Moderate hydraulic conductivity $2 \cdot 10^{-8}$ m/s throughout the interval.

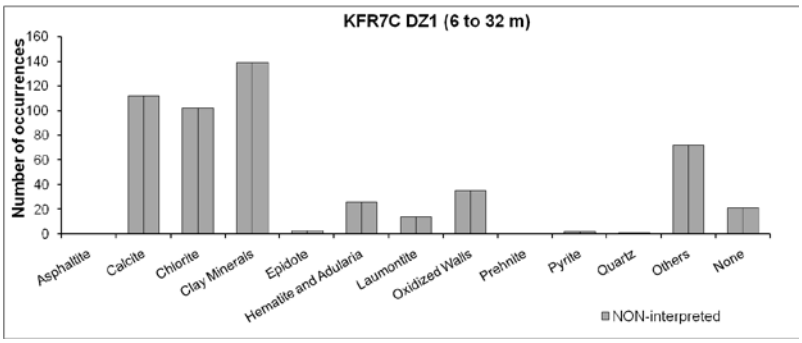

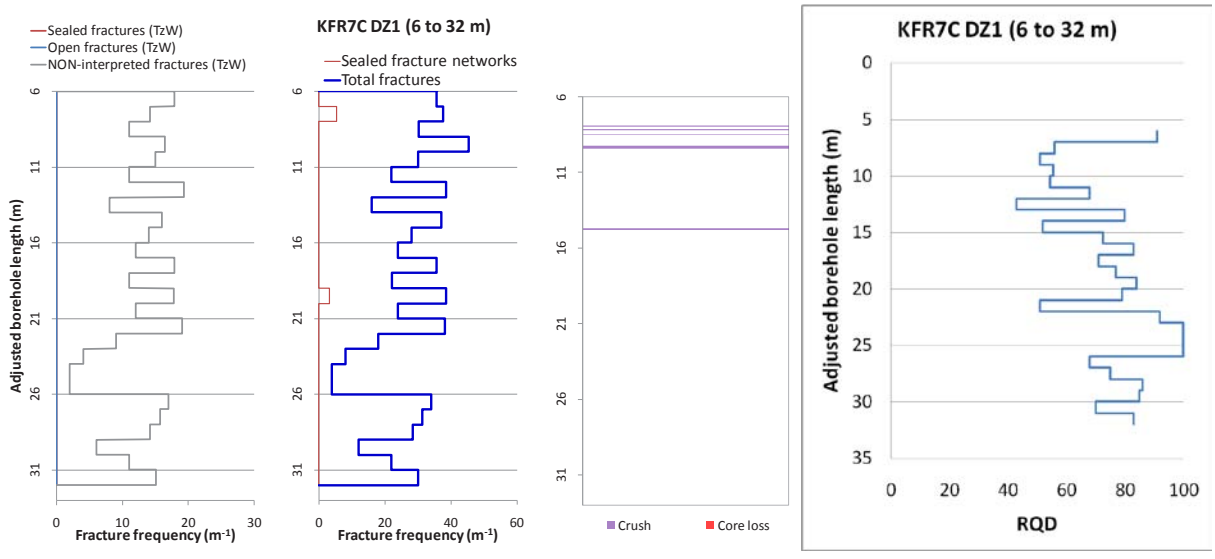

Borehole intersections for ZFM871				
BH	Geometrical Intercept		Target intercept	
	Sec_up BH length (m) [z (-m)]	Sec_low BH length (m) [z (-m)]	Sec_up BH length (m) [z (-m)]	Sec_low BH length (m) [z (-m)]
KFR12	14.73 [101.85]	36.77 [123.89]	21.25	31.50
SHI DZ1 21.25–31.50 m: Increased frequency of broken fractures. The section 24.30–25.64 m is generally crushed. α-angles > 55°. Weak oxidation throughout the interval. Predominant fracture minerals are clay minerals, Fe-hydroxide/hematite and chlorite. Fine- to medium-grained granite (111058). Confidence level = 3. Relatively high transmissivity of the section 20.0–33.0 m ($3 \cdot 10^{-6}$ m^2/s). The transmissivity of this section is significantly elevated compared with the rest of the tested borehole sections.				
KFR13	53.36 [176.70]	74.99 [198.33]	61	68
SHI DZ4: 61–68 m: Increased frequency of unbroken and especially broken fractures. Predominant fracture filling minerals are laumontite, chlorite and calcite. A number of broken fractures with clay minerals are concentrated along the section 60.1–64.5 m length. Their α–angles range between 42 and 78°. Moderately foliated metagranite-granodiorite (101057) and fine- to medium-grained metagranodiorite-tonalite (101051). Confidence level = 1. Increased hydraulic conductivity ($1–2 \cdot 10^{-7}$ m/s) throughout the interval.				

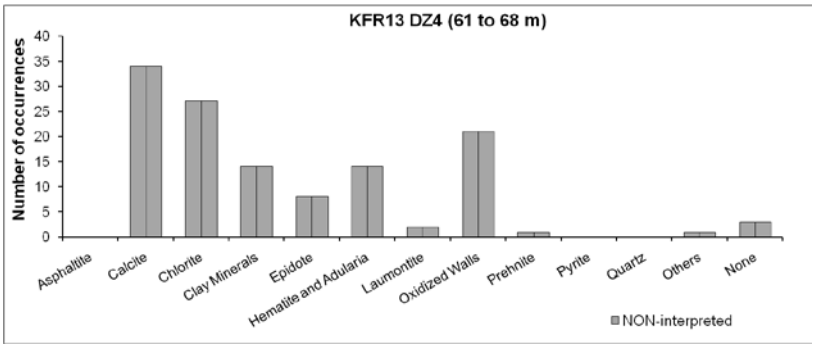

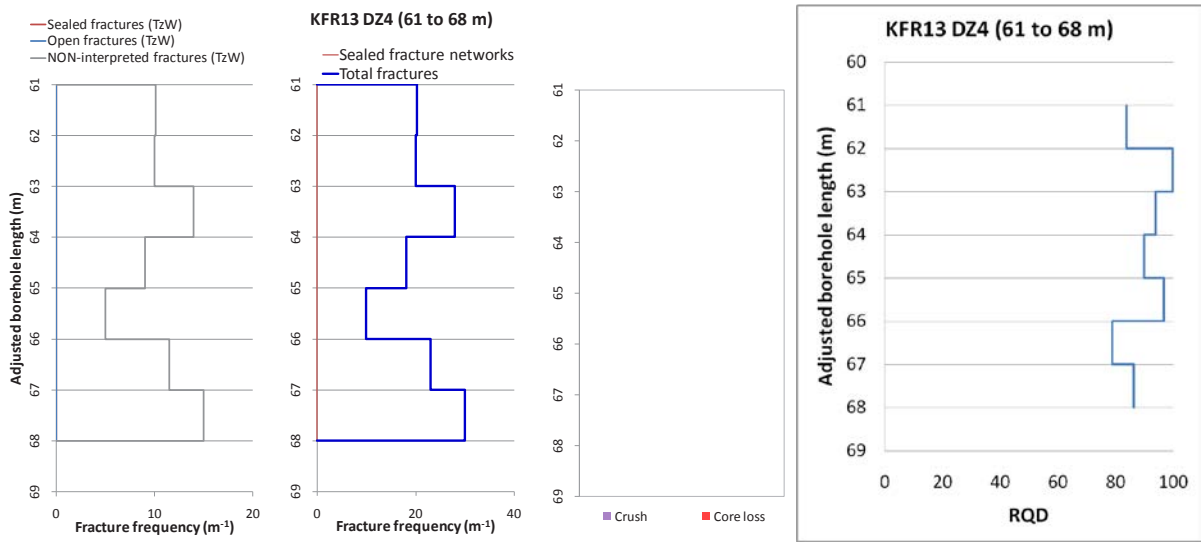

Borehole intersections for ZFM871				
BH	**Geometrical Intercept**		**Target intercept**	
	Sec_up BH length (m) [z (-m)]	**Sec_low BH length (m) [z (-m)]**	**Sec_up BH length (m) [z (-m)]**	**Sec_low BH length (m) [z (-m)]**
KFR31	217.28 [143.72]	eoh [160.73]	228.76	232.00
SHI DZ2 228.76–232.00 m: Increased frequency of broken fractures and several crushed intervals. α-angles generally > 45° and typically parallel with the tectonic foliation. Generally faint to weak oxidation of the metagranite and faint to weak chloritization of the amphibolites. Predominant minerals in broken fractures are clay minerals, hematite, chlorite and calcite. Fine- to medium-grained metagranite-granodiorite (101057) and amphibolite (102017). Confidence level = 3. Moderate transmissivity of the interval 204–242 m ($9 \cdot 10^{-7}$ m^2/s).				
KFR32	161.72 [112.29]	186.25 [130.08]	163.10	186.10
SHI DZ2 163.10–186.10 m: Increased frequency of unbroken fractures and especially broken fractures. More than 10 broken fractures/m throughout the interval. α-angles generally > 45°. Locally minor crushes. Weak to medium oxidation throughout the interval and weak to medium chloritization of amphibolites (102017). Predominant minerals in broken fractures are clay minerals, hematite, chlorite and calcite, and in unbroken fractures laumontite. Fine- to medium-grained metagranite-granodiorite (101057) and amphibolite (102017). Confidence level = 3. High transmissivity of the interval 163–176 m ($4 \cdot 10^{-5}$ m^2/s) and moderate transmissivity of the interval 176–187 m ($2 \cdot 10^{-6}$ m^2/s).				
KFR37	172.25 [148.38]	200.89 [173.79]	183.43	193.60
SHI DZ2 183.43–193.60 m: Increased frequency of broken fractures with an average of c. 10 broken fractures/m outside crushes. Variable α-angles, but generally > 45°. Crushed interval at 191.00–192.35 m. Generally weak to medium oxidation. Predominant minerals in broken fractures are clay minerals, hematite/Fe-hydroxide and locally chlorite. Fine- to medium-grained metagranite-granodiorite (101057) and pegmatitic granite (101061). Confidence level = 3. High transmissivity of the interval 183–194 m ($4 \cdot 10^{-5}$ m^2/s). The dominating transmissivity is contained in the in the section 191–194 m.				
KFR57	6.00 [93.60]	eoh [112.98]	15.85	25.38
Comment:				
SHI DZ1 15.85–25.38 m: Increased frequency of broken fractures. Varying α-angles with generally low angles (< 30°) in the cental part of the interval. Generally faint to moderate oxidation and at 16.80–21.50 m argillization, locally of strong intensity. Predominant minerals in broken fractures are clay minerals. Pegmatitic granite (101061), fine- to medium-grained granite (111058) and amphibolite (102017). Confidence level = 3. No hydraulic test data from this borehole.				

Borehole intersections for ZFM871				
BH	**Geometrical Intercept**		**Target intercept**	
	Sec_up BH length (m) [z (-m)]	**Sec_low BH length (m) [z (-m)]**	**Sec_up BH length (m) [z (-m)]**	**Sec_low BH length (m) [z (-m)]**
KFR21	108.57 [108.57]	129.26 [129.26]	–	–
Comment: No drill core available.				
KFR22	139.98 [121.22]	eoh [138.65]	–	–
Comment: No drill core available.				
KFR23	81.75 [70.80]	105.07 [90.99]	–	–
Comment: No drill core available.				
KFR33	158.04 [104.28]	eoh [110.49]	–	–
Comment: No drill core available.				
KFR80	0.00 [136.00]	13.29 [148.49]	–	–
Comment: No drill core available.				
KFR83	5.28 [90.23]	eoh [98.67]	–	–
Comment: No drill core available.				

Tunnel intersections for ZFM871				
Tunnel	**Geometrical Intercept**		**Target intercept**	
	Start ch.(m)	**End ch. (m)**	**Start ch.(m)**	**End ch. (m)**
NBT	0+380	0+432 (End of tunnel)	0+405	0+432

Comment: Target intercept defined by (tDZ101, tDZ102, tDZ103 and tDZ104 0+405–0+432) in Appendix 2. 2009/.Control point added at chainage 0+405. Due to the gentle dip and nature of the zone the selected central point, representing the zone position, is approximate

Note: /Axelsson and Hansen 1997/ estimate NBT 8+405 to 8+435 and that the zone also occurs in the connecting rock drainage basin (BB).

The modelled zone geometry also encompasses the rock drainage basin (BB), the support shaft (FS) and nearby niches (connection to the NBT at 0+405) but no detailed survey measurements are available for chainage estimates.

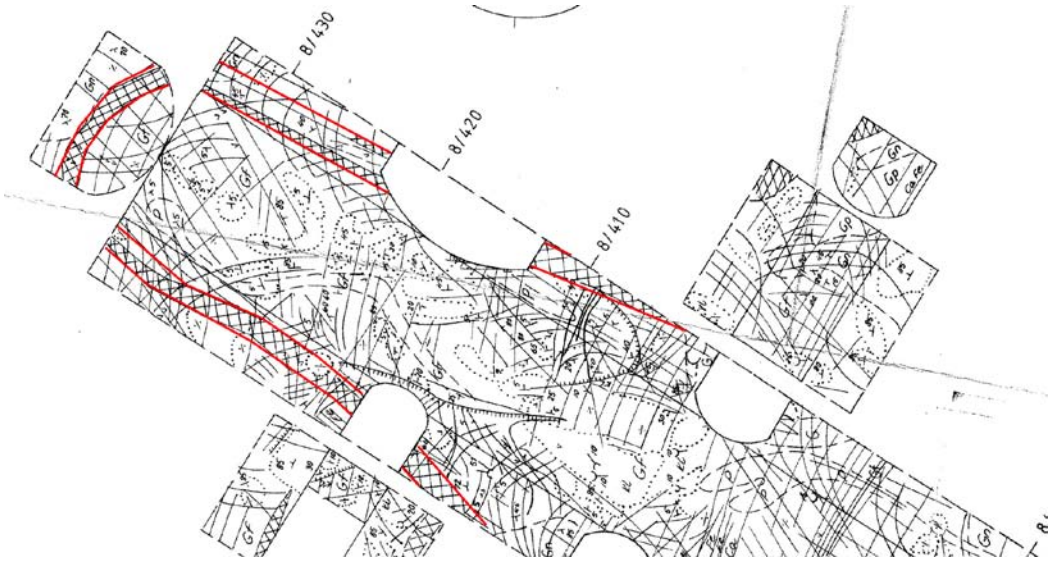

Position of ZFM871 in the NBT shown by red outline and original cross hatching from detailed mapping drawing –17 of /Christiansson and Bolvede 1987/.

Deformation zone ZFMA1

Borehole and tunnel intersections (metres along borehole/tunnel)

None

Deformation style, alteration and geometry

Deformation style: Assumed to be brittle

Alteration: No data

Strike/dip (span) right-hand-rule: 082 / 45 (–7/±5)

Trace length at ground surface (span): Does not intersect the surface

Model thickness (span) : 40 m (9–45 m)

Confidence in existence: Medium

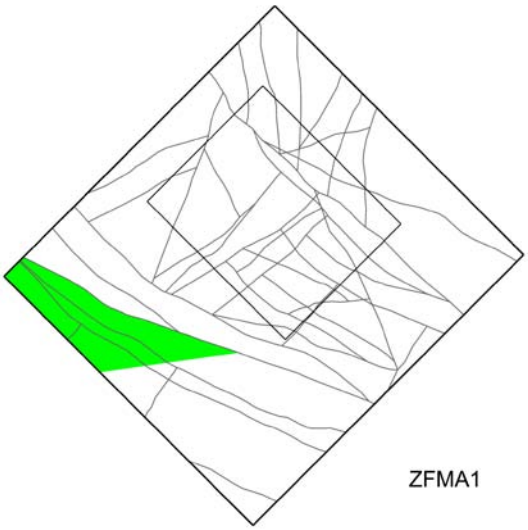

No intersection with the ground surface

Modelling procedure*:* Corresponds to seismic reflector A1/A0 /Juhlin et al. 2002/, the position of which in 3D space has been attained from /Cosma et al. 2003/. Properties adopted from /Stephens et al. 2007/. Selective reprocessing and review of the seismic data along profiles 5b and 8 /Juhlin and Zhang 2010/ resulted in a slight modification of the original reflector orientation from 082°/45° to 075°/45°, but this minor strike adjustment falls within the earlier stated uncertainty range presented in /Stephens et al. 2007/. The earlier modelled zone extent, orientation, thickness and uncertainty thickness span have been maintained after /Stephens et al. 2007/.

Fractures in the deformation zone

General characteristics

Fracture orientation: No data

Fracture frequency: No data

Fracture filling mineralogy: No data

Deformation zone ZFMB10

Borehole and tunnel intersections (metres along borehole/tunnel)

None

Deformation style, alteration and geometry

Deformation style: No data

Alteration: No data

Strike/dip (span) right-hand-rule): 025 / 35 (±15/±10)

Trace length at ground surface: The interpreted extent of the reflector does not intercept the ground surface

Model thickness: 10 m (a 1% default value based on an estimated equivalent length of 950 m)

Confidence in existence: Low

No intersection with the ground surface

Modelling procedure*:* The modelled zone is based on the reprocessed seismic data and resulting reflector geometry as reported by /Juhlin and Zhang 2010/. The main conclusion from the report is that a new reflection (B10) has been identified that may extend below the SFR site. This reflection was not clearly observed in the previous processing /Juhlin and Palm 2005/. The reflection is oriented approximately 025°/35°. This orientation is similar to the set B group identified earlier /Juhlin and Palm 2005/. Note that the dip of the reflection is uncertain. On shot gathers it appears to dip at a slightly shallower angle while on the stacked sections it appears to dip at a greater angle. This discrepancy is probably due to the crooked nature of the profiles. However, reflections are clearly observed in shot gathers and its presence below SFR is highly probable. See /Juhlin and Zhang 2010/ for further details.

In accordance with earlier modelling work at Forsmark, ZFMB10 has been terminated against the major WNW-ESE and NW-SE, composite ductile and brittle deformation zones (ZFMWNW0001, ZFMWNW1035, ZFMNW0805A and ZFMNW0805B).

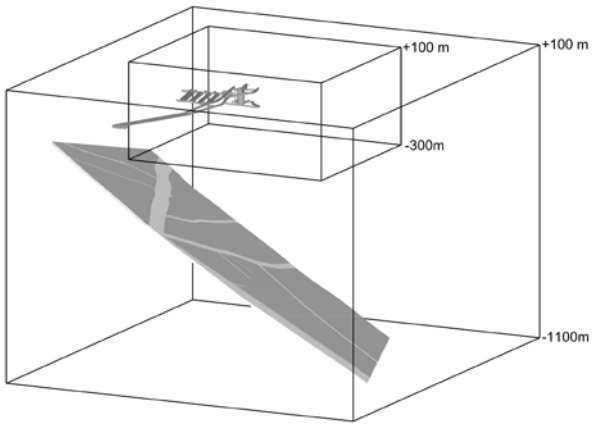

ZFMB10 (grey slab) lies entirely outside and below the local model volume.

Fractures in the deformation zone

General characteristics

Fracture orientation: No data

Fracture frequency: No data

Fracture filling mineralogy: No data

Steeply dipping NNE to ENE deformation zones

Deformation zone ZFMENE3115

Borehole and tunnel intersections (metres along borehole/tunnel)

KFR102A: 422–503 m (DZ3 422–503 m)
KFR104: 149–154 m (DZ2 149–154 m)
KFR105: 45–52 m (DZ1 45–52 m)

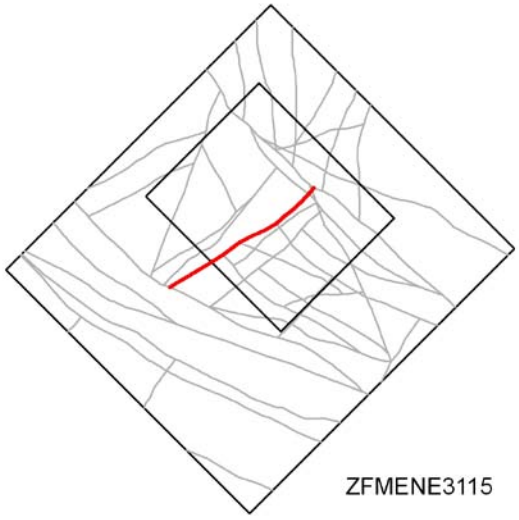

Deformation style, alteration and geometry

Deformation style: Brittle. Cohesive breccias present in all BH intercepts

Alteration: Locally red-stained bedrock with fine-grained hematite dissemination and argillization. Vuggy rock with quartz dissolution at 440.39–440.91, 441.64–441.76, 448.85–458.65, 473.15–474.14 and 478.35–478.42 m in KFR102A DZ3

Strike/dip (span) right-hand-rule: 236 / 84 (±5 / ±5)

Trace length at ground surface (span): 793 m (750–850 m)

Model thickness (span): 28 m (3–30 m)

Confidence in existence: High

Modelling procedure*:* The position of the zone on the ground surface is based on the lineaments MFM3115G, MSFR08116 and MSFR10001 defined by magnetic minima (/Isaksson et al. 2007/ and SFR model version 1.0) with further extension to the south-west to allow termination at ZFMWNW1035. Forward modelling of magnetic data along profiles 20 and 42 (see Appendix 6) provide weak support for the modelled zone thickness and the sub-vertical dip to the north-west.

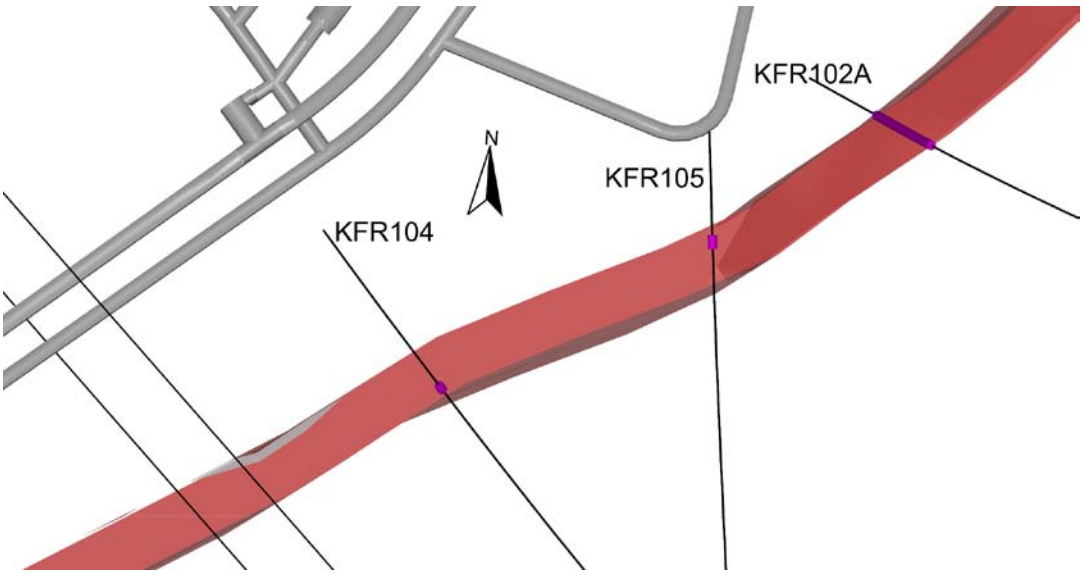

View of ZFMENE3115 looking down dip showing the SHI PDZ intercepts (pink cylinders) in KFR102A, KFR104 and KFR105. It should be noted that the modelled zone thickness of 28 m is based on KFR102A DZ3. An alternative interpretation of DZ3 is that it represents more than one zone and this would result in a reduction of ZFMENE3115 thickness to around 10 m.

Deformation zone ZFMENE3115

Fractures in the deformation zone

General characteristics

Fracture orientation:

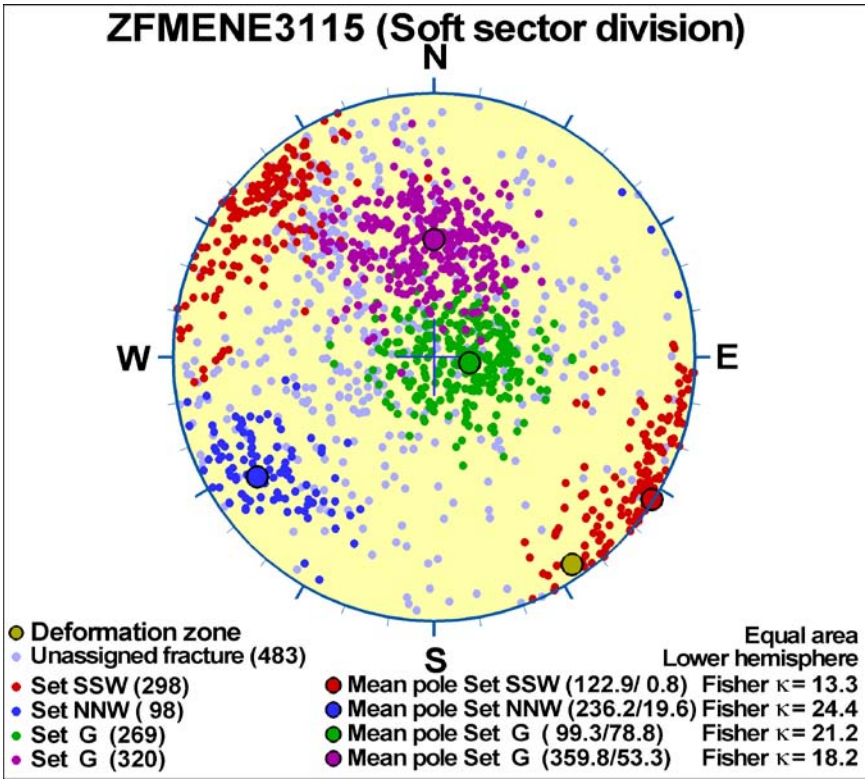

Fracture frequency: Open 10 m^{-1}, Sealed 31 m^{-1}

Fracture filling mineralogy:

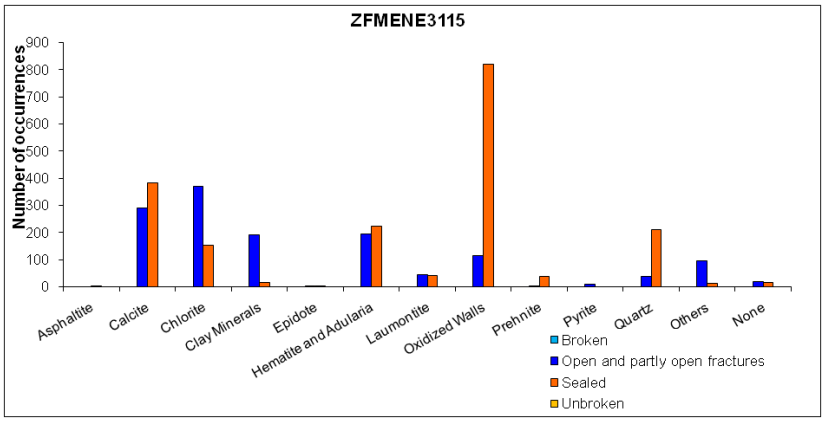

KFR104 DZ2 (149–154 m)

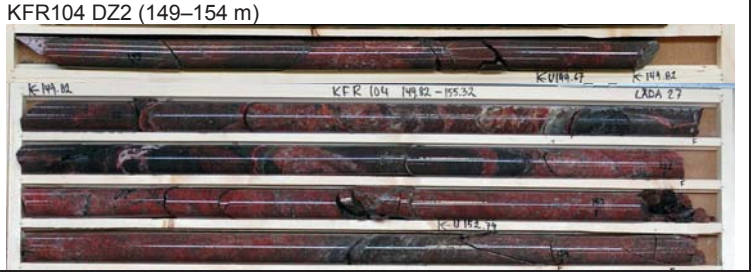

Deformation zone ZFMENE3115	
	KFR105 DZ1 (45–52 m) 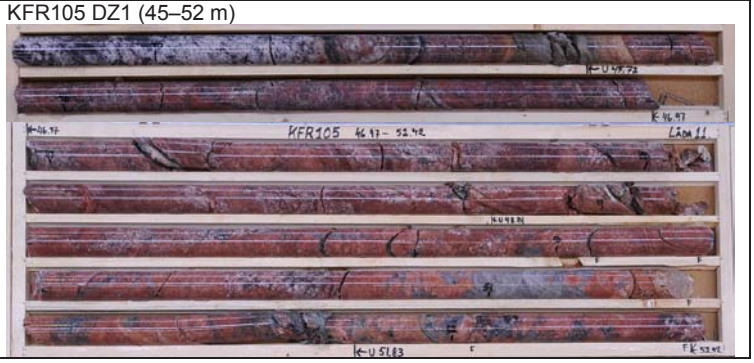

BOREHOLE AND TUNNEL INTERCEPT DETAILS

Borehole intersections for ZFMENE3115				
BH	**Geometrical Intercept**		**Target intercept**	
	Sec_up BH length (m) [z (-m)]	**Sec_low BH length (m) [z (-m)]**	**Sec_up BH length (m) [z (-m)]**	**Sec_low BH length (m) [z (-m)]**
KFR102A	423.71 [380.72]	503.36 [451.30]	422	503

SHI DZ3 422–503 m: Increased frequency of open and sealed fractures in the intervals 422–444 and 461–503 m. Eight crushes with the most extensive at 434.65–435.90 m. Two slickensides. Fracture apertures generally up to 0.5 mm with a few ranging up to 2 mm and a local maximum up to 10 mm. Locally weak to strong oxidation, rarely argillisation, laumontitisation and carbonatitisation. Five intervals with quarts dissolution at 440.39–440.91, 441.64–441.76, 448.85–458.65, 473.15–474.14 and 478.35–478.42 m. Ductile deformation recorded at 466.46–466.09 m (019°/81°) and brittle ductile deformation recorded at 488.86–489.10 m (320°/41°). Predominant minerals in open fractures are chlorite, calcite, hematite, clay minerals, in sealed fractures calcite, quarts, adularia and chlorite and in sealed fracture networks calcite, quartz, chlorite and clay minerals. The entire possible deformation zone is characterised by poor radar penetration. The entire interval 422–503 m is characterized by significantly decreased bulk resistivity, several distinct caliper anomalies and decreased magnetic susceptibility. The most prominent low resistivity anomalies occur in the intervals 434–443, 451–458 and 471–475 m. In the section 450–457 m the density is significantly decreased, c. 2,570 kg/m^3. Starting at 427 m the fluid temperature is characterized by several anomalies, and this pattern of anomalies continues through out the entire borehole length. Metagranite-granodiorite (101057), pegmatitic granite (101061) and amphibolite (102017). Confidence level = 3.

No flow anomalies above 427 m. Increased frequency of flow anomalies in the interval 427–458 m. No flow anomalies below 458 apart from one single flow anomaly at 474 m. The total transmissivity of the section is $2 \cdot 10^{-6}$ m^2/s, where the transmissivity is dominated by one single flow anomaly at 427 m (T = $1 \cdot 10^{-6}$ m^2/s) and a number of flow anomalies at the section 435–441 m (T = $8 \cdot 10^{-7}$ m^2/s). The character of the inflow indicates porous rock at 451–458 m.

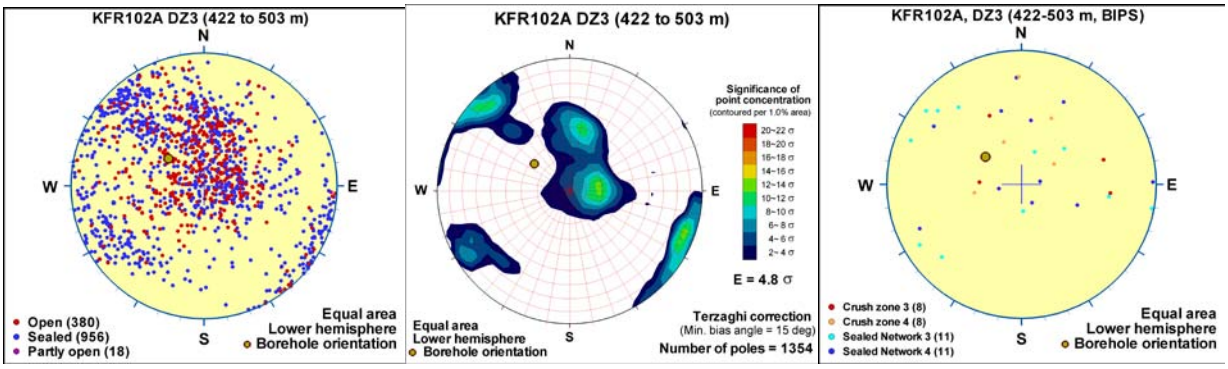

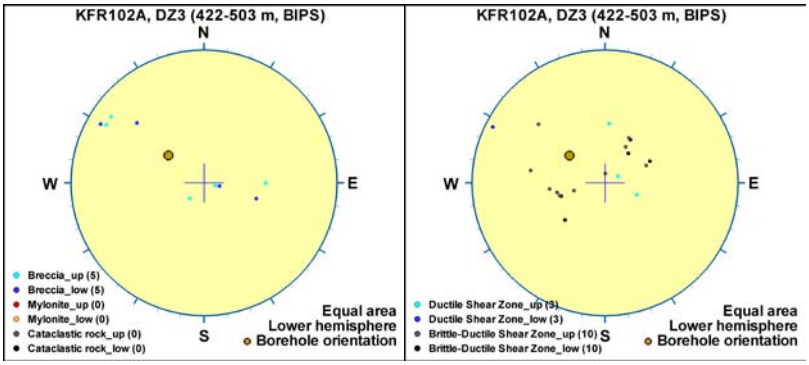

Borehole intersections for ZFMENE3115
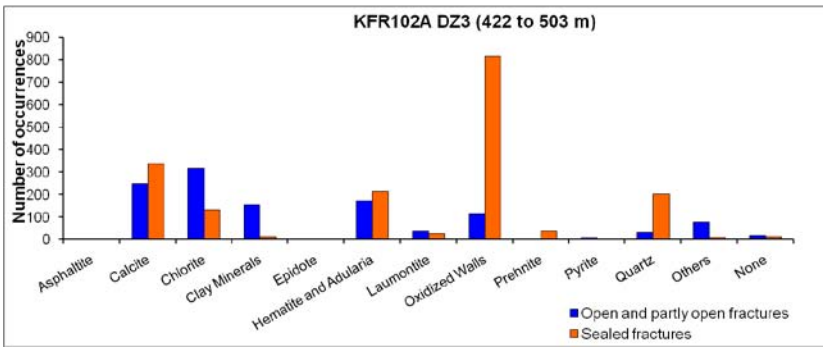
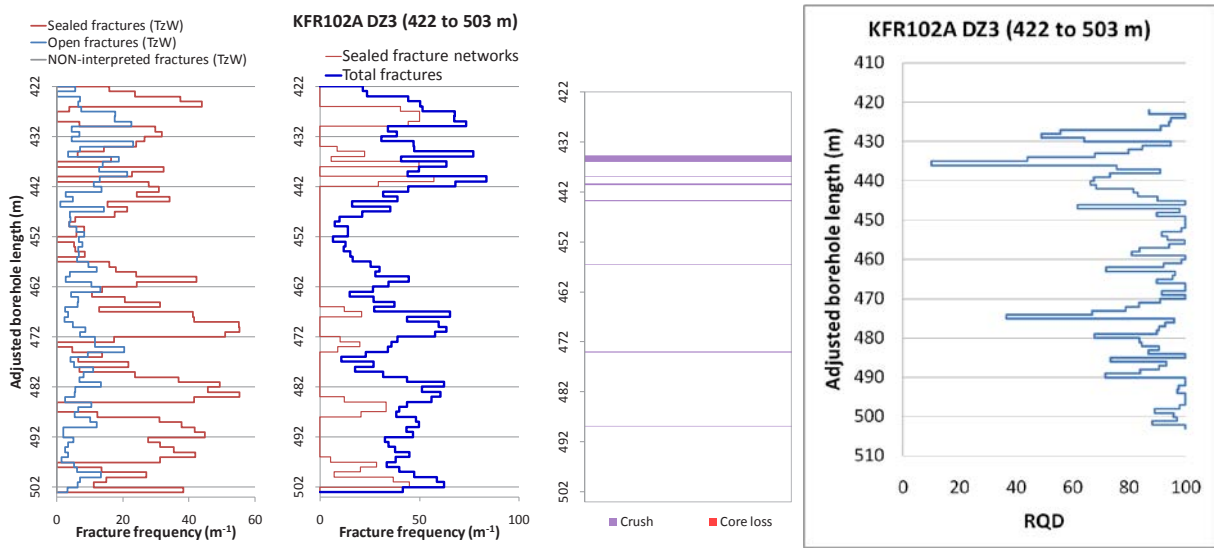

Borehole intersections for ZFMENE3115				
BH	**Geometrical Intercept**		**Target intercept**	
	Sec_up BH length (m) [z (-m)]	**Sec_low BH length (m) [z (-m)]**	**Sec_up BH length (m) [z (-m)]**	**Sec_low BH length (m) [z (-m)]**
KFR104	117.33 [92.42]	168.86 [133.40]	149	154
SHI DZ2 149–154 m: Increased frequency of open and sealed fractures. Fractures aperture up to 1 mm. A few moderately altered open fractures. Minor intervals of brecciation at 150.96–151.38 and 153.64–153.80 m. Locally weak to moderate argillization. Predominant minerals in sealed fractures are calcite, chlorite and laumontite and in open fractures are chlorite, calcite and hematite. Low electric resistivity. One distinct radar reflector at the lower end of the interval oriented 105°/15°. Pegmatitic granite (101061), metagranite-granodiorite (101057) and amphibolite (102017). Confidence level = 3. Low transmissivity of the interval ($4 \cdot 10^{-9}$ m^2/s).				

Borehole intersections for ZFMENE3115

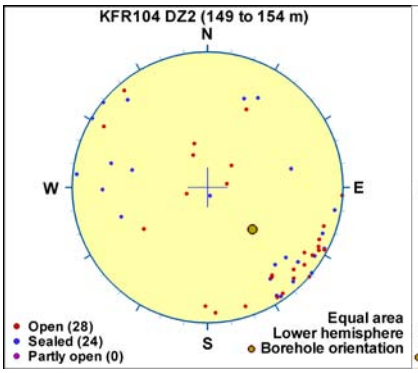

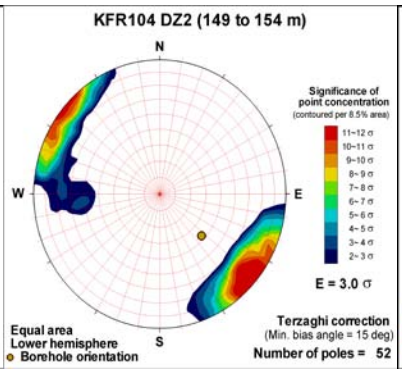

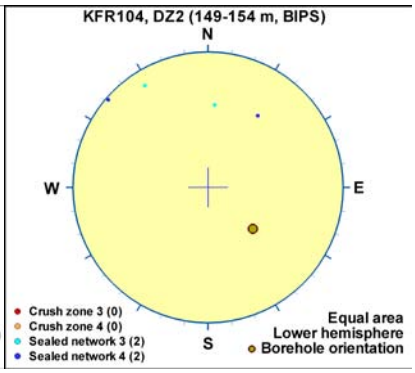

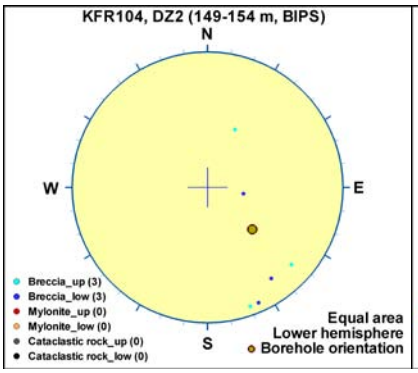

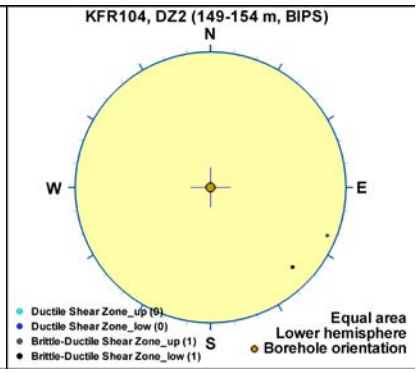

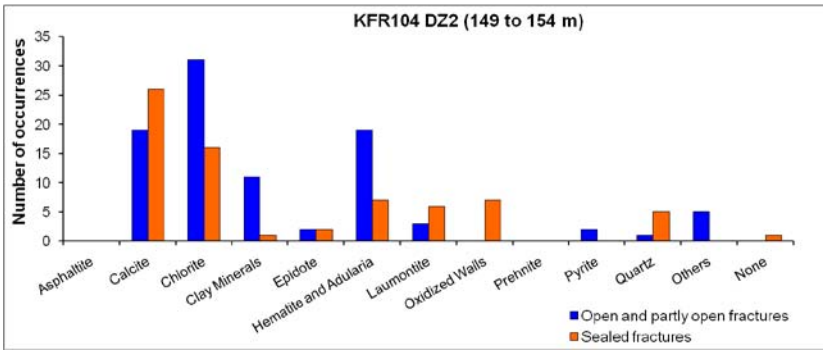

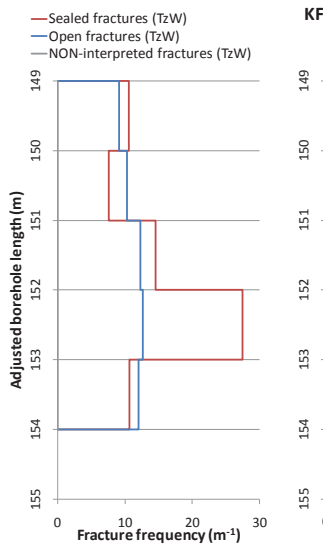

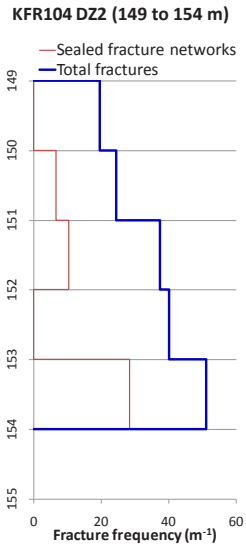

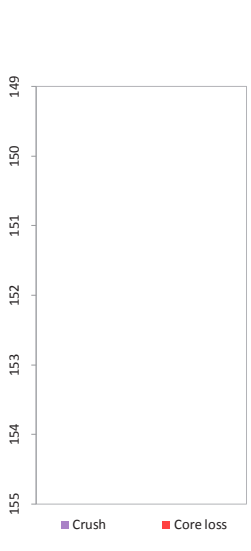

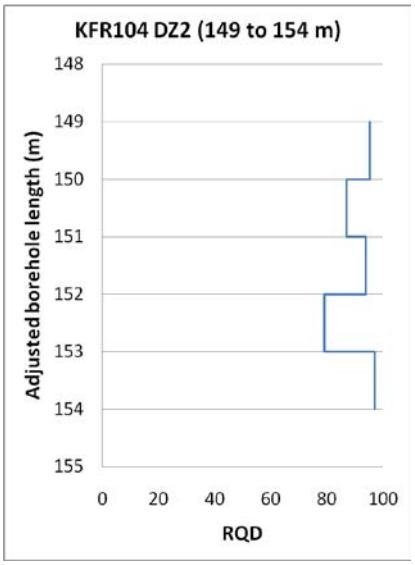

Borehole intersections for ZFMENE3115				
BH	Geometrical Intercept		Target intercept	
	Sec_up BH length (m) [z (-m)]	Sec_low BH length (m) [z (-m)]	Sec_up BH length (m) [z (-m)]	Sec_low BH length (m) [z (-m)]
KFR105	32.87 [112.53]	62.47 [117.58]	45	52

SHI DZ1 45–52 m: Increased frequency of open and sealed fractures and sealed networks. Three minor crushes at 45.58–45.66, 47.97–48.01 and 51.67–51.73 m and one cataclasite at 45.59–45.75 m. Zone cores defined at 45.55–45.85 and 51.65–51.95 m. Fracture apertures in general up to 1mm, with one aperture at 5 mm. Predominant minerals in open fractures are clay minerals, calcite, chlorite and muscovite and in sealed fractures calcite, laumontite and clay minerals. Very local argillization at 45.52–45.75, 49.01–49.04 and 51.67–51.74 m. The entire interval is characterized by several low resistivity anomalies and decreased bulk resistivity (< 1,000 Ohm-m). One radar reflector at 47.6 m, oriented 062°/72° or 282°/54°. Pegmatitic granite (101061). Confidence level = 3.

Two low-transmissive flow anomalies at 45.8 m and 49.0 m (T = $5 \cdot 10^{-9}$ and $1 \cdot 10^{-9}$ m^2/s, respectively). The total transmissivity of the section 43–53 m is about $1 \cdot 10^{-8}$ m^2/s.

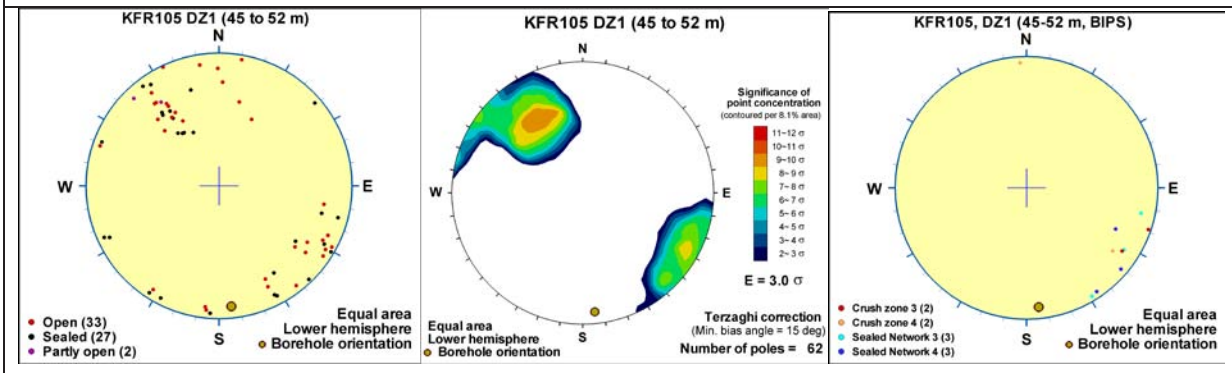

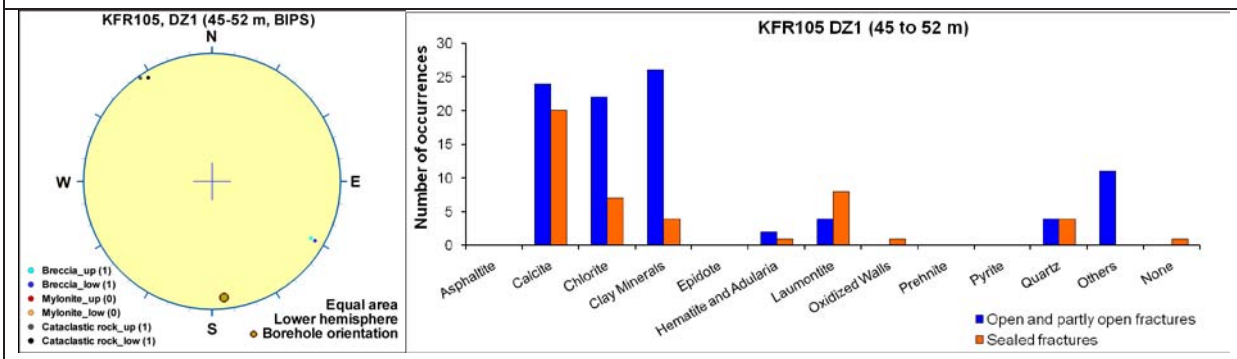

Borehole intersections for ZFMENE3115

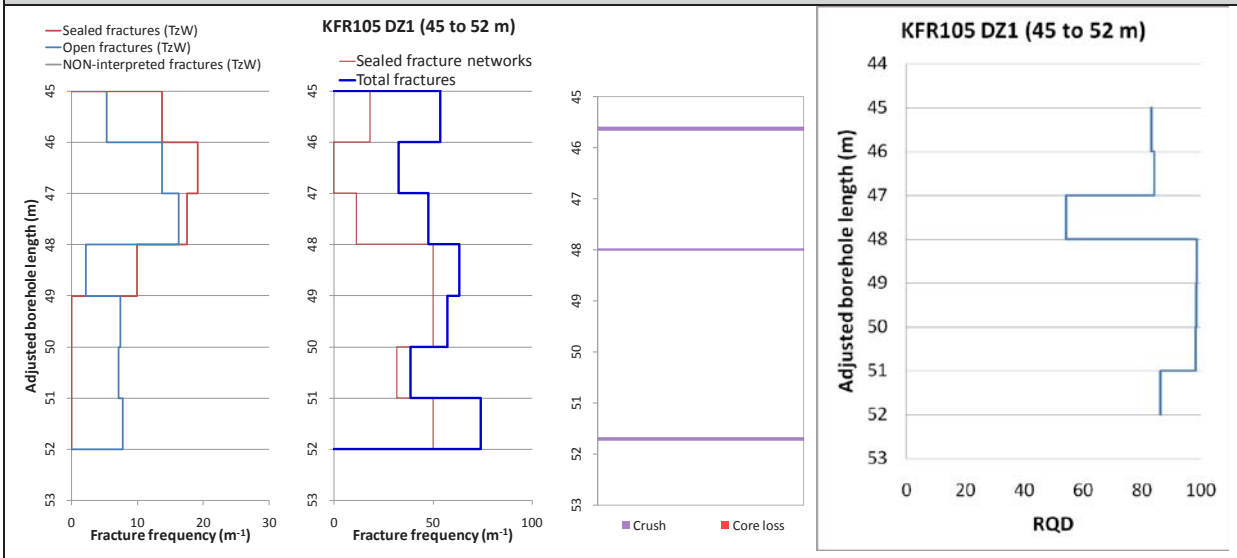

Deformation zone ZFMNE3135

Borehole and tunnel intersections (metres along borehole/tunnel)

None

Deformation style, alteration and geometry

Deformation style: Brittle (no direct evidence – inferred association with other NE-SW trending deformation zones)

Alteration: No data

Strike/dip (span) right-hand-rule: 81 / 90 (±5 / ±10)

Trace length at ground surface (span) : 368 m (200–380 m)

Model thickness: 5 m (1% default)

Confidence in existence: Medium

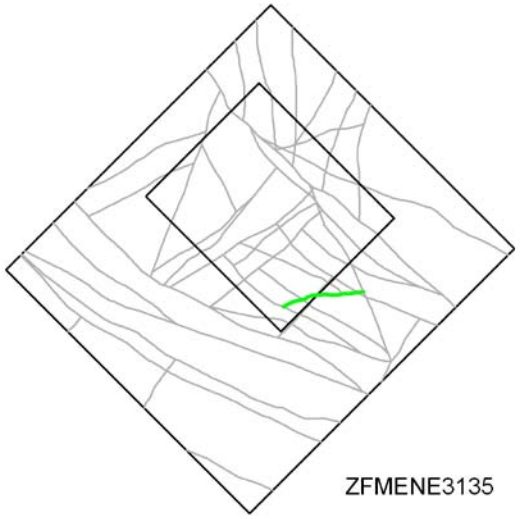

Modelling procedure*:* Based on magnetic lineament MSFR08113 in SFR model version 1.0 that is a modification of lineament MFM3135G in Forsmark model stage 2.3 /Isaksson et al. 2007/.

Fractures in the deformation zone

General characteristics

Fracture orientation: No data

Fracture frequency: No data

Fracture filling mineralogy: No data

Deformation zone ZFMENE3151

Borehole and tunnel intersections (metres along borehole/tunnel)

None

Deformation style, alteration and geometry

Deformation style: Brittle (no direct evidence – inferred association with other ENE-WSW trending deformation zones)

Alteration: No data

Strike/dip (span) right-hand-rule: 74 / 90 (±5 / ±10)

Trace length at ground surface (span) : 421 m (300–470 m)

Model thickness: 5 m (1% default)

Confidence in existence: Medium

Modelling procedure*:* The position of the zone at the ground surface is based on a modification to the magnetic lineament MSFR08005 (SFR modelling work). The lineament was originally inferred to cross ZFMNW0805A and to continue a short distance on the western side of the zone. This extension was not considered likely conceptually and the zone was terminated against ZFMNW0805A. The number from the associated, Forsmark stage 2.3 lineament MFM3151G /Isaksson et al. 2007/ has been maintained for traceability between the different versions of the lineament interpretation.

Forward modelling of magnetic data along profiles 7, 8 and 34 (see Appendix 6) support the inferred vertical dip of the inferred zone, whereas profile 9 indicates a very steep dip to the north-west.

Deformation zone ZFMENE8031

Borehole and tunnel intersections (metres along borehole/tunnel)

None

Deformation style, alteration and geometry

Deformation style: Brittle (no direct evidence – inferred association with other ENE-WSW trending deformation zones)

Alteration: No data

Strike/dip (span) right-hand-rule: 63 / 90 (±5 / ±10)

Trace length at ground surface: 537 m (530−670 m)

Model thickness / model thickness span : 5 m (1% default)

Confidence in existence: Medium

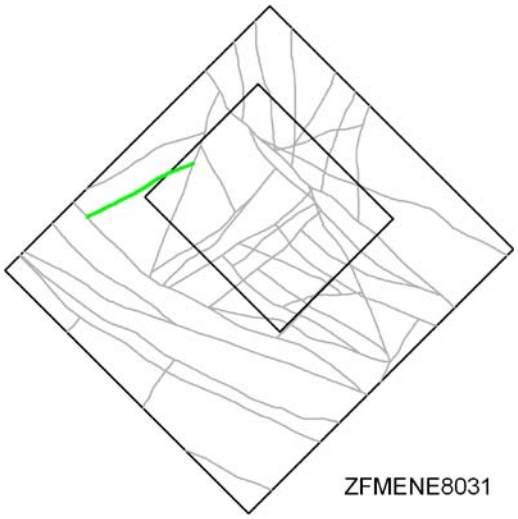

Modelling procedure*:* The position of the zone at the ground surface is based on a modification of the SFR version 1.0 lineament MSFR08031. The DZ trace terminates at ZFMNNE0869 to the NE whereas the lineament extends further to the NE. However, the existence of a zone coupled with the lineament in this position is not supported by tunnel mapping. The DZ trace has a greater extent in the SW where it terminates at ZFMWNW1035, whereas the lineament ends at the general boundary of an area where the magnetic field is 'disturbed' and prevents further interpretation.

The initial hypothesis was that the zone dips gently to moderately to the SE. However, any dip between 20 and 70° to the SE would generate a significant intercept in the SFR tunnels and caverns as well as boreholes and nothing significant with such an orientation has been noted. The remaining alternatives are a subvertical to northwards dip. The zone has been modelled as vertical since there is no actual evidence for a northerly dip.

Forward magnetic modelling has been performed along profiles 27, 28, 29 and 30 (see Appendix 6). The anomaly pattern is weak and the results have a high uncertainty. The clearest indicator is from profile 27 where the modelling supports a subvertical dip to the inferred zone. No real indications of orientation can be obtained from profile 28, while profiles 29 and 30 indicate a "slight dip towards the south-east" though the uncertainty is high. The inversion modelling gives no clear indications as regards orientation.

Fractures in the deformation zone

General characteristics

Fracture orientation: No data

Fracture frequency: No data

Fracture filling mineralogy: No data

Deformation zone ZFMENE8034

Borehole and tunnel intersections (metres along borehole/tunnel)

None

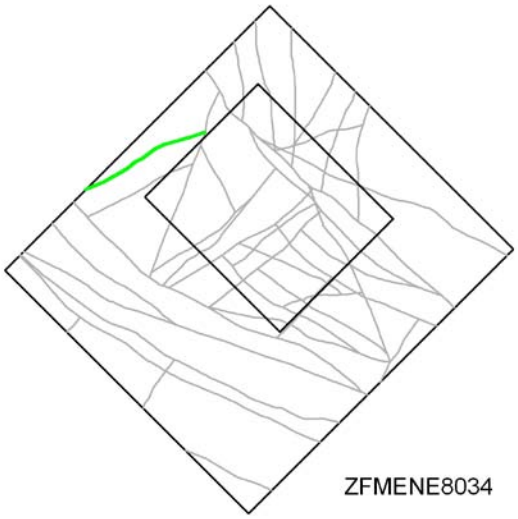

Deformation style, alteration and geometry

Deformation style: Brittle (no direct evidence – inferred association with other ENE-WSW trending deformation zones)

Alteration: No data

Strike/dip (span) right-hand-rule: 67 / 90 (±5 / ±10)

Trace length at ground surface (span): 1203 m (1200−1300 m)

Model thickness: 10 m (1% default)

Confidence in existence: Medium

Modelling procedure*:* In the early stage of the modelling work, the main supporting evidence for the inferred dip and general orientation of this zone was seismic reflector A1 /Juhlin and Palm 2005/. Subsequently, after the re-processing of the seismic data /Juhlin and Zhang 2010/, the existence of this reflector to the north of the Singö zone has been discounted, in accordance with the interpretation already made in Forsmark model stage 2.2 /Stephens et al. 2007/. Consequently the dip and detailed alignment of the zone were also revaluated.

Attempts have been made, in combination with the interpretation of H1 and H3 /Carlsson et al.1985/, to generate a sub-horizontal zone lying above the existing SFR facility. This geometry was not supported by the position of the lineament. Other dips to the south were also investigated but the main range would generate intercepts in the existing facility that are not supported by the tunnel and cavern geological mapping. Consequently, the zone has been modelled as vertical and is interpreted as being a member of the ENE sub-set with properties similar to the other zones in this sub-set.

Fractures in the deformation zone

General characteristics

Fracture orientation: No data

Fracture frequency: No data

Fracture filling mineralogy: No data

Deformation zone ZFMNE0870

Borehole and tunnel intersections (metres along borehole/tunnel)

HFR101: 28–41 m (DZ1 8.04–58 m)
KFR02: 32.5–37.5 m (DZ1 32.5–37.5 m)
KFR03: 48.00–95.95 m (DZ2 48.00–53.65 m, DZ3 70.42–72.75 m and DZ4 81.86–95.95 m)
KFR04: 14–63 m (DZ2 14–63 m)
KFR7C: 6.23–7.15 m (DZ1 6–32 m)
KFR31: 228.76–232 m (DZ2 228.76–232 m)
KFR54: 27–40 m (DZ2 27–40 m)
KFR55: 17–38 m (DZ2 8–38 m)
KFR68: 71.59–105.13 m (DZ1 71.59–78.11 m and DZ2 102.83–105.13 m)
DT: 0+535–0+570 (tDZ40)
DT: DT-BT connection tunnel at 0+610 (tDZ40)
BT: 0+640–0+690 (tDZ40)
BT: 0+888–0+907 (tDZ56)
BT: 1+020–1+050 (tDZ66)
NBT: 0+352 (tDZ80)
STT: 0+810–0+820 (tDZ66)
IST: 0+088 (tDZ80)

Deformation style, alteration and geometry

Deformation style: Brittle. Cohesive breccia present in KFR03 DZ2. A possible ductile precursor is recorded by /Carlsson et al. 1986/

Alteration: Red-stained bedrock with fine-grained hematite dissemination and locally minor argillization

Strike/dip (span) right-hand-rule: 232 / 76 (±5 / 70−90)

Trace length at ground surface (span): 559 m (500−730 m)

Model thickness (span): 16 m (2−20 m)

Confidence in existence: High

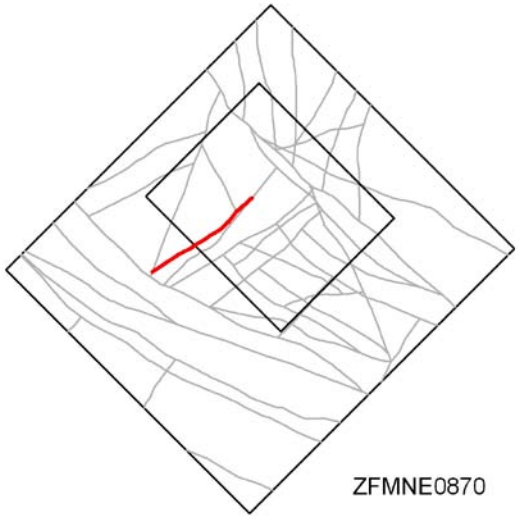

Modelling procedure*:* This zone corresponds to zone 9 in earlier SFR models (see, for example, Axelsson and Hansen 1997/). It was renamed ZFMNE0870 in the Forsmark stage 2.2 model /Stephens et al. 2007/. It has been remodelled in SFR model version 1.0 to extend from ZFMNW1035 and ZFMNNE0869 in the south-west to ZFMNW0805A/B and ZFMNE3118 in the north-east. The earlier subdivision into two sections (ZFMNE0870A and ZFMNE0870B) with an offset at ZFMWNW3262 has been rejected, based on a lack of support from new borehole data. /Axelsson and Hansen 1997/ state that this zone is, for most of its length, a water-bearing gouge-filled joint. Mylonitization was also recorded and, if correctly interpreted (cataclastic rock?), indicates a ductile origin whilst the clay gouge indicates brittle reactivation. Flush-water loss and water leakage in the BT from 5/640-5/690 were also recorded.

The surface position, based on a projection of tunnel mapping results, lacks a corresponding magnetic lineament and ZFMNE0870 is not crossed by a seismic refraction survey profile. The central part of the zone lies beneath the pier corresponding to an area where the magnetic field is disturbed. The zone has been modelled as an undulating surface based on multiple tunnel intercepts and correlation with borehole SHI results.

Deformation zone ZFMNE0870

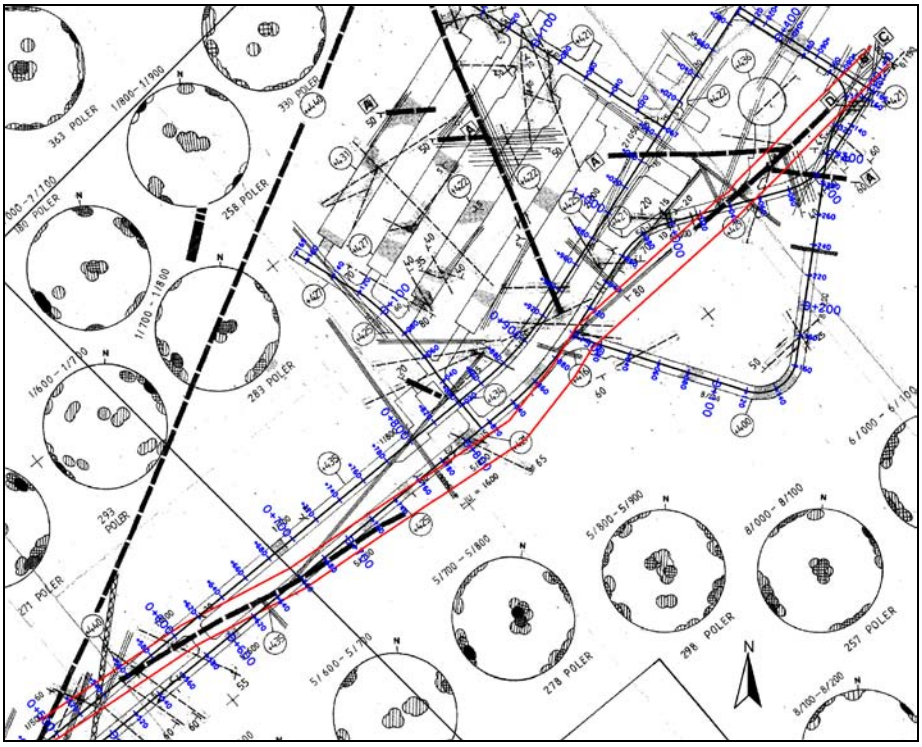

A horizontal section through ZFMNE0870 at general tunnel level, –75 m elevation. The modelled zone position is shown by the two parallel red lines. The earlier interpreted position and extent by /Christiansson and Bolvede 1987/ is seen on the original overview drawing of the tunnel mapping results as bold dashed black lines. The modelled thickness of the zone, 16 m, is based on SHI borehole results.

Deformation zone ZFMNE0870

Fractures in the deformation zone

General characteristics

Fracture orientation:

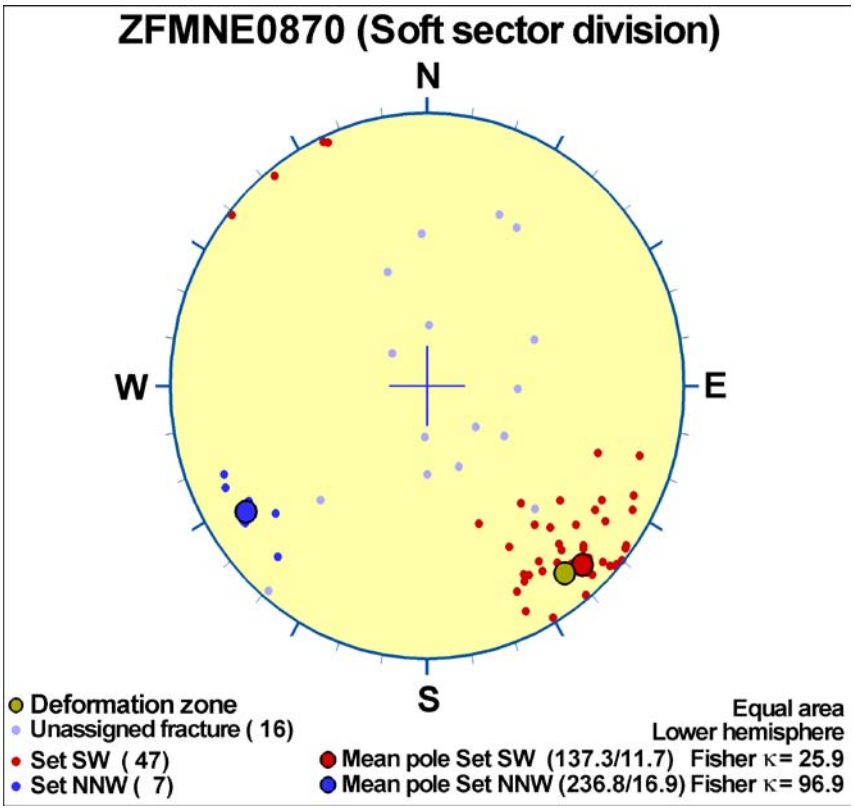

Note that the stereogram only is based on data from HFR101 (28–41 m). The number of points for the NNW set is only 7 and the corresponding low significance of the cluster is described by the Kamb plot presented for the relevant HFR101 borehole section below.

Fracture frequency: No orientaion corrected data from cored drillholes available. See HFR101 for a general indication.

Fracture filling mineralogy:

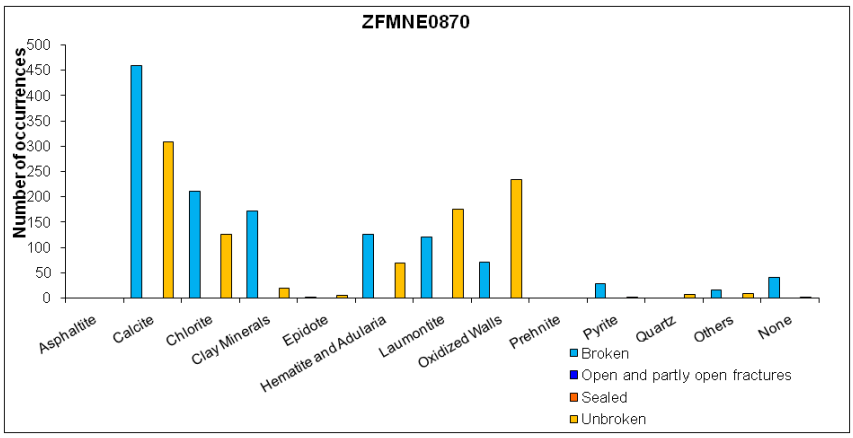

KFR02 DZ1 (32.5–37.5 m)

Deformation zone ZFMNE0870

KFR03 DZ2 (48.00–53.65 m)

KFR03 DZ3 (70.42–72.75 m)

KFR03 DZ4 (81.86–95.95 m)

Deformation zone ZFMNE0870	
	

BOREHOLE AND TUNNEL INTERCEPT DETAILS

Borehole intersections for ZFMNE0870				
BH	**Geometrical Intercept**		**Target intercept**	
	Sec_up BH length (m) [z (-m)]	**Sec_low BH length (m) [z (-m)]**	**Sec_up BH length (m) [z (-m)]**	**Sec_low BH length (m) [z (-m)]**
HFR101	19.17 [15.39]	46.17 [40.57]	28	41

Comment: An interval with slightly increased frequency of steeply dipping (> 65°) fractures, striking SW occurs at approximately 28–41 m length. Both sealed and open fractures. Control point added at 33.02 m.

(Note DZ1 = 8.04–58 m, see below)

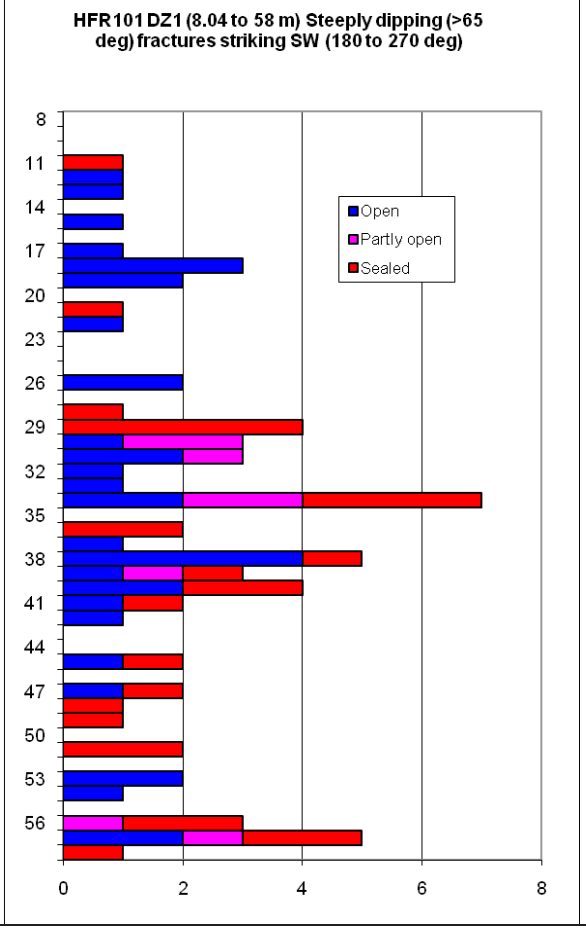

SHI DZ1 8.04–58 m: Increased frequency of open and sealed fractures. Fracture aperture up to 2 mm. Locally weak to medium oxidation. Significantly decreased bulk resistivity along the entire section and minor caliper anomalies. Metagranite-granodiorite (101057), pegmatitic granite (101061), fine- to medium-grained granite (111058), amphibolite (102017) and felsic to intermediate metavolcanic rock (103076). Confidence level = 3.

No flow anomaly in this interval.

Borehole intersections for ZFMNE0870

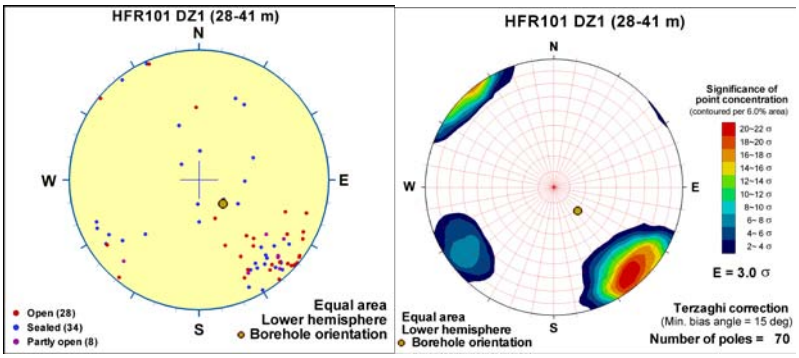

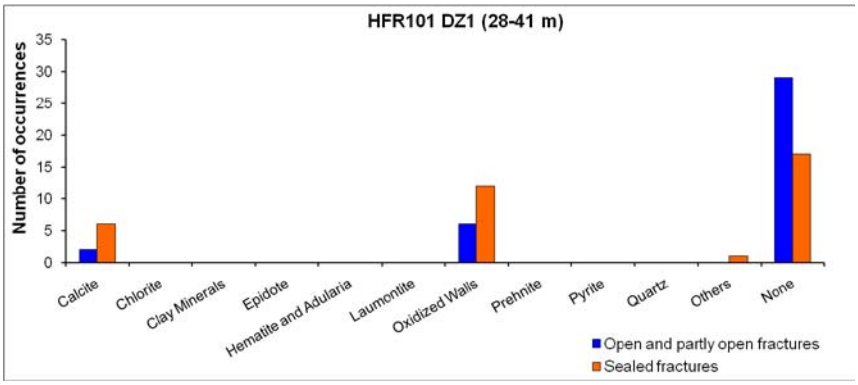

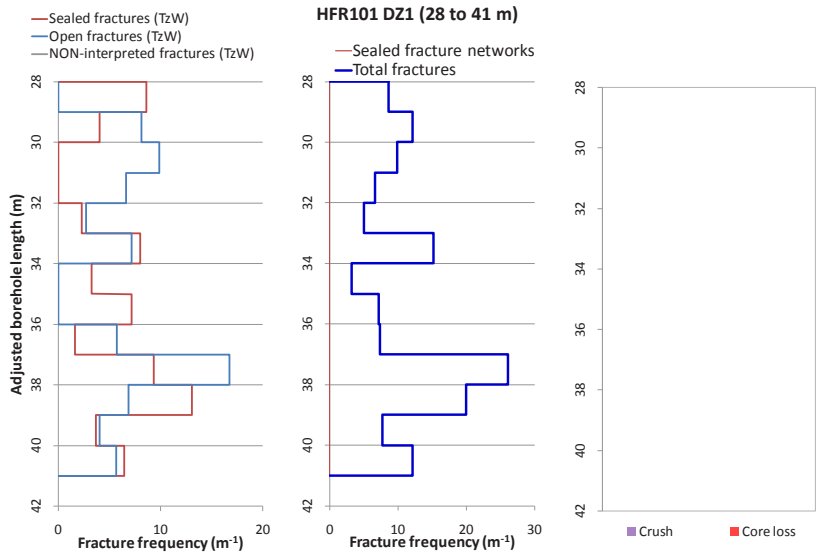

Borehole intersections for ZFMNE0870				
BH	**Geometrical Intercept**		**Target intercept**	
	Sec_up BH length (m) [z (-m)]	**Sec_low BH length (m) [z (-m)]**	**Sec_up BH length (m) [z (-m)]**	**Sec_low BH length (m) [z (-m)]**
KFR02	0 [85.43]	60.99 [146.42]	32.5	37.5
SHI DZ1 32.5–37.5: Only defined by geophysical data. Distinctly decreased levels in the resistivity and SPR data along the entire interval. In the fluid temperature data there is a significant anomaly centered at c. 34.0 m, which indicates in or out flow of water. Pegmatitic granite (101061), fine- to medium-grained metagranite-granodiorite (101057) and felsic to intermediate metavolcanic rock (103076). Confidence level = 2. Moderate but increased transmissivity of the sections 26–36 m and 36–46 m ($7 \cdot 10^{-7}$ and $4 \cdot 10^{-7}$ m^2/s, respectively).				
KFR03	36.39 [118.76]	eoh [183.97]	48	95.95
SHI DZ2 48.00–53.65 m: Increased frequency of broken and unbroken fractures. Generally α-angles > 45°. Crushed section at 50.85–51.20 m. A 4 dm long laumontite-sealed breccia at approximately 49.5 m. Generally faint oxidation. Predominant fracture minerals are laumontite, calcite, clay minerals, chlorite and hematite. Distinct decrease in the SPR logging data along the entire interval. Moderately foliated metagranite-granodiorite (101057) and pegmatitic granite (101061). Confidence level = 2. Moderate transmissivity of the section 45–56 m ($3 \cdot 10^{-7}$ m^2/s).				
SHI DZ3 70.42–72.75 m: Slightly increased frequency of broken and unbroken fractures. Generally α-angles < 45°. Faint to weak oxidation and in most of the interval strong laumontization. Predominant fracture minerals are laumontite, hematite/Fe-hydroxide, clay minerals and chlorite. Distinct decrease in the SPR logging values along the entire interval. Fine- to medium-grained granite (111058) and amphibolite (102017). Confidence level = 3. Low transmissivity of the section 57–80 m ($4 \cdot 10^{-8}$ m^2/s).				
SHI DZ4 81.86–95.95 m: Increased frequency of broken and unbroken fractures, which locally forms sealed networks. Approximately 9 broken fractures/m outside crushed intervals. Varying α-angles with several conspicuous, clay-dominated fractures at angles < 30°. Four minor crushes. Faint to weak oxidation and minor argillization associated with clay-dominated fractures. Predominant fracture minerals are clay minerals, Fe-hydroxide/hematite, chlorite and calcite, and in unbroken fractures also adularia. Distinct decrease in the SPR logging values along the section 85.0–93.0 m. Fine- to medium-grained granite (111058) and pegmatitic granite (101061). Confidence level = 3. Low transmissivity of the section 81–101.6 m ($2 \cdot 10^{-8}$ m^2/s).				

Borehole intersections for ZFMNE0870				
BH	Geometrical Intercept		Target intercept	
	Sec_up BH length (m) [z (-m)]	Sec_low BH length (m) [z (-m)]	Sec_up BH length (m) [z (-m)]	Sec_low BH length (m) [z (-m)]
KFR04	2.73 [79.83]	67.69 [142.57]	14	63

SHI DZ2 14–63 m: Increased frequency of broken and unbroken fractures. One crush at 32.60–32.77 m and one breccia at 33.00–33.22 m. Predominant fracture minerals are laumontite and calcite. Registered α–angles for laumontite-bearing fractures in the interval are generally gently to moderately dipping (< 53°). The occurrence of clay minerals is mainly concentrated to two short sections at 20–23 and 32–36 m length, which corresponds to low single point resistivity anomalies (SPR). The α–angles of these clay filled fractures are moderately to steeply dipping. Generally weak to moderately oxidized. Fine to medium grained granite (111058), amphibolite (102017) and felsic to intermediate metavolcanic rock (103076). Confidence level = 2.

The hydraulic conductivity (measured in sections of about 20–40 m) is low in the whole interval (about $1 \cdot 10^{-8}$ m/s).

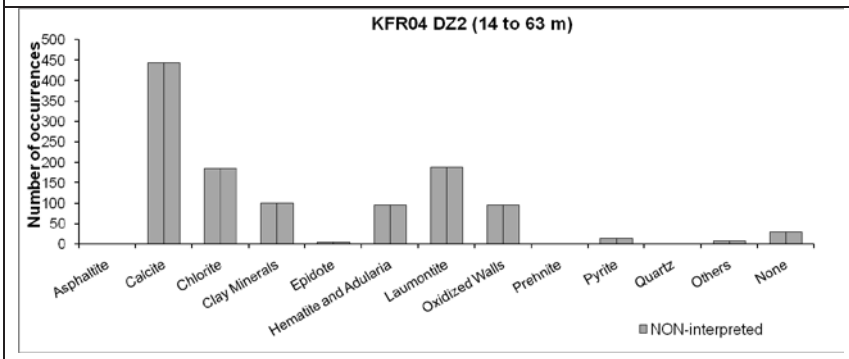

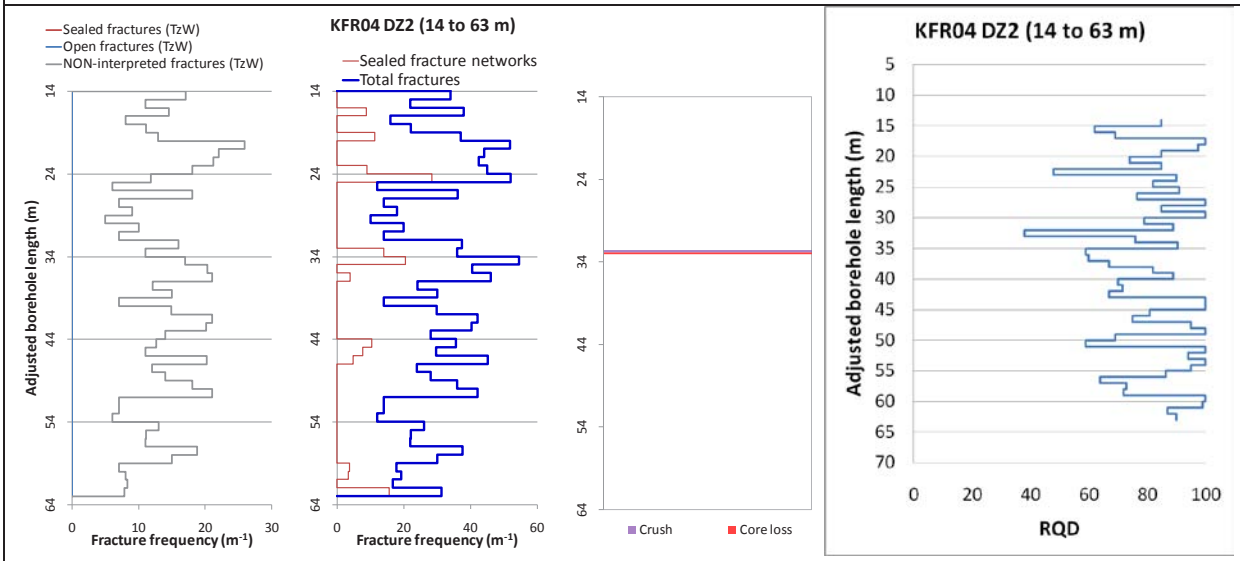

KFR7C	0.00 [133.40]	28.72 [160.39]	6.23	7.15

Comment: The intercept is considered to be dominated by ZFM871. However a short section between 6.23–7.15 m contains laumontite filled fractures with low alpha angles that could represent ZFMNE0870

Borehole intersections for ZFMNE0870				
BH	**Geometrical Intercept**		**Target intercept**	
	Sec_up BH length (m) [z (-m)]	**Sec_low BH length (m) [z (-m)]**	**Sec_up BH length (m) [z (-m)]**	**Sec_low BH length (m) [z (-m)]**
KFR31	222.79 [147.50]	eoh [160.73]	228.76	232
SHI DZ2 228.76–232.00 m: Increased frequency of broken fractures and several crushed intervals. α-angles generally > 45° and typically parallel with the tectonic foliation. Generally faint to weak oxidation of the metagranite and faint to weak chloritization of the amphibolites. Predominant minerals in broken fractures are clay minerals, hematite, chlorite and calcite. Fine- to medium-grained metagranite-granodiorite (101057) and amphibolite (102017). Confidence level = 3. Moderate transmissivity of the interval 204–242 m ($9 \cdot 10^{-7}$ m^2/s).				
KFR53	18.72 [89.91]	37.01 [98.33]	–	–
KFR54	25.31 [100.37]	42.18 [112.85]	27	40
Comment: **SHI DZ2 27–40 m:** Increased frequency of broken and to a lesser extent unbroken fractures and sealed networks. Decreased frequency of broken fractures between 28.6–33.7 m. Hematite stained clay minerals are restricted to two intervals of anomalously high fracture frequencies at 26.9–28.2 and 31.1–37.4 m, whereas laumontite mainly is restricted to 28.0–31.2 and 37.3–39.1 m. Both assemblages often include calcite. The chlorite content, on the other hand, is very low relative to that in other parts of the drill core. The α–angles of the clay-bearing fractures are typically dipping gently to moderately (30, 37, 60 and 71°). Generally weak to medium oxidation. Generally strongly foliated metagranite-granodiorite (101057) and one occurrence of pegmatitic granite (101061) in the lower most part of the section. Confidence level = 3. The hydraulic conductivity is low to very low (10^{-9}–10^{-10} m/s). 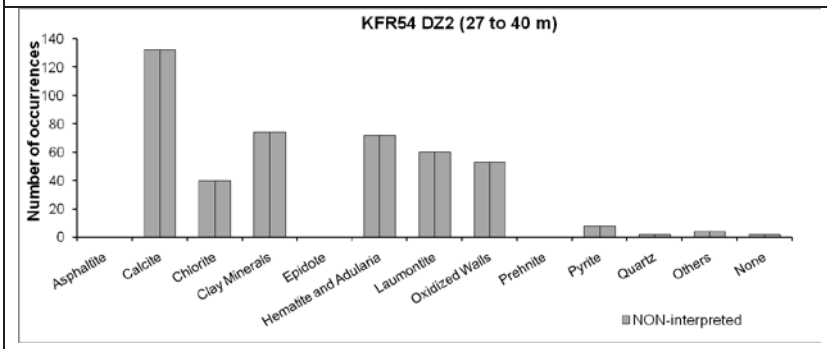 				

Borehole intersections for ZFMNE0870

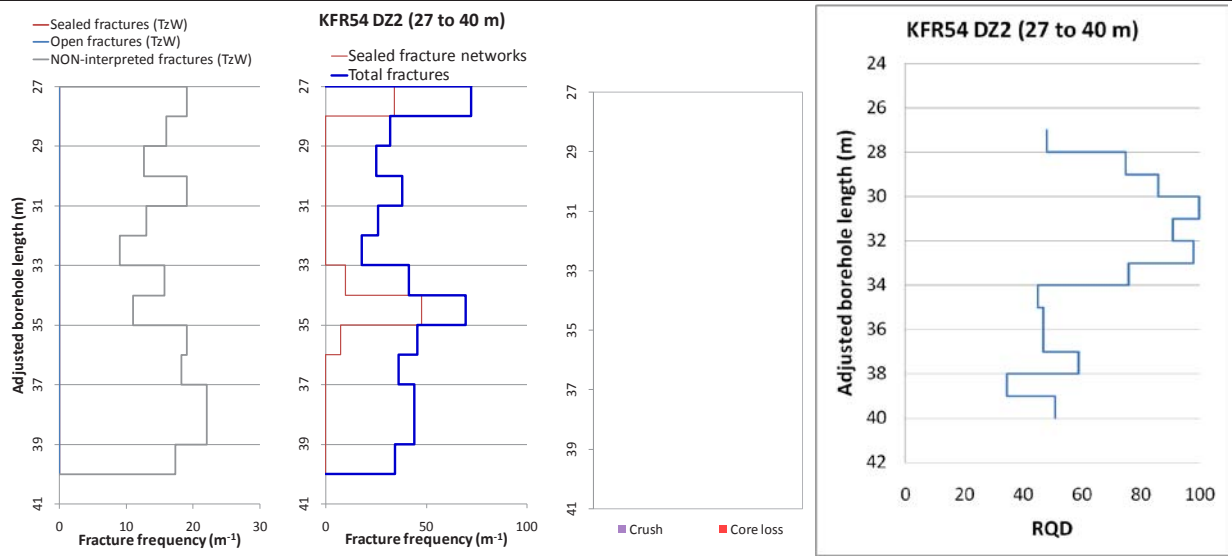

BH	Geometrical Intercept		Target intercept	
	Sec_up BH length (m) [z (-m)]	Sec_low BH length (m) [z (-m)]	Sec_up BH length (m) [z (-m)]	Sec_low BH length (m) [z (-m)]
KFR55	17.09 [128.84]	42.69 [133.72]	17	38

Comment: The quoted target intercept is based on a straightforward geometrical subdivision of DZ2 between ZFMNE0870 and ZFMNE3118. It is not expected that their character can be distinguished.

SHI DZ2 8–38 m: Increased frequency of broken and unbroken fractures and sealed networks, especially in the intervals 8–21 m and 32–38 m. Core loss at 17.86–18.51, 19.13–19.37, 33.48–33.60 and 34.89–35.33 m. The most frequent fracture filling minerals, which occur throughout the interval, are calcite, and to some extent chlorite. Fractures with clay minerals as the primary infilling are generally restricted to the interval at 16.8–19.5 m, with α–angles of 69°. Laumontite ± calcite filled fractures, on the other hand, occur along three intervals at 8.0–12.6, 16.0–16.5 and 20.4–28.1 m length. Two α–angles are registered in the uppermost (68 and 77°) and three in the lowermost (50, 57 and 65°) intervals. Locally faint to medium oxidation. Strongly foliated metagranite-granodiorite (101057) and one occurrence of fine- to medium-grained granite (111058). Confidence level = 3.

No hydrogeological investigation data from the upper 22 m of the borehole. The hydraulic conductivity is low in the measured section 22–38 m (10^{-8} m/s).

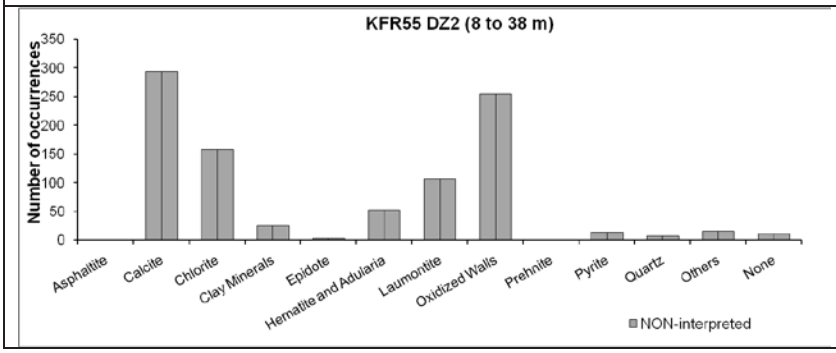

Borehole intersections for ZFMNE0870

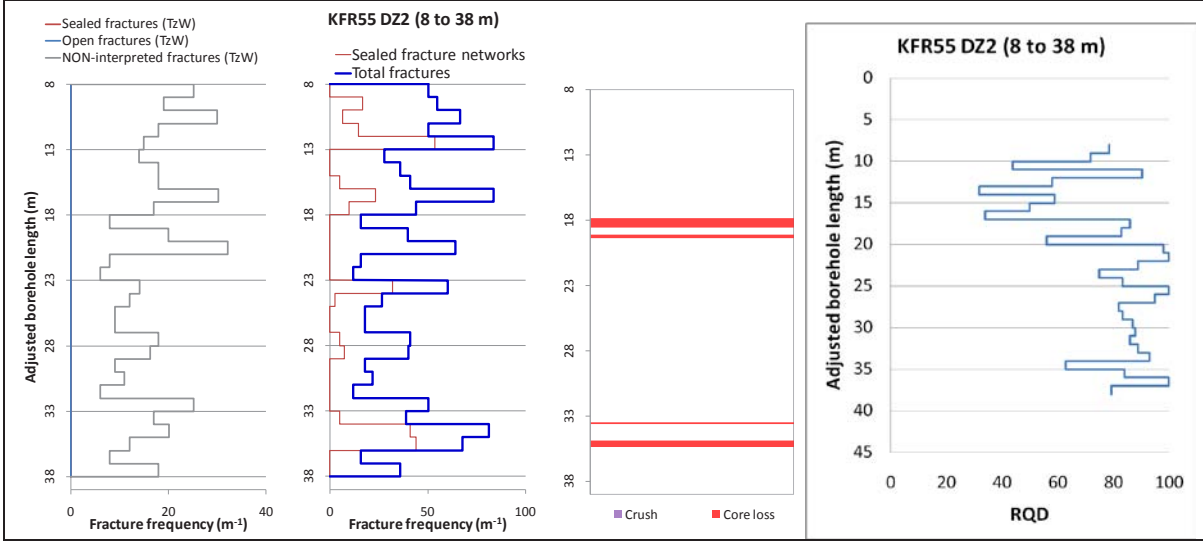

BH	Geometrical Intercept		Target intercept	
	Sec_up BH length (m) [z (-m)]	**Sec_low BH length (m) [z (-m)]**	**Sec_up BH length (m) [z (-m)]**	**Sec_low BH length (m) [z (-m)]**
KFR68	60.25 [42.60]	93.99 [66.45]	71.59	105.13
Comment: Combined SHI DZ1 and DZ2. Note: KFR68 is interpreted as intercepting the meeting point between ZFMNNE0869 and ZFMNE0870. Since the BH lacks fracture orientation data it is impossible to correlate the PDZ with any specific steeply dipping zone. Thus, the PDZ is taken as target intercept for both ZFMNE0870 and ZFMNNE0869.				
SHI DZ1 71.59–78.11 m: Increased frequency of broken fractures, locally also sealed fracture networks. Variable α-angles, but generally > 45°. Locally faint to weak argillization. Weak muscovitization throughout the interval. Predominant minerals in broken and unbroken fractures are clay minerals, calcite and chlorite. Pegmatitic granite (101061) and aplitic metagranite (101058). Confidence level = 3. Transmissivity below the measurement limit ($7 \cdot 10^{-7}$ m^2/s).				
SHI DZ2 102.83–105.13 m: Increased Increased frequency of broken fractures and crushes. Variable α-angles. Weak to moderate oxidation throughout the interval. Predominant minerals in broken fractures are clay minerals, chlorite, hematite and calcite. Fine- to medium-grained granite (111058) and pegmatitic granite (101061). Confidence level = 1. Moderate transmissivity of the interval 102.51–105.51 m ($8 \cdot 10^{-7}$ m^2/s).				
KFR7B	20.27 [152.83]	eoh [153.63]	–	–
Comment: The geometrical intercept is at the modelled zone margin. No target intercept is defined.				
KFR70	34.91 [24.74]	92.80 [69.92]	–	–
Comment: No DZ identified by SHI. Judging from the photographs of the drill cores there is no obvious indication of a possible zone along the geometric intercept. The fracture frequency is generally less than 10 fractures/m and				

BH	Geometrical Intercept		Target intercept	
	Sec_up BH length (m) [z (-m)]	Sec_low BH length (m) [z (-m)]	Sec_up BH length (m) [z (-m)]	Sec_low BH length (m) [z (-m)]
oxidation or other alterations cannot be distinguished. No target intercept has been defined.				

Borehole intersections for ZFMNE0870				
BH	Geometrical Intercept		Target intercept	
	Sec_up BH length (m) [z (-m)]	Sec_low BH length (m) [z (-m)]	Sec_up BH length (m) [z (-m)]	Sec_low BH length (m) [z (-m)]
KFR104	0.00 [2.83]	1.88 [1.29]	–	–
Comment: The geometrical intercept is at the modelled zone margin. No target intercept is defined.				

Tunnel intersections for ZFMNE0870				
Tunnel	Geometrical Intercept		Target intercept	
	Start ch.(m)	End ch. (m)	Start ch.(m)	End ch. (m)
DT	0+470	0+600	0+535	0+570
Comment: Target intercept defined by tDZ40 in Appendix 2. Earlier interpreted as 1+530–1+570 /Axelsson and Hansen 1997/.				
DT	DT-BT connection tunnel at 0+610		DT-BT connection tunnel at 0+610	
Comment: Target intercept defined by tDZ40 in Appendix 2. Earlier interpreted as DT-BT connection tunnel at 0+610 /Axelsson and Hansen 1997/.				
BT	0+620	0+780	0+640	0+690
Comment: Target intercept defined by tDZ40 in Appendix 2. Earlier interpreted as 5+640–5+690 /Axelsson and Hansen 1997/.				
BT	0+860	0+925	0+888	0+907
Comment: Connection with NBT. Target intercept defined by tDZ56 in Appendix 2.				
BT	1+017	1+050	1+020	1+050
Comment: Target intercept defined by tDZ66 in Appendix 2. Earlier interpreted as 6+025–6+050 /Axelsson and Hansen 1997/.				
NBT	0+000	0+010	–	–

Tunnel intersections for ZFMNE0870				
Tunnel	**Geometrical Intercept**		**Target intercept**	
	Start ch.(m)	**End ch. (m)**	**Start ch.(m)**	**End ch. (m)**
Comment: Connection with BT.				
NBT	0+350	0+365	0+352	0+352
Comment: Target intercept defined by tDZ80 in Appendix 2. Earlier interpreted as 8+290–8+350 (as a branch of zone 9) /Axelsson and Hansen 1997/.				
STT	0+800	0+820	0+810	0+820
Comment: Target intercept defined by tDZ66 in Appendix 2.				
IST	0+078	0+095	0+088	0+088
Comment: Target intercept defined by tDZ80 in Appendix 2. This location is at the connection between ST and STT an extension of this. Earlier interpreted as 4+090 (as a branch of zone 9) /Axelsson and Hansen 1997/.				

Deformation zone ZFMNE3112

Borehole and tunnel intersections (metres along borehole/tunnel)

KFR102A: 302–325 m (DZ2 302–325 m)
KFR102B: 173–180 m (DZ4 173–180 m)
KFR104: 268–283 m (DZ3 268–283 m)
KFR105: 88.5–96.5 m (DZ2 88.5–96.5 m)

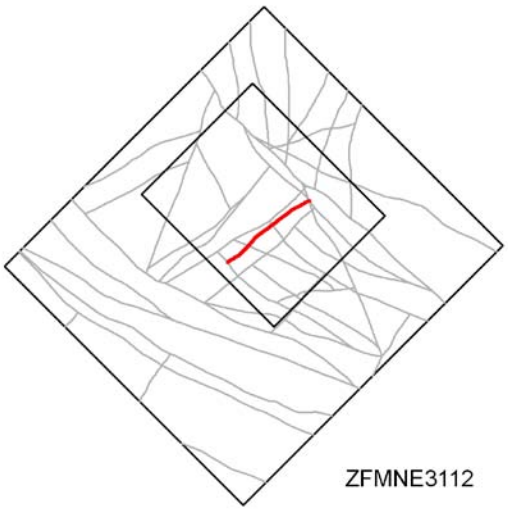

Deformation style, alteration and geometry

Deformation style: Brittle. Minor cohesive breccias present in three of the BH intercepts.

Alteration: Generally red-stained bedrock with fine-grained hematite dissemination with minor intervals of laumontization and carbonatization in KFR104 DZ3 and argillization in KFR102A DZ2.

Strike/dip (span) right-hand-rule: 233 / 89 (±5 / ±10)

Trace length at ground surface (span): 474 m (400−710 m)

Model thickness (span): 10 m (5−12 m)

Confidence in existence: High

Modelling procedure*:* The position of the zone at the ground surface is based on a projection from the interpreted borehole correlations, with only a weak and partial agreement with the lineament MFM3112G defined by a magnetic minimum /Isaksson et al. 2007/. The central part of this zone lies beneath the pier where the magnetic field is disturbed and hinders lineament interpretation.

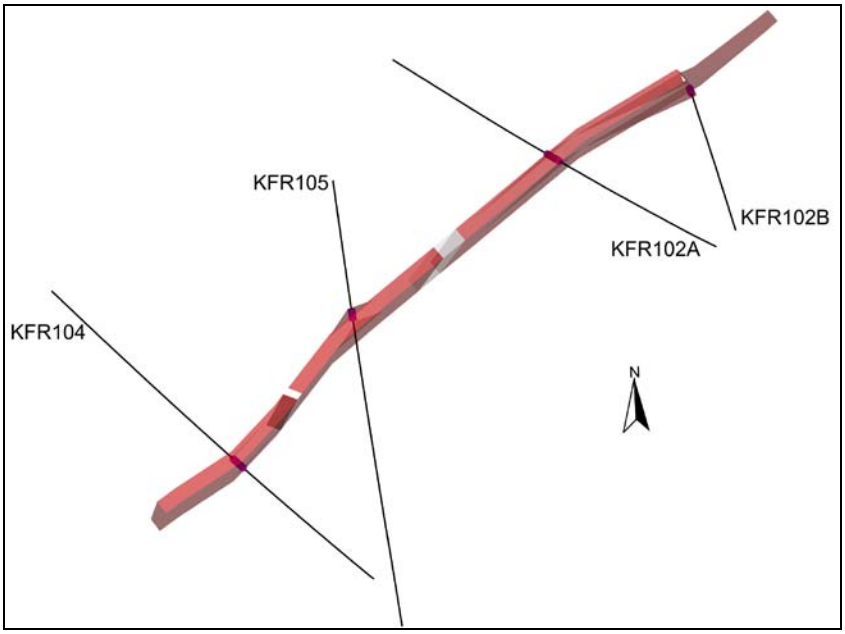

ZFMNE3112 looking down dip. The relevant borehole SHI PDZs are shown as pink cylinders. The modelled zone thickness is 10 m.

Deformation zone ZFMNE3112

Fractures in the deformation zone

General characteristics

Fracture orientation:

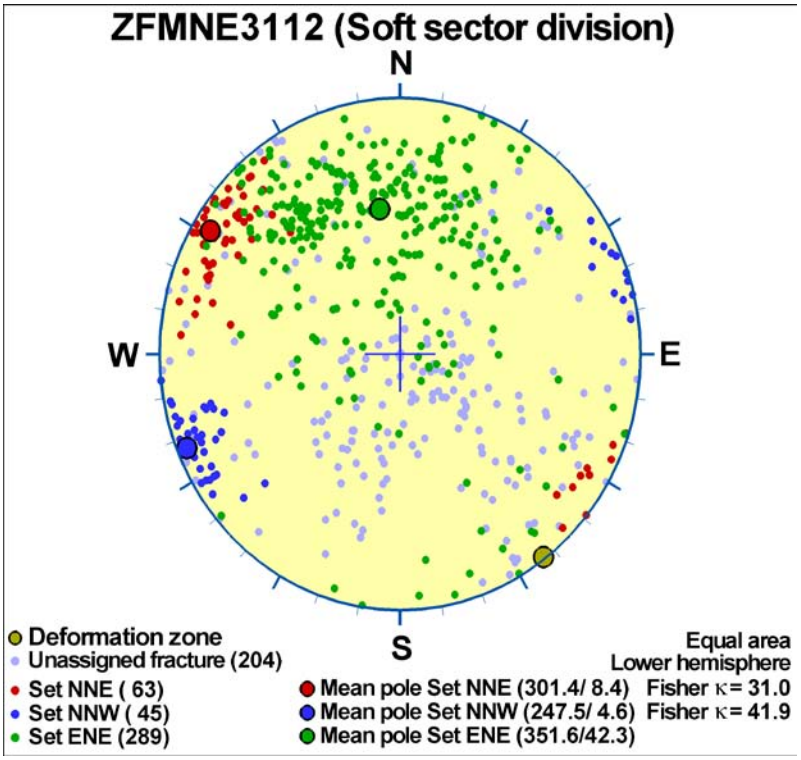

Fracture frequency: Open 10 m^{-1}, Sealed 28 m^{-1}

Fracture filling mineralogy:

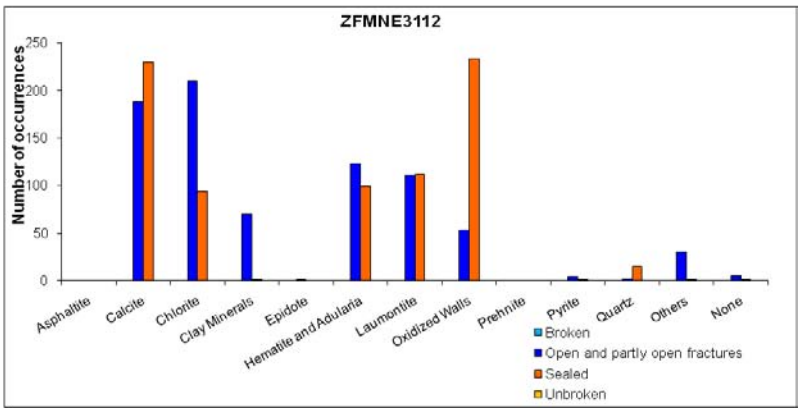

Deformation zone ZFMNE3112

KFR102B DZ4 (173–180 m)

BOREHOLE AND TUNNEL INTERCEPT DETAILS

Borehole intersections for ZFMNE3112				
BH	**Geometrical Intercept**		**Target intercept**	
	Sec_up BH length (m) [z (-m)]	**Sec_low BH length (m) [z (-m)]**	**Sec_up BH length (m) [z (-m)]**	**Sec_low BH length (m) [z (-m)]**
KFR102A	299.70 [269.82]	323.05 [290.81]	302	325

SHI DZ2 302–325 m: Increased frequency of open and sealed fractures. Fractures aperture generally less than 0.5 mm. Locally faint to medium oxidation. Predominant minerals in open fractures are chlorite, calcite, hematite, clay minerals and laumontite and in sealed fractures calcite, laumontite, chlorite and adularia. The possible deformation zone core 308–310 m is characterized by two fractures with five mm aperture, three minor crushes, argillisation and clay minerals as predominant mineral in open fractures. Two radar reflectors without orientation at 302 and 311 m, and one oriented reflector at 325 m (033°/83° or 213°/32°). The magnetic susceptibility is decreased along the entire section. In the section 307–310 m the resistivity is significantly decreased and there is also a distinct caliper anomaly. There is another clear low resistivity anomaly in the interval 322–325 m. In the section 312–318 m there is a fluid temperature anomaly indicating the occurrence of a water bearing fracture. Metagranite-granodiorite (101057), fine- to medium-grained granite (111058) and pegmatitic granite (101061). Confidence level = 3.

One single medium-transmissive flow anomaly (T = $2 \cdot 10^{-8}$ m^2/s) at 309 m, probably related to one, or both, of the 5 mm aperture fractures. Transmissivity below the measurement limit in the rest of the section.

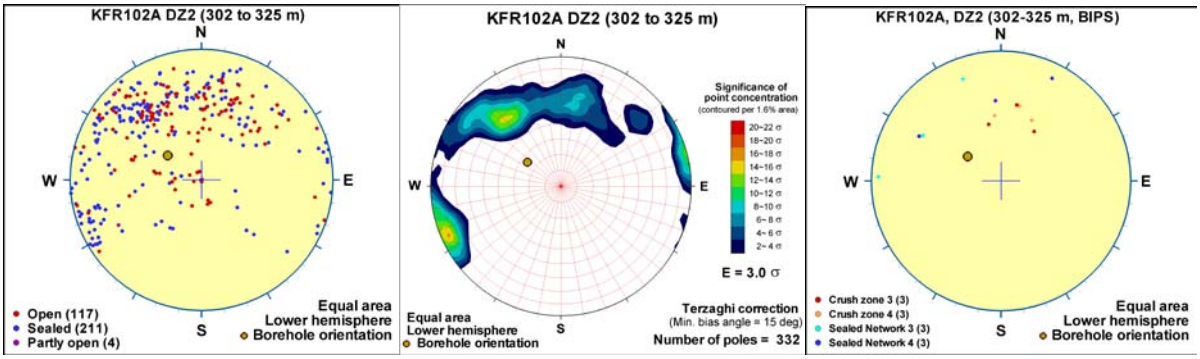

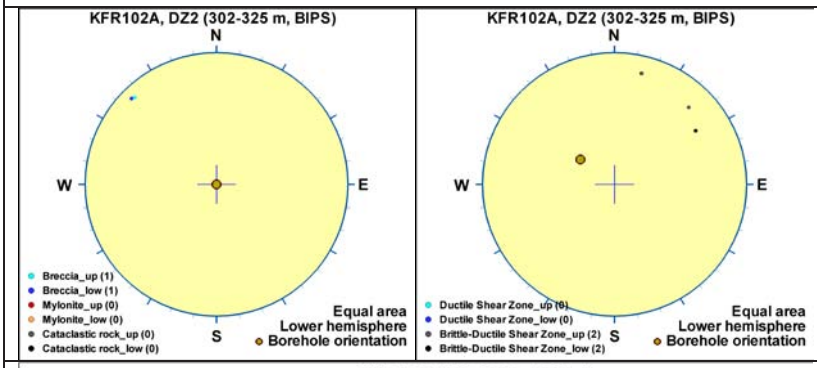

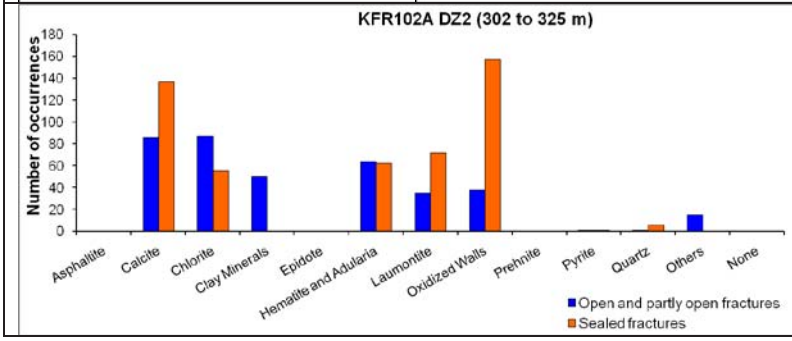

Borehole intersections for ZFMNE3112

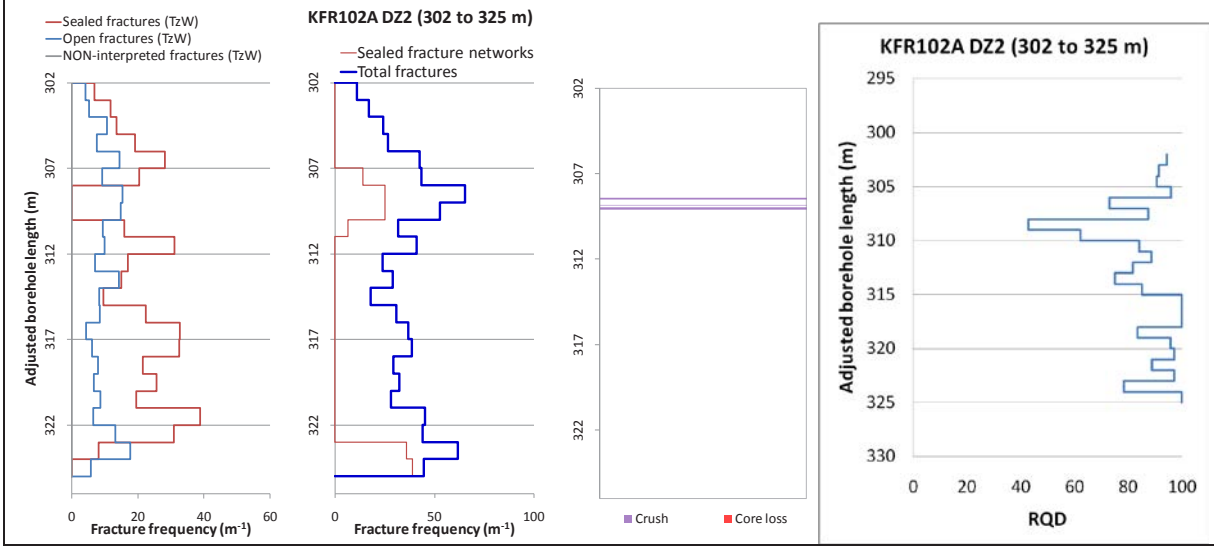

BH	Geometrical Intercept		Target intercept	
	Sec_up BH length (m) [z (-m)]	Sec_low BH length (m) [z (-m)]	Sec_up BH length (m) [z (-m)]	Sec_low BH length (m) [z (-m)]
KFR102B	170.32 [135.07]	eoh [180.08]	173	180

SHI DZ4 173–180 m: Increased frequency of sealed fractures and sealed fracture networks. Brecciated intervals at 176.01–176.04, 178.92–179.10 and 179.66–179.74 m. Predominant minerals in sealed fractures and sealed fracture networks are calcite, chlorite, laumontite and adularia. Minor interval of medium oxidation. Significantly decreased resistivity and magnetic susceptibility in the interval 172.0–173.5 m. In the remaining part of the section the resistivity and magnetic susceptibility are partly decreased along minor intervals. Pegmatitic granite (101061), metagranite-granodiorite (101057), felsic to intermediate metavolcanic rock (103076), fine- to medium-grained granite (111058) and amphibolite (102017). Confidence level = 3.

An isolated cluster of relatively high-transmissive flow anomalies at 172.0–173.6 m. Total transmissivity of $2 \cdot 10^{-6}$ m^2/s. No flow logging data below approximately 173.8 m.

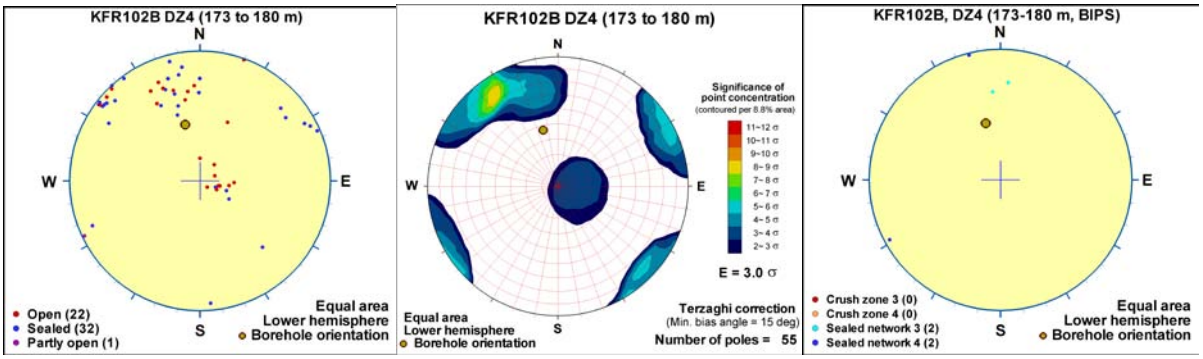

Borehole intersections for ZFMNE3112

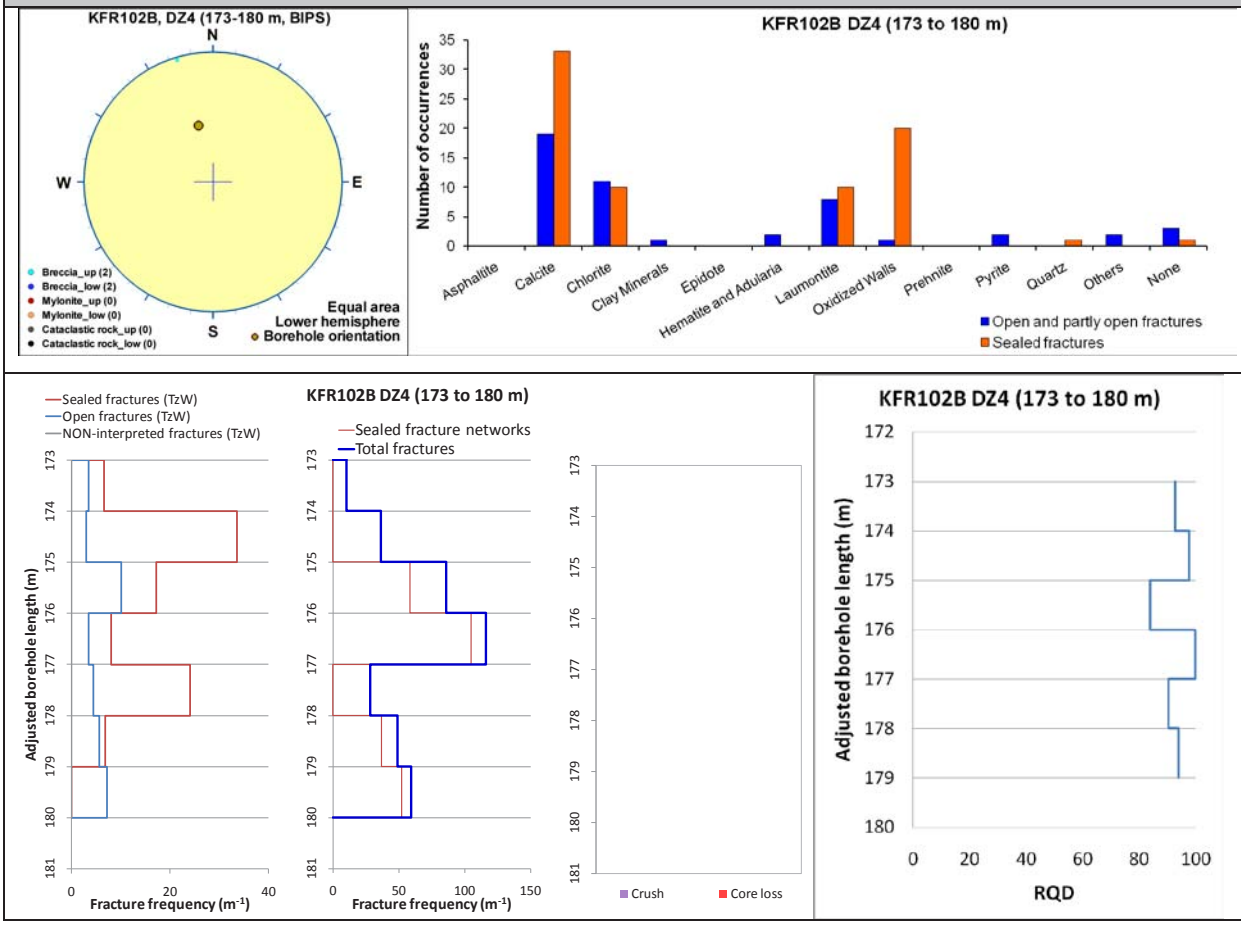

BH	Geometrical Intercept		Target intercept	
	Sec_up BH length (m) [z (-m)]	Sec_low BH length (m) [z (-m)]	Sec_up BH length (m) [z (-m)]	Sec_low BH length (m) [z (-m)]
KFR104	265.84 [209.12]	282.99 [222.33]	268	283

SHI DZ3 268–283 m: Increased frequency of open fractures and sealed fracture network. Two crushes at 276.36–276.64 and 277.46–277.75 m. Fracture apertures up to 0.5 mm with a single aperture at 3 mm. Generally weak to moderate oxidation and one interval of carbonatization at 275.06–275.95 m. Predominant minerals in open fractures are chlorite, laumontite, hematite and calcite. Very low electric resistivity and one caliper anomaly. Two radar reflectors of which one is oriented (109°/20° or 232°/85°). Pegmatitic granite (101061), aplitic metagranite (101058), metagranite-granodiorite (101057) and amphibolite (102017). Confidence level = 3.

Two single flow anomalies where the transmissivity of the interval ($1 \cdot 10^{-7}$ m^2/s) is dominated by the anomaly at 276 m.

Borehole intersections for ZFMNE3112

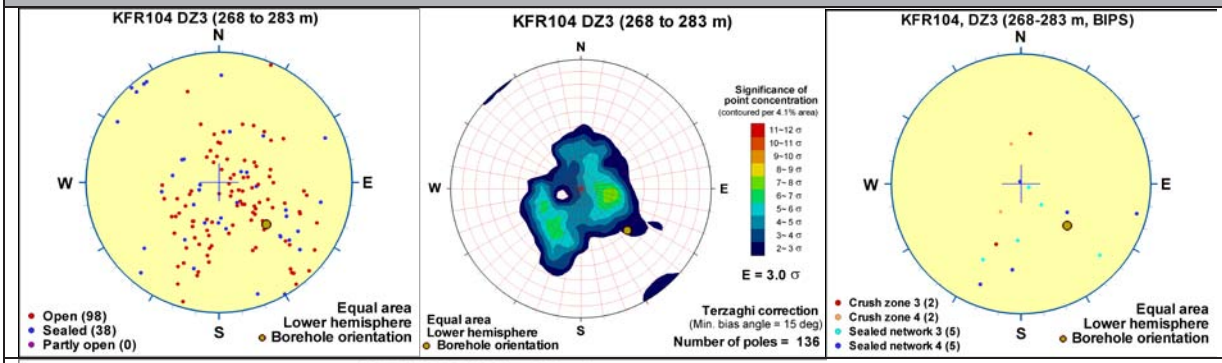

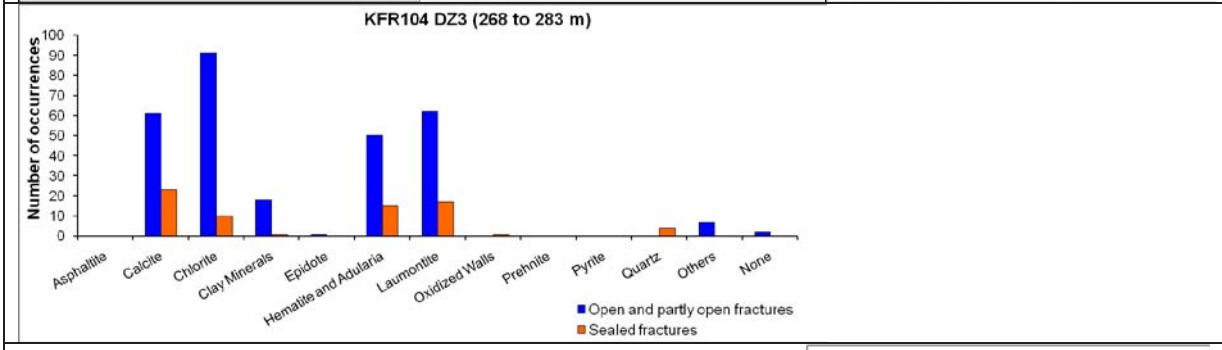

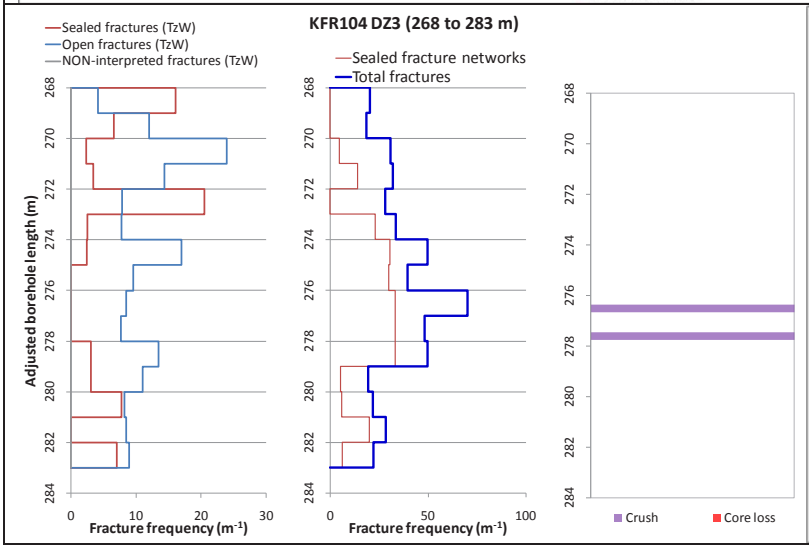

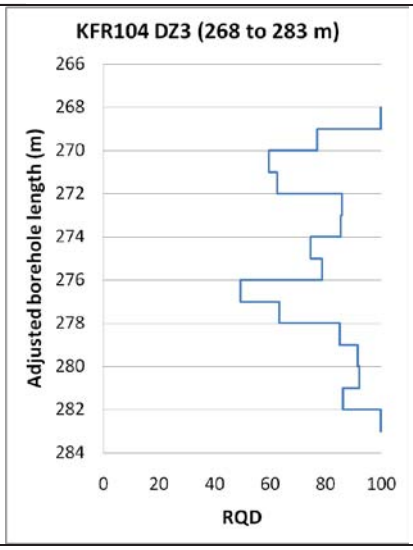

Borehole intersections for ZFMNE3112				
BH	Geometrical Intercept		Target intercept	
	Sec_up BH length (m) [z (-m)]	Sec_low BH length (m) [z (-m)]	Sec_up BH length (m) [z (-m)]	Sec_low BH length (m) [z (-m)]
KFR105	87.69 [121.86]	99.69 [123.87]	88.5	96.5

SHI DZ2 88.5–96.5 m: Increased frequency of sealed fractures and sealed networks. Fracture apertures in general up to 0.5 mm. Predominant fracture minerals are calcite, chlorite, adularia and oxidized walls. Generally weakly oxidized. A minor decrease in resistivity along the interval but no other indications in the geophysical logging data. Fine- to medium-grained metagranite-granodiorite (101057) and pegmatitic granite (101061). Confidence level = 3.

Three low-transmissive flow anomalies at 88.7, 94.9 and 95.7 m. The total transmissivity of the section is very low, about $2 \cdot 10^{-9}$ m^2/s.

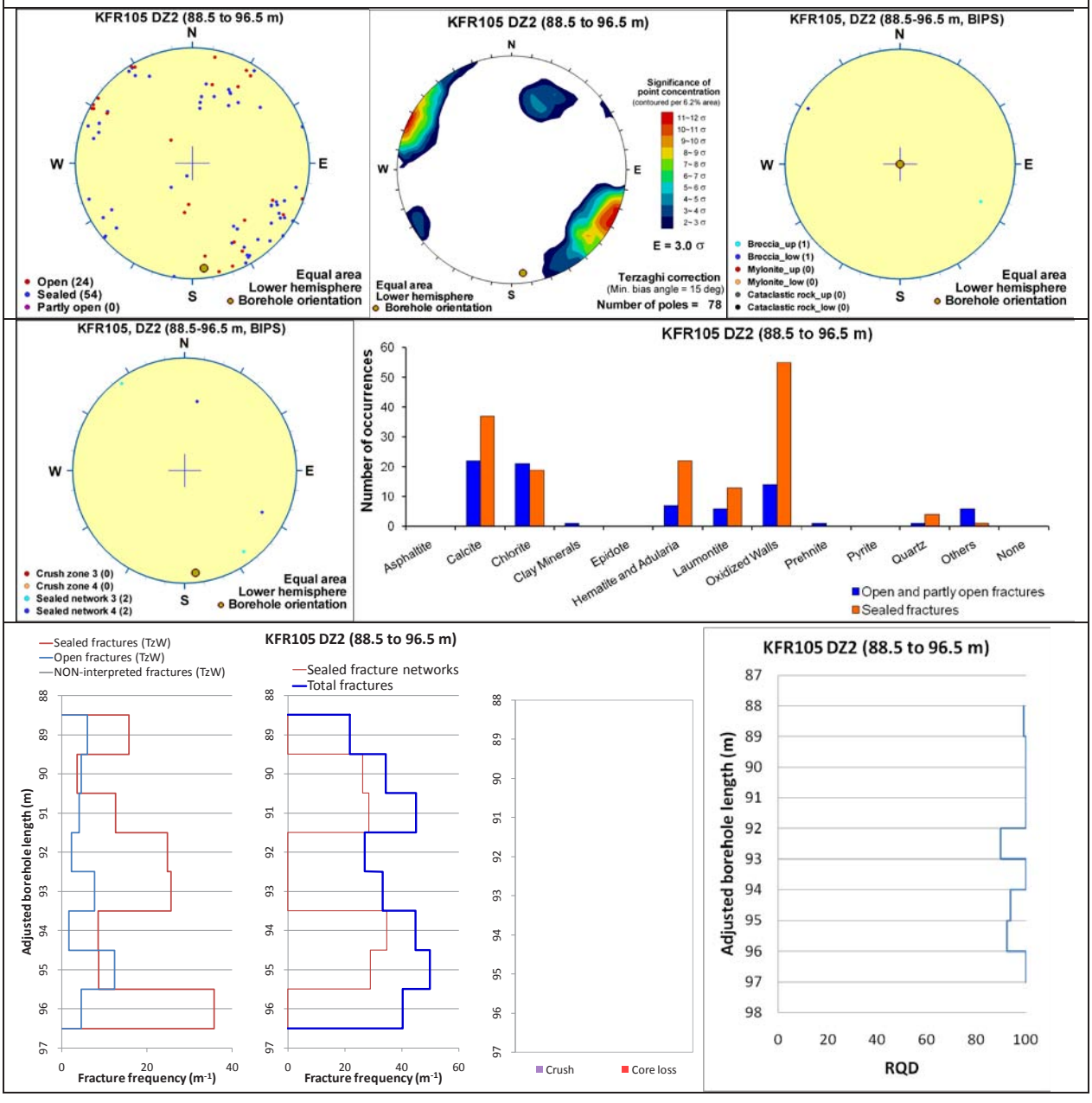

Deformation zone ZFMNE3118

Borehole and tunnel intersections (metres along borehole/tunnel)

HFR101: 190–202 m (DZ3 190–202 m)
KFR13: 47.5–61 m (DZ3 47.5–61 m)
KFR54: 0–2.5 m (DZ1 0–2.5 m)
KFR55: 8–17 m (DZ2 8–38 m)
KFR104: 30–45.5 m (DZ1 30–45.5 m)
BT: 1+095 (tDZ73)
BT/ST: 1+166 (tDZ73)
NBT: 0+055–0+059
NBT: 0+295–340 (tDZ73)

Deformation style, alteration and geometry

Deformation style: Brittle. Inferred minor brittle-ductile shear zone at 200.25–200.54 m in HFR101 DZ3. Cohesive breccia in KFR104 DZ1.

Alteration: Locally red-stained bedrock with fine-grained hematite dissemination. Altered vuggy rock with quartz dissolution at 38.30–40.75 m along KFR104 DZ1.

Strike/dip (span) right-hand-rule: 44 / 84 (±5 / ±10)

Trace length at ground surface (span): 743 m (720−760 m)

Model thickness (span): 8 m (2−10 m)

Confidence in existence: High

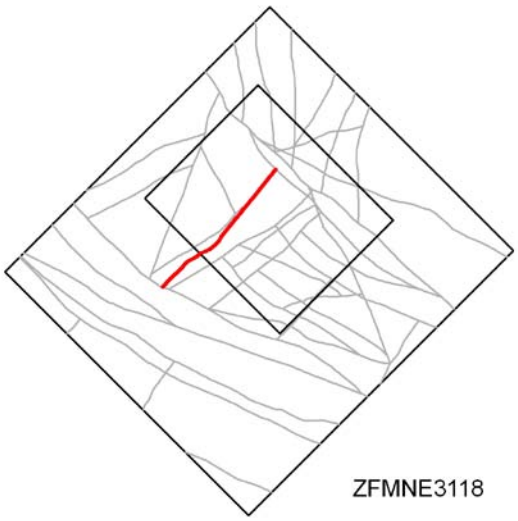

Modelling procedure*:* Modified after zone 12 /Carlsson et al. 1985/. The position of the zone at the ground surface in the south-west coincides with the magnetic lineament MSFR08111 in SFR model version 1.0, itself an update of MFM3118G /Isaksson et al. 2007/. The main central section of the zone lies beneath the pier in an area where the magnetic field is disturbed and hinders lineament interpretation.

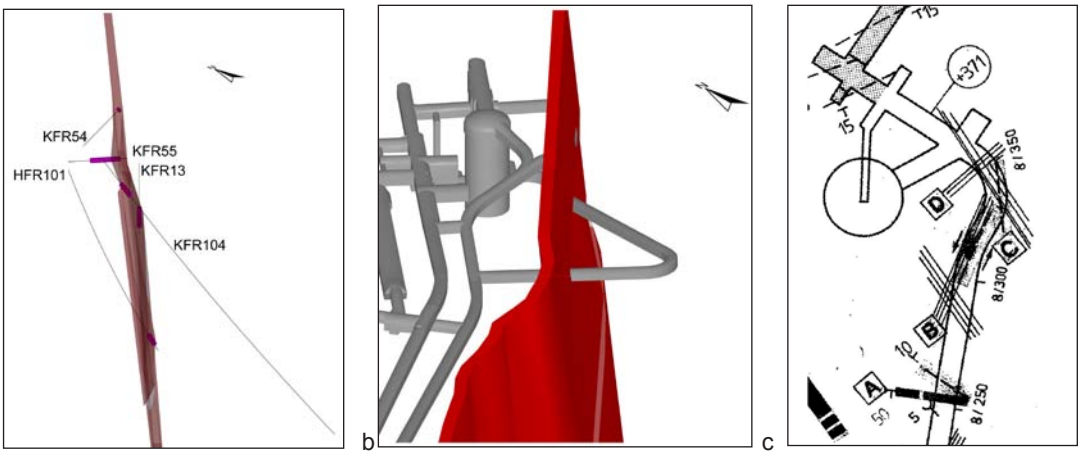

a b c

a. The central section of ZFMNE3118 looking along the strike to NE. The relevant SHI PDZs are shown as pink cylinders. Note only part of KFR55 DZ2 correlates with the zone.

b. ZFMNE3118 looking along the strike to NE showing the tunnel intercept positions.

c. Overview mapping drawing of the NBT. ZFMNE3118 corresponds to the approximate B alignment.

Deformation zone ZFMNE3118

Fractures in the deformation zone

General characteristics

Fracture orientation:

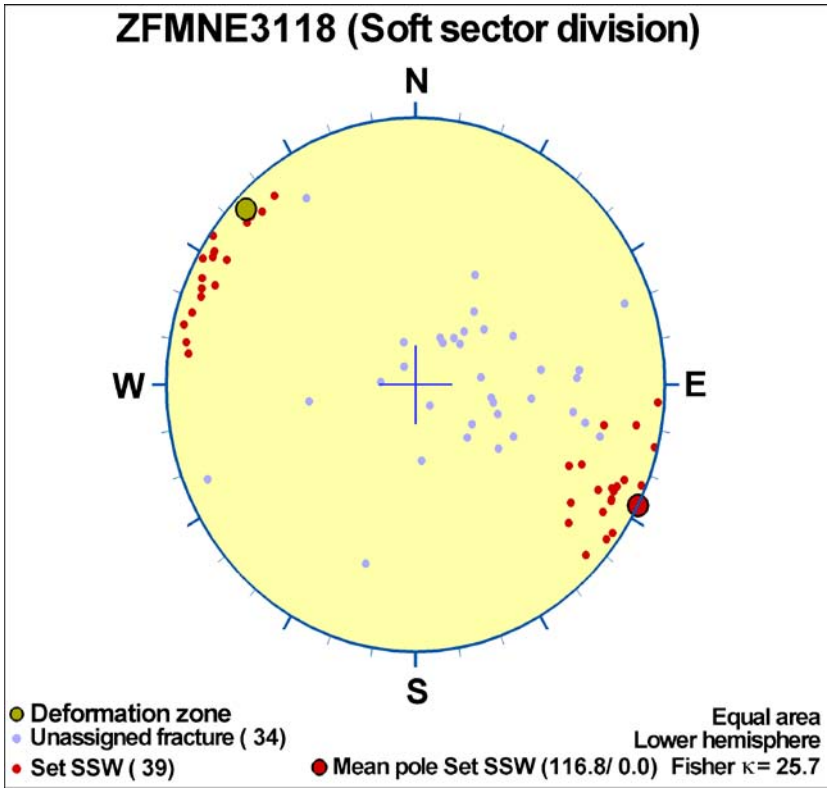

Fracture frequency: Open 8 m^{-1}, Sealed 23 m^{-1}

Fracture filling mineralogy:

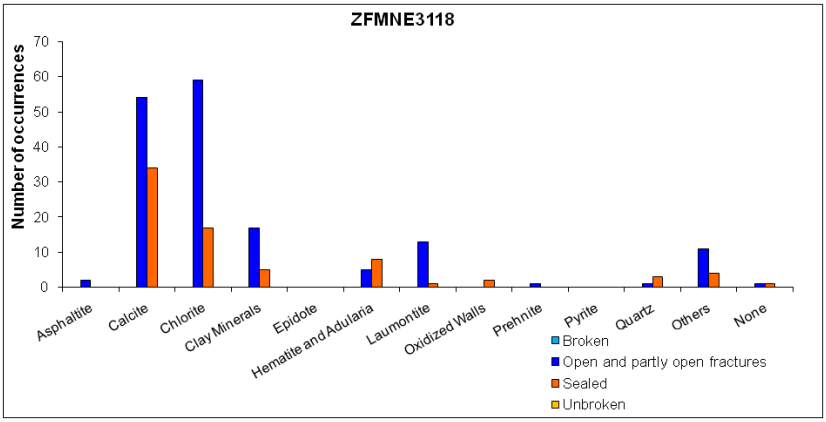

Deformation zone ZFMNE3118

KFR104 DZ1 (30–45.5 m)

BOREHOLE AND TUNNEL INTERCEPT DETAILS

Borehole intersections for ZFMNE3118				
BH	**Geometrical Intercept**		**Target intercept**	
	Sec_up BH length (m) [z (-m)]	**Sec_low BH length (m) [z (-m)]**	**Sec_up BH length (m) [z (-m)]**	**Sec_low BH length (m) [z (-m)]**
HFR101	183.85 [164.70]	203.09 [181.46]	190	202

SHI DZ3 190–202 m: Increased frequency of open fractures, sealed fractures and sealed fracture network. Fracture aperture up to 1 mm. Locally weak to medium oxidation. Inferred minor brittle-ductile shear zone at 200.25–200.54 m. Partly decreased bulk resistivity and caliper anomalies. Metagranite-granodiorite (101057), pegmatitic granite (101061) and amphibolite (102017). Confidence level = 1.

One flow anomaly at 196.0–197.0 m with a moderate transmissivity (about $3 \cdot 10^{-7}$ m^2/s). Corresponds to an increased estimated fracture frequency. This is one of the two observed flow anomalies in the borehole.

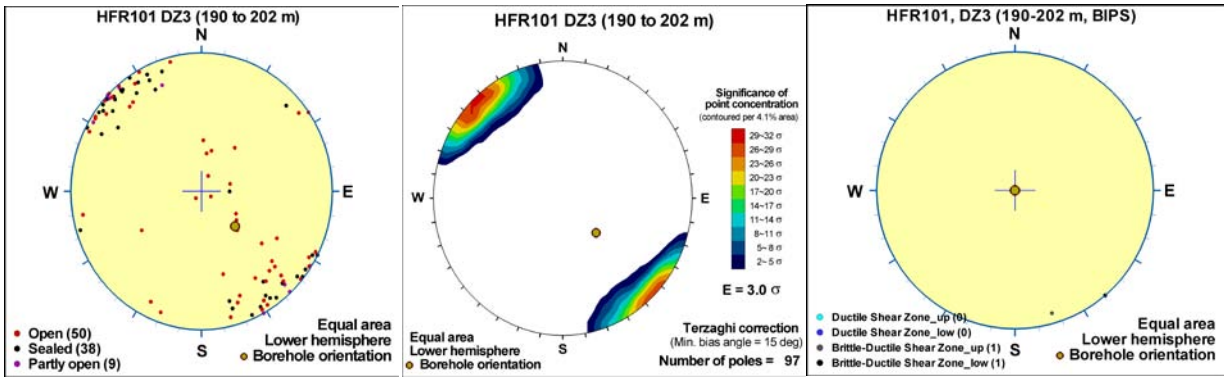

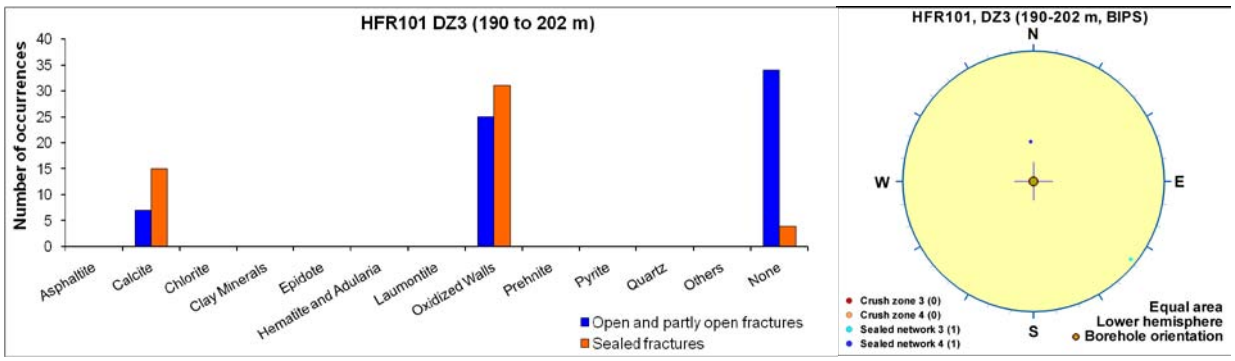

Borehole intersections for ZFMNE3118

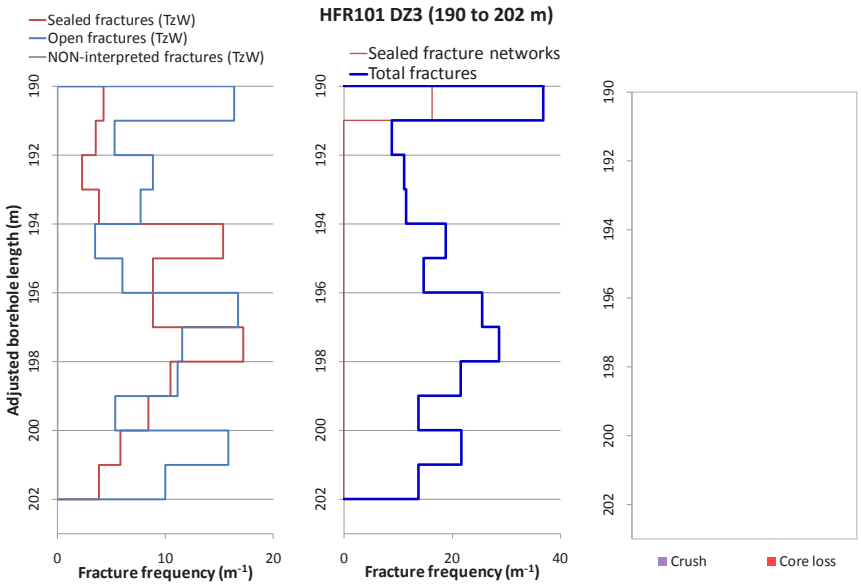

BH	Geometrical Intercept		Target intercept	
	Sec_up BH length (m) [z (-m)]	Sec_low BH length (m) [z (-m)]	Sec_up BH length (m) [z (-m)]	Sec_low BH length (m) [z (-m)]
KFR13	44.37 [167.71]	eoh [199.94]	47.5	61

SHI DZ3 47.5–61 m: Increased frequency of broken and unbroken fractures and sealed networks. Predominant fracture filling minerals are laumontite, chlorite and calcite. α–angles are generally small. Locally faint to moderate oxidation. Moderately foliated metagranite-granodiorite (101057) and fine- to medium-grained granite (111058). Confidence level = 2.

Increased hydraulic conductivity ($1 \cdot 10^{-7}$ m/s) in the interval 54–61 m.

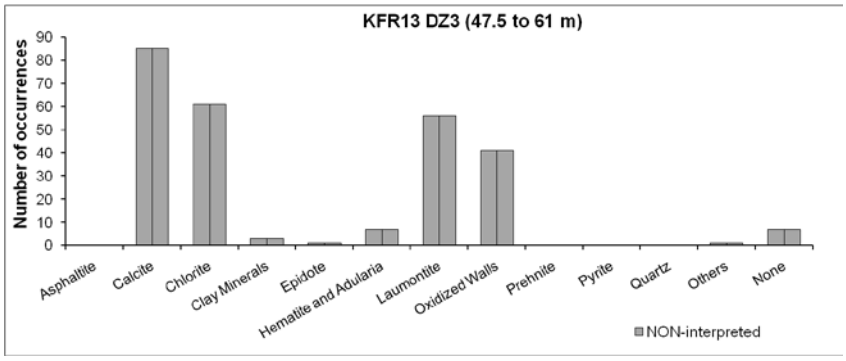

Borehole intersections for ZFMNE3118

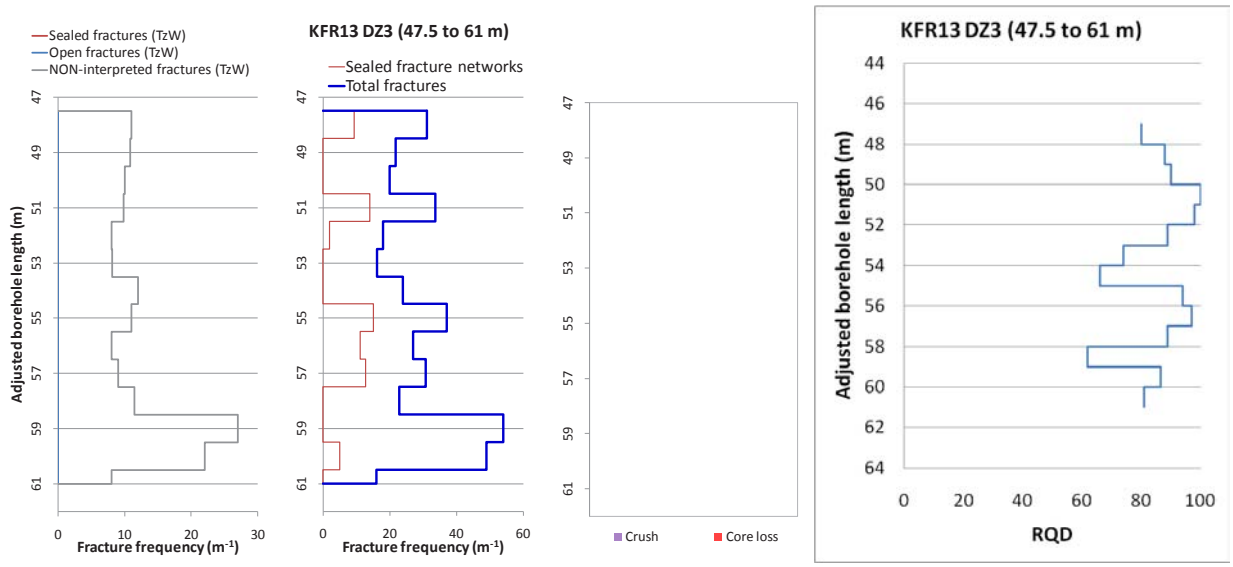

BH	Geometrical Intercept		Target intercept	
	Sec_up BH length (m) [z (-m)]	Sec_low BH length (m) [z (-m)]	Sec_up BH length (m) [z (-m)]	Sec_low BH length (m) [z (-m)]
KFR54	0.00 [81.65]	7.42 [87.14]	0	2.5

Comment:

SHI DZ1 0–2.5 m: Increased frequency of broken and unbroken fractures and sealed networks. Predominant fracture minerals are chlorite, calcite and laumontite. Strongly foliated metagranite-granodiorite (101057). Confidence level = 3.

No hydrogeological investigation data from this interval.

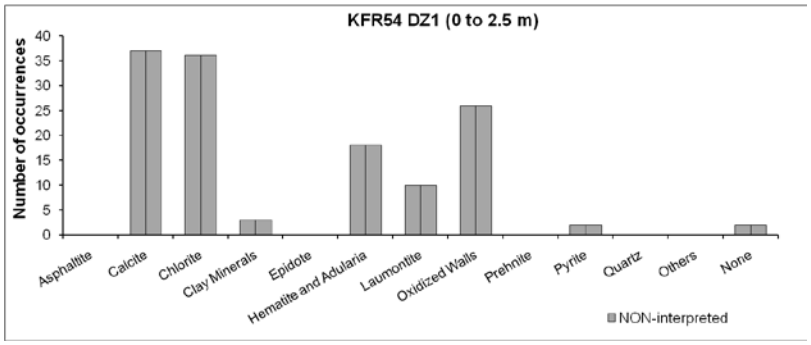

Borehole intersections for ZFMNE3118

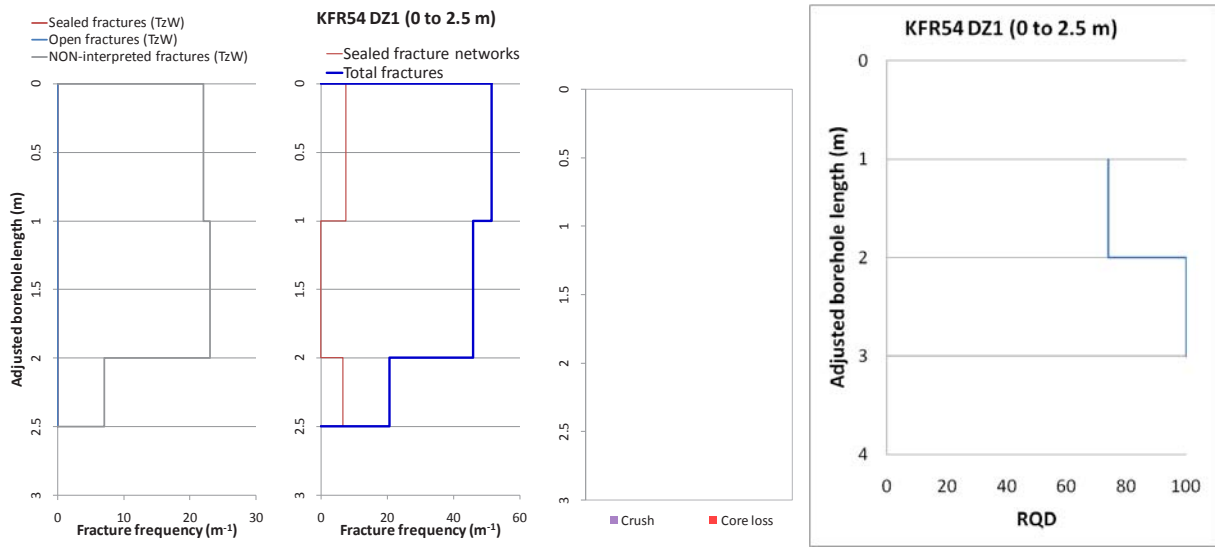

BH	Geometrical Intercept		Target intercept	
	Sec_up BH length (m) [z (-m)]	Sec_low BH length (m) [z (-m)]	Sec_up BH length (m) [z (-m)]	Sec_low BH length (m) [z (-m)]
KFR55	8.65 [127.23]	16.80 [128.78]	8	17

Comment: The quoted target intercept is based on a straightforward geometrical subdivision of DZ2 between ZFMNE0870 and ZFMNE3118. It is not expected that their character can be distinguished.

SHI DZ2 8–38 m: Increased frequency of broken and unbroken fractures and sealed networks, especially in the intervals 8–21 m and 32–38 m. Core loss at 17.86–18.51, 19.13–19.37, 33.48–33.60 and 34.89–35.33 m. The most frequent fracture filling minerals, which occur throughout the interval, are calcite, and to some extent chlorite. Fractures with clay minerals as the primary infilling are generally restricted to the interval at 16.8–19.5 m, with α–angles of 69°. Laumontite ± calcite filled fractures, on the other hand, occur along three intervals at 8.0–12.6, 16.0–16.5 and 20.4–28.1 m length. Two α–angles are registered in the uppermost (68 and 77°) and three in the lowermost (50, 57 and 65°) intervals. Locally faint to medium oxidation. Strongly foliated metagranite-granodiorite (101057) and one occurrence of fine- to medium-grained granite (111058). Confidence level = 3.

No hydrogeological investigation data from the upper 22 m of the borehole. The hydraulic conductivity is low in the measured section 22–38 m (10^{-8} m/s).

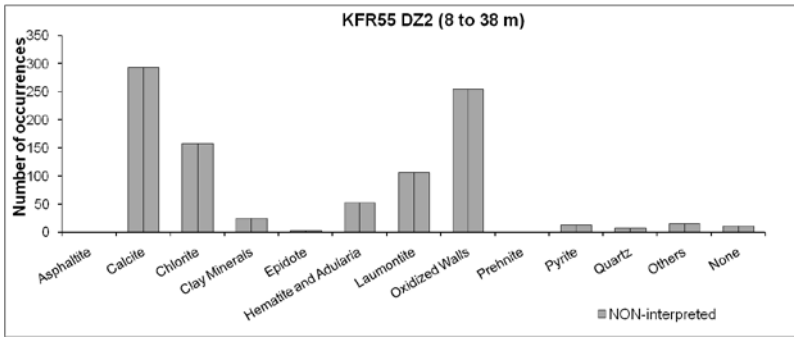

Borehole intersections for ZFMNE3118

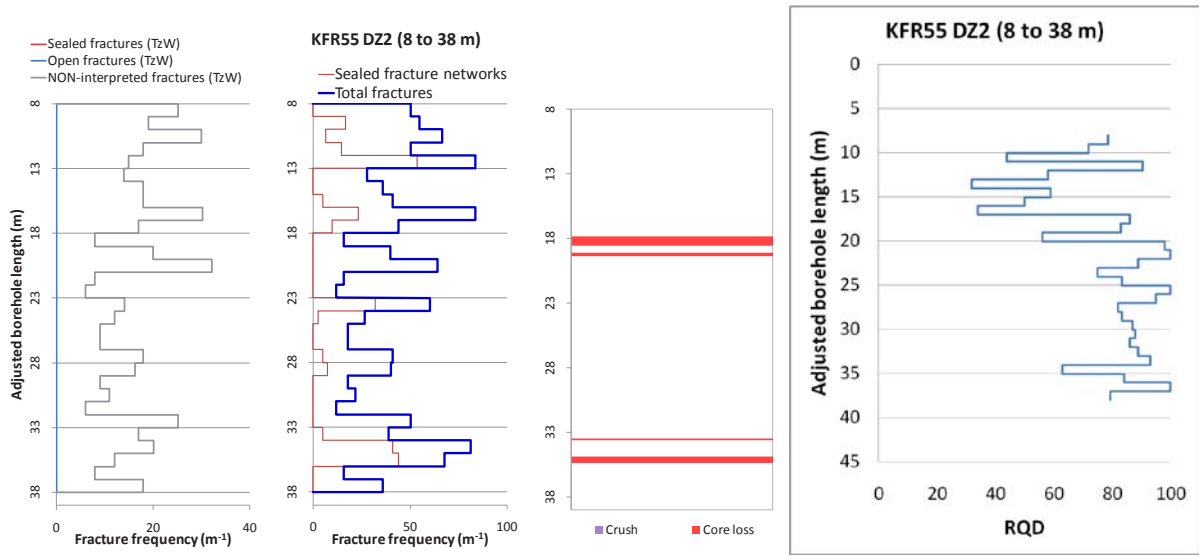

BH	Geometrical Intercept		Target intercept	
	Sec_up BH length (m) [z (-m)]	Sec_low BH length (m) [z (-m)]	Sec_up BH length (m) [z (-m)]	Sec_low BH length (m) [z (-m)]
KFR104	29.73 [21.50]	45.95 [34.72]	30	45.5

SHI DZ1 30–45.5 m: Increased frequency of sealed fracture networks. Faint oxidation in the lower half of the interval and quarts dissolution at 38.30–40.75 m where vugs are filled with calcite. Fracture apertures up to 1 mm with a single aperture at 3 mm. Predominant minerals in sealed fracture networks are chlorite, adularia and hematite. Low electric resistivity. Pegmatitic granite (101061) and metagranite-granodiorite (101057). Confidence level = 1.

Rather high, but not anomalous, transmissivity of the interval ($2 \cdot 10^{-7}$ m^2/s).

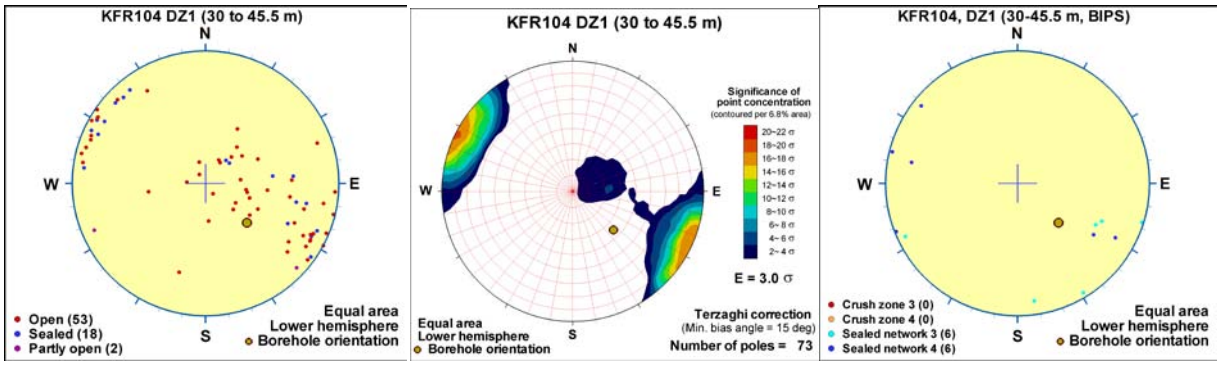

Borehole intersections for ZFMNE3118

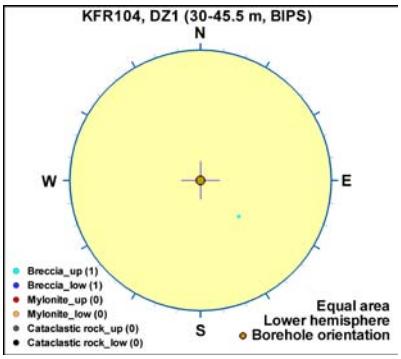

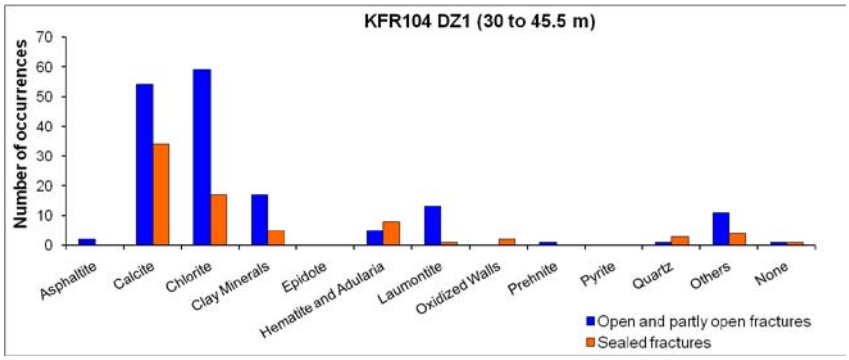

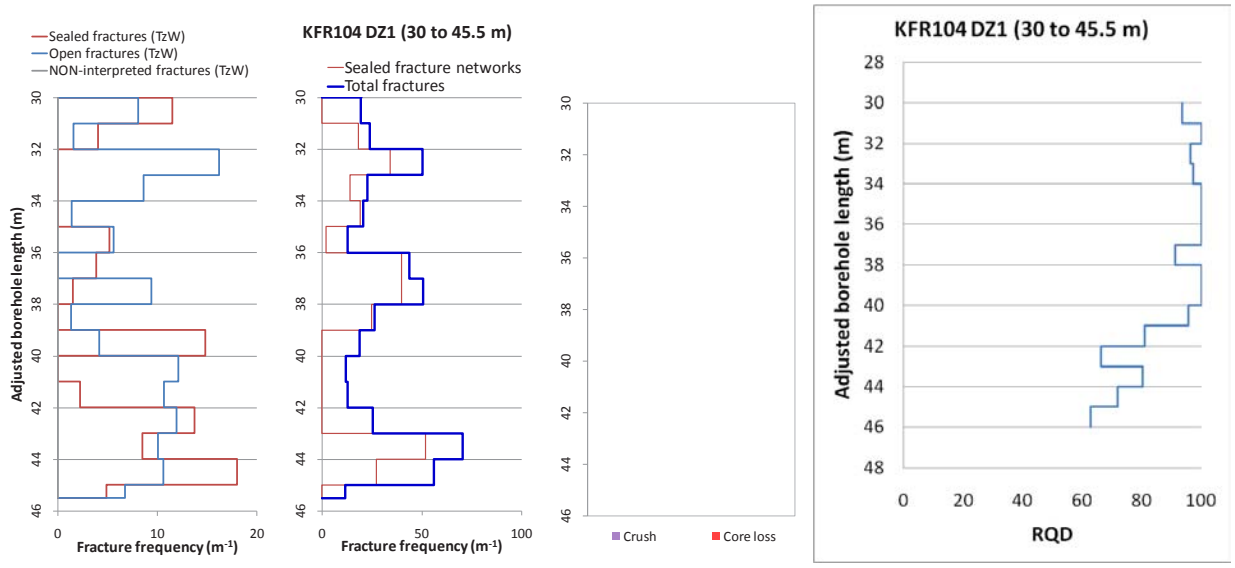

Tunnel intersections for ZFMNE3118

Tunnel	Geometrical Intercept		Target intercept	
	Start ch.(m)	End ch. (m)	Start ch.(m)	End ch. (m)
BT	1+075	1+095	1+095	1+095

Comment: Target intercept defined by tDZ73 in Appendix 2.

Tunnel intersections for ZFMNE3118				
Tunnel	**Geometrical Intercept**		**Target intercept**	
	Start ch.(m)	**End ch. (m)**	**Start ch.(m)**	**End ch. (m)**
BT/ST	1+130	1+166	1+166	–
Comment: Target intercept defined by tDZ73 at 0+88 in ST in Appendix 2.				
NBT	0+055	0+063	0+055	0+059
Comment: Target intercept based on shotcrete coverage marked in the detailed tunnel mapping. Earlier interpreted as zone 12 by /Carlsson et al. 1985/ with an intercept of 8+060.				
NBT	0+295	0+315	0+295	0+340
Comment: Target intercept defined by tDZ73 in Appendix 2.				

Deformation zone ZFMNE3134

Borehole and tunnel intersections (metres along borehole/tunnel)

None

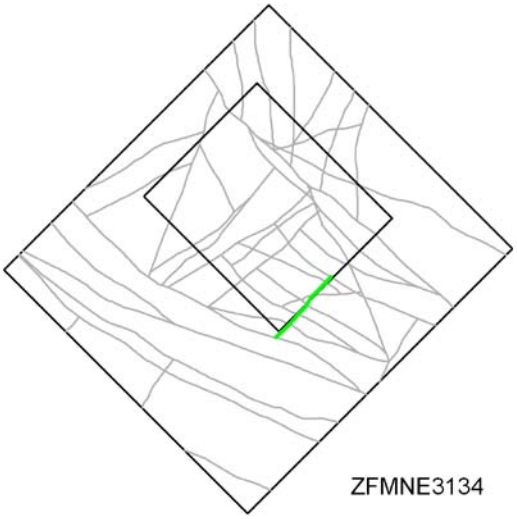

Deformation style, alteration and geometry

Deformation style: Brittle (no direct evidence – inferred association with other NE-SW trending deformation zones)

Alteration: No data

Strike/dip (span) right-hand-rule: 41 / 90 (±5 / ±10)

Trace length at ground surface (span): 370 m (350−700 m)

Model thickness: 5 m (1% default)

Confidence in existence: Medium

Modelling procedure*:* The position of the zone at the ground surface is based on a linking of lineaments MSFR10005 and MSFR10011 defined by magnetic minima in the SFR model version 1.0, earlier represented by MFM3134G in Forsmark stage 2.3 /Isaksson et al. 2007/. The zone modelled thickness and vertical dip are default values.

Fractures in the deformation zone

General characteristics

Fracture orientation: No data

Fracture frequency: No data

Crush zone: No data

Fracture filling mineralogy: No data

Deformation zone ZFMNE3137

Borehole and tunnel intersections (metres along borehole/tunnel)

KFR102A: 149–161 m (DZ1 149–161 m)
KFR102B: 109–114 m (DZ2 109–114 m)
KFR104: 382–387 m (DZ4 382–387 m)
KFR105: 191–205 m

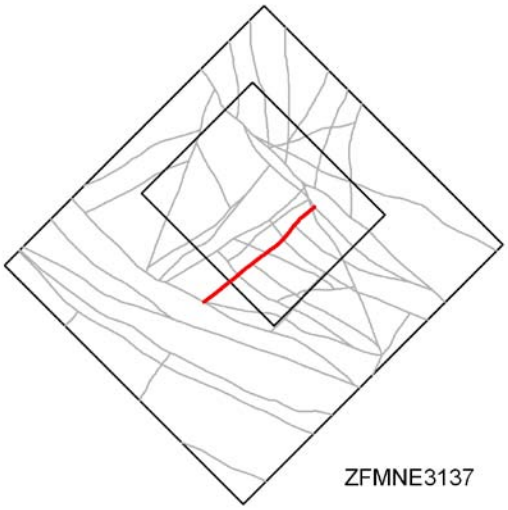

Deformation style, alteration and geometry

Deformation style: Brittle. Minor cataclasite in KFR104 DZ4

Alteration: Locally red-stained bedrock with fine-grained hematite dissemination

Strike/dip (span) right-hand-rule: 230 / 90 (±5 / ±5)

Trace length at ground surface (span): 672 m (570−680 m)

Model thickness (span): 5 m (1−8 m)

Confidence in existence: High

Modelling procedure*:* The position of the zone at the ground surface is based on the magnetic lineament MSFR10004 in SFR model version 1.0, i.e. modified lineament MFM3137G in Forsmark stage 2.3 /Isaksson et al. 2007/, with an extension through the disturbed magnetic area below the pier allowing correlation with new borehole information. Forward modelling of magnetic data along profile 40 (see Appendix 6) supports the modelled vertical dip of the zone.

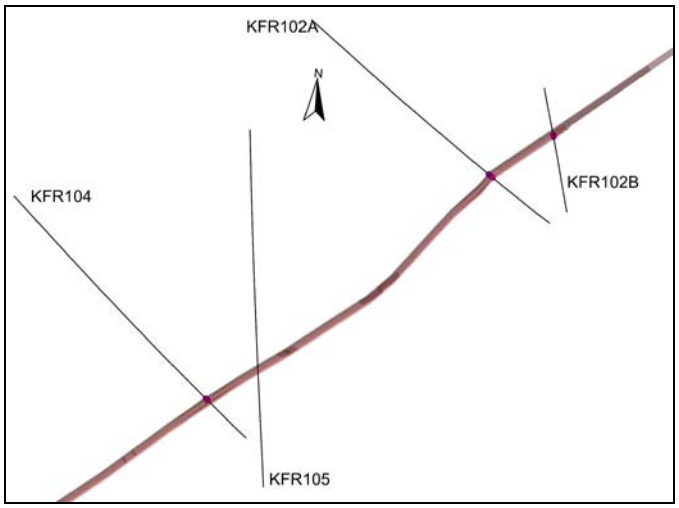

ZFMNE3137, top view (dip vertical) in relation to penetrating boreholes. Relevant SHI PDZs are shown as pink cylinders. The modelled zone thickness is 5 m.

Deformation zone ZFMNE3137

Fractures in the deformation zone

General characteristics

Fracture orientation:

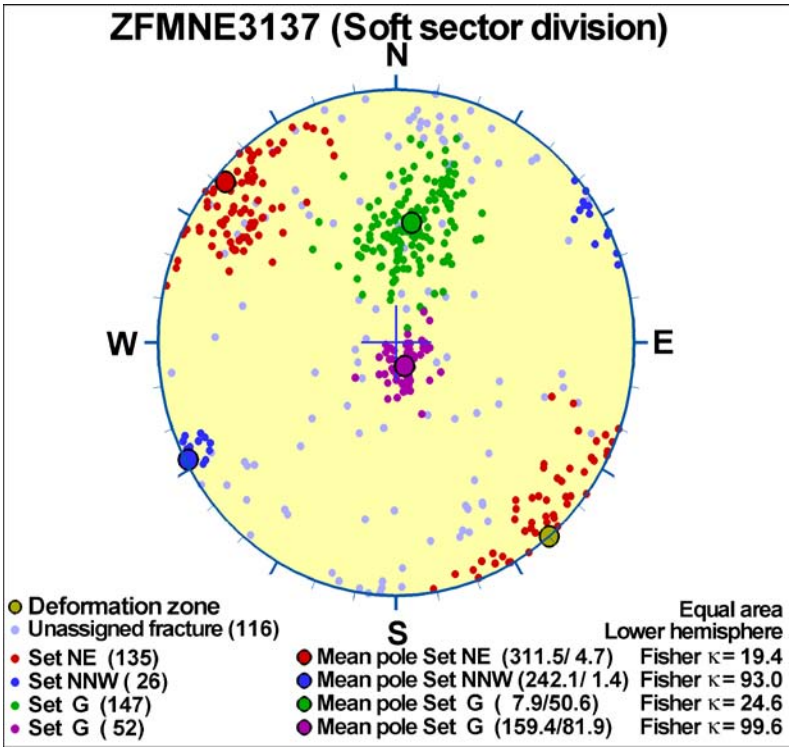

Fracture frequency: Open 7 m^{-1}, Sealed 32 m^{-1}

Fracture filling mineralogy:

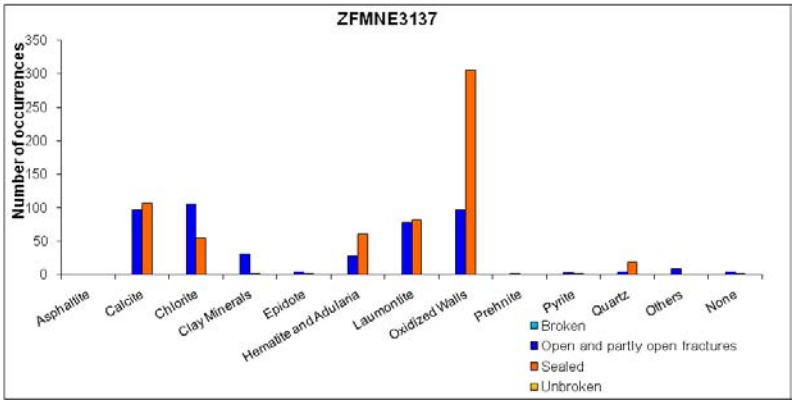

KFR102A DZ1 (149–161 m)

Deformation zone ZFMNE3137

BOREHOLE AND TUNNEL INTERCEPT DETAILS

Borehole intersections for ZFMNE3137

BH	Geometrical Intercept		Target intercept	
	Sec_up BH length (m) [z (-m)]	Sec_low BH length (m) [z (-m)]	Sec_up BH length (m) [z (-m)]	Sec_low BH length (m) [z (-m)]
KFR102A	147.83 [132.22]	160.74 [143.97]	149	161

SHI DZ1 149–161 m: Increased frequency of open and particularly sealed fractures. No alteration. Fracture apertures 0.5 mm or less. Predominant minerals in sealed and open fractures are laumontite, adularia, calcite and chlorite. One oriented radar reflector at 154 m (315°/63° or 108°/63°). The magnetic susceptibility is decreased along the entire section. There are no other significant anomalies related to increased fracturing in the geophysical logging data. Metagranite-granodiorite (101057). Confidence level = 2.

Two flow anomalies and rather low transmissivity of the section (T = $1 \cdot 10^{-8}$ m^2/s).

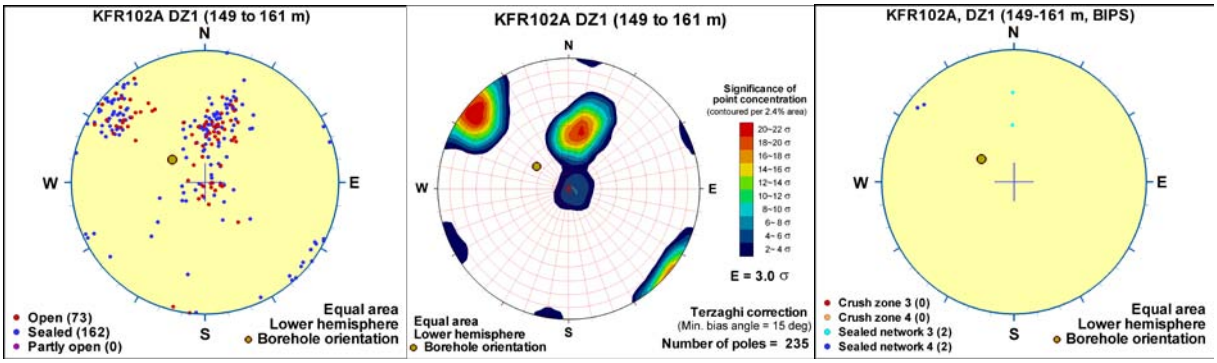

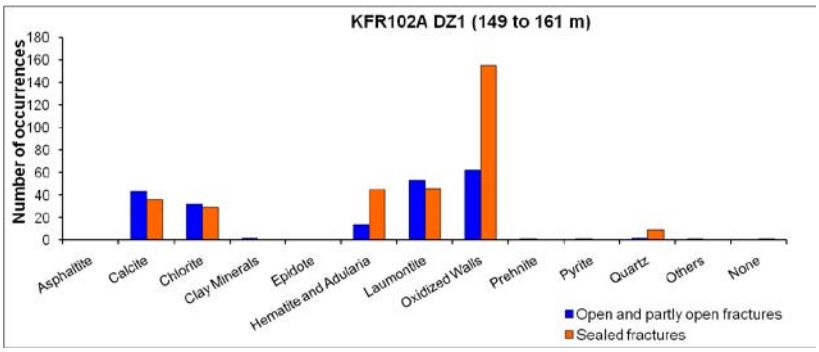

Borehole intersections for ZFMNE3137

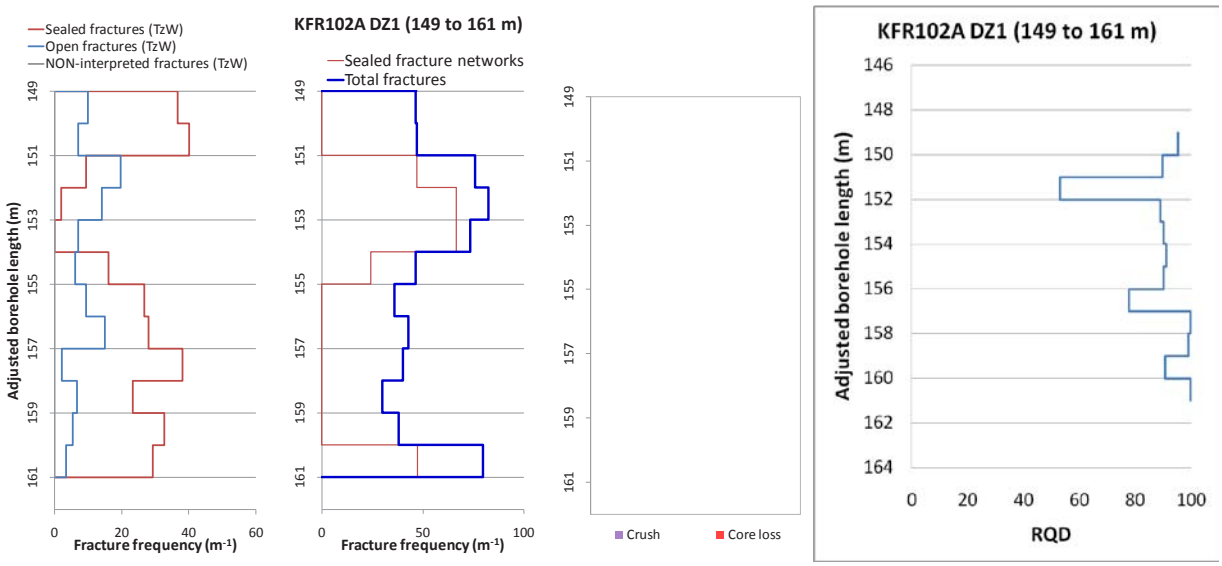

BH	Geometrical Intercept		Target intercept	
	Sec_up BH length (m) [z (-m)]	Sec_low BH length (m) [z (-m)]	Sec_up BH length (m) [z (-m)]	Sec_low BH length (m) [z (-m)]
KFR102B	106.92 [84.13]	116.23 [91.63]	109	114

SHI DZ2 109–114 m: Increased frequency of open and sealed fractures and sealed fracture networks. Fracture apertures up to 1.5 mm. Locally weak to medium oxidation. Predominant minerals in sealed fractures are calcite, chlorite, laumontite, adularia and quartz and in open fractures chlorite, calcite, laumontite and clay minerals. Significantly decreased resistivity and magnetic susceptibility in the interval 109–111 m. In the remaining part of the section the resistivity and magnetic susceptibility are partly decreased along minor intervals. Metagranite-granodiorite (101057), pegmatitic granite (101061) and amphibolite (102017). Confidence level = 3.

The transmissivity of the interval is about $1 \cdot 10^{-7}$ m^2/s and is dominated by two flow anomalies at 109.1 and 109.7 m, the latter corresponding to several open fractures.

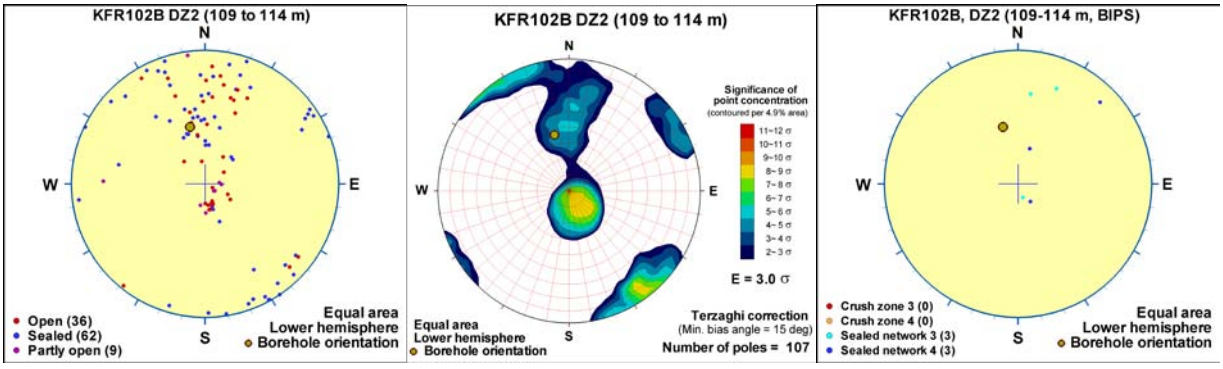

Borehole intersections for ZFMNE3137

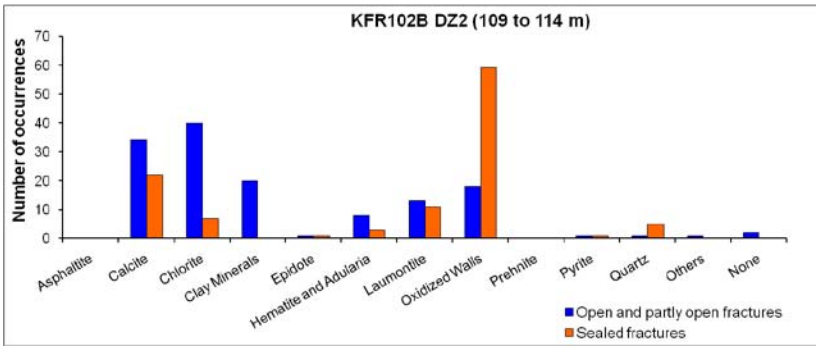

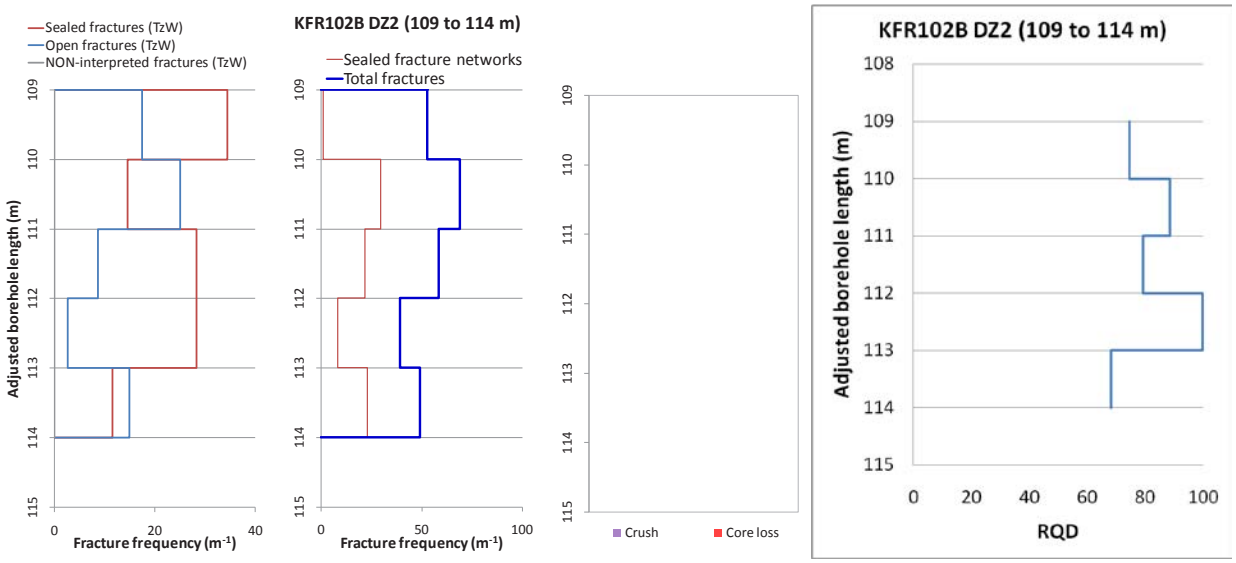

BH	Geometrical Intercept		Target intercept	
	Sec_up BH length (m) [z (-m)]	Sec_low BH length (m) [z (-m)]	Sec_up BH length (m) [z (-m)]	Sec_low BH length (m) [z (-m)]
KFR104	380.85 [296.78]	388.50 [302.51]	382	387

Comment:

SHI DZ4 382–387 m: Increased frequency of sealed fracture networks. One minor cataclasite at 383.34–383.36 m. Locally faint to moderate oxidation. Fracture aperture up to 1mm. Predominant minerals in sealed fracture networks are adularia, laumontite, chlorite and calcite. One minor resistivity anomaly. One oriented radar reflector (216°/70° or 184°/11°). Felsic to intermediate metavolcanic rock (103076) and pegmatitic granite (101061). Confidence level = 3.

No flow anomaly and transmissivity below the measurement limit in this interval.

Borehole intersections for ZFMNE3137

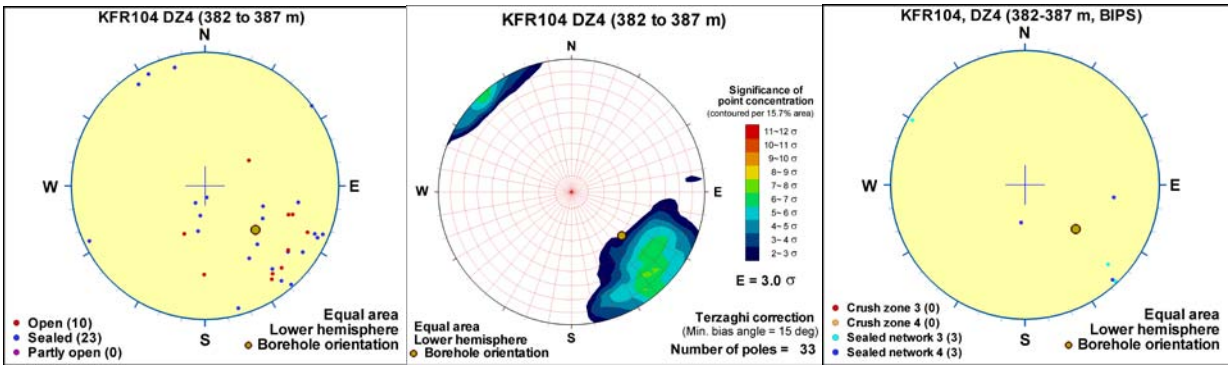

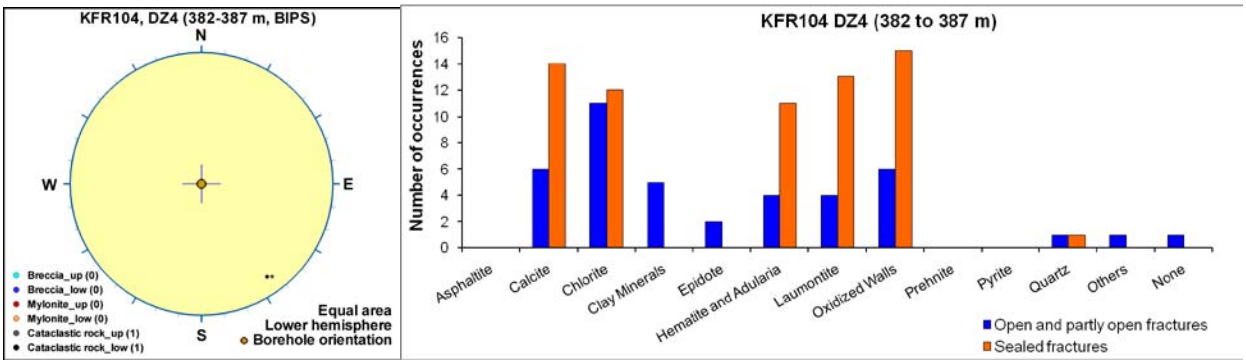

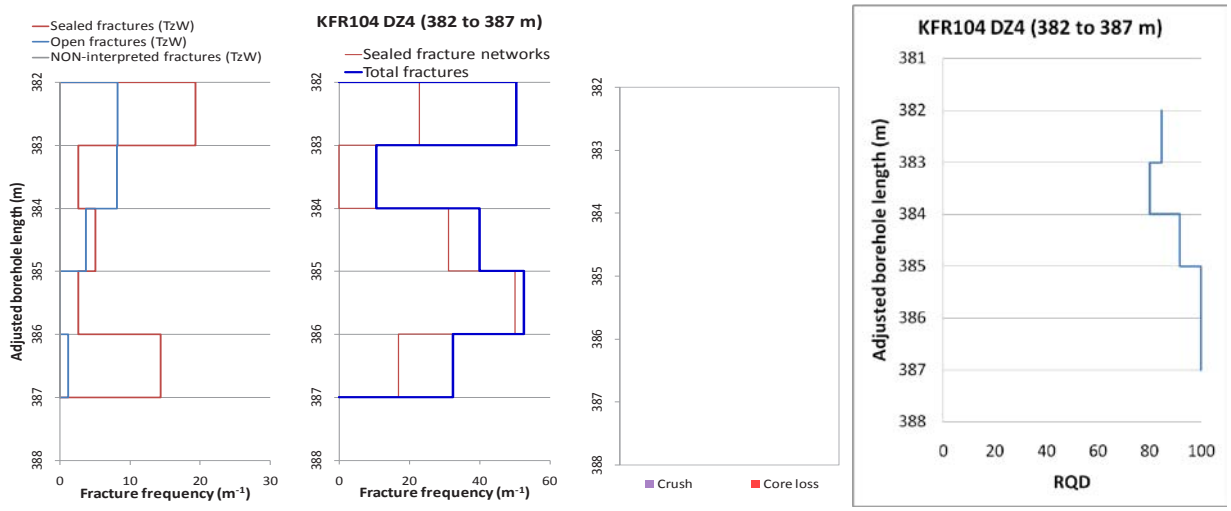

BH	Geometrical Intercept		Target intercept	
	Sec_up BH length (m) [z (-m)]	Sec_low BH length (m) [z (-m)]	Sec_up BH length (m) [z (-m)]	Sec_low BH length (m) [z (-m)]
KFR105	203.99 [140.86]	209.71 [141.77]	191	205

Borehole intersections for ZFMNE3137

Comment: There is no SHI DZ interpreted in the position of the target intercept in KFR105. However, the modelled geometry generates an intercept in KFR105 with a section of core that coincides with an interval of increased frequency of steeply dipping fractures that strike NE at 191 to 193 m length. In addition, two NE-striking sealed networks at 202.7–203.8 and 204.2–204.8 m with piece lengths of 30 and 15 mm, respectively, along with NE-striking crush at 205.0–205.05 m. No control point has been added for this borehole.

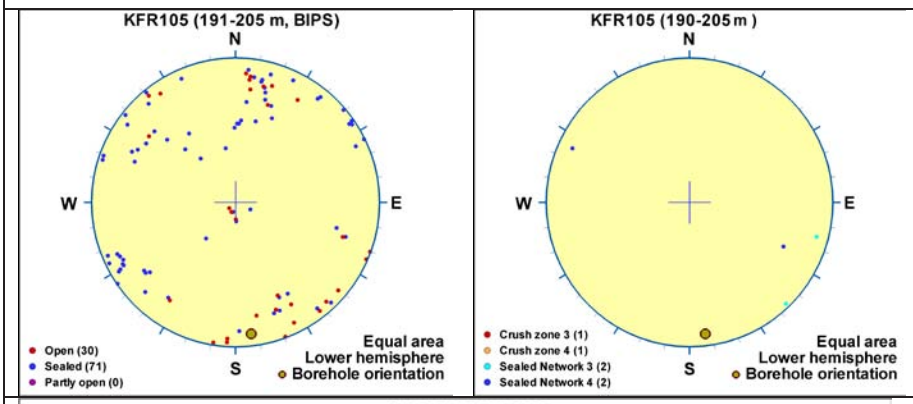

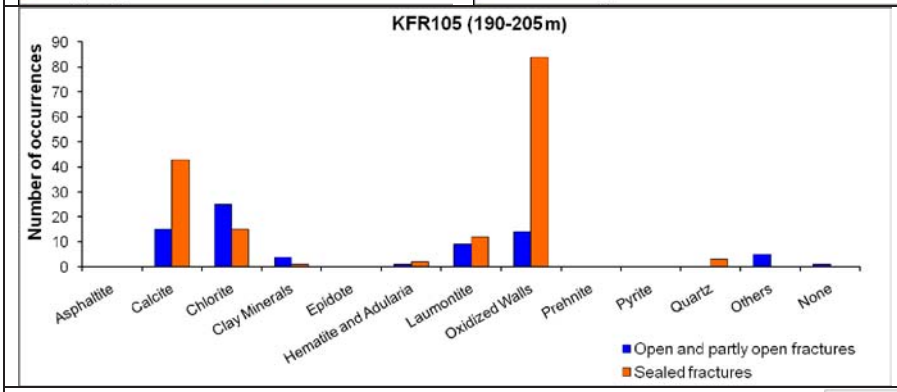

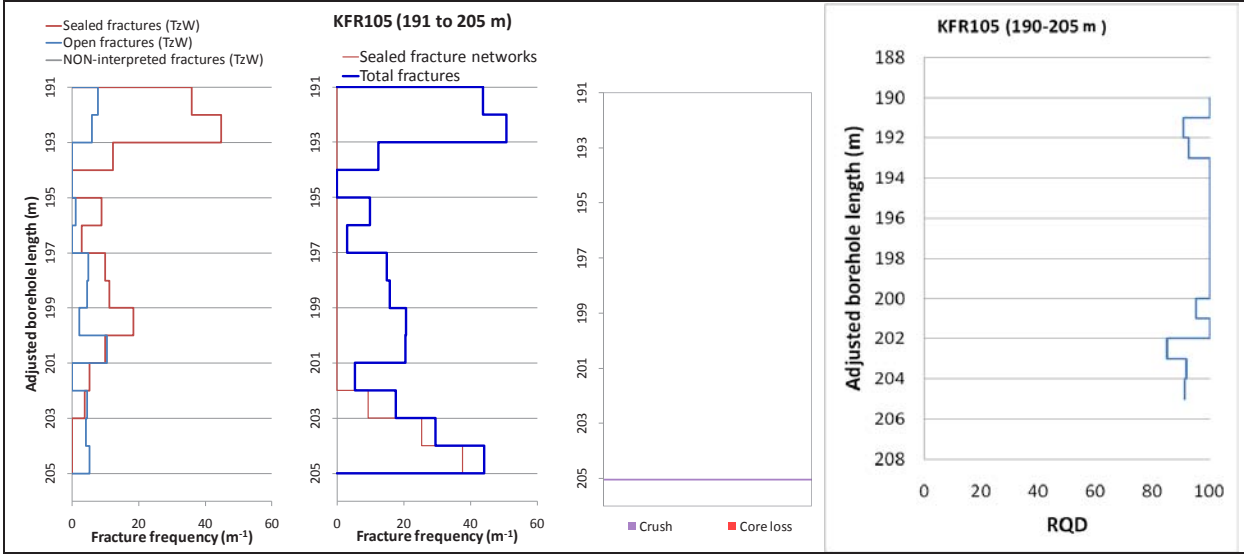

Deformation zone ZFMNNE0725

Borehole and tunnel intersections (metres along borehole/tunnel)

KFM06A: 740–775 m (DZ7 740–775 m)

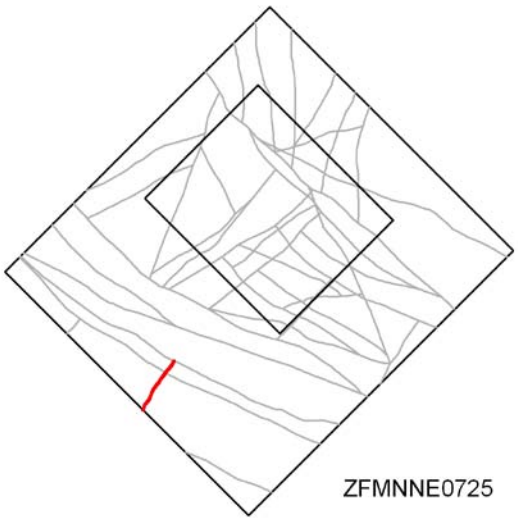

Deformation style, alteration and geometry

Deformation style: Brittle, including cohesive breccia.

Alteration: Red-stained bedrock with fine-grained hematite dissemination. Vuggy rock with quartz dissolution at 770.8–770.9 m in KFM06A DZ7

Strike/dip (span) right-hand-rule: 201 / 84 (±5 / ±10)

Trace length at ground surface (span): 1763 m (1760−1900 m)

Model thickness (span) : 12 m (3–45 m)

Confidence in existence: High

Modelling procedure*:* The position of the zone at the ground surface is based on the lineament MFM0725G, defined by a magnetic minimum in Forsmark stage 2.3 /Isaksson et al. 2007/, which was extended c. 500 m in a NNE direction during stage 2.3 compared with that available in the modelling work during stage 2.2 /Stephens et al. 2007/. The zone was included as a high confidence zone in the stage 2.2 model based on an interception in borehole KFM06A /Stephens et al. 2007/. With the exception of the trace length of the zone at the ground surface and the strike of the zone, steered by the extension of the corresponding lineament, the properties are identical to those presented in /Stephens et al. 2007/. The minor change in strike lies within the uncertainty interval presented in /Stephens et al. 2007/.

Fractures in the deformation zone

General characteristics

Fracture orientation: See sterographic projections and statistics (based on DZ7 in KFM06A in /Stephens et al. 2007/).

Fracture frequency: Mean 16 m^{-1} with a span of 3–107 m^{-1} (based on DZ7 in KFM06A in /Stephens et al. 2007/).

Fracture filling mineralogy: Chlorite, calcite, quartz, hematite/adularia and laumontite (based on DZ7 in KFM06A in /Stephens et al. 2007/).

BOREHOLE AND TUNNEL INTERCEPT DETAILS

Borehole intersections for ZFMNNE0725

BH	Geometrical Intercept		Target intercept	
	Sec_up BH length (m) [z (-m)]	Sec_low BH length (m) [z (-m)]	Sec_up BH length (m) [z (-m)]	Sec_low BH length (m) [z (-m)]
KFM06A	749.14	781.69	740	775

Comment: For identification and description of DZ7 in KFM06A, see /Carlsten et al. 2005/. For more details on the character and kinematics of DZ7 in KFM06A, see /Nordgulen and Saintot 2006/. Two intervals around 745 m and 770 m contain calcite-cemented fault breccias with angular, rotated rock fragments, sealed fracture networks and a crush zone. These intervals are considered to form zone cores. The geometrical intercept comes directly from the DZ_PFM_Loc_v22_01.rvs model since this intercept is located outside the SFR regional model boundary.

Deformation zone ZFMNNE0869

Borehole and tunnel intersections (metres along borehole/tunnel)

KFR09: 0–58.7 m (DZ1 0–58.7 m)
KFR36: 45–115.5 m (DZ1 45–115.5 m)
KFR68: 71.59– 105.13 m (DZ1 71.59–78.11 m and DZ2 102.83–105.13 m)
DT 0+430–0+540 (tDZ30 0+430, tDZ31 0+475, tDZ32 0+478 and tDZ34 0+525
BT 0+355–0+450 (tDZ30 0+355, tDZ31 0+400, tDZ32 0+414 and tDZ34 0+450)

Deformation style, alteration and geometry

Deformation style: Brittle. Cohesive breccias present in KFR36 DZ1

Alteration: Red-stained bedrock with fine-grained hematite dissemination

Strike/dip (span) right-hand-rule: 201 / 86 (±5 / ±10)

Trace length at ground surface (span): 898 m (550−900 m)

Model thickness (span): 60 m (20−60 m)

Confidence in existence: High

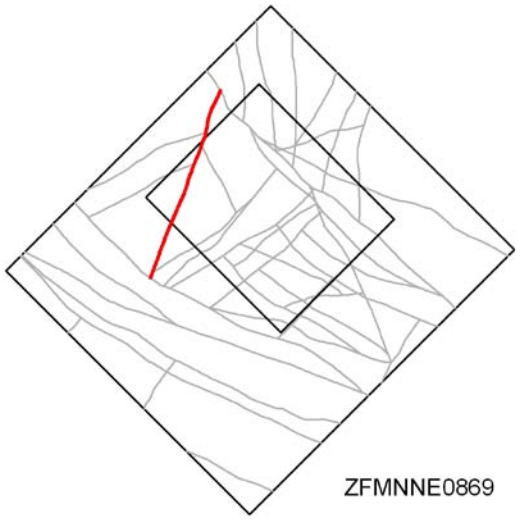

Modelling procedure*:* This zone corresponds to zone 3 in earlier SFR models (see for example /Axelsson and Hansen 1997/). It was renamed ZFMNNE0869 in the Forsmark stage 2.2 model /Stephens et al. 2007/. The position of the central section of the zone at the ground surface is based on the lineament MSFR08089 in SFR model version 1.0 that corresponds to a magnetic minimum. The zone has been extended further to the NNE to terminate against ZFMNW0805A based on the reprocessing and re-evaluation of magnetic data. The NNE termination to ZFMNW0805A is consistent with the extension modelled by /Axelsson and Hansen 1997/, which was adopted subsequently by /Stephens et al. 2007/. However, adjustments to zone ZFMNW0805A have resulted in a minor adjustment of the trace length of zone ZFMNNE0869 at the ground surface compared with that presented in /Stephens et al. 2007/. In the SSE, the zone terminates at the surface at ZFMWNW1035 and at depth at ZFMNW0002.

The orientation 201/86 involves only a slight adjustment compared with earlier models (200/80 in /Stephens et al. 2007/). However, the zone thickness has been modified considerably in accordance with current SKB SHI based methodology. The thickness has been increased from 10 m to 60 m based on the results of the geological SHI from KFR09 and KFR36 and the indications as presented on the tunnel mapping overview drawings, all of which support an increased modelled thickness. The earlier thinner interpretation /Axelsson and Hansen 1997/ did not include the mapped parallel structures shown in the tunnel mapping though the reasoning is not clear. The zone is interpreted to be a composite zone consisting of several narrower high-strain segments (sub-zones) that diverge and converge in a complex pattern /Axelsson and Hansen 1997/. In the tunnels the zone has been reported as associated with moisture, dripping and occasionally running water.

The zone is crossed by four seismic refraction profiles /Keisu and Isaksson 2004/. Two profiles indicate minor low velocity anomalies while velocities generally lie in the range of 4000–5000 m/s. Forward modelling of magnetic data along profile 18 (see Appendix 6) suggests a sub-vertical dip. It should be noted that the width of the anomaly is much narrower than the modelled zone thickness. The anomaly is taken to represent one member of a broader group of sub-parallel, narrow zones represented by the greater modelled thickness.

Deformation zone ZFMNNE0869

a. 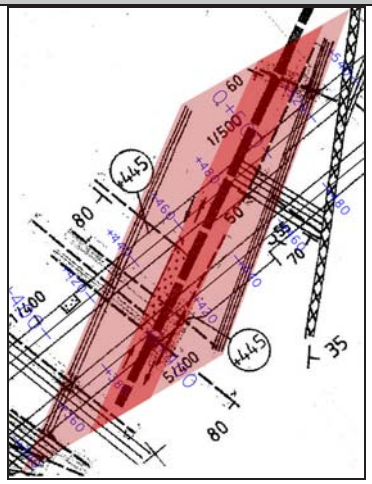

b. 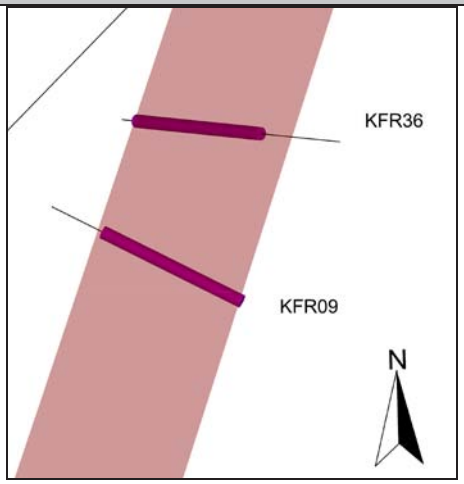

a. Plan view of ZFMNNE0869 as interpreted in the DT and BT tunnels. The possible zone core is shown in dark pink with the bordering damage zones shown in a lighter pink.

b.ZFMNNE0869, looking down dip, as interpreted in KFR36 and KFR09. The relevant SHI PDZs are shown as pink cylinders.

Fractures in the deformation zone

General characteristics

Fracture orientation: No orientation fracture data is available

Fracture frequency: No orientation corrected data is available. See individual borehole intercepts for general indications.

Fracture filling mineralogy:

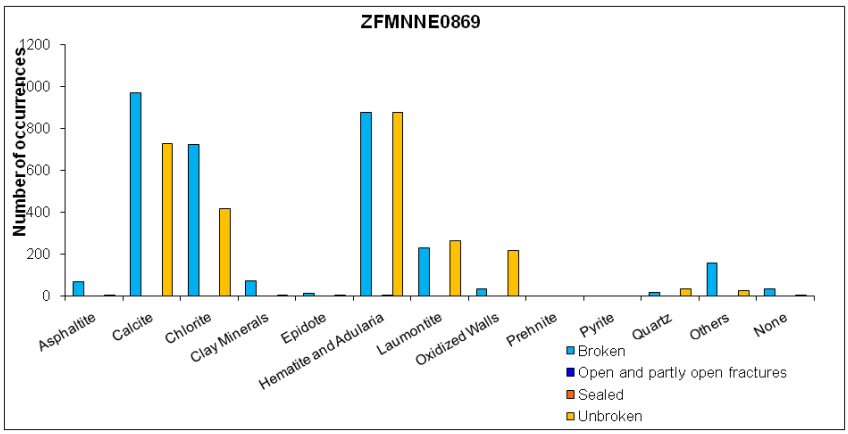

Deformation zone ZFMNNE0869

KFR09 DZ1 (0–58.7 m)

BOREHOLE AND TUNNEL INTERCEPT DETAILS

Borehole intersections for ZFMNNE0869				
BH	Geometrical Intercept		Target intercept	
	Sec_up BH length (m) [z (-m)]	Sec_low BH length (m) [z (-m)]	Sec_up BH length (m) [z (-m)]	Sec_low BH length (m) [z (-m)]
KFR09	0.00 [77.44]	59.19 [82.60]	0	58.7

SHI DZ1 0–58.7 m: Increased frequency of broken and unbroken fractures and sealed networks. Most intensely fractured between 16–58.7 m. Seven minor intervals of crush. Calcite, chlorite, adularia and laumontite, variably discoloured by microscopic hematite, are the most frequent fracture filling minerals. The occurrence of laumontite is, generally restricted to two distinct sections at 0–24 and 40–45 m, and their α–angles are typically dipping moderately (57–78°). None of the other major mineral phases exhibit such a distinct distribution pattern. Numerous asphalt-bearing fractures have been registered in the length interval 26–61 m. The occurrence of clay mineral fillings is rather scarce. Generally faint to weak oxidation. Felsic to intermediate volcanic rock (103076) with minor occurrences of pegmatitic granite (101061), fine- to medium-grained granite (111058) and amphibolite (102017). Confidence level = 3.

No hydrogeological investigation data from the upper 7 m of the borehole. The hydraulic conductivity (measured in sections of about 20 m) is moderate to high in the whole interval (above $4 \cdot 10^{-8}$ m/s). The maximum measured hydraulic conductivity is $2 \cdot 10^{-6}$ m/s in the interval 43–62 m.

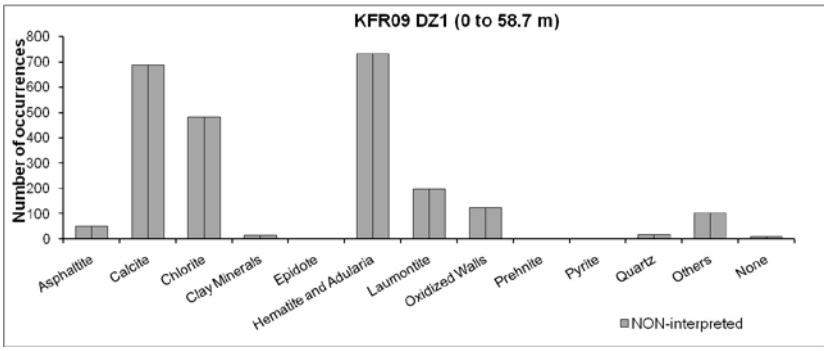

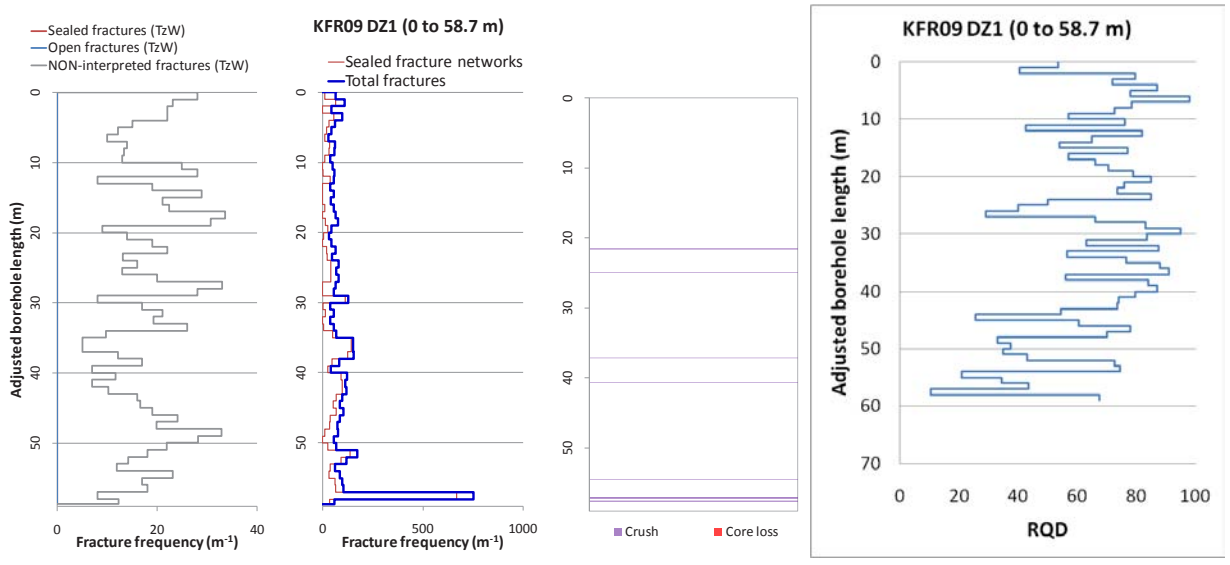

Borehole intersections for ZFMNNE0869				
BH	Geometrical Intercept		Target intercept	
	Sec_up BH length (m) [z (-m)]	Sec_low BH length (m) [z (-m)]	Sec_up BH length (m) [z (-m)]	Sec_low BH length (m) [z (-m)]
KFR36	27.80 [14.99]	118.84 [80.48]	45	115.5

SHI DZ1 45–115.5 m: Increased frequency of broken and unbroken fractures and sealed networks. Decreased frequency of broken fractures between 63.5–70 m, which corresponds to the occurrence of pegmatitic granite. The section between 98–115.5 m is the most highly fractured part, with nine crushed sections. The primary infilling minerals in the interval are adularia, calcite and laumontite, together with trace amounts of hematite. Three breccias at 57.09–57.10, 104.81–105.56 and 107.95–108.04 m occur in the interval. α–angles are generally small to moderate (<67°). In the intensely fractured interval at 44–53 m length, there is a majority of fractures filled by calcite and chlorite, with subordinate amounts of hematite. The interval includes one minor crush zone at 49.11–49.15 m. A distinct peak of broken fractures with adularia and chlorite together with a white unidentifiable mineral that might be kaolinite or a zeolite occurs at 60–62 m. Two α–angles at 12 and 30° are registered in the interval. Asphaltite-bearing fractures, concentrated to the interval between 105–114 m. Generally faint to weak oxidation through out the possible zone. Strongly foliated metagranite-granodiorite (101057) with occurrences of fine- to medium-grained granite (111058), intermediate metavolcanic rock (103076), pegmatitic granite (101061), amphibolites (102017) and metagabbro-diorite (101033). Confidence level = 3.

The hydraulic conductivity (measured in 3-m sections) is quite high in the whole interval ($6 \cdot 10^{-6}$–$5 \cdot 10^{-8}$ m/s). Hydraulic conductivity above $1 \cdot 10^{-6}$ m/s at 48–51, 54–57, 96–99 and 102–108 m.

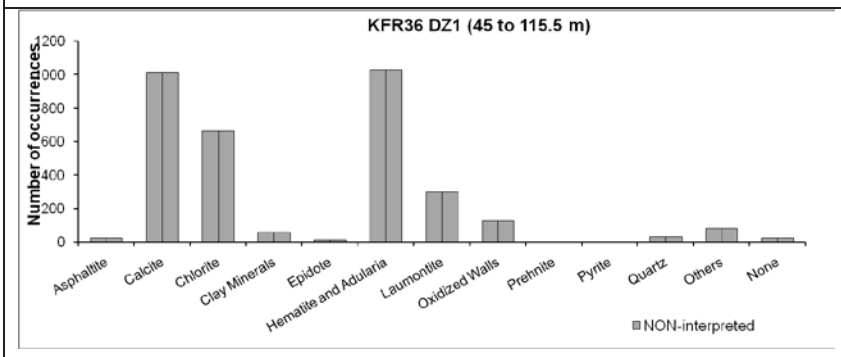

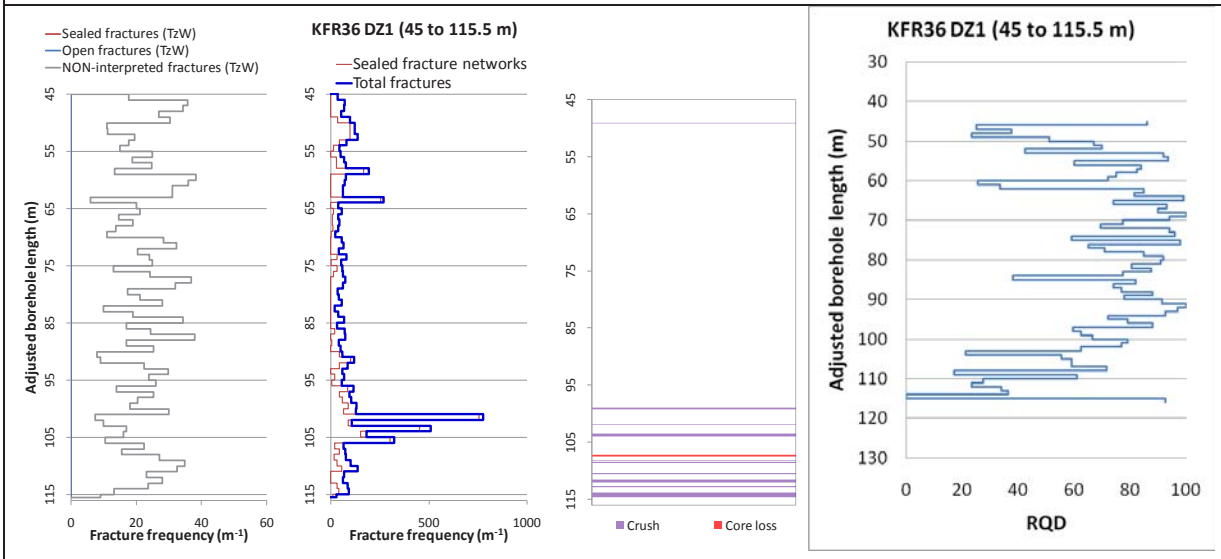

Borehole intersections for ZFMNNE0869				
BH	**Geometrical Intercept**		**Target intercept**	
	Sec_up BH length (m) [z (-m)]	**Sec_low BH length (m) [z (-m)]**	**Sec_up BH length (m) [z (-m)]**	**Sec_low BH length (m) [z (-m)]**
KFR68	43.94 [31.06]	eoh [90.82]	71.59	105.13
Comment: KFR68 is interpreted as intercepting the meeting point between ZFMNNE0869 and ZFMNE0870. Since the BH lacks fracture orientation data, it is impossible to correlate the PDZ with any specific steeply dipping zone. Thus, the PDZs are taken as target intercepts for both ZFMNE0870 and ZFMNNE0869.				
SHI DZ1 71.59–78.11 m: Increased frequency of broken fractures, locally also sealed fracture networks. Variable α-angles, but generally > 45°. Locally faint to weak argillization. Weak muscovitization throughout the interval. Predominant minerals in broken and unbroken fractures are clay minerals, calcite and chlorite. Pegmatitic granite (101061) and aplitic metagranite (101058). Confidence level = 3. Transmissivity below the measurement limit ($7 \cdot 10^{-7}$ m^2/s).				
SHI DZ2 102.83–105.13 m: Increased frequency of broken fractures and crushes. Variable α-angles. Weak to moderate oxidation throughout the interval. Predominant minerals in broken fractures are clay minerals, chlorite, hematite and calcite. Fine- to medium-grained granite (111058) and pegmatitic granite (101061). Confidence level = 1. Moderate transmissivity of the interval 102.51–105.51 m ($8 \cdot 10^{-7}$ m^2/s).				
KFR10	0.00 [78.30]	97.49 [147.24]	–	–
Comment: Judging from the photographs of the drill cores, there is a frequency of broken fractures that locally exceeds 10 fractures/m along the interval 0–97 m. Oxidation of varying degrees occurs frequently throughout the interval 0–97 m. Both the fracture frequency and occurrence of oxidation resembles that for DZ1 in KFR09 and for DZ1 in KFR36, but is generally slightly lower and less conspicuous, respectively. Thus, ZFMNNE0869 may well have its intersection in this interval, but a specific target intercept cannot be defined.				
SHI DZ1 0–5.00 m: Increased frequency of broken and locally unbroken fractures. α-angles > 45°. Weak to medium oxidation outside amphibolites. Predominant fracture minerals are chlorite, laumontite, calcite and clay minerals. Moderately foliated metagranite-granodiorite (101057) and amphibolite (102017). Confidence level = 1. No hydraulic test data from this section of the borehole.				

Tunnel intersections for ZFMNNE0869				
Tunnel	**Geometrical Intercept**		**Target intercept**	
	Start ch.(m)	**End ch. (m)**	**Start ch.(m)**	**End ch. (m)**
DT	0+430	0+555	0+430	0+540
Comment: Target intercept defined by tDZ30 0+430, tDZ31 0+475, tDZ32 0+478, tDZ34 0+525 and tDZ36 0+540 in Appendix 2 of /Curtis et al. 2009/. Clay, crushed rock, alteration, water and injection /Carlsson et al. 1985/.				
BT	0+357	0+482	0+350	0+450
Comment: Target intercept defined by (tDZ30 0+355, tDZ31 0+400, tDZ32 0+414 and tDZ34 0+450) in Appendix 2.				

Deformation zone ZFMNNE2308

Borehole and tunnel intersections (metres along borehole/tunnel)

None

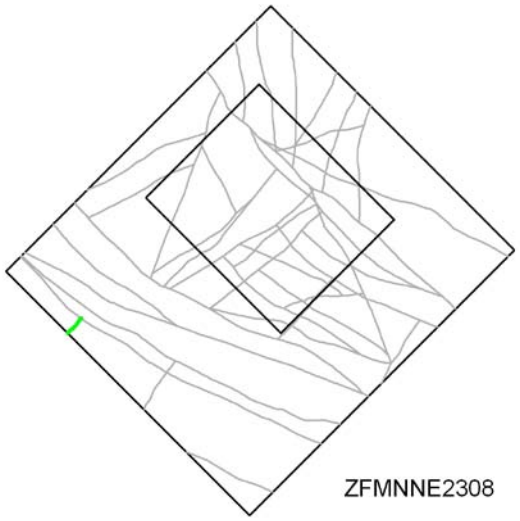

Deformation style, alteration and geometry

Deformation style: Brittle (no direct evidence – inferred association with other NNE-SSW trending deformation zones)

Alteration: No data

Strike/dip (span) right-hand-rule: 214 / 80 (±5 / ±10)

Trace length at ground surface (span): 1250 m (1250−1390 m)

Model thickness : 15 m (3−45 m)

Confidence in existence: Medium

Modelling procedure*:* Apart from a minor modification in the termination of this zone against ZFMWNW0813 rather than ZFMWNW0001 and, as a result, a minor reduction in the trace length of the zone at the ground surface, the modelling procedure and properties for zone ZFMNNE2308 follow those presented in /Stephens et al. 2007/.

Fractures in the deformation zone

General characteristics

Fracture orientation: No data

Fracture frequency: No data

Fracture filling mineralogy: No data

Deformation zone ZFMNNE3130

Borehole and tunnel intersections (metres along borehole/tunnel)

None

Deformation style, alteration and geometry

Deformation style: Brittle (no direct evidence – inferred association with other NNE-SSW trending deformation zones)

Alteration: No data

Strike/dip (span) right-hand-rule: 30 / 90

Trace length at ground surface (span): 411 m (390−420 m)

Model thickness: 5 m (1% default)

Confidence in existence: Medium

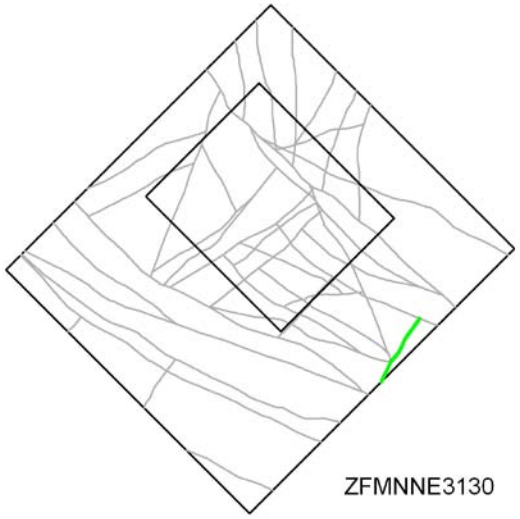

Modelling procedure*:* The position of the zone at the ground surface is based on the magnetic lineament MFM3130G in Forsmark stage 2.3 /Isaksson et al. 2007/. The modelled thickness and vertical dip are default values.

Fractures in the deformation zone

General characteristics

Fracture orientation: No data

Fracture frequency: No data

Fracture filling mineralogy: No data

Deformation zone ZFMNNE3264

Borehole and tunnel intersections (metres along borehole/tunnel)

None

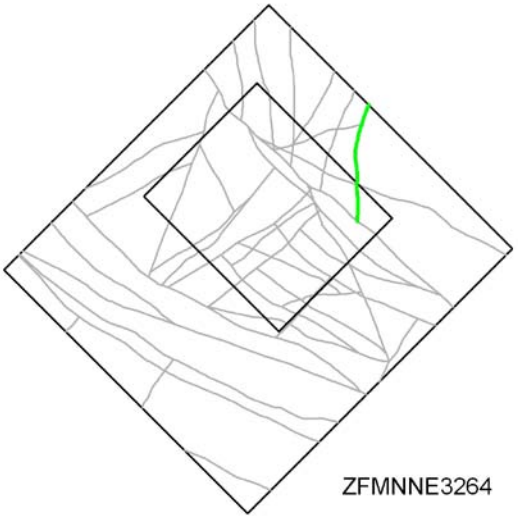

Deformation style, alteration and geometry

Deformation style: Brittle (no direct evidence – inferred association with other NNE-SSW trending deformation zones)

Alteration: No data

Strike/dip (span) right-hand-rule: 031 / 90 (005−035 / ±10)

Trace length at ground surface (span): 1128 m (525−1130 m)

Model thickness: 10 m (1% default)

Confidence in existence: Medium

Modelling procedure*:* The position of the zone at the ground surface is based on the magnetic lineament MSFR08001 in SFR model version 1.0, itself an update of lineament MFM3264G in Forsmark stage 2.3 /Isaksson et al. 2007/. The stage 2.3 number in the zone name has been maintained for traceability of the zone between different versions of lineament interpretation. Forward modelling of magnetic data along profile 36 (see Appendix 6) weakly supports the inferred vertical dip of the inferred zone, while profile 35 (see Appendix 6) gives a weak indication of a subvertical dip towards the west. The modelled zone thickness is a default value.

Fractures in the deformation zone

General characteristics

Fracture orientation: No data

Fracture frequency: No data

Fracture filling mineralogy: No data

Deformation zone ZFMNNE3265

Borehole and tunnel intersections (metres along borehole/tunnel)

None

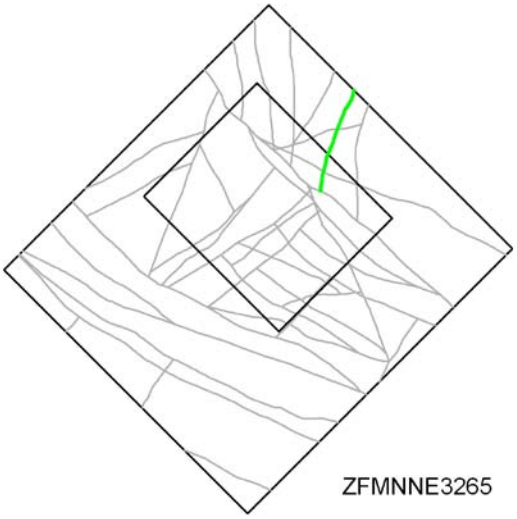

Deformation style, alteration and geometry

Deformation style: Brittle (no direct evidence – inferred association with other NNE-SSW trending deformation zones)

Alteration: No data

Strike/dip (span) right-hand-rule: 032 / 90 (015−035 / ±10)

Trace length at ground surface (span): 1103 m (475−1103 m)

Model thickness: 10 m (1% default)

Confidence in existence: Medium

Modelling procedure*:* The position of the zone at the ground surface is based on the magnetic lineament MFM3265G /Isaksson et al. 2007/, itself essentially the same as a linking of lineaments MSFR08002 and MSFR08003 in the SFR model version 1.0 interpretation. The forward modelling of magnetic data along profiles 9, 35 and 36 (see Appendix 6) support the inferred vertical dip of the zone. The modelled zone thickness is a default value.

Fractures in the deformation zone

General characteristics

Fracture orientation: No data

Fracture frequency: No data

Fracture filling mineralogy: No data

Deformation zone ZFMNNE3266

Borehole and tunnel intersections (metres along borehole/tunnel)

None

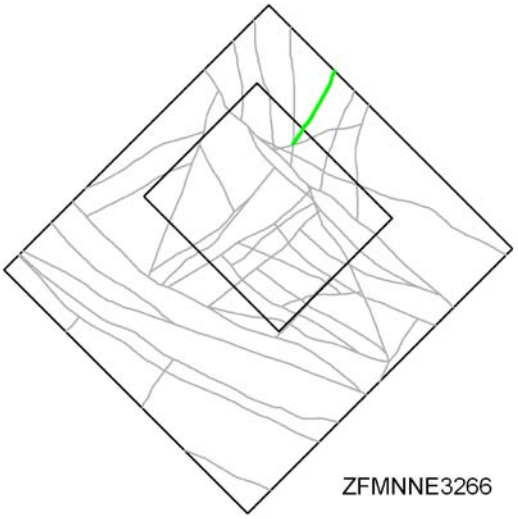

Deformation style, alteration and geometry

Deformation style: Brittle (no direct evidence – inferred association with other NNE-SSW trending deformation zones)

Alteration: No data

Strike/dip (span) right-hand-rule: 034 / 90 (025–035 / ±10)

Trace length at ground surface (span): 1015 m (695−1015 m)

Model thickness: 10 m (1% default)

Confidence in existence: Medium

Modelling procedure*:* The position of the zone at the ground surface is based on the magnetic lineament MFM3266G in Forsmark stage 2.3 /Isaksson et al. 2007/. There has been a very minor update resulting in lineament MSFR08009 in the SFR model version 1.0 interpretation. The stage 2.3 number has been maintained to aid traceability between different versions of the lineament interpretation.

Fractures in the deformation zone

General characteristics

Fracture orientation: No data

Fracture frequency: No data

Fracture filling mineralogy: No data

Steeply dipping WNW to NW deformation zones

Deformation zone ZFMNW0002

Borehole and tunnel intersections (metres along borehole/tunnel)

HFM34: 180– 192 (DZ2 180–184 m and DZ3 188–192 m)
HFM35: 24–52.5 m (DZ1 24–33 m and DZ2 47.2–52.5 m)
DT: 0+309 to 0+372 (tDZ19 0+309–0+372, tDZ20 0+322 and tDZ21 0+355)
BT: 0+297 to 0+347 (tDZ19 0+297–0+347, tDZ20 0+302, tDZ21 0+339 and tDZ22 0+345)

Deformation style, alteration and geometry

Deformation style: Ductile and brittle

Alteration: Very local red-stained bedrock with fine-grained hematite dissemination, chloritization

Strike/dip (span) right-hand-rule: 134 / 90 (±5 / 70−90)

Trace length at ground surface: 18,000 m

Model thickness (span): 50 m (10−80 m)

Confidence in existence: High

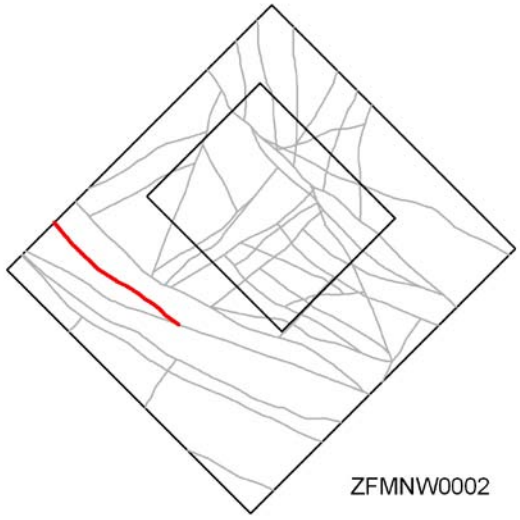

Modelling procedure*:* The properties of zone ZFMNW0002 are based on and have been modified slightly after Forsmark model stage 2.2 /Stephens et al. 2007/. Zone ZFMNW0002, a splay of the major, regionally significant Singö zone, is itself a regional deformation zone interpreted as having a length of 18 km /Stephens et al. 2007/. The position of the zone as it crosses the SFR regional model area is based on the magnetic lineament MSFR08085 in SFR model version 1.0, which has a slightly modified alignment at its south-east end, both in relation to MFM0804G in the stage 2.3 lineament interpretation /Isaksson et al. 2007/ and lineament MFM0804 used in the modelling work during model stage 2.2 /Stephens et al. 2007/.

The zone was identified in tunnel 3 at Forsmark (see Fig. 5-9 in /Carlsson and Christiansson 1987/). The zone was also reported earlier at SFR in /Carlsson et al. 1985/ as ‘zone 1’ who noted that the zone had been identified by tunnel mapping and seismic investigations. The zone was noted as not being very pronounced in the SFR tunnel, consisting of sheet fractured rock and partly crushed rock. The zone was attributed a thickness of 7 to 10 m.

The zone has been interpreted as having a close association with the neighbouring ZFMWNW0001 /Stephens et al. 2007/ and being part of the same tectonic belt within the SFR regional model area. The thickness has been modified solely on the basis of reference to the mapping in the SFR DT (operation) and BT (construction) tunnels, with the Singö zone corresponding to the complex series of crush zones and ZFMNW0002 corresponding to a secondary, more isolated crush zone lying within a section of closely spaced, sub-vertical parallel fractured rock mapped in the tunnels. Outside of the SFR regional model volume, in Forsmark tunnel 3 the zone thickness was reported as 75 m. Boreholes KFM11A, HFM34 and HFM35 were drilled to provide information on the Singö zone and neighbouring splays at depth. An evaluation of the data from these three boreholes was presented in /Stephens et al. 2008b/.

The property assessment by /Stephens et al. 2007/ for ZFMNW0002 was mainly based on information from the cooling water tunnel of Forsmark reactor 3. In this, ZFMNW0002 is described in terms of low fracture frequency (1 m^{-1}) and ductile deformation characterized by zones of foliated rocks and chlorite schist. Recorded alterations are chloritization and red-stained bedrock with fine-grained hematite dissemination.

Deformation zone ZFMNW0002

Fractures in the deformation zone

General characteristics

Fracture orientation:

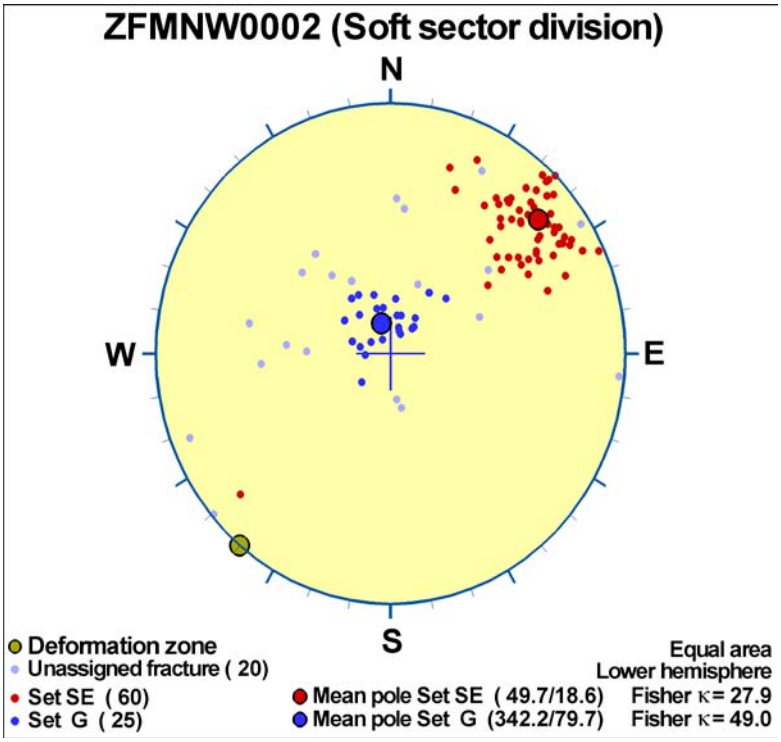

The above is based on the intercept in percussion borehole HFM35. General reference can be made to ZFMWNW0001 for probable typical fracture orientation sets.

Fracture frequency: See HFM35 DZ2 and DZ3 below for low confidence indications of fracture frequency.

Fracture filling mineralogy: Chlorite and calcite /Stephens et al. 2007/

BOREHOLE AND TUNNEL INTERCEPT DETAILS

Borehole intersections for ZFMNW0002

BH	Geometrical Intercept		Target intercept	
	Sec_up BH length (m) [z (-m)]	Sec_low BH length (m) [z (-m)]	Sec_up BH length (m) [z (-m)]	Sec_low BH length (m) [z (-m)]
HFM34	170.32 [138.81]	eoh [200.75]	180	192

Comment: Two low confidence SHI DZs fall within this interval. However, there are no BIPS data available for this borehole. In addition the entire BH falls within the modelled ZFMWNW0001

DZ2 180–184 m: Low resistivity, low P-wave velocity, low magnetic susceptibility and several calliper anomalies. One identified radar reflector with an intersection angle of 53°. Due to **poor BIPS image**, mapping of fractures and rock types has not been carried out. Judgement of possible deformation zone has been based only on geophysical data. Confidence level = 1.

Borehole intersections for ZFMNW0002
DZ3 188–192 m: Low resistivity, low P-wave velocity, low magnetic susceptibility and several calliper anomalies. One identified radar reflector with an intersection angle of 57°. Due to **poor BIPS image**, mapping of fractures and rock types has not been carried out. Judgement of possible deformation zone has been based only on geophysical data. Confidence level = 1.

BH	Geometrical Intercept		Target intercept	
	Sec_up BH length (m) [z (-m)]	**Sec_low BH length (m) [z (-m)]**	**Sec_up BH length (m) [z (-m)]**	**Sec_low BH length (m) [z (-m)]**
HFR35	0.00 [1.90]	54.54 [42.92]	24	52.5

Comment: Vertical to subvertical dip to the SW fits with the HFM35 DZ1 and DZ2 intercepts and is also supported by the fracture orientations in DZ1 and at least not contradicted by DZ2.

SHI DZ1 24–33 m: Increased frequency of open fractures and one crush zone in the upper part of the possible zone. Fractures that strike SE and dip steeply to the SW and fractures that are gently dipping dominate. Fracture apertures are generally less than 1 mm, with a few ranging up to 3 mm. Low resistivity, low P-wave velocity, low magnetic susceptibility and several caliper anomalies. Four identified radar reflectors with an intersection angle of 45–74°. Zone situated in metavolcanic rock and subordinate pegmatitic granite. Confidence level = 3.

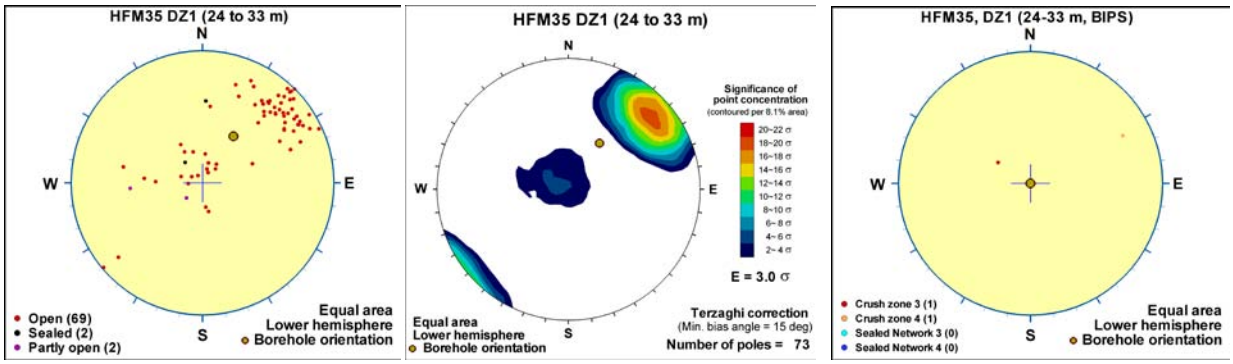

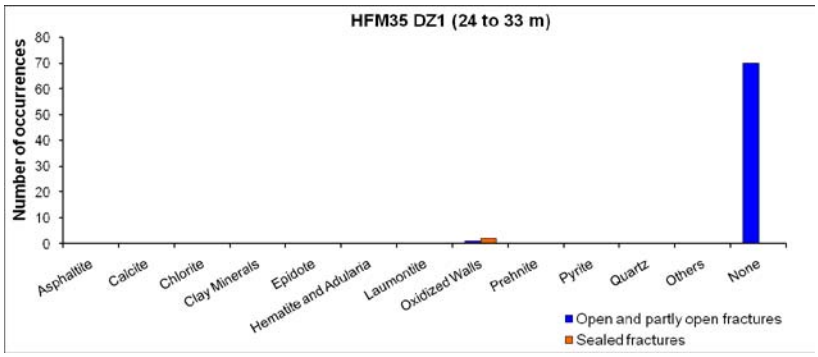

Borehole intersections for ZFMNW0002

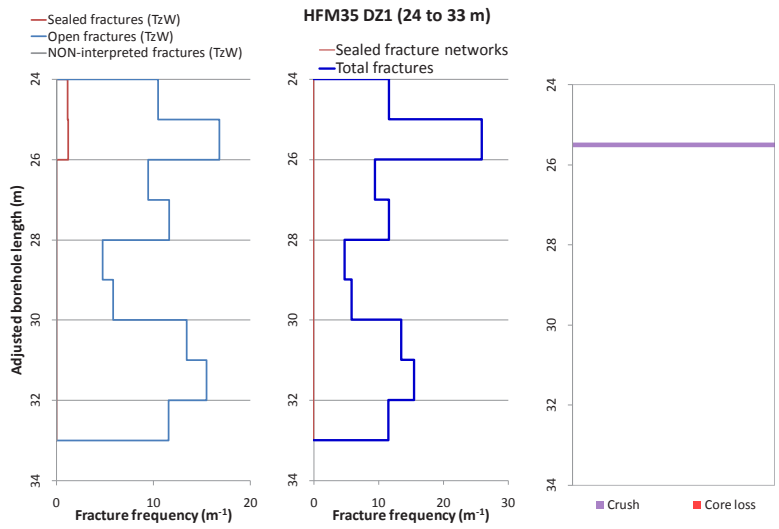

SHI DZ2 47.2–52.5 m: Open fractures strike SSE and dip variably to the WSW. Two crush zones. Apertures are generally less than 1 mm. Low resistivity, low P-wave velocity, low magnetic susceptibility and several caliper anomalies. Two identified radar reflector with an intersection angle of 50º and 72º. Zone situated in metavolcanic rock and subordinate pegmatitic granite. Confidence level = 3.

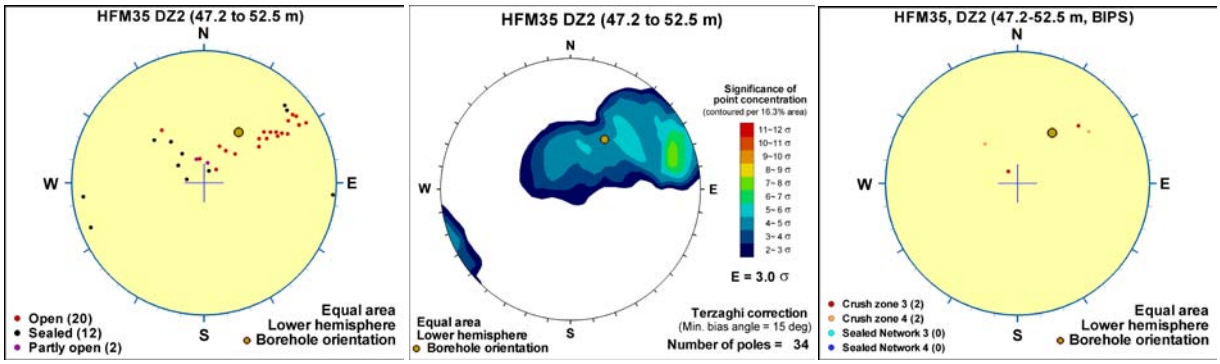

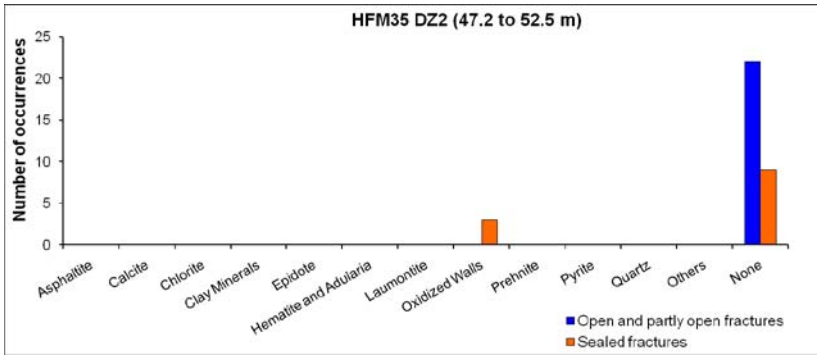

Borehole intersections for ZFMNW0002
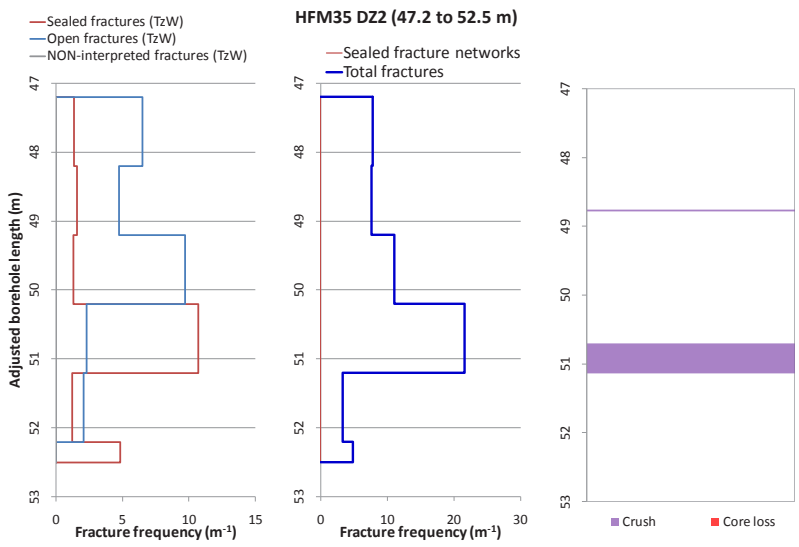

BH	Geometrical Intercept		Target intercept	
	Sec_up BH length (m) [z (-m)]	Sec_low BH length (m) [z (-m)]	Sec_up BH length (m) [z (-m)]	Sec_low BH length (m) [z (-m)]
KFM11A	652.50 [555.69]	735.42 [622.02]	-	-
Comment: The intercept in KFM11A falls within the extensive DZ1 (245–824 m) and can be taken to be a general intercept position within the Singö 'tectonic belt' rather than based on specific evidence from the drillcore. Due to the orientation and inferred origin, it is anticipated that zone ZFMNW0002 has a character similar to the larger zone ZFMWNW0001.				

Tunnel intersections for ZFMNW0002				
Tunnel	Geometrical Intercept		Target intercept	
	Start ch.(m)	End ch. (m)	Start ch.(m)	End ch. (m)
DT	0+313	0+365	0+309	0+372
Comment: Target intercept defined by tDZ19 0+309–0+372, tDZ20 0+322 and tDZ21 0+355 in Appendix 2.				
BT	0+292	0+345	0+297	0+347
Comment: Target intercept defined by tDZ19 0+297–0+347, tDZ20 0+302, tDZ21 0+339 and tDZ22 0+345 in Appendix 2.				

Tunnel intersections for ZFMNW0002

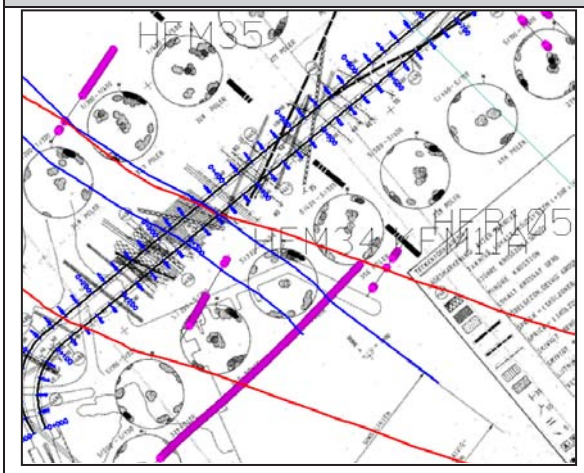

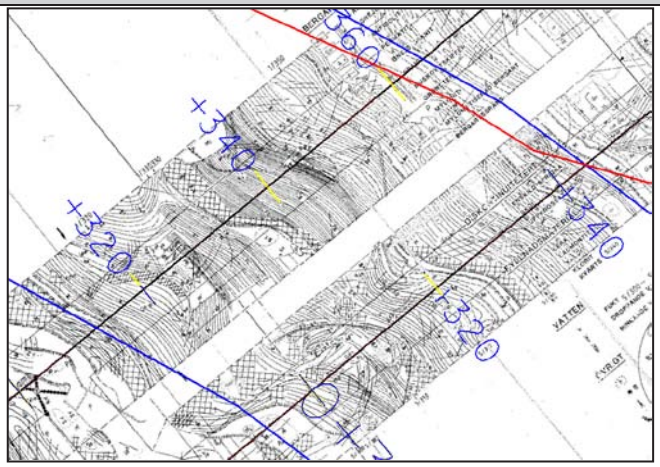

Left: Overview drawing of tunnel mapping showing ZFMWNW0001 (red parallel lines) and a nearby splay ZFMNW0002 (blue parallel lines) as interpreted to intercept the SFR operations and construction tunnels. Note the position coincides with a section of very closely planar jointed rock – part of the Singö zone interpreted by /Christiansson and Bolvede 1987/ and Zone 1 by /Carlsson et al. 1985/. Note that in this position ZFMNW0002 coincides with the northern damage zone of ZFMWNW0001. Boreholes HFM35, HFM34, KFM11A and HFR105 are visible and SHI PDZs are shown as pink cylinders. The modelled zone thickness, seen as blue parallel lines is 50 m.

Right: Extract from detailed mapping covering the ZFMNW0002 intercept (blue parallel lines)

Deformation zone ZFMNW0805A

Borehole and tunnel intersections (metres along borehole/tunnel)

KFR7A: 43–74.45 m (DZ1 3.5–74.45 m)
KFR08: 41–104.4 m (DZ2 41–104.4 m)
KFR11: 41.45–95.65 m (DZ1 41.45–95.65 m)
KFR101: 242–341.76 m (DZ5 242–341.76 m)

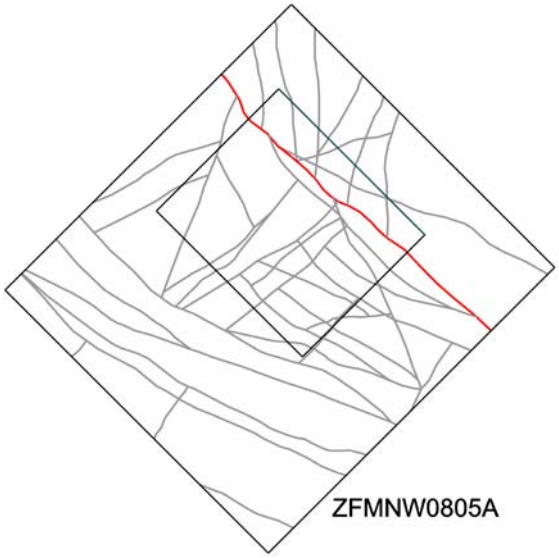

Deformation style, alteration and geometry

Deformation style: Ductile and brittle. Sections of brittle-ductile deformation, including cohesive breccias and cataclasites present in all BH intercepts.

Alteration: Red-stained bedrock with fine-grained hematite dissemination. Altered vuggy rock with quartz dissolution at 72.55–73.30 and 77.95–79.55 m in KFR08 DZ2, 66.58–67.15 and 70.45–70.60 m in KFR11 DZ1 and 300.76–301.25 m in KFR101 DZ5.

Strike/dip (span) right-hand-rule: 312 / 82 (±5 / ±5)

Trace length at ground surface (span): 3643 m (3600–>3643 m)

Model thickness (span): 60 m (30−70 m)

Confidence in existence: High

Modelling procedure*:* This zone corresponds to zone 8 in earlier SFR models (see for example /Axelsson and Hansen 1997/). It was renamed ZFMNW0805 in the Forsmark stage 2.2 model /Stephens et al. 2007/ and is referred to as zone ZFMNW0805A in the current SFR model.

Zone ZFMNW0805A is a local major zone interpreted as having a length of greater than 3 km /Stephens et al. 2007/. The zone crosses the entire regional model volume. The current interpretation of the zone at the ground surface is based on the magnetic lineaments MFM0805G0, MSRF08095, MSFR10008, MSFR10007, MSFR08033 and MSFR08094 (/Isaksson et al 2007/ and SFR model version 1.0).

/Carlsson et al. 1985/ reported that the zone could be identified by seismic investigations. However, the position of the zone does not seem to correspond with any clear low velocity anomalies. The zone was identified in boreholes KFR24 (Kb4) and KFR25 (Kb5) with a dip of 80–90° towards the north-east and a width of 5–10 m. Both /Carlsson et al. 1985/ and /Axelsson and Hansen 1997/ interpreted the zone as dipping steeply to the north-east, with a thickness of 5–15 m (10–45 m including rim zones) /Carlsson et al 1985/. The zone was presented in /Stephens et al 2007/ with an orientation of 134°/90° (uncertainty in strike/dip of ±5°/±10°) and a thickness of 10 m with a span of 10–64 m. The possible deformation zones included in the SHI's reported in the current SFR modelling work are at the base of the boreholes. For this reason, it is inferred that the full thickness of the zone has not been penetrated in these boreholes. The zone has been reported as being characterized by mylonitization, highly fractured rock, alteration and core loss.

The modelled zone thickness and orientation show a good fit with the magnetic forward modelling along profiles 2, 3, 31 and the inversion modelling (see Appendix 6). Profiles 4 and 21 also cross ZFMNW0805A and ZFMNW0805B but do not have such a clear correlation due to possible interference from other structures. These two profiles indicate a more sub-vertical pair of structures.

The radar reflector at 302 m borehole length in KFR101 has an orientation of 299°/87° which gives a reasonable fit with ZFMNW0805A.

Deformation zone ZFMNW0805A

Fractures in the deformation zone

General characteristics

Fracture orientation:

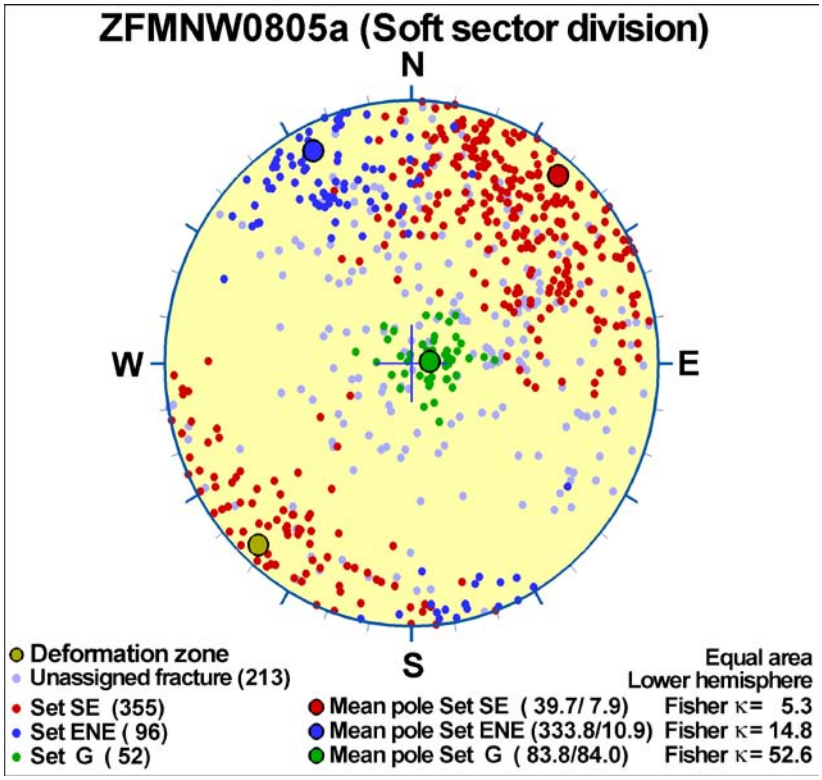

Fracture frequency: Open 10 m^{-1}, Sealed 31 m^{-1}

Fracture filling mineralogy:

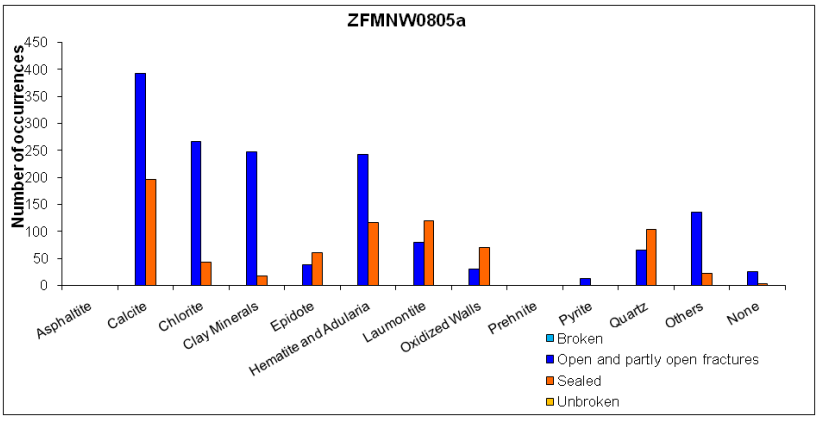

Deformation zone ZFMNW0805A

KFR101 DZ5 292 m–313 m (around fault core position)

BOREHOLE AND TUNNEL INTERCEPT DETAILS

Borehole intersections for ZFMNW0805A				
BH	Geometrical Intercept		Target intercept	
	Sec_up BH length (m) [z (-m)]	Sec_low BH length (m) [z (-m)]	Sec_up BH length (m) [z (-m)]	Sec_low BH length (m) [z (-m)]
KFR7A	43.61 [133.81]	eoh [134.89]	43	74.45

Comment: The target interval corresponds to the lower half of DZ1 and the borehole is interpreted not to penetrate the full thickness of the zone. The remainder of DZ1 is interpreted as intercepting ZFMNW0805B.

SHI DZ1 3.5–74.45 m: Increased frequency of unbroken fractures, sealed networks and especially broken fractures. Nineteen crushes with the most extensive sections at 49.09–74.45 m. Brittle-ductile section characterized by fault breccias and cataclasite at 21–24 m and 64.83–71.29 m. Predominant fracture minerals are clay minerals, calcite and Fe-hydroxide/hematite. The registered α–angles of clay filled fractures are highly variable, ranging from 0 to 85°. Fractures filled with laumontite form swarms throughout the drill core, with the most extensive occurrence at 56.9–64.8 m length. Most of these fractures have gently dipping α–angles less than 25°, with a few ranging up to 55° towards the drill core length axis. Moderately to strongly foliated metagranite-granodiorite (101057), pegmatitic granite (101061), aplitic metagranite (101058), fine- to medium-grained granite (111058) and amphibolite (102017). Confidence level = 3.

Low hydraulic conductivity $6 \cdot 10^{-9}$ m/s in the interval 3.5–19 m. Moderate hydraulic conductivity of $5 \cdot 10^{-7}$ m/s in the interval 20–47 m. High hydraulic conductivity of $3 \cdot 10^{-6}$ m/s in the interval 48–74.45 m.

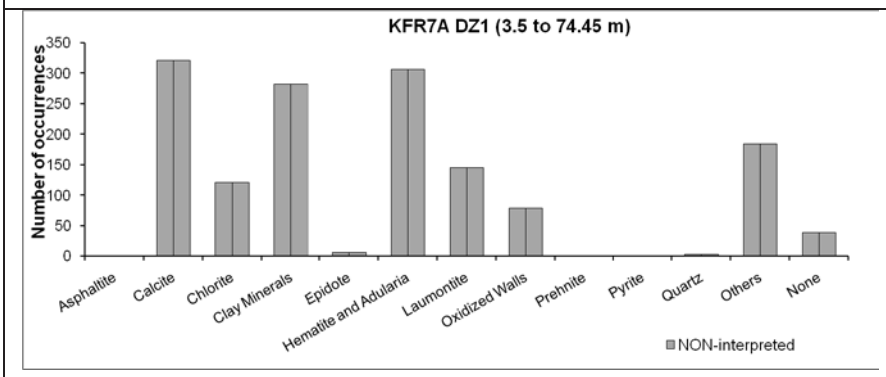

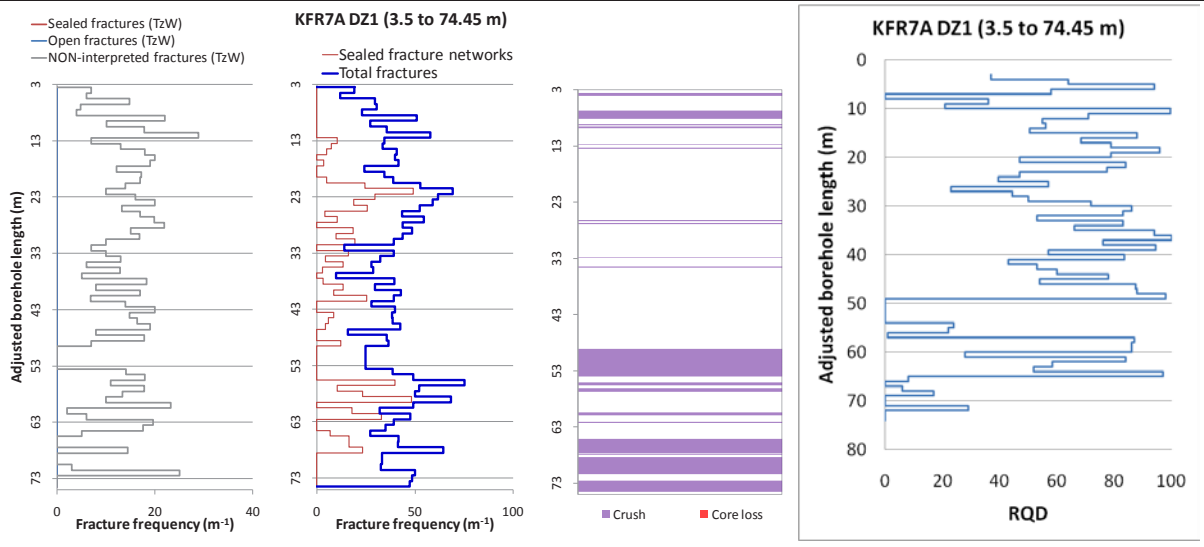

Borehole intersections for ZFMNW0805A				
BH	Geometrical Intercept		Target intercept	
	Sec_up BH length (m) [z (-m)]	Sec_low BH length (m) [z (-m)]	Sec_up BH length (m) [z (-m)]	Sec_low BH length (m) [z (-m)]
KFR08	40.32 [89.53]	101.46 [94.86]	41	104.4

Comment: /Carlsson et al. 1986/ described the zone in the following manner: rim 41–62 m, core 62–80, rim 80–90 m. *Note rim is defined as a zone of increased hydraulic conductivity compared to the general rock mass*.

SHI DZ2 41–104.4 m: Very high frequency of sealed networks and broken fractures. Nineteen crushed sections. Brittle- to ductile section characterised by fault breccias and cataclasite at 42.25–49.80, 53.83–59.1 and 76–80 m. The predominant fracture filling minerals are calcite, chlorite, laumontite and adularia, typically discoloured by hematite. Registered α–angles for fractures in this interval are variable, but generally moderately dipping. Generally weakly to moderately oxidized with two short sections of quartz dissolution (vuggy rock) at 72.55–73.30 and 77.95–79.55 m. Pegmatitic granite (101061), fine- to medium-grained granite (111058) and moderately foliated metagranite-granodiorite (101057). Confidence level = 3.

Moderate hydraulic conductivity (measured in sections of about 20–40 m) of 2–5·10^{-7} m/s throughout the interval.

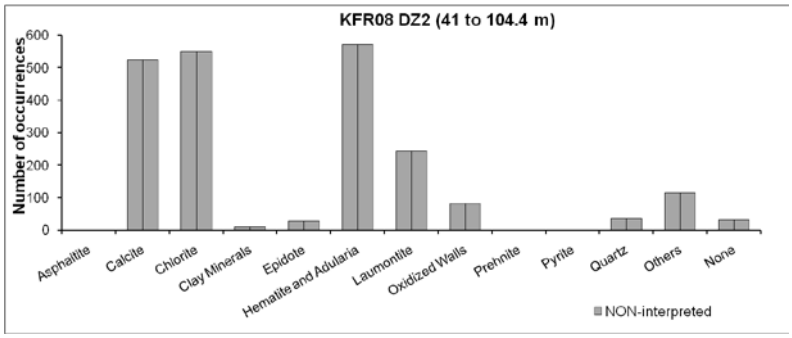

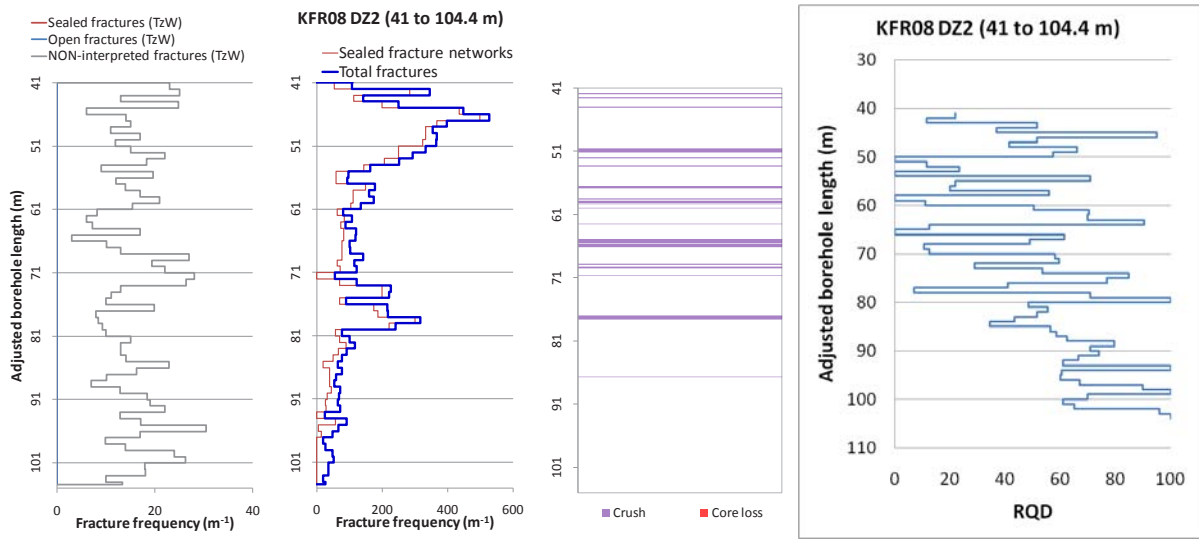

Borehole intersections for ZFMNW0805A				
BH	**Geometrical Intercept**		**Target intercept**	
	Sec_up BH length (m) [z (-m)]	**Sec_low BH length (m) [z (-m)]**	**Sec_up BH length (m) [z (-m)]**	**Sec_low BH length (m) [z (-m)]**
KFR11	32.63 [92.17]	eoh [103.53]	41.45	95.65
Comment: /Carlsson et al. 1986/ described the zone in the following manner: rim 42–65 m, core 65–84, rim 84–92 m. Note rim is defined as a zone of increased hydraulic conductivity compared to the general rock mass.				
SHI DZ1 41.45–95.65 m: Increased frequency of broken fractures. In the section 61.90–92.12 m more highly increased frequency, several crushes, breccias and locally brittle-ductile deformation, particularly at 66.58–74.30 m. Varying α-angles, but generally > 45°. A considerable amount of the fractures are parallel with the tectonic foliation. Occurrences of quartz dissolution ('vuggy granite') at 66.58–67.15 and 70.45–70.60 m. Faint to weak oxidation throughout the interval. Predominant fracture minerals are chlorite, calcite, laumontite and in the core of the possible zone clay minerals, asphaltite and quartz. Pegmatitic granite (101061) and fine- to medium-grained granite (111058). Confidence level = 3. High transmissivity of the section 40.0–98.07 m ($6 \cdot 10^{-5}$ m^2/s). The absolutely dominating transmissivity is contained in the in the section 56–98.07 m.				
KFR101	217.39 [171.55]	334.48 [256.96]	242	341.76
Comment: Note radar reflector at 302 m BH length has an orientation of 299/87 which gives a reasonable fit with ZFMNW0805A.				
SHI DZ5 242–341.76 m: Increased frequency of broken and unbroken fractures and sealed networks. More highly increased frequency of broken fractures at 294–304 m. Five crushed interval at 261.58–261.60, 294.18–294.26, 295.14–295.23, 300.03–300.05 and 338.67–338.71 m. Occasional slickensides. Fractures aperture up to 5 mm. Locally weak to medium oxidation. Interval of vuggy granite affected by argillization at 300.76–301.25 m. Several intervals of breccias, cataclasites and brittle-ductile shear zones, ranging up to a few decimeters in length. One more extensive brittle-ductile shear zones at 326.32–329.91 m. Predominant minerals in sealed fractures are calcite, laumontite, quartz, adularia, epidote and chlorite and in open fractures and crushed intervals calcite, chlorite, clay minerals, hematite, adularia, muscovite, laumontite and quartz. Increased frequency of low resistivity anomalies in the section c. 242–276 m and there is a significant decrease in bulk resistivity in the interval 293–336 m. At 295 m there is one distinct caliper anomaly. Two distinct radar reflector oriented 041°/47°, 296°/16° or 296°/87°, and a prominent radar wave attenuation from c. 290 m to the end of the borehole. Pegmatitic granite (101061), aplitic metagranite (101058), fine- to medium-grained granite (111058), moderately foliated metagranite-granodiorite (101057) and amphibolite (102017). Confidence level = 3. Increased frequency of flow anomalies in the section, particularly in the interval 294–304 m. No flow anomalies below c. 326 m and no flow logging data available below 332 m. The total transmissivity of the interval is quite high (about $9 \cdot 10^{-6}$ m^2/s) where about 90% is concentrated to the interval 294–304 m.				

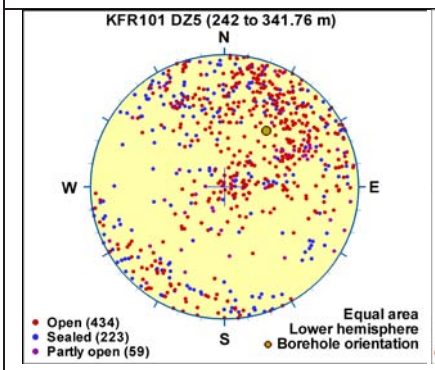

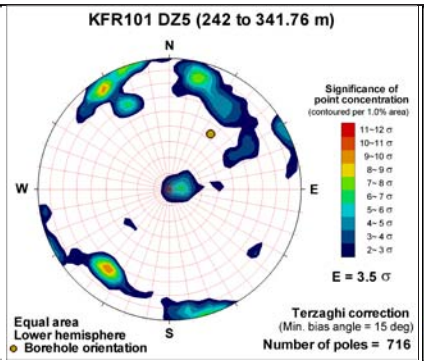

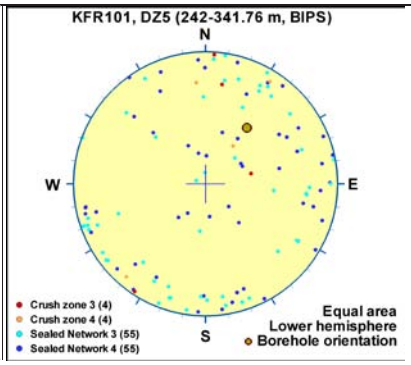

Borehole intersections for ZFMNW0805A

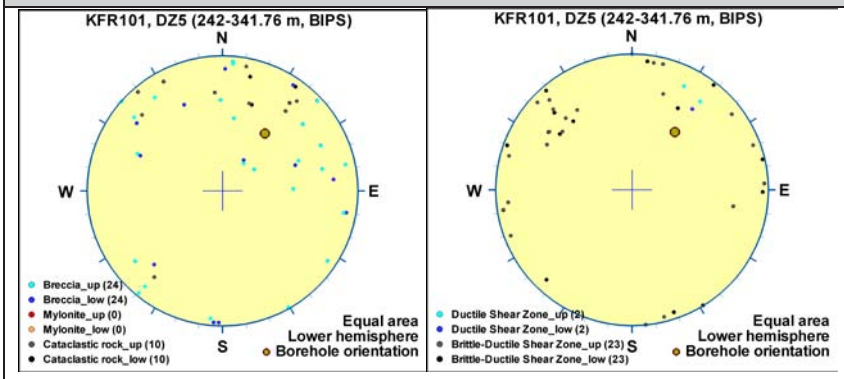

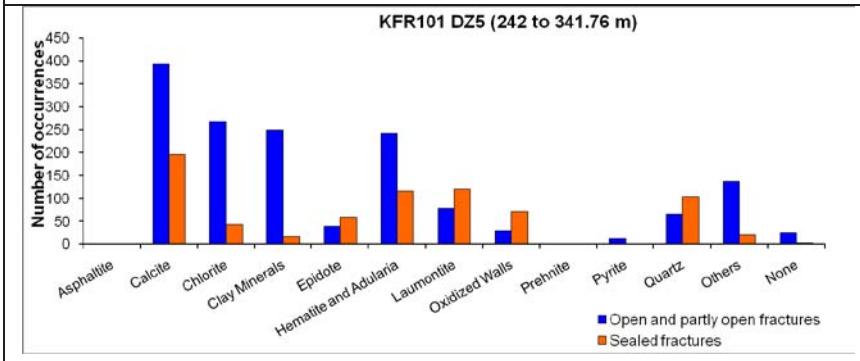

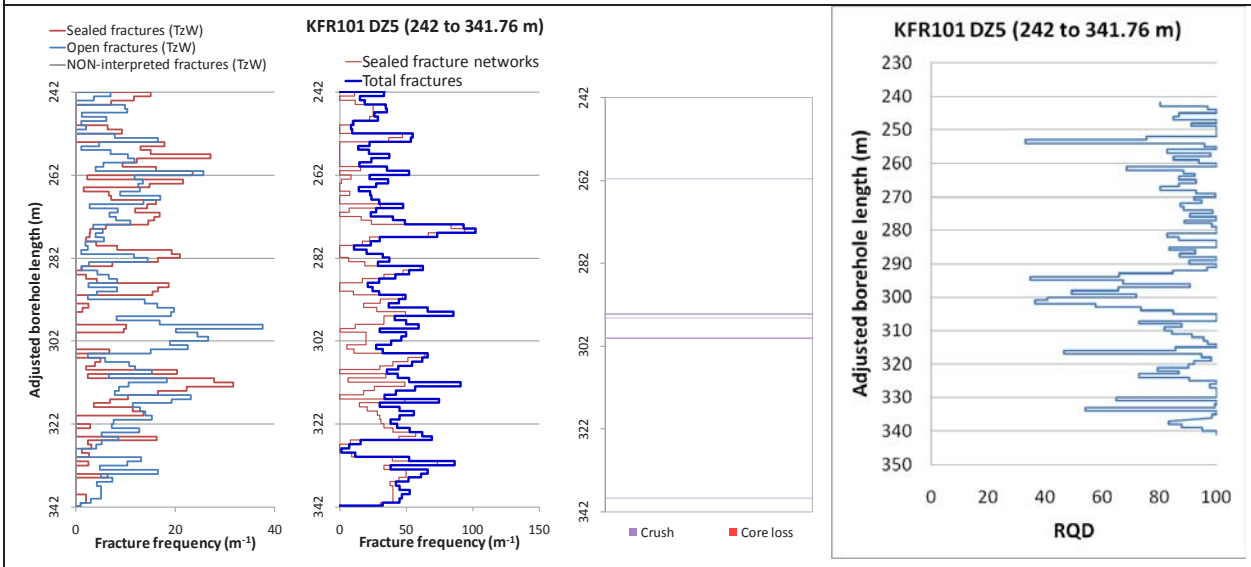

Borehole intersections for ZFMNW0805A				
BH	**Geometrical Intercept**		**Target intercept**	
	Sec_up BH length (m) [z (-m)]	**Sec_low BH length (m) [z (-m)]**	**Sec_up BH length (m) [z (-m)]**	**Sec_low BH length (m) [z (-m)]**
KFR23	10.16 [8.80]	11.36 [9.84]	–	–
Comment: There is a marginal geometrical intercept with this borehole but no information is available.				
KFR24	48.99 [41.08]	156.64 [131.36]	–	–
Comment: The earlier quoted position of the zone fits well with the currently modelled position. However, no control point has been added since more weight has been placed on the boreholes that still have drill core available. /Axelsson and Hansen 1997/ report an approximate position of correlation with the zone at 137 m borehole length (385 m level). This borehole has not been assessed during the current modelling phase since no drill core is available for review. /Carlsson et al. 1986/ described the zone in the following manner: rim zone to SW 126–131m, core 131–135 m borehole length. Note rim is defined as a zone of increased hydraulic conductivity compared to the general rock mass.				
KFR25	50.13 [36.06]	195.09 [140.32]	–	–
Comment: No drill core available and therefore no control point has been used from this borehole. The earlier definitions of the zone fall within the current modelled zone boundaries. /Axelsson and Hansen 1997/ report an approximate position of correlation as 174 m borehole length (375 m level). This borehole has not been assessed during the current modelling phase since no drill core is available for review. /Carlsson et al. 1986/ described the zone in the following manner: rim 172–175 m, core 175–184 m, rim 184–188 m. Note rim is defined as a zone of increased hydraulic conductivity compared to the general rock mass.				
KFR56	57.18 [59.48]	eoh [48.72]	–	–
Comment: No drill core available and therefore no control point has been used from this borehole. The earlier definition of the zone fall within the current modelled zone boundaries. /Axelsson and Hansen 1997/ report an approximate position of correlation as 68 m borehole length (445 m level). This Intercept is not listed by /Carlsson et al. 1985/				

Deformation zone ZFMNW0805B

Borehole and tunnel intersections (metres along borehole/tunnel)

KFR08: 3–19 m (DZ1 3–19 m)
KFR38: 153.60–181.65 m (DZ1 153.60–181.65 m)
KFR101: 97–116 m (DZ2 97–116 m)
KFR7A: 3.5–43 m (DZ1 3.5–74.45 m)

Deformation style, alteration and geometry

Deformation style: Ductile and brittle. Several minor cohesive breccias, cataclasites and brittle-ductile shear zones along KFR101 DZ2 and KFR7A DZ1.

Alteration: Red-stained bedrock with fine-grained hematite dissemination, along with chloritization of amphibolite

Strike/dip (span) right-hand-rule: 315 / 75 (±5 / 70−90)

Trace length at ground surface (span): 1181 m (1170−1200 m)

Model thickness (span): 30 m (5−30 m)

Confidence in existence: High

Modelling procedure*:* The position of the zone on the ground surface is based on the magnetic lineaments MFM0805G1, MSFR08104 and MSFR08098 (/Isaksson et al. 2007/ and SFR model version 1.0), with further adjustment being made based on borehole data.

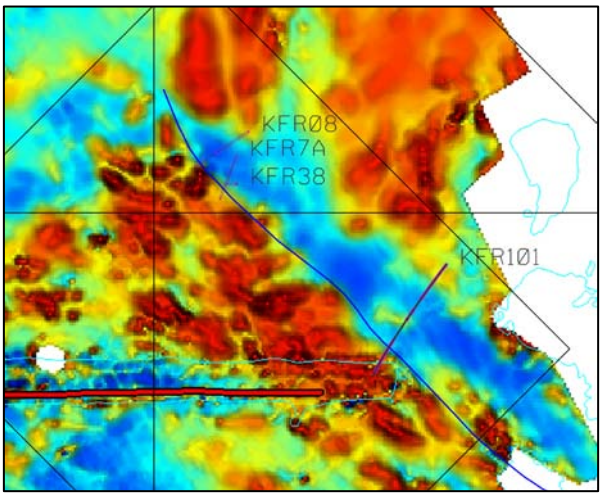

Modified surface position of ZFMNW0805B (blue) shown together with the magnetic map (first vertical derivative of the total field)

The modelled zone thickness is based on the listed SHI PDZ intervals while the modelled convergence of ZFMNW0805B with ZFMNW0805A at depth within the regional model volume is largely conceptual rather than strictly deterministic, with 3D convergence at depth consistent with the 2D convergence of the inferred zone traces at the ground surface. ZFMNW0805B is considered to form a splay of zone ZFMNW0805A. This interpretation is supported by the similar fracture characteristics along these two zones.

The forward modelling of magnetic data along profile 3 and the inversion modelling (Appendix 6) support the steep dip to the north-east. The magnetic modelling along profile 2 indicates the possibility of a more gently dipping structure possibly lying within the wedge between ZFMNW0805A and ZFMNW0805B. However, this is considered most likely to be a very local feature (see Appendix 6).

An alternative to the geometry presented in the model would be to more strictly follow lineament MFM0805G1 and correlate it with KFR08 DZ2 rather than KFR08 DZ1. Although KFR08 DZ2 is currently inferred as being dominated by ZFMNW0805A, it should be emphasized that DZ1 has a confidence level of 1. Such a modelled zone geometry would also include a more restricted target intercept in KFR7A DZ1. The brittle-ductile deformation style inferred to be associated with ZFMNW0805B is limited to 21–24 m length and it cannot be excluded that some of the brittle deformation outside this interval, at least in part, is alternatively related to zone ZFM871.Such an alternative would

eliminate the current geometric intercepts with the SFR tunnels (BT and 1B), where there is no strong evidence to support the presence of the zone. However, heterogeneity along the length of a zone can also adequately account for this feature.

Fractures in the deformation zone

General characteristics

Fracture orientation:

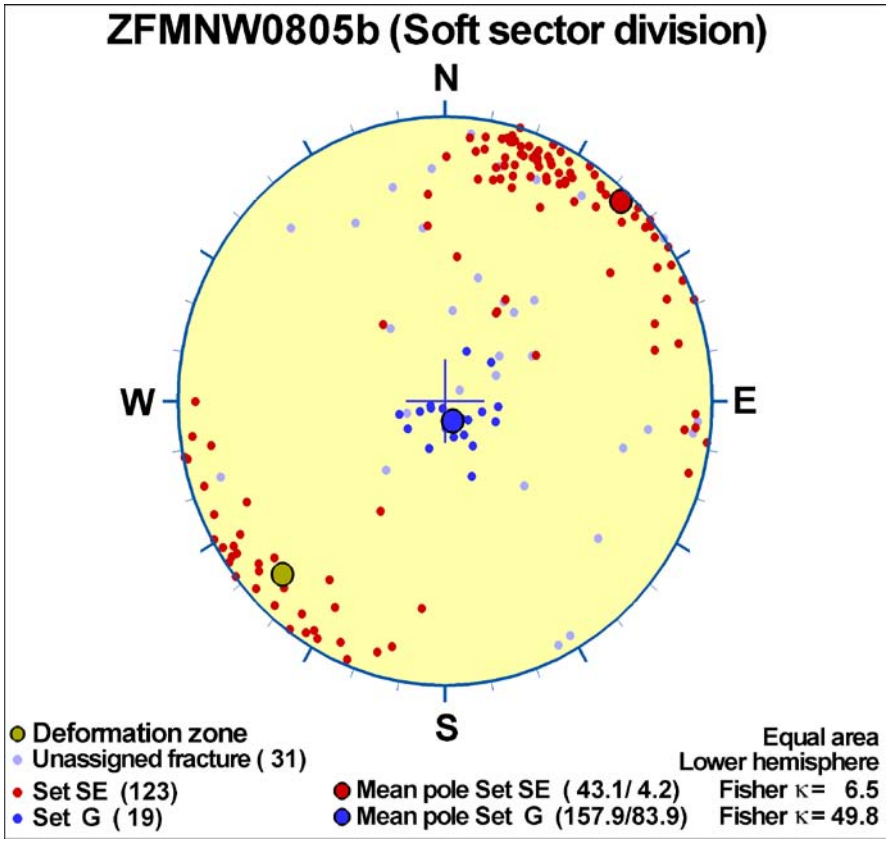

Fracture frequency: Open 13 m^{-1}, Sealed 57 m^{-1}

Fracture filling mineralogy:

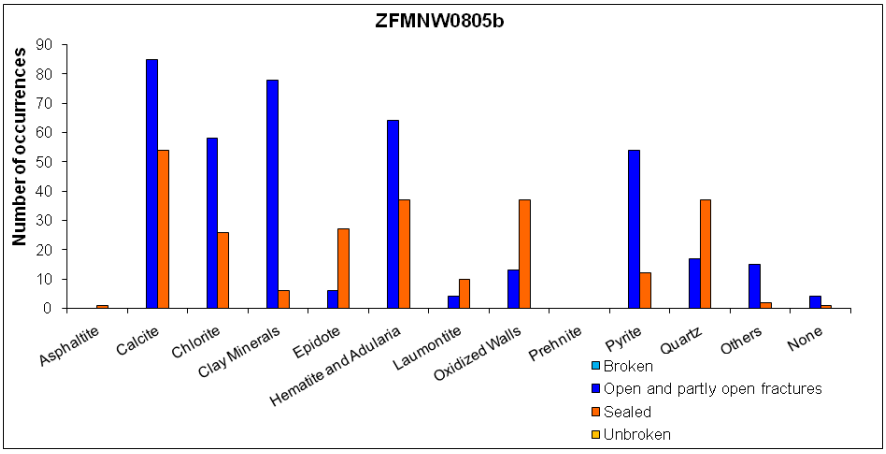

Deformation zone ZFMNW0805B

KFR101 DZ2 (97–116 m)

BOREHOLE AND TUNNEL INTERCEPT DETAILS

Borehole intersections for ZFMNW0805B				
BH	**Geometrical Intercept**		**Target intercept**	
	Sec_up BH length (m) [z (-m)]	**Sec_low BH length (m) [z (-m)]**	**Sec_up BH length (m) [z (-m)]**	**Sec_low BH length (m) [z (-m)]**
KFR7A	11.13 [132.68]	43.20 [133.79]	3.5	43.00

Comment: The target interval corresponds to the upper half of DZ1. The remainder of DZ1 is interpreted as intercepting ZFMNW0805A. There is also geometric intercept with ZFM871, which includes the uppermost part of DZ1. The brittle-ductile deformation style inferred to be associated with ZFMNW0805B is limited to 21–24 m length and it cannot be excluded that some of the brittle deformation outside this interval, at least in part, is related to ZFM871, although no target intercept has been defined. Such an alternative interpretation would reduce the zone thickness and hence limit the geometric intercepts with the SFR tunnels (BT and 1B).

Borehole intersections for ZFMNW0805B
DZ1 3.5–74.45 m: Increased frequency of unbroken fractures, sealed networks anB especially broken fractures. Nineteen crushes with the most extensive sections at 49.09–74.45 m. Brittle-ductile section characterised by fault breccias and cataclasite at 21–24 m and 64.83–71.29 m. Predominant fracture minerals are clay minerals, calcite and Fe-hydroxide/hematite. The registered α–angles of clay filled fractures are highly variable, ranging from 0 to 85°. Fractures filled with laumontite form swarms throughout the drill core, with the most extensive occurrence at 56.9–64.8 m length. Most of these fractures have gently dipping α–angles less than 25°, with a few ranging up to 55° towards the drill core length axis. Moderately to strongly foliated metagranite-granodiorite (101057), pegmatitic granite (101061), aplitic metagranite (101058), fine- to medium-grained granite (111058) and amphibolite (102017). Confidence level = 3. Low hydraulic conductivity $6 \cdot 10^{-9}$ m/s in the interval 3.5–19 m. Moderate hydraulic conductivity of $5 \cdot 10^{-7}$ m/s in the interval 20–47 m. High hydraulic conductivity of $3 \cdot 10^{-6}$ m/s in the interval 48–74.45 m.
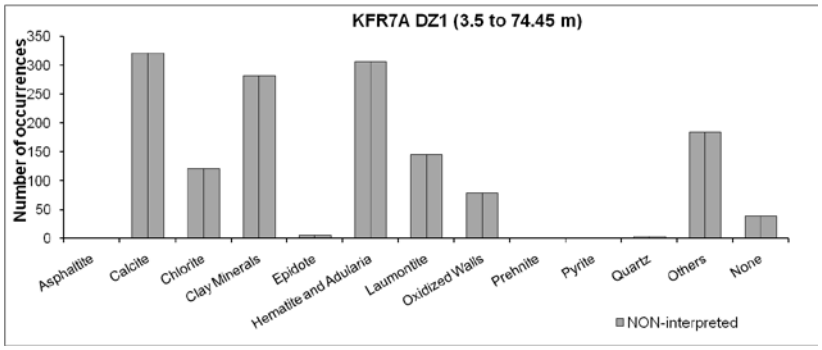
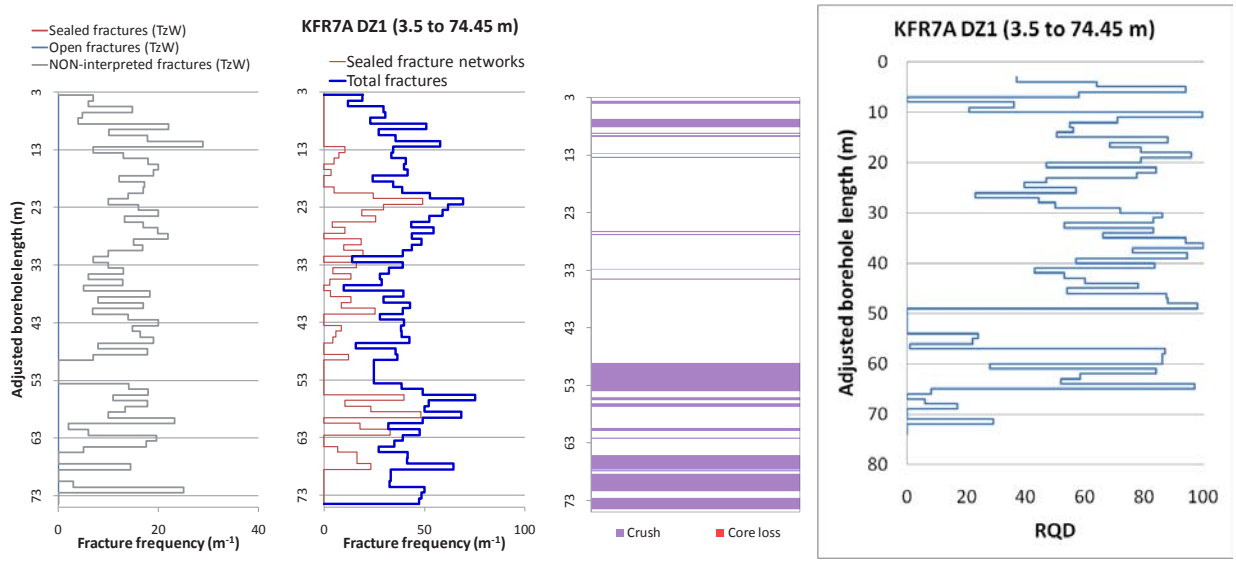

Borehole intersections for ZFMNW0805B				
BH	**Geometrical Intercept**		**Target intercept**	
	Sec_up BH length (m) [z (-m)]	**Sec_low BH length (m) [z (-m)]**	**Sec_up BH length (m) [z (-m)]**	**Sec_low BH length (m) [z (-m)]**
KFR08	2.8 [86.26]	32.35 [88.84]	3	19
DZ1 3–19 m: Increased frequency of broken fractures, sealed networks and especially unbroken fractures. Predominant fracture fillings are chlorite, calcite and laumontite. Registered α–angles are highly variable between 10 and 81°. Minor weak chloritization and faint oxidation occurs. Moderately to strongly foliated metagranite-				

Borehole intersections for ZFMNW0805B
granodiorite (101057) and pegmatitic granite (101061). Confidence level = 1. No hydrogeological investigation data from the upper 6 m of the borehole. Moderate hydraulic conductivity of 2 ·10^{-8} m/s in the section 6–19 m.

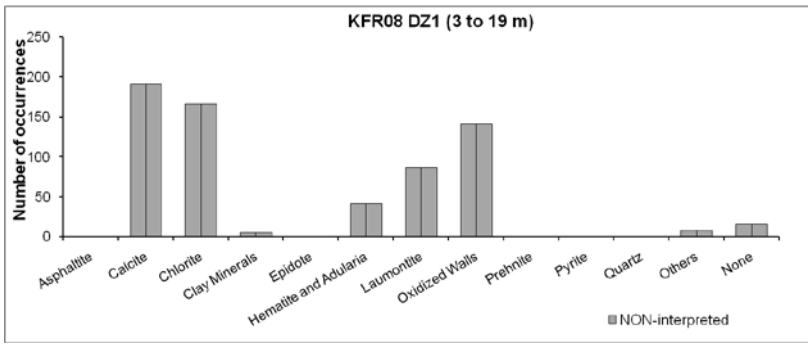

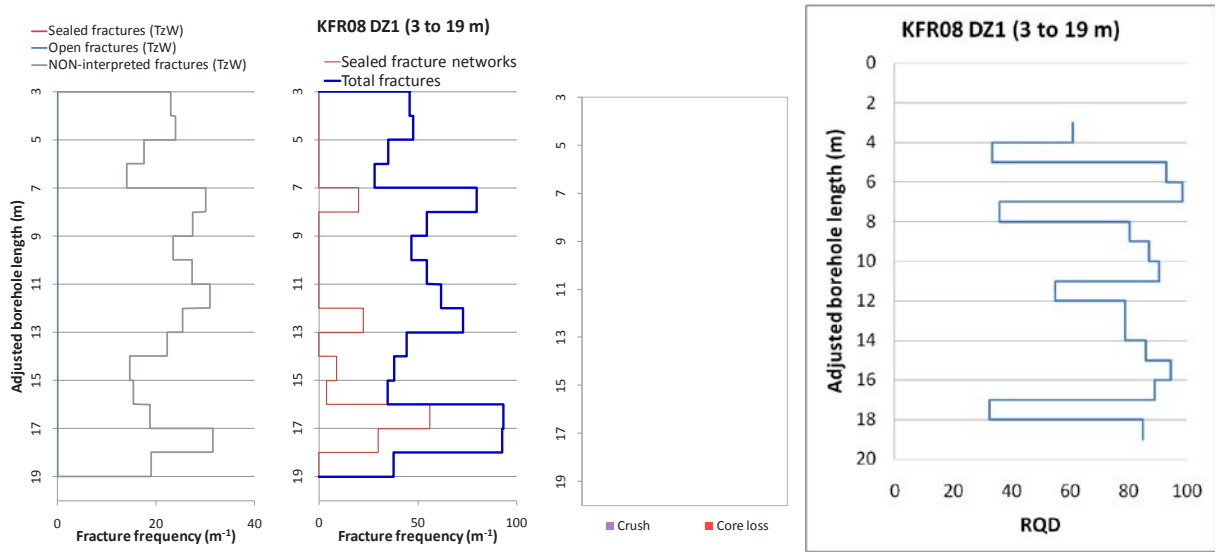

BH	Geometrical Intercept		Target intercept	
	Sec_up BH length (m) [z (-m)]	Sec_low BH length (m) [z (-m)]	Sec_up BH length (m) [z (-m)]	Sec_low BH length (m) [z (-m)]
KFR38	105.19 [84.31]	eoh [152.04]	153.60	181.65

DZ1 153.60–181.65 m: Increased frequency of broken and unbroken fractures. Several crushes, of which the most extensive occurs at 178.90–186.00 m. Generally α-angles > 45°. Locally weak oxidation. Amphibolites are consistently weakly chloritized. Predominant minerals in broken fractures are clay minerals, chlorite, hematite, calcite and laumontite and in unbroken fractures laumontite, calcite and hematite. Pegmatitic granite (101061), fine- to medium-grained metagranite-granodiorite (101057), aplitic metagranite (101058) and amphibolite (102017). Confidence level = 3.

High transmissivity of the interval 153–182 m (4·10^{-5} m^2/s). The dominating transmissivity is contained in the in the section 179–182 m.

Borehole intersections for ZFMNW0805B				
BH	Geometrical Intercept		Target intercept	
	Sec_up BH length (m) [z (-m)]	Sec_low BH length (m) [z (-m)]	Sec_up BH length (m) [z (-m)]	Sec_low BH length (m) [z (-m)]
KFR101	80.26 [63.23]	131.55 [104.67]	97	116

Comment: Radar reflector at 106 m BH length (316°/87°) has an orientation and position that fits well with ZFMNW0805B.

SHI DZ2 97–116 m: Increased frequency of broken and unbroken fractures and sealed networks. One crushed interval at 108.07–108.32 m. Occasional slickensides. Fractures aperture up to 2 mm. Generally weak to medium oxidation. Intervals exceeding a few centimeters of breccia at 108.03–108.51 and of mylonite at 108.51–108.71 and 109.21–109.32 m. Brittle-ductile shear zones at 102.86–102.97 and 107.30–109.64 m. Predominant minerals in sealed fractures are calcite, quartz, adularia, epidote, chlorite and pyrite and in open fractures are calcite, clay minerals, chlorite, pyrite, adularia, hematite and quartz. Significantly decreased resistivity along the entire section and one distinct caliper anomaly at c. 108.5 m. One distinct radar reflector oriented 313°/87° or 331°/30°, and a prominent radar wave attenuation in the interval c. 100–110 m. Moderately foliated metagranite-granodiorite (101057), fine- to medium-grained granite (111058), amphibolite (102017) and pegmatitic granite (101061). Confidence level = 3.

One single high-transmissive flow anomaly (about $8 \cdot 10^{-6}$ m^2/s) at c. 108.3 m corresponding to the caliper anomaly.

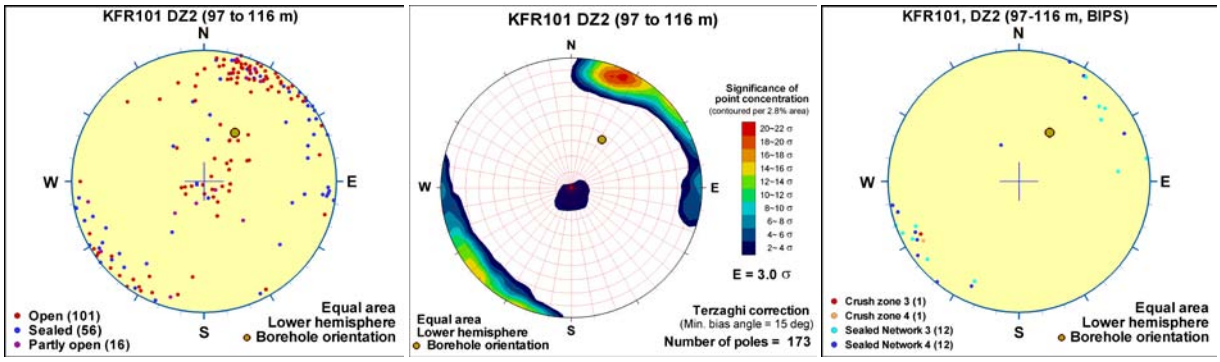

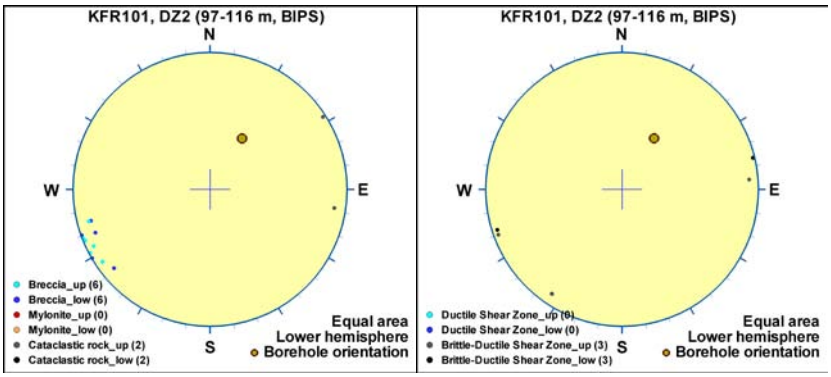

Borehole intersections for ZFMNW0805B

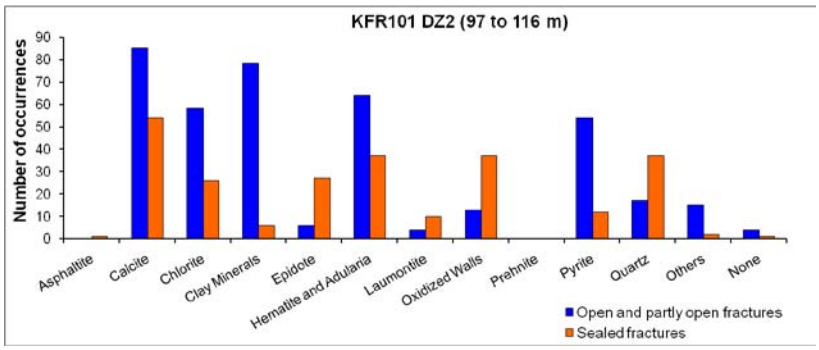

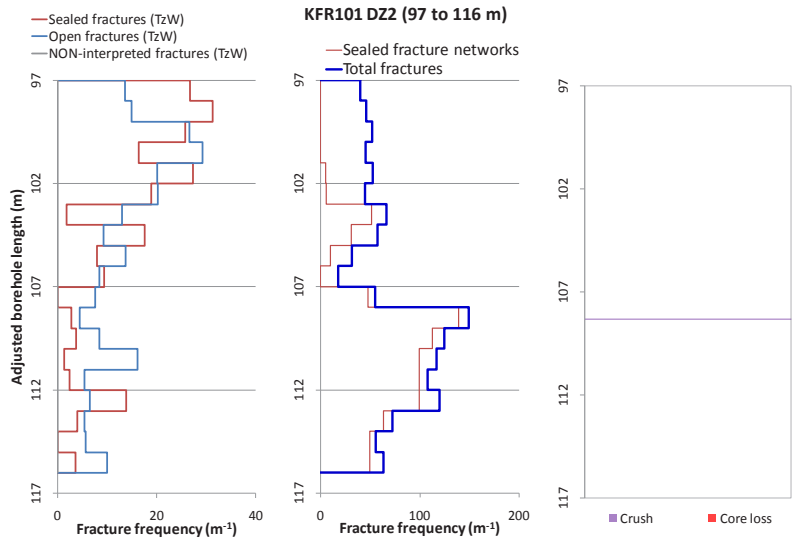

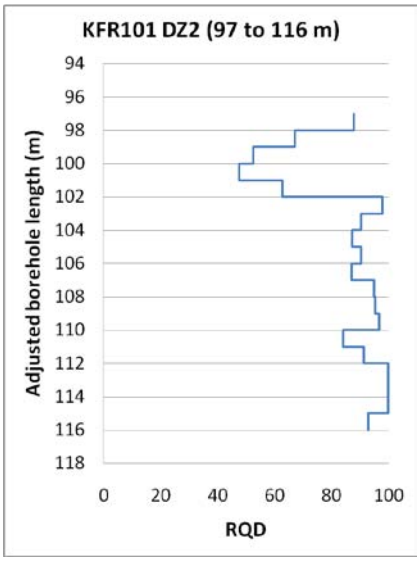

BH	Geometrical Intercept		Target intercept	
	Sec_up BH length (m) [z (-m)]	Sec_low BH length (m) [z (-m)]	Sec_up BH length (m) [z (-m)]	Sec_low BH length (m) [z (-m)]
KFR11	0.00 [86.50]	18.77 [89.76]	–	–
Comment: Judging from the photographs of the drill cores there is no obvious indication of a zone with the dignity of ZFMNW0805B along the geometric intercept. The only conspicuous feature is an approximately 2 dm long, intensely fractured interval with moderate oxidation/laumontization at 16 m length. No target intercept is defined.				
KFR24	0.00 [0.00]	40.81 [34.22]	–	–
Comment: No drill core is available for review.				
KFR25	0.00 [0.00]	62.04 [44.62]	–	–
Comment: No drill core is available for review.				

Borehole intersections for ZFMNW0805B				
BH	**Geometrical Intercept**		**Target intercept**	
	Sec_up BH length (m) [z (-m)]	**Sec_low BH length (m) [z (-m)]**	**Sec_up BH length (m) [z (-m)]**	**Sec_low BH length (m) [z (-m)]**
KFR11	0.00 [86.50]	18.77 [89.76]	–	–
Comment: Judging from the photographs of the drill cores there is no obvious indication of a zone with the dignity of ZFMNW0805B along the geometric intercept. The only conspicuous feature is an approximately 2 dm long, intensely fractured interval with moderate oxidation/laumontization at 16 m length. No target intercept is defined.				
KFR24	0.00 [0.00]	40.81 [34.22]	–	–
Comment: No drill core is available for review.				
KFR25	0.00 [0.00]	62.04 [44.62]	–	–
Comment: No drill core is available for review.				
KFR56	3.92 [82.83]	44.46 [65.06]	–	–
Comment: No drill core is available for review.				

Tunnel intersections for ZFMNW0805B				
BH	**Geometrical Intercept**		**Target intercept**	
	Sec_up BH length (m) [z (-m)]	**Sec_low BH length (m) [z (-m)]**	**Sec_up BH length (m) [z (-m)]**	**Sec_low BH length (m) [z (-m)]**
BT	1+178	1+193	1+182	1+185
Comment: Several vertical NNW-SSE striking fractures (approximately 160°/90°) that penetrate the entire tunnel perimeter at 6/182–6/185. Some of the fractures are marked as "damp" in the detailed drawing –11 of /Christiansson and Bolvede 1987/. This is taken as a target intercept for ZFMNW0805B. Note that the extent of the geometric intercept mainly is based on the target intercepts in KFR7A DZ1 and KFR08 DZ1, with confidence level = 1.				
1B	0+023	0+044	–	–
Comment: Generally a high frequency of vertical NW-SE striking fractures (approximately 130°/90°) from the connection with IST and onwards towards north. The fracture set is conspicuous in all parts included in detailed drawing –12 of /Christiansson and Bolvede 1987/ and it is not possible to define a specific target intercept. Note that the extent of the geometric intercept mainly is based on the target intercepts in KFR7A DZ1 and KFR08 DZ1, with confidence level = 1.				

Deformation zone ZFMWNW0001

Borehole and tunnel intersections (metres along borehole/tunnel)

HFM34: 37–192 m (DZ1 37–133 m, DZ2 180–184 m and DZ3 188–192 m)
HFM35: 24–52.5 m (DZ1 24–33 m and DZ2 47.2–52.5 m)
HFR105: 21.12–92 m (DZ1 21.12–31 m and 88–92 m)
KFM11A: 498–824 m (DZ1 245–824 m)
KFR01: 0–62.30 m (DZ1 0–62.30 m)
KFR61: 1.40–70.90 m (DZ1 1.40–70.90 m)
KFR62: 45.64–82.80 m (DZ1 45.64–82.80 m)
KFR64: 12.79–54.17 m (DZ1 12.79–54.17 m)
KFR65: 17.63–39.68 m (DZ1 17.63–39.68 m)
KFR66: 14.99–29.17 m (DZ1 14.99–29.17 m)
KFR67: 13.74–48.95 m (DZ1 13.74–48.95 m)
KFR71: 65.67–120.90 m (DZ1 65.67–69.50 m and 72.14–120.90 m)

DT: 0+212 to 0+295 (tDZ7 0+212, tDZ8 0+243, tDZ9 0+255, tDZ10 0+257, tDZ12 0+259, tDZ13 0+260, tDZ14 0+258–0+271, tDZ15 0+275, tDZ16 0+278–0+295 and tDZ17 0+291)
BT: 0+189 to 0+283 (tDZ7 0+189, tDZ8 0+220, tDZ9 0+228, tDZ10 0+229, tDZ11 0+231, tDZ12 0+234, tDZ13 0+238, tDZ14 0+238–0+249, tDZ15 0+248, tDZ16 0+267–0+283, tDZ17 0+268 and tDZ18 0+280)

Deformation style, alteration and geometry

Deformation style: Ductile origin followed by brittle reactivation. Intense brittle-ductile deformation, including cohesive breccias, cataclasites, brecciated cataclasites present in virtually all BH intercepts

Alteration: Red stained bedrock with fine-grained hematite dissemination. Locally muscovitization, argillization and chloritization. An interval of steatitisation (talc alteration) at 510–525 m in KFM11A DZ1

Strike/dip (span) right-hand-rule: 120 / 90 (±5 / ±10)

Trace length at ground surface: 30 km

Model thickness (span): 185 m (100−240 m)

Confidence in existence: High

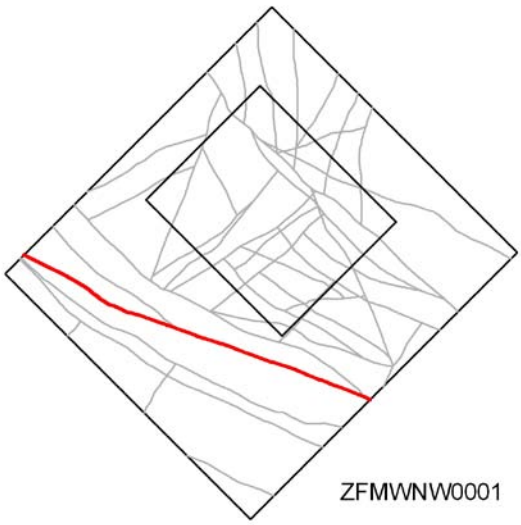

Modelling procedure*:* Zone ZFMWNW0001, referred to as the Singö zone in earlier SFR models, is a major regional deformation zone interpreted as having a total length of 30 km /Stephens et al. 2007/. The zone crosses the entire regional model volume. The interpretation is largely based on that presented in /Stephens et al. 2007/, itself based on earlier work by /Christianson 1986, Axelsson and Hansen 1997/.

The interpretation of zone ZFMWNW0001 has been re evaluated during version 1.0. The underlying magnetic lineament MFM0803G0 remains unchanged from the geometry presented in Forsmark stage 2.3 /Isaksson et al. 2007/. However, minor changes were made between the modelling phase during stage 2.2 /Stephens et al. 2007/ and the revision of lineaments in stage 2.3 /Isaksson et al. 2007/. Other input data have included the results of the tunnel mapping /Glamheden et al. 2007/. The main focus concerning tunnel mapping has been placed on the SFR tunnels since these lie in the area of interest for the current project. The SHI results from boreholes KFM11A, HFM34 and HFM35 also provided key input data with higher confidence being placed in the cored borehole KFM11A. The data from these boreholes were not available for use in model stage 2.2 /Stephens et al. 2007/ but the SHI results from these three boreholes were evaluated in /Stephens et al. 2008b/. Reference has also been made to this work, in particular the attempted subdivision of the very extensive DZ1 from KFM11A.

The northern boundary of the zone coincides with the earlier interpreted boundary of the zone in the tunnel (/Christiansson and Bolvede 1985/ and tunnel intersections section below) and provides a reasonable fit and correlation when extrapolated with the base of DZ1 in KFM11A. The southern boundary of the zone has been estimated based on an examination of details from KFM11A DZ1 and a subdivision of this PDZ. The subdivision and subsequent position of this boundary in the borehole (498 m BH length target intercept) is in agreement with a possible boundary identified by /Stephens et al. 2008b/. The tunnel data provide no clear evidence to establish a

distinction between the Singö zone and the immediately abutting zones, ZFMWNW3259, ZFMWNW0813 and ZFMNW0002. It should be noted that the current position for this boundary is some 30 m further south-west compared with that reported in /Christiansson and Bolvede 1985/. The older boreholes from the construction of SFR (KFR01, KFR61, KFR62, KFR64, KFR65, KFR66 and KFR67) along with the percussion drilled borehole HFM34 and their associated PDZs are interpreted as lying wholly within the ZFMWNW0001 modelled zone boundaries.

Forward modelling of magnetic data along profiles 24, 25 and 26 (see Appendix 6) suggests a vertical to steep dip to the south-west. Due to the uncertainty of the modelling result and likely local variations, a vertical dip, based on the tunnel and KFM11A data, has been retained in the model.

Fractures in the deformation zone

General characteristics

Fracture orientation:

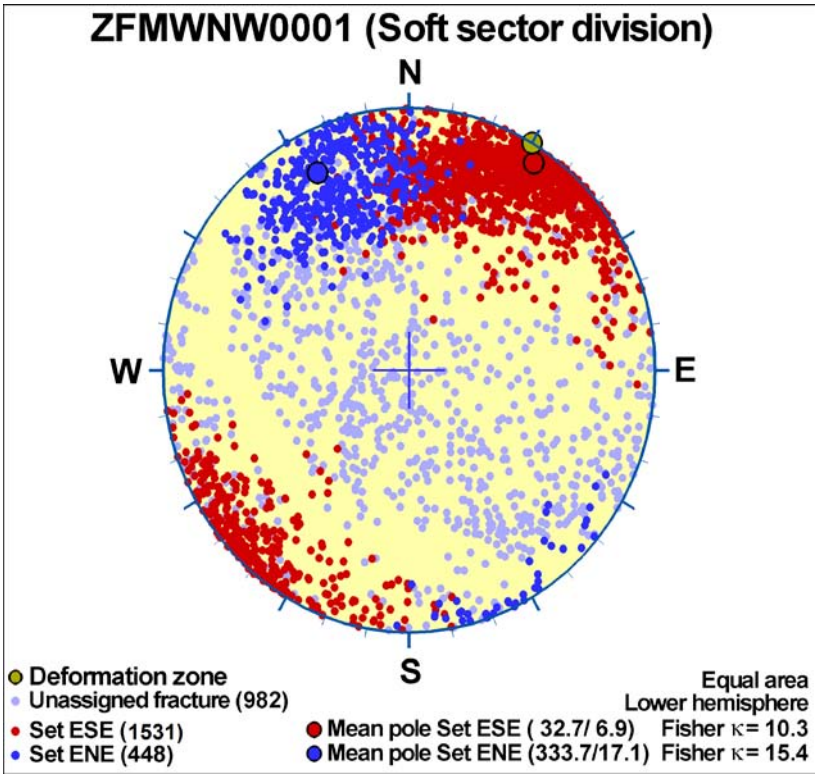

Fracture frequency: Open 10 m^{-1}, Sealed 42 m^{-1}

Fracture filling mineralogy:

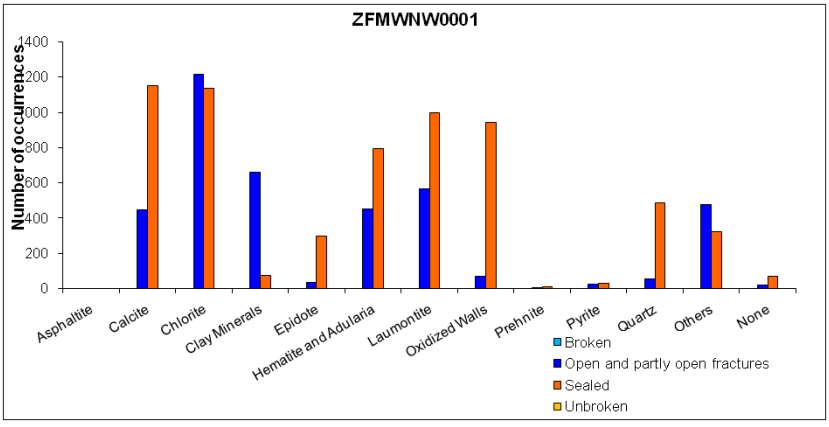

Deformation zone ZFMWNW0001	
	KFR01 DZ1 (fault core) 

BOREHOLE AND TUNNEL INTERCEPT DETAILS

Borehole intersections for ZFMWNW0001				
BH	**Geometrical Intercept**		**Target intercept**	
	Sec_up BH length (m) [z (-m)]	**Sec_low BH length (m) [z (-m)]**	**Sec_up BH length (m) [z (-m)]**	**Sec_low BH length (m) [z (-m)]**
HFM34	0.00 [2.45]	eoh [161.28]	37	192

Comment: The entire borehole lies within the modelled zone boundaries.

SHI DZ1 37–113 m: Increased frequency of sealed fractures in the upper half of the possible deformation zone, and low resistivity, low P-wave velocity, low magnetic susceptibility and several calliper anomalies in the lower half of the possible zone (82–133 m). Fractures that strike ESE and dip steeply to the SSW and fractures that are gently dipping dominate. The lower half of the possible zone contains three crush zones and several low radar amplitude anomalies. In the possible deformation zone, there are 23 identified radar reflectors with an intersection angle of 34–90°. Fracture apertures are generally less than 1 mm. Zone situated in metavolcanic rock and pegmatitic granite with subordinate amounts of amphibolite. Confidence level = 2.

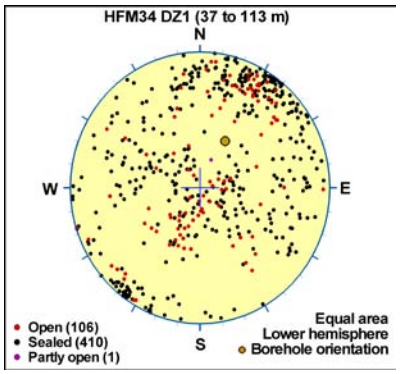

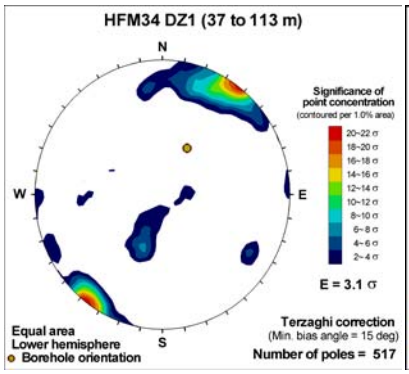

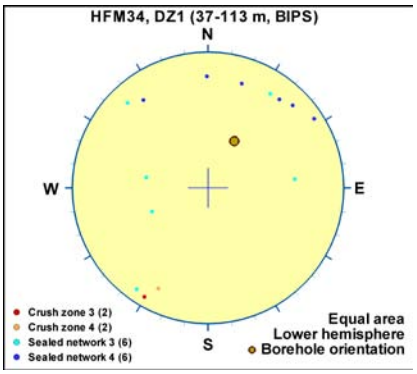

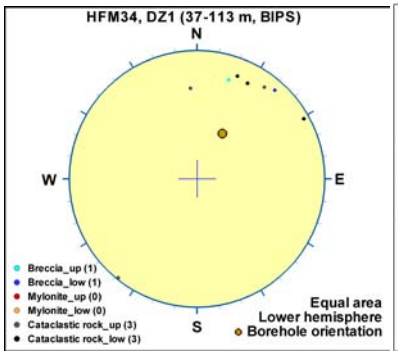

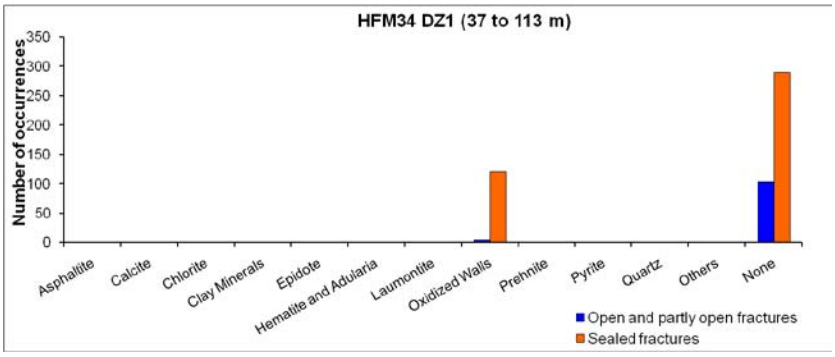

Borehole intersections for ZFMWNW0001

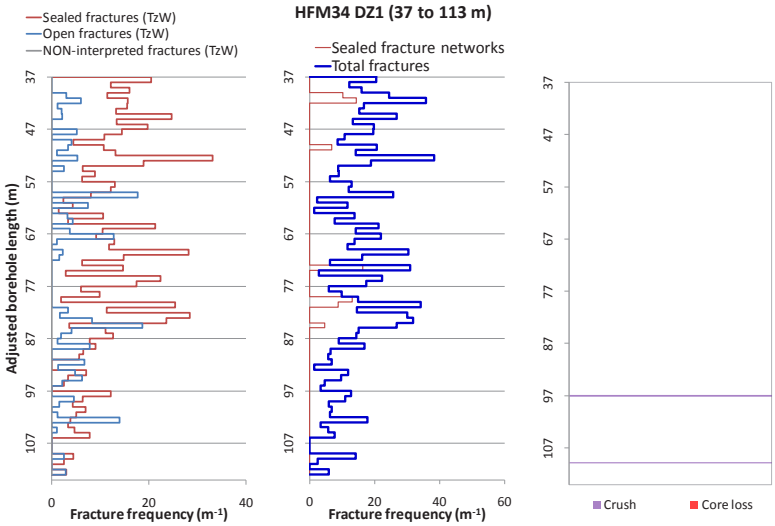

SHI DZ2 180–184 m: Low resistivity, low P-wave velocity, low magnetic susceptibility and several calliper anomalies. One identified radar reflector with an intersection angle of 53°. Due to **poor BIPS image**, mapping of fractures and rock types has not been carried out. Judgement of possible deformation zone has been based only on geophysical data. Confidence level = 1.

SHI DZ3 188–192 m: Low resistivity, low P-wave velocity, low magnetic susceptibility and several calliper anomalies. One identified radar reflector with an intersection angle of 57°. Due to **poor BIPS image**, mapping of fractures and rock types has not been carried out. Judgement of possible deformation zone has been based only on geophysical data. Confidence level = 1.

BH	Geometrical Intercept		Target intercept	
	Sec_up BH length (m) [z (-m)]	Sec_low BH length (m) [z (-m)]	Sec_up BH length (m) [z (-m)]	Sec_low BH length (m) [z (-m)]
HFM35	0.00 [1.90]	49.27 [38.79]	24	52.5

DZ1 24–33 m: Increased frequency of open fractures and one crush zone in the upper part of the possible zone. Fractures that strike SE and dip steeply to the SW and fractures that are gently dipping dominate. Fracture apertures are generally less than 1 mm, with a few ranging up to 3 mm. Low resistivity, low P-wave velocity, low magnetic susceptibility and several caliper anomalies. Four identified radar reflectors with an intersection angle of 45–74°. Zone situated in metavolcanic rock and subordinate pegmatitic granite. Confidence level = 3.

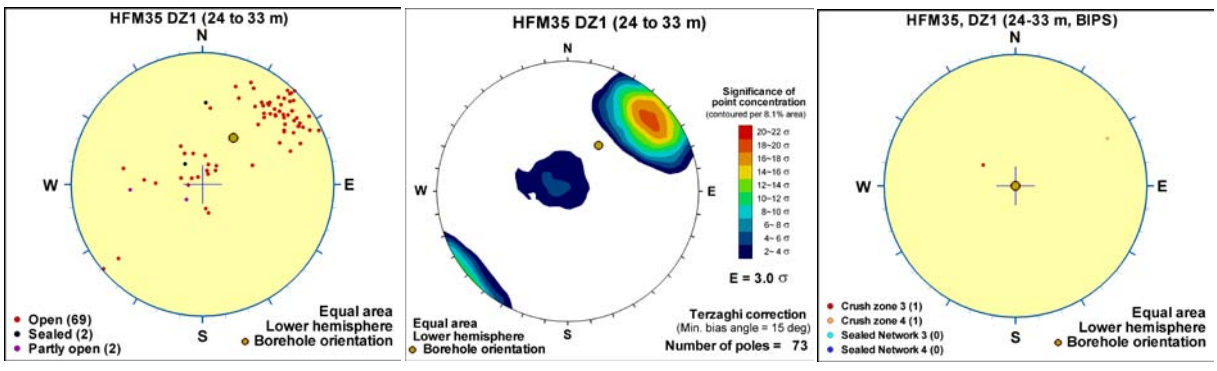

Borehole intersections for ZFMWNW0001

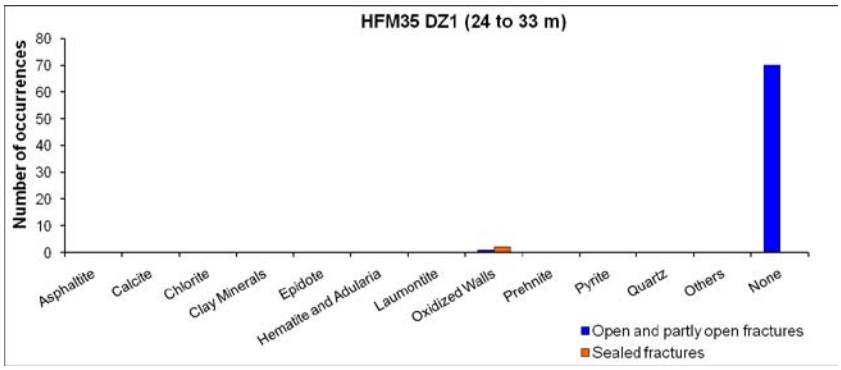

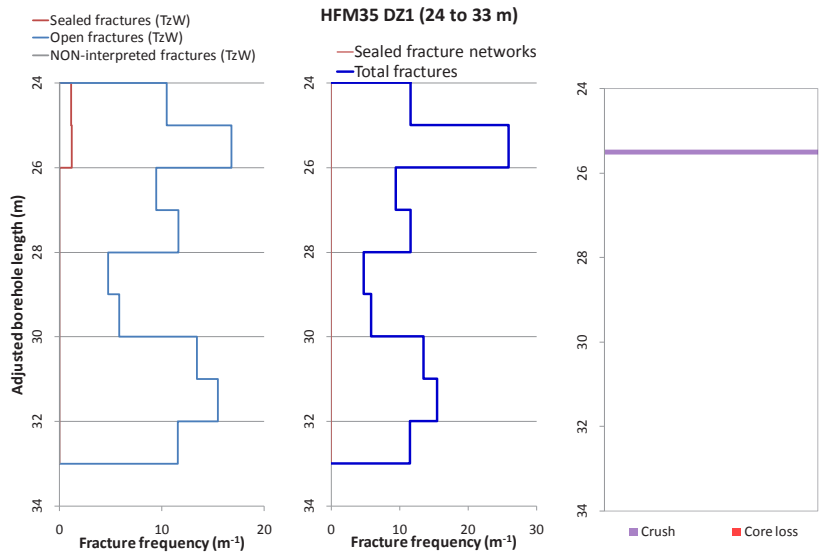

DZ2 47.2–52.5 m: Open fractures strike SSE and dip variably to the WSW. Two crush zones. Apertures are generally less than 1 mm. Low resistivity, low P-wave velocity, low magnetic susceptibility and several caliper anomalies. Two identified radar reflector with an intersection angle of 50° and 72°. Zone situated in metavolcanic rock and subordinate pegmatitic granite. Confidence level = 3.

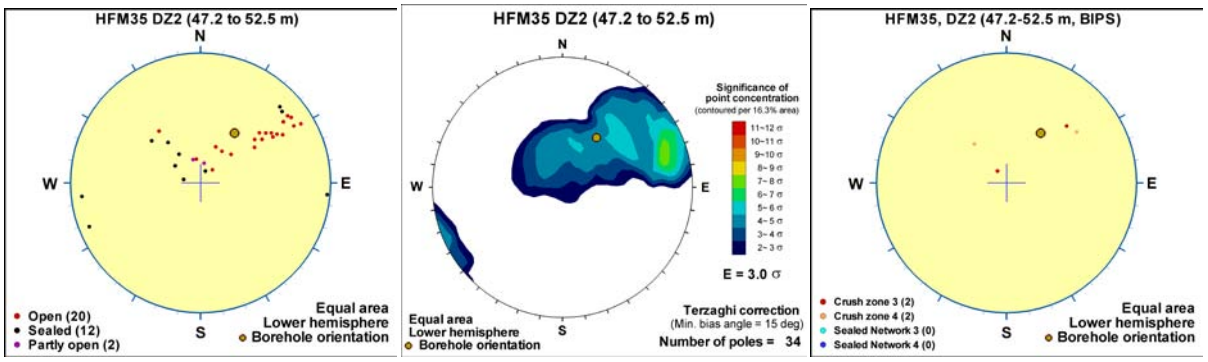

Borehole intersections for ZFMWNW0001
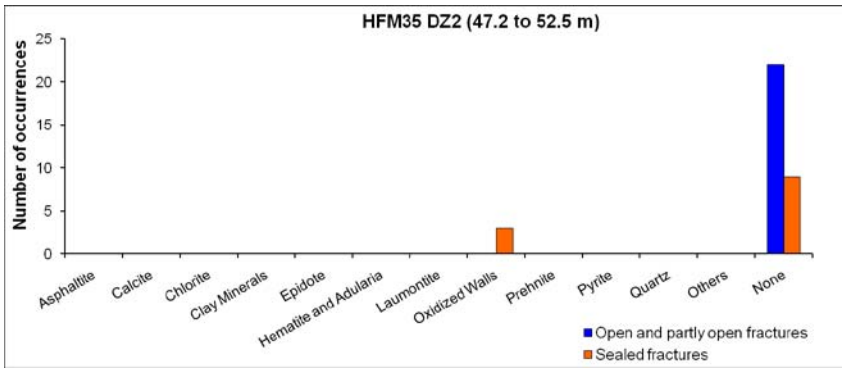
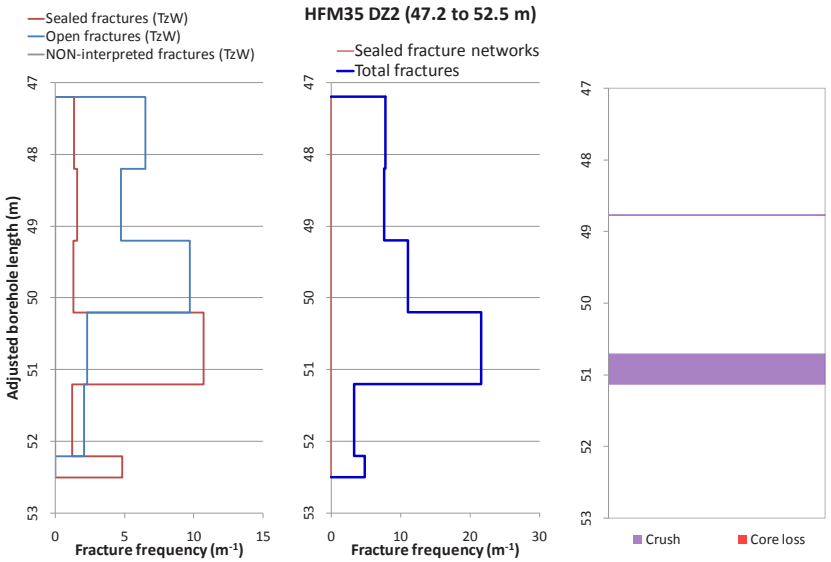

Borehole intersections for ZFMWNW0001				
BH	**Geometrical Intercept**		**Target intercept**	
	Sec_up BH length (m) [z (-m)]	**Sec_low BH length (m) [z (-m)]**	**Sec_up BH length (m) [z (-m)]**	**Sec_low BH length (m) [z (-m)]**
HFR105	0.00 [3.27]	83.64 [71.62]	21.12	92
DZ1 21.12–31 m: Increased frequency of open fractures. Three crushed intervals at 22.16–22.31, 27.48–27.53 and 29.45–29.95 m. Fracture aperture up to 5 mm, with one aperture 20 mm. Weak to medium oxidation throughout the interval. Significantly decreased bulk resistivity and major caliper anomalies along the entire section. Metagranite-granodiorite (101057), pegmatitic granite (101061) and amphibolite (102017). Confidence level = 1. No flow anomaly in this interval. Also a complimentary pumping test in the section above 38 m showed that the transmissivity of this interval is low.				

Borehole intersections for ZFMWNW0001

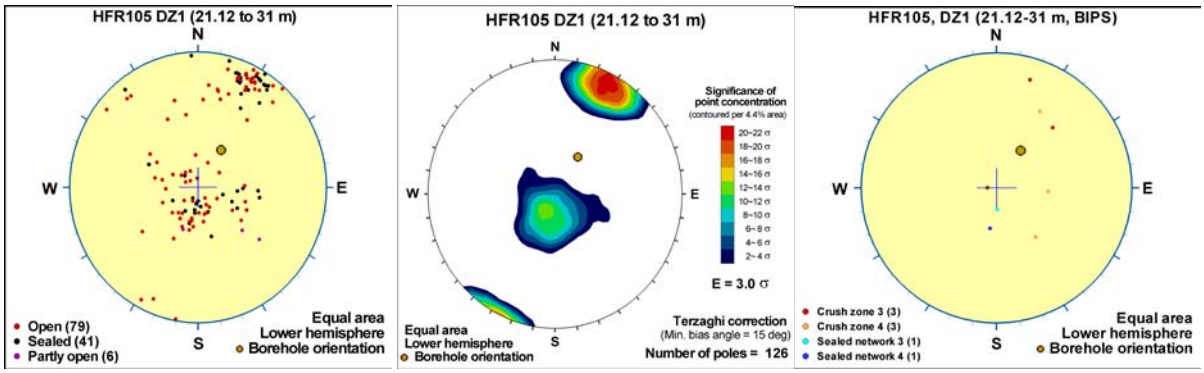

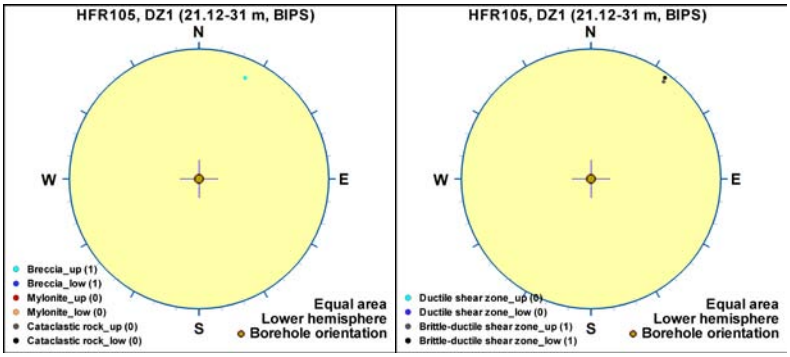

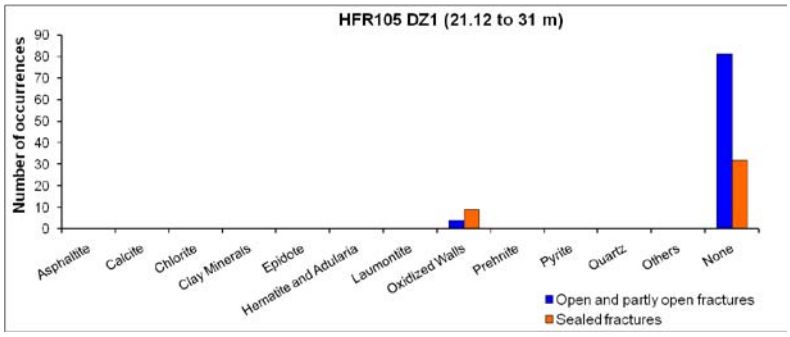

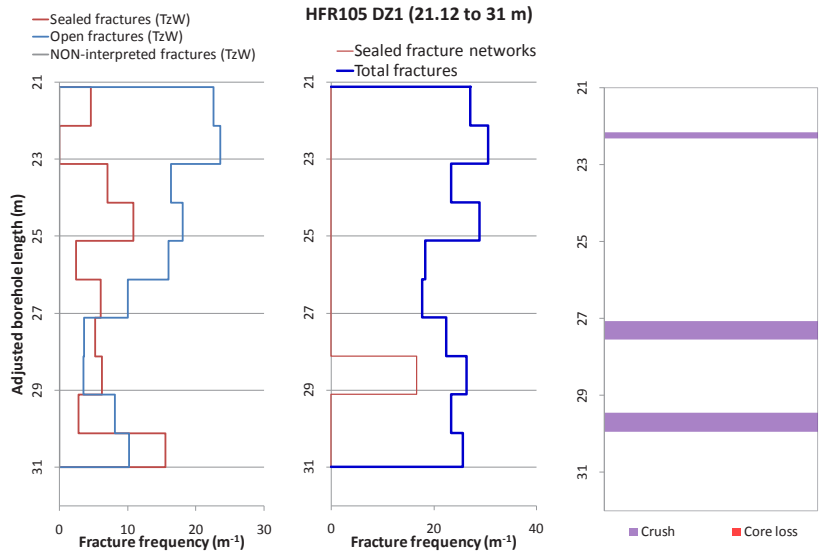

Borehole intersections for ZFMWNW0001

DZ2 88–92 m: Increased frequency of open and sealed fractures and sealed networks. Two crushed intervals at 89.73–89.75 and 91.37–92.32 m. Fracture aperture 0.7 mm or less. Generally medium to strong oxidation. Minor brecciated interval at 89.75–89.90 m. The geophysical logging data show significantly decreased bulk resistivity and major caliper anomalies along the entire section. Metagranite-granodiorite (101057) and pegmatitic granite (101061). Confidence level = 3.

One flow anomaly at 89.1–89.5 m with a quite high transmissivity (about $6 \cdot 10^{-6}$ m^2/s). This is one of three observed flow anomalies in the borehole.

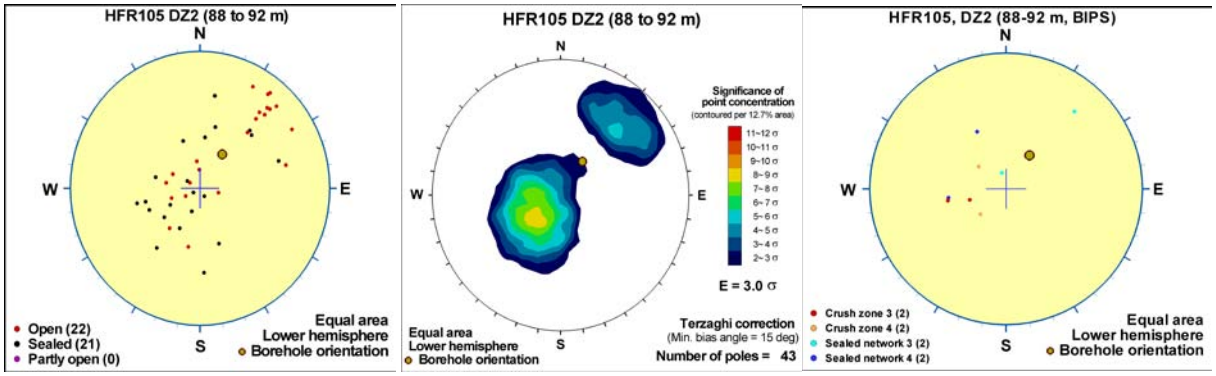

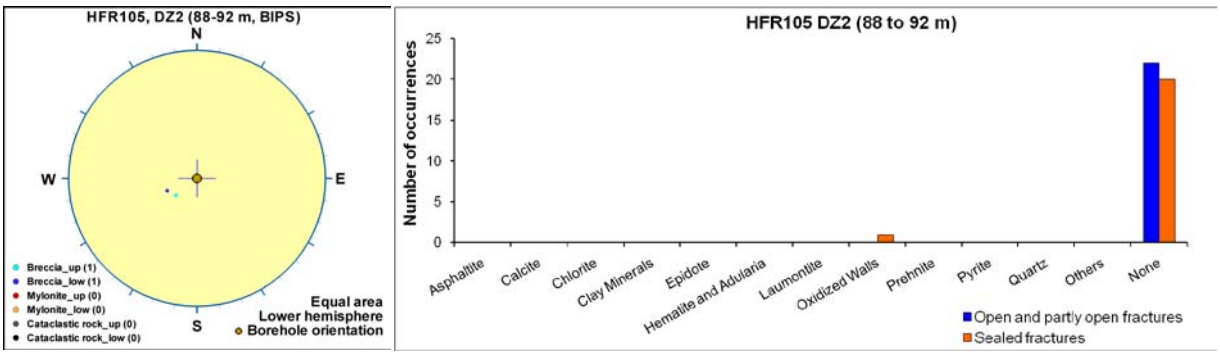

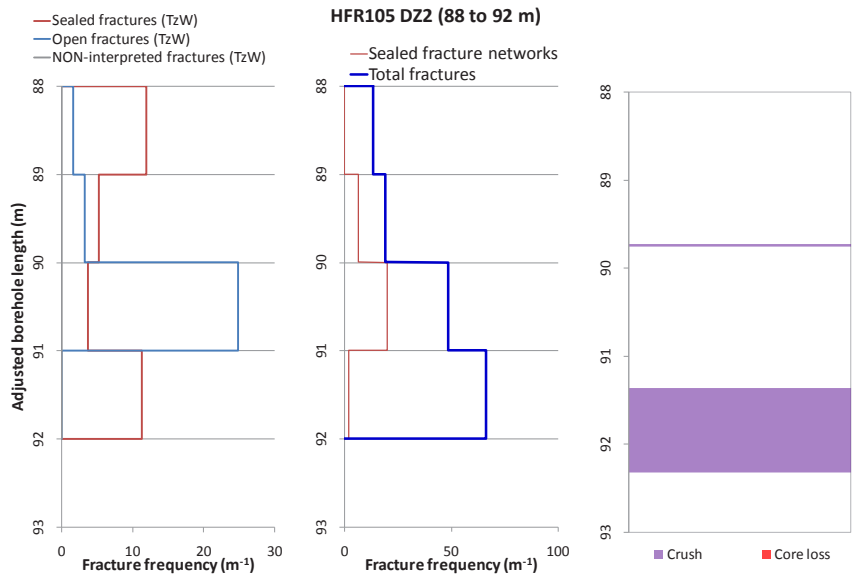

Borehole intersections for ZFMWNW0001				
BH	**Geometrical Intercept**		**Target intercept**	
	Sec_up BH length (m) [z (-m)]	**Sec_low BH length (m) [z (-m)]**	**Sec_up BH length (m) [z (-m)]**	**Sec_low BH length (m) [z (-m)]**
KFM11A	492.66 [424.66]	831.43 [697.77]	498	824

Comment:

SHI DZ1 245–824 m: *The description as follows has been modified from /Carlsten et al. 2007/ to match the target intercept (i.e. details that concern the SHI interval outside the target intercept has been omitted).*

Generally increased frequency of sealed fractures, sealed fracture networks and open fractures, and several intervals with one or more crush zones (505–522 m, 580–615 m, 649–661 m, 686–696 m and 774–801 m). Fractures that strike ESE and dip moderately to steeply to the SSW dominate. Gently dipping fractures are also present. Fracture apertures are generally less than 1 mm, with a few ranging up to 10 mm. Faint to medium oxidation is present along short intervals throughout the possible zone. Predominant fracture minerals are chlorite, calcite, laumontite, adularia, quartz, clay minerals and epidote. Four intervals with low radar amplitude, low bulk resistivity with low resistivity anomalies, low magnetic susceptibility and scattered low P-wave velocity anomalies can be recognized at 498–630 m, 653–664 m, 676–723 m and 787–824 m. The interval 498–630 m is characterised by very low bulk resistivity, several caliper anomalies and generally low P-wave velocity. Twenty-nine radar reflectors of which five are oriented (011/16, 086/72, 168/77, 188/49 and 204/21) and a more distinct low radar amplitude also characterise this interval. Furthermore, muscovite alteration of faint to medium intensity more or less affects the whole interval, while steatitisation (talc alteration) occurs in the interval 510–525 m. Between 515 and 575 m, the frequency of particularly sealed fractures decreases relative to the remaining part of the possible zone. Furthermore, calcite, adularia and epidote are generally absent in this interval, while laumontite is prominent. From c. 700 m and downwards, the bulk resistivity diminishes significantly without a relationship to other geophysical anomalies. The possible zone occurs in felsic to intermediate metavolcanic rock, aplitic metagranite and fine- to medium-grained granite with subordinate amphibolite, pegmatitic granite, medium-grained metagranite-granodiorite and medium-grained metagranodiorite. The base of the possible zone corresponds to the contact between aplitic metagranite (RU6b) and fine- to medium-grained metagranitoid (RU9). Confidence level = 3.

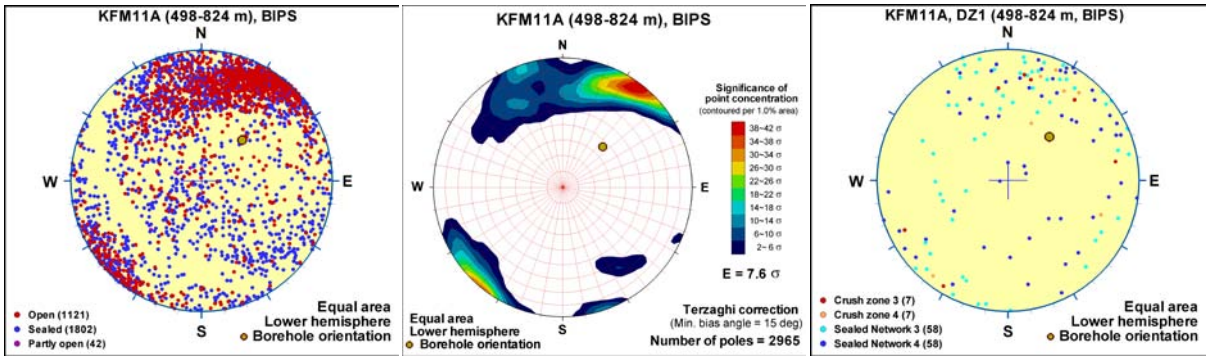

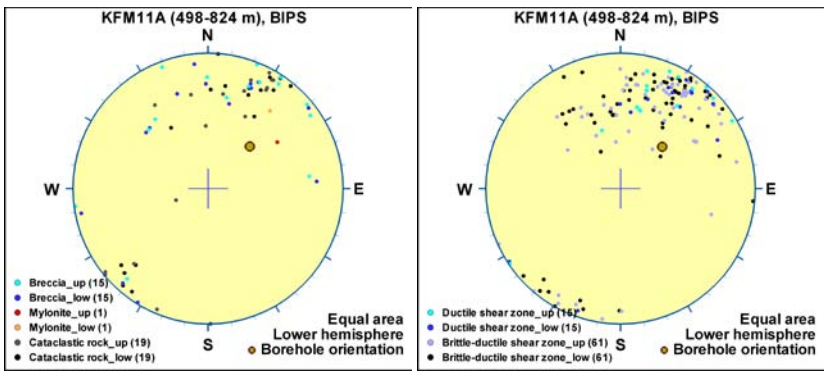

Borehole intersections for ZFMWNW0001

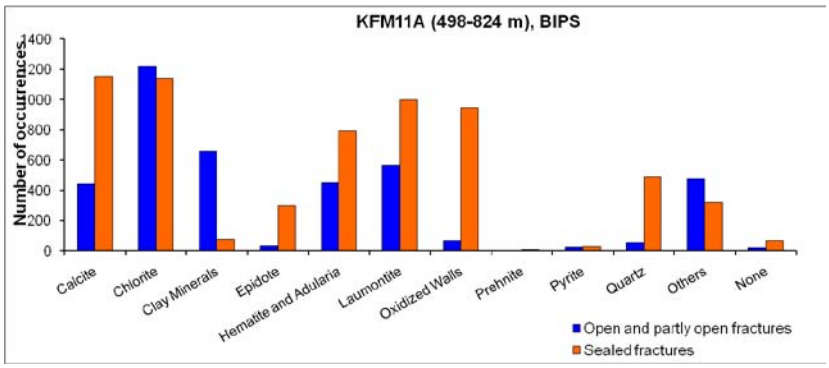

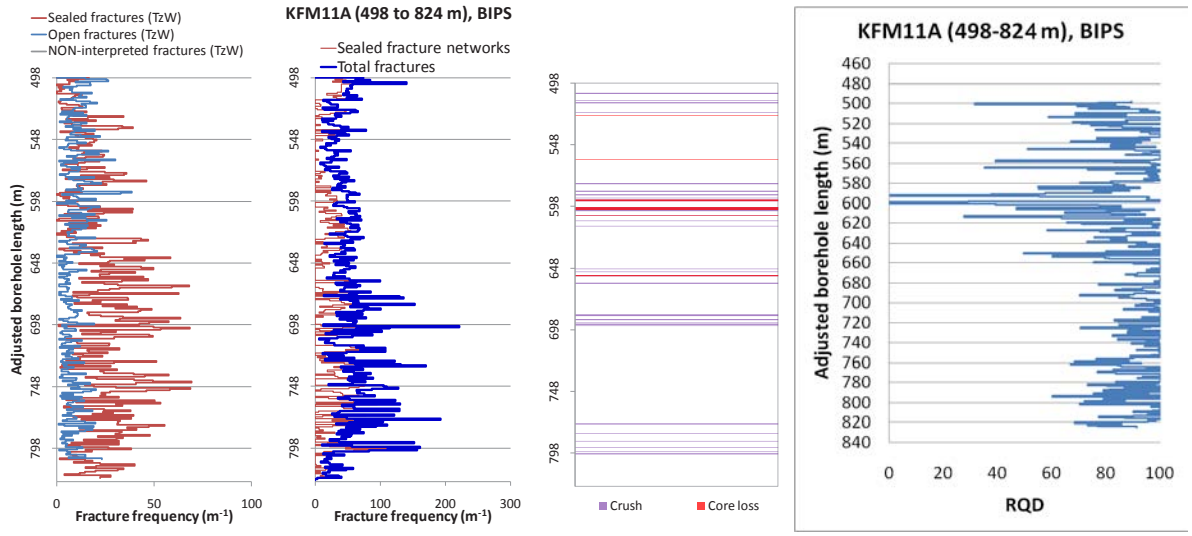

BH	Geometrical Intercept		Target intercept	
	Sec_up BH length (m) [z (-m)]	Sec_low BH length (m) [z (-m)]	Sec_up BH length (m) [z (-m)]	Sec_low BH length (m) [z (-m)]
KFR01	0.00 [47.98]	eoh [101.93]	0.00	62.30

Comment: The entire borehole lies within the modelled zone boundaries.

SHI DZ1 0–62.30 m: High frequency of broken fractures, with consistently more than 10 broken fractures per metre; locally considerably more, especially in the lowermost 18 m, which consists of pegmatitic granite (101061). α-angles in the pegmatitic granite (101061) are generally high and in the strongly foliated felsic to intermediate volcanic rock (103076) generally parallel with the foliation. In the interval 18.25–29.40 m there is brittle-ductile deformation and intense foliation, locally cataclasite in the pegmatitic granite (101061). Several crushes, especially between 49 m and the end of the borehole. Muscovitization and faint to weak argillization of the felsic to intermediate metavolcanic rock (103076). Predominant minerals in broken fractures are calcite, clay minerals and locally chlorite; in the pegmatitic granite (101061) mainly calcite. The SPR log is generally decreased along the entire borehole (200 ohm relative to the 'normal' background of 1,000 ohm), which indicates a high frequency of open fractures. Felsic to intermediate metavolcanic rock (103076) and pegmatitic granite (101061). Confidence level = 3.

No hydraulic test data from the section 0–11.0 m. The transmissivity of the section 11.0–43.5 m is low ($4 \cdot 10^{-8}$ m^2/s). Increased transmissivity ($1 \cdot 10^{-6}$ m^2/s) of the section 44.5–62.3 m.

Borehole intersections for ZFMWNW0001				
BH	**Geometrical Intercept**		**Target intercept**	
	Sec_up BH length (m) [z (-m)]	**Sec_low BH length (m) [z (-m)]**	**Sec_up BH length (m) [z (-m)]**	**Sec_low BH length (m) [z (-m)]**
KFR61	0.00 [1.40]	eoh [47.85]	1.40	70.90
Comment: The entire borehole lies within the modelled zone boundaries.				
SHI DZ1 1.40–70.90 m: Generally 10–15 broken fractures/m. Varying α-angles but generally >45°. A considerable proportion of the fractures are oriented parallel with the tectonic foliation. More highly fractured with several crushes, cataclasite and brecciation in the approximate section between 50 and 65 m. Very local argillization and the amphibolite is affected by chloritisation. Predominant minerals in broken fractures are chlorite, calcite, laumontite and clay minerals. In the section 50–60 m clay minerals and asphaltite dominate the fracture mineralogy. Cataclasite (108003), high strained pegmatitic granite (101061), recrystallized metagranite-granodiorite (101057) and amphibolite (102017). Confidence level = 3. No hydraulic test data from this borehole.				
KFR62	0.00 [0.60]	eoh [57.95]	45.64	82.80
Comment: The entire borehole lies within the modelled zone boundaries.				
DZ1 45.64–82.80 m: Increased frequency of unbroken and particularly broken fractures, with 10–20 broken fractures/m. Several crushes in the section 51.90–77.00 m. Generally high α-angles with a considerable amount parallel with the tectonic foliation. Locally brittle-ductile deformation. Cataclasite and locally breccia between 53.00 and c. 73 m. Minor occurrences of faint oxidation and moderate to strong argillization. Predominant in broken fractures are clay minerals, chlorite, calcite and locally asphaltite. Strongly foliated pegmatitic granite (101061), cataclasite (108003), strongly foliated metagranite-granodiorite (101057) and amphibolite (102017). Confidence level = 3. No hydraulic test data from this borehole.				
KFR64	0.00 [0.03]	eoh [46.61]	12.79	54.17
Comment: The entire borehole lies within the modelled zone boundaries.				
SHI DZ1 12.79–54.17 m: Highly fractured, locally with > 20 broken fractures/m. Several crushed sections. α-angles generally > 45° and parallel with the tectonic foliation. Unbroken fractures with aperture occur locally. Strong brittle-ductile deformation throughout the borehole. Brecciated cataclasite. Locally strong argillization and in the lowermost 10 m also muscovitization and chloritization. Predominant minerals in broken fractures are clay minerals, chlorite and more subordinate laumontite, calcite and asphaltite. Pegmatitic granite (101061), cataclasite (108003), amphibolite (102017), strongly foliated metagranite-granodiorite (101057) and possibly felsic to intermediate metavolcanic rock (103076). Confidence level = 3. No hydraulic test data from the section 12.79–17.29 m. The transmissivities of the sections 17.29–21.29 m and 41.29–53.29 are low (below detection limit). Increased transmissivities (>$1 \cdot 10^{-6}$ m^2/s) of the sections 25.29–27.29 m, 29.29–33.29 m, and 35.29–41.29 m, especially of the section 35.29–37.29 m ($1 \cdot 10^{-5}$ m^2/s).				

Borehole intersections for ZFMWNW0001				
BH	**Geometrical Intercept**		**Target intercept**	
	Sec_up BH length (m) [z (-m)]	**Sec_low BH length (m) [z (-m)]**	**Sec_up BH length (m) [z (-m)]**	**Sec_low BH length (m) [z (-m)]**
KFR65	0.00 [0.00]	eoh [39.68]	17.63	39.68
Comment: The entire borehole lies within the modelled zone boundaries.				
SHI DZ1 17.63–39.68 m: Increased frequency of unbroken and broken fractures. Highly variable α-angles. Note that the tectonic foliation is sub-parallel with the borehole direction. Locally faint oxidation. Predominant minerals in broken and unbroken fractures are laumontite and calcite. Recrystallised metagranite-granodiorite (101057). Confidence level = 2. The transmissivities of the sections 16.13–24.13 m, 28.13–36.13 m, and 38.13–40.13 are low (below detection limit). Increased transmissivities (>$1 \cdot 10^{-6}$ m^2/s) of the sections 24.13–28.23 m and 36.13–38.13 m, especially of the section 26.13–28.13 m ($1 \cdot 10^{-5}$ m^2/s).				
KFR66	0.00 [0.00]	eoh [29.17]	14.99	29.17
Comment: The entire borehole lies within the modelled zone boundaries.				
SHI DZ1 14.99–29.17 m: Increased frequency of broken fractures. Crushes predominate down to 6.08 m with several minor crushes below that drill core length. Generally high, but variable α-angles. Virtually the entire interval consists of brecciated cataclasite. Chloritization of amphibolites and locally some argillization of granitic material. Generally faint to moderate oxidation and at 16.80–21.50 m argillization, locally of strong intensity. Predominant minerals in broken fractures are clay minerals, calcite, chlorite and locally asphaltite. Cataclasite (108003) in the uppermost metre with a pegmatitic precursor and in the lowermost meter of amphibolitic composition. Confidence level = 3. No hydraulic test data from the sections 14.99–18.09 m and 29.09–29.17 m. Transmissivity below the measurement limit in the section 28.09–29.09 m. High transmissivity of the rest of the interval ($4 \cdot 10^{-5}$ m^2/s), with the transmissivity concentrated to the section 18.09–22.09 m.				
KFR67	0.00 [0.00]	eoh [44.36]	13.74	48.95
Comment: The entire borehole lies within the modelled zone boundaries.				
SHI DZ1 13.74–48.95 m: High frequency of broken fractures with > 10 broken fractures/m, locally up to 30 fractures/m. Fracture orientations generally parallel with the tectonic foliation with α-angles at 45–50°. Several minor crushes. Locally faint oxidation and amphibolites affected by weak to moderate chloritization. Strong ductile strain throughout the drill core. Predominant minerals in broken fractures are chlorite, clay minerals and calcite. Pegmatitic granite (101061), amphibolite (102017) and strongly foliated metagranite-granodiorite (101057). Confidence level = 3. No hydraulic test data from the section 13.74–17.54 m. The transmissivities of the sections 19.64–21.64 m, 23.54–29.54 m, and 37.54–39.54 m are low (below detection limit). Increased transmissivities (>$1 \cdot 10^{-6}$ m^2/s) of the rest of DZ1, with the exception of 29.54–31.54 m where the transmissivity is lower ($4 \cdot 10^{-7}$ m^2/s).				

Borehole intersections for ZFMWNW0001				
BH	**Geometrical Intercept**		**Target intercept**	
	Sec_up BH length (m) [z (-m)]	**Sec_low BH length (m) [z (-m)]**	**Sec_up BH length (m) [z (-m)]**	**Sec_low BH length (m) [z (-m)]**
KFR71	0.00 [33.30]	eoh [29.08]	65.67	120.90
DZ1 65.67–69.50 m: Increased frequency of unbroken fractures. Generally brittle-ductile deformation and locally minor crushes. α-angles generally parallel with the foliation (i.e. > 50°). Moderate chloritization of amphibolites and weak to moderate oxidation of pegmatitic granites. Predominant minerals in broken fractures are clay minerals, calcite, chlorite and laumontite and in unbroken fractures epidote. Pegmatitic granite (101061), metagranite-granodiorite (101057), and amphibolite (102017). Confidence level = 3. Relatively high transmissivity of the interval 60–70 m ($3 \cdot 10^{-6}$ m^2/s).				
DZ2 72.14–120.90 m: Increased frequency of broken and locally unbroken fractures, with fracture frequencies exceeding 15 and locally 30 fractures/m. Consistently strong brittle-ductile deformation and extensive intervals of cataclasite. Several crushed sections of which the most extensive exceeds one metre. The majority of the fractures are parallel with the foliation with α-angles > 45°. Predominant fracture minerals are clay minerals, chlorite and calcite. Locally, occurrences of asphaltite. Amphibolites are generally chloritized. Muscovitization from 109 m to the end of the interval. Local argillization. Fine- to medium-grained metagranite-granodiorite (101057), cataclasite (108003), amphibolite (102017) and pegmatitic granite (101061). Confidence level = 3. Very high transmissivity of the interval 70–120.90 m ($2 \cdot 10^{-4}$ m^2/s). The absolutely dominating transmissivity is contained in the in the section 80–120.93 m.				

Tunnel intersections for ZFMWNW0001				
Tunnel	**Geometrical Intercept**		**Target intercept**	
	Start ch.(m)	**End ch. (m)**	**Start ch.(m)**	**End ch. (m)**
DT	0+155	0+362	0+212	0+295
Comment: Target intercept defined by tDZ7 0+212, tDZ8 0+243, tDZ9 0+255, tDZ10 0+257, tDZ12 0+259, tDZ13 0+260, tDZ14 0+258–0+271, tDZ15 0+275, tDZ16 0+278–0+295 and tDZ17 0+291 in Appendix 2.				
BT	0+140	0+345	0+189	0+283
Comment: Target intercept defined by tDZ7 0+189, tDZ8 0+220, tDZ9 0+228, tDZ10 0+229, tDZ11 0+231, tDZ12 0+234, tDZ13 0+238, tDZ14 0+238–0+249, tDZ15 0+248, tDZ16 0+267–0+283, tDZ17 0+268 and tDZ18 0+280 in Appendix 2.				

Tunnel intersections for ZFMWNW0001

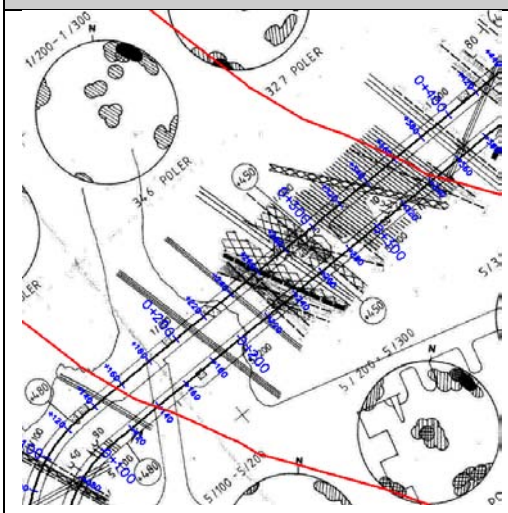

Overview drawing of tunnel mapping and poles to fracture planes in the SFR operational (above) and construction (below) tunnels in the area of intersection with ZFMWNW0001, chainage scale is in metres. Pole concentrations in %: black ≥12; grid 6-12; lines 3-6; no fill >3. /Christiansson and Bolvede 1987/.

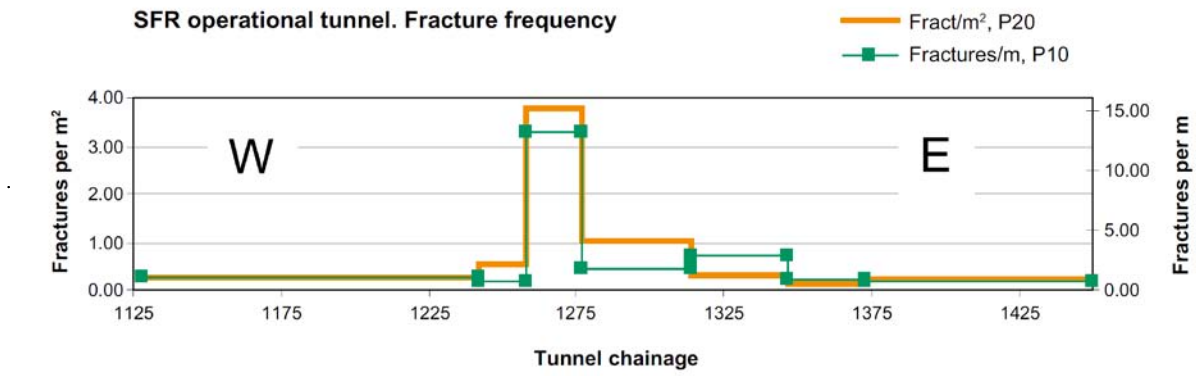

Observed fracture intensity in the SFR operational tunnel. P10 is the amount of fractures per metre crossing the right-hand spring-line. P20 is the amount of fractures per square metre within the tunnel envelope surface. Cut-off length: 3 m. /Glamheden et al. 2006/. SFR V1.0 modelled zone position in the operational tunnel is 1155–1360 m.

Deformation zone ZFMWNW0813

Borehole and tunnel intersections (metres along borehole/tunnel)

KFM11A: 245–400 m (DZ1 245–824 m)
DT: 0+065–0+128
BT: 0+042–0+082 (tDZ3 0+070, tDZ4 0+076 and tDZ5 0+072)

Deformation style, alteration and geometry

Deformation style: Ductile and brittle. Cohesive breccia, mylonite and several ductile and brittle-ductile shear zones present in the target intercept of KFM11A DZ1.

Alteration: Red-stained bedrock with fine-grained hematite dissemination. Locally chloritization and muscovitization

Strike/dip (span) right-hand-rule: 115 / 90 (±5 / ±10)

Trace length at ground surface (span): 2715 m (2700−2750 m)

Model thickness (span): 75 m

Confidence in existence: High

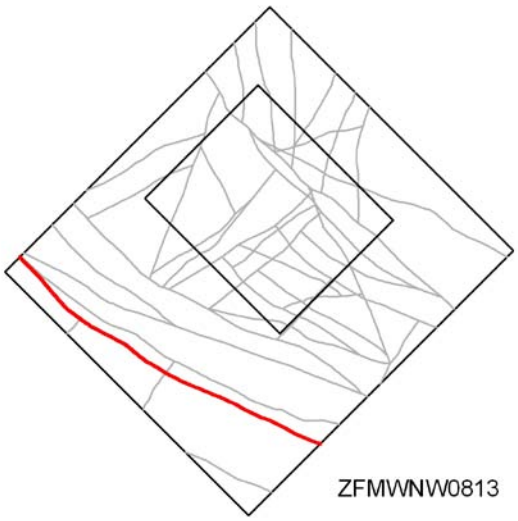

Modelling procedure*:* The deformation zone position on the ground surface is based on lineament MFM0813G /Isaksson et al. 2007/, with some modification in the current modelling work based on tunnel and borehole evidence in the area where the magnetic field is disturbed due to man-made structures. The original lineament and zone trace diverge in the area of the tunnel, with the zone extended to cross the SFR construction and operation tunnels before terminating at ZFMWNW0001. The modification was based on the existence of deformation seen in the upper level of KFM11A DZ1 and significant deformation seen in the BT and DT detailed tunnel mapping results.

Forward modelling of magnetic data along profiles 24, 25 and 26 (see Appendix 6) suggests a vertical to steep dip to the south-west. Due to the uncertainty of the modelling result and probable local variations, a vertical dip, based on the tunnel and KFM11A data, has been retained in the model.

Deformation zone ZFMWNW0813

Fractures in the deformation zone

General characteristics

Fracture orientation:

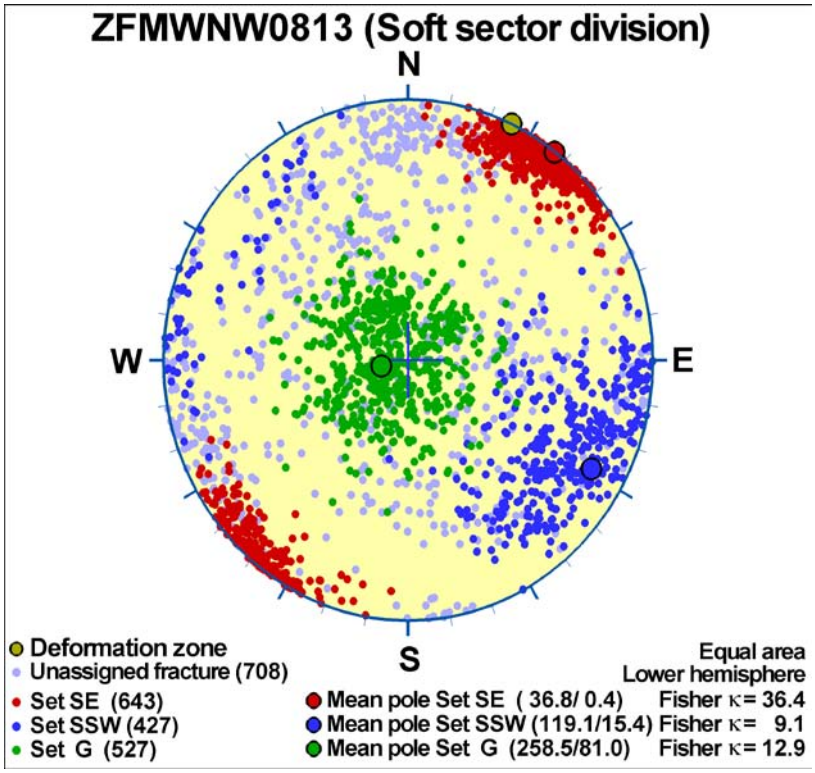

Fracture frequency: Open 7 m^{-1}, Sealed 38 m^{-1}

Fracture filling mineralogy:

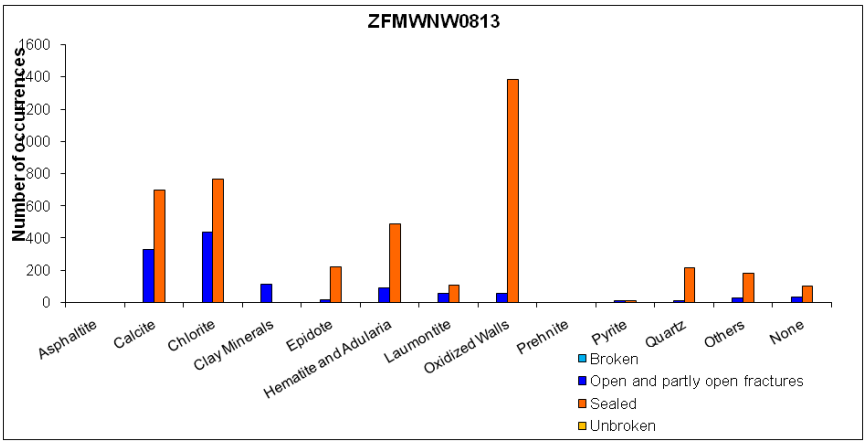

Deformation zone ZFMWNW0813

KFM11A 339–382 m (as an example of poorer rock quality within the longer 245–400 m section of DZ1)

BOREHOLE AND TUNNEL INTERCEPT DETAILS

Borehole intersections for ZFMWNW0813				
BH	**Geometrical Intercept**		**Target intercept**	
	Sec_up BH length (m) [z (-m)]	**Sec_low BH length (m) [z (-m)]**	**Sec_up BH length (m) [z (-m)]**	**Sec_low BH length (m) [z (-m)]**
KFM11A	247.68 [215.31]	391.95 [339.54]	245	400
Comment: The upper intercept corresponds to the upper boundary of DZ1 from KFM11A SHI. The lower boundary does not correspond to any specific evidence at this level within DZ1 but rather reflects a more general subdivision of the portion of DZ1 lying outside of ZFMWNW0001 between ZFMWNW0813 and ZFMWNW3259 based on the lineament size and position with reference to the high resolution magnetic map.				

Borehole intersections for ZFMWNW0813

SHI DZ1 245–824 m: *The description as follows has been modified from /Carlsten et al. 2007/ to match the target intercept (i.e. details that concern the SHI interval outside the target intercept has been omitted).*

Generally increased frequency of sealed fractures, sealed fracture networks and open fractures, and several intervals with one or more crush zones (317 m and 376–384 m). Gently dipping fractures and fractures that strike ESE and dip steeply to the SSW dominate. Gently dipping fractures are also present. Fracture apertures are generally less than 1 mm, with a few ranging up to 10 mm. Faint to medium oxidation is present along short intervals throughout the possible zone. Predominant fracture minerals are chlorite, calcite, laumontite, adularia, quartz, clay minerals and epidote. Two intervals with low radar amplitude, low bulk resistivity with low resistivity anomalies, low magnetic susceptibility and scattered low P-wave velocity anomalies can be recognized at 248–279 and 345–382 m. Furthermore, muscovite alteration of faint to medium intensity more or less affects the whole interval. The possible zone occurs in felsic to intermediate metavolcanic rock, with subordinate fine- to medium-grained granite, amphibolites and pegmatitic granite. The possible zone corresponds to the contact between felsic to intermediate metavolcanic rocks with different densities. Confidence level = 3.

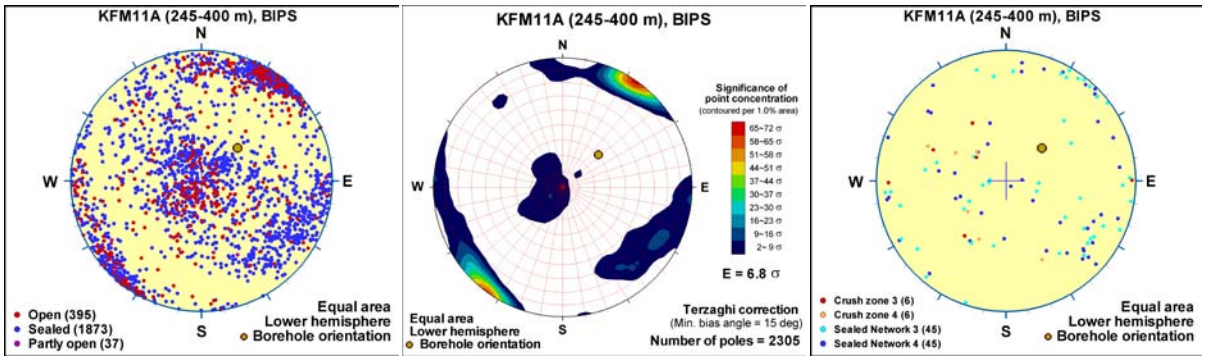

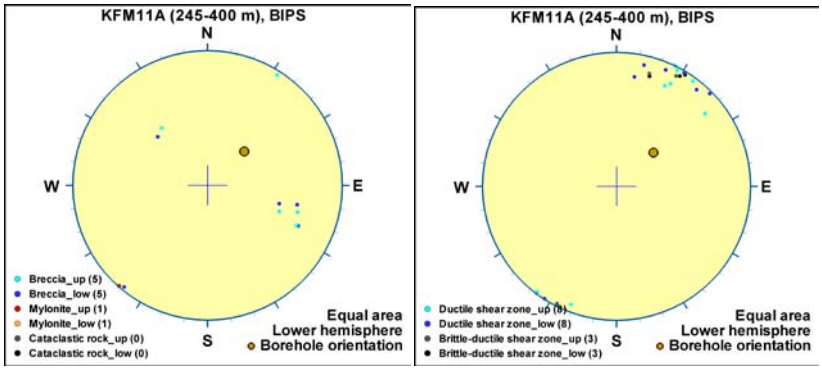

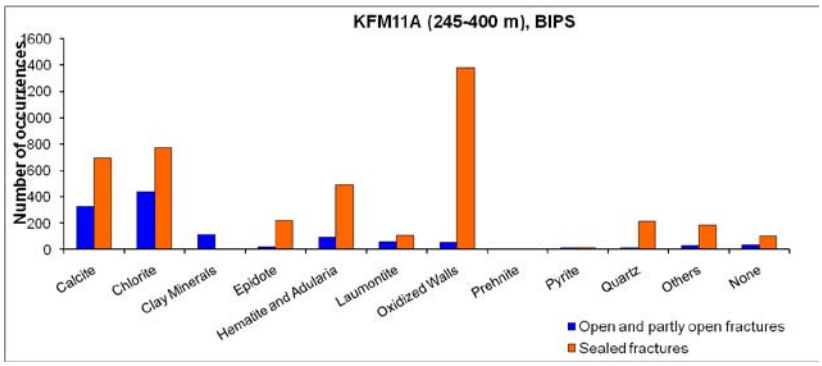

Borehole intersections for ZFMWNW0813

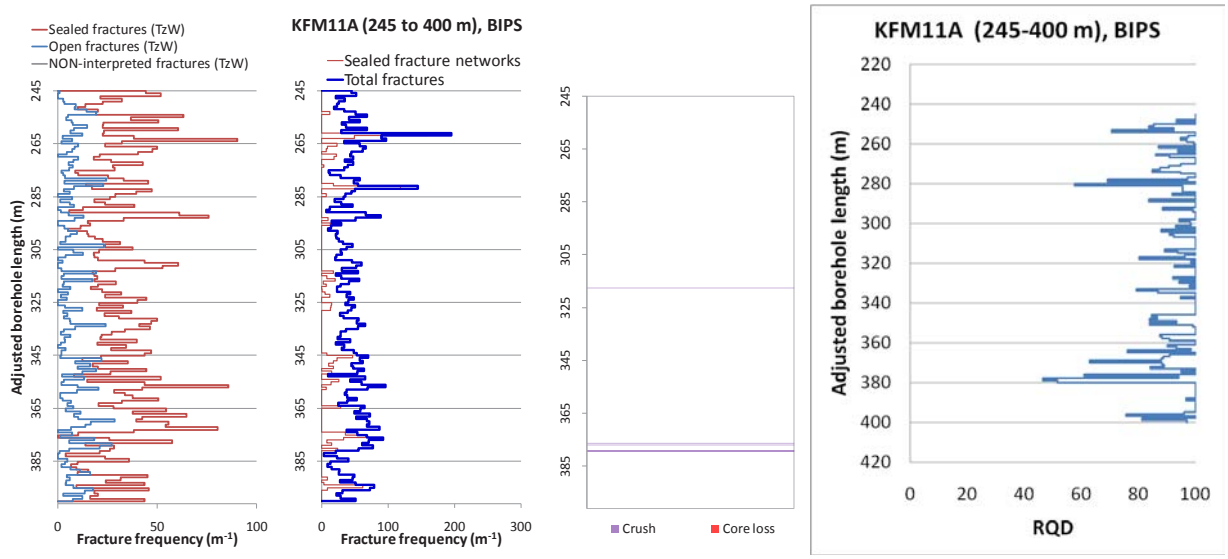

Tunnel intersections for ZFMWNW0813

Tunnel	Geometrical Intercept		Target intercept	
	Start ch.(m)	End ch. (m)	Start ch.(m)	End ch. (m)
DT	0+062	0+138	0+065	0+128
Comment: Target intercept mainly based on the shotcrete coverage marked in the detailed tunnelmapping /Christiansson and Bolvede 1987/.				
BT	0+042	0+120	0+042	0+082
Comment: Target intercept defined by tDZ3 0+070, tDZ4 0+076 and tDZ5 0+072 in Appendix 2.				

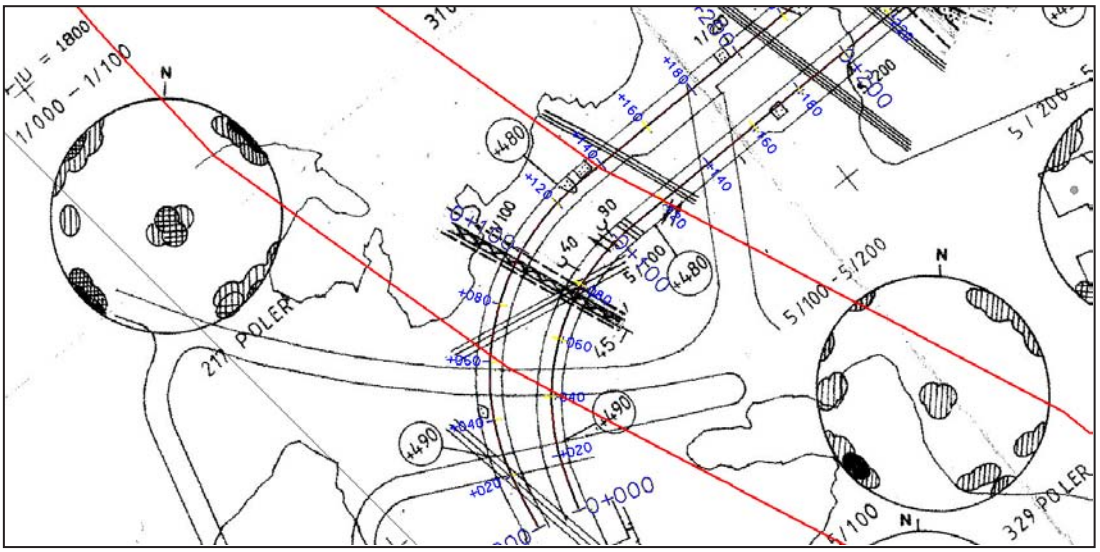

Tunnel intersections for ZFMWNW0813

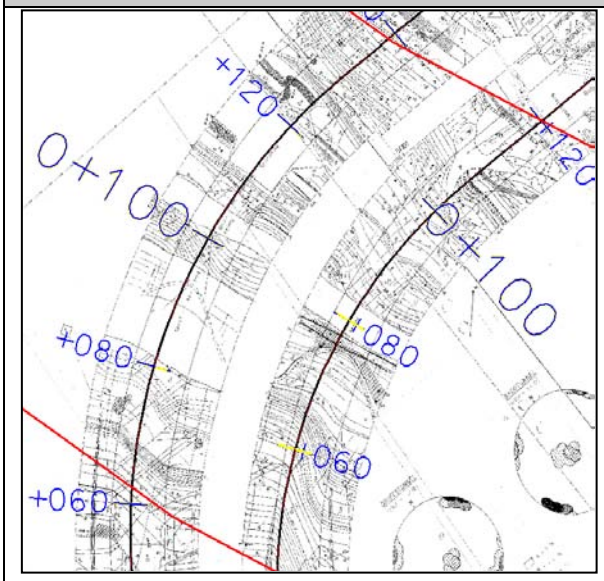

Overview and detailed drawing of tunnel mapping in the SFR operational and construction tunnels in the area of intersection with ZFMWNW0813, chainage scale is in meters. /Christiansson and Bolvede 1987/. Note the extensive areas of shotcrete. Considerable deformation occurs in the tunnel in this general area but the actual specific boundary positions of the zone are uncertain and only approximate.

Deformation zone ZFMWNW0835

Borehole and tunnel intersections (metres along borehole/tunnel)

KFR27: 108–120 m (DZ1 108–120 m) and 323–469 m (DZ2 323–379.5 m, DZ3 389–401 m and DZ4 421–469 m)

Deformation style, alteration and geometry

Deformation style: Brittle. Several minor ductile and brittle-ductile shear zones in KFR27 DZ2, DZ3 and especially DZ4.

Alteration: Locally red-stained bedrock with fine-grained hematite dissemination and argillization. Altered vuggy rock with quartz dissolution at 424.55–428.70, 431.01–451.64 and 457.64–463.08 m in KFR27 DZ4

Strike/dip (span) right-hand-rule: 118 / 88 (±5 / ±10)

Trace length at ground surface (span): 1044 m (1044−1580 m)

Model thickness: 21 m (5−22 m)

Confidence in existence: High

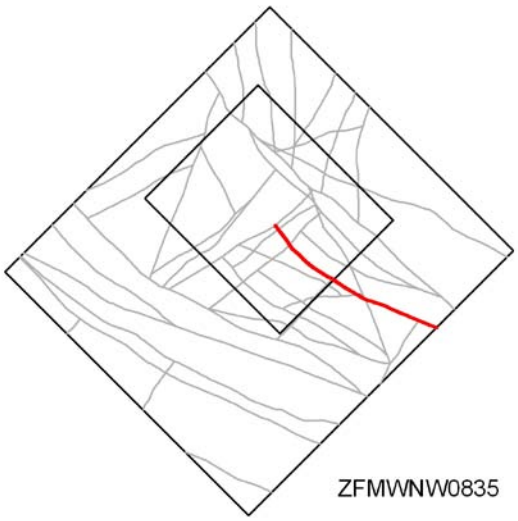

Modelling procedure*:* The position of the zone on the ground surface is based on a linking of magnetic lineaments MSFR08107 and MSFR08106 (updated from lineament MFM0835BG in Forsmark stage 2.3 /Isaksson et al. 2007/) with a further minor extension to the WNW. The large quoted length range reflects the uncertainty in a further possible extension of the zone to the north-west. Forward modelling of magnetic data along profiles 2 and 44 (see Appendix 6) suggest a steep dip to the north-east whereas inversion modelling supports the more vertical dip.

Section view of ZFMNWW0835 looking along the strike to the WNW, showing intersections with KFR27. The KFR27 SHI PDZs are shown as pink cylinders.

Deformation zone ZFMWNW0835

Fractures in the deformation zone

General characteristics

Fracture orientation: The apparent dominance of gently dipping fractures is considered to be due to data bias along the more or less vertical borehole KFR27.

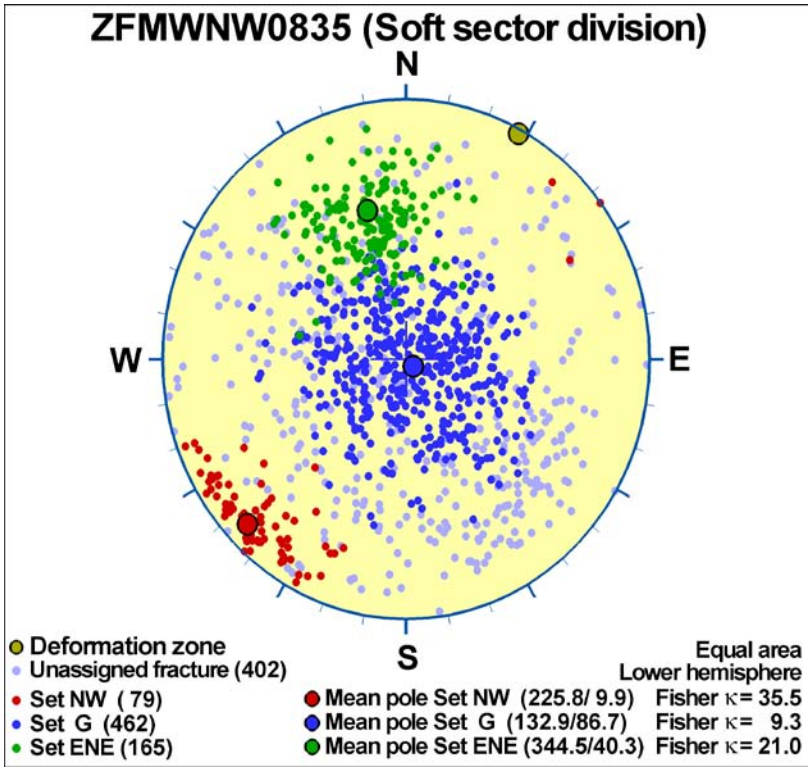

Fracture frequency: Open 14 m^{-1}, Sealed 21 m^{-1}

Fracture filling mineralogy:

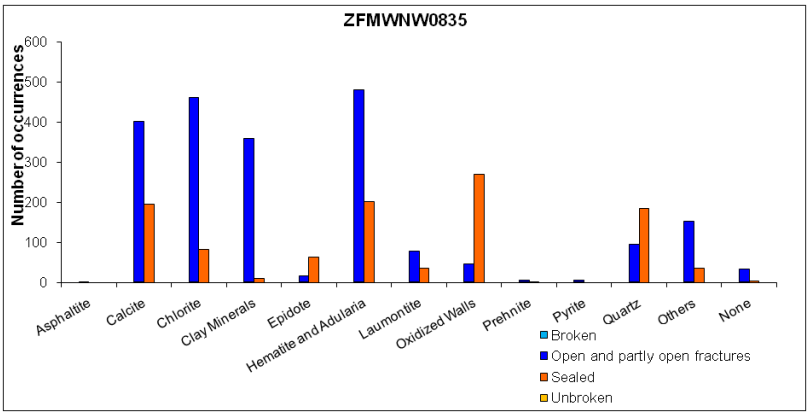

Deformation zone ZFMWNW0835

KFR27 DZ2 (323–379.5 m)

BOREHOLE AND TUNNEL INTERCEPT DETAILS

Borehole intersections for ZFMWNW0835				
BH	**Geometrical Intercept**		**Target intercept**	
	Sec_up BH length (m) [z (-m)]	**Sec_low BH length (m) [z (-m)]**	**Sec_up BH length (m) [z (-m)]**	**Sec_low BH length (m) [z (-m)]**
KFR27	0 [2.87]	153.31 [150.43]	108	120

DZ1 108–120 m: Increased frequency of sealed fractures and sealed fracture networks. Locally weak to moderate oxidation. No core available. Moderate resistivity anomalies. One distinct radar reflector at approximately 118 m. Pegmatitic granite (101061), metagranite-granodiorite (101057) and felsic to intermediate metavolcanic rock (103076). Confidence level = 1.

Medium transmissivity of this interval (T = $8 \cdot 10^{-8}$ m^2/s).

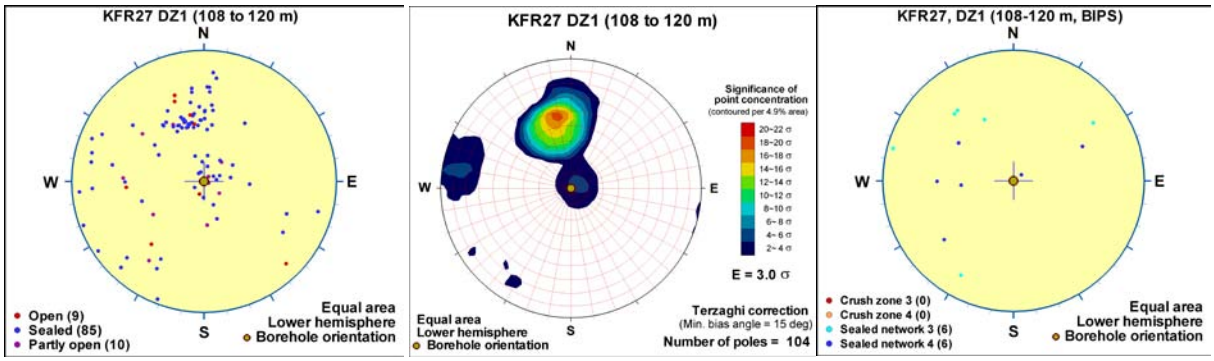

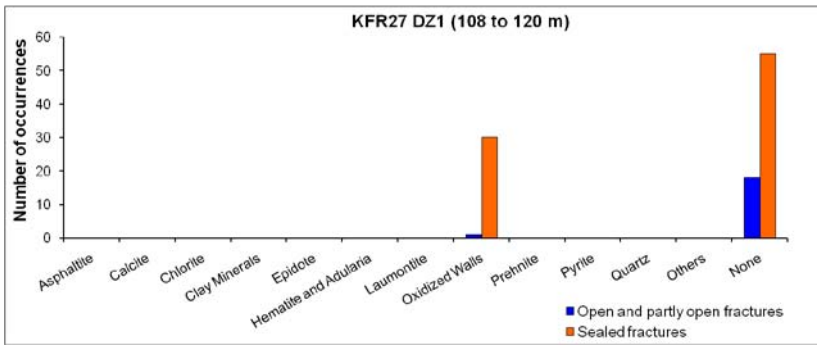

Borehole intersections for ZFMWNW0835

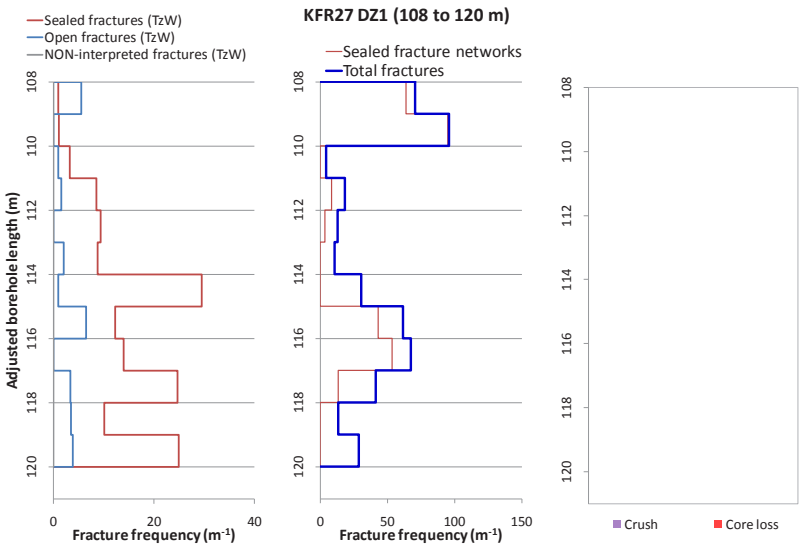

Borehole intersections for ZFMWNW0835

BH	Geometrical Intercept		Target intercept	
	Sec_up BH length (m) [z (-m)]	Sec_low BH length (m) [z (-m)]	Sec_up BH length (m) [z (-m)]	Sec_low BH length (m) [z (-m)]
KFR27	195.98 [193.06]	470.56 [466.08]	323	469

SHI DZ2 323–379.5 m: Several shorter intervals with increased frequency of open and sealed fractures and a more extensive interval in the lower most part of the possible deformation zone. Thirteen crush sections throughout the interval and one minor breccia at 338.51–338.52 m. Fracture aperture up to 1mm. Locally faint to moderate oxidation and faint to weak argillization. Predominant minerals in open fractures are calcite, chlorite, clay minerals and hematite. Low electric resistivity especially in the lower part of the section. A minor deflection in the temperature gradient. Two radar reflectors (352°/01° or 332°/11° and 334°/65° or 154°/53°). Fine- to medium-grained granite (111058), metagranite-granodiorite (101057), pegmatitic granite (101061) and amphibolite (102017). Confidence level = 3.

Increased frequency of flow anomalies. The total transmissivity of the interval is $1 \cdot 10^{-6}$ m^2/s.

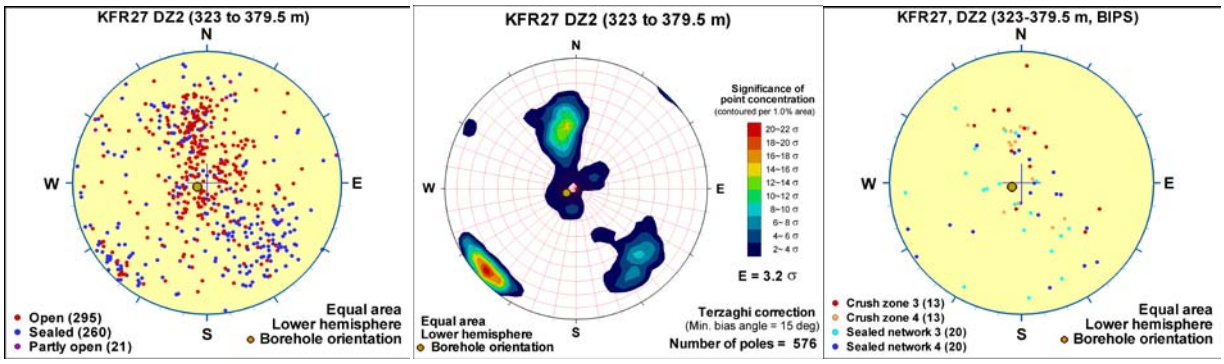

Borehole intersections for ZFMWNW0835

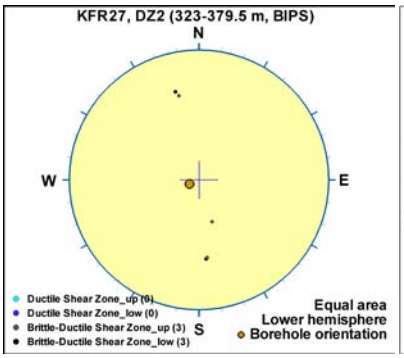

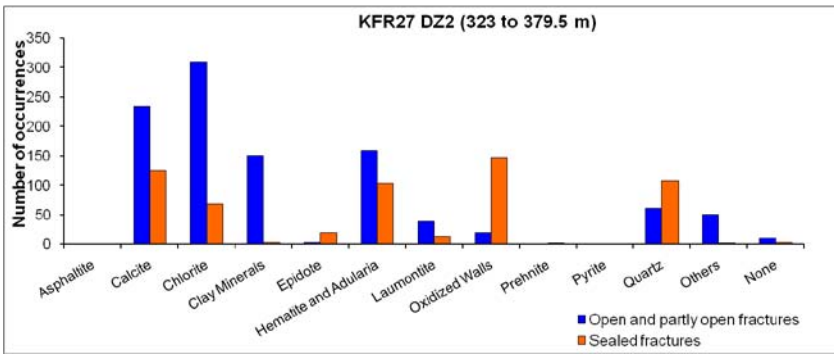

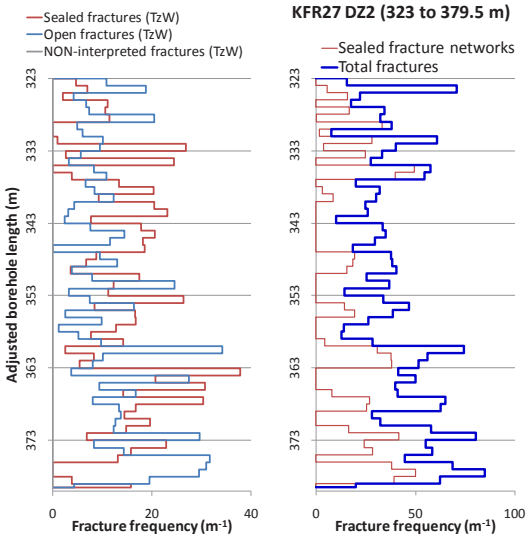

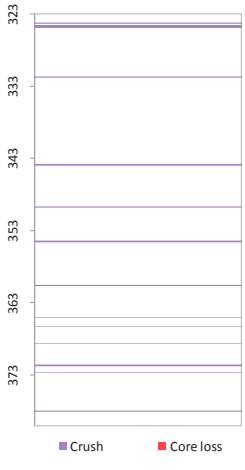

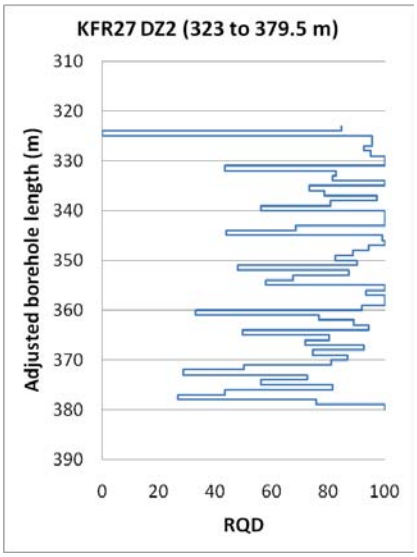

DZ3 389–401 m: Increased frequency of sealed and open fractures and sealed fracture networks. One crush at the interval 394.71–394.75 m. Fracture aperture up to 0.5 mm and one single aperture at 3 mm. Generally weak to moderate oxidation. Predominant minerals in open fractures are chlorite, laumontite and clay minerals, in sealed fractures calcite, laumontite and quartz and in the crushed interval chlorite and clay minerals. Moderate resistivity anomalies. Metagranite-granodiorite (101057), pegmatitic granite (101061) and amphibolite (102017). Confidence level = 2.

One single low-transmissive (T = $1 \cdot 10^{-9}$ m^2/s) flow anomaly at 392.1 m.

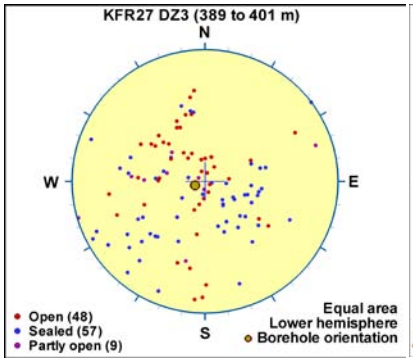

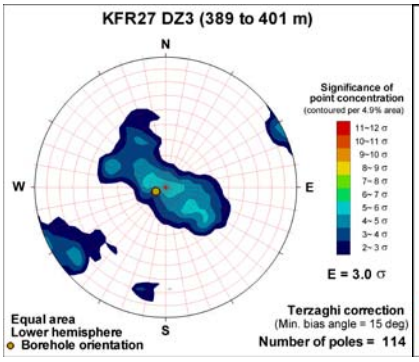

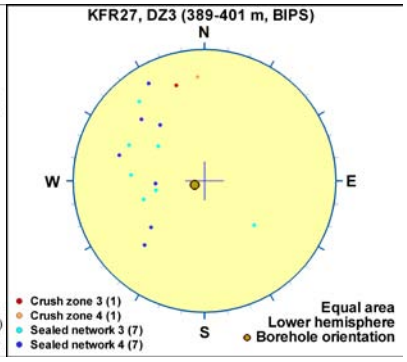

Borehole intersections for ZFMWNW0835

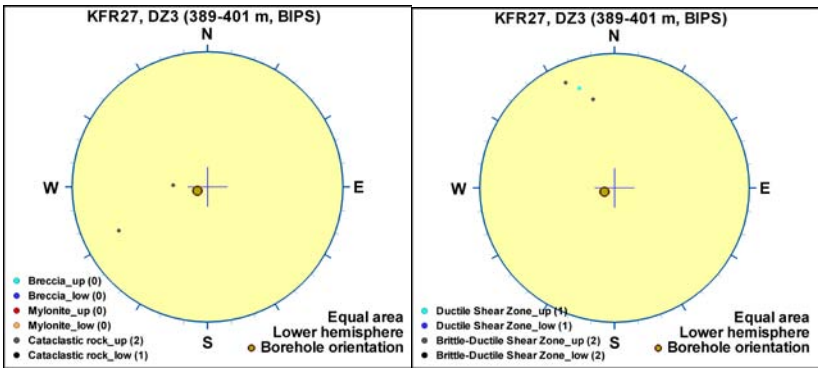

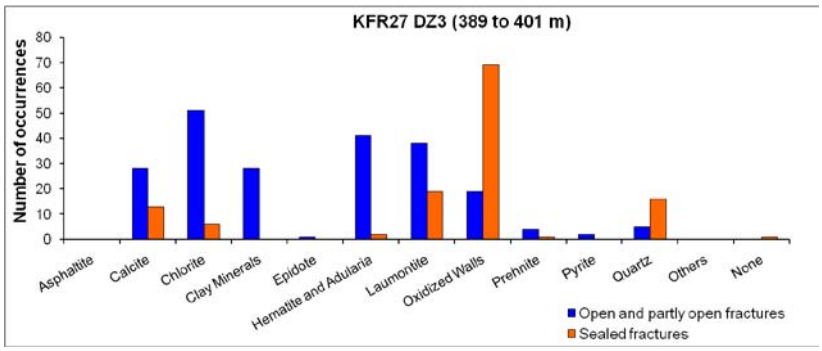

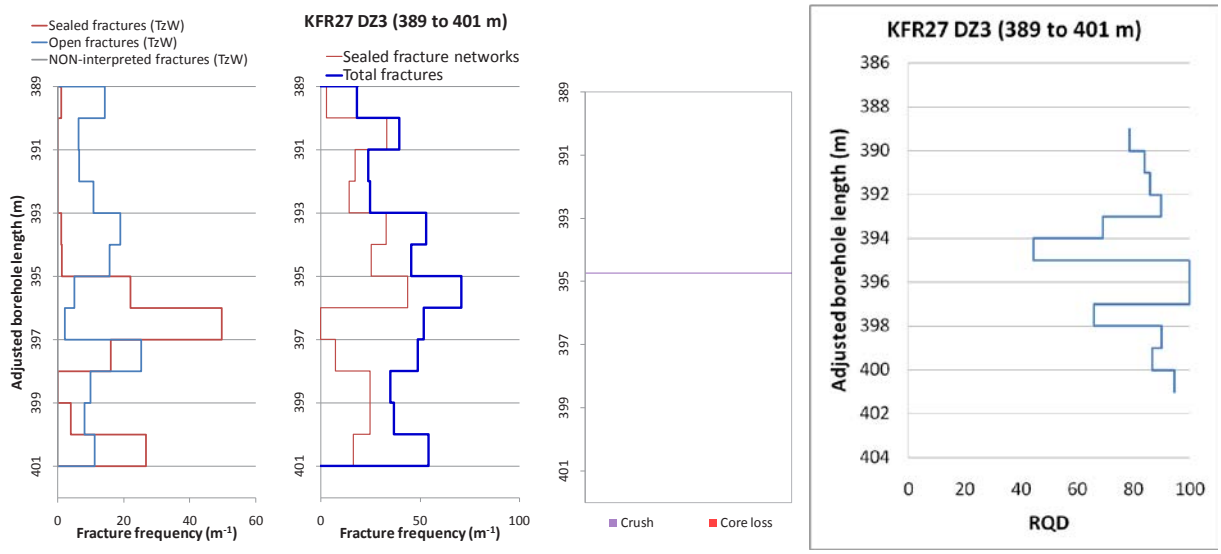

Borehole intersections for ZFMWNW0835

DZ4 421–469 m: The possible deformation zone can be divided in to three different characteristic intervals. The uppermost interval, extending down to c.442 m, is characterized by increased frequency of sealed and especially open fractures. Six crushed sections with a concentration between 431.4–433.5 m. Fracture aperture up to 3 mm Generally faint to moderate oxidation and faint to strong quarts dissolution. Predominant minerals in open fractures are hematite, calcite, clay minerals and adularia, in sealed fractures adularia, epidote, calcite and quartz and in crushed intervals clay minerals and adularia. Very low resistivity especially in the central part. Several calliper anomalies and a moderate deflection in the temperature gradient. The central sub interval extends from c. 442 m to c. 463 m, is characterized by strong brittle-ductile deformation and intense alteration that includes oxidation, quarts dissolution, argillization, chloritization and epidotization. Three crushes at 446.86–446.91, 448.12–448.14 and 458.30–458.33 m. Several moderately altered open fractures. Apertures ranging up to 2 mm. Predominant mineral in open fractures are clay minerals. The lower most interval, from c.463m, is characterized by increased frequency of sealed and open fractures. A few moderately to strongly altered open fractures. Generally weak oxidation and locally chloritization. Apertures ranging up to 3 mm. Predominant minerals in open fractures are chlorite and clay minerals and in sealed fractures adularia, laumontite and calcite. Very low resistivity especially in the central part. Several calliper anomalies and a moderate deflection in the temperature gradient. Amphibolite (102017), metagranite-granodiorite (101057), fine- to medium-grained granite (111058) and pegmatitic granite (101061). Confidence level = 3.

A cluster of flow anomalies at 410–436 m. The transmissivity is concentrated to the section 423–429 m. No flow anomaly below 436 m. The total transmissivity of the interval is $4 \cdot 10^{-6}$ m^2/s.

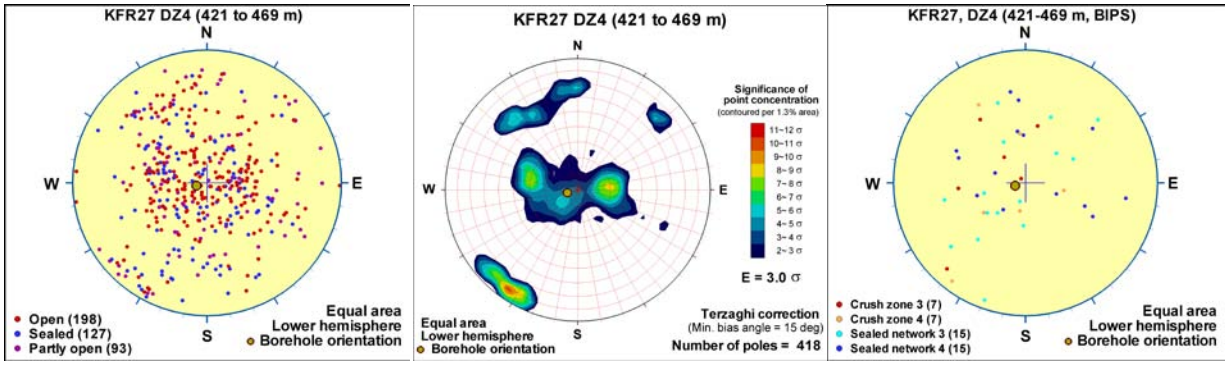

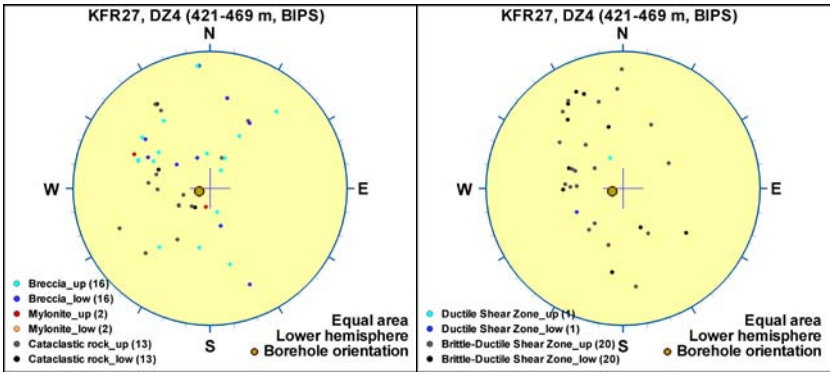

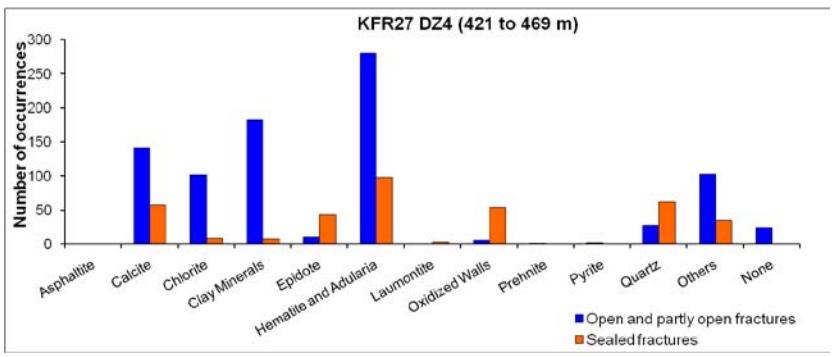

Borehole intersections for ZFMWNW0835

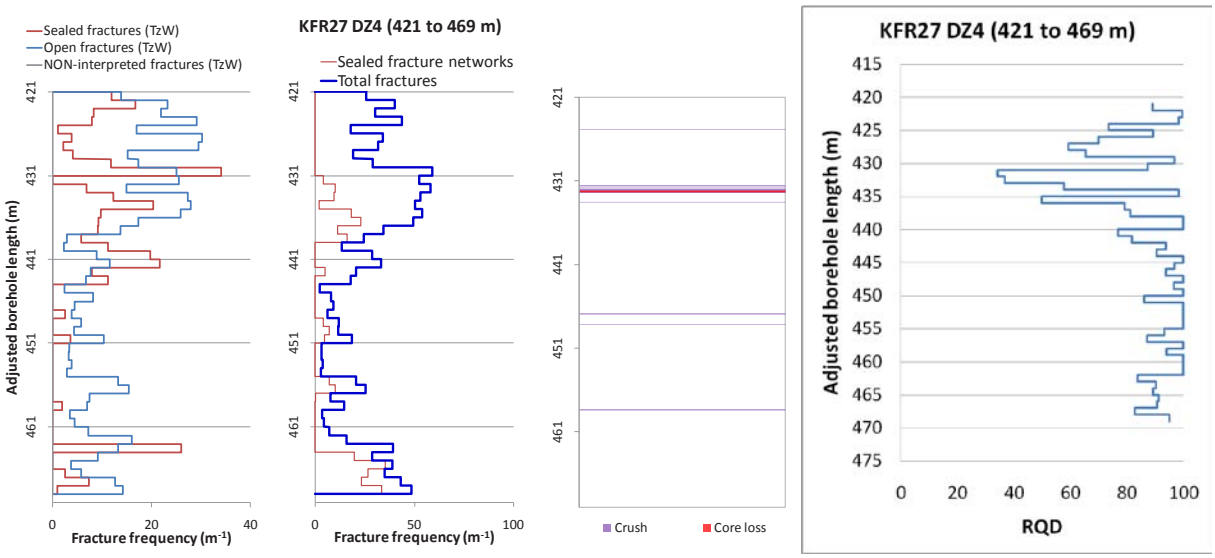

Deformation zone ZFMWNW0836

Borehole and tunnel intersections (metres along borehole/tunnel)

None

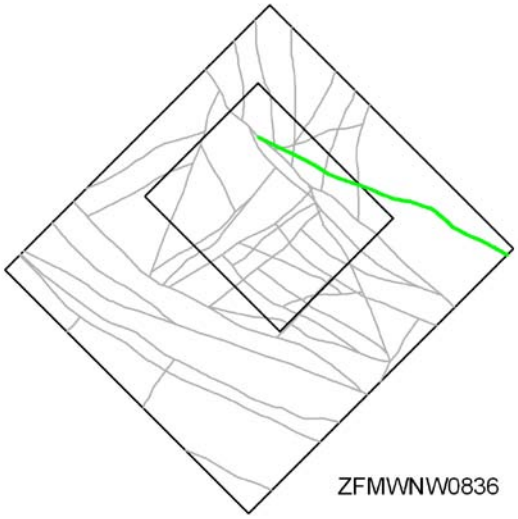

Deformation style, alteration and geometry

Deformation style: No data

Alteration: No data

Strike/dip (span) right-hand-rule: 117 / 90 (±5 / ±10)

Trace length at ground surface (span): 4868 m (4868−>4868 m)

Model thickness: 50 m (1% default)

Confidence in existence: Medium

Modelling procedure*:* The surface position of the zone is based on magnetic lineaments MFM0836G, MSFR08007 and MSFR10010 (/Isaksson et al 2007/ and SFR model version 1.0). The zone has been given a significant extension to the north-west compared with the lineament, to allow a better fit with the concept that the zone is a splay of ZFMNW0805A. The extension is not in any conflict with the magnetic data (see below).

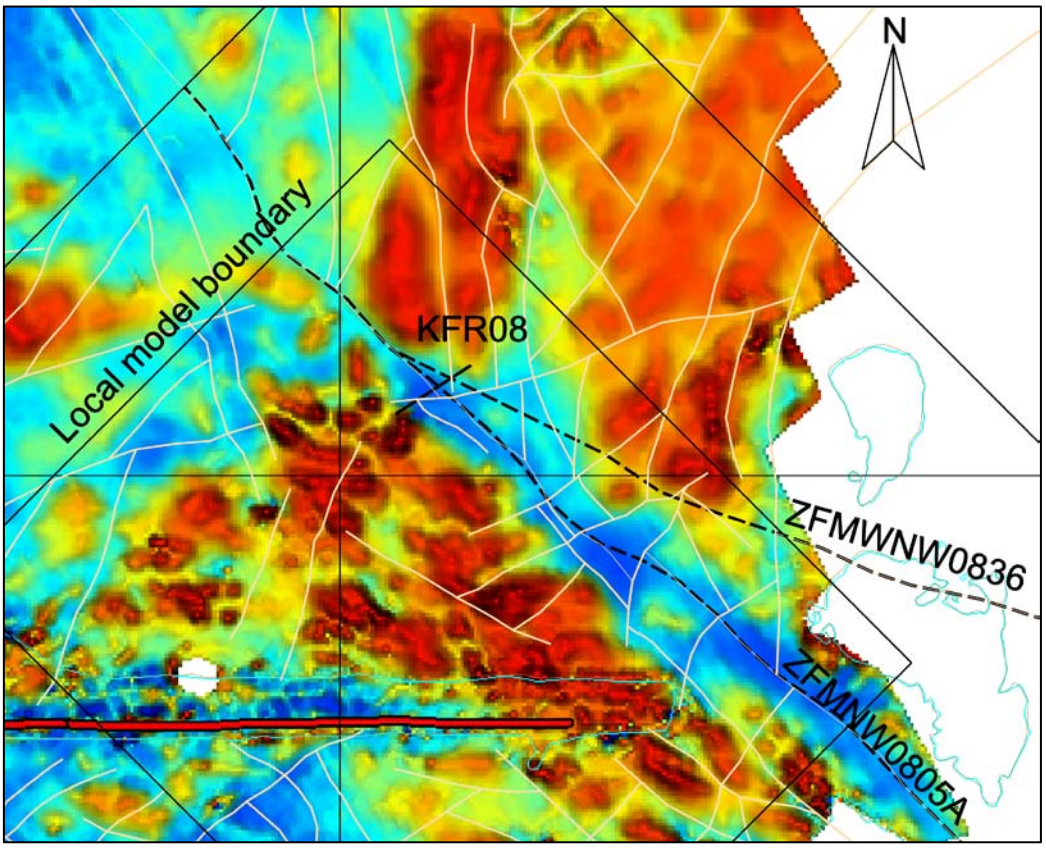

Map of the first vertical derivative of the magnetic total field, the deformation zone ground surface traces for ZFMWNW0836 and ZFMNW0805A, and the SFR version 1.0 lineaments, with a focus on the local model area where the ZFMWNW0836 zone trace diverges from the lineaments.

The zone is associated with two geometrical borehole intercepts. In KFR08 the geometrical intercept fits well with the magnetic surface data and the SHI (DZ1 41–104 m). However, KFR08 DZ1 is currently interpreted as being dominated by ZFMNW0805A. No drill core or SHI is available for KFR25. Since there is no confidently supportive borehole or tunnel information, the zone is only assigned a medium confidence.

Deformation zone ZFMWNW0836

Fractures in the deformation zone

General characteristics

Fracture orientation: No data

Fracture frequency: No data

Fracture filling mineralogy: No data

BOREHOLE AND TUNNEL INTERCEPT DETAILS

Borehole intersections for ZFMWNW0836				
BH	**Geometrical Intercept**		**Target intercept**	
	Sec_up BH length (m) [z (-m)]	**Sec_low BH length (m) [z (-m)]**	**Sec_up BH length (m) [z (-m)]**	**Sec_low BH length (m) [z (-m)]**
KFR08	46.04 [90.03]	104.12 [95.10]	–	–
Comment: Geometrical intercept fits well with the magnetic surface data and the SHI (DZ2 41–104 m). However, KFR08 DZ2 is currently interpreted as being dominated by ZFMNW0805A.				
KFR25	64.07 [46.08]	144.25 [103.76]	–	–
Comment: No core available				

Deformation zone ZFMWNW1035

Borehole and tunnel intersections (metres along borehole/tunnel)

HFR105: 119–147 m (DZ3 119–147 m)
DT: 0+420 to 0+433 (tDZ25 0+420, tDZ26 0+422, tDZ27 0+425 and tDZ28 0+433)
BT: 0+398 to 0+416 (tDZ26 0+398 and tDZ28 0+416)

Deformation style, alteration and geometry

Deformation style: Ductile origin with brittle reactivation based on tunnel mapping and inferred association with other WNW-ESE trending deformation zones

Alteration: Locally red-stained bedrock with fine-grained hematite dissemination

Strike/dip (span) right-hand-rule: 120 / 80 (±5 / ±10)

Trace length at ground surface (span): 1622 m (1622−>2000 m)

Model thickness (span): 15 m (5−20 m)

Confidence in existence: High

Modelling procedure*:* The surface position of ZFMNW1035 is based on the magnetic lineaments MFM1035G, MSFR08112, MSFR08110 and MSFR08123 (/Isaksson et al. 2007, SFR model version 1.0) with some adjustments based on correlation with SFR tunnel mapping and borehole information.

There are a number of structures mapped in the tunnels with strikes parallel to the trends of the lineaments and with a steep dip to the south-west. A thickness of 15 m has been defined by the thickness of HFR105 DZ3, as well as to reflect the spread of the inferred related structures seen in the tunnel mapping. In a similar manner as other parallel-oriented zones in the vicinity of SFR, tunnel mapping suggests that the zone consists of an associated group of sub-parallel smaller structures and the different zones together, in the area around SFR, define the complex Singö tectonic belt.

The forward modelling of magnetic data along profile 1 (see Appendix 6) data suggests a sub-vertical to steep dip to the north-east but the lateral continuity of the anomaly and, as a result, how representative it is for zone ZFMNW1035 are uncertain. Other modelled profiles (24, 25, 26 and 33) indicate a general steep dip to the south-west, as inferred by linking the lineaments to borehole and tunnel intersections in the modelling procedure.

Deformation zone ZFMWNW1035

Fractures in the deformation zone

General characteristics

Fracture orientation:

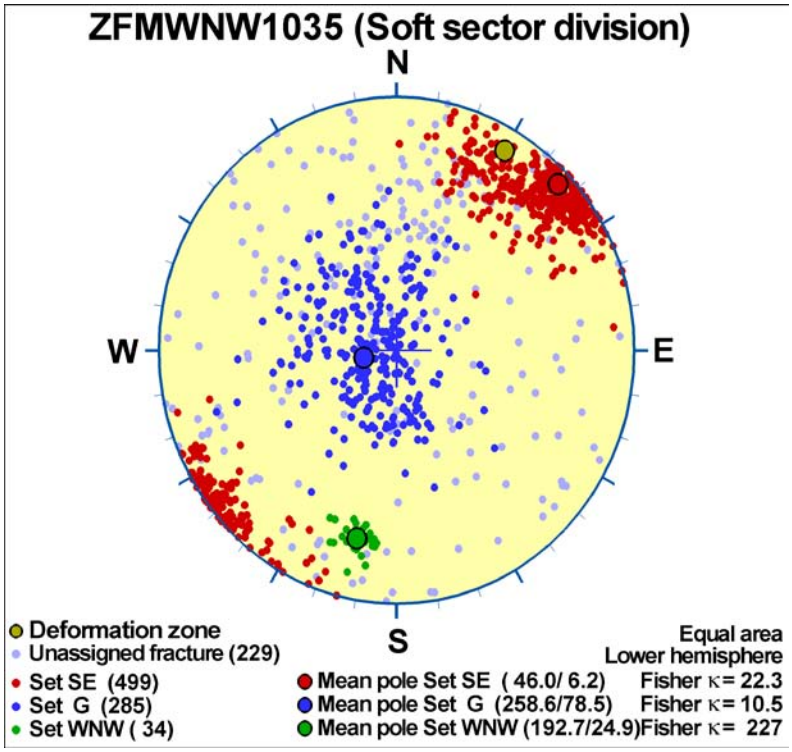

Fracture frequency: A general indication is available from HFR105 presented below.

Fracture filling mineralogy:

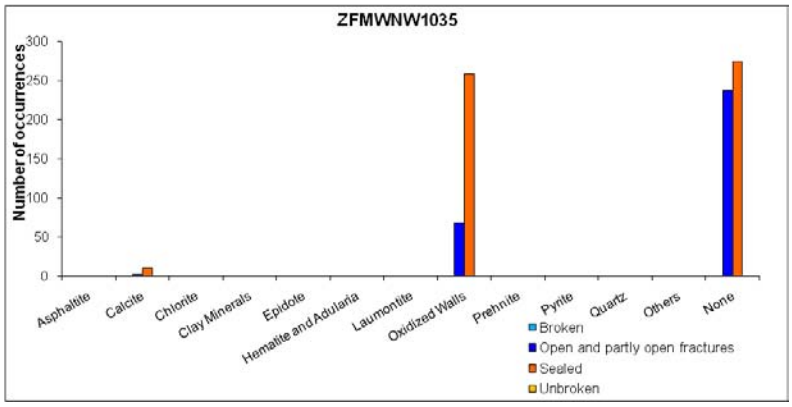

BOREHOLE AND TUNNEL INTERCEPT DETAILS

Borehole intersections for ZFMWNW1035				
BH	**Geometrical Intercept**		**Target intercept**	
	Sec_up BH length (m) [z (-m)]	**Sec_low BH length (m) [z (-m)]**	**Sec_up BH length (m) [z (-m)]**	**Sec_low BH length (m) [z (-m)]**
HFR105	117.03 [102.03]	146.16 [128.59]	119	147

Comment: This BH has been used to define the zone thickness.

DZ3 119–147 m: Increased frequency of open fractures, sealed fractures and sealed fracture network. Four crushed intervals at 120.16–120.34, 120.90–121.06, 129.49–129.51 and 142.58–142.75 m. Fracture aperture 0.7 mm or less. Locally weak to medium oxidation. Significantly decreased bulk resistivity and major caliper anomalies along the intervals c. 118–120 m and c. 141–147 m. At c. 118 m the density is significantly decreased. Metagranite-granodiorite (101057), pegmatitic granite (101061), fine- to medium-grained granite (111058), amphibolite (102017) and fine- to medium-grained metagranodiorite-tonalite (101051). Confidence level = 2.

One flow anomaly at 119.4–120.0 m with a high transmissivity (about 1·10–5 m^2/s). This is one of three observed flow anomalies in the borehole.

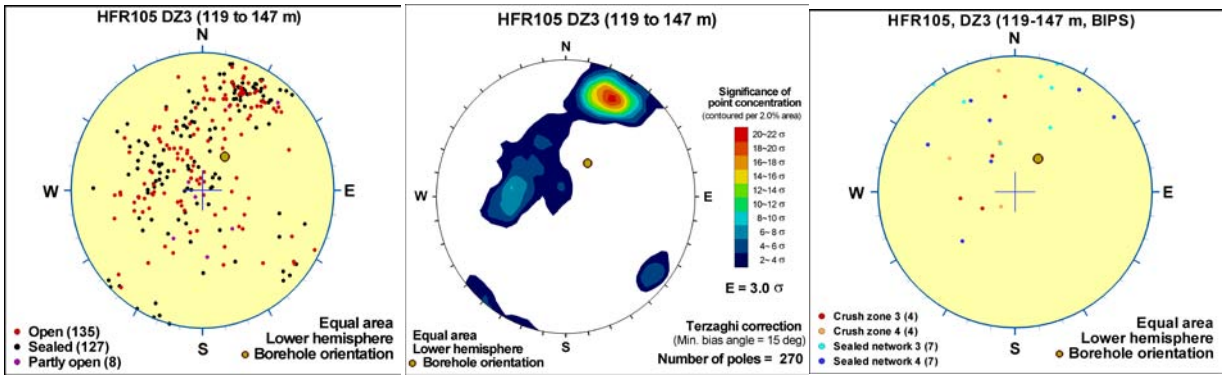

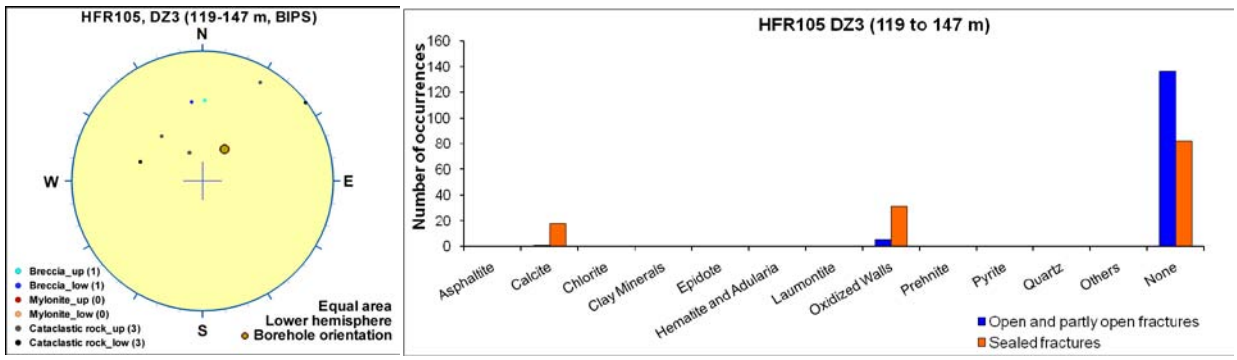

Borehole intersections for ZFMWNW1035

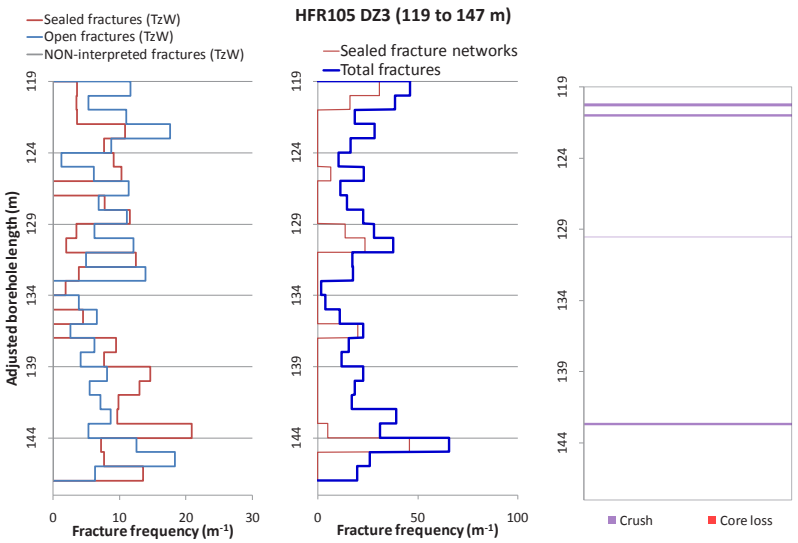

BH	Geometrical Intercept		Target intercept	
	Sec_up BH length (m) [z (-m)]	Sec_low BH length (m) [z (-m)]	Sec_up BH length (m) [z (-m)]	Sec_low BH length (m) [z (-m)]
HFM35	180.90 [136.56]	199.19 [149.33]	–	–

Comment: HFR105 DZ3 rather than HFM35 DZ3 has been given a higher priority for defining the zone geometry of ZFMWNW1035 and no specific target intercept has been defined. DZ3 is inferred to represent a series of parallel lying smaller structures that form part of the so-called Singö tectonic belt.

SHI DZ3104–200 m: Increased frequency of open and sealed fractures. Fractures that strike SE and dip steeply to the SW and fractures that are gently dipping dominate. Five crush zones in the lower half. Fracture apertures are generally less than 1 mm, with a few ranging up to 6 mm. Below 114 m, low resistivity, low P-wave velocity, low magnetic susceptibility and several caliper anomalies. 39 identified radar reflectors with intersection angles ranging from 31° to 90°. Several low radar amplitude intervals. Zone situated in aplitic metagranite with subordinate pegmatitic granite, metavolcanic rock, amphibolite and fine- to medium-grained granite. Confidence level = 3.

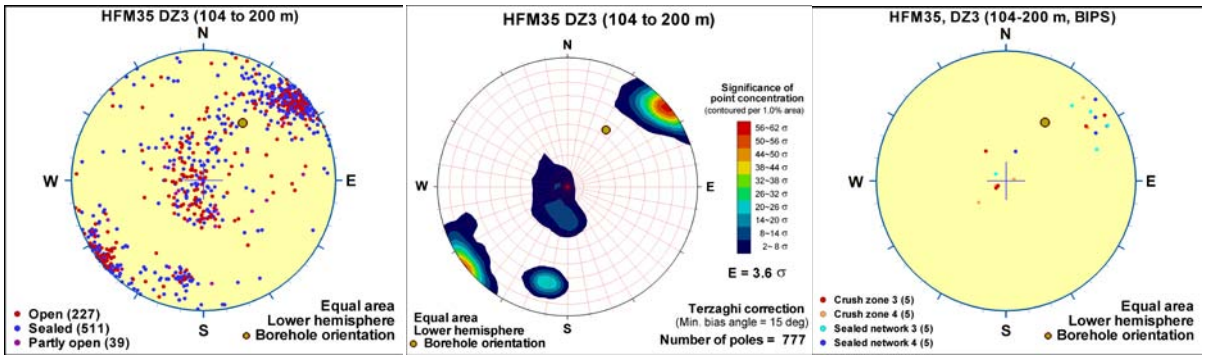

Borehole intersections for ZFMWNW1035

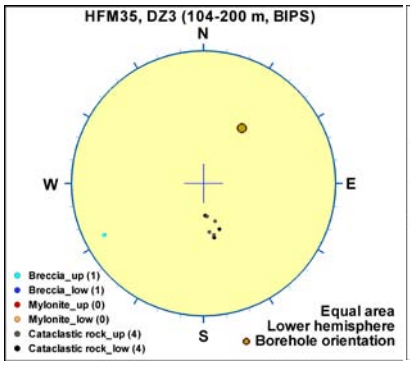

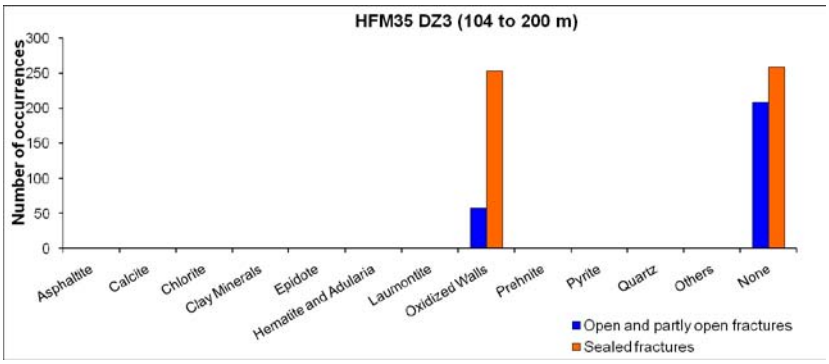

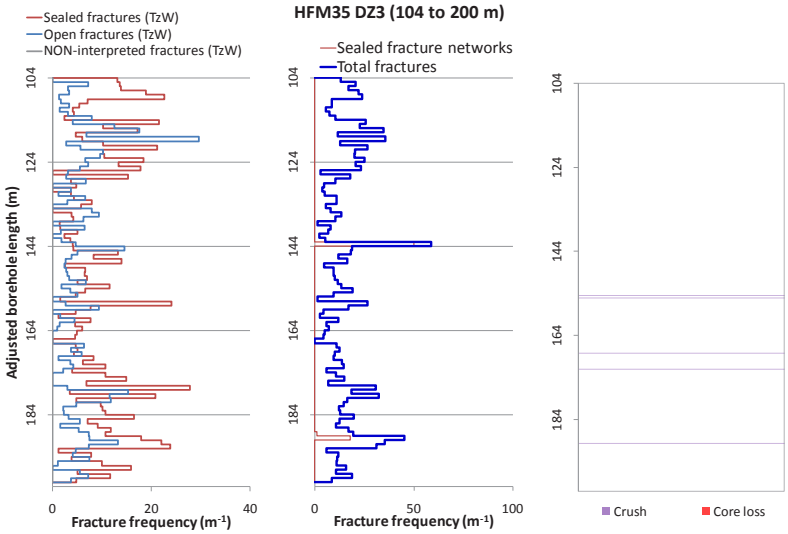

BH	Geometrical Intercept		Target intercept	
	Sec_up BH length (m) [z (-m)]	Sec_low BH length (m) [z (-m)]	Sec_up BH length (m) [z (-m)]	Sec_low BH length (m) [z (-m)]
KFM11A	714.86 [605.63]	736.38 [622.78]	–	–
Comment: The geometrical BH intersection lies within the very extensive SHI DZ1 (245–824 m). BH section 715–736 m falls within the modelled Singö zone, ZFMWNW0001 itself. The interpreted deformation is attributed to the belt in general without any more specific subdivision. The information from this BH has not been used to define the zone thickness.				
KFR68	0.00 [0.00]	5.19 [3.67]	–	–
Comment: No target intercept defined. No PDZ has been defined in this position though note the very shallow depth. Higher priority given to tunnel and HFR105 when defining the zone geometry.				

Tunnel intersections for ZFMWNW1035				
Tunnel	**Geometrical Intercept**		**Target intercept**	
	Start ch.(m)	**End ch. (m)**	**Start ch.(m)**	**End ch. (m)**
DT	0+420	0+435	0+420	0+433
Comment: Target intercept defined by tDZ25 0+420, tDZ26 0+422, tDZ27 0+425 and tDZ28 0+433 in Appendix 2.				
BT	0+398	0+412	0+398	0+416
Comment: Target intercept defined by tDZ26 0+398 and tDZ28 0+416 in Appendix 2.				

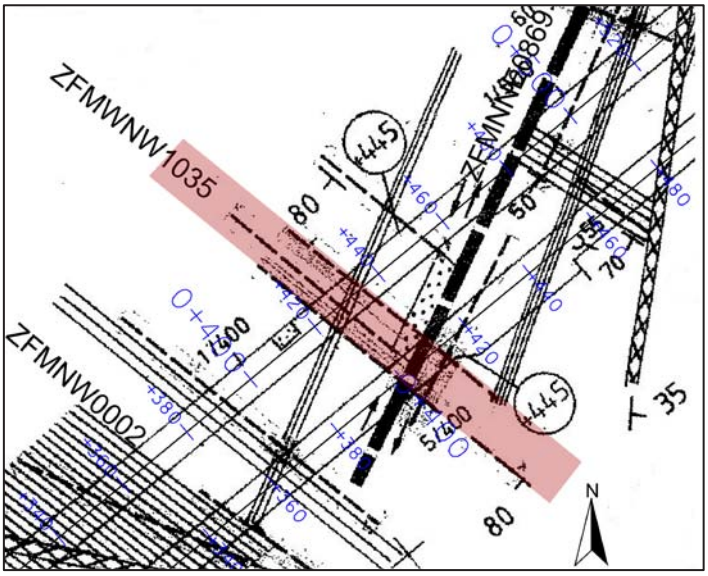

Overview drawing of the tunnel mapping /Christiansson and Bolvede 1987/ along with the interpreted intersection of ZFMWNW1035. The approximate positions of ZFMNW0002 and ZZFMNNE0869 are also indicated for reference.

Deformation zone ZFMWNW1056

Borehole and tunnel intersections (metres along borehole/tunnel)

None

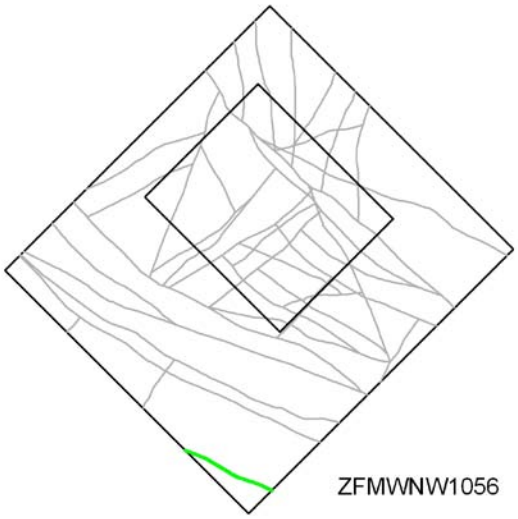

Deformation style, alteration and geometry

Deformation style: Ductile and brittle (no direct evidence – inferred association with other WNW-ESE trending deformation zones)

Alteration: No data

Strike/dip (span) right-hand-rule: 110 / 90 (±5 / ±10)

Trace length at ground surface (span): 2758 m (2750−2800 m)

Model thickness: 10 m (1% default)

Confidence in existence: Medium

Modelling procedure*:* The position of the zone on the ground surface is based on magnetic lineament MFM1056G /Isaksson et al. 2007/. No other information is available. The vertical dip and thickness are default values.

Fractures in the deformation zone

General characteristics

Fracture orientation: No data

Fracture frequency: No data

Fracture filling mineralogy: No data

Deformation zone ZFMWNW3259

Borehole and tunnel intersections (metres along borehole/tunnel)

KFM11A: 400–498 m (DZ1 245–824 m)
DT: 0+142 to 0+170 (tDZ6 0+143)
BT: 0+120 to 0+150

Deformation style, alteration and geometry

Deformation style: Ductile and brittle. Several brittle-ductile shear zones, cataclasites and cohesive breccias in all BH intercepts

Alteration: Red-stained bedrock with fine-grained hematite dissemination. Locally chloritization, muscovitization, epidotization and argillization

Strike/dip (span) right-hand-rule: 117 / 90 (±5 / ±10)

Trace length at ground surface (span): 2174 m (2150−2190 m)

Model thickness (span): 50 m (20−60 m)

Confidence in existence: High

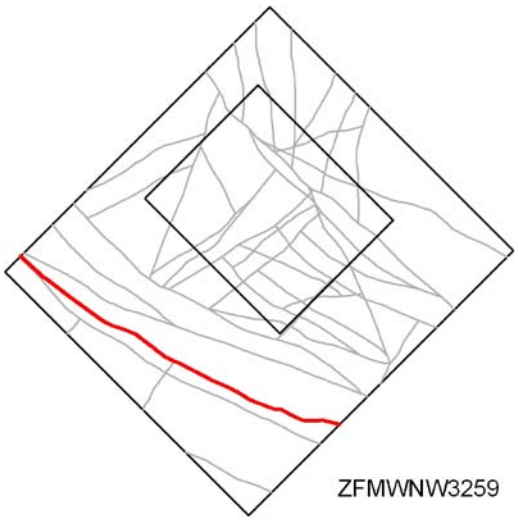

Modelling procedure: The position of the zone at the ground surface is based on magnetic lineament MFM3259G /Isaksson et al. 2007/, with a slight lateral adjustment in position as it traverses KFM11A and a further extension to the north-west coupled to a re-linking of the connection with MFM0813G. MFM3259G is taken to be the equivalent of linking the series of much shorter SFR version 1.0 lineaments MSFR08073, MSFR08074 and MSFR08075 in SFR model version 1.0 and is considered to be a more suitable length of trace to use in the regional model area.

Forward modelling of magnetic data along profiles 24, 25 and 26 (see Appendix 6) suggests a vertical to steep dip to the south-west. Due to the uncertainty of the modelling result and probable local variations, a vertical dip, based on the tunnel and KFM11A data, has been retained in the model.

Deformation zone ZFMWNW3259

Fractures in the deformation zone

General characteristics

Fracture orientation:

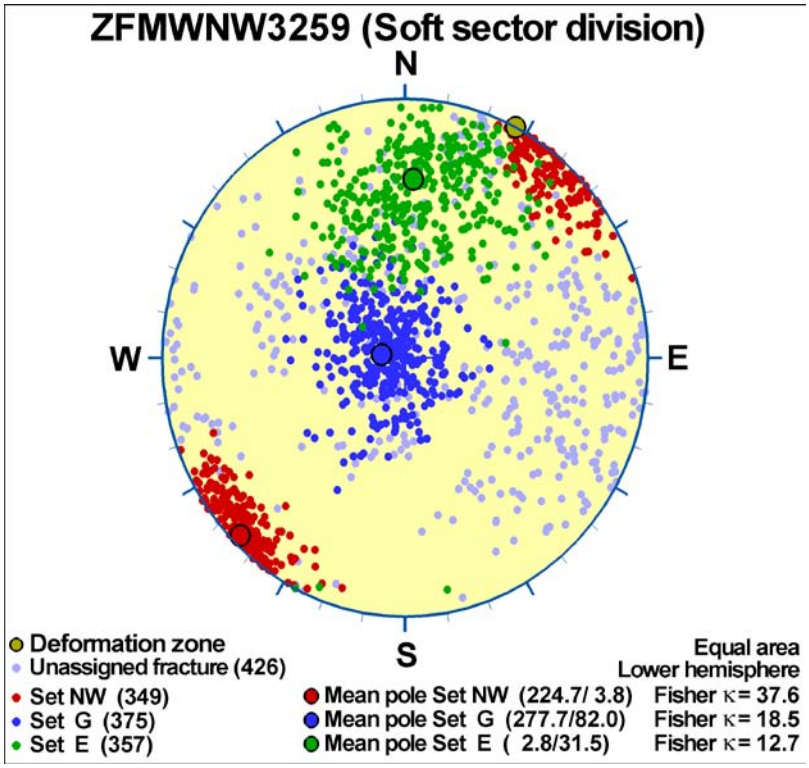

Fracture frequency: Open 8 m^{-1}, Sealed 43 m^{-1}

Fracture filling mineralogy:

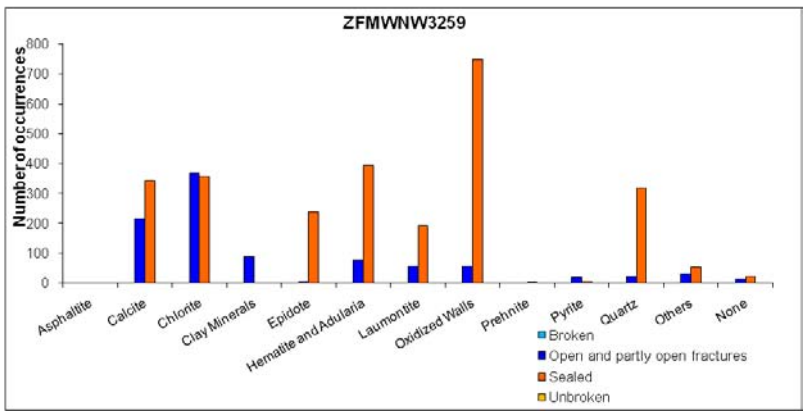

BOREHOLE AND TUNNEL INTERCEPT DETAILS

Borehole intersections for ZFMWNW3259				
BH	**Geometrical Intercept**		**Target intercept**	
	Sec_up BH length (m) [z (-m)]	**Sec_low BH length (m) [z (-m)]**	**Sec_up BH length (m) [z (-m)]**	**Sec_low BH length (m) [z (-m)]**
KFM11A	401.86 [347.99]	495.48 [427.02]	400	498

Comment: The upper intercept falls within DZ1 from KFM11A SHI. However, no specific evidence at this level within DZ1 has been identified but rather the position reflects a more general subdivision of the portion of DZ1 lying outside of ZFMWNW0001 between ZFMWNW0813 and ZFMWNW3259 based on the lineament size and position with reference to the magnetic map. The lower boundary corresponds to a subdivision earlier suggested by /Stephens et al. 2008b/.

SHI DZ1 245–824 m: *The description as follows has been modified from /Carlsten et al. 2007/ to match the target intercept (i.e. details that concern the SHI interval outside the target intercept have been omitted).*

Generally increased frequency of sealed fractures, sealed fracture networks and open fractures, and one interval with three crush zones at 437–464 m. Gently dipping fractures and fractures that strike ESE and dip steeply to the SSW dominate. Gently dipping fractures are also present. Fracture apertures are generally less than 1 mm, with a few ranging up to 4 mm. Faint to medium oxidation is present along short intervals throughout the possible zone. Predominant fracture minerals are chlorite, calcite, laumontite, adularia, quartz, clay minerals and epidote. Laumontite is common beneath 410 m. One interval with low radar amplitude, low bulk resistivity with low resistivity anomalies, low magnetic susceptibility and scattered low P-wave velocity anomalies can be recognized at 405–468 m. Furthermore, muscovite alteration of faint to medium intensity more or less affects the whole interval. The possible zone occurs in felsic to intermediate metavolcanic rock, with subordinate fine- to medium-grained granite, amphibolite, pegmatitic granite and medium-grained metagranite-granodiorite. The possible zone corresponds to the contact between felsic to intermediate metavolcanic rocks with different densities. Confidence level = 3.

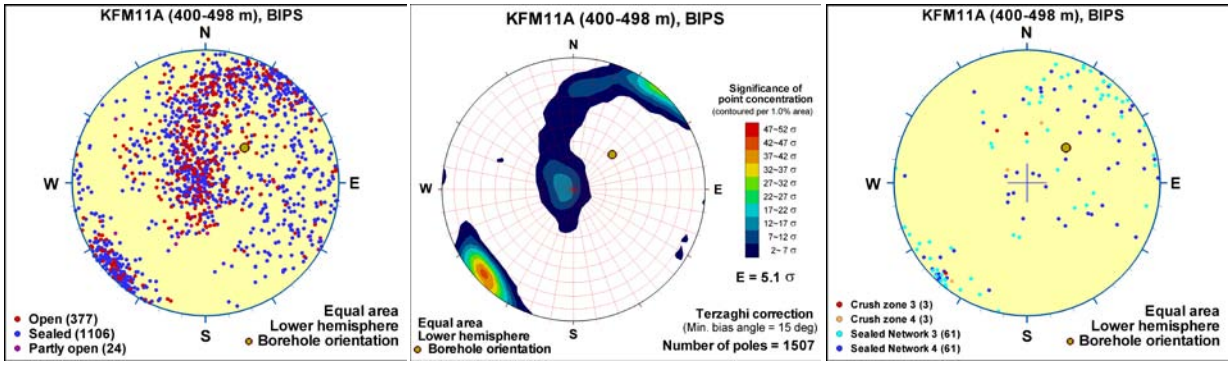

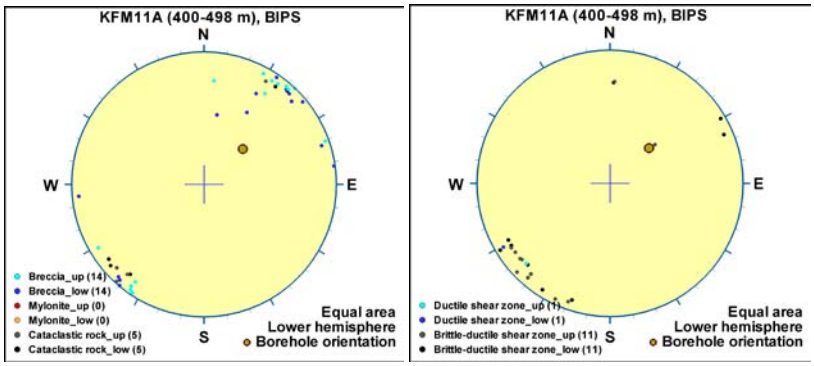

Borehole intersections for ZFMWNW3259

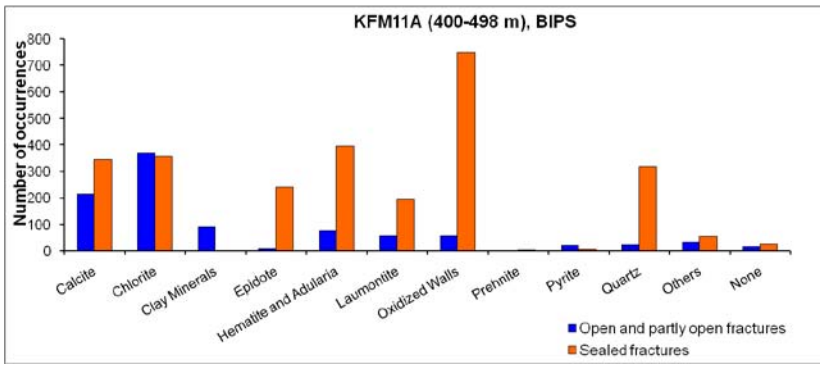

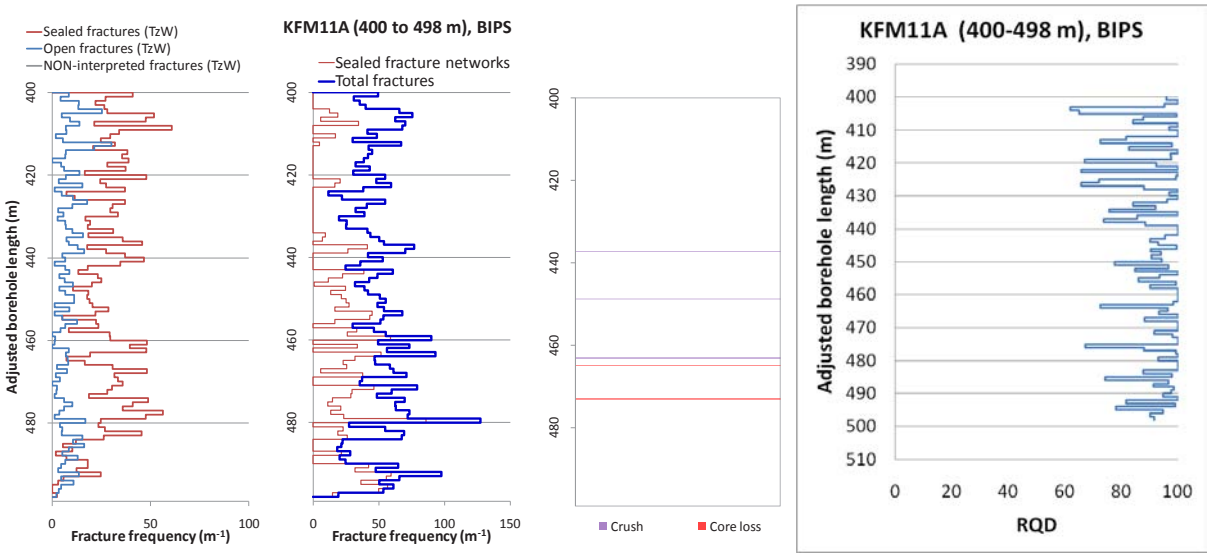

Tunnel intersections for ZFMWNW3259

Tunnel	Geometrical Intercept		Target intercept	
	Start ch.(m)	End ch. (m)	Start ch.(m)	End ch. (m)
DT	0+128	0+180	0+142	0+170
Comment: Target intercept defined by tDZ6 0+143 in Appendix 2.				
BT	0+108	0+158	0+120	0+150
Comment: Target intercept mainly based on the shotcrete coverage marked in the tunnel mapping by /Christiansson and Bolvede 1987/. No specific evidence is taken to define the boundaries of this zone in the tunnel but similar to in KFM11A there is clear evidence of deformation and the modelled zone represents a more general subdivision of deformation seen in the tunnel between ZFMWNW0813, ZFMWNW3259, ZFMWNW0001 and ZFMNW0002.				

Tunnel intersections for ZFMWNW3259

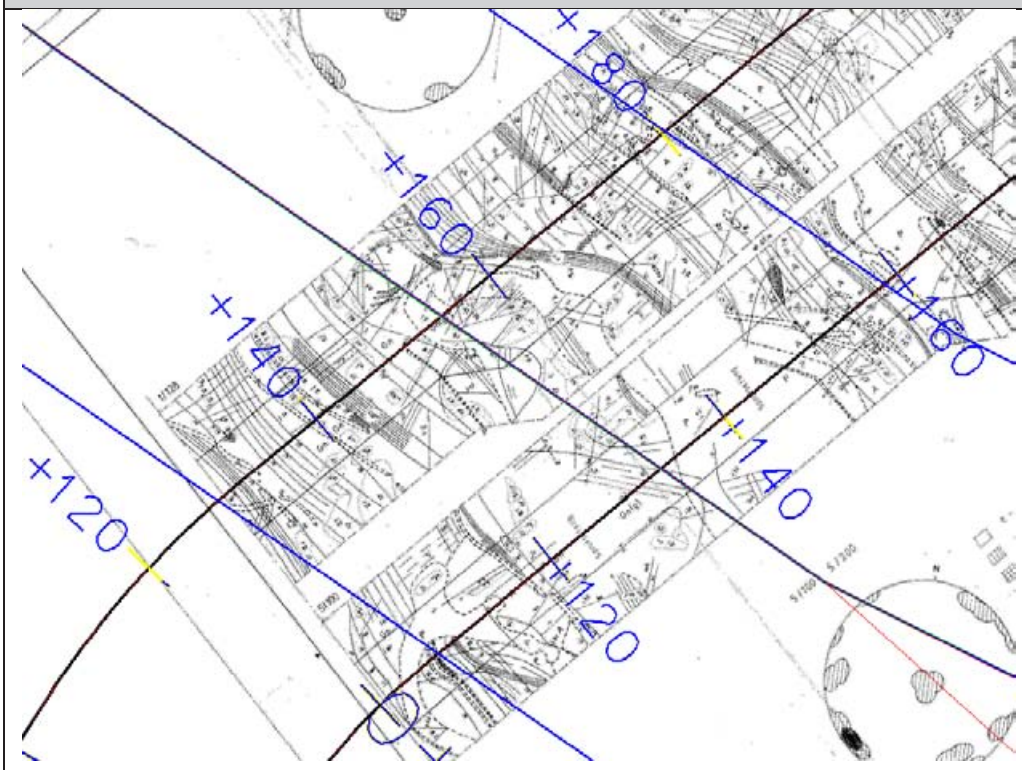

Deformation zone ZFMWNW3262

Borehole and tunnel intersections (metres along borehole/tunnel)

KFR103: 180–182.5 m (DZ3 180–182.5 m)
KFR106: 67–73 m (DZ3 67–73 m)

Deformation style, alteration and geometry

Deformation style: Brittle. Minor ductile and brittle-ductile shear zones present in KFR106 DZ3 and KFR103 DZ3, respectively

Alteration: Locally red-stained bedrock with fine-grained hematite dissemination

Strike/dip (span) right-hand-rule: 116 / 86 (±10 / ±10)

Trace length at ground surface (span): 610 m (300−1000 m)

Model thickness (span) : 2 m (<1−3 m)

Confidence in existence: High

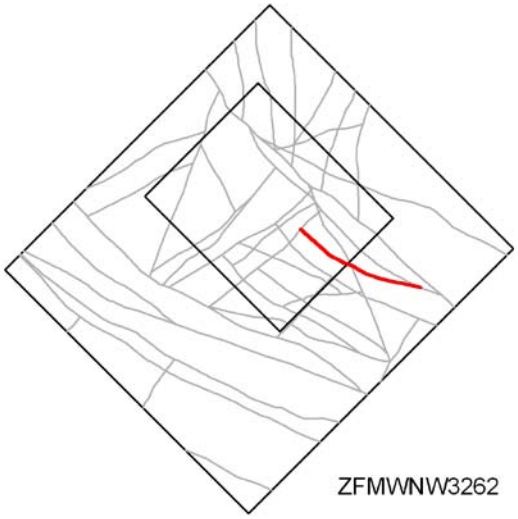

Modelling procedure*:* The position of the zone on the ground surface is based on magnetic lineament MSFR08105 in SFR model version 1.0, itself a modification of lineament MFM3262G from /Isaksson et al. 2007/. The earlier number has been retained in the zone name to assist traceability. There has been an extension to the WNW, through an area where the magnetic field is disturbed, to allow termination at zone ZFMNE3137. Thickness is based on the SHI PDZ borehole intercepts. Forward modelling of magnetic data along profile 2 (Appendix 6) indicates a very steep dip to the north-east whereas inversion modelling indicates a vertical to sub-vertical dip towards the south-west that corresponds to the modelled geometry.

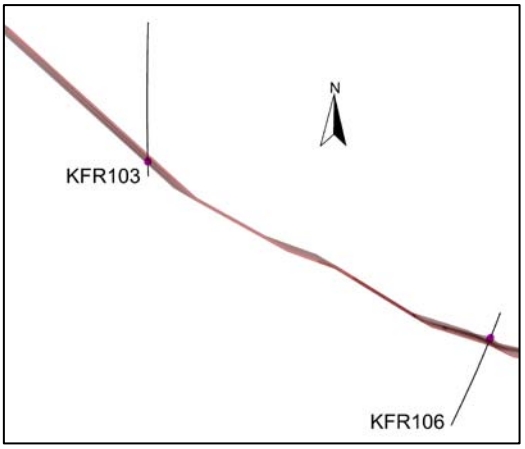

ZFMWNW3262, looking down dip (sub-vertical) with the relevant SHI PDZs shown as pink cylinders. The modelled zone thickness is 2 m.

Deformation zone ZFMWNW3262

Fractures in the deformation zone

General characteristics

Fracture orientation:

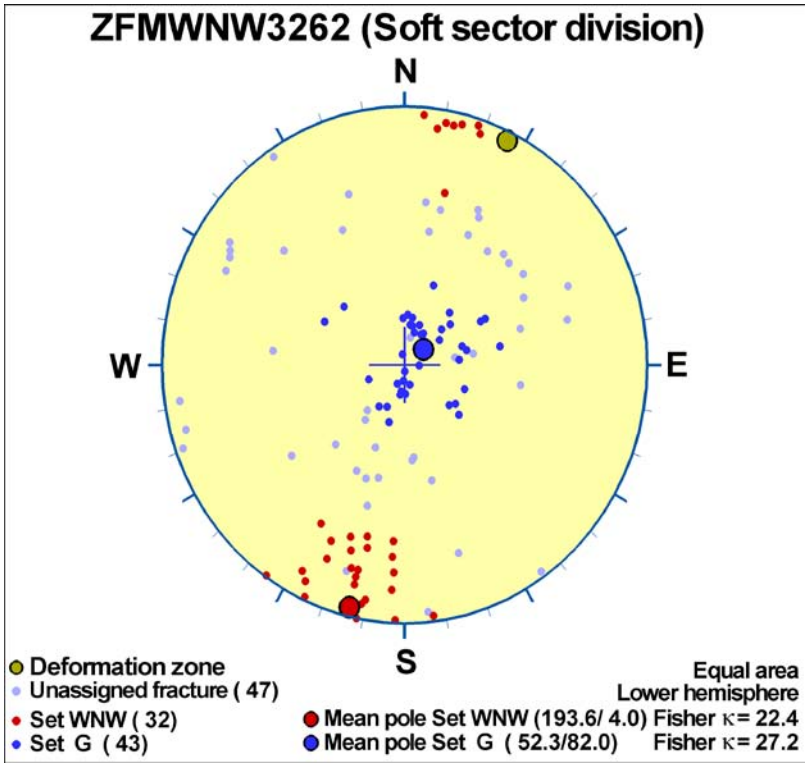

Fracture frequency: Open 19 m^{-1}, Sealed 20 m^{-1}

Fracture filling mineralogy:

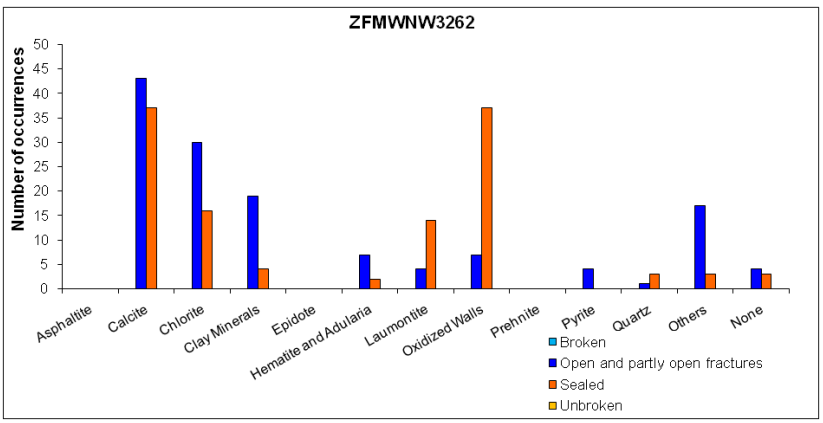

Deformation zone ZFMWNW3262

KFR106 DZ3 (67–73 m)

BOREHOLE INTERCEPT DETAILS

Borehole intersections for ZFMWNW3262				
BH	**Geometrical Intercept**		**Target intercept**	
	Sec_up BH length (m) [z (-m)]	**Sec_low BH length (m) [z (-m)]**	**Sec_up BH length (m) [z (-m)]**	**Sec_low BH length (m) [z (-m)]**
KFR103	178.46 [141.30]	183.59 [145.39]	180	182.5

DZ3 180–182.5 m: Increased frequency of open fractures and two crushed intervals at 180.69–180.73 and 181.89–182.01 m. Three intervals of core loss at 181.16–181.22, 181.28–181.40 and 181.96–182.00 m. Fracture apertures 0.5 mm or less. Faint to moderate oxidation. Predominant minerals in open fractures and crushed intervals are chlorite, calcite, clay minerals, iron hydroxide and muscovite. Significantly decreased bulk resistivity and magnetic susceptibility along the entire section. Metagranite-granodiorite (101057), pegmatitic granite (101061) and amphibolite (102017). Confidence level = 3.

An isolated cluster of flow anomalies at 180.7–187.9 m. The flow anomalies correspond to crushes and core losses. Total transmissivity of $1 \cdot 10^{-5}$ m^2/s.

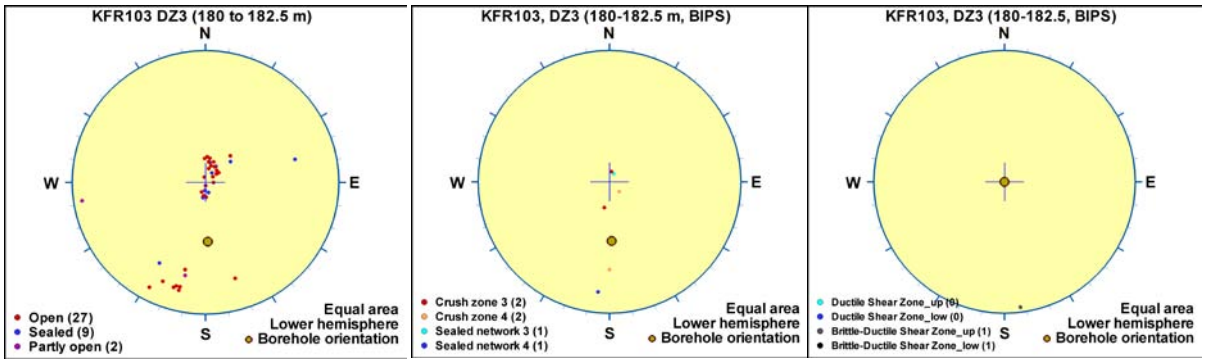

Borehole intersections for ZFMWNW3262

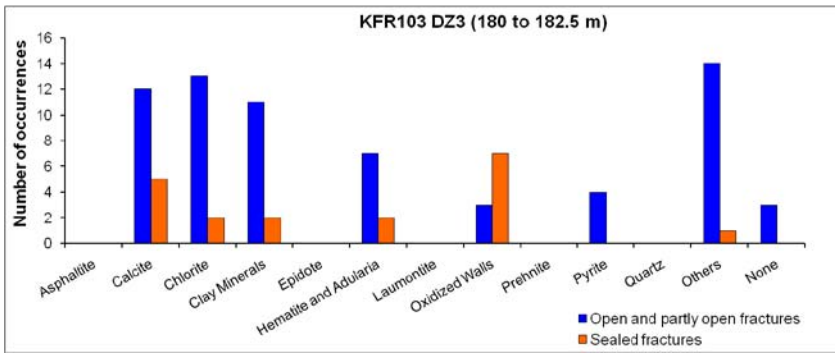

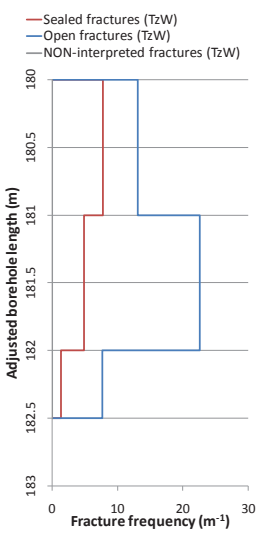

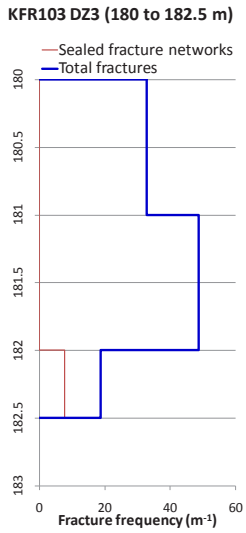

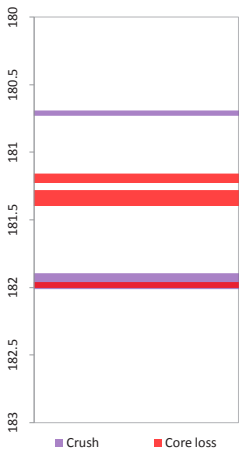

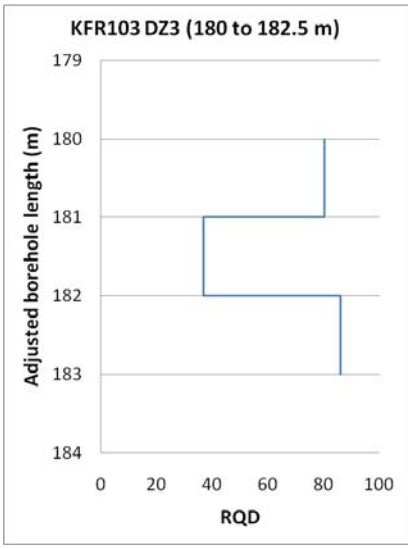

BH	Geometrical Intercept		Target intercept	
	Sec_up BH length (m) [z (-m)]	Sec_low BH length (m) [z (-m)]	Sec_up BH length (m) [z (-m)]	Sec_low BH length (m) [z (-m)]
KFR106	67.04 [61.90]	73.35 [69.69]	67	73

DZ3 67–73 m: Locally increased frequency of open and sealed fractures. One minor crush at 69.58–69.61 m and one ductile shear zone at 69.45–70.19 m (256°/44°). Fracture apertures generally between 0.5 and 1.5mm with one example up to 12 mm. No alteration. Predominant minerals in open fractures are calcite, chlorite, clay minerals, laumontite and oxidized walls. In sealed fractures calcite, oxidized walls, laumontite and chlorite. One radar reflector interpreted without orientation at 72 m. A few narrow low resistivity anomalies and one distinct fluid temperature anomaly, that in combination indicate the occurrence of water bearing fractures. Metagranite-granodiorite (101057), felsic to intermediate metavolcanic rock (103076) and pegmatitic granite (101061). Confidence level = 3.

Very high transmissivity of the interval 68–73 m. A number of flow anomalies, with the dominating anomaly at 68.3 m. The total transmissivity of the section is $3 \cdot 10^{-5}$ m^2/s.

Borehole intersections for ZFMWNW3262

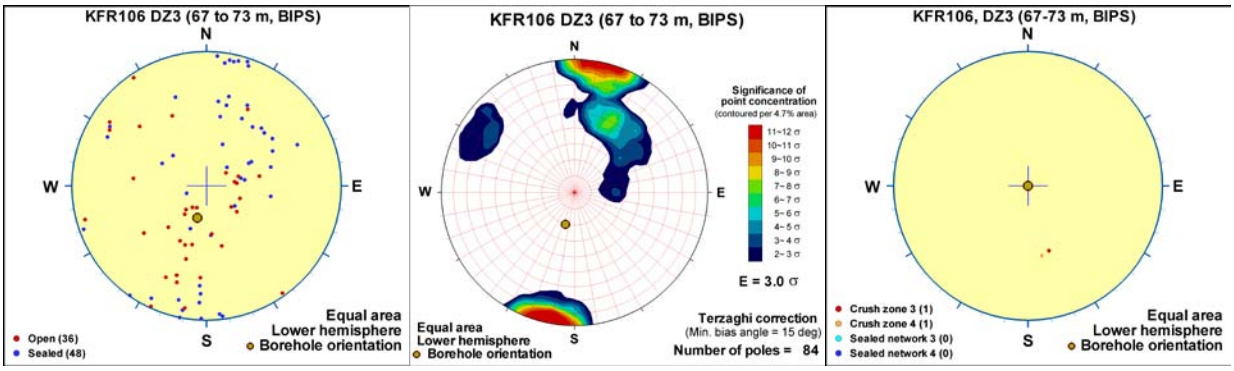

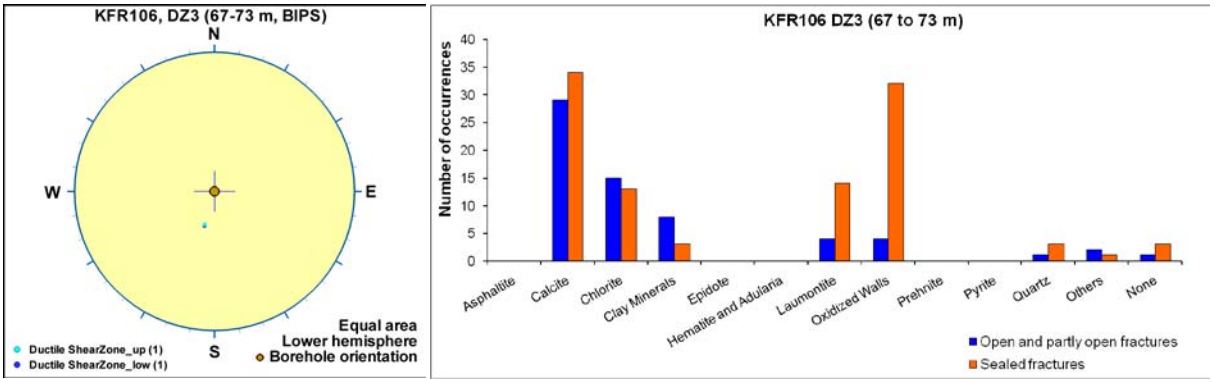

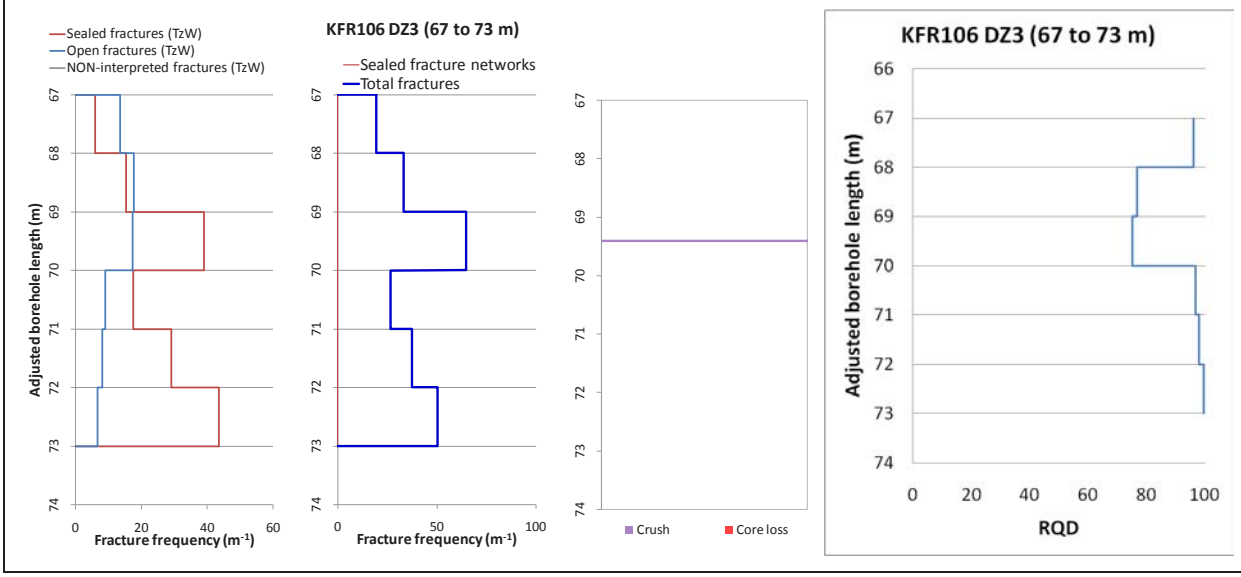

Deformation zone ZFMWNW3267

Borehole and tunnel intersections (metres along borehole/tunnel)

KFR104: 396–454.57 m (DZ5 396–405 m and DZ6 447–454.57 m)
KFR105: 258–283 m (DZ4 258–283 m)

Deformation style, alteration and geometry

Deformation style: Brittle. Minor cohesive breccia and cataclasite in target intercept along KFR104

Alteration: Locally red-stained bedrock with fine-grained hematite dissemination, argillization, laumontitization and epidotization

Strike/dip (span) right-hand-rule: 122 / 90 (±5 / ±10)

Trace length at ground surface (span): 698 m (500−1000 m)

Model thickness (span): 18 m (2−20 m)

Confidence in existence: High

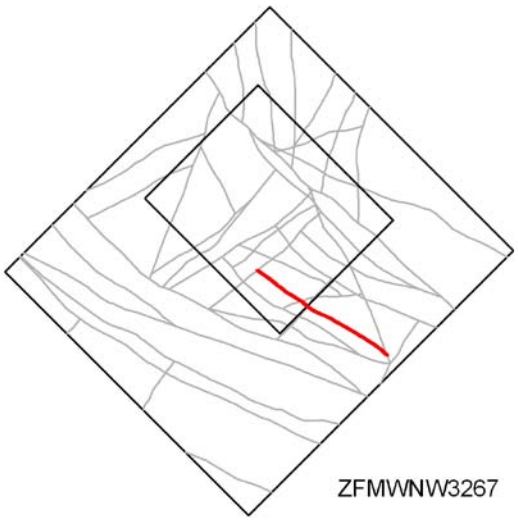

Modelling procedure*:* In the current SFR model version 1.0, this zone is based on a modification of the Forsmark stage 2.3 lineament MFM3267G /Isaksson et al. 2007/. In the SFR model version 0.1 lineament interpretation, this lineament was replaced by MSFR08121 and MSFR08115. The dip of the zone is based on a link with the borehole interceptions in KFR104 and KFR105. The forward modelling of magnetic data along profile 1 (see Appendix 6) data suggests a sub-vertical to a very steep dip to the north-east, while profile 39 modelling suggests a vertical dip.

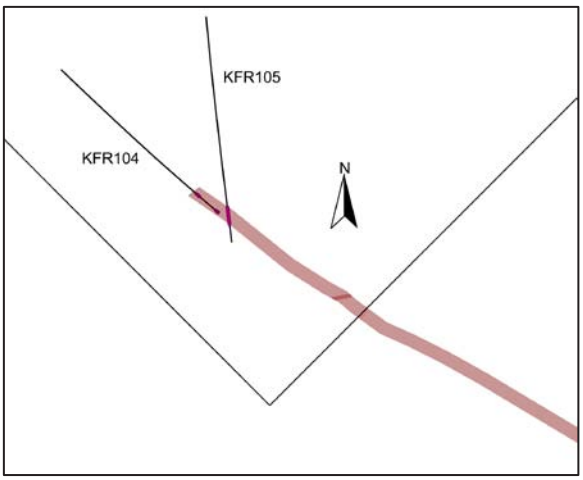

Plan view of ZFMWNW3267 with the relevant SHI PDZs shown as pink cylinders. The modelled zone thickness is 18 m

Deformation zone ZFMWNW3267

Fractures in the deformation zone

General characteristics

Fracture orientation:

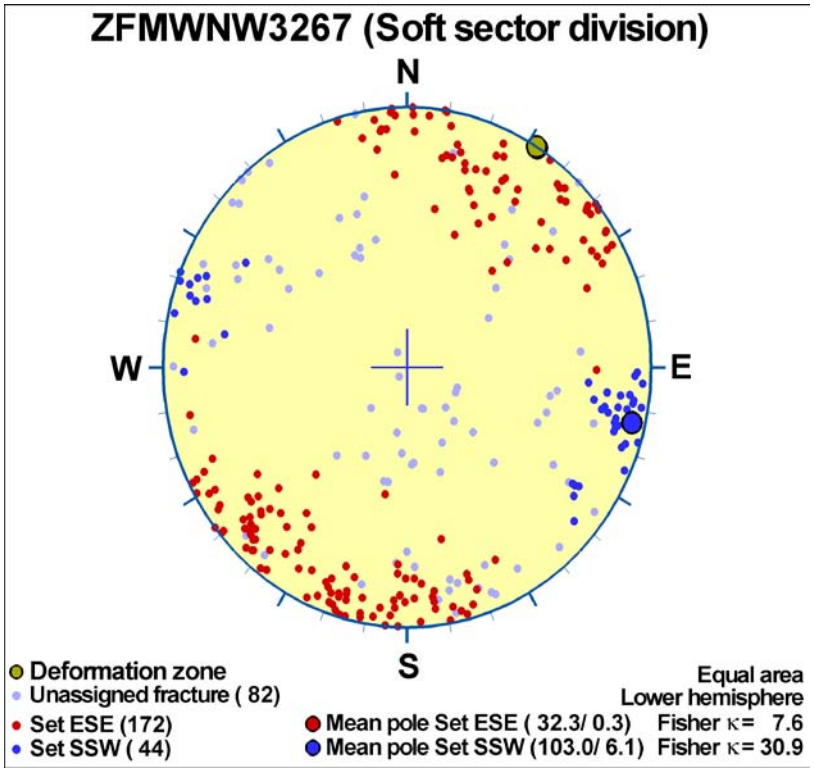

Fracture frequency: Open 10 m^{-1}, Sealed 26 m^{-1}

Fracture filling mineralogy:

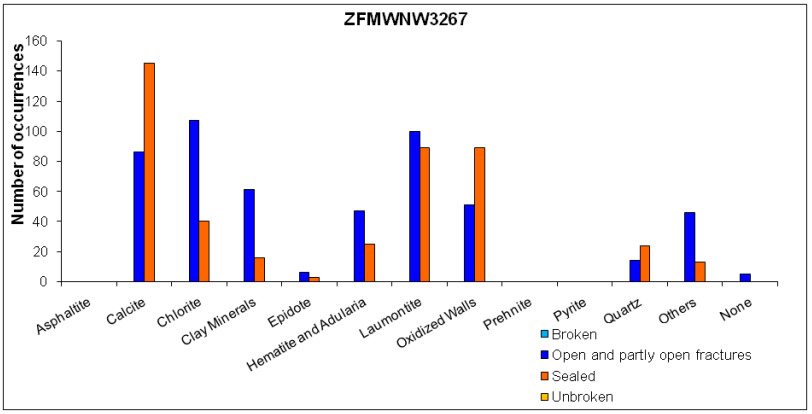

KFR105 DZ4 (258–283 m)

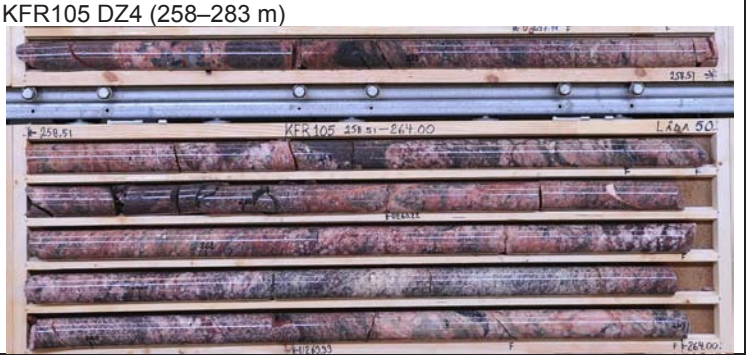

Deformation zone ZFMWNW3267

BOREHOLE AND TUNNEL INTERCEPT DETAILS

Borehole intersections for ZFMWNW3267				
BH	**Geometrical Intercept**		**Target intercept**	
	Sec_up BH length (m) [z (-m)]	**Sec_low BH length (m) [z (-m)]**	**Sec_up BH length (m) [z (-m)]**	**Sec_low BH length (m) [z (-m)]**
KFR104	388.50 [302.51]	eoh [351.72]	396	454.57

Comment: Fracture plots show that NW striking fractures dominate the interval between DZ5 and DZ6.

DZ5 396–405 m: Increased frequency of open fractures. One minor cataclasite along the lower limit of the possible zone at 400.39–400.41 m. Fracture apertures up to 2 mm. Several moderately altered open fractures. Varying degrees of argillization and epidotization in the lower half of the interval. Predominant minerals in open fractures are clay minerals, chlorite and calcite. Low electric resistivity and one minor caliper anomaly. Pegmatitic granite (101061) and amphibolite (102017). Confidence level = 3.

One single flow anomaly (T = $1 \cdot 10^{-8}$ m^2/s) at 405 m. This is the only flow anomaly in the borehole below 350 m.

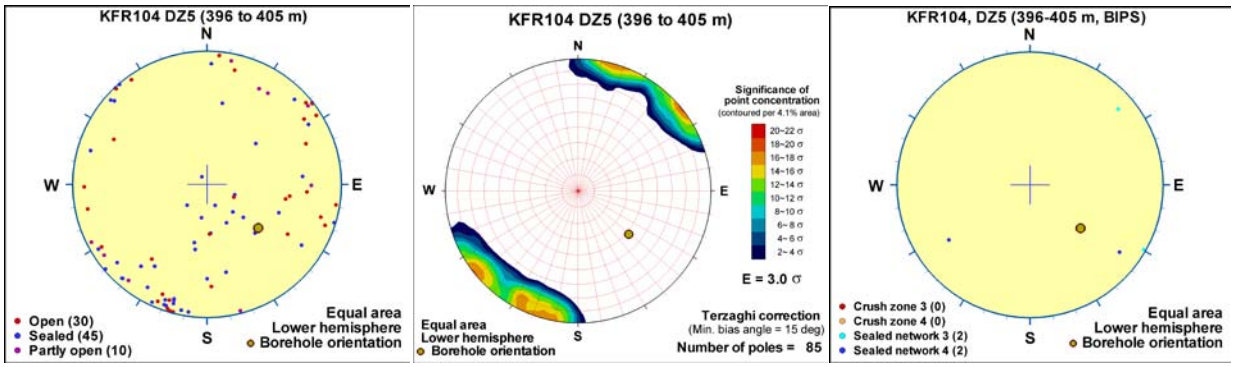

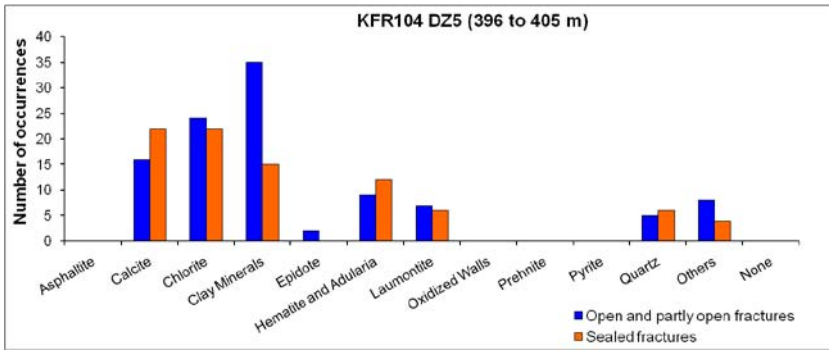

Borehole intersections for ZFMWNW3267

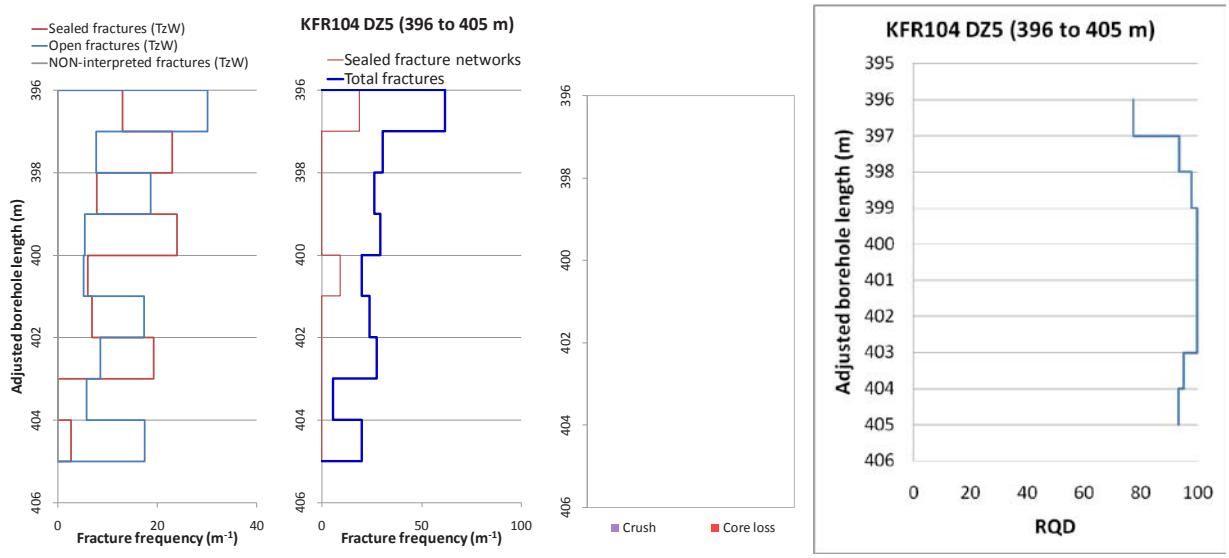

DZ6 447–454.57 m: Increased frequency of sealed fractures and sealed fracture network in the upper half of the interval. One brecciated interval at 452.97–453.05 m. Locally faint to strong oxidation and laumontization. No BIPS image of the interval. Predominant minerals in sealed fractures are laumontite, calcite and chlorite. Low electric resistivity and one major caliper anomaly. Fine to medium grained granite (111058), pegmatitic granite (101061) and metagranite-granodiorite (101057). Confidence level = 3.

No hydraulic data from this interval.

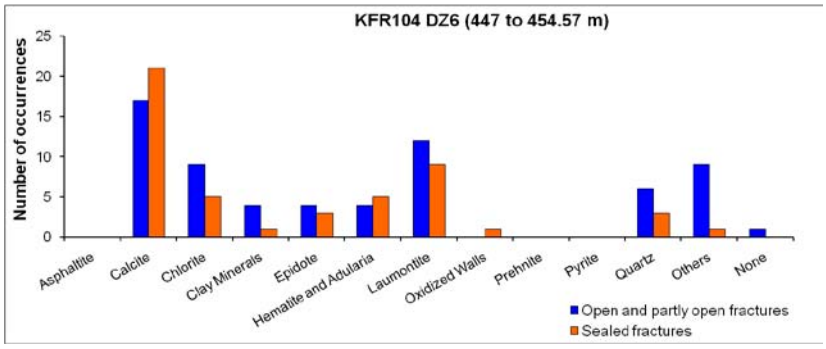

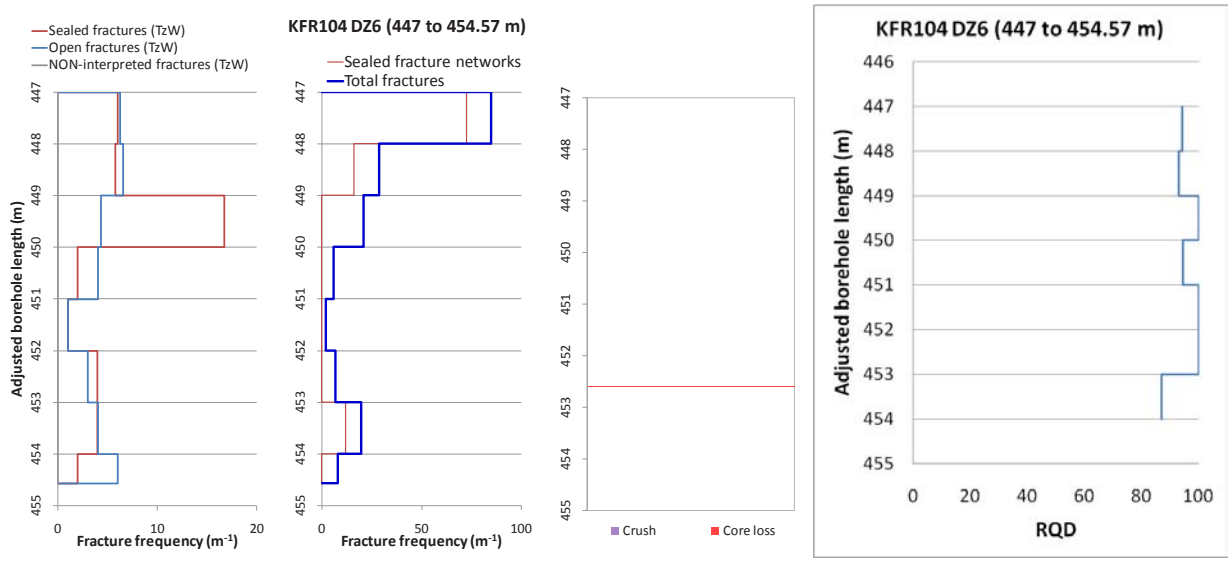

Borehole intersections for ZFMWNW3267				
BH	Geometrical Intercept		Target intercept	
	Sec_up BH length (m) [z (-m)]	Sec_low BH length (m) [z (-m)]	Sec_up BH length (m) [z (-m)]	Sec_low BH length (m) [z (-m)]
KFR105	257.84 [149.34]	282.99 [153.16]	258	283

DZ4 258–283 m: Increased frequency of open fractures and especially sealed fractures along with sealed fracture networks. Two minor crushes at 259.80–259.82 and 270.31–270.38 m. Zone core defined at 279.7–281.0 m. Fracture apertures in general up to 0.5 mm. Very local moderate to strong oxidation and moderate laumontite alteration. Predominant fracture minerals in open fractures are laumontite, chlorite, calcite, oxidized walls, hematite and clay minerals and in sealed fractures laumontite, calcite and oxidized walls. Several significant low resistivity anomalies (< 2,000 Ohm-m), and two distinct anomalies in the fluid temperature data indicating water-bearing fractures. In the section 278–286 m there are significant caliper anomalies. One radar reflector at 268.6 m oriented 316°/33° or 039°/45°. Pegmatitic granite (101061), fine- to medium-grained metagranite-granodiorite (101057) and felsic to intermediate metavolcanic rock (103076). Confidence level = 3.

Low transmissivity of the section (T = $4 \cdot 10^{-8}$ m^2/s). The main flow anomaly is located at 267.3 m.

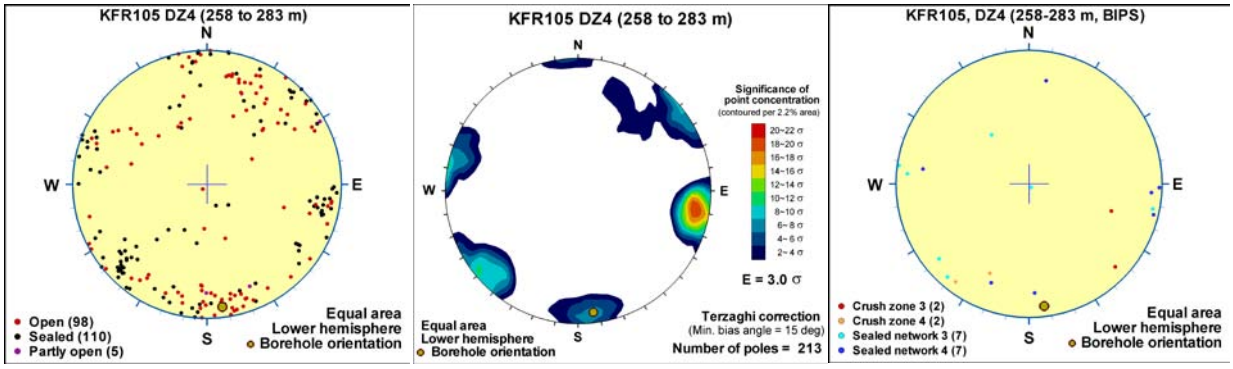

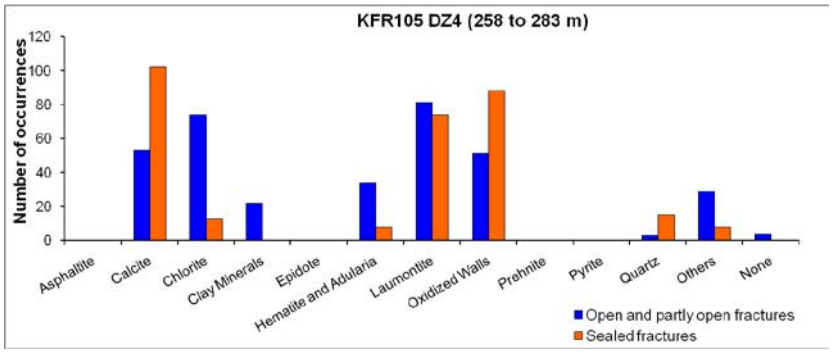

Borehole intersections for ZFMWNW3267

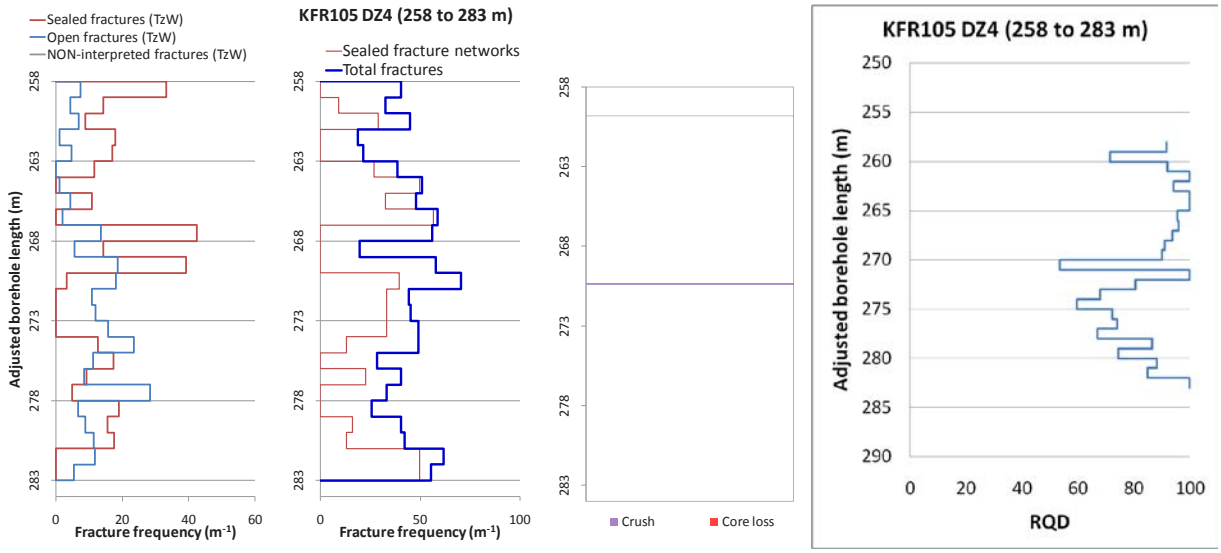

Deformation zone ZFMWNW3268

Borehole and tunnel intersections (metres along borehole/tunnel)

None

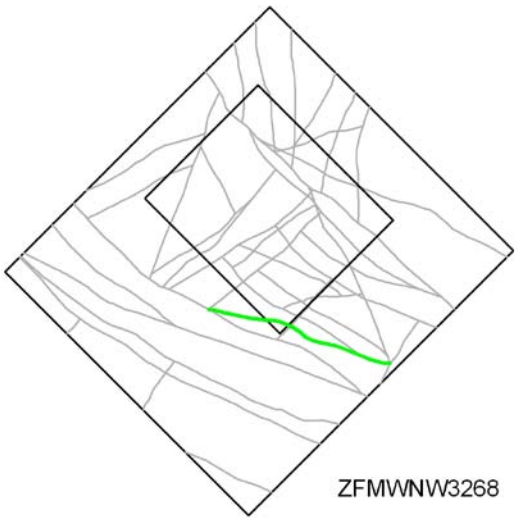

Deformation style, alteration and geometry

Deformation style: Ductile and brittle (no direct evidence – inferred association with other WNW-ESE trending deformation zones)

Alteration: No data

Strike/dip (span) right-hand-rule: 109 / 90 (±5 / ±10)

Trace length at ground surface (span): 861 m (700−870 m)

Model thickness: 5 m*

Confidence in existence: Medium

Modelling procedure*:* The position of the zone at the ground surface is based on magnetic lineament MSFR80006 (SFR model version 1.0), itself an update of lineament MFM3268G /Isaksson et al. 2007/, with a further extension to the WNW to allow termination at ZFMNE3137 and ZFMWNW1035. The vertical dip is a default value.

*The modelled thickness is a 1% default value based on the traceable zone length of 709 m. However, in the model the zone geometry has been extended to terminate at ZFMWNW1035 to ensure connectivity giving an rvs modelled length of 861 m.

Fractures in the deformation zone

General characteristics

Fracture orientation: No data

Fracture frequency: No data

Fracture filling mineralogy: No data

Deformation zone ZFMWNW8042

Borehole and tunnel intersections (metres along borehole/tunnel)

KFR105: 170.8–176 m (DZ3 170.8–176 m)

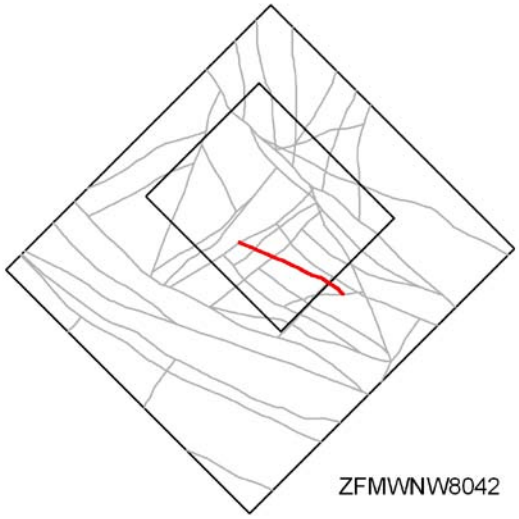

Deformation style, alteration and geometry

Deformation style: Brittle

Alteration: Locally red-stained bedrock with fine-grained hematite dissemination and chloritization of amphibolite.

Strike/dip (span) right-hand-rule: 116 / 89 (±5 / ±10)

Trace length at ground surface (span): 524 m (250−800 m)

Model thickness (span): 5 m (1−7 m)

Confidence in existence: High

Modelling procedure*:* The position of the zone at the ground surface is based on magnetic lineament MSFR08042 (SFR model version 1.0) with a further extension to the WNW to allow termination at ZFMENE3115. The zone thickness is based on the borehole intercept and the dip is based on linking the lineament to the borehole intercept. Forward modelling of magnetic data along profiles 12 and 44 supports the vertical dip and limited thickness of the zone, while inversion modelling suggests a very steep dip to the north-east (see Appendix 6)

Fractures in the deformation zone

General characteristics

Fracture orientation:

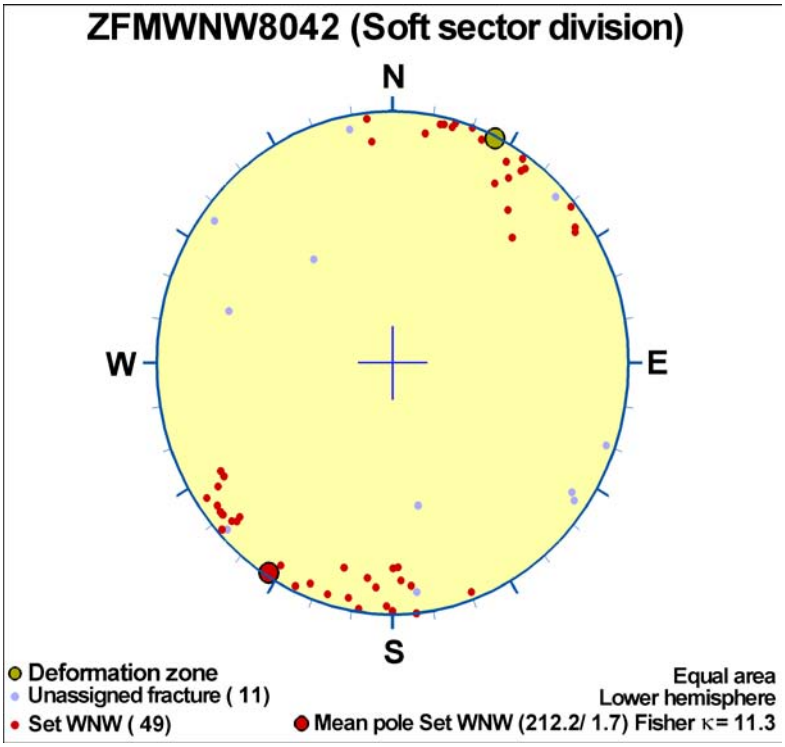

Fracture frequency: Open 14 m^{-1}, Sealed 55 m^{-1}

Deformation zone ZFMWNW8042

Fracture filling mineralogy:

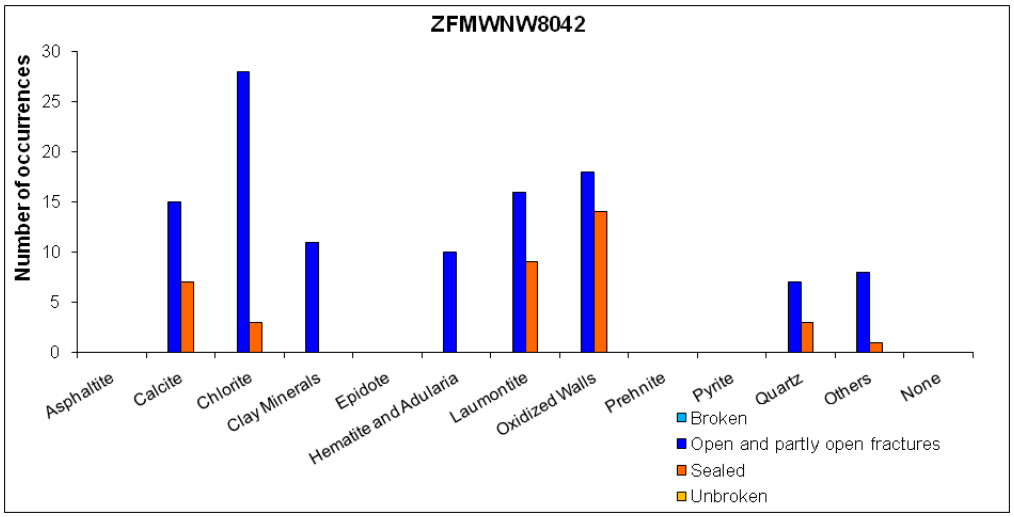

KFR105 DZ3 (170.8–176 m)

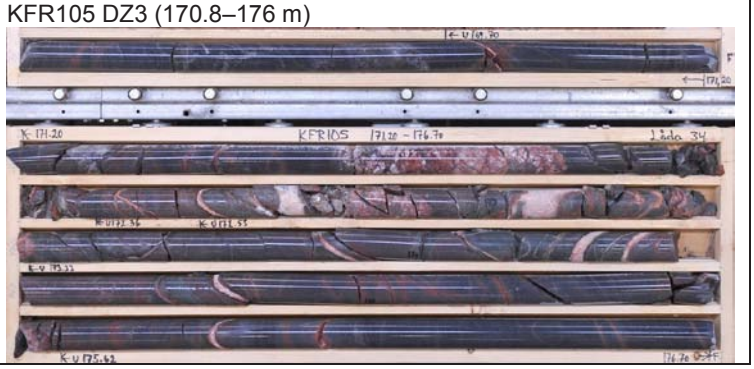

BOREHOLE AND TUNNEL INTERCEPT DETAILS

Borehole intersections for ZFMWNW8042				
BH	**Geometrical Intercept**		**Target intercept**	
	Sec_up BH length (m) [z (-m)]	**Sec_low BH length (m) [z (-m)]**	**Sec_up BH length (m) [z (-m)]**	**Sec_low BH length (m) [z (-m)]**
KFR105	170.49 [135.48]	176.34 [136.42]	170.8	176

SHI DZ3 170.8–176 m: Increased frequency of sealed and open fractures and sealed networks. Zone core defined at 172.5–173.4 m. One minor crush at 172.82–172.86 m and one breccia at 173.11–173.19 m. Fracture apertures in general up to 0.5 mm. Predominant fracture minerals in open fractures are chlorite, oxidized walls, laumontite, calcite and clay minerals and in sealed fractures laumontite, calcite and oxidized walls. Local faint to moderate oxidation and chloritization. The section 172–176 m is characterized by significantly decreased bulk resistivity, < 1,000 Ohm-m in the zone core and a distinct anomaly in the fluid temperature data indicating a water bearing fracture. One distinct radar reflector at 173.6 m oriented 270°/38°. Felsic to intermediate metavolcanic rock (103076) and pegmatitic granite (101061). Confidence level = 3.

Increased frequency of flow anomalies, the two most significant at 172.7 and 173.0 m. The total transmissivity of the section is moderate, about $3 \cdot 10^{-7}$ m^2/s.

Borehole intersections for ZFMWNW8042

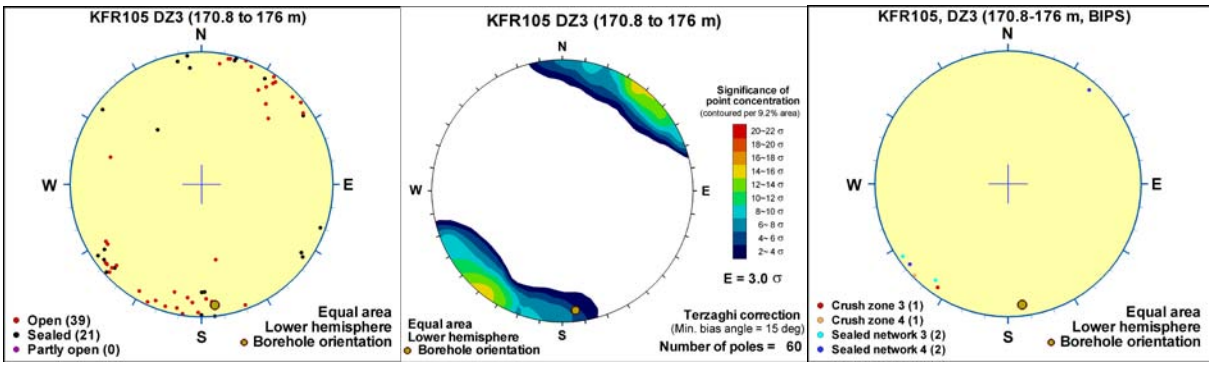

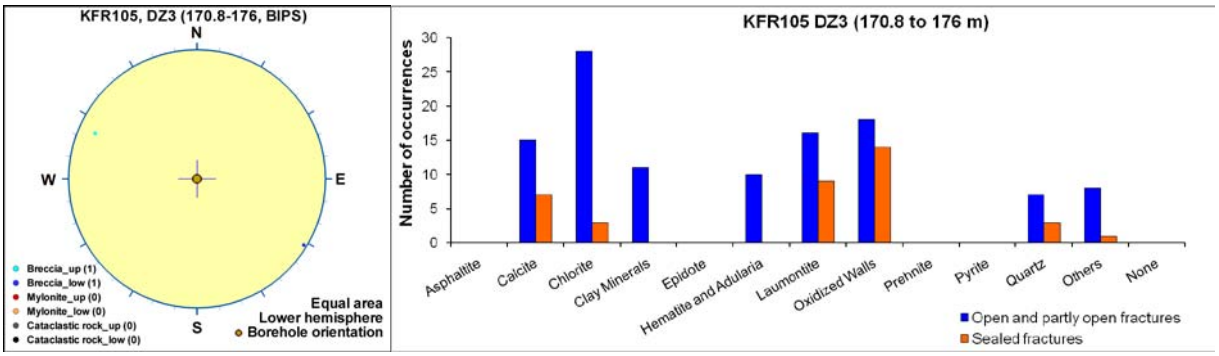

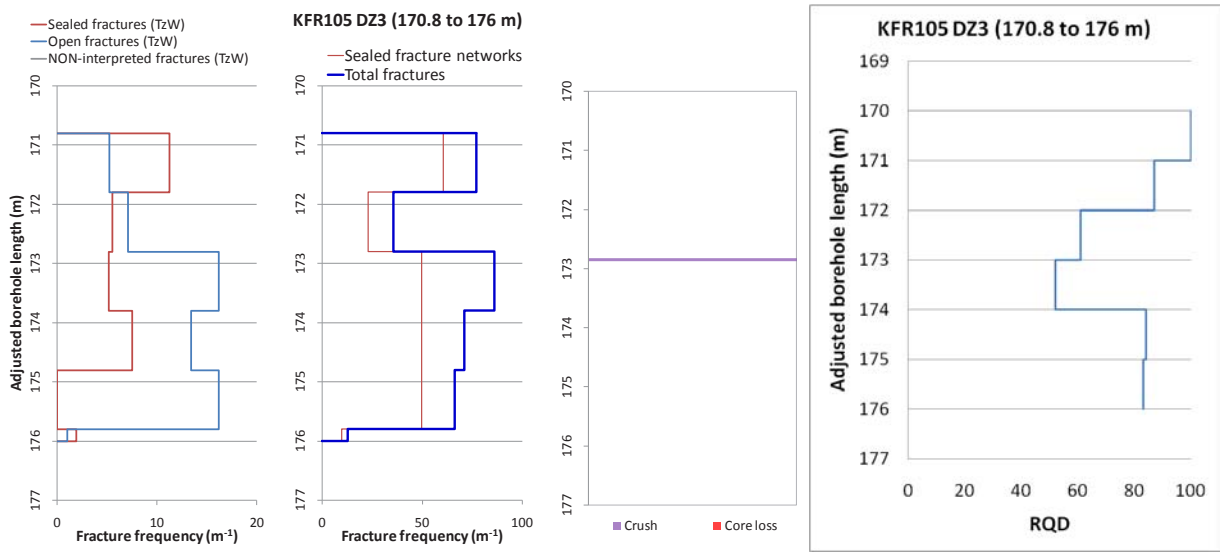

Deformation zone ZFMWNW8043

Borehole and tunnel intersections (metres along borehole/tunnel)

None

Deformation style, alteration and geometry

Deformation style: Brittle (no direct evidence – inferred association with other neighbouring WNW-ESE trending deformation zones)

Alteration: No data

Strike/dip (span) right-hand-rule: 124 / 90 (±5 / ±10)

Trace length at ground surface (span): 775 m (625−925 m)

Model thickness: 10 m (1% default)

Confidence in existence: Medium

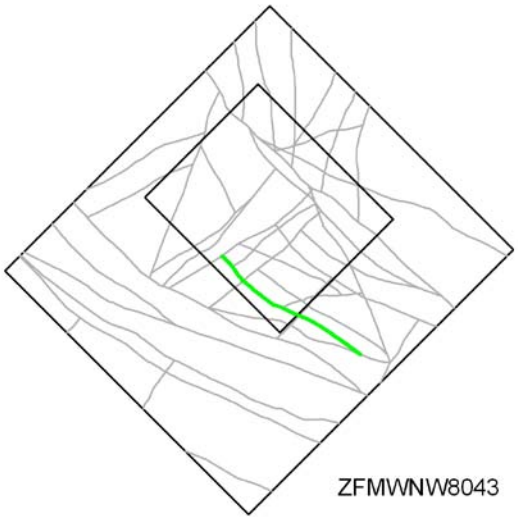

Modelling procedure*:* The position of the zone at the ground surface is based on version 1.0 magnetic lineament MSFR10002 that replaces version 0.1 lineaments MSFR08043 and MSFR08045. The earlier number has been kept in the zone name to assist traceability between different model versions. The modelled dip and thickness are default values.

Fractures in the deformation zone

General characteristics

Fracture orientation: No data

Fracture frequency: No data

Crush zone: No data

Fracture filling mineralogy: No data

Steeply dipping NNW to N-S deformation zones

Deformation zone ZFMNNW0999

Borehole and tunnel intersections (metres along borehole/tunnel)

None

Deformation style, alteration and geometry

Deformation style: No data

Alteration: No data

Strike/dip (span) right-hand-rule: 170 / 90 (± 5 / ±10)

Trace length at ground surface (span): 692 m (692−>692 m)

Model thickness: 5 m (1% default)

Confidence in existence: Medium

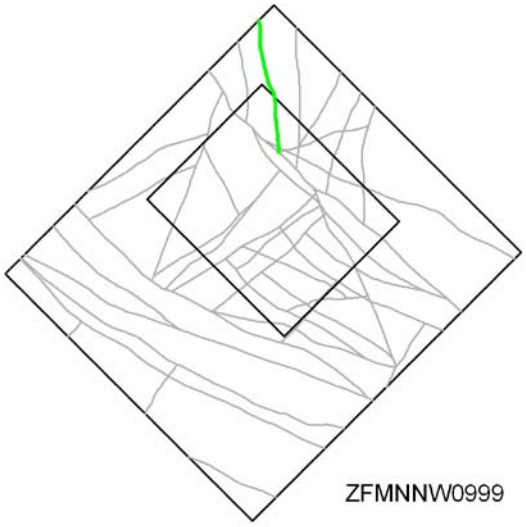

Modelling procedure: ZFMNNW0999 is based on the magnetic lineament MFM0999G in the Forsmark stage 2.3 interpretation /Isaksson et al. 2007/. The zone has a length of 692 m terminating at ZFMNW0805A in the south and extending outside of the regional model area to the north, where MFM0999G terminates at lineament MSFR08078 in the SFR model version 1.0 (an update of Forsmark stage 2.3 lineament MFM3149G in /Isaksson et al. 2007/). The modelled zone geometry results in an intersection in KFR08 SHI DZ2. However, this interval is inferred as being dominated by ZFMNW0805A and no exclusive evidence for the existence of ZFMNNW0999 has been identified. For this reason, ZFMNNW0999 has been classed as medium confidence. The general thickness and vertical to sub-vertical dip are supported by the forward modelling of magnetic data along profiles 5 and 6 (see Appendix 6).

Fractures in the deformation zone

General characteristics

Fracture orientation: No data

Fracture frequency: No data

Fracture filling mineralogy: No data

BOREHOLE AND TUNNEL INTERCEPT DETAILS

Borehole intersections for ZFMNNW0999

BH	Geometrical Intercept		Target intercept	
	Sec_up BH length (m) [z (-m)]	Sec_low BH length (m) [z (-m)]	Sec_up BH length (m) [z (-m)]	Sec_low BH length (m) [z (-m)]
KFR08	75.72 [92.62]	81.46 [93.12]	-	-

Comment: This interval is inferred as being dominated by ZFMNW0805A and no exclusive evidence for the existence of ZFMNNW0999 has been identified.

Deformation zone ZFMNNW1034

Borehole and tunnel intersections (metres along borehole/tunnel)

HFR106: 158–182 m (DZ2 158–162 m and DZ3 177–182 m)
KFR101: 13.72–88 m (DZ1 13.72–88 m)
KFR106: 256–266 m (DZ7 256–266 m)

Deformation style, alteration and geometry

Deformation style: Brittle, including minor cohesive breccias. Inferred brittle-ductile shear zone registered in HFR106 DZ3. Ductile and brittle-ductile shear zones present in KFR101 DZ1.

Alteration: Locally red-stained bedrock with fine-grained hematite dissemination. Very locally argillization and epidotization

Strike/dip (span) right-hand-rule: 337 / 78 (±5 / ±10)

Trace length at ground surface (span): 883 m (880−1130 m)

Model thickness (span): 17 m (5−20 m)

Confidence in existence: High

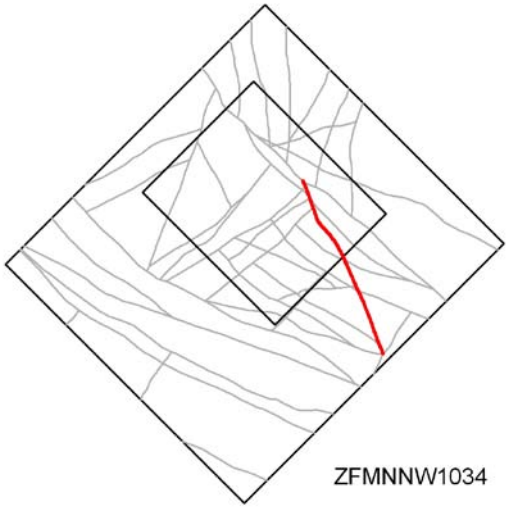

Modelling procedure*:* Based on magnetic lineament MFM1034G in Forsmark stage 2.3 /Isaksson et al. 2007/ that has been adjusted slightly and updated as lineaments MSFR08100 and MSFR08101 in SFR model version 1.0. Further modification took place in the modelling work at the north-west end, based on information from KFR101 DZ1, where the zone passes through the magnetically disturbed pier area. The general thickness and steep dip to the north-east are supported by the forward modelling of magnetic data along profile 2 (see Appendix 6).

Fractures in the deformation zone

General characteristics

Fracture orientation:

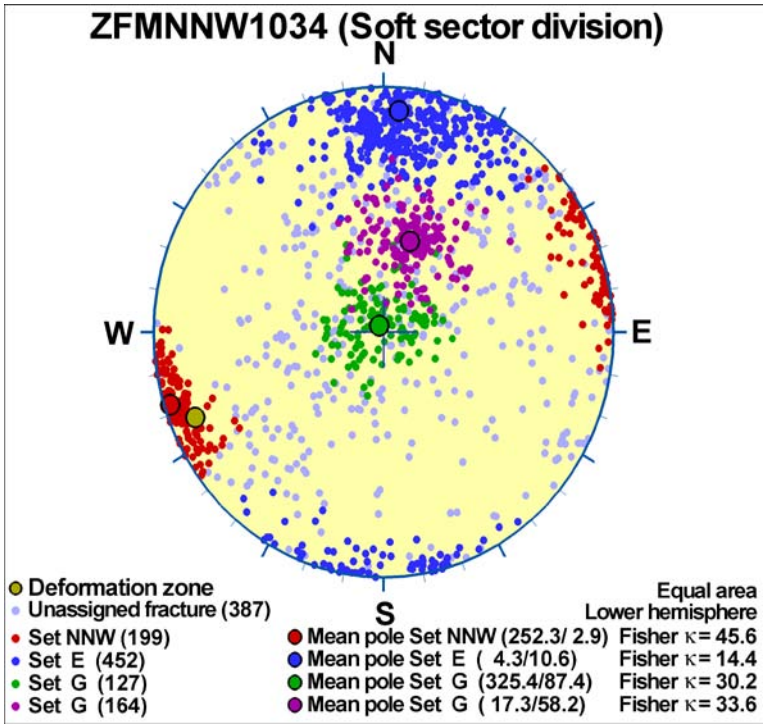

Fracture frequency: Open 9 m^{-1}, Sealed 43 m^{-1}

Deformation zone ZFMNNW1034

Fracture filling mineralogy:

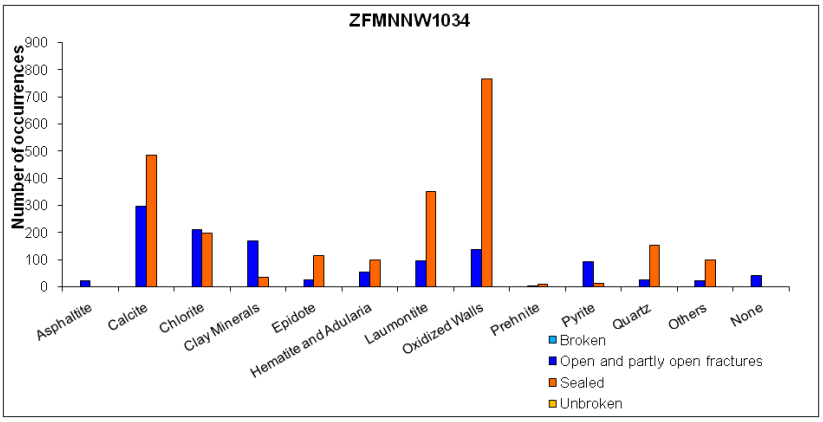

KFR106 DZ7 (256–266 m)

BOREHOLE AND TUNNEL INTERCEPT DETAILS

Borehole intersections for ZFMNNW1034				
BH	**Geometrical Intercept**		**Target intercept**	
	Sec_up BH length (m) [z (-m)]	**Sec_low BH length (m) [z (-m)]**	**Sec_up BH length (m) [z (-m)]**	**Sec_low BH length (m) [z (-m)]**
HFR106	136.61 [110.02]	179.79 [144.56]	158	182

SHI DZ2 158–162 m: No clear indications in the BIPS-image. However, there is a distinct decrease in the bulk resistivity and there are significant caliper anomalies. Metagranite-granodiorite (101057), pegmatitic granite (101061) and felsic to intermediate metavolcanic rock (103076). Confidence level = 1.

No flow anomaly observed in this section (however, there may be flow below the lower measurement limit which was relatively high in this case).

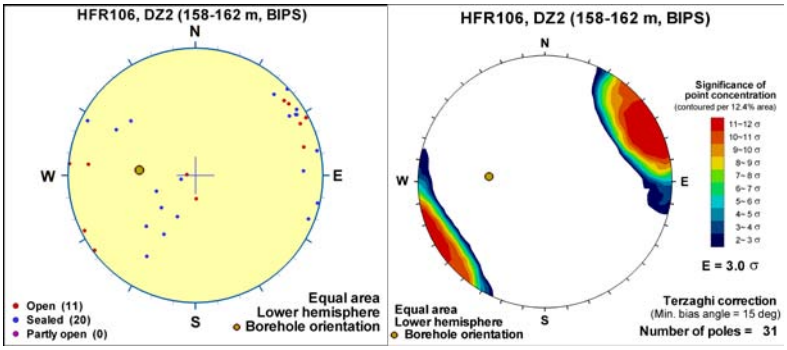

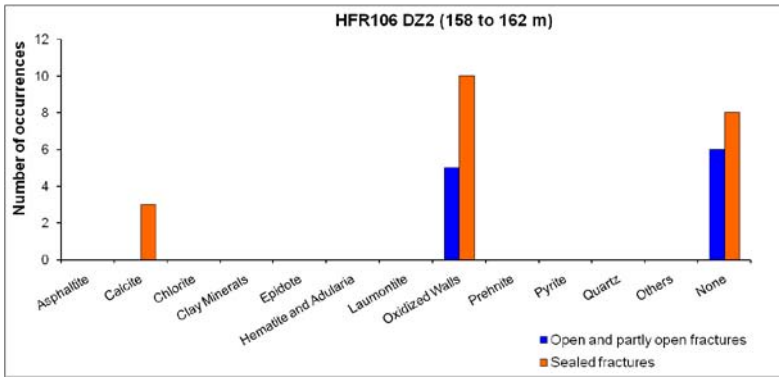

Borehole intersections for ZFMNNW1034

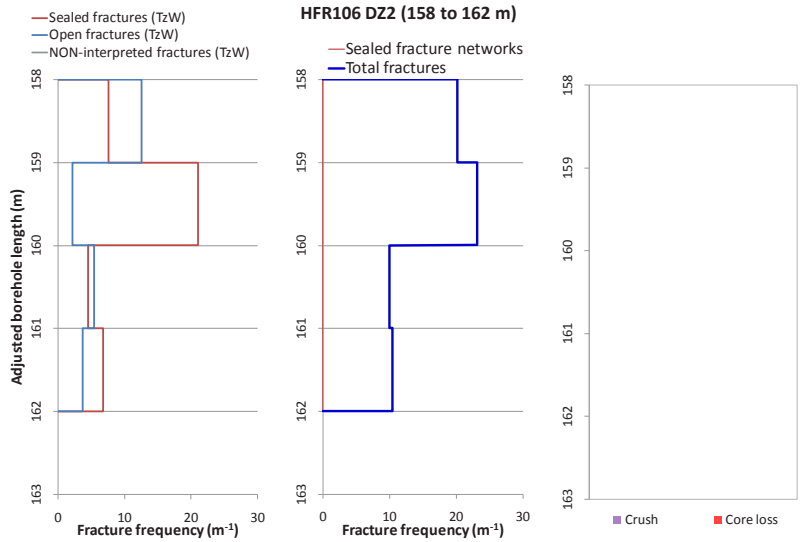

SHI DZ3 177–182 m: Distinct increase in fracture frequency. One brittle-ductile shear zone at 178.05 m (322°/88°) –178.27 m (331°/84°) and one breccia at 178.39 m (332°/82°) –178.74 m (326°/82°). Fracture apertures generally 0.5 to 2 mm, with one example of 8 mm. Locally weak oxidation. At 179.0 m borehole length there is one narrow low resistivity anomaly, one caliper anomaly and a minor but distinct fluid temperature anomaly, that in combination indicate the occurrence of water bearing fractures. Metagranite-granodiorite (101057), pegmatitic granite (101061). Confidence level = 3.

One flow anomaly at 177.3–178.5 m. The transmissivity of the section is very high, $2 \cdot 10^{-5}$ m^2/s.

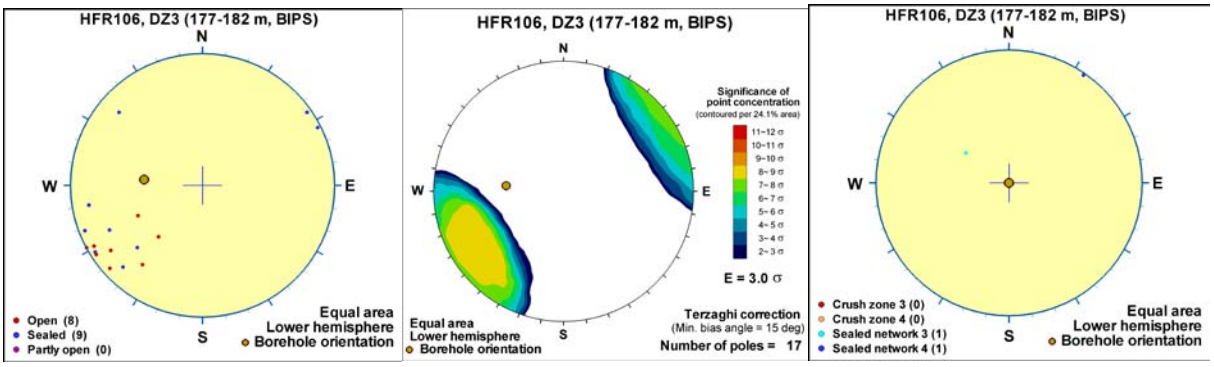

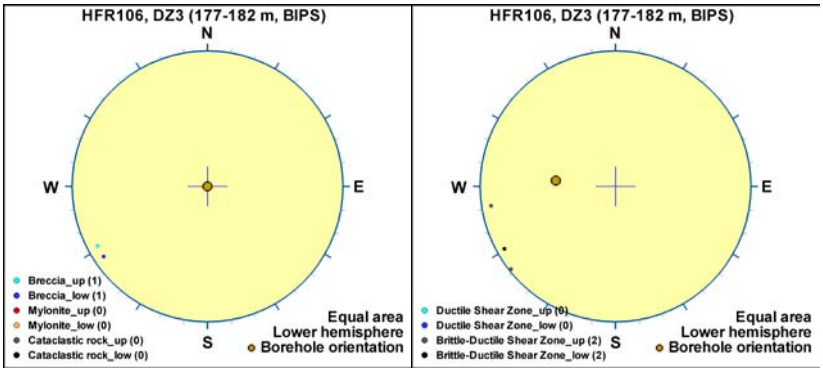

Borehole intersections for ZFMNNW1034

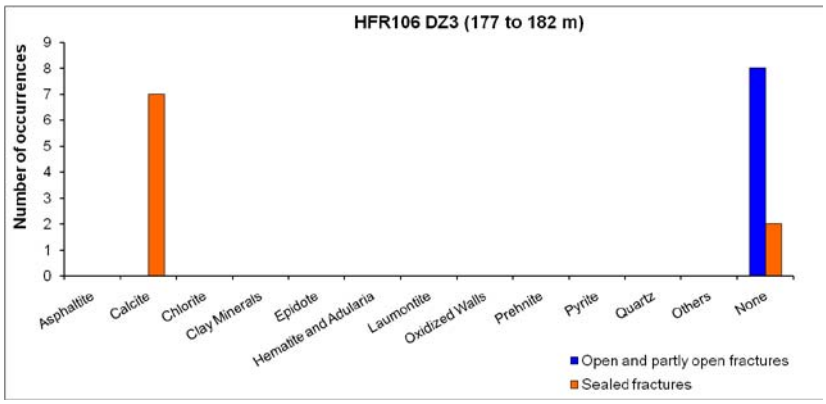

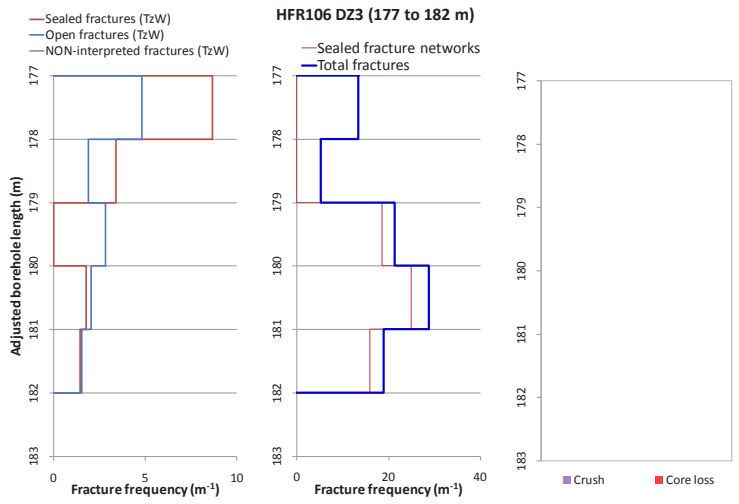

BH	Geometrical Intercept		Target intercept	
	Sec_up BH length (m) [z (-m)]	Sec_low BH length (m) [z (-m)]	Sec_up BH length (m) [z (-m)]	Sec_low BH length (m) [z (-m)]
KFR101	8.42 [4.50]	79.85 [62.90]	13.72	88

SHI DZ1 13.72–88 m: Increased frequency of open fractures, sealed fracture networks and especially sealed fractures. Occasional slickensides. Fractures aperture up to 1.5 mm. Locally faint to medium oxidation. Several minor intervals (< 1 dm) of breccias, cataclasites, mylonite and brittle-ductile shear zones. Predominant minerals in sealed fractures are calcite, laumontite, chlorite, quartz and epidote, and in open fractures are calcite, chlorite, clay minerals, laumontite and pyrite. Decreased resistivity in the section c. 30–50 m and one distinct caliper anomaly at c. 33 m. The magnetic susceptibility is increased along the entire interval defining the deformation zone. Moderately foliated metagranite-granodiorite (101057), amphibolite (102017), pegmatitic granite (101061) and felsic to intermediate metavolcanic rock (103076). Confidence level = 3.

Increased frequency of flow anomalies in the section 14–65 m but no flow anomalies below 65 m. The total transmissivity of the interval is quite high (about $5 \cdot 10^{-6}$ m^2/s if the dominating flow at the lower edge of the casing is removed). The caliper anomaly at c. 33 m corresponds to a single high-transmissive flow anomaly.

Borehole intersections for ZFMNNW1034

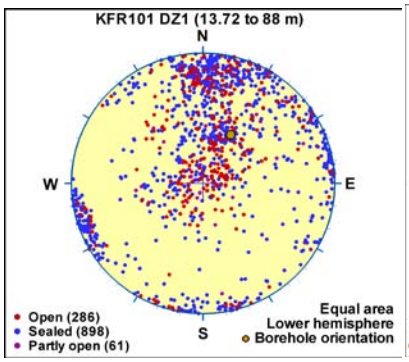

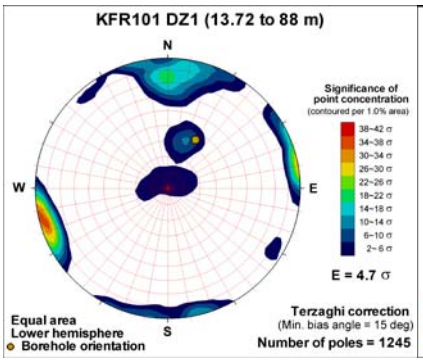

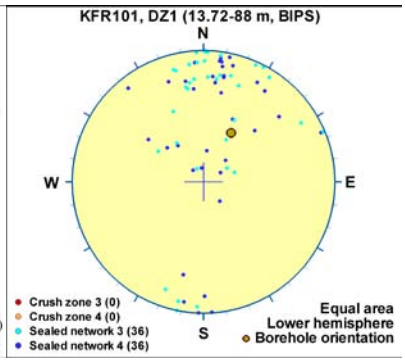

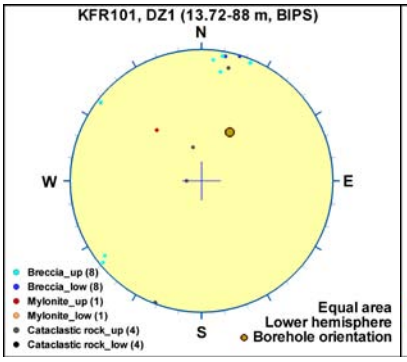

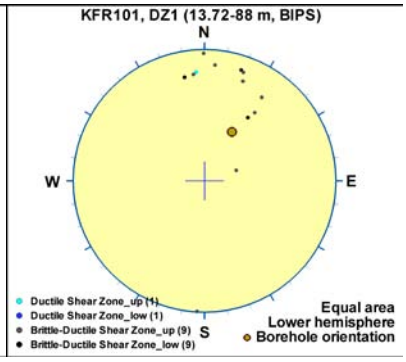

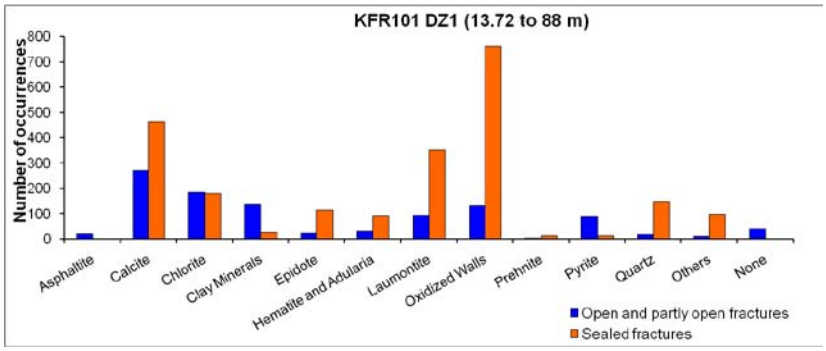

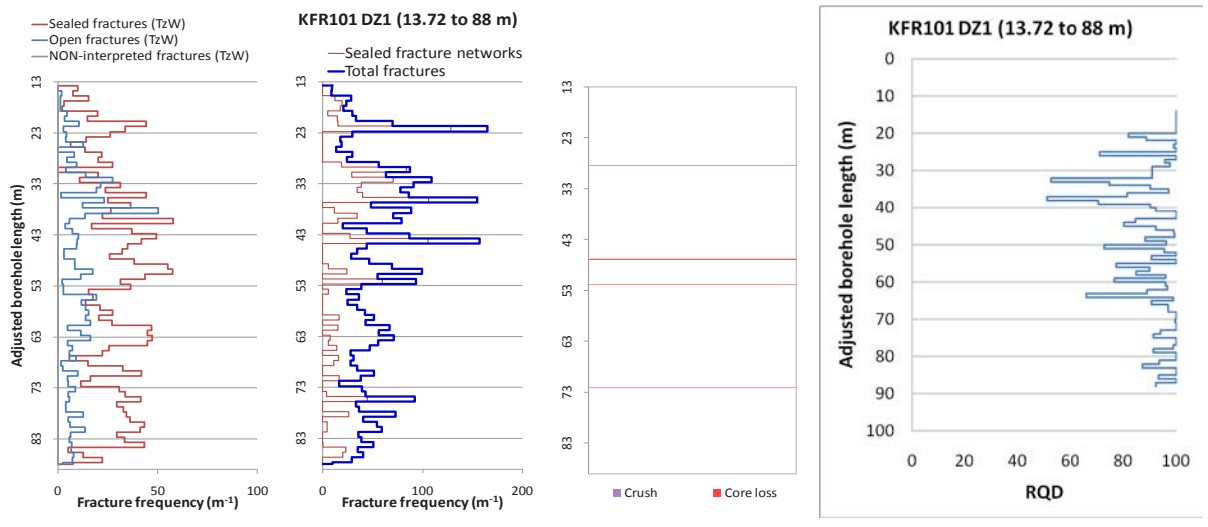

Borehole intersections for ZFMNNW1034				
BH	Geometrical Intercept		Target intercept	
	Sec_up BH length (m) [z (-m)]	Sec_low BH length (m) [z (-m)]	Sec_up BH length (m) [z (-m)]	Sec_low BH length (m) [z (-m)]
KFR106	200.93 [187.19]	271.05 [252.67]	256	266

SHI DZ7 256–266 m: Increased frequency of sealed and locally open fractures. One crush at 263.16–263.31 m, and one breccia at 263.29 m (294°/55°) – 263.91 m (327°/70°). Fracture apertures generally 0.5 mm or less, locally up to 3 mm. Locally faint to weak oxidation, faint argillization and faint epidotization. Dominating minerals in sealed fractures are calcite, chlorite, clay minerals, oxidized walls, quartz, epidote and hematite; in open fractures clay minerals, calcite, chlorite and hematite. Three radar reflectors of which one is oriented at 262 m (330°/81°). Significantly decreased bulk resistivity, one significant caliper anomaly and a minor, but distinct fluid temperature anomaly. Metagranite-granodiorite (101057) and pegmatitic granite (101061). Confidence level = 3.

One high-transmissive flow anomaly at 262.7 m. The transmissivity of the section is $8 \cdot 10^{-6}$ m^2/s.

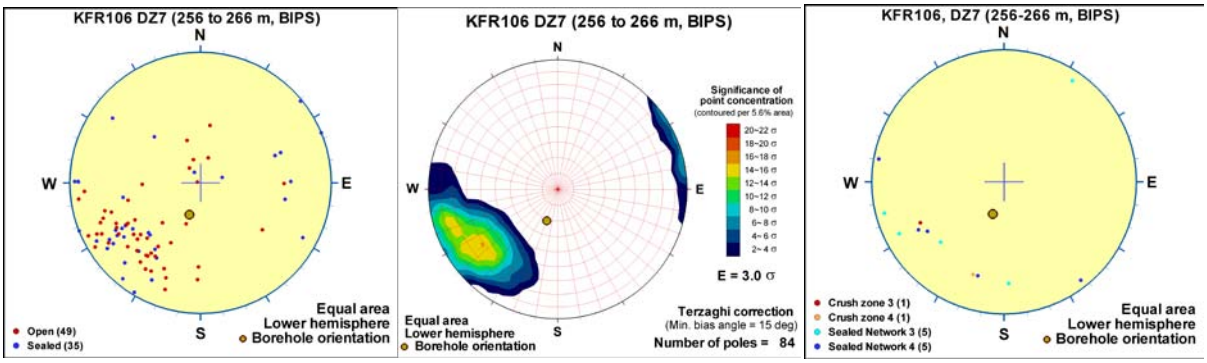

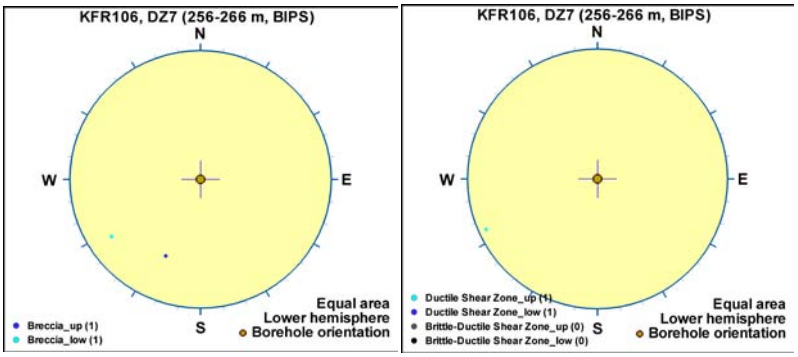

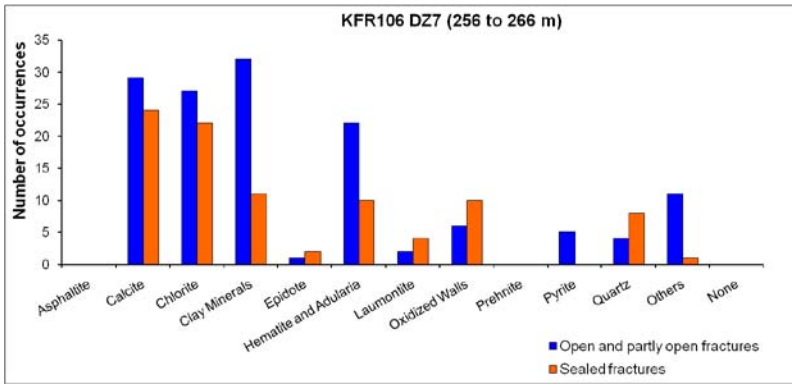

Borehole intersections for ZFMNNW1034

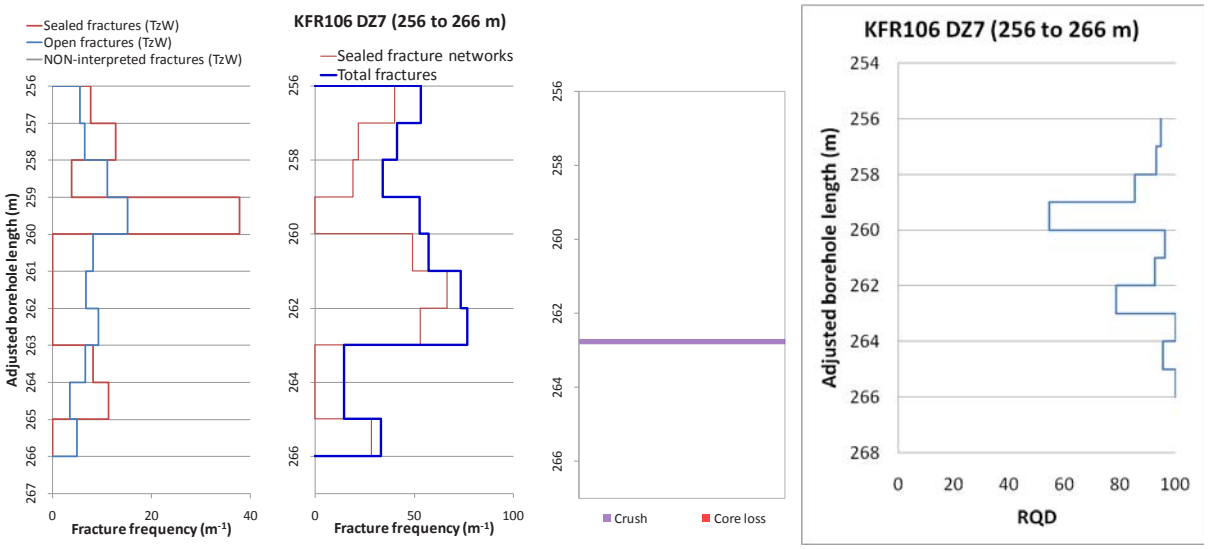

Deformation zone ZFMNNW1209

Borehole and tunnel intersections (metres along borehole/tunnel)

KFR35: 32.7–70 m (DZ1 32.7–70 m)
DT: 0+930 (tDZ59 0+930)
BT: 0+893
1 BTF: 0+100 (tDZ59 0+100)
2 BTF: 0+078 to 0+080 (tDZ59 0+080 and tDZ126 0+078)
BLA: 0+055 to 0+060 (tDZ59 0+060 and tDZ126 0+055)
BMA: 0+030 (tDZ59 0+030)

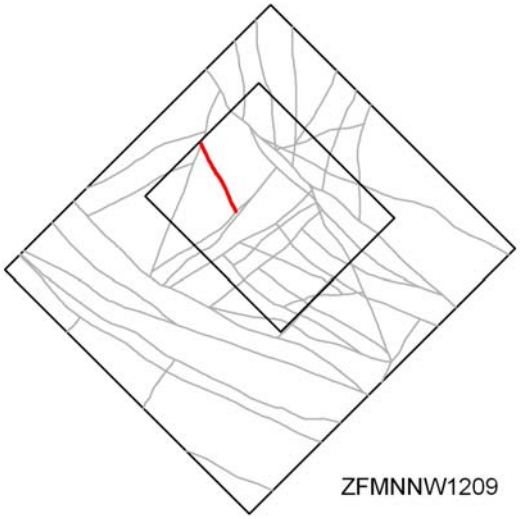

Deformation style, alteration and geometry

Deformation style: Brittle, including minor cohesive breccias and cataclasites present in KFR35 DZ1.

Alteration: Locally red-stained bedrock with fine-grained hematite dissemination.

Strike/dip (span) right-hand-rule: 151 / 83 (±10 / ±10)

Trace length at ground surface (span): 341 m (340−400 m)

Model thickness (span): 18 m (2−18 m)

Confidence in existence: High

Modelling procedure*:*

This zone corresponds to zone 6 in earlier SFR models (see, for example, Axelsson and Mærsk Hansen 1997/). It was renamed ZFMNNW1209 in the Forsmark stage 2.2 model /Stephens et al. 2007/. In the same manner as that carried out in Forsmark stage 2.2 /Stephens et al. 2007/, the zone has essentially been adopted from the earlier geological model for SFR by /Axelsson and Mærsk Hansen 1997/. The surface position is based on a combination of magnetic lineament and tunnel mapping results. The zone is crossed by a single seismic refraction profile /Keisu and Isaksson 2004/. However, it does not have a seismic refraction anomaly associated with it, probably due to its diffuse character.

The extent of the zone at the ground surface is based on a modification to the Forsmark stage 2.3 magnetic lineament MFM3114G /Isaksson et al. 2007/. A further extension to the south-east was examined. However, although possible correlation is suggested by the fracture patterns of KFR104 DZ5 and KFR105 DZ4 and DZ5, the resulting projected surface trace does not fit well with the magnetic data. In addition, HFR102 should intercept the zone at an intermediary position and there is no PDZ recorded in this BH. For this reason, the southern extension is possible, but is only weakly supported and has not been implemented.

Based on inspection of the tunnel mapping results and their visualization in RVS, the existence of this apparently ‘well established’ zone reported in /Axelsson and Mærsk Hansen 1997/ and earlier reports is difficult to follow as a single discrete structure. It is judged most likely to be a group of loosely associated thin discontinuous structures with a similar trend spread out over a thickness of around 18 m. The evidence quoted in the northernmost BMA cavern by /Axelsson and Mærsk Hansen 1997/ shows a structure that dips steeply (c. 70°) to the NE, whereas indicators in the other caverns (BLA, 2BTF and 1 BTF) are more consistent and dip steeply to the west. Modelling work has adopted the steep dip to the west. The existence of the same structure in the DT is uncertain, while extension of the DT structure as a fracture swarm along the BT is present but was discounted in earlier work /Axelsson and Hansson 1997/.

The modelled geometry has been kept simple based on a partial agreement with the magnetic lineament MFM3114G, three control points from BLA, 2BTF and 1BTF, along with the SHI DZ1 in KFR35, giving a dip of 83° towards west. The zone has been modelled with a thickness of 18 m to correlate with the thickness indicated by the geological SHI DZ1 in KFR35 and the geometrical spread of the individual, gouge-filled fractures. Individually mapped tunnel locations yield earlier recorded thicknesses between 0.5 and 2 m. Similar and parallel, clay-filled fractures have been reported to the north of the defined zone /Christiansson 1986/. As pointed out in the main text in this report, estimates of zone thickness in the earlier SFR work were underestimated according to current SKB methodology.

Fractures in the deformation zone

General characteristics

Fracture orientation: No data

Fracture frequency: See KFR35 DZ1 for general indication of fracture frequency (no Terzarghi correction)

Fracture filling mineralogy: See KFR35 DZ1 below

KFR35 52–70 m

BOREHOLE AND TUNNEL INTERCEPT DETAILS

Borehole intersections for ZFMNNW1209				
	Sec_up BH length (m) [z (-m)]	**Sec_low BH length (m) [z (-m)]**	**Sec_up BH length (m) [z (-m)]**	**Sec_low BH length (m) [z (-m)]**
KFR35	32.90 [20.65]	71.04 [50.49]	32.7	70

Borehole intersections for ZFMNNW1209

SHI DZ1 32.7–70 m: Increased frequency of broken and unbroken fractures and sealed networks. Six crushed intervals in the lower part of the section (57.37–68.15 m). Three intervals at 44.83–46.07, 55.92–56.01 and 60.37–61.60 m include fault breccias and cataclasite. Predominant fracture minerals are adularia, calcite and quartz. α–angles are generally small to moderate (21–61°). Asphaltite, typically associated with calcite, is more or less limited to this section. Occurrence of a black unknown mineral that resembles asphaltite is registered in the interval between 20.1 and 71.6 m. Locally faint to weak oxidation. One minor core loss at 63.84–64.15 m. Pegmatitic granite (101061) with occurrences of felsic to intermediate metavolcanic rock (103076), fine- to medium-grained granite (111058) and strongly foliated metagranite-granodiorite (101057). Confidence level = 3.

Hydraulic conductivity (measured in 3-m sections) above the lower measurement limit ($1.7 \cdot 10^{-8}$) in the intervals 36–39 and 54–63 m. Hydraulic conductivity slightly above $1 \cdot 10^{-6}$ m/s at 54–60 m.

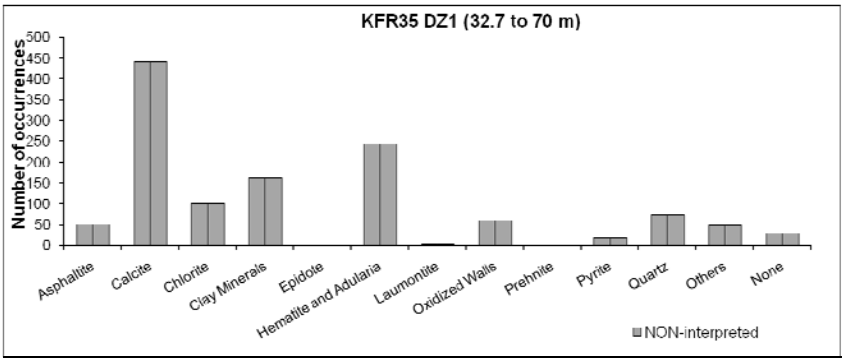

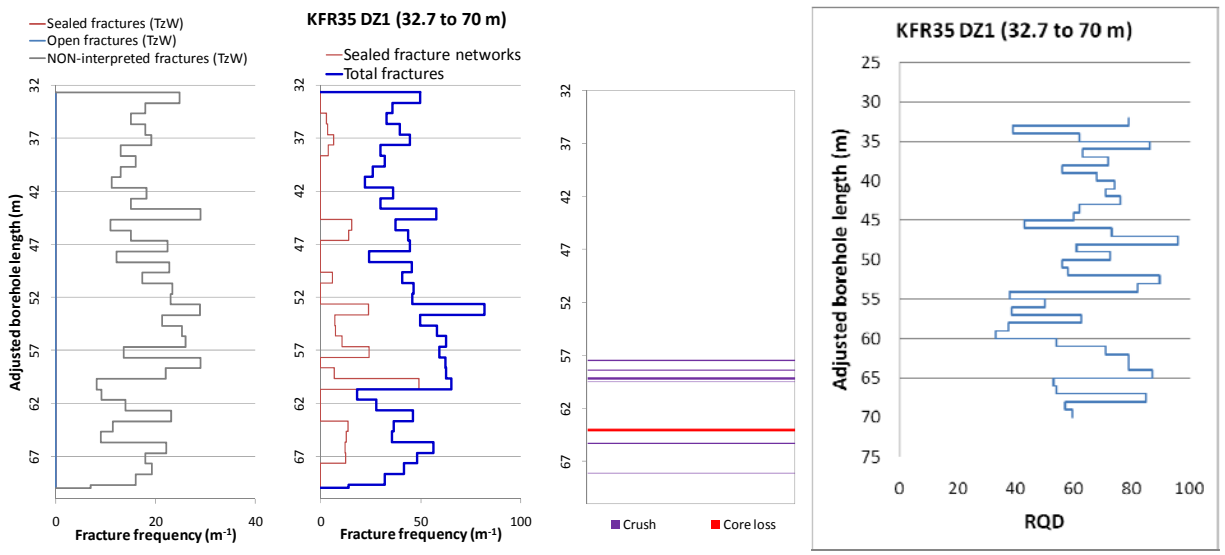

BH	Geometrical Intercept		Target intercept	
	Sec_up BH length (m) [z (-m)]	Sec_low BH length (m) [z (-m)]	Sec_up BH length (m) [z (-m)]	Sec_low BH length (m) [z (-m)]
KFR33	46.19 [26.87]	114.64 [74.24]	–	–

Comment: /Axelsson and Hansen 1997/ approximate position of correlation was 465 m level. /Carlsson et al. 1986/ quote direct BH lengths and these have been judged a more reliable indicator of the zones interpreted position in the borehole (67–72 m). They describe the character in terms of mylonitization, crushed rock, highly fractured and alteration.

Tunnel intersections for ZFMNNW1209				
Tunnel	**Geometrical Intercept**		**Target intercept**	
	Start ch.(m)	**End ch. (m)**	**Start ch.(m)**	**End ch. (m)**
DT	0+920	0+945	0+930	0+930
Comment: Target intercept defined by tDZ59 in Appendix 2. 1/920 Sheet fractured rock. Shotcrete before mapping /Carlsson et al. 1985/				
BT	0+885	0+907	0+893	0+893
Comment: Additional possible low confidence observation based on detailed drawing –09 /Christiansson and Bolvede 1987/ 5/890 to a lesser degree sheet fractured rock /Carlsson et al. 1985/				
NBT	0+000	0+010	-	-
Comment:				
1 BTF	0+090	0+117	0+100	0+100
Comment: Target intercept defined by tDZ59 in Appendix 2.				
2 BTF	0+070	0+090	0+078	0+080
Comment: Target intercept defined by tDZ59 and tDZ126 in Appendix 2.				
BLA	0+048	0+068	0+055	0+060
Comment: Target intercept defined by tDZ59 and tDZ126 in Appendix 2.				
BMA	0+030	0+055	0+030	0+030
Comment: Target intercept defined by tDZ59 in Appendix 2.				

Tunnel intersections for ZFMNNW1209

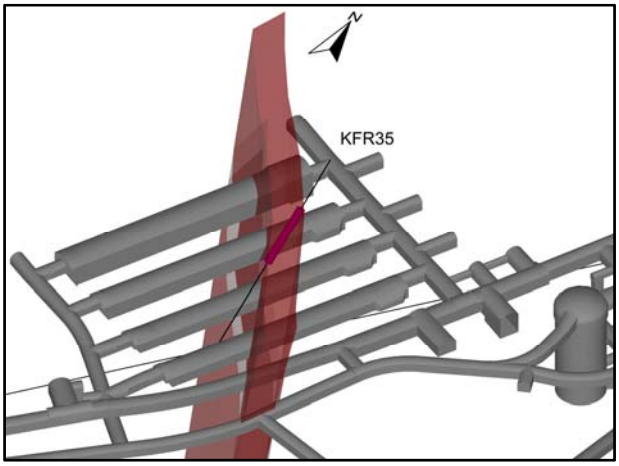

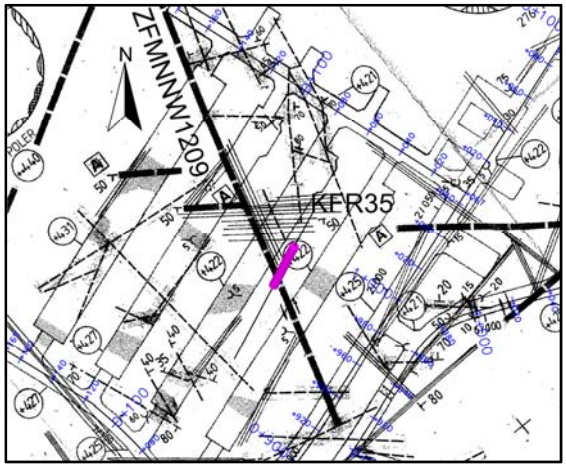

ZFMNNW1209 crossing the rock caverns and intercepted by KFR35 as it appears in the model (left) and the original overview mapping /Christiansson and Bolvede 1987/. The zone is modelled with a thickness of 18 m based on KFR35 SHI.

Deformation zone ZFMNNW3113

Borehole and tunnel intersections (metres along borehole/tunnel)

None

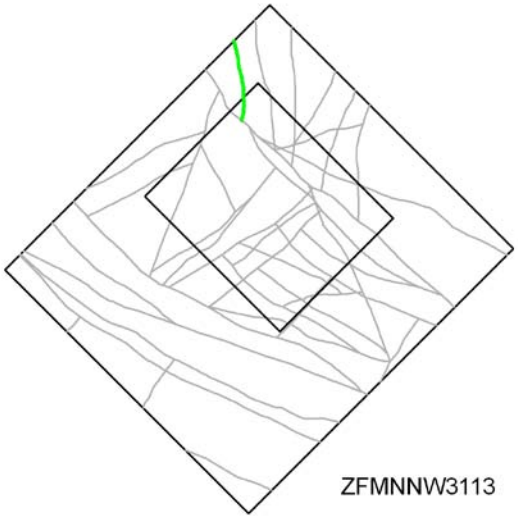

Deformation style, alteration and geometry

Deformation style: No data

Alteration: No data

Strike/dip (span) right-hand-rule: 173 / 90 (170−180 / ±10)

Trace length at ground surface (span): 376 m (360−380 m)

Model thickness: 5 m (1% default)

Confidence in existence: Medium

Modelling procedure*:* The position of the zone at the ground surface is based on magnetic lineament MSFR08079 in SFR model version 1.0, being a very minor revision of lineament MFM3113G in Forsmark stage 2.3 /Isaksson et al. 2007/. The earlier number has been maintained for traceability purposes in different lineament interpretations. The modelled thickness and dip are default values.

Fractures in the deformation zone

General characteristics

Fracture orientation: No data

Fracture frequency: No data

Fracture filling mineralogy: No data

Deformation zone ZFMNS3154

Borehole and tunnel intersections (metres along borehole/tunnel)

None

Deformation style, alteration and geometry

Deformation style: No data

Alteration: No data

Strike/dip (span) right-hand-rule: 180 / 90 (±5 / ±10)

Trace length at ground surface (span): 757 m (500−760 m)

Model thickness: 10 m (1% default)

Confidence in existence: Medium

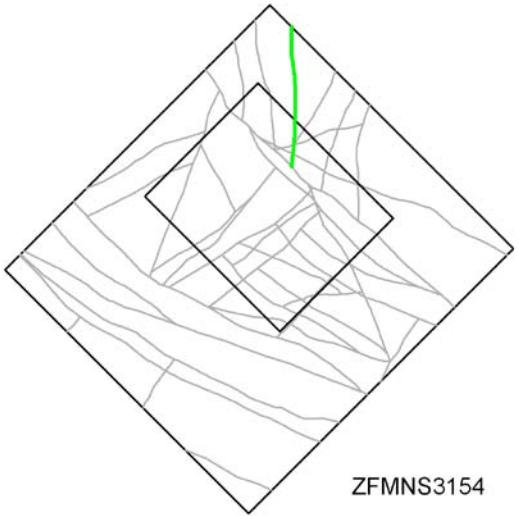

Modelling procedure*:* The position of the zone at the ground surface is based on the magnetic lineament MFM3154G /Isaksson et al. 2007/. This lineament was subsequently broken up and modelled at a higher resolution as lineaments MSFR08012, MSFR08013, MSFR08014 and MSFFR08015 during SFR model version 1.0. The SFR model version 1.0 interpretation is considered as equally valid as the earlier stage 2.3 interpretation. However, the latter suits more favourably the DZ modelling resolution in the SFR regional model and, for this reason, the earlier name has been maintained. Forward modelling of magnetic data along profiles 5 and 6 (see Appendix 6) supports the earlier assumed vertical dip of the zone. The modelled thickness and dip of the zone are default values.

Fractures in the deformation zone

General characteristics

Fracture orientation: No data

Fracture frequency: No data

Fracture filling mineralogy: No data

Appendix 12

Structures not included in the deterministic deformation zone model

Possible deformation zones (PDZ) in the single-hole interpretation (SHI)

In addition to the SHI PDZ borehole data upon which the deterministic deformation zone models are based, there are a number of PDZ's that lack a correlation with any of the modelled deformation zones. These PDZ's typically show thin apparent and, as a consequence, even thinner true thicknesses and a considerable proportion of them were defined with a low or medium confidence level during the SHI work. In total, there are 31 such PDZ's distributed among 22 boreholes (Table A12-1). The possible geological character of three of these minor structural features is included in the following section.

Table A12-1. Summary of SHI possible deformation zones (PDZ) not linked to deterministic deformation zones (SFR model version 1.0).

BH	SHIPDZ	BH length Sec_up (m)	BH length Sec_low (m)	SHI Conf. level	Estimated orientation (alt. est)	Apparent thickness (m)	Estimated true thickness (m) (alt. est)	Comment
HFR101	DZ2	101	115	1	–	14	–	Too much scatter in the data to enable estimation of orientation.
HFR106	DZ1	38	40	1	–	2	–	Limited data set and too much scatter to enable estimation of orientation.
KFR02	DZ2	99.2	100.2	1	–	1	–	No orientation data.
KFR03	DZ1	6	12	2	–	6	–	No orientation data.
KFR04	DZ1	0	3	1	–	3	–	No orientation data.
KFR09	DZ2	69	74.3	3	–	5.3	–	No orientation data.
KFR10	DZ2	95.65	107.28	3	–	11.63	–	No orientation data.
KFR13	DZ1	20	30	3	–	10	–	No orientation data.
KFR13	DZ2	36	41	1	–	5	–	No orientation data.
KFR19	DZ1	38.53	49.32	2	–	10.79	–	No orientation data.
KFR20	DZ1	48.50	52.00	1	–	3.50	–	No orientation data.
KFR31	DZ1	82.05	91.70	2	–	9.65	–	No orientation data.
KFR32	DZ1	155.70	159.00	3	–	3.3	–	No orientation data.
KFR37	DZ1	36.60	45.60	2	–	9.00	–	No orientation data.
KFR51	DZ1	9.84	11.15	1	–	1.31	–	No orientation data.
KFR52	DZ1	19.85	22.40	2	–	2.55	–	No orientation data.
KFR55	DZ1	0	3.3	2	–	3.3	–	No orientation data.
KFR69	DZ1	52.38	79.00	2	–	26.62	–	No orientation data.
KFR69	DZ2	121.60	146.10	3	–	24.5	–	No orientation data.
KFR101	DZ3	179	186	3	–	7	–	Too much scatter in the data to enable estimation of orientation.
KFR101	DZ4	197	213	2	120/90	16	10.5	Interpreted as a short splay between ZFMNW0805A and ZFMNW0805B.
KFR102B	DZ1	67	70	3	098/81	3	2	
KFR102B	DZ3	149.5	150.5	2	229/08	1	< 1	
KFR103	DZ1	24.5	26.5	3	–	2	–	Too much scatter in the data to enable estimation of orientation.
KFR103	DZ2	84	91	3	298/86 (343/12)	7	4 (6)	
KFR105	DZ5	293.6	304	2	319/88	10.4	6	
KFR106	DZ1	15	20	3	216/90	5	< 1	
KFR106	DZ2	36.5	52	2	–	15.5	–	Too much scatter in the data to enable estimation of orientation.
KFR106	DZ4	84.5	86	3	181/14	1.5	1.5	
KFR106	DZ5	100.5	101	3	012/12	0.5	< 1	
KFR106	DZ6	153	157	3	098/19	4	3	

Sub-horizontal stress release structures

/Carlsson et al. 1985/ proposed the existence of two horizontal structures H1 and H3, of limited lateral extent, lying above the existing silo (Table A12-2 and Figure A12-1). These structures have been reported earlier in /Curtis et al. 2009/ and the supporting evidence for them has been re-evaluated during the current modelling work. No new borehole information is available.

The original interpretation was based on the identification of drill core sections with a slightly raised frequency of open fractures with occasional clay infilling and, most importantly, in terms of the original interpretation, hydraulic connection between a number of the boreholes involved. The new evaluation resulted in a structure with essentially the same extent, position and thickness, although H1 and H3 have been modelled as a single structure rather than being split as in the original model (Figure A12-1). The structure is horizontal, lies at a depth of c. 25 m, has a hydraulic thickness of c. 10 m and is interpreted as a stress release feature rather than a deformation zone related to regional-scale tectonic activity. Such features are considered to be relatively ubiquitous in the uppermost part of the bedrock in the Forsmark region /SKB 2008b/.

Table A12-2. Borehole intercepts for potential sub-horizontal stress release structures delivered in RVS format as 'possible hydraulic features' to aid hydrological modelling work.

ID	BH	Control point (BH length m)	Intercept defined by /Carlsson et al. 1985/ (BH length m)		Intercept defined by geological SHI (BH length m)			Comment
			Sec_up	Sec_low	PDZ	Sec_up	Sec_low	
H1	KFR21	29.5	26	33	–	–	–	
H1	KFR22	39	39	39	–	–	–	
H1	KFR23	23	23	23	–	–	–	
H1	KFR24	35	35	35	–	–	–	
H1	KFR25	48.5	42	55	–	–	–	
H1	KFR37	33	31	35	DZ1	36.60	45.60	
H1	KFR38	40	39	41	–	–	–	
H3	KFR31	60	56	64	–	–	–	
H3	KFR32	62.5	60	65	–	–	–	
H3	KFR33	57.5	55	60	–	–	–	
H3	KFR35	40	39	41	–	–	–	Carlsson's intercept lie within the much more extensive SHI DZ1 (32.70–70 m), as being ZFMNNW1209.
H5	HFR105	133	–	–	DZ3	119	147	
H5	HFR106	179.5	–	–	DZ3	177	182	
H5	KFR27	114	–	–	DZ1	108	120	
H5	KFR101	182.5	–	–	DZ3	179	186	
H5	KFR102A	155	–	–	DZ1	149	161	
H5	KFR102B	176.5	–	–	DZ4	173	180	
H5	KFR103	181.25	–	–	DZ3	180	182.5	
H5	KFR104	127.5	–	–	–	–	–	Increased frequency of open sub-horizontal fractures in the interval 120–135 m.
H5	KFR105	–	–	–	–	–	–	Radar reflector no 8 has a sub-parallel leg at ~195–220 m, at a distance of 15–20 m from the BH.
H5	KFR106	155	–	–	DZ6	153	157	
H6	KFR27	114	–	–	DZ1	108	120	
H6	KFR102B	150	–	–	DZ3	149.5	150.5	

Some attempts have also been made to investigate alternative interpretations of the PDZ's listed in Table A12-1 and model them deterministically as potential horizontal structures formed in connection with release of bedrock stress and not as tectonically steered deformation zones (Table A12-2 and Figure A12-2). These possible structures consist of an increased frequency of horizontal or sub-horizontal fracturing with a certain amount of hydraulic connection as indicated by testing in and between various boreholes. They are not included in the deformation zone model but have been provided for further assessment and consideration by the hydrogeology modelling team. They are referred to as H5 (008°/03°, approximate elevation –130 masl) and H6 (200°/07° approximate elevation –110 masl).The geometry and nature of these sub-horizontal structures were further investigated and developed by /Öhman and Follin 2010/.

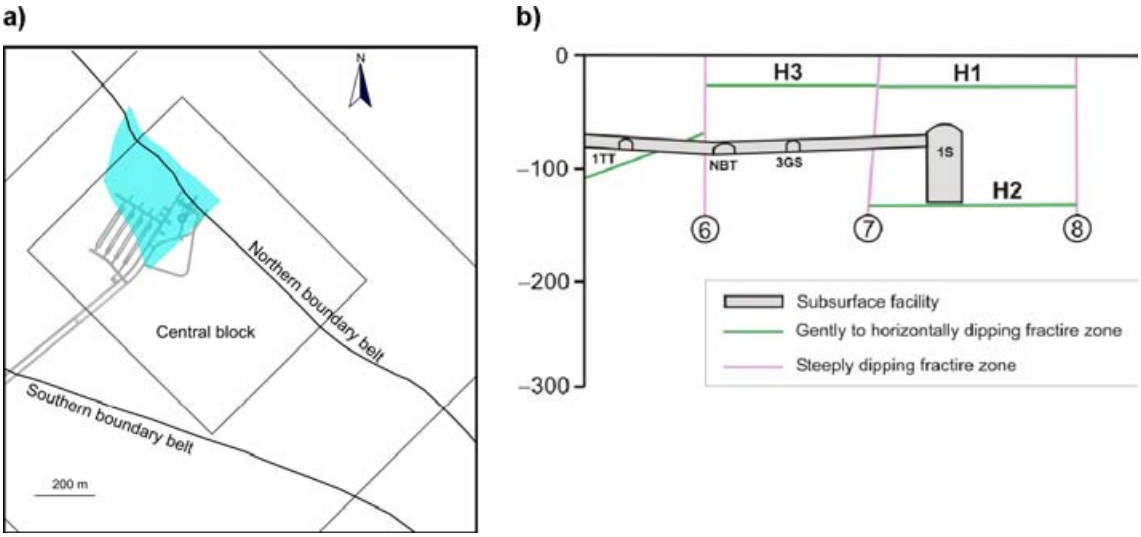

Figure A12-1. *a) Plan view of H1+H3 from the current modelling work. b) H1 and H3 as represented in the earlier model by /Carlsson et al. 1985/.*

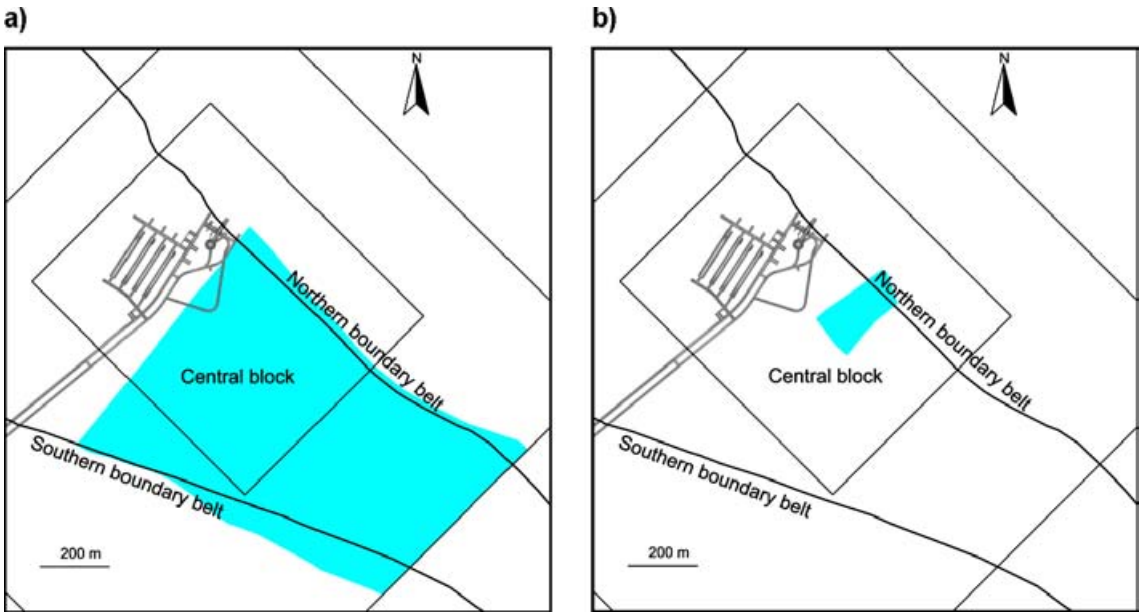

Figure A12-2. *Plan view of a) H5 and b) H6 as delivered for further evaluation by hydrogeological modelling.*

Appendix 13

Summary of borehole and tunnel intercepts for rock domains RFR01 and RFR02 in SFR model version 1.0

The terms *Target borehole/tunnel intercept* and *Geometrical borehole/tunnel intercept*, as defined in Section 5.1.2 for deformation zones, are quoted in Appendix 13. A target borehole intercept is the interpreted position of a rock domain in an individual borehole, whereas a geometrical borehole intercept is the intercept between a modelled domain boundary and an individual borehole as they exist in the RVS model. Target intercepts conform to the geological SHI rock unit intercepts. A target/geometrical tunnel intercept is defined in the same manner, but by chainage intervals along a tunnel centre line rather than borehole length.

Contents

Table A13-1. Summary of borehole intercepts for rock domains RFR01 and RFR02 (SFR model version 1.0). Eoh = end of borehole; mb = boundary of model volume.

Borehole	Geometrical intercept (v1.0) (BH length m)		Target intercept (v1.0) (BH length m)		Intercept defined by geological SHI (BH length m)			Comment
	Sec_up	Sec_low	Sec_up	Sec_low	RU	Sec_up	Sec_low	
RFR01								
HFR101	0.00	eoh	8.04	eoh	RU1, RU2a, RU3, RU2b, RU4a, RU5, RU4b, RU6	8.04	eoh	
HFR102	0.00	eoh	9.04	eoh	RU1, RU2	9.04	eoh	
KFR02	0.00	eoh	0.00	eoh	RU1, RU2, RU3, RU4	0.00	eoh	
KFR27	0.00	207.84	11.82	207.84	RU1, RU2a, RU3a, RU2b	11.82	207.84	
KFR69	0.00	159.96	11.68	159.96	RU1a, RU2, RU1b	11.68	159.96	
KFR70	0.00	eoh	9.24	eoh	RU1a, RU2a, RU1b, RU2b, RU3	9.24	eoh	
KFR104	0.00	385.15	8.73	mb	RU1a, RU2a, RU1b, RU3, RU2b	8.73	mb	The borehole penetrates the model boundary at 385.15 m length.
KFR105	0.00	83.46	0.00	83.46	RU1a, RU2, RU1b	0.00	83.46	
KFR105	183.20	eoh	183.20	eoh	RU5, RU1c, RU6, RU7	183.20	eoh	
RFR02								
KFR03	0.00	eoh	0.00	eoh	RU1, RU2, RU3a, RU4, RU3b, RU5	0.00	eoh	
KFR04	0.00	eoh	0.00	eoh	RU1, RU2a, RU3, RU2b, RU4	0.00	eoh	
KFR05	0.00	eoh	0.60	eoh	RU1, RU2, RU3, RU4, RU5	0.60	eoh	
KFR08	0.00	eoh	0.00	eoh	RU1, RU2, RU3	0.00	eoh	
KFR09	0.00	eoh	0.00	eoh	RU1, RU2, RU3	0.00	eoh	
KFR10	0.00	eoh	0.00	eoh	RU1, RU2	0.00	eoh	
KFR11	0.00	eoh	0.00	eoh	RU1, RU2, RU3, RU4	0.00	eoh	
KFR12	0.00	eoh	0.00	eoh	RU1, RU2, RU3	0.00	eoh	
KFR13	0.00	eoh	0.00	eoh	RU1, RU2	0.00	eoh	
KFR14	0.00	eoh	0.00	eoh	RU1	0.00	eoh	
KFR19	0.00	eoh	0.00	eoh	RU1, RU2a, RU3, RU4, RU2b	0.00	eoh	
KFR20	0.00	eoh	0.00	eoh	RU1, RU2, RU3, RU4,RU5, RU6	0.00	eoh	
KFR27	207.84	303.41	207.84	mb	RU3b, RU4a	207.84	mb	The borehole penetrates the model boundary at 303.41 m length.
KFR31	0.00	eoh	16.60	eoh	RU1, RU2, RU3, RU4, RU5, RU6, RU7	16.60	eoh	
KFR32	0.00	eoh	16.55	eoh	RU1, RU2, RU3, RU4, RU5, RU6	16.55	eoh	
KFR34	0.00	eoh	13.55	eoh	RU1, RU2a, RU3, RU2b	13.55	eoh	
KFR35	0.00	eoh	18.00	eoh	RU1, RU2, RU3, RU4, RU5	18.00	eoh	
KFR36	0.00	eoh	16.10	eoh	RU1, RU2	16.10	eoh	

Borehole	Geometrical intercept (v1.0) (BH length m)		Target intercept (v1.0) (BH length m)		Intercept defined by geological SHI (BH length m)			Comment
	Sec_up	Sec_low	Sec_up	Sec_low	RU	Sec_up	Sec_low	
KFR37	0.00	eoh	12.23	eoh	RU1, RU2, RU3, RU4	12.23	eoh	
KFR38	0.00	eoh	13.45	eoh	RU1, RU2a, RU3, RU2b	13.45	eoh	
KFR51	0.00	eoh	0	eoh	RU1, RU2	0	eoh	
KFR52	0.00	eoh	0	eoh	RU1	0	eoh	
KFR54	0.00	eoh	0	eoh	RU1	0	eoh	
KFR55	0.00	eoh	0	eoh	RU1	0	eoh	
KFR57	0.00	eoh	0.00	eoh	RU1, RU2	0.00	eoh	
KFR69	159.96	eoh	159.96	eoh	RU3	159.96	eoh	
KFR101	0.00	eoh	13.72	eoh	RU1, RU2, RU3, RU4, RU5, RU6, RU7, RU8, RU9	13.72	eoh	
KFR102A	0.00	333.28	70.44	mb	RU1, RU2a, RU3, RU4a, RU5, RU4b	70.44	mb	The borehole penetrates the model boundary at 333.28 m length.
KFR102B	0.00	eoh	13.94	eoh	RU1, RU2, RU3, RU4	13.94	eoh	
KFR103	0.00	eoh	13.03	eoh	RU1, RU2, RU3a, RU4a, RU3b, RU5, RU4b, RU3c	13.03	eoh	
KFR105	83.46	183.20	83.46	183.20	RU3, RU4	83.46	183.20	
KFR7A	0.00	eoh	0.00	eoh	RU1, RU2, RU3	0.00	eoh	
KFR7B	0.00	eoh	0.00	eoh	RU1	0.00	eoh	
KFR7C	0.00	eoh	0.00	eoh	RU1, RU2	0.00	eoh	

Table A13-2. Summary of tunnel intercepts for rock domains RFR01 and RFR02 (SFR model version 1.0). Target intercepts are quoted as tunnel centreline intercepts and are based on inspection of the detailed geological tunnel mapping results as presented in /Christiansson and Bolvede 1987/. mb = boundary of model volume.

SFR Facility part	Geometrical intercept (v1.0) (chainage m)		Target intercept (v1.0) (chainage m)		Comment
RFR01					
DT	mb	0+906	mb	0+910	
BT	mb	0+900	mb	0+907	
NBT	0+000	0+133	0+000	0+130	
TT	0+000	0+074	0+000	0+040	
1 BTF	0+185	0+210	–	–	
RFR02					
DT	0+906	1+126	0+910	1+126	
BT	0+900	1+166	0+907	1+166	
NBT	0+133	0+432	0+130	0+432	
TT	0+074	0+169	0+040	0+169	
1 BTF	0+000	0+185	–	–	

Appendix 14

Properties of rock domains RFR01 and RFR02 in SFR model version 1.0

The geological properties of two of the four rock domains in the SFR model version 1.0 (Figure A14-1), for which geological data are available (i.e. RFR01 and RFR02), are presented here. Descriptions of the domains are provided in Section 6.3 in the main text of this report. All properties addressed in the two rock domains (Table A14-1) and for the dominant rock type in each domain (Table A14-2) are based solely on analyses of samples from the local SFR model volume.

Table A14-1. Properties assigned to rock domains RFR01 and RFR02.

Property
Rock domain ID. RFRxx.
Dominant rock type with quantitative proportion. The latter has been divided into two separate estimates in RFR02 for boreholes from the construction of SFR and for boreholes from the latest drilling campaign connected with the future expansion of SFR.
Quantitative proportion of subordinate rock types, divided in RFR02 into two separate estimates as for the dominant rock type.
Degree of homogeneity.
Metamorphism/alteration.
Mineral fabric. Type of orientation with Fisher mean and κ value (where statistically appropriate).

Table A14-2. Properties assigned to the dominant rock type in rock domains RFR01 and RFR02.

Property of dominant rock type
Grain-size (classification according to the terminology used by the Geological Survey of Sweden).
Structure.
Texture.
Density (kg/m^3). Range/mean/standard deviation.
Magnetic susceptibility (10^{-5} SI units). Range/geometric mean/standard deviation.
Natural exposure rate (μR/h). Range/mean/standard deviation.

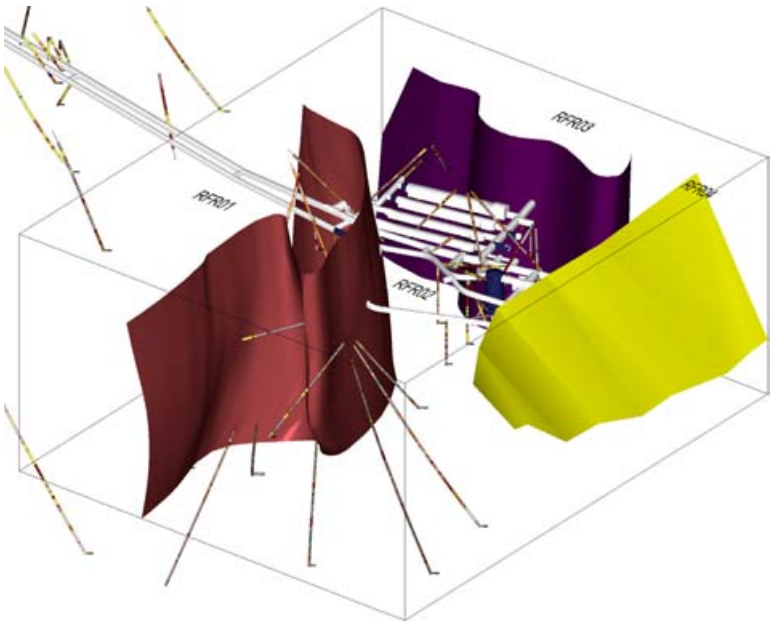

Figure A14-1. *Three dimensional model (SFR version 1.0) showing the boundaries between the four rock domains within the local SFR model volume relative to the boreholes and the SFR underground facility. The colour choice is only for legibility.*

RFR01

Property	Character	Quantitative estimate	Confidence	Comment
Dominant rock type	Pegmatite, pegmatitic granite (101061)	60%	High	Tunnel data from SFR. KFR and HFR borehole data. Quantitative estimate from all KFR and HFR boreholes including rock occurrences.
	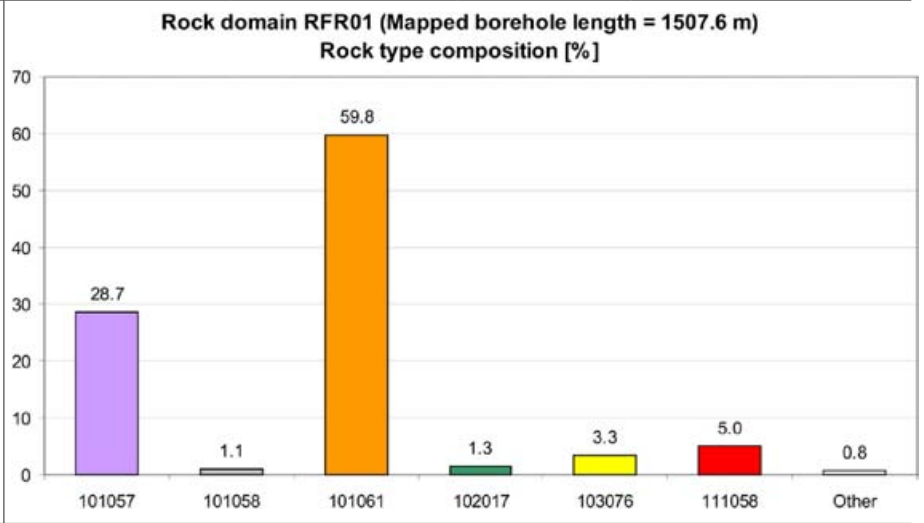			
Grain-size	Medium- to coarse-grained		High	KFR and HFR borehole data.
Structure	Massive, locally faint to weak foliation or lineation distinguishable		High	KFR and HFR borehole data.
Texture	Non-eqiugranular		High	KFR and HFR borehole data.
Density (kg/m^3)	2,537–2,804	2,643	28	KFR27, KFR104 and KFR105 borehole data, N=2790. Range/geometric mean/standard deviation.
Magnetic susceptibility (10^{-5} SI units)	0–5109	16	46/12	KFR27, KFR104 and KFR105 borehole data, N=2788. Range/geometric mean/standard deviation above/below mean.
Natural exposure (microR/h)	22–262	82	33	KFR104 and KFR105 borehole data, N=2605. Range/geometric mean/standard deviation
Subordinate rock type(s) Only the more important components listed	Granite (to granodiorite, metamorphic) (101057)	29%	High	Tunnel data from SFR. KFR and HFR borehole data. Quantitative estimate from all KFR and HFR boreholes including rock occurrences.
	Granite, fine- to medium-grained (111058)	5%		
	Felsic to intermediate metavolcanic rock (103076)	3%		
	Amphibolite (102017)	1%		
	Granite, metamorphic, aplitic (101058)	1%		

Property	Character	Quantitative estimate	Confidence	Comment
Degree of heterogeneity	Medium		High	Tunnel data from SFR. KFR and HFR borehole data.
Metamorphism/ alteration	Amphibolite-facies metamorphism. In part, unaffected by metamorphism		High	Tunnel data from SFR. KFR and HFR borehole data.
Mineral fabric (type/orientation)	Tectonic foliation/ banding (pole to best-fit great circle)	104/4	Medium	KFR and HFR borehole data from boreholes drilled 2008–2009, N=58.
	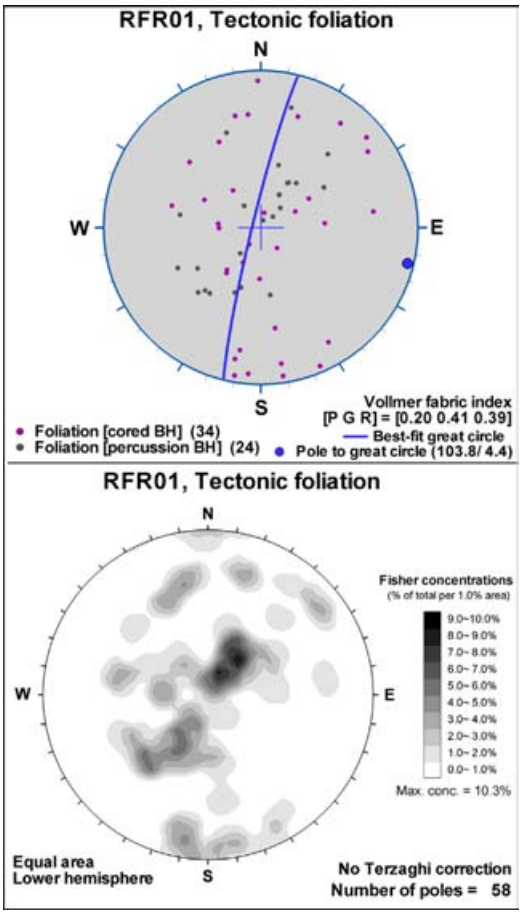			
	Mineral stretching lineation	094/60	Medium	KFR and HFR borehole data from boreholes drilled 2008–2009, N=17.
	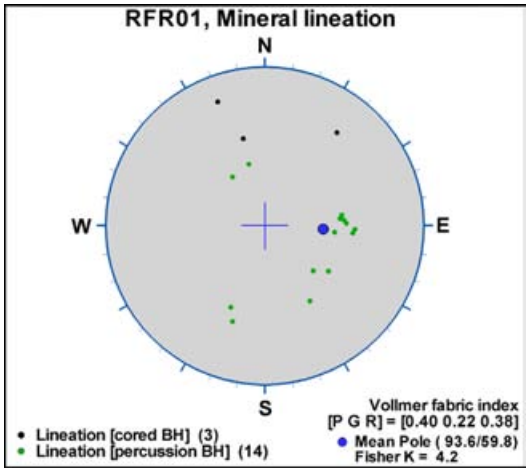			

RFR02

Property	Character	Quantitative estimate		Confidence	Comment
Dominant rock type	Granite to granodiorite, metamorphic (101057)	50%	32%	High	Tunnel data from SFR. KFR borehole data. Quantitative estimate from all KFR boreholes including rock occurrences. Boreholes drilled 2008–2009 (south of SFR)/*boreholes drilled during the construction of SFR (within and close to SFR).*
	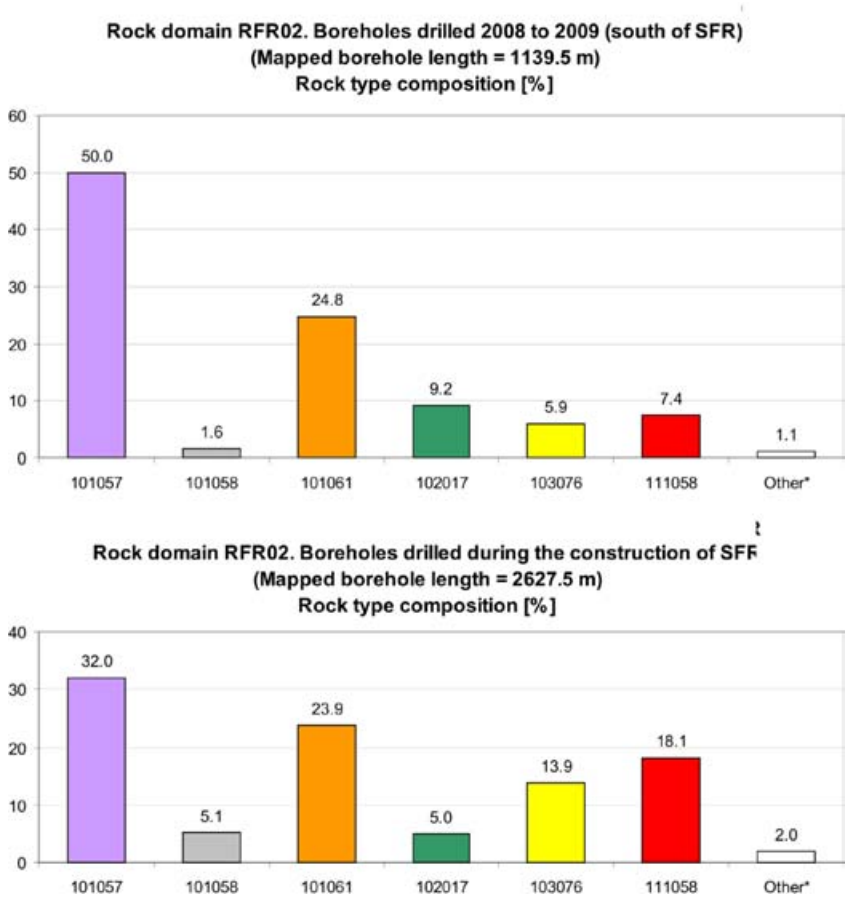				
Grain-size	Fine- to finely medium-grained			High	Tunnel data from NBT in SFR. KFR borehole data.
Structure	Moderate to strong foliation, locally mineral lineation. In part banded and folded			High	Tunnel data from NBT in SFR. KFR borehole data.
Texture	Eqiugranular			High	Tunnel data from NBT in SFR. KFR borehole data.
Density (kg/m^3)	2,595–2,880	2,706		25	KFR27, KFR101, KFR102A, KFR102B, KFR103, KFR105 borehole data, N=2766. Range/geometric mean/standard deviation.
Magnetic susceptibility (10^{-5} SI units)	0–10617	137		748/116	KFR27, KFR101, KFR102A, KFR102B, KFR103, KFR105 borehole data, N=2764. Range/geometric mean/standard deviation above/below mean.
Natural exposure (microR/h)	17–260	36		10	KFR101, KFR102A, KFR102B, KFR103, KFR105 borehole data, N=2561. Range/mean/standard deviation

Property	Character	Quantitative estimate		Confidence	Comment
Subordinate rock type(s). Only the more important components listed	Pegmatite, pegmatitic granite (101061)	25%	24%	High	Tunnel data from SFR. KFR borehole data. Quantitative estimate from all KFR boreholes including rock occurrences. Boreholes drilled 2008–2009 (south of SFR)/*boreholes drilled during the construction of SFR (within and close to SFR)*.
	Granite, fine- to medium-grained (111058)	7%	18%		
	Felsic to intermediate metavolcanic rock (103076)	6%	14%		
	Amphibolite (102017)	9%	5%		
	Granite, metamorphic, aplitic (101058)	2%		5%	
Degree of heterogeneity	High			High	Tunnel data from SFR. KFR borehole data.
Metamorphism/ alteration	Amphibolite-facies metamorphism. In part, unaffected by metamorphism			High	Tunnel data from SFR. KFR borehole data.
Mineral fabric (type/orientation)	Tectonic foliation/banding (pole to best-fit great circle)	110/17		Medium	Tunnel data from NBT in SFR, N=60. KFR borehole data from boreholes drilled 2008–2009 (south of SFR), N=149.
	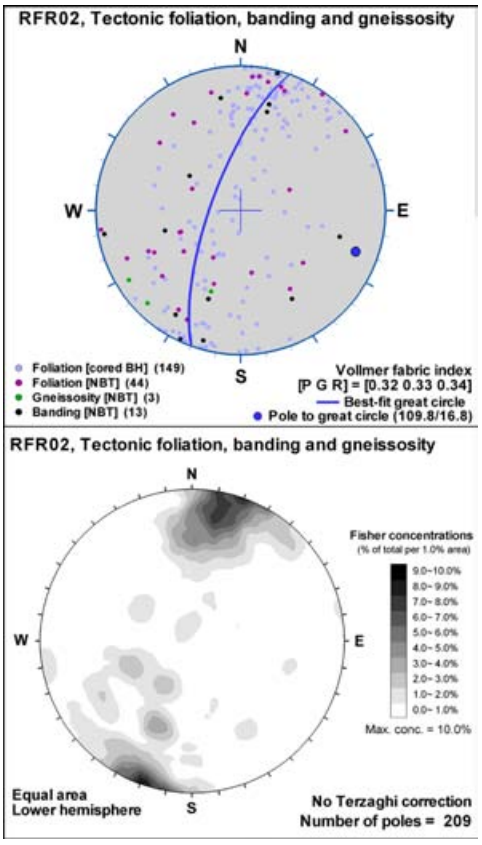				
	Mineral stretching lineation	151/84		High	KFR borehole data from boreholes drilled 2008–2009 (south of SFR), N=13.

Property	Character	Quantitative estimate	Confidence	Comment
	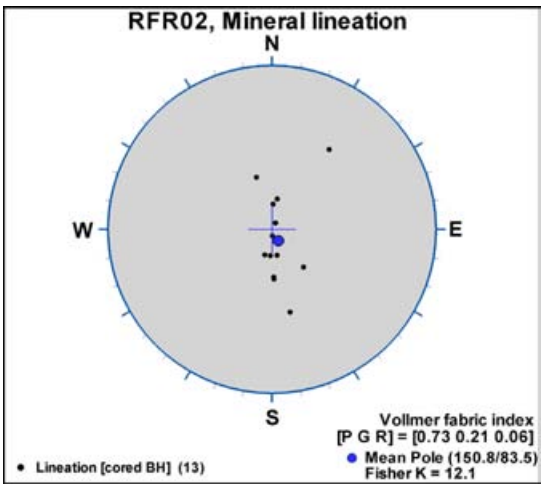			
	Fold axis	Variable and insufficient data.		Tunnel data from NBT in SFR, N=5.
	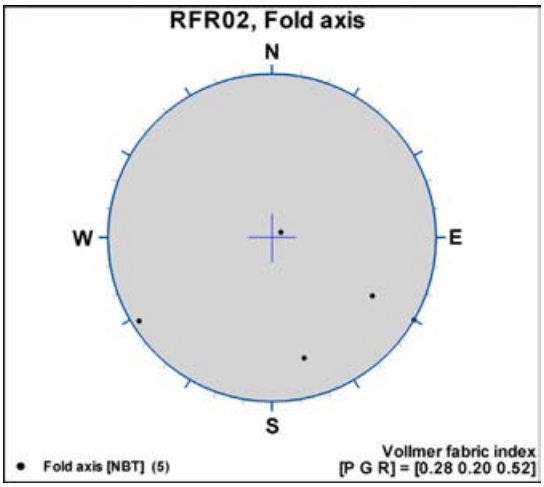			

Appendix 15

Distribution of rock types in rock domains RFR01 and RFR02 on a borehole by borehole basis

Contents

Table A15-1. Translation of rock codes to rock names. The different groups (A to D) are described in Section 4.3.1.

Rock code	Rock composition	Complementary characteristics		
1051	Granitoid			
1058	Granite			
1062	Aplite			
5105	Hybrid rock			
6005	Breccia			
8003	Cataclastic rock			
8004	Mylonite			
8020	Hydrothermal vein/segregation, unspecified			
8021	Quartz-dominated hydrothermal vein/segregation			
101004	Ultramafic rock	Metamorphic		Group B
101054	Tonalite to granodiorite	Metamorphic		Group B
101057	Granodiorite (to granite)	Metamorphic	Fine- to finely medium-grained	Group B
101058	Granite	Metamorphic	Aplitic	Group B
101061	Pegmatite, pegmatitic granite			Group D
102017	Amphibolite			Group B
103076	Felsic to intermediate metavolcanic rock	Metamorphic		Group A
108019	Calc-silicate rock (skarn)			Group A
111058	Granite		Fine- to medium-grained	Group D

Table A15-2. Distribution of rock types in boreholes included within RFR01.

Borehole	Rock type [m]							
	101057	101058	101061	102017	103076	111058	Other	Total
HFR101	42.23	–	120.73	2.57	14.24	20.44	0.09	200.29
HFR102	16.72	–	21.06	0.79	–	–	7.39	45.96
KFR02	60.06	–	97.87	0.04	8.71	2.95	0.70	170.33
KFR104	119.61	13.66	209.20	9.30	14.88	8.08	1.68	376.42
KFR105	54.58	–	126.35	1.79	1.89	22.28	0.18	207.07
KFR27	70.23	0.83	97.37	1.39	9.68	14.96	1.48	195.96
KFR69	44.93	1.36	94.05	0.69	–	7.25	–	148.28
KFR70	24.68	–	135.15	3.43	–	–	–	163.26
Total	433.03	15.85	901.78	20.01	49.40	75.96	11.52	1,507.56
%	28.72	1.05	59.82	1.33	3.28	5.04	0.76	100.00

*Other includes 1058, 1062, 6005, 8003, 8021.

Table A15-3. Distribution of rock types in boreholes included within RFR02 (data set GE043 for boreholes from the latest drilling campaign, GE038 for remapped boreholes from the construction of SFR and GE044 for other old SFR boreholes).

Borehole	Rock type [m]							
	101057	101058	101061	102017	103076	111058	Other*	Total
KFR03	11.73	30.43	34.81	5.01	11.60	–	8.02	101.60
KFR04	25.33	–	1.20	8.39	25.09	38.79	1.71	100.50
KFR05	–	–	14.74	4.63	62.50	47.57	1.36	130.80
KFR08	19.94	–	46.14	–	1.26	31.41	5.65	104.40
KFR09	3.63	–	18.96	1.16	50.21	6.28	–	80.24
KFR10	2.15	–	20.34	3.59	47.08	28.90	5.21	107.28
KFR11	18.68	–	23.75	2.58	1.50	39.05	12.51	98.07
KFR12	22.04	–	16.55	0.07	1.13	8.52	1.95	50.26
KFR13	43.83	–	16.11	1.17	–	11.36	4.13	76.60
KFR14	–	–	3.09	13.48	9.22	2.83	0.05	28.67
KFR19	8.39		30.82	2.59	41.66	26.10	0.60	110.17
KFR20	20.26	0.57	26.00	13.03	29.69	20.02	0.12	109.70
KFR27	41.69	–	36.54	13.39	0.72	2.61	0.62	95.57
KFR31	76.63	15.94	65.42	10.58	13.18	43.75	–	225.50
KFR32	97.39	5.89	49.51	18.65	–	21.71	–	193.15
KFR34	47.69	–	51.09	3.00	24.25	2.42	–	128.45
KFR35	39.80	–	43.78	8.49	17.64	6.92	5.53	122.17
KFR36	35.89	8.70	15.23	4.54	11.07	29.73	2.64	107.80
KFR37	71.80	33.92	22.34	7.60	–	55.91	1.10	192.67
KFR38	65.61	26.31	37.39	15.51	–	27.13	–	171.95
KFR51	20.41	–	19.90	1.52	4.45	–	–	46.28
KFR52	3.96	–	20.40	0.33	–	4.86	0.40	29.95
KFR54	42.05	–	3.56	2.59	–	4.81	0.29	53.30
KFR55	52.65	–	5.08	–	1.72	2.44	–	61.89
KFR57	2.48	–	6.44	2.06	10.58	3.82	–	25.38
KFR69	30.36	–	6.73	0.40	1.35	1.47	0.93	41.24
KFR101	156.79	18.52	84.66	21.32	7.83	31.28	7.64	328.04
KFR102A	138.78	–	62.45	19.77	5.74	33.94	2.16	262.84
KFR102B	81.99	0.04	30.17	30.16	13.97	9.04	0.76	166.13
KFR103	86.91	–	52.49	19.25	22.90	4.60	1.02	187.16
KFR105	63.47	–	15.89	0.80	16.20	3.05	0.32	99.73
KFR7A	41.08	13.54	16.87	1.04	–	1.91	–	74.45
KFR7B	17.13	–	3.97	–	–	–	–	21.10
KFR7C	19.36	–	6.69	–	–	7.95	–	34.00
Total	1,409.90	153.86	909.10	236.70	432.55	560.18	64.64	3,767.00
%	37.43	4.08	24.13	6.28	11.48	14.87	1.72	100.00

* Other includes 1051, 1058, 1062, 5105, 6005, 8003, 8004, 8020, 8021, 101004, 101054, 108019.